# SYSTEMS PHARMACOLOGY AND TRADITIONAL CHINESE MEDICINE

EDITED BY: Aiping Lu, Yonghua Wang and Wei Zhou
PUBLISHED IN: Frontiers in Pharmacology

frontiers Research Topics

# frontiers



ISSN 1664-8714
ISBN 978-2-88966-885-4
DOI 10.3389/978-2-88966-885-4

## About Frontiers

Frontiers is more than just an open-access publisher of scholarly articles: it is a pioneering approach to the world of academia, radically improving the way scholarly research is managed. The grand vision of Frontiers is a world where all people have an equal opportunity to seek, share and generate knowledge. Frontiers provides immediate and permanent online open access to all its publications, but this alone is not enough to realize our grand goals.

## Frontiers Journal Series

The Frontiers Journal Series is a multi-tier and interdisciplinary set of open-access, online journals, promising a paradigm shift from the current review, selection and dissemination processes in academic publishing. All Frontiers journals are driven by researchers for researchers; therefore, they constitute a service to the scholarly community. At the same time, the Frontiers Journal Series operates on a revolutionary invention, the tiered publishing system, initially addressing specific communities of scholars, and gradually climbing up to broader public understanding, thus serving the interests of the lay society, too.

## Dedication to Quality

Each Frontiers article is a landmark of the highest quality, thanks to genuinely collaborative interactions between authors and review editors, who include some of the world's best academicians. Research must be certified by peers before entering a stream of knowledge that may eventually reach the public - and shape society; therefore, Frontiers only applies the most rigorous and unbiased reviews.
Frontiers revolutionizes research publishing by freely delivering the most outstanding research, evaluated with no bias from both the academic and social point of view. By applying the most advanced information technologies, Frontiers is catapulting scholarly publishing into a new generation.

## What are Frontiers Research Topics?

Frontiers Research Topics are very popular trademarks of the Frontiers Journals Series: they are collections of at least ten articles, all centered on a particular subject. With their unique mix of varied contributions from Original Research to Review Articles, Frontiers Research Topics unify the most influential researchers, the latest key findings and historical advances in a hot research area! Find out more on how to host your own Frontiers Research Topic or contribute to one as an author by contacting the Frontiers Editorial Office: frontiersin.org/about/contact

# SYSTEMS PHARMACOLOGY AND TRADITIONAL CHINESE MEDICINE

Topic Editors:
**Aiping Lu,** Hong Kong Baptist University, Hong Kong, SAR China
**Yonghua Wang,** Northwest A and F University, China
**Wei Zhou,** The Affiliated Hospital of Shenzhen University Shenzhen, China

**Citation:** Lu, A., Wang, Y., Zhou, W., eds. (2021). Systems Pharmacology and Traditional Chinese Medicine. Lausanne: Frontiers Media SA. doi: 10.3389/978-2-88966-885-4

# Table of Contents

frontiers in Pharmacology

ORIGINAL RESEARCH
published: 12 November 2019
doi: 10.3389/fphar.2019.01356

# Anti-Hypoxic Molecular Mechanisms of *Rhodiola crenulata* Extract in Zebrafish as Revealed by Metabonomics

*Yi Ma[1], Yi Wu[1], Zhengchao Xia[1], Jingyi Li[1,3], Xiaorong Li[1,2], Pingxiang Xu[1,2], Xuelin Zhou[1,2]* and Ming Xue[1,2]**

[1] *Department of Pharmacology, Beijing Laboratory for Biomedical Detection Technology and Instrument, School of Basic Medical Sciences, Capital Medical University, Beijing, China,* [2] *Beijing Engineering Research Center for Nerve System Drugs, Capital Medical University, Beijing, China,* [3] *Beijing Tropical Medicine Research Institute, Beijing Friendship Hospital, Capital Medical University, Beijing, China*

OPEN ACCESS

**Edited by:**
*Aiping Lu,*
*Hong Kong Baptist University, Hong Kong*

**Reviewed by:**
*Shih-Yu Lee,*
*National Defense Medical Center, Taiwan*
*Guangguo Tan,*
*Fourth Military Medical University, China*

***Correspondence:**
*Ming Xue*
*xuem@ccmu.edu.cn*
*Xuelin Zhou*
*peterxlzhou@gmail.com;*
*zhouxuelin@ccmu.edu.cn*

**Specialty section:**
*This article was submitted to Ethnopharmacology, a section of the journal Frontiers in Pharmacology*

**Received:** *03 July 2019*
**Accepted:** *25 October 2019*
**Published:** *12 November 2019*

**Citation:**
*Ma Y, Wu Y, Xia Z, Li J, Li X, Xu P, Zhou X and Xue M (2019) Anti-Hypoxic Molecular Mechanisms of Rhodiola crenulata Extract in Zebrafish as Revealed by Metabonomics. Front. Pharmacol. 10:1356. doi: 10.3389/fphar.2019.01356*

The health supplement of *Rhodiola crenulata* (*RC*) is well known for its effective properties against hypoxia. However, the mechanisms of its anti-hypoxic action were still unclear. The objective of this work was to evaluate the molecular mechanisms of RC extract against hypoxia in a hypoxic zebrafish model through metabonomics and network pharmacology analysis. The hypoxic zebrafish model in the environment with low concentration (3%) of oxygen was constructed and used to explore the anti-hypoxic effects of RC extract, followed by detecting the changes of the metabolome in the brain through liquid chromatography–high resolution mass spectrometry. An *in silico* network for metabolite-protein interactions was further established to examine the potential mechanisms of RC extract, and the mRNA expression levels of the key nodes were validated by real-time quantitative PCR. As results, RC extract could keep zebrafish survive after 72-h hypoxia *via* improving lactate dehydrogenase, citrate synthase, and hypoxia-induced factor-1α in brains. One hundred and forty-two differential metabolites were screened in the metabonomics, and sphingolipid metabolism pathway was significantly regulated after RC treatment. The constructed protein-metabolites network indicated that the HIF-related signals were recovered, and the mRNA level of AMPK was elevated. In conclusion, RC extract had markedly anti-hypoxic effects in zebrafish *via* changing sphingolipid metabolism, HIF-related and AMPK signaling pathways.

**Keywords: *Rhodiola crenulata*, anti-hypoxia, zebrafish, metabonomics, network analysis**

## INTRODUCTION

Oxygen homeostasis is a survival prerequisite for most of the living creatures on the earth. Oxygen participates in the oxidation reaction for contributing necessary biology processing, and a suitable concentration of oxygen may drive carbon metabolism for energy production. When oxygen level reduces, some important pathways may be disturbed which could induce organ damage (Chaillou, 2018). Hypoxia, as a reduced oxygen environment, can induce the changes of physiology and

**Abbreviations:** RC, *Rhodiola crenulata*; LDH, citrate synthase; HIF-1α, hypoxia-induced factor-1α.

pathology in the body. People existing at high altitude are damaged by hypoxia environment, and organ ischemia with low oxygen supply can also impair their health (Hiraga, 2018).

*Rhodiolae crenulatae* radix et rhizoma ("Hong-Jing-Tian" in Chinese; abbreviated as RC) is the rhizoma of *Rhodiola crenulata* (Hook. f. et Thoms.) H. Ohba which is widely grown in plateau and mountainous areas at high altitude. The health supplement and nutraceuticals of RC are widely used to treat hypoxia during hypoxia environment in Tibet of China (Li et al., 2015). People arriving at high altitude area from the plain have to take RC product for some days to conquer altitude stress, since there is no other effective medicine for anti-hypoxia except oxygen inhalation. RC also shows some potential pharmacological effects, such as anti-inflammation, neuroprotection, and anti-fatigue action (Lee et al., 2013; Chang et al., 2018). RC extract contains active components, such as salidroside, herbacetin, and quercetin, which are possibly responsible for anti-hypoxic activity (Gupta et al., 2010; Zheng et al., 2012). However, up to date, the anti-hypoxic mechanisms of RC are not fully explored.

Metabonomics obtains the profiles of endogenous metabolites to illustrate the significant disturbance of molecular and metabolism pathways (Laíns et al., 2018). After environmental stress or drug treatment, the metabolomes in the cell, tissue, organ, and/or body are changed. Compared to the genomics and proteomics, the metabonomic approach is an increasingly active tool to explore the key biological mechanisms which is most closely linking to phenotype. Herbal extracts have multiple active components for treating diseases *via* various targets. It's unsuitable for herbs that only single protein target and pathway are explored for studying their mechanisms of action. Protein-protein interactions or protein-metabolite interactions are extensively used to investigate the pharmacological mechanisms of the herbs *via* multiple targets.

Zebrafish (*Danio rerio*) is a kind of model animals. Because of its short generation time, small size, and perfect fecundity, zebrafish model provides an excellent and wide application in pharmacological research (Jensen et al., 2011; Santos et al., 2017). Moreover, compared to other mammals, zebrafish model has a potential ability to adapt to hypoxia environment (Long et al., 2015). In recent researches, zebrafish embryos and larvae as animal models have been used to study hypoxia stress (Long et al., 2015). Thus, in our current study, we developed an adult zebrafish model under hypoxia to reveal the biological mechanisms of RC extract by using metabonomics and bioinformatics tools (**Figure 1**).

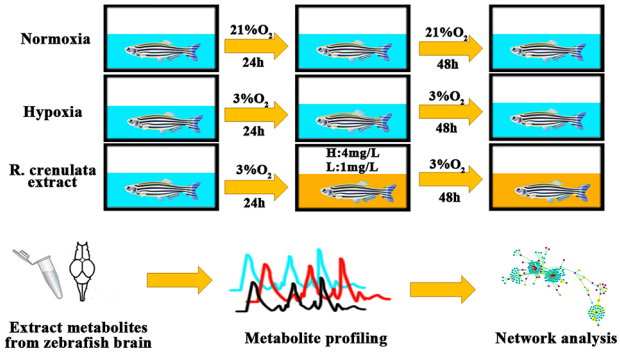


**FIGURE 1 |** The process of zebrafish handling with different concentrations of oxygen. Background in blue indicates the normoxia or hypoxia environment and background in yellow shows RC extract treatment.

# MATERIALS AND METHODS

## Chemicals and Materials

Acetonitrile (LC-MS grade), water (LC-MS grade), and formic acid (LC-MS grade) were purchased from the Fisher Scientific (Fair Lawn, NJ, USA). Methanol (HPLC grade) was obtained from the Fisher Scientific (Fair Lawn, NJ, USA). Power-up SYBGREEN was purchased from the Invitrogen Co. (Carlsbad, CA, USA). Authentic standard of salidroside (purity >98%) was purchased from the ChromaBio Co. (Chengdu, Sichuan, China). Authentic standards of rhodiosin, herbacetin, and kaempferol (purity >98%) were obtained from the YuanYe Co. (Shanghai, China).

## Plant Material and Herbal Extraction

The radix et rhizoma of *Rhodiola crenulata* (Hook. f. et Thoms.) H. Ohba was collected from the Xinjiang Region of China and supplied by the Kailai Biological Engineering Co., Ltd. (Xi'an, China). It was identified by Dr. Rong Luo (School of Chinese Medicine, Capital Medical University). A specimen (voucher number 2016-EJ819) was deposited in the Department of Materia Medica, School of Chinese Medicine, Capital Medical University.

The raw materials were powdered, and then extracted by heating reflux with 75% ethanol for two hours and repeated twice. After filtered, the combined solution was dried in vacuum for the collection of dry extract. The dried extract was stored in the desiccator before use. The yield of the dried extract was more than 20%.

## Chemical Composition Analysis

For the qualitation of the major components in the RC extract, Agilent 1100 HPLC-UV was used with a Grace Alltima $C_{18}$ column (4.6 × 250 mm, 5μm). The mobile phase contained solution A (water with 0.2% formic acid) and solution B (acetonitrile). The gradient elution program was set as followed: 0–15 min, 5%–12% B; 15–40 min, 12%–15% B; 40–50 min, 15%–20% B; 50–80 min, 20%–25% B; 80–95 min, 25%–30% B; 95–110 min, 30%–35% B. The flow rate and detection wavelength were set at 1 ml/min and 280 nm, respectively. A typical HPLC-UV chromatogram of RC extract was shown in **Figure S1**.

For the quantitation of its major components, 1 mg of RC extract was weighed and dissolved in the solvent (methanol/water = 1:1) to the final volume of 1 ml. After sonicated for 30 min and centrifuged at 13,000 g for 10 min, the supernatant was collected. UPLC-MS/MS analysis was carried out using an Agilent 1290 system coupled with a triple-quadrupole Agilent 6490 mass spectrometer which was equipped with an ESI ionization source. The negative mode was used to quantify the amounts of active

components. Chromatographic separation was performed by using the Waters Acquity HSS T3 column (2.1 × 150 mm, 1.8 μm). A gradient elution program separated all compounds with mobile phase A solution (0.1% formic acid in water) and B solution (0.1% formic acid in acetonitrile). The gradient elution program was performed as followed: 0–7 min, 10%–60% B; 7–8 min, 60%–100% B; 8–8.1 min, 100% B; 8.1–9 min, 100%–10% B; 9–10 min, 10% B. The total run time was 10 min. The ion pairs of standard active components and parameters of CE were listed as followed: salidroside, m/z 345.2→289.9, CE -10V; rhodiosin, m/z 609.1→301, CE -20V; herbacetin, m/z 300.9→255, CE -35V; kaempferol, m/z 285.0→92.8, CE -40V. The dwell time was 50 ms and fragmentor was 380V. The sample was tested in triplicate.

As shown in **Figure S1**, four components were identified with their respective authentic standards by LC-MS in the negative mode. The contents (w/w extract) of salidroside, rhodiosin, kaempferol, and herbacetin were 15.7 ± 0.1‰, 8.4 ± 0.1‰, 1.42 ± 0.06‰, and 0.95 ± 0.03‰, respectively.

## Zebrafish Handling

The wild-type TU zebrafish (mixed gender, 6 months old, 5 cm in length, 0.25 g in mass) were obtained from the Laboratory Animals Center of Capital Medical University (LACCMU, Beijing, China). Prior to the experiments, all zebrafish were acclimated under 14:10 h light-dark cycle and constant temperature (25 ± 2°C) for at least two weeks in a zebrafish feeding system (Far East Instrument Co., Ltd., Taiwan, China). The feeding system was equipped with 10-L tanks, a recirculating freshwater supplier, an air pump, a biological and mechanical filtration system, and ultraviolet lamps. The zebrafish husbandry and experiments were conducted by following the protocols approved by the Animal Experimentation Ethics Committee of Capital Medical University (AEEC No. AEEI-2016-016).

## Hypoxia Model and Drug Treatment

Adult zebrafish were placed in the chamber with pipes connecting with nitrogen gas flowing. After the environment has reached 3% of $O_2$, the water chambers were pre-equilibrated with nitrogen gas for at least 2 h. The concentration of oxygen in the water and air was validated by an oxygen sensor (SX716, SANXIN, Shanghai, China). When nitrogen gas was balanced, the model group was exposed under hypoxia for 72 h. For RC treatment, the zebrafish were exposed to 24-h hypoxic treatment (3% oxygen), followed by administration of RC extract for 24-h and repeated administration for another 24 h. RC extract (lower than 100 mg/L) was totally dissolved in the water without observed precipitate. The $LC_{50}$ value of RC extract in adult zebrafish was about 43 mg/L, and the two selected concentrations 4 mg/L and 1 mg/L of RC extract without observed toxicity were used for the above-mentioned treatment.

## Hypoxia-Related Biomarkers

After RC treatment, the zebrafish were sacrificed through putting into liquid nitrogen. The frozen brain samples were collected by forceps, weighed, and homogenized with cold phosphate buffered saline (PBS) solution. The activities of lactate dehydrogenase (LDH) and citrate synthase (CS) were tested by using the LDH and CS kit (Nanjing Jiancheng Co., China), respectively. HIF-1α was detected by the ELISA kit (Nanjing Jiancheng Co., China).

## Sample Preparation for Metabonomics

For metabonomic analysis, the frozen brain samples of another batch were weighed and homogenized with cold methanol and water (4:1, v/v) (Yuan et al., 2012). After incubated for 20 min and centrifuged at 13,000 rpm for 20 min at 4°C, the metabolites in brain were extracted in the supernatant. The samples were pooled as a quality control (QC) group. All samples were subjected to liquid chromatography–high resolution mass spectrometry (LC-HRMS).

## Metabonomics Analysis

LC-HRMS analyses were performed by using the Waters Acquity ultra-performance liquid chromatography (UPLC) coupled with Synapt G2-Si mass spectrometer which was equipped with data independent analysis (DIA) mode. The separation of polar metabolites was achieved through Waters Acquity HSS T3 (2.1 × 150 mm, 1.8 μm) column, while the nonpolar metabolites were separated by the Waters CSH $C_{18}$ (2.1 × 150 mm, 1.7 μm) column. The parameters for mass spectrometry were listed as followed: capillary 3 kV for positive mode and 2.5kv for negative mode; sampling cone, 40V; source offset, 80V; cone gas, 50 L/h; desolvation gas flow, 600 L/h; source temperature, 120°C.

For the analysis of polar metabolites, the mobile phase program was set with 0.1% formic acid in water as mobile phase A and 0.1% formic acid in acetonitrile as mobile phase B. The gradient elution program for positive mode was performed as followed: 0–7.0 min, 0.1%–33% B; 7.0–12.0 min, 33%–44% B; 12.0–14.0 min, 44%–64% B; 14.0–18.0 min, 64%–100% B; 18.0–20.0 min, 100% B; 20.1–22.0 min, 0.1% B. Gradient elution program for negative mode was set as followed: 0–3.0 min, 0.1%–35% B; 3.0–6.0 min, 35%–44% B; 6.0–8.0 min, 44%–64% B; 8.0–13.0 min, 64%–100% B; 13.0–15.0 min, 100% B; 15.1–17.0 min, 0.1% B.

For the analysis of non-polar metabolites, the parameters were set with solution A (acetonitrile/water [60:40] containing 10 mM ammonium formate and 0.1% formic acid), and solution B (Isopropanol/acetonitrile [90:10] containing 10 mM ammonium formate and 0.1% formic acid). The gradient elution program for positive and negative modes was set as followed: 0–2.0 min, 40%–43% B; 2.0–2.1 min, 43%–50% B; 2.1–12.0 min, 50%–54% B; 12.0–12.1 min, 54%–70% B; 12.1–18.0 min, 70%–99% B; 18.1–20.0 min, 40% B.

The continuum data were collected from 50–1200 Da and the scan rate was 0.2 s. The representative chromatograms for metabonomics are presented in **Figure S2**. The QC samples were inserted to evaluate the stability of LC-MS system.

## Data Analysis

LC-MS data were analyzed using the Progenesis QI software (Nonlinear Dynamics, Newcastle, U.K.). After retention time and

*m/z* were calculated, the peaks from each sample were aligned and picked. The isotope and adduct deconvolution were used to validate that the numbers of peaks were detected. Total ions were used for normalization. To obtain the metabolites from groups with significant differentials, the metabolites were scaled by the Pareto transformed. Ezinfo (3.0, Umetrics, Umea, Sweden) and SIMCA-P (13.0, Umetrics, Umea, Sweden) were used to achieve principle components analysis (PCA) and orthogonal partial least-squares discriminant analysis (OPLS-DA). The variable importance in the projection (VIP) value, *p*-value, and fold change from these metabolites were combined as the features to screen the differential metabolites. In addition, Benjamini and Hochberg method was used for the correction of false discovery rate (FDR). The compounds (VIP > 1, FDR < 0.05) were identified from Human Metabolome Database (HMDB), Kyoto Encyclopedia of Genes and Genomes (KEGG), and LipidMaps databases. Pathway analysis and enrichment for metabolites were analyzed by Metaboanalyst 4.0 (www.metaboanalyst.ca) (Chong et al., 2018). The QC samples were conducted for PCA score to assess LC-MS stability.

## Interaction Network Construction Between Protein and Metabolites

To reveal the anti-hypoxic mechanisms of action of RC extract, MBROLE v.2.0 (http://csbg.cnb.csic.es/mbrole) was used to construct potential protein-metabolite interaction and enrichment analysis (López-Ibáñez et al., 2016). The likely proteins of hypoxia interacting with metabolites were collected for further analysis using the OMIM, HDMB, and STRING protein-protein interaction databases. The visualization of the formed network was achieved by Cytoscape v.3.6. In order to realize the function of a disturbing protein in the hypoxia group or treatment group, the clusters were applied to show protein functions.

## Validation of Potential Targets

Total RNA from the brain was extracted using Trizol (Sigma-Aldrich, USA). RNA was reversely transcripted to cDNA by ReverTra Ace (TOYOBO, Japan) *via* the Oligo dT primers. PCR SYBR master mix (Invitrogen, USA) was used for amplification of each potential target. The cycling conditions were listed as followed: 50°C, 2 min for activation; 95°C, 2 min for DNA polymerase; 95°C, 15 s for denaturing; and 60°C, 1 min for annealing. Processes of denaturing and extending were repeated for 40 times. The sequences of primers are available in **Table S1**. Relative mRNA expression was calculated through normalization with the housekeeping gene *gapdh*.

# RESULTS

## Hypoxia Biomarkers

RC extract could markedly improve the survival of zebrafish in the hypoxic environment (3% oxygen). Meanwhile, the activities of LDH and HIF-1α were significantly declined in the RC group, when compared to those in the hypoxia group (**Figure 2**). The activity of CS was rapidly reduced which may be due to the injury in the hypoxic environment. However, the levels of LDH, HIF-1α, and CS in the normoxia group were stable during the measurements. In the RC treatment group under normoxia, as illustrated in **Figure S2**, the hypoxic biomarkers showed no significant change. Thus, RC extract could keep homeostasis for the hypoxia-related biomarkers, indicating that RC had excellent anti-hypoxia effect under hypoxic environment.

## Multivariate Data Analysis in Metabonomics

To evaluate the anti-hypoxic mechanisms of RC extract, the metabolites in different groups were separated and analyzed by the positive and negative modes of base peak intensity chromatograms which were obtained from LC-HRMS. The profiles of base peak intensity were illustrated in **Figure S3**. The closely gathered plots of the QC group showed good stability of the LC-MS system, as illustrated in **Figure S4**. After normalization and peaks alignment *via* the QI software, these peaks were picked from the different groups to construct multivariate analysis in EZinfo and SIMCA-P, followed by multivariate statistical approaches of PCA. The PCA plots ($R^2 = 0.79$, $Q^2 = 0.50$) clearly separated normoxia and hypoxia group in the metabolic state, and the changes of metabolome were in a time-dependent manner, as depicted in **Figure S5A**. After RC extract treatment, the metabolite traces became similar to the normal group. As depicted in **Figure S5B**, the different metabolites were recovered after RC treatment as the PCA plots illustrated. Moreover, the plots of 24-h treatments of 4 mg/L and 1 mg/L of RC were similar to that of hypoxia group in **Figure 3A**, whereas the plots of 72-h RC treatment at 4 mg/L were almost similar with that of normoxia group in **Figure 3B**. The results indicated that RC had a better effect at higher concentration (4 mg/mL).

## Pathway Analysis

Potential biomarkers with VIP value more than 1 and FDR value lower than 0.05 were selected from loading plots *via* OPLS-DA and ANOVA analysis. The metabolites with fold change over 1.2 were collected. Several databases (e.g. HMDB, KEGG, and LipidMaps) were used to identify these compounds *via* fragment peaks by data-independent acquisition mode. One hundred and forty-two of the total metabolites were identified when compared with the metabolomes among the normoxia, hypoxia, and 4 mg/L of RC groups, and their chemical information was shown in **Table S2**. Besides, as depicted in **Figure 4**, the relative concentration trends of numerous differential metabolites were recovered by RC treatment. The enrichment and pathway analysis showed that the pathways of sphingolipid metabolism, glycerophospholipid metabolism, and citrate cycle were obviously disturbed under hypoxia and re-adjusted after RC extract treatment (**Figure 5**). The taurine and hypotaurine metabolism, as well as alanine, aspartate, and glutamate metabolism, were also changed after RC extract treatment under hypoxia.

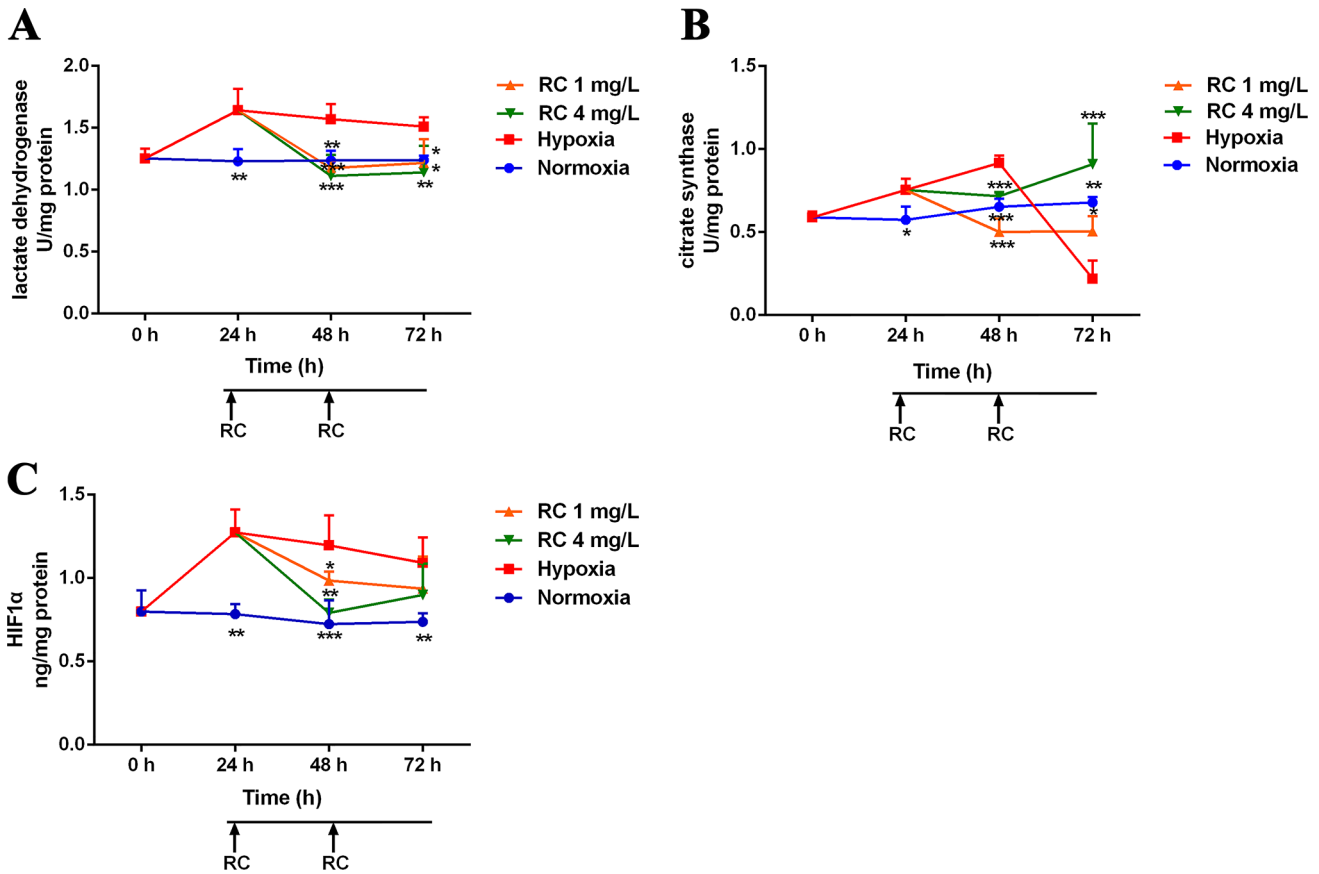


**FIGURE 2 |** The activities of hypoxic biomarkers including **(A)** lactate dehydrogenase, **(B)** citrate synthase, and **(C)** hypoxia-induced factor-1α in different RC extract treatment groups under hypoxia when compared to the hypoxia and the normoxia groups. *$p < 0.05$, **$p < 0.01$, and ***$p < 0.001$ versus the hypoxia control group. Data are presented as the mean ± SD (n = 4).

## Network Construction of Protein and Metabolites Interaction

The cluster analyses were established to reveal several functions influenced by RC treatment as depicted in **Figure 6**. The most influenced part is oxidoreductase and lipase activity. Moreover, O-acyltransferase and phospholipase may also participate in the anti-hypoxic function of RC extract. The metabolite-protein-hypoxia interaction network was built to explore the hub nodes of RC extract treatment. In order to directly obtain interaction with the metabolites in hypoxia, the first neighbor nodes of interaction network were conducted. As associated with RC treatment under hypoxia, there were some key proteins including histone lysine demethylase (PHF8), hypoxia-inducible factor 1-alpha (HIF-1α), Egl nine homolog 1 (EGLN1), Egl nine homolog 2 (EGLN2), Egl nine homolog 3 (EGLN3), transmembrane prolyl 4-hydroxylase (P4HTM), 5'-AMP-activated protein kinase catalytic subunit alpha-1 (PRKAA1), and cytosolic phospholipase A2 (PLA2G4A).

To verify this network, the mRNA levels were quantified by real-time PCR. The results showed that these genes obviously changed in different treatment groups (**Figure 7**). The encoded genes of HIF prolyl-hydroxylase (PHD) including *egln1b* and *egln3* were elevated under hypoxia, whereas their expressions were decreased after RC treatment, while *egln2* had a reverse tendency. As shown in the protein-metabolite network, *p4htm* was connected with succinic acid, and its mRNA level was decreased by RC treatment. As encoding AMPK kinase, the mRNA expression levels of *prkab1b* and *prkab1a* were improved in RC treatment group when compared to hypoxia group. Moreover, the mRNA level of *phf8* was decreased *via* RC treatment when compared to the hypoxia group. As important hub nodes interacted with the multiple differential metabolites including phosphatidylcholine and phosphatidylethanolamine, the mRNA levels of *pla2g4aa* and *pla2g4ab* were disturbed under hypoxia, and reversed after RC treatment.

## DISCUSSION

*Rhodiola crenulata* is a well-known traditional Chinese medicine (TCM) reported to enhance hypoxia endurance capacity. RC extract was widely used to treat high altitude illness and mountain sickness (Chen et al., 2014). Our results supported the anti-hypoxic

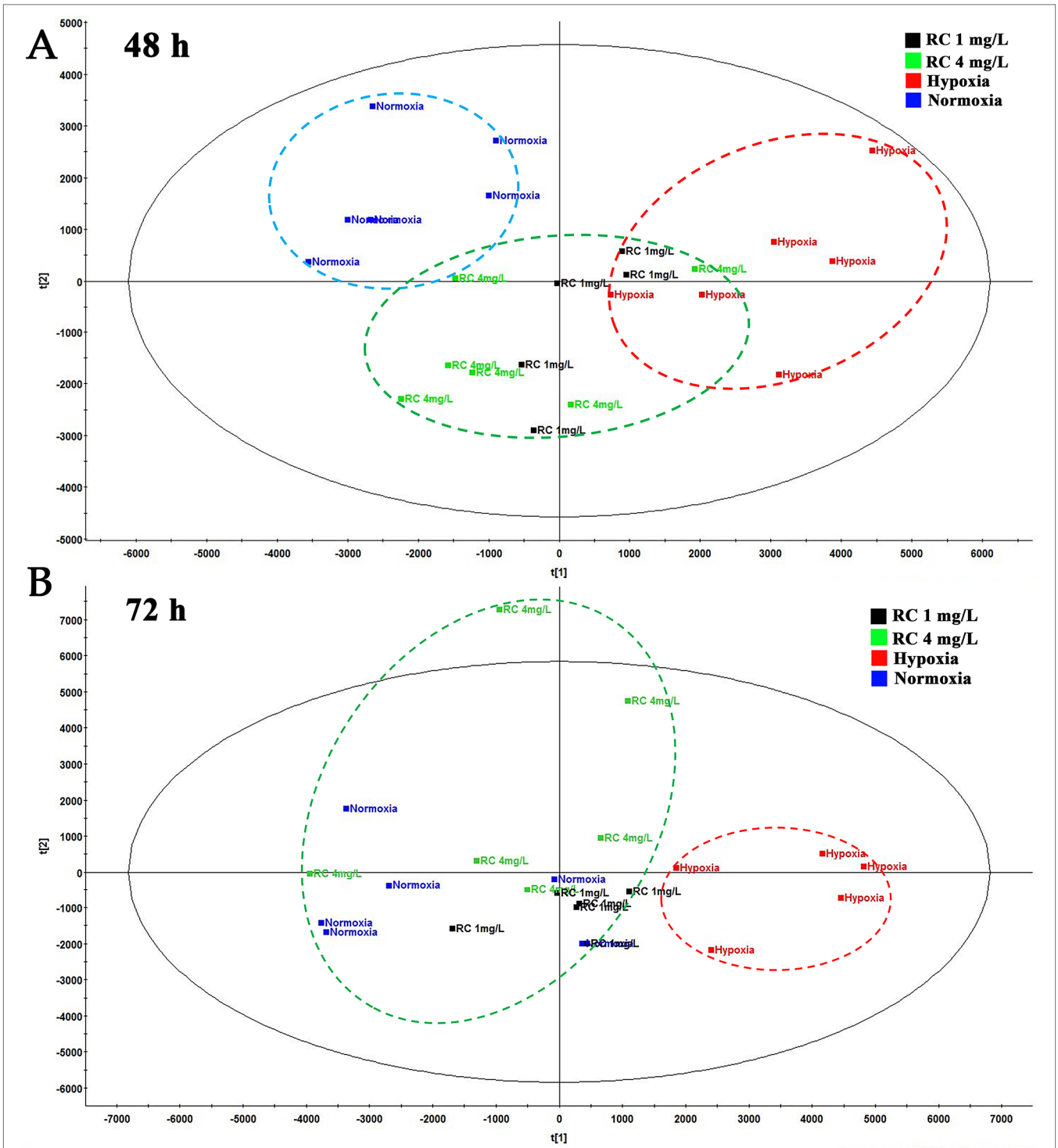


**FIGURE 3 |** The PCA plot among normal, hypoxia, and RC extract treatment groups. The red dash circle shows hypoxia control. Blue dash circle shows normoxia control. **(A)** The PCA score among normal, hypoxia and treatment after 48-h treatment. **(B)** The PCA score among three groups after 72-h treatment (n = 5).

effects of RC in hypoxic environments, and RC could maintain zebrafish survival, which are consistent to its clinical effect.

LDH, HIF-1α, and CS possess different functions in the hypoxic environment. LDH, reflecting the degree of hypoxia, is a potential biomarker for hypoxic injury in clinical diagnosis (Fineschi et al., 2017). HIF-1α is a sensitive oxygen sensor that has different biological functions in hypoxia. Our results indicated that RC extract could decrease LDH activities and HIF-1α

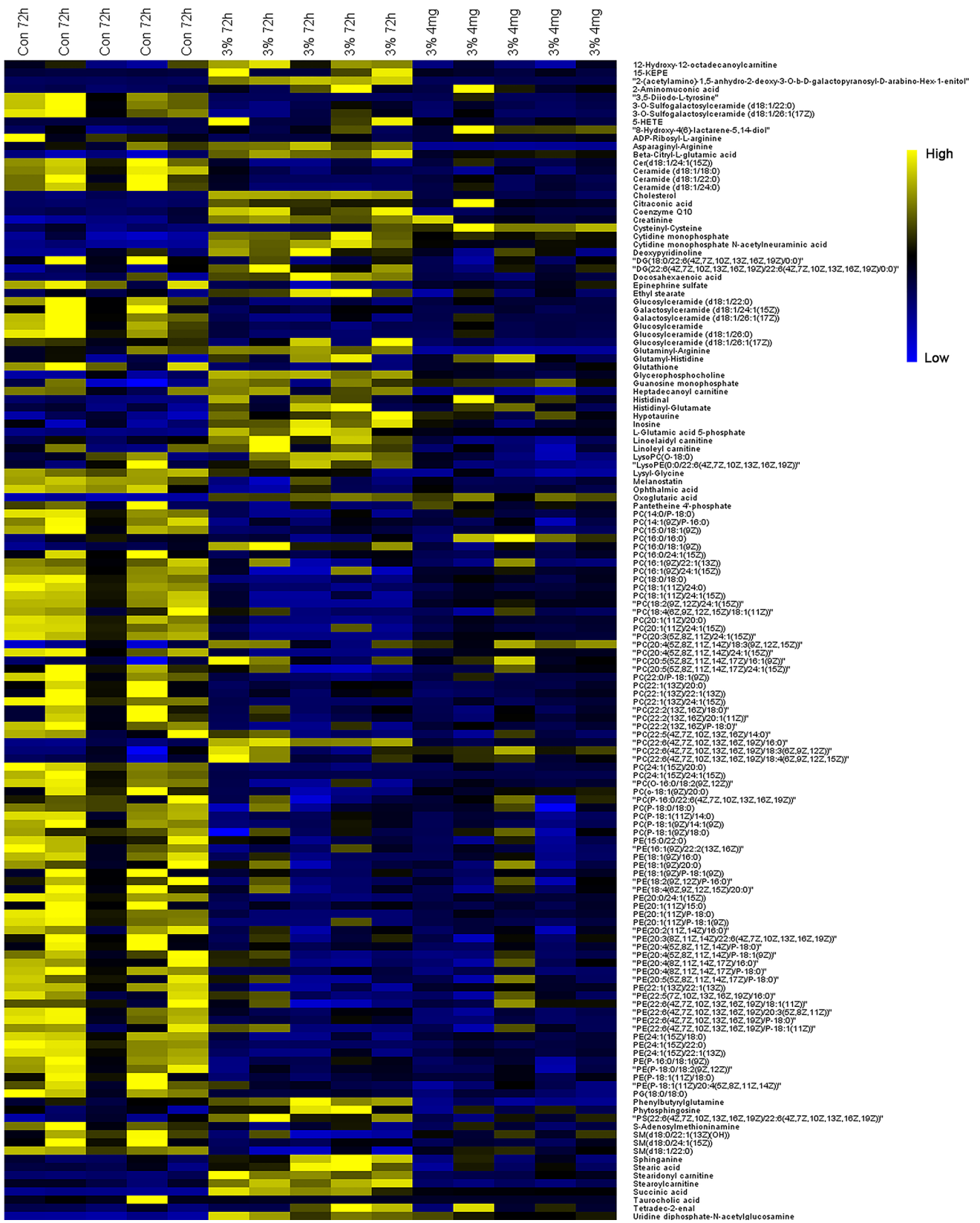


**FIGURE 4 |** The heatmap of metabolites among normoxia, 72-h hypoxia and RC extract (4 mg/L) treatment. Metabolites labeled in yellow or blue indicate the high or low levels, respectively.

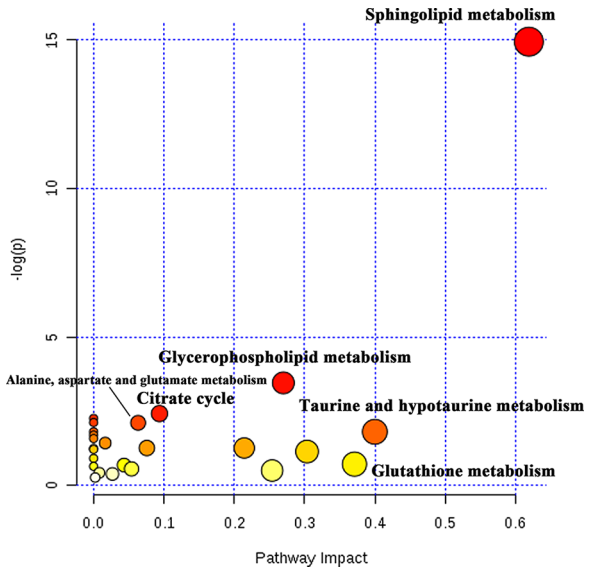


**FIGURE 5 |** The pathway analysis of differential metabolites. The tendency of red circles shows the importance of metabolism pathway.

expression which were elevated under hypoxia. The activity of citrate synthase, a crucial enzyme to produce citrate, indicates the capacity of aerobic respiration and mitochondrial function (Larsen et al., 2012). Mikaela et al. showed that high altitude and chronic hypoxia could increase CS activities (Mandic et al., 2013; Lui et al., 2015). Similar to our data, the CS activity in hypoxia group increased after 48-h hypoxia condition, indicating that the zebrafish enhanced the CS activity to conquer hypoxia in the first 48-h hypoxic treatment. However, if mitochondria were injured, CS would decrease in hypoxic environment (Warren et al., 2017). This is similar to our results on CS activity which was rapidly declined after 72-h serious hypoxia, showing that after 72-h hypoxic treatment, the mitochondria of zebrafish possibly were damaged. Meanwhile, to resemble with the tendency of normoxia group, CS activity was kept to be steady by RC extract treatment. In brief, our results indicated that RC treatment improved these direct hypoxia-related indicators, suggesting that RC could keep zebrafish adaptation in hypoxia environments.

The PCA scores in metabonomics illustrated that the plots of higher concentration of RC extract were closed to the plot of normoxia group, meaning that RC had an excellent effect on anti-hypoxia through regulating endogenous metabolites. Because TCM contains multiple active components, the network pharmacology provides an appropriate approach, as a tool for system biology, to fully understand the mechanisms of actions (Zhang et al., 2019). For RC extract, the multiple molecular targets could be influenced by RC treatment to improve the anti-hypoxic ability of organs. In our study, the pathway analysis and metabolite-protein interaction network

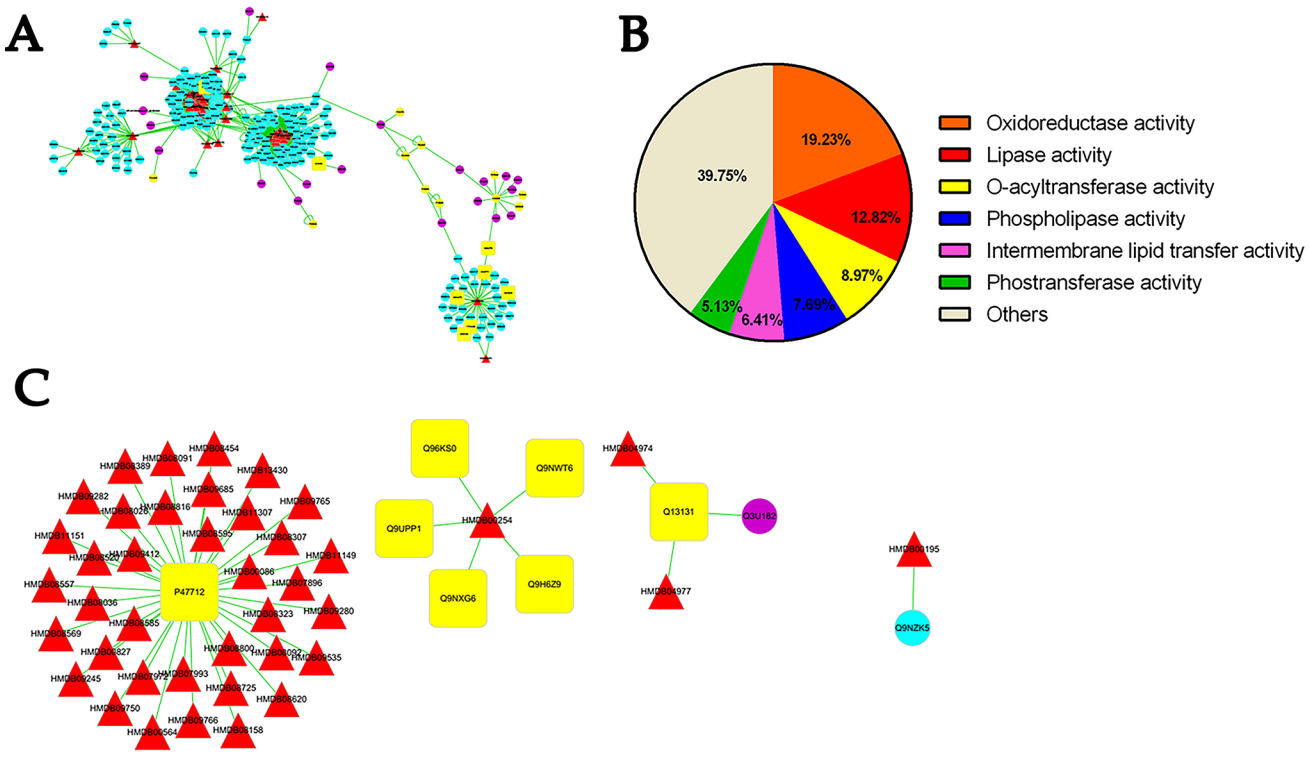


**FIGURE 6 |** The analysis of protein-metabolite interaction network. Whole network **(A)**, the molecular functions of the selected proteins **(B)**, and the first neighbor node of proteins linking to metabolites **(C)** indicate the interactions between protein and metabolites. Red triangle shows differential metabolites *via* metabonomics and blue circle shows their interacting proteins listed in the MBRole database. Yellow circle indicated interacting proteins with metabolites straightly correlated to hypoxia. Q9UPP1: PHF8; Q9NWT6: HIF1α; Q9GZT9: EGLN1; Q96KS0: EGLN2; Q9H6Z9: EGLN3; Q9NXG6: P4HTM; Q13131: PRKAA1; P47712: PLA2G4A.

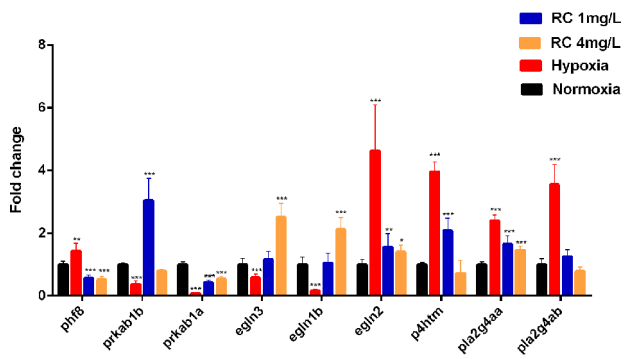


**FIGURE 7 |** The mRNA expression of key node in zebrafish brain tissue after different RC extract treatment under hypoxia, as detected by real-time PCR. *$p < 0.05$, **$p < 0.01$, ***$p < 0.001$ versus hypoxia groups. Data are presented as mean ± SD (n = 6).

were conducted, indicating that sphingolipid metabolism, HIF-1α related and AMPK signaling pathways were obviously regulated under hypoxia.

Sphingolipid metabolism is implicated in various signaling pathways and pathological changes such as cell membrane injury and inflammation. Sphingomyelin (SM), an important molecule in sphingolipid metabolic pathway, is essential for the formation of plasma membrane and involves in cell proliferation and growth (Adada et al., 2016; Bienias et al., 2016). So far, several studies have proved that the elevated concentration of SM plays a vital role in the stabilization of cell membrane against hypoxia injury (Zager, 2000; Moschetta et al., 2000). LDH activity is a common biomarker to reflect cell injury and cell integrity, and it decreased *via* RC treatment. In addition, low concentration of oxygen could reduce the SM level, however, RC could recover its level. Thus, as change of sphingolipid metabolic pathway after RC treatment, the increased level of SM was consisted with the decrease of LDH activity, indicating that RC treatment might enhance cell protection to resist hypoxia. Meanwhile, the activities of lipase and phospholipase were also altered obviously with regulation of sphingolipids. Several researches have provided that sphingolipid metabolism influences not only lipase activity, but also the activity of cytosolic phospholipase A2 (cPLA2) (Nakamura et al., 2010; Nakamura and Murayama, 2014). The cPLA2 increases the level of arachidonic acid, leading to inflammatory reactions by disrupting endogenous metabolic balance (Meirer et al., 2014). Two genes *pla2g4aa* and *pla2g4ab*, encoding cPLA2 in zebrafish, were up-regulated in hypoxic environment, but recovered after RC treatment. In addition, two metabolites, 5-hydroxyeicosatetraenoic acid (5-HETE) and 15-Oxo-ETE (15-KETE), were enriched in arachidonic acid metabolic pathway, which were inflammatory factors (Samuel et al., 1993; Powell and Rokach, 2015). With declining of cPLA2, they were suppressed *via* RC treatment, indicating that inflammation was alleviated. In summary, RC treatment could increase cellular sphingomyelin as a critical molecule in sphingolipid metabolism, and finally cause the decline of cPLA2, an inflammatory producer.

HIF-1α is a well known and hub biomarker for hypoxia. Our results indicated that the level of HIF-1α decreased after RC treatment, which was consistent to the data of the mRNA expression levels of genes regulating HIF-1α. PHF8 plays an essential role in hypoxia stress, and its knockdown can reduce the activation of HIF-1α (Maina et al., 2017). EGLN1, EGLN2, and EGLN3 are a family of proteins which can influence hypoxia process (Schofield and Ratcliffe, 2004; Ivan and Kaelin, 2017). The *egln1*, as called *egln1b* in zebrafish, encodes PHD2 to degrade HIF-1α by prolyl hydroxylation in an aerobic environment (Schofield and Ratcliffe, 2004). The mRNA expression of *egln1b* in treatment group was elevated when compared to hypoxic group. PHD1 and PHD3 were also encoded by *egln2* and *egln3*, respectively. Similar to the expression tendency of *egln1b*, the mRNA level of *egln3* was reduced under hypoxia but increased after RC treatment. However, *egln2* had an opposite trend in an aerobic environment when compared to hypoxia. It is possible that PHD2 is main regulator and PHD3 is most relevant isoform for HIF-1α (Appelhoff et al., 2004). P4HTM also plays essential roles in the HIF-related signaling pathway to balance oxygen homeostasis, and inhibition of P4HTM is regarded as a potential target for treating ischemia (Hyvärinen et al., 2010). Our work showed that the mRNA expression of *p4htm* was almost four-fold changes under hypoxia whereas its expression level in RC (4 mg/L) group were similar to that in the normoxia group.

Alternatively, citrate cycle has a critical role in essential energy metabolism. Succinate, as a key metabolic intermediate in TCA circle (Tretter et al., 2016; Lukyanova et al., 2018), regulates the transcription of HIF-1α both in the Krebs cycle and in GABA shuttle. After RC treatment, the treatment group declined the concentration of succinate so as to increase HIF-1α degradation, which was consistent to the above-mentioned ELISA results. By elevating HIF-1α signal pathway, some researchers have revealed that it could increase inflammatory cytokines to up-regulate the formation of arachidonic acids which are inflammatory factors (Pchejetski et al., 2010; Tannahill et al., 2013; Guo et al., 2017). Thus, the declined HIF-1α could cause down-regulation of arachidonic acid, which partly may reduce the inflammatory effect and subsequently alleviate hypoxia damage.

In addition, *in silico* network construction indicated that AMP-related signaling pathway was also elevated. AMPK involved in regulating energy metabolism in hypoxic environment. As an AMP-activated protein kinase and an analog with PRKAB1B

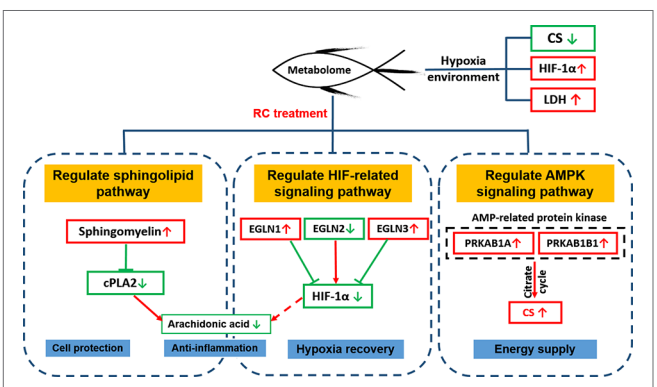


**FIGURE 8 |** The molecular mechanisms of RC extract against hypoxia in zebrafish revealed by metabonomics and *in silico* network construction.

and PRKAB1A in zebrafish, PRKAA1 can improve hypoxia tolerance under nutrient-deprived conditions (Sun et al., 2018). Lee et al. showed that RC extract has potential to exert the glucose-lowering effect *via* activating AMPK signaling pathway (Lee et al., 2015). This evidence was consistent with our results, and supported that AMPK signaling pathway played a crucial role in the regulation of RC extract against hypoxia. During hypoxia for three days, *prkab1a* and *prkab1b* were inhibited. It's likely exhausted in the hypoxic environment due to the acceleration of energy consumption. In contrast, the expressions of these genes were increased after RC treatment, suggesting that these genes had actions on energy homeostasis. After 72-h hypoxia treatment, CS activity was obviously suppressed in the hypoxic group which may be due to the inhibition of AMPK and the exhaustion of energy, whereas RC treatment could keep energy homeostasis.

Nevertheless, we confirmed some important metabolites based on the databases. A further study should be performed for the exact mechanisms of RC extract to anti-hypoxia action *via* the molecular and systemic biology approaches.

## CONCLUSION

Taken together, our work firstly used metabonomics and hypoxic zebrafish model to reveal the metabolic pathway recovered by RC extract. Differential metabolites based on the databases were screened and the interaction network between the protein and metabolites, as regulated by RC treatment, was constructed. As depicted in **Figure 8**, RC shows an excellent effect on anti-hypoxia *via* multiple molecular mechanisms. Sphingolipid metabolism, HIF-related and AMPK signaling pathways were regulated by RC extract to keep zebrafish survive under hypoxia. Our investigations provided not only an insight that zebrafish could be a tool to study hypoxia, but also a systematic understanding of anti-hypoxic molecular mechanisms of RC extract.

## DATA AVAILABILITY STATEMENT

All datasets generated for this study are included in the article/ **Supplementary Material**.

## ETHICS STATEMENT

The animal study was reviewed and approved by Animal Experimentation Ethics Committee of Capital Medical University.

## AUTHOR CONTRIBUTIONS

YM and MX designed the study and wrote the article. YW, ZX, and JL carried out experiments. XL and PX developed analysis tools. XZ and MX gave advice and careful revision.

## ACKNOWLEDGMENTS

This study was financially supported by the National Natural Science Foundation of China (Grant Nos. 81573683 and 81773803).

## SUPPLEMENTARY MATERIAL

The Supplementary Material for this article can be found online at: https://www.frontiersin.org/articles/10.3389/fphar.2019.01356/full#supplementary-material

## REFERENCES

Adada, M., Luberto, C., and Canals, D. (2016). Inhibitors of the sphingomyelin cycle: sphingomyelin synthases and sphingomyelinases. *Chem. Phys. Lipids* 197, 45–59. doi: 10.1016/j.chemphyslip.2015.07.008

Appelhoff, R. J., Tian, Y. M., Raval, R. R., Turley, H., and Harris, A. L. (2004). Differential function of the prolyl hydroxylases PHD1, PHD2, and PHD3 in the regulation of hypoxia-inducible factor. *J. Biol. Chem.* 279, 38458–38465. doi: 10.1074/jbc.M406026200

Bienias, K., Fiedorowicz, A., Sadowska, A., Prokopiuk, S., and Car, H. (2016). Regulation of sphingomyelin metabolism. *Pharmacol. Rep.* 68, 570–581. doi: 10.1016/j.pharep.2015.12.008

Chaillou, T. (2018). Skeletal muscle fiber type in hypoxia: adaptation to high-altitude exposure and under conditions of pathological hypoxia. *Front. In Physiol.* 9, 1450. doi: 10.3389/fphys.2018.01450

Chang, P., Yen, I., Tsai, W., Chang, T., and Lee, S. (2018). Protective effects of rhodiola crenulata extract on hypoxia-induced endothelial damage *via* regulation of ampk and erk pathways. *Int. J. Mol. Sci.* 19, 2286. doi: 10.3390/ijms19082286

Chen, C., Hou, C., Bernard, J. R., Chen, C., and Hung, T. (2014). Rhodiola crenulata andcordyceps sinensis-based supplement boosts aerobic exercise performance after short-term high altitude training. *High Alt. Med. Biol.* 15, 371–379. doi: 10.1089/ham.2013.1114

Chong, J., Soufan, O., Li, C., Caraus, I., and Li, S. (2018). Metaboanalyst 4.0: towards more transparent and integrative metabolomics analysis. *Nucleic Acids Res.* 46, 486–494. doi: 10.1093/nar/gky310

Fineschi, V., Viola, V. V., Russa, R. L., Santurro, A., and Frati, P. (2017). A controversial medicolegal issue: timing the onset of perinatal hypoxic-ischemic brain injury. *Mediators Inflammation* 2017, 6024959. doi: 10.1155/2017/6024959

Guo, X. K., Zhu, Z. Q., Zhang, W. J., Meng, X. X., and Zhu, Y. (2017). Nuclear translocation of HIF-1α induced by influenza A (H1N1) infection is critical to the production of proinflammatory cytokines. *Emerg. Microbes Infect.* 6, 1–8. doi: 10.1038/emi.2017.21

Gupta, V., Lahiri, S. S., Sultana, S., Tulsawani, R. K., and Kumar, R. (2010). Anti-oxidative effect of rhodiola imbricata root extract in rats during cold, hypoxia and restraint (C–H–R) exposure and post-stress recovery. *Food Chem. Toxicol.* 48, 1019–1025. doi: 10.1016/j.fct.2010.01.012

Hiraga, T. (2018). Hypoxic microenvironment and metastatic bone disease. *Int. J. Mol. Sci.* 19, 3523. doi: 10.3390/ijms19113523

Hyvärinen, J., Hassinen, I. E., Sormunen, R., Mäki, J. M., and Kivirikko, K. I. (2010). Hearts of hypoxia-inducible factor prolyl 4-hydroxylase-2 hypomorphic mice show protection against acute ischemia-reperfusion injury. *J. Biol. Chem.* 285, 13646–13657. doi: 10.1074/jbc.M109.084855

Ivan, M., and Kaelin, W. G. (2017). The egln-hif o2-sensing system: multiple inputs and feedbacks. *Mol. Cell* 66, 772–779. doi: 10.1016/j.molcel.2017.06.002

Jensen, L. D., Rouhi, P., Cao, Z., Länne, T., and Wahlberg, E. (2011). Zebrafish models to study hypoxia-induced pathological angiogenesis in malignant and nonmalignant diseases. *Birth Defects Res. Part C: Embryo Today: Rev.* 93, 182– 193. doi: 10.1002/bdrc.20203

López-Ibáñez, J., Pazos, F., and Chagoyen, M. (2016). Mbrole 2.0—functional enrichment of chemical compounds. *Nucleic Acids Res.* 44, 201–204. doi: 10.1093/nar/gkw253

Laíns, I., Gantner, M., Murinello, S., Lasky-Su, J. A., and Miller, J. W. (2018). Metabolomics in the study of retinal health and disease. *Prog. In Retin. Eye Res.* 69, 57–79. doi: 10.1016/j.preteyeres.2018.11.002

Larsen, S., Nielsen, J., Hansen, C. N., Nielsen, L. B., and Wibrand, F. (2012). Biomarkers of mitochondrial content in skeletal muscle of healthy young human subjects. *J. Physiol.* 590, 3349–3360. doi: 10.1113/jphysiol.2012.230185

Lee, S., Shi, L., Chu, H., Li, M., and Ho, C. (2013). Rhodiola crenulata and its bioactive components, salidroside and tyrosol, reverse the hypoxia-induced reduction of plasma-membrane-associated na,k-atpase expression *via* inhibition of ros-ampk-pkcξpathway. *Evidence-Based Complement. Altern. Med.* 2013, 1–15. doi: 10.1155/2013/284150

Lee, S., Lai, F., Shi, L., Chou, Y., and Yen, I. (2015). Rhodiola crenulata extract suppresses hepatic gluconeogenesis *via* activation of the ampk pathway. *Phytomedicine* 22, 477–486. doi: 10.1016/j.phymed.2015.01.016

Li, L., Wang, H., and Zhao, X. (2015). Effects of rhodiola on production, health and gut development of broilers reared at high altitude in tibet. *Sci. Rep.* 4, 7166. doi: 10.1038/srep07166

Long, Y., Yan, J., Song, G., Li, X., and Li, X. (2015). Transcriptional events co-regulated by hypoxia and cold stresses in zebrafish larvae. *BMC Genomics* 16, 385. doi: 10.1186/s12864-015-1560-y

Lui, M. A., Mahalingam, S., Patel, P., Connaty, A. D., and Ivy, C. M. (2015). High-altitude ancestry and hypoxia acclimation have distinct effects on exercise capacity and muscle phenotype in deer mice. *Am. J. Physiol. Regulat. Integr. Comp. Physiol.* 308, 779–791. doi: 10.1152/ajpregu.00362.2014

Lukyanova, L. D., Kirova, Y. I., and Germanova, E. L. (2018). The role of succinate in regulation of immediate hif-1α expression in hypoxia. *Bull. Exp. Biol. Med.* 164, 298–303. doi: 10.1007/s10517-018-3976-2

Maina, P. K., Shao, P., Jia, X., Liu, Q., and Umesalma, S. (2017). Histone demethylase phf8 regulates hypoxia signaling through hif1α and h3k4me3. *Biochim. Et Biophys. Acta (BBA) - Gene Regul. Mech.* 1860, 1002–1012. doi: 10.1016/j.bbagrm.2017.07.005

Mandic, M., Speers-Roesch, B., and Richards, J. G. (2013). Hypoxia tolerance in sculpins is associated with high anaerobic enzyme activity in brain but not in liver or muscle. *Physiol. Biochem. Zool.* 86, 92–105. doi: 10.1086/667938

Meirer, K., Steinhilber, D., and Proschak, E. (2014). Inhibitors of the arachidonic acid cascade: interfering with multiple pathways. *Basic Clin. Pharmacol. Toxicol.* 114, 83–91. doi: 10.1111/bcpt.12134

Moschetta, A., VanBerge-Henegouwen, G. P., Portincasa., P., Portincasa, G., and Groen, A. K. (2000). Sphingomyelin exhibits greatly enhanced protection compared with egg yolk phosphatidylcholine against detergent bile salts. *J. Lipid Res.* 41, 916–924.

Nakamura, H., and Murayama, T. (2014). The role of sphingolipids in arachidonic acid metabolism. *J. Pharmacol. Sci.* 124, 307–312. doi: 10.1254/jphs.13R18CP

Nakamura, H., Wakita, S., Suganami, A., Tamura, Y., and Hanada, K. (2010). Modulation of the activity of cytosolic phospholipase a2α (cpla2α) by cellular sphingolipids and inhibition of cpla2α by sphingomyelin. *J. Lipid Res.* 51, 720– 728. doi: 10.1194/jlr.M002428

Pchejetski, D., Nunes, J., Coughlan, K., Lall, H., and Pitson, S. M. (2010). The involvement of sphingosine kinase 1 in LPS-induced Toll-like receptor 4-mediated accumulation of HIF-1α protein, activation of ASK1 and production of the pro-inflammatory cytokine IL-6. *Immunol. Cell Biol.* 89, 268–274. doi: 10.1038/icb.2010.91

Powell, W. S., and Rokach, J. (2015). Biosynthesis, biological effects, and receptors of hydroxyeicosatetraenoic acids (hetes) and oxoeicosatetraenoic acids (oxo-etes) derived from arachidonic acid. *Biochim. Et Biophys. Acta (BBA) - Mol. Cell Biol. Lipids* 1851, 340–355. doi: 10.1016/j.bbalip.2014.10.008

Samuel, S., Edwin, B. S., Sharie, L., LaMarche, B. S., and David, T. (1993). 5-Hydroxyeicosatetraenoic acid biosynthesis by gestational tissues: Effects of inflammmatory cytokines. *Am. J. Obstest. Gynecol.* 169, 1467–1471. doi: 10.1016/0002-9378(93)90420-N

Santos, D., Luzio, A., and Coimbra, A. M. (2017). Zebrafish sex differentiation and gonad development: a review on the impact of environmental factors. *Aquat. Toxicol.* 191, 141–163. doi: 10.1016/j.aquatox.2017.08.005

Schofield, C. J., and Ratcliffe, P. J. (2004). Oxygen sensing by hif hydroxylases. *Nat. Rev. Mol. Cell Biol.* 5, 343–354. doi: 10.1038/nrm1366

Sun, S., Gu, Z., Fu, H., Zhu, J., and Ge, X. (2018). Hypoxia induces changes in amp-activated protein kinase activity and energy metabolism in muscle tissue of the oriental river prawn macrobrachium nipponense. *Front. In Physiol.* 9, 751. doi: 10.3389/fphys.2018.00751

Tannahill, G. M., Curtis, A. M., Adamik, J., Palsson-McDermott, E. M., and McGettrick, A. F. (2013). Succinate is an inflammatory signal that induces il-1β through hif-1α. *Nat.* 496, 238–242. doi: 10.1038/nature11986

Tretter, L., Patocs, A., and Chinopoulos, C. (2016). Succinate, an intermediate in metabolism, signal transduction, ROS, hypoxia, and tumorigenesis. *Biochim. Et Biophys. Acta (BBA) - Bioenergetics* 1857, 1086–1101. doi: 10.1016/j.bbabio.2016.03.012

Warren, M., Subramani, K., Schwartz, R., and Raju, R. (2017). Mitochondrial dysfunction in rat splenocytes following hemorrhagic shock. *Biochim. Et Biophys. Acta (BBA) - Mol. Basis Dis.* 1863, 2526–2533. doi: 10.1016/j.bbadis.2017.08.024

Yuan, M., Breitkopf, S. B., Yang, X., and Asara, J. M. (2012). A positive/negative ion-switching, targeted mass spectrometry-based metabolomics platform for bodily fluids, cells, and fresh and fixed tissue. *Nat. Protoc.* 7, 872–881. doi: 10.1038/nprot.2012.024

Zager, R. A. (2000). Sphingomyelinase and membrane sphingomyelin content:determinants of proximal tubule cell susceptibility to injury. *J. Am. Soc. Nephrol.* 11, 849–902.

Zhang, R., Zhu, X., Bai, H., and Ning, K. (2019). Network pharmacology databases for traditional chinese medicine: review and assessment. *Front. In Pharmacol.* 10, 123. doi: 10.3389/fphar.2019.00123

Zheng, K. Y., Zhang, Z., Guo, A. J., Bi, C. W., and Zhu, K. Y. (2012). Salidroside stimulates the accumulation of hif-1α protein resulted in the induction of epo expression: a signaling *via* blocking the degradation pathway in kidney and liver cells. *Eur. J. Pharmacol.* 679, 34–39. doi: 10.1016/j.ejphar.2012.01.027

**Conflict of Interest:** The authors declare that the research was conducted in the absence of any commercial or financial relationships that could be construed as a potential conflict of interest.

frontiers in Pharmacology

ORIGINAL RESEARCH
published: 27 November 2019
doi: 10.3389/fphar.2019.01435

# Network Pharmacology-Based Prediction of Active Ingredients and Mechanisms of *Lamiophlomis rotata* (Benth.) Kudo Against Rheumatoid Arthritis

*Yunbin Jiang[1]*†, Mei Zhong[1†], Fei Long[2], Rongping Yang[1], Yanfei Zhang[3]* and Tonghua Liu[3,4]**

[1] College of Pharmaceutical Sciences and Chinese Medicine, Southwest University, Chongqing, China, [2] College of Pharmacy, Chengdu University of Traditional Chinese Medicine, Chengdu, China, [3] Institute of Tibetan Medicine, Tibetan Traditional Medical College, Lhasa, China, [4] Key Laboratory on Health Cultivation of the Ministry of Education, Beijing University of Chinese Medicine, Beijing, China

OPEN ACCESS

**Edited by:**
Yonghua Wang,
Northwest A&F University, China

**Reviewed by:**
Jingxiao Zhang,
Luoyang Normal University, China
Lilei Zhang,
Luoyang Normal University, China

***Correspondence:**
Yunbin Jiang
yunbinjiang@swu.edu.cn
Yanfei Zhang
1301379170@qq.com
Tonghua Liu
thliu@vip.163.com

†These authors have contributed equally to this work

**Specialty section:**
This article was submitted to Ethnopharmacology, a section of the journal Frontiers in Pharmacology

**Received:** 21 June 2019
**Accepted:** 11 November 2019
**Published:** 27 November 2019

**Citation:**
Jiang Y, Zhong M, Long F, Yang R, Zhang Y and Liu T (2019) Network Pharmacology-Based Prediction of Active Ingredients and Mechanisms of Lamiophlomis rotata (Benth.) Kudo Against Rheumatoid Arthritis. Front. Pharmacol. 10:1435. doi: 10.3389/fphar.2019.01435

**Background:** *Lamiophlomis rotata* (LR) showed favorable clinical effect and safety on rheumatoid arthritis (RA), but its active ingredients and mechanisms against RA remain unknown. The aim of this work was to explore the active ingredients and mechanisms of LR against RA by network pharmacology.

**Methods:** Compounds from LR were identified using literature retrieval and screened by absorption, distribution, metabolism, excretion, and toxicity (ADMET) evaluation. Genes related to the selected compounds or RA were identified using public databases, and the overlapping genes between compounds and RA target genes were identified using Venn diagram. Then, the interactions network between compounds and overlapping genes was constructed, visualized, and analyzed by Cytoscape software. Finally, pathway enrichment analysis of overlapping genes was carried out on Database for Annotation, Visualization, and Integrated Discovery (DAVID) platform.

**Results:** A total of 148 compounds in LR were identified, and ADMET screen results indicated that 67 compounds exhibited good potential as active ingredients. A total of 90 compounds-related genes and 1,871 RA-related genes were identified using public databases, and 48 overlapping genes between them were identified. Cytoscape results suggested that the active ingredients and target genes of LR against RA consisted of 23 compounds and 48 genes, and luteolin and AKT1 were the uppermost active ingredient and hub gene, respectively. DAVID results exhibited that the mechanisms of LR against RA were related to 34 signaling pathways, and the key mechanism of LR against RA might be to induce apoptosis of synovial cells by inactivating PI3K-Akt signaling pathway.

**Conclusion:** The active ingredients and mechanisms of LR against RA were firstly investigated using network pharmacology. This work provides scientific evidence to support the clinical effect of LR on RA, and a research basis for further expounding the active ingredients and mechanisms of LR against RA.

**Keywords: *Lamiophlomis rotata*, rheumatoid arthritis, network pharmacology, active ingredient, mechanism, luteolin, PI3K-Akt signaling pathway**

## INTRODUCTION

Rheumatoid arthritis (RA), a chronic autoimmune disease, can cause cartilage and bone damage as well as disability. RA is characterized by joint inflammation, but is more like a syndrome that consists of extra-articular manifestations, such as rheumatoid nodules, pulmonary involvement or vasculitis, and systemic comorbidities (Smolen et al., 2016). RA can present at any age, affects about 1% of the population, and carries a huge emotional and financial burden for both the individual and society (McInnes and Schett, 2017). Because inflammation is the main driving factor to cause clinical symptoms, joint damage, disability, and comorbidity in RA patients, anti-inflammation is a key therapeutic strategy (Smolen et al., 2007). At present, the anti-RA drugs include disease-modifying antirheumatic drugs and non-steroidal anti-inflammatory drugs in western country (Smolen et al., 2016). However, traditional Chinese medicine (TCM) plays a vital complementary role in treating RA in China (Zhang et al., 2010). For the past few years, TCM has been increasingly important strategy for treatment of RA in China due to its good therapeutic effect and low toxic side effects.

Chinese Pharmacopoeia shows that *Lamiophlomis rotata* (Benth.) Kudo (LR) can be used to treat RA, and LR patent medicines (Duyiwei capsule or tablet) are legally allowed to trade in China. It was reported that LR showed favorable clinical effect and safety on RA (Ye et al., 2007), and a meta-analysis indicated that LR was effective and safe in treating bleeding, pain, and inflammation (Wang et al., 2008). In addition, animals experiment indicated that LR could significantly inhibit the formation of primary and secondary arthritis in rats (Wang et al., 2013). At present, the active ingredients and mechanisms of LR against RA has not been reported. Therefore, the studies on active ingredients and mechanisms of LR against RA should be strengthened to provide scientific evidence to support its clinical application in treating RA.

Network pharmacology, a systematic analytical method, can analyze the interaction network of multiple factors such as drugs, protein target, diseases, and genes (Hopkins, 2007). Network pharmacology can decipher the mechanism of drugs action with a holistic perspective, which emphasizes the paradigm shift from "one target, one drug" to "network target, multicomponent therapeutics" (Hopkins, 2008). The characteristic is also shared by TCM, and the holistic theory has long been central to TCM treatments of various diseases (Li et al., 2014). Therefore, network pharmacology is a very advantageous technology to explore TCM-related issues. At present, network pharmacology has been widely used to investigate the active ingredients and mechanisms of TCM against various diseases (Tang et al., 2015; Chen et al., 2018).

In this work, network pharmacology was used to investigate the active ingredients and mechanisms of LR against RA. First, compounds from LR were identified using literature retrieval, and were screened by absorption, distribution, metabolism, excretion, and toxicity (ADMET) evaluation. Then, genes related to selected compounds or RA were identified using public databases, and the overlapping genes between compounds and RA target genes were identified. Third, the key active ingredients and hub genes of LR against RA were identified by analyzing the interactions between compounds and overlapping genes. Finally, pathway enrichment analysis of overlapping genes was carried out to explore the molecular mechanisms of LR against RA. The workflow is shown in **Figure 1**.

## MATERIALS AND METHODS

### Compounds Database Construction and ADMET Evaluation

The information of compounds from LR were collected by retrieving literatures in CNKI (http://www.cnki.net/), WANFANG DATA (http://www.wanfangdata.com.cn/), Baidu Xueshu (http://xueshu.baidu.com/), Web of Science and Google Scholar, and the SMILES and molecular formulas of compounds were identified using SciFinder (https://scifinder.cas.org/), PubChem (https://pubchem.ncbi.nlm.nih.gov/), or ChemSpider (http://www.chemspider.com/) with the aid of compounds names or structure. Then, compounds were screened by applying ADMET criteria of FAFDrugs4 (http://fafdrugs4.mti.univ-paris-diderot.fr/) (Miteva et al., 2006) with the aid of SMILES, and the "PhysChem Filters" of FAFDrugs4 was set as "*Drug-Like Soft*." Compounds were selected out as potential active ingredients when the result of ADMET evaluation was "Accepted."

### Target Genes Linked to Selected Compounds or RA

Based on SMILES, target genes of the identified compounds were predicted using STITCH (http://stitch.embl.de/) (Szklarczyk et al., 2016) with the "*Homo sapiens*" setting. To get more credible target genes of each compound, compound with the highest "Tanimoto score," usually 1.000 (match *via* InChIKey), was used to predict the genes of target compound, and the target genes were screened by setting "minimum required interaction score" as "high confidence (0.700)" during performing STITCH prediction (Lee et al., 2018).

RA-related target genes were identified by retrieving public databases including Online Mendelian Inheritance in Man (OMIM, https://omim.org/), Therapeutic Target Database (TTD, http://bidd.nus.edu.sg/group/cjttd/) (Li et al., 2018), Traditional Chinese Medicine Systems Pharmacology Database and Analysis Platform (TCMSP, http://lsp.nwu.edu.cn/tcmsp.php) (Ru et al., 2014), and DisGeNET (http://www.disgenet.org/). The overlapping genes between compounds and RA target genes were identified and visualized by Venn diagram, plotted using the OmicShare tools, a free online platform for data analysis (www.omicshare.com/tools).

### Network Construction of Interactions Between Compounds and Overlapping Genes

The interactions between compounds and overlapping genes were obtained based on the results of STITCH prediction, and the network of the interactions was constructed, visualized, and analyzed by Cytoscape ver. 3.7.1 (https://cytoscape.org/). Nodes in network indicate compounds and genes, and edges suggest

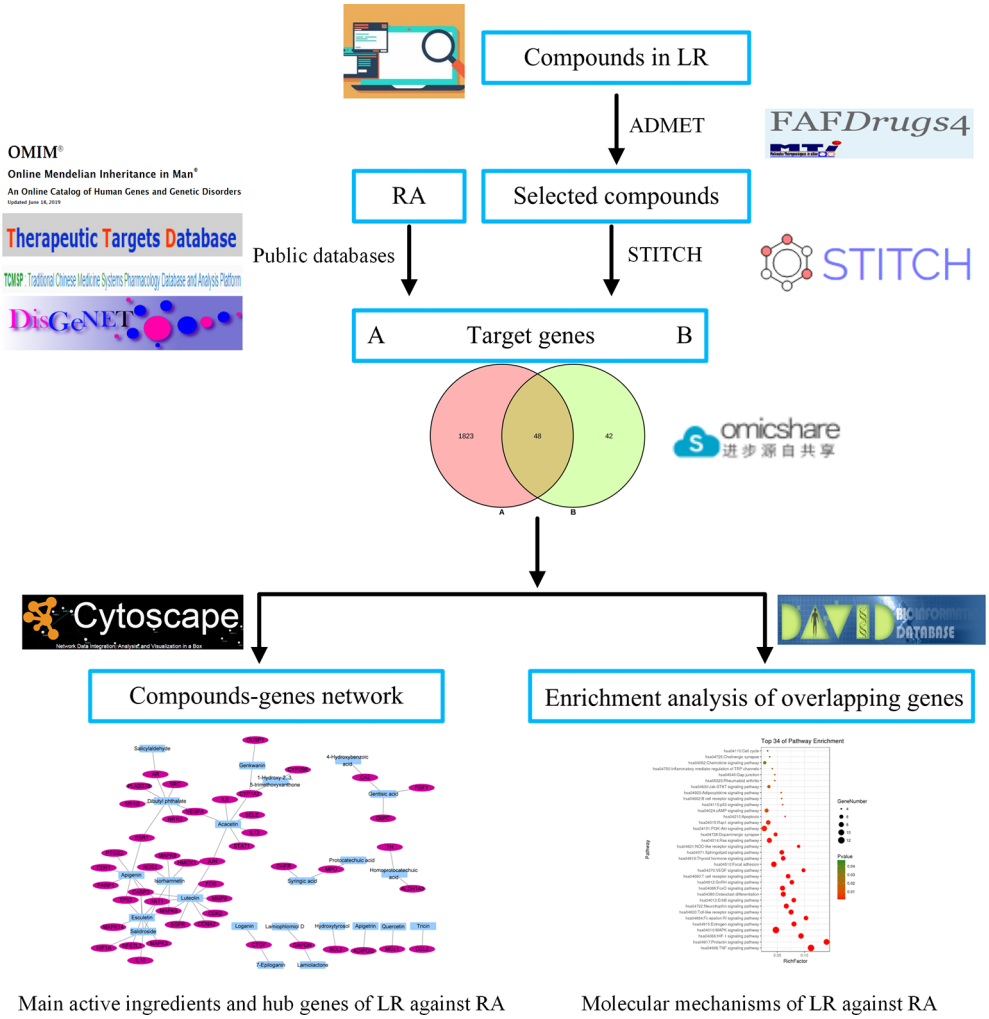


**FIGURE 1 |** Workflow of network pharmacology analysis.

interactions between compounds and genes (Lee et al., 2018). The key active ingredients and hub genes of LR against RA were selected out by setting "Degree value" of compounds or genes, identified by analyzing topological structure of network. Degree value of compounds or genes represents the edges numbers of compounds or genes in network. The bigger degree value of compounds or genes are, the more important compounds or genes are for the therapeutic effect of LR on RA.

## Pathway Enrichment Analysis of Overlapping Genes

Kyoto Encyclopedia of Genes and Genomes (KEGG) pathway enrichment analysis of overlapping genes was carried out on Database for Annotation, Visualization, and Integrated Discovery ver. 6.8 (https://david.ncifcrf.gov/) with the "*Homo sapiens*" setting. The results of KEGG pathway enrichment were used to decipher the potential molecular mechanisms of LR against RA. Bubble chart of interested KEGG pathways was plotted by the OmicShare tools.

# RESULTS

## Potential Active Ingredients From LR

A total of 148 compounds in LR were identified by literatures retrieval, and the names, molecular formulas of these compounds are listed in **Supplementary Table S1**. The ADMET screen results of 148 compounds showed that the results of 67 compounds were "Accepted," indicating that the 67 compounds exhibited good potential as active ingredients. These compounds are listed in **Table 1**.

## Target Genes Linked to the 67 Compounds or RA

As shown in **Supplementary Table S2**, a total of 90 genes related to 25 compounds from abovementioned 67 compounds were identified using STITCH prediction, and no genes linked to another 42 compounds were identified based on STITCH prediction. As listed in **Supplementary Table S3**, a total of 1,871 RA-related genes were identified by retrieving OMIM, TTD, TCMSP, and

**TABLE 1 |** A list of the final selected 67 compounds in LR for network analysis based on ADMET screen.

| No. | Compound | No. | Compound |
|---|---|---|---|
| 1 | (–)-α-terpineol-8-O-β-D-glucopyranoside | 35 | gentisic acid |
| 2 | (+)-α-terpineol-8-O-β-D-glucopyranoside | 36 | hexanoic acid |
| 3 | (2Z)-2,6-dimethyl-6-hydroxyocta-2,7-dienyl-O-β-D-glucopyranoside | 37 | homoprotocatechuic acid |
| 4 | (E)-4-hydroxyhex-2-enoic acid | 38 | hydroxytyrosol |
| 5 | (Z)-3-hexenyl glucopyranoside | 39 | icariside H1 |
| 6 | 1-hydroxy-2,3,5-trimethoxyxanthone | 40 | isololiolide |
| 7 | 2,4,5-trihydroxycinnamic acid | 41 | isorhamnetin |
| 8 | 3,4-dihydroxybenzaldehyde | 42 | lamiolactone |
| 9 | 3β-hydroxy-5α,6α-epoxy-7-megastigmen-9-one | 43 | lamiophlomiol A |
| 10 | 4'-(p-carbonylphenyl)-luteolin | 44 | lamiophlomiol B |
| 11 | 4-hydroxybenzoic acid | 45 | lamiophlomiol C |
| 12 | 5-hydroxyloganin | 46 | lamiophlomiol D |
| 13 | 7,8-dehydropenstemonoside | 47 | lamiophlomiol E |
| 14 | 7,8-dehydropenstemoside | 48 | lamiophlomiol F |
| 15 | 7-dehydroxyzaluzioside | 49 | lamiophlomis alkali |
| 16 | 7-deoxyloganic acid | 50 | loganin |
| 17 | 7-deoxyloganin | 51 | loliolide |
| 18 | 7-epiloganin | 52 | luteolin |
| 19 | 8-deoxyshanzhiside | 53 | n-butyl-β-D-fructofuranoside |
| 20 | 8-epi-7-deoxyloganin | 54 | n-butyl-β-D-fructopyranoside |
| 21 | 8-epideoxyloganic acid | 55 | notohamosin B |
| 22 | acacetin | 56 | penstemoside |
| 23 | apigenin | 57 | phlorigidoside C |
| 24 | apigetrin | 58 | protocatechuic acid |
| 25 | caffeic acid | 59 | quercetin |
| 26 | cedrol | 60 | rhexifoline |
| 27 | chlorogenic acid | 61 | salicylaldehyde |
| 28 | chlorotuberoside | 62 | salidroside |
| 29 | cyclohexylglycine | 63 | salviifoside A |
| 30 | dibutyl phthalate | 64 | shanzhiside methyl ester |
| 31 | dodecanoic acid | 65 | syringic acid |
| 32 | esculetin | 66 | tricin |
| 33 | eugenyl-O-β-D-glucopyranoside | 67 | vanillyl-O-β-D-glucopyranoside |
| 34 | genkwanin | | |

*ADMET, absorption, distribution, metabolism, excretion and toxicity; LR, Lamiophlomis rotate.*

DisGeNET databases. The results of Venn diagram (**Figure 2**) suggested 48 overlapping genes were identified by matching 90 compounds-related genes with 1,871 RA-related genes.

## Key Active Ingredients and Hub Genes of LR Against RA

The interactions between 48 overlapping genes and compounds were identified based on the results of STITCH prediction, and 23 compounds were finally identified. The interactions between 48 overlapping genes and 23 compounds are listed in **Table 2**, and were visualized by network, which includes with 71 nodes and 68 edges (**Figure 3**). The results suggested that the therapeutic effect of LR on RA was directly related to the 23 compounds and 48 genes. The 23 compounds were categorized as nine flavonoids (luteolin, apigenin, acacetin, isorhamnetin, genkwanin, 1-hydroxy-2,3,5-trimethoxyxanthone, quercetin, tricin, and apigetrin), five phenolic acids (gentisic acid, syringic acid, homoprotocatechuic acid, protocatechuic acid, and 4-hydroxybenzoic acid), four iridoids (loganin, 7-epiloganin,

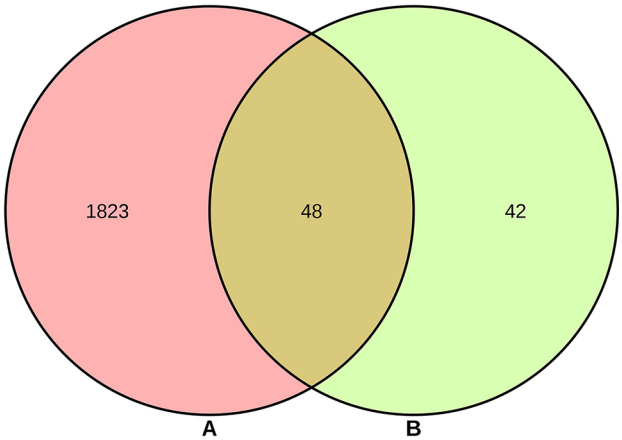


**FIGURE 2 |** Overlapping genes between 1,871 rheumatoid arthritis (RA)-related genes **(A)** and 90 compounds-related genes **(B)**.

lamiophlomiol D, and lamiolactone), two volatile oil (dibutyl phthalate and salicylaldehyde), one coumarin (esculetin), one phenylethanoid glycoside (salidroside), and one polyphenol (hydroxytyrosol). Based on the degree value of each compound or gene (**Table 3**), it was very easy to distinguish the contribution difference of 23 compounds and 48 genes to LR against RA. Luteolin (**Figure 4**), connected to nine genes, was considered as the uppermost active ingredient of LR against RA. AKT1, connected to five compounds, was considered as the hub gene of LR against RA.

## Potential Molecular Pathways of LR Against RA

The results of KEGG pathway enrichment analysis indicated that 48 overlapping genes were significantly enriched in 74 signaling pathways ($p < 0.05$). Based on the extensive literature retrieval, the 34 signaling pathways (**Figure 5**) were directly related to occurrence and development of RA, indicating that these signaling pathways might be the mechanisms of LR against RA. The detailed information of top 10 pathways is shown in **Table 4**. In addition, the hub gene AKT1 of LR against RA was directly enriched in 27 signaling pathways of the 34 signaling pathways. Coincidently, AKT1 plays a role in almost all of the 27 signaling pathways by PI3K-Akt signaling pathway, suggesting that PI3K-Akt signaling pathway might be the hub signaling pathway of LR against RA.

# DISCUSSION

Compounds-genes network suggested that the therapeutic effect of LR on RA was directly related to 23 compounds, including nine flavonoids, five phenolic acids, four iridoids, two volatile oil, one coumarin, one phenylethanoid glycoside, and one polyphenol. The ratio of flavonoids to 23 compounds was close to 40%, suggesting that flavonoids were more important than other kinds of compounds for the therapeutic effect of LR on RA. Based on the

**TABLE 2 |** A list of the interactions between 23 compounds in LR and 48 target genes related to RA.

| No. | Compound | Gene | No. | Compound | Gene |
|---|---|---|---|---|---|
| 1 | 1-hydroxy-2,3,5-trimethoxyxanthone | CYP1A2 | 35 | genkwanin | CYP1A2 |
| 2 | 1-hydroxy-2,3,5-trimethoxyxanthone | CYP2B6 | 36 | gentisic acid | FGF1 |
| 3 | 4-hydroxybenzoic acid | CA2 | 37 | gentisic acid | G6PD |
| 4 | 7-epiloganin | CTGF | 38 | gentisic acid | CA2 |
| 5 | acacetin | IL5 | 39 | homoprotocatechuic acid | TH |
| 6 | acacetin | SELE | 40 | homoprotocatechuic acid | ALDH1A3 |
| 7 | acacetin | VEGFA | 41 | hydroxytyrosol | BCL2 |
| 8 | acacetin | IL13 | 42 | isorhamnetin | NOS2 |
| 9 | acacetin | STAT1 | 43 | isorhamnetin | MAPK9 |
| 10 | acacetin | CYP1A2 | 44 | isorhamnetin | HMOX1 |
| 11 | acacetin | JUN | 45 | isorhamnetin | MAPK8 |
| 12 | apigenin | CDK1 | 46 | isorhamnetin | AKT1 |
| 13 | apigenin | PTGS2 | 47 | lamiolactone | GAPDH |
| 14 | apigenin | ESR1 | 48 | lamiophlomiol D | GAPDH |
| 15 | apigenin | CASP3 | 49 | loganin | CTGF |
| 16 | apigenin | PARP1 | 50 | luteolin | CCNA2 |
| 17 | apigenin | TP53 | 51 | luteolin | CASP3 |
| 18 | apigenin | AKT1 | 52 | luteolin | EGFR |
| 19 | apigetrin | ADIPOQ | 53 | luteolin | FOS |
| 20 | dibutyl phthalate | NR1I3 | 54 | luteolin | MAPK8 |
| 21 | dibutyl phthalate | ESR1 | 55 | luteolin | CDK2 |
| 22 | dibutyl phthalate | VEGFA | 56 | luteolin | AKT1 |
| 23 | dibutyl phthalate | PLA2G1B | 57 | luteolin | JUN |
| 24 | dibutyl phthalate | SRC | 58 | luteolin | MMP9 |
| 25 | dibutyl phthalate | NR1I2 | 59 | protocatechuic acid | MPO |
| 26 | dibutyl phthalate | AR | 60 | quercetin | MCL1 |
| 27 | esculetin | NFE2L2 | 61 | salicylaldehyde | AR |
| 28 | esculetin | MAPK14 | 62 | salidroside | CASP3 |
| 29 | esculetin | CASP3 | 63 | salidroside | IL10 |
| 30 | esculetin | MAPK8 | 64 | salidroside | HIF1A |
| 31 | esculetin | MAPK3 | 65 | salidroside | AKT1 |
| 32 | esculetin | TP53 | 66 | syringic acid | DHFR |
| 33 | esculetin | AKT1 | 67 | syringic acid | MPO |
| 34 | genkwanin | DUSP1 | 68 | tricin | CCL2 |

*LR, Lamiophlomis rotate; RA, rheumatoid arthritis.*

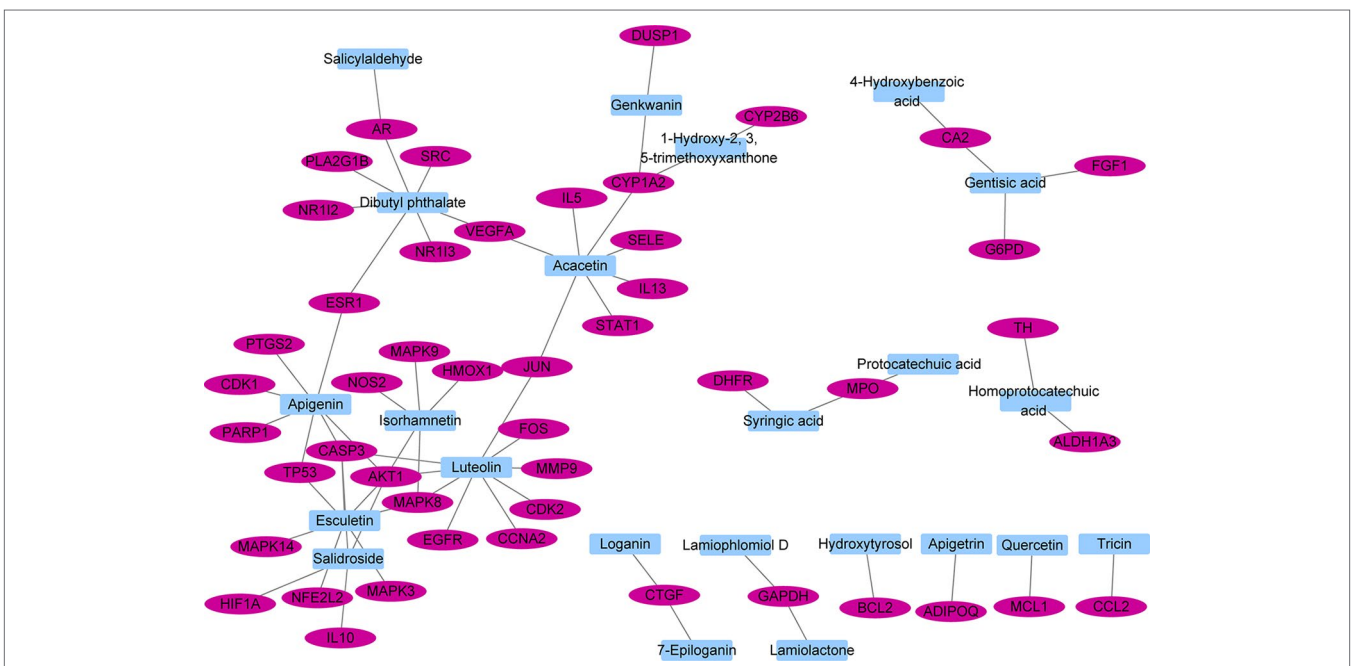


**FIGURE 3 |** Network with 71 nodes and 68 edges linking 23 compounds in *Lamiophlomis rotata* and 48 target genes related to rheumatoid arthritis.

**TABLE 3 |** Degree value of 23 compounds and 48 target genes in network.

| No. | Compound | Value | No. | Gene | Value | No. | Gene | Value |
|---|---|---|---|---|---|---|---|---|
| 1 | luteolin | 9 | 1 | AKT1 | 5 | 25 | TH | 1 |
| 2 | apigenin | 7 | 2 | CASP3 | 4 | 26 | PTGS2 | 1 |
| 3 | acacetin | 7 | 3 | CYP1A2 | 3 | 27 | DUSP1 | 1 |
| 4 | esculetin | 7 | 4 | MAPK8 | 3 | 28 | CCNA2 | 1 |
| 5 | dibutyl phthalate | 7 | 5 | MPO | 2 | 29 | IL13 | 1 |
| 6 | isorhamnetin | 5 | 6 | ESR1 | 2 | 30 | MCL1 | 1 |
| 7 | salidroside | 4 | 7 | VEGFA | 2 | 31 | CCL2 | 1 |
| 8 | gentisic acid | 3 | 8 | CTGF | 2 | 32 | STAT1 | 1 |
| 9 | syringic acid | 2 | 9 | CA2 | 2 | 33 | PARP1 | 1 |
| 10 | homoprotocatechuic acid | 2 | 10 | TP53 | 2 | 34 | HMOX1 | 1 |
| 11 | genkwanin | 2 | 11 | GAPDH | 2 | 35 | IL10 | 1 |
| 12 | 1-hydroxy-2,3,5-trimethoxyxanthone | 2 | 12 | JUN | 2 | 36 | PLA2G1B | 1 |
| 13 | hydroxytyrosol | 1 | 13 | AR | 2 | 37 | EGFR | 1 |
| 14 | protocatechuic acid | 1 | 14 | NOS2 | 1 | 38 | FOS | 1 |
| 15 | quercetin | 1 | 15 | CDK1 | 1 | 39 | G6PD | 1 |
| 16 | tricin | 1 | 16 | BCL2 | 1 | 40 | MAPK3 | 1 |
| 17 | loganin | 1 | 17 | IL5 | 1 | 41 | HIF1A | 1 |
| 18 | 7-epiloganin | 1 | 18 | FGF1 | 1 | 42 | SRC | 1 |
| 19 | 4-hydroxybenzoic acid | 1 | 19 | MAPK9 | 1 | 43 | CDK2 | 1 |
| 20 | lamiophlomiol D | 1 | 20 | SELE | 1 | 44 | ALDH1A3 | 1 |
| 21 | lamiolactone | 1 | 21 | DHFR | 1 | 45 | CYP2B6 | 1 |
| 22 | salicylaldehyde | 1 | 22 | NFE2L2 | 1 | 46 | NR1I2 | 1 |
| 23 | apigetrin | 1 | 23 | NR1I3 | 1 | 47 | MMP9 | 1 |
| | | | 24 | MAPK14 | 1 | 48 | ADIPOQ | 1 |

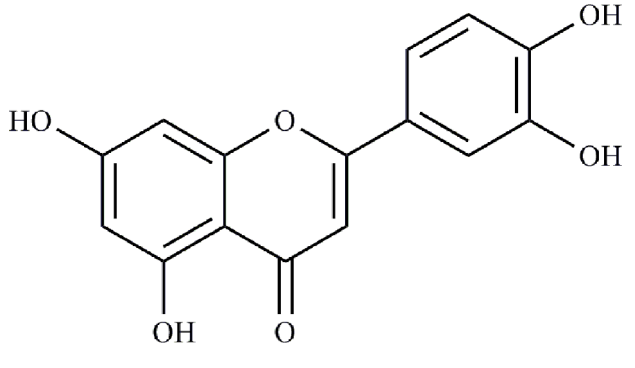


**FIGURE 4 |** Chemical structure of luteolin.

degree value of each compound in compounds-genes network, luteolin was considered as the uppermost active ingredient of LR against RA. It was reported that flavonoids were the key active ingredients group of LR (Lin et al., 2003), and flavonoids are used to control the quality of LR patent medicines (Duyiwei capsule or tablet) in Chinese Pharmacopoeia. Studies suggested that luteolin inhibited the proliferation and partially blocked the pathogenic function of synovial fibroblasts in RA (Hou et al., 2009; Lou et al., 2015). Meanwhile, TCMSP suggests that luteolin is related to occurrence and development of RA (Ru et al., 2014). Additionally, it was reported that the quantity of luteolin in LR was about 0.9% (Yi and Sun, 2016), and the clinical dosage of LR patent medicines is 9 g/day based on Chinese Pharmacopoeia, suggesting that the daily intake of luteolin 81 mg in clinic. Study indicated that luteolin showed obvious anti-RA effect on mice

**TABLE 4 |** Target genes in top 10 of pathway enrichment related to occurrence and development of RA.

| Pathway ID | Term | Target genes |
|---|---|---|
| hsa04668 | TNF signaling pathway | AKT1, FOS, CASP3, CCL2, PTGS2, MAPK14, JUN, MMP9, MAPK3, MAPK9, MAPK8, SELE |
| hsa04917 | Prolactin signaling pathway | AKT1, FOS, MAPK14, MAPK3, TH, ESR1, MAPK9, MAPK8, STAT1, SRC |
| hsa04066 | HIF-1 signaling pathway | AKT1, EGFR, HIF1A, HMOX1, BCL2, MAPK3, VEGFA, NOS2, GAPDH |
| hsa04010 | MAPK signaling pathway | AKT1, EGFR, FOS, CASP3, DUSP1, MAPK14, JUN, MAPK3, TP53, MAPK9, MAPK8, FGF1 |
| hsa04915 | Estrogen signaling pathway | AKT1, EGFR, FOS, JUN, MMP9, MAPK3, ESR1, SRC |
| hsa04664 | Fc epsilon RI signaling pathway | AKT1, IL5, MAPK14, MAPK3, MAPK9, IL13, MAPK8 |
| hsa04620 | Toll-like receptor signaling pathway | AKT1, FOS, MAPK14, JUN, MAPK3, MAPK9, MAPK8, STAT1 |
| hsa04722 | Neurotrophin signaling pathway | AKT1, MAPK14, JUN, BCL2, MAPK3, TP53, MAPK9, MAPK8 |
| hsa04012 | ErbB signaling pathway | AKT1, EGFR, JUN, MAPK3, MAPK9, MAPK8, SRC |
| hsa04380 | Osteoclast differentiation | AKT1, FOS, MAPK14, JUN, MAPK3, MAPK9, MAPK8, STAT1 |

*RA, rheumatoid arthritis.*

with collagen type II-induced RA at a dose of 1 mg/kg/day (Impellizzeri et al., 2013), which is far lower than the equivalent dose of luteolin in mice, suggesting that the quantity of luteolin in LR is high enough to be of pharmacological relevance.

Compounds-genes network showed that the therapeutic effect of LR on RA was directly related to 48 genes. The results of KEGG pathway enrichment analysis of 48 genes suggested that 34 signaling pathways were directly linked to occurrence and development of RA, indicating that these signaling pathways might be the mechanisms of LR against RA. The relationships of the top 10 pathways with RA were briefly discussed as follows. TNF signaling pathway: The occurrence and development of RA can be suppressed by inhibiting the overexpression of TNF-α, and antibody therapy against TNF-α can effectively reduce the arthritis and synovitis symptoms of RA patients (Matsuno et al., 2002). Prolactin signaling pathway and estrogen signaling pathway: Sex hormones such as estrogen and prolactin have long been thought to be directly related to occurrence and development of RA, and recent evidence indicated that estrogen and prolactin showed both anti- and pro-inflammatory effects in RA (Tang et al., 2017). HIF-1 signaling pathway: Clinical research exhibited that HIF-1alpha level was strongest in the sub-lining layer of RA synovium and was linked to synovium inflammation and angiogenesis in RA patients (Brouwer et al., 2009). MAPK signaling pathway: It was reported that andrographolide showed protective effects on RA through inhibiting MAPK pathways, suggesting that MAPK signaling pathway was related to occurrence and development of RA (Li et al., 2017). Fc epsilon RI signaling pathway: Report indicated that IgE, the initiation factor in Fc epsilon RI signaling pathway, may be involved in some extra-articular manifestations of RA (Meretey et al., 1982). Toll-like receptor signaling pathway: Previous reports indicated that Toll-like receptor and the signaling

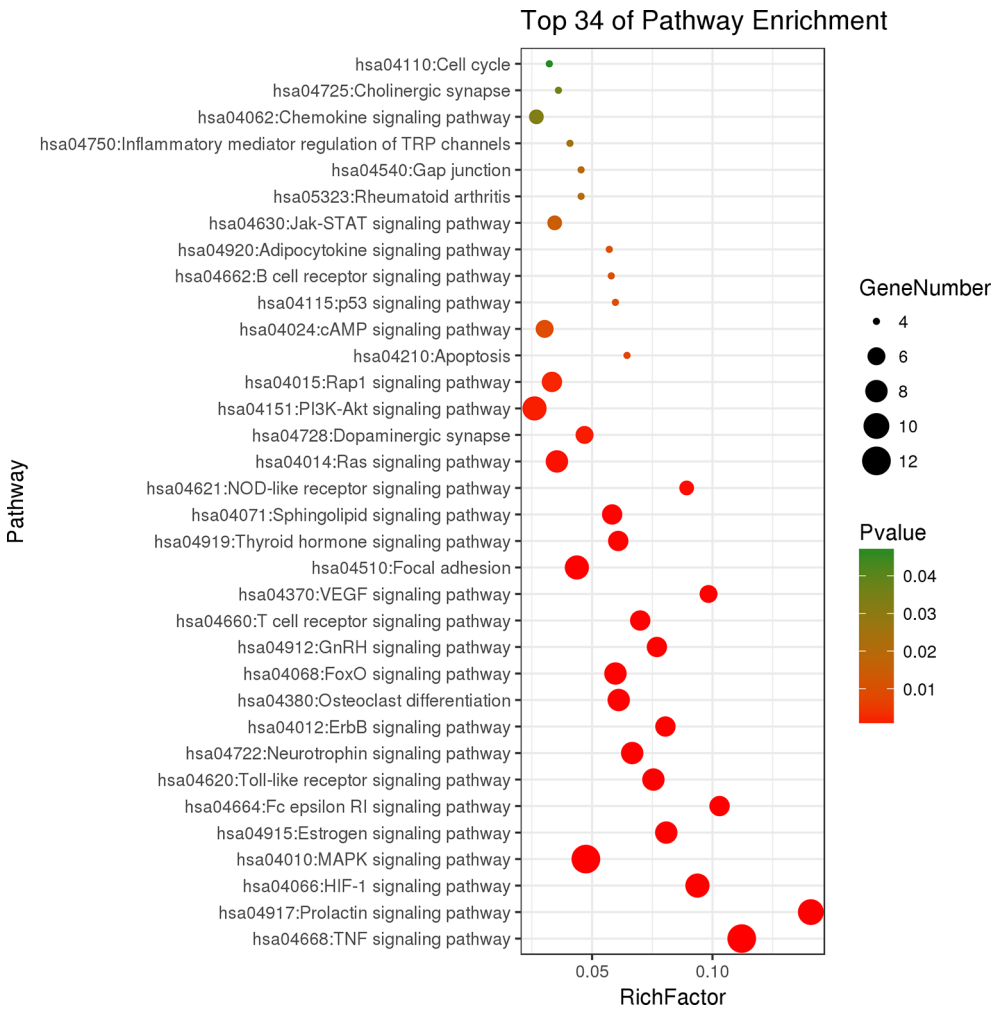


**FIGURE 5 |** Bubble chart of 34 signaling pathways related to occurrence and development of rheumatoid arthritis.

pathway were intensively linked to RA pathogenesis (Takagi, 2011). Neurotrophin signaling pathway: Report suggested that the level of mesencephalic astrocyte-derived neurotrophic factor was closely related to occurrence and development of RA (Ma et al., 2018). ErbB signaling pathway: It was reported that ErbB-2 was involved in occurrence and development of RA (Jiang et al., 2012). Osteoclast differentiation: Reports exhibited that activated RA synovial fibroblasts played a vital role in rheumatoid bone destruction by expressing osteoclast differentiation factor (Shigeyama et al., 2000).

Based on the degree value of each gene in compounds-genes network, AKT1 was considered as the hub gene of LR against RA. AKT1 was directly enriched in 27 signaling pathways of the abovementioned 34 signaling pathways. Coincidently, AKT1 plays a role in almost all of the 27 signaling pathways by PI3K-Akt signaling pathway, suggesting that PI3K-Akt signaling pathway might be the hub signaling pathway of LR against RA. Joint synovium is the main diseased region in RA patients, and its out-of-control proliferation to cartilage and bone causes release of inflammatory cytokines, resulting in occurrence of RA. Therefore, inducing apoptosis of synovial cells is also a feasible strategy for treating RA by preventing development of inflammation (Park et al., 2010). It was reported that PI3K-Akt signaling pathway was abnormally activated in RA synovium, resulting in the overexpression of anti-apoptotic genes such as FLIP, Bcl-2, and Mcl-1 (Harris et al., 2009). The overexpression of these anti-apoptotic genes lead to out-of-balance apoptosis of synovial cells, which induced occurrence and development of RA (Smith et al., 2010). Reports indicated that luteolin, the uppermost active ingredient of LR against RA, inhibited the proliferation of synovial fibroblasts in RA by blocking PI3K-Akt signaling pathway (Hou et al., 2009). Therefore, the key mechanism of LR against RA might be to induce apoptosis of synovial cells by inactivating PI3K-Akt signaling pathway.

## CONCLUSION

The active ingredients and mechanisms of LR against RA were firstly investigated using network pharmacology. The findings

of this work suggested that the active ingredients and target genes of LR against RA consisted of 23 compounds and 48 genes, and luteolin and AKT1 were the uppermost active ingredient and hub gene of LR against RA, respectively. The mechanisms of LR against RA were related to 34 signaling pathways, and the key mechanism of LR against RA might be to induce apoptosis of synovial cells by inactivating PI3K-Akt signaling pathway. This work provides scientific evidence to support the clinical effect of LR on RA, and a research basis for further expounding the active ingredients and mechanisms of LR against RA.

## DATA AVAILABILITY STATEMENT

The raw data supporting the conclusions of this manuscript will be made available by the authors, without undue reservation, to any qualified researcher.

## AUTHOR CONTRIBUTIONS

YJ, YZ, and TL conceived and designed this work, and wrote and revised the whole manuscript. MZ collected the data. YJ, MZ, FL, and RY analyzed the data.

## FUNDING

This work was supported by the Regional Collaborative Innovation Center Project of Tibetan Medicine (No. 2018XTCX045).

## SUPPLEMENTARY MATERIAL

The Supplementary Material for this article can be found online at: https://www.frontiersin.org/articles/10.3389/fphar.2019.01435/full#supplementary-material

## REFERENCES


Brouwer, E., Gouw, A. S., Posthumus, M. D., van Leeuwen, M. A., Boerboom, A. L., Bijzet, J., et al. (2009). Hypoxia inducible factor-1-alpha (HIF-1alpha) is related to both angiogenesis and inflammation in rheumatoid arthritis. *Clin. Exp. Rheumatol.* 27, 945–951.

Chen, L., Cao, Y., Zhang, H., Lv, D., Zhao, Y., Liu, Y., et al. (2018). Network pharmacology-based strategy for predicting active ingredients and potential targets of Yangxinshi tablet for treating heart failure. *J. Ethnopharmacol.* 219, 359–368. doi: 10.1016/j.jep.2017.12.011

Harris, S. J., Foster, J. G., and Ward, S. G. (2009). PI3K isoforms as drug targets in inflammatory diseases: lessons from pharmacological and genetic strategies. *Curr. Opin. Investig. Drugs* 10, 1151–1162.

Hopkins, A. L. (2007). Network pharmacology. *Nat. Biotechnol.* 25, 1110–1111. doi: 10.1038/nbt1007-1110

Hopkins, A. L. (2008). Network pharmacology: the next paradigm in drug discovery. *Nat. Chem. Biol.* 4, 682–690. doi: 10.1038/nchembio.118

Hou, Y., Wu, J., Huang, Q., and Guo, L. (2009). Luteolin inhibits proliferation and affects the function of stimulated rat synovial fibroblasts. *Cell Biol. Int.* 33, 135–147. doi: 10.1016/j.cellbi.2008.10.005

Impellizzeri, D., Esposito, E., Di Paola, R., Ahmad, A., Campolo, M., Peli, A., et al. (2013). Palmitoylethanolamide and luteolin ameliorate development of arthritis caused by injection of collagen type II in mice. *Arthritis Res. Ther.* 15, R192. doi: 10.1186/ar4382

Jiang, Y., Tu, S. H., Xia, Y. K., Chen, Z., Chang, D., Yang, H. W., et al. (2012). Regulatory effect of tripterygium wilfordii polyglycoside on expression of epidermal growth factor receptor family in collagen induced arthritis rats. *Chin. J. Rheumatol.* 16, 187–190. (in Chinese). doi: 10.3760/cma.j.issn.1007-7480.2012.03.010

Lee, A. Y., Park, W., Kang, T. W., Cha, M. H., and Chun, J. M. (2018). Network pharmacology-based prediction of active compounds and molecular targets in Yijin-Tang acting on hyperlipidaemia and atherosclerosis. *J. Ethnopharmacol.* 221, 151–159. doi: 10.1016/j.jep.2018.04.027

Li, S., Fan, T. P., Jia, W., Lu, A., and Zhang, W. (2014). Network pharmacology in traditional chinese medicine. *Evid. Based Complement. Alternat. Med.* 2014, 138460. doi: 10.1155/2014/138460

Li, Z. Z., Tan, J. P., Wang, L. L., and Li, Q. H. (2017). Andrographolide benefits rheumatoid arthritis *via* inhibiting MAPK pathways. *Inflammation* 40, 1599–1605. doi: 10.1007/s10753-017-0600-y

Li, Y. H., Yu, C. Y., Li, X. X., Zhang, P., Tang, J., Yang, Q., et al. (2018). Therapeutic target database update 2018: enriched resource for facilitating bench-to-clinic research of targeted therapeutics. *Nucleic Acids Res.* 46, D1121–D1127. doi: 10.1093/nar/gkx1076

Lin, T. M., Gu, Y., Fang, K. Q., Zhang, S. Q., and Jiang, Y. P. (2003). Analgesic effects of different extraction components from *Lamiophlomis rotata* (Benth.) kudo, a medicinal plant in XiZang (Tibet) in mice. *J. Fourth Mil. Med. Univ.* 24, 444–446. (in Chinese). doi: 10.3321/j.issn:1000-2790.2003.05.021

Lou, L., Liu, Y., Zhou, J., Wei, Y., Deng, J., Dong, B., et al. (2015). Chlorogenic acid and luteolin synergistically inhibit the proliferation of interleukin-1β-induced fibroblast-like synoviocytes through regulating the activation of NF-κB and JAK/STAT-signaling pathways. *Immunopharmacol. Immunotoxicol.* 37, 499–507. doi: 10.3109/08923973.2015.1095763

Ma, Y. Y., Di, Z. M., Cao, Q., Shen, Y. J., Shen, Y. X., and Feng, L. J. (2018). Expression characterization of MANF during course of rat adjuvant arthritis and its relationship with inflammation. *Chin. Pharmacol. Bull.* 34, 537–543. (in Chinese). doi: 10.3969/j.issn.1001-1978.2018.04.020

Matsuno, H., Yudoh, K., Katayama, R., Nakazawa, F., Uzuki, M., Sawai, T., et al. (2002). The role of TNF-alpha in the pathogenesis of inflammation and joint destruction in rheumatoid arthritis (RA): a study using a human RA/SCID mouse chimera. *Rheumatol. (Oxford)* 41, 329–337. doi: 10.1093/rheumatology/41.3.329

McInnes, I. B., and Schett, G. (2017). Pathogenetic insights from the treatment of rheumatoid arthritis. *Lancet* 389, 2328–2337. doi: 10.1016/S0140-6736(17)31472-1

Meretey, K., Falus, A., Erhardt, C. C., and Maini, R. N. (1982). IgE and IgE-rheumatoid factors in circulating immune complexes in rheumatoid arthritis. *Ann. Rheumatol. Dis.* 41, 405–408. doi: 10.1136/ard.41.4.405

Miteva, M. A., Violas, S., Montes, M., Gomez, D., Tuffery, P., and Villoutreix, B. O. (2006). FAF-Drugs: free ADME/tox filtering of compound collections. *Nucleic Acids Res.* 34, W738–W744. doi: 10.1093/nar/gkl065

Park, S. Y., Lee, S. W., Shin, H. K., Chung, W. T., Lee, W. S., Rhim, B. Y., et al. (2010). Cilostazol enhances apoptosis of synovial cells from rheumatoid arthritis patients with inhibition of cytokine formation *via* Nrf2-linked heme oxygenase 1 induction. *Arthritis Rheumatol.* 62, 732–741. doi: 10.1002/art.27291

Ru, J., Li, P., Wang, J., Zhou, W., Li, B., Huang, C., et al. (2014). TCMSP: a database of systems pharmacology for drug discovery from herbal medicines. *J. Cheminform.* 6, 13. doi: 10.1186/1758-2946-6-13

Shigeyama, Y., Pap, T., Kunzler, P., Simmen, B. R., Gay, R. E., and Gay, S. (2000). Expression of osteoclast differentiation factor in rheumatoid arthritis. *Arthritis Rheumatol.* 43, 2523–2530. doi: 10.1002/1529-0131(200011)43:11 < 2523::AID-ANR20 > 3.0.CO;2-Z

Smith, M. D., Weedon, H., Papangelis, V., Walker, J., Roberts-Thomson, P. J., and Ahern, M. J. (2010). Apoptosis in the rheumatoid arthritis synovial membrane: modulation by disease-modifying anti-rheumatic drug treatment. *Rheumatol. (Oxford)* 49, 862–875. doi: 10.1093/rheumatology/kep467

Smolen, J. S., Aletaha, D., Koeller, M., Weisman, M., and Emery, P. (2007). New therapies for the treatment of rheumatoid arthritis. *Lancet* 370, 1861–1874. doi: 10.1016/S0140-6736(07)60784-3

Smolen, J. S., Aletaha, D., and Mclnnes, I. B. (2016). Rheumatoid arthritis. *Lancet* 388, 2023–2038. doi: 10.1016/S0140-6736(16)30173-8

Szklarczyk, D., Santos, A., von Mering, C., Jensen, L. J., Bork, P., and Kuhn, M. (2016). STITCH 5: augmenting protein-chemical interaction networks with tissue and affinity data. *Nucleic Acids Res.* 44, D380–D384. doi: 10.1093/nar/gkv1277

Takagi, M. (2011). Toll-like receptor–a potent driving force behind rheumatoid arthritis. *J. Clin. Exp. Hematop.* 51, 77–92. doi: 10.3960/jslrt.51.77

Tang, F., Tang, Q., Tian, Y., Fan, Q., Huang, Y., and Tan, X. (2015). Network pharmacology-based prediction of the active ingredients and potential targets of Mahuang Fuzi Xixin decoction for application to allergic rhinitis. *J. Ethnopharmacol.* 176, 402–412. doi: 10.1016/j.jep.2015.10.040

Tang, M. W., Garcia, S., Gerlag, D. M., Tak, P. P., and Reedquist, K. A. (2017). Insight into the Endocrine system and the immune system: a review of the inflammatory role of prolactin in rheumatoid arthritis and psoriatic arthritis. *Front. Immunol.* 8, 720. doi: 10.3389/fimmu.2017.00720

Wang, L., Xu, L., Li, Y. L., Ai, C. L., and Li, J. (2008). Efficacy and safety of Lamiophlomis Rotata (Benth) Kudo: a systematic review of randomized controlled trials. *Chin. J. Evid.-based Med.* 8, 1060–1078. (in Chinese). doi: 10.3969/j.issn.1672-2531.2008.12.011

Wang, L. J., Wang, Y., Yang, J., Chu, Y. P., and Zhang, S. J. (2013). Experimental study of Lamiophlomis rotate preventing and treatment function on rat adjuvant arthritis. *Chin. J. Basic Med. Trad. Chin. Med.* 19, 763–766. (in Chinese).

Ye, F., Yang, H., and Xu, Y. (2007). Clinical observation of 69 cases of arthritis deformans treated with Duyiwei capsule. *World Chin. Med.* 2, 339–340. (in Chinese). doi: 10.3969/j.issn.1673-7202.2007.06.007

Yi, Y., and Sun, L. (2016). Simultaneous determination of dipsacoside B, luteolin and apigenin in zang medicine *Lamiophlomis rotata* by HPLC. *Chin. Pharma.* 27, 4733–4735. (in Chinese). doi: 10.6039/j.issn.1001-0408.2016.33.42

Zhang, P., Li, J., Han, Y., Yu, X. W., and Qin, L. (2010). Traditional Chinese medicine in the treatment of rheumatoid arthritis: a general review. *Rheumatol. Int.* 30, 713–718. doi: 10.1007/s00296-010-1370-0

**Conflict of Interest:** The authors declare that the research was conducted in the absence of any commercial or financial relationships that could be construed as a potential conflict of interest.

frontiers in Pharmacology

REVIEW
published: 15 January 2020
doi: 10.3389/fphar.2019.01461

# Effects of Berberine and Its Derivatives on Cancer: A Systems Pharmacology Review

*Chaohe Zhang[1], Jiyao Sheng[1], Guangquan Li[1], Lihong Zhao[1], Yicun Wang[1], Wei Yang[1], Xiaoxiao Yao[1]*, Lihuan Sun[1]*, Zhuo Zhang[2] and Ranji Cui[1]**

[1] Jilin Provincial Key Laboratory on Molecular and Chemical Genetic, Second Hospital of Jilin University, Changchun, China, [2] China-Japan Union Hospital of Jilin University, Changchun, China

OPEN ACCESS

**Edited by:**
Yonghua Wang,
Northwest A & F University,
China

**Reviewed by:**
Qin Mingze,
Shenyang Pharmaceutical University,
China
Anna-Mart Engelbrecht,
Stellenbosch University,
South Africa

***Correspondence:**
Xiaoxiao Yao
Yaoxx@jlu.edu.cn
Lihuan Sun
lihua.sun@163.com
Ranji Cui
cuiranji@jlu.edu.cn

**Specialty section:**
This article was submitted to Ethnopharmacology, a section of the journal Frontiers in Pharmacology

**Received:** 27 June 2019
**Accepted:** 13 November 2019
**Published:** 15 January 2020

**Citation:**
Zhang C, Sheng J, Li G, Zhao L, Wang Y, Yang W, Yao X, Sun L, Zhang Z and Cui R (2020) Effects of Berberine and Its Derivatives on Cancer: A Systems Pharmacology Review. Front. Pharmacol. 10:1461. doi: 10.3389/fphar.2019.01461

Numerous studies have shown that berberine and its derivatives demonstrate important anti-tumor effects. However, the specific underlying mechanism remains unclear. Therefore, based on systems pharmacology, this review summarizes the information available on the anti-tumor effects and mechanism of berberine and its derivatives. The action and potential mechanism of action of berberine and its derivatives when used in the treatment of complex cancers are systematically examined at the molecular, cellular, and organismic levels. It is concluded that, with further in-depth investigations on their toxicity and efficacy, berberine and its derivatives have the potential for use as drugs in cancer therapy, offering improved clinical efficacy and safety.

**Keywords: berberine, tumor, systems pharmacology, liver cancer, breast cancer**

## INTRODUCTION

Berberine (chemical formula: $C_{20}H_{18}NO_4$, slowly soluble in water), the main alkaloid in the herbal medicine coptis, has been widely used in China (Alolga et al., 2016; Li et al., 2019). It also exists in many Berberidaceae, Papaveraceae, and Rutaceae plants. Based on its chemical structure, berberine is a protozoan morphinane alkaloid (Ruan et al., 2017). In addition to extensive biological activities, such as anti-inflammation, antioxidative, and anti-diabetic, berberine demonstrates anti-tumor activity by means of interference in tumorigenesis and in multiple features of tumor development. Therefore, berberine is widely used in the prevention and treatment of tumors (Refaat et al., 2015; Li et al., 2017a; Liao et al., 2018; Liu et al., 2019a). In addition, it is difficult for berberine to penetrate cytomembrane and to be assimilate into the gastrointestinal tract due to its poor lipid solubility (Lu et al., 2006; Ge et al., 2016; Zhu et al., 2017). Therefore, a series of berberine derivatives have been designed by transforming and modifying its chemical structure (Sagar et al., 2006; Xiao et al., 2018). Simultaneously, the pharmacological activities of berberine derivatives were also widely studied.

Numerous studies have revealed that berberine has anti-tumor activity in many cancers (Wen et al., 2016; Zou et al., 2017). This mainly consists of inhibiting tumor cell proliferation and tumor angiogenesis, inducing apoptosis of tumor cells, and delaying the transfer of tumor cells (Li et al., 2018; Dai et al., 2019; Liu et al., 2019b). In contrast, in a leukemia mouse model, berberine reportedly inhibited the growth of the spleen by inhibiting the differentiation of nicotinate mononucleotide pyrophosphorylase and granulocyte (Yu et al., 2007; Gu et al., 2008; Wang Z. et al., 2016). In the SCC-4 tumor mouse model, the number of tumors in mice treated with berberine

was obviously less than that observed in the control group (Jantova et al., 2003; Yu et al., 2007; Ho et al., 2009). In this review, we focus on the anti-cancer mechanisms and signaling pathways of berberine (**Figure 1**).

## EFFECTS OF BERBERINE ON P53 AND THE CELL CYCLE

Berberine alters cellular processes through interactions with nucleic acids and various proteins. The effect of berberine on cell cycle progression has also been observed through cell cycle arrest at the G1 phase, G0/G1 phase, or G2/M phase (Eo and Kim, 2014; Gu et al., 2015). For example, berberine induced G2/M phase arrest in T47D and in G0/G1 in MCF-7 cells (Barzegar et al., 2015). Computational and experimental data demonstrated that CaM potentially plays a crucial role in the anti-tumor effect induced by berberine. A biological assay revealed that berberine induced G1 cell cycle arrest in Bel7402 cells partially by interacting with CaM and blocking subsequent signal cascades (Ma et al., 2013).

p53 is one of the key tumor suppressor genes and is very important in the process of apoptosis in various tumor cells. The protein encoded by this gene is a transcriptional factor that controls the initiation of the cell cycle. Therefore, p53 plays a critical role in whether to start cell division or not. If the cell is damaged and cannot be repaired, p53 protein will participate in the initiation process, allowing the cell to initiate apoptosis. For example, p53 can inhibit BCL2 by BAX, which increases the BAX/BCL2 ratio and can also induce cell apoptosis by Apaf-1 regulation of the underlying signal caspase 3 (Babiker et al., 2018; Liu et al., 2018; Ma et al., 2019; Nkpaa et al., 2019). The tumor suppressor p53 was reported to play a key role in the anti-tumor action of berberine. A recent study has revealed that berberine may up-regulate p53 expression by suppressing the inner inhibitor MDM2 at the post-transcriptional level (Shukla et al., 2016; Wang et al., 2016; Chrysovergis et al., 2019; Draganov et al., 2019). In addition, berberine may increase the expression of the primary precursor, precursor, and mature forms of miR-23a, which could enhance berberine-induced G2/M cell cycle arrest. Orally administered berberine inhibits p53 expression and non-expression in lung cancer xenografts, increasing the level of p53 and therefore inhibiting the G1 phase of tumor cells. CDK (Cyclin-Dependent Kinase) is a heterodimeric protein that promotes the progression of the cell cycle by modulating the kinase cascade. Inhibition of cell cycle G1 is also observed when CDK inhibitors are over-expressed. Berberine induces the over-expression of CIP1/p21 and Kip1/p27 proteins and downregulates cyclin-dependent kinases (cdk2, cdk4, cdk6), leading to G1 arrest of tumor cells (Eom et al., 2008; Lan et al., 2014; Li et al., 2017b).

An interesting study has shown that berberine exerts different effects on p53 expression in breast cancer cell lines MCF-7 and MDA-MB231. MCF-7 cells express the wild-type tumor protein p53 (TP53), while MDA-MB-231 cells express the mutant TP53. In both cell lines, p53 mRNA levels are down-regulated by TPA (12-O-tetradecano-13-acetate, a tumor promoter) (Kim and Jung, 2012). After coptis, the level of p53 expression increased in TPA-induced MCF-7 cells. However, the expression of p53 remained unaltered in TPA-treated MDA-MB231 cells (Yan and Asmah, 2017). Studies have demonstrated that berberine does not directly affect the expression of p53 when p53 is mutated and mediates p53-dependent inhibition of tumor cells in the G2 phase. Therefore, berberine can affect the mutation of p53 and non-mutant p53 in cancer cells through different pathways.

Berberine has been seen to activate TP53, which increased the expression of miR-23a in HCC. This TP53, in turn, stimulated p21Cip1 and GADD45alpha expression. Suppression of miR-23a blocked the binding of TP53 to the chromatin and blocked transcriptional activation of p21Cip1 and GADD45alpha (Wang et al., 2014b; Sujitha et al., 2018). Berberine induced miR-23a, which may not be suppressed in mitosis A (NIMA) kinase 6 (NEK6) and resulted in blocking of the cell cycle in G2/M (Jee et al., 2010). In addition, NEK6 may have an impact on TP53. NEK6 antagonized TP53 and induced senescence (Sheng et al., 2015). RNA-Seq analysis revealed that berberine modified the expression of genes in the TP53 and cell cycle pathways (Li et al., 2015).

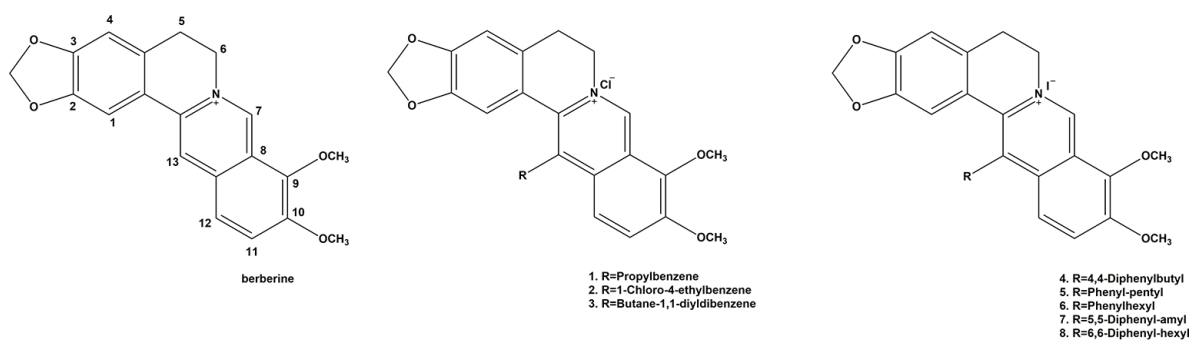


**FIGURE 1 |** Possible mechanism of the anti-tumor effects induced by berberine based on systems pharmacology. VEGFR, vascular endothelial growth factor receptor; Akt, serine/threonine kinase; ERK, extracellular regulated protein kinases activation; MMP, Matrix Metalloproteinase; AMPK, AMP-activated protein kinase; BAX, Bcl-2-associated X protein; Bcl-2, B-cell lymphoma 2; ROS, reactive oxygen species.

TP53 plays an important role in the induction of tumor cell apoptosis. In another study, the effects of berberine on the arachidonic acid (AA) metabolic pathway in HCC were examined. Berberine altered the viability and apoptosis of HCC cells in a dose-dependent fashion by inducing the translocation of apoptosis-inducing factors between the mitochondria and nucleus. Berberine also suppressed the levels of cytosolic phospholipase A2 (cPLA) and COX-2, which increased the ratio of AA to PEG-2 (Feng et al., 2012). Collectively, these findings suggest that tumor protein p53 (TP53) is closely associated with the anti-tumor effects induced by berberine (**Figure 1** and **Table 1**).

## EFFECTS OF BERBERINE ON TUMOR PROLIFERATION AND APOPTOSIS

Apoptosis is a multi-gene, strictly controlled process. These genes are highly conserved among species, including the Bcl-2 family and caspase family. Berberine may down-regulate the expression of XIAP, an X-linked inhibitor of apoptotic proteins, triggering apoptosis in leukocyte-depleted p53 genes (Liu et al., 2013). Berberine can also induce apoptosis by increasing reactive oxygen species (ROS) in certain breast cancer cells (MCF-7 and MDA-MBA-231). Berberine and tumor necrosis factor-related apoptosis-inducing ligand (TRAIL) demonstrated synergistic effects on apoptosis-induction in TNBC, with p38 MAPK activated in response to the combined treatment. Hence, berberine/TRAIL induced apoptosis by regulating p38 MAPK pathways (Refaat et al., 2015).

Several studies have reported the anti-tumor effects of berberine in the human hepatocellular carcinoma (HCC) cell line by inducing apoptosis. Berberine activates mitochondrial apoptosis in HCC cells by increasing Bax expression, PT pore formation, Cyto C release into the cytosol, and the subsequent activation of caspase 3- and 9-signaling pathways (Wang et al., 2010). CD147 was shown to up-regulate the expression of classic MDR-related transporter MDR1, and it affects apoptotic pathways in cancer cells, enhancing drug sensitivity. CD147 is highly expressed in HCC cells, promoting tumor invasion, metastasis, and tumor angiogenesis, and also inhibiting apoptosis and anoikis (Kuang et al., 2009). Furthermore, Hou et al. (2011) reported that berberine induces both apoptosis and cell death in HepG2 cells, which correlates with the down-regulation of CD147. Hepatic nuclear factor 4 alpha (HNF4alpha), a key liver transcription factor, can transactivate the Exo 70 promoter region. Berberine-mediated cell cycle arrest occurred through the down-regulation of HNF4alpha and Exo-70 (Yu et al., 2014). This demonstrates that berberine induces pyroptosis in HCC. Pyroptosis is a caspase-1 dependent programmed cell death program (Chen et al., 2016). In addition, MiR-22-3p was lower in HCC. Berberine demonstrated an ability to increase miR-22-3p in HCC. In these studies, high doses of berberine inhibited cell growth at the 24 h time interval. Berberine treatment decreased the expression of SP1, cyclin D1, and BCL2. Berberine induced miR-22-3p, which bound SP1 and suppressed cyclinD1 and BCL2.

Berberine has exhibited the ability to overcome multidrug resistance, indicating its potential in tumor chemotherapy. Coadministration of berberine and cisplatin resulted in potentiation, and berberine sensitized the cells to cisplatin. Furthermore, berberine increased the extent of DNA damage and apoptosis normally induced by cisplatin (Zhao et al., 2016). Berberine decreased breast cancer cell migration and chemokine expression. This was determined by wound healing assays and RNA analysis of chemokine receptors in MCF-7 breast cancer cells (Ahmadiankia et al., 2016). Berberine has been proven to increase the anti-tumor effects of tamoxifen (TAM) in drug-sensitive MCF-7 and drug-resistant MCF-7/TAM cells. The combined treatment of berberine and TAM enhanced cytotoxic activity and induced G1 arrest and apoptosis, potentially due to p21Cip-1 induction and increase of the BAX/BCL2 ratio (Wen et al., 2016). The combination of berberine and curcumin has been shown to effectively suppress growth in certain breast cancer cell lines. The combined treatment was more effective than treatment with either berberine or curcumin alone. The combined treatment resulted in phosphorylation of c-Jun N-terminal kinase (JNK) and Beclin1 and reduced the phosphorylation of BCL-2 (Wang K. et al., 2016).

AMPK, an AMP-dependent protein kinase, is a critical molecule in the regulation of bioenergetic metabolism and core metabolic-related diseases. Its activation is accompanied by an apoptotic effect in a caspase-dependent manner *via* the mitochondrial pathway. Activation of AMPK leads to the

**TABLE 1** | Effects of berberine on various cancer cell lines.

| Cell lines | Origin | Effects |
|---|---|---|
| MCF-7, MDA-MB-231 | Breast cancer | Increased BAX/BCL2 ratio and ROS; Decreased VEGFR, Akt, ERK1,2 activation and the expression of MMP-2,9, IL-8; Cycle arrest and cell apoptosis |
| HCC, MHCC97-L, HepG2, SMMC-7721, Be-l7402 | Liver cancer | Down-regulation of HNF4alpha and Exo-70, COX-2, NF-kappaB, MMP-9, TNF-α, CD147; MAPK and ERK1,2 inactivation; TP53, mTORC1 inhibition; Cell cycle arrest |
| HTB-94 | Chondrosarcoma | Increased TP53 and $p21^{Cip1}$ expression; Decreased cyclin B1, CDC2, CDC25c, and pRB expression. |
| A549, H1299 | Lung cancer | Caspase-3 activation; Decrease in Bcl-2/Bcl-xL levels; Increase in Bax/Bak levels |
| LNCaP, PC-3 | Prostate carcinoma | Caspase-9 and -3 activation; Decrease in Bcl-2/Bcl-xL levels; Up-regulation of p21 and p27 |

*VEGFR, vascular endothelial growth factor receptor; Akt, serine/threonine kinase; ERK, extracellular regulated protein kinases activation; AMPK, AMP-activated protein kinase; BAX, Bcl-2-associated X protein; Bcl-2, B-cell lymphoma 2.*

induction of apoptosis in various human cancer cell types (Ji et al., 2010). Furthermore, berberine promoted AMPK phosphorylation and inhibited Akt phosphorylation in HepG2 cells, leading to caspase-dependent mitochondrial pathway apoptosis (Yang and Huang, 2013). Synergistic antitumor effects were observed when berberine was employed in combination with other agents to treat hepatomas. The combined use of berberine and evodiamine could significantly enhance the apoptosis of SMMC-7721 cells, which is related to the up-regulation of TNF-α (Wang et al., 2008). In addition, the use of berberine in combination with the microtubule poison vincristine has proved efficient against hepatoma cell lines by potentiating the pro-apoptotic effect of the individual drug (Wang et al., 2014a). Other studies have demonstrated that the interstitial implantation of radioactive seed $^{125}I$ induced hepatoma cell apoptosis. This effect was enhanced when $^{125}I$ was combined with berberine, which induces apoptosis, cell degeneration, and necrosis (Wang et al., 2012). Furthermore, the anti-tumor activity of gamma radiation is significantly enhanced by berberine *via* the activation of the p38 MAPK pathway and ROS generation in human hepatoma cells (Ma et al., 2013). Berberine can induce apoptosis and autophagic cell death in HEP-G2 HCC cells. Induction of apoptosis and autophagy require AMP-activated protein kinase (AMPK), resulting in the elevated expression of inactive acetyl-CoA carboxylase (ACC). Inhibition of AMPK by RNAi or the AMPK inhibitor (compound C) suppressed the effects of berberine. In contrast, the AMPK activator AICAR stimulated cytotoxic effects. It has been shown that berberine inhibits mTORC1 activation by stimulating AMPK (Choi et al., 2009). Therefore, these findings suggest that berberine alone or in combination with other drugs possesses an anti-tumor effect mediated *via* AMPK activation.

## EFFECTS OF BERBERINE ON TUMOR METASTASIS INHIBITION

Berberine has exhibited its ability to suppress tumor metastasis (Lin et al., 2006; Serafim et al., 2008; Cai et al., 2014). Matrix metalloproteinases (MMPs) degrade the tissue matrix, allowing tumor cells to break through the normal tissue barrier and invade the surrounding normal tissue and distant organs. *In vitro* studies have demonstrated that the inhibition of FAK, IKK, NF-kB, u-PA, MMP-2, and MMP-9 significantly reduced metastasis. Berberine inhibits the release of MMP-2 from tumor cells and thus inhibits tumor cell destruction of the tissue matrix.

Berberine increased the activities of numerous proteins involved in proliferation, such as Janus Kinase 2 (JAK2), Phosphoinositide 3-kinase (PI3K), activator protein-1 (AP-1), and NF-kappaB (Mahata et al., 2011; Fu et al., 2013; Wu et al., 2013; Belanova et al., 2019; El-Zeftawy et al., 2019; Jiang et al., 2019). These proteins decreased IL-8 expression in the TNBC cell line, MDA-MB-231. The IL-8 stimulated invasion was also suppressed by berberine (Kim et al., 2018). Berberine also decreased MMP-2, MMP-9, E-cadherin, EGF, bFGF, and fibronectin in the breast cancer cells. The effect of berberine was inhibited by JNK and p38 MAPK inhibitors and was increased by p38 MAPK activators (Zheng et al., 2014; Zhou et al., 2015; Zhao et al., 2019).

Berberine can also bind to the vasodilator-stimulated phosphoprotein (VASP). VASP is over-expressed in breast cancer cells with high mobility and inhibits polymerization. Berberine binds VASP in MDA-MB-231 cells and suppresses proliferation and tumor growth (Su et al., 2016).

## STRUCTURAL MODIFICATION OF BERBERINE

### Modification Transformation and Antineoplastic Activity of C-13-Substituted Berberine Derivatives

The diverse pharmacological properties exhibited by berberine indicate that the alkaloid has definite potential as a drug in a wide spectrum of clinical applications. The structure of berberine (**Figure 2**) represents a biologically essential skeleton and also a natural lead compound for the introduction of various chemical modifications at appropriate positions. The structural

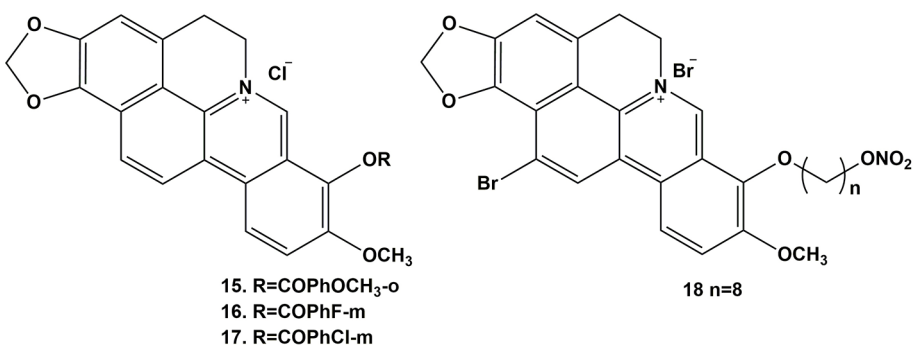


**FIGURE 2 |** Structure of berberine and compounds 1-8.

modification of berberine for antineoplastic activity has mainly focused on C-9 (Iwasa et al., 1996; Krishnan and Bastow, 2000; Pang et al., 2005; Pang et al., 2007; Cui et al., 2010; Huang et al., 2010) and C-13 (Park et al., 2006; Ortiz et al., 2014). Therefore, to examine the anticancer activity of the berberine derivatives, three berberine derivatives were prepared and bioassayed on human colon carcinoma cell lines. The results revealed that the derivatives also induced cell cycle arrest and cell death by apoptosis. Furthermore, the effect of the derivatives was more potent than that of the parent compound.

To further improve the efficacy and bioavailability of the derivatives, Yang et al. designed several cycloberberine derivatives (Yang et al., 2008; Jin et al., 2015; Yang et al., 2019). Among them, some compounds showed strong inhibition on human HepG2 cells. Another researcher also synthesized a series of cycloberberine derivatives and evaluated their anti-cancer activity (Franceschin et al., 2006). Among them, five compounds exhibited strong inhibition on human HepG2 cells, respectively.

In addition, 13-ethylpyridine hydrochloride berberine derivatives produced by the Franceschin group selectively combined with the G-quadruplex DNA in the cell growth cycle and inhibited the activity of telomerase, demonstrating good anti-tumor activity (Gornall et al., 2007). They also observed that this kind of compound not only increased the stability of G-quadruplex DNA but can also inhibit polymerases (Jin et al., 2015). Gornall et al. studied the interaction between 13-indolyl supersede berberine and G-quadruplex DNA and found that the former can selectively combine with G-quadruplex DNA but not with double-strand DNA, which was meaningful for exploring new measures for inhibiting tumor amplification (Li et al., 2013). These findings indicate that berberine derivatives, like berberine, have anti-tumor effects.

## Modification Transformation and Antineoplastic Activity of C-9-Substituted Berberine Derivatives

Shi et al. designed and synthesized a series of new triazole berberine derivatives (Shi et al., 2011). Most of the compounds displayed stronger anti-tumor activity in SMMC-7721 cells than berberine (Lo et al., 2013). Among these derivatives, compounds 12 and 13 exhibited the strongest inhibition activity in SMMC-7721 cell lines. New 1,13-cycloprotoberberine derivatives were designed and synthesized and their cytotoxicity evaluated in HCT 116 (Pang et al., 2005). The results were reported to demonstrate that the replacement of 9-methoxyl with an ester moiety strengthened *in vitro* antiproliferative activity. Further research indicated that compound 14 inhibited the activity of DNA topoisomerase I (Top I), leading to stasis of G2/M phase to decrease the growth of tumor cells. This group also compounded a series of cycloberberine derivatives and evaluated their anticancer activity *in vitro*. The results demonstrated that compounds 15-17 could inhibit human HepG2 cell proliferation induced by the inhibition of DNA Top I at the G2/M phase (**Figure 3**). In addition, they designed and

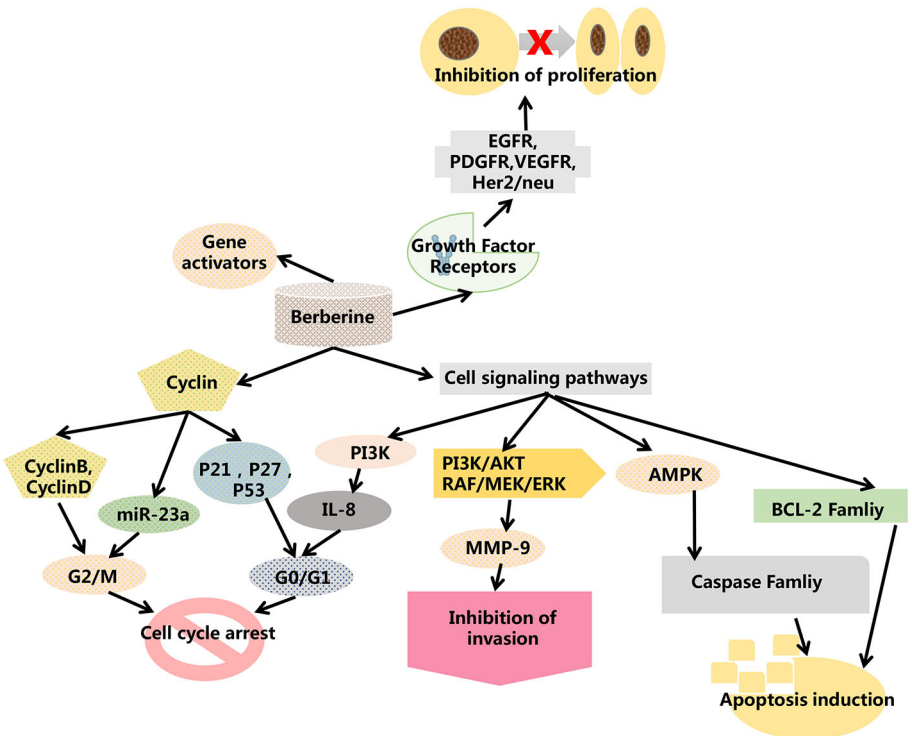


**FIGURE 3 |** Structure of compounds 15-17.

synthesized 9-O-bile acid berberine, which displayed much stronger inhibition on hepatoma carcinoma cells than berberine. This derivative also had higher reported bioavailability (Chen et al., 2005).

Lo's team observed that lipotropic substitutive derivatives, such as 9-O-alkyl supersede berberine and 9-O-Terpenyl substituted berberine, could induce apoptosis in HepG2 tumor cells and that their inhibitory activity against HepG2 and HT-29 tumor cells could be further enhanced with the extension of the alkyl chain. Moreover, berberine can produce a series of 9-O-berberine derivatives by pyrogenic and alkylation reaction (Mistry et al., 2017). The reaction can convert the methyl in the C (9) methoxy group into ethyl to compound 9-O-ethylamine berberine, demonstrating a strong affinity with CT DNA. Furthermore, compared to the parent berberine, the affinity of berberine red dimer, compounded by Chen's team (Qin et al., 2006), for DNA increased by 100 times. Protein POT1 is another important protein associated with telomere extension and protection. It has been identified as a potential drug target for cancer treatment. Xiao's team observed that the interaction between 9-N-supersede berberine derivatives and POT1 could influence the effect of POT1 and telomeric DNA. This result may provide a potential new pathway for future cancer therapies.

Mistry and colleagues combined the C-9 replacement of berberine and substituted 2-aminobenzothiazoles by a pentyl side chain, which was assessed for *in vitro* antioxidant and anticancer activities against tumor cells (Sun et al., 2009; Mistry et al., 2017). The results suggest that compounds with methoxy or cyano functional groups were the most active radical scavengers to DPPH and ABTS. Furthermore, they also exhibited the strongest anti-tumor activity against the HeLa and CaSki cervical cancer cell lines, including the SK-OV-3 ovarian cancer cell line.

Notably, the G-quadruplex in the promoter region of c-myc took effect as a transcriptional repressor. The c-myc transcriptional repressor 1,5-7 controlled by G-quadruplex structure is considered an attractive target for anti-cancer therapeutic strategies. Ma et al. (2008) explored the interaction between 9-N-substituted berberine derivatives and G-quadruplex DNA using electrophoretic mobility shift assay (EMSA), circular dichroism spectroscopy (CD), the fluorescence resonance energy transfer-melting (FRET-melting) method, polymerase chain reaction-stop assay (PCR-stop assay), the competition dialysis method, cell proliferation assay, and reverse transcription-polymerase chain reaction (RT-PCR). The results indicated that these derivatives could selectively induce and stabilize the formation of the c-myc in the parallel molecular G-quadruplex. Accordingly, transcription of c-myc was down-regulated in the cancer cell line. Moreover, this result could be effective with or without metal cations. In addition, the different structural derivatives reported different abilities to stabilize the c-myc G-quadruplex. Therefore, 9-N-substitutes, such as a 1,6-diaminohexyl side chain, at the 9-position of berberine improved the selective binding with G-quadruplex, increased the inhibition of hybridization, and thus blocked gene expression.

Nitric oxide (NO) is also important in various physiological and pathophysiological processes (Chiu and Chien, 2011). Based on recent studies, decreased levels of NO in liver tissues may be conducive to the progression of HCC. In addition, NO donors, such as sodium nitroprusside (SNP), arrested the cell cycle and induced apoptosis in HepG2 cells, suppressing proliferation, migration, and invasion of cancer cells effectively. Therefore, in anti-tumor studies, NO donors are usually used as substitutes for NO. Moreover, numerous reports have demonstrated that the anti-tumor activity of NO-donating hybrids was greater than that of sole NO donors, parent drugs, or their combinations (Bauer et al., 2010; van der Stoep et al., 2009; Wang et al., 2013; Dzinic et al., 2014). Furthermore, NO-donating anti-tumor drugs do not induce any drug resistance in tumor cells. In addition, the hydrophilic nature of the quaternary ammonium salt is the main cause of impaired intestinal absorption. Different lengths of alkyl linkages can be used to improve lipophilicity and enhance effectiveness. Hence, it is necessary to design and synthesize a series of berberine derivatives for the treatment of HCC. Several results have demonstrated that the majority of derivatives with antiproliferative activity against HepG2 cells have been a dramatic improvement on the parent compounds (Nechepurenko et al., 2011). Among these derivatives, compound 15a, superior to the positive control cisplatin, exhibited the most promising activity. In structure-activity relationship analysis, the concentration of released NO increased slightly with the extension of the chain length. A more detailed study indicated that compound 18 resulted in the stasis of the G2 phase in the cell cycle and induced apoptosis in HepG2 cells by the depolarization of the mitochondria. Furthermore, the *in vivo* anti-tumor activity of compound 18 was observed in an H22 liver cancer xenograft mouse model. Therefore, it can be stated that berberine derivatives demonstrate anti-tumor activities (Mei et al., 2015; Zou et al., 2017) and could be promising therapeutic agents in cancer therapy.

## CONCLUSION

Berberine and its derivatives have extensive pharmacological actions. In this review, their anti-tumor effects and underlying mechanisms were systemically outlined based on systems pharmacology. This review also revealed the efficacy and potential mechanism of action of berberine and its derivatives when used in the treatment of complex cancers at the molecular, cellular, and organism levels. Furthermore, several signaling pathways were also outlined. However, there are limitations in the study of berberine, as its anti-tumor mechanism has yet to be fully elucidated. More importantly, there have only been a few *in vivo* and pre-clinical studies evaluating berberine. However, in-depth investigations on the efficacy of berberine and its derivatives are ongoing, and a growing number of studies have started focusing on the potential anti-tumor role of berberine,

possibly mediated through immune regulation. The ability of berberine to increase chemosensitivity and reduce the side effects of chemosensitizers has also been emphasized. Berberine and its derivatives may be promising drugs in cancer therapy, possibly improving clinical efficacy and safety.

## AUTHOR CONTRIBUTIONS

CZ and LZ wrote the first draft. WY, JS, and XY provided the organization and framework of the article. ZZ, LS, YW, RC, and GL provided critical revisions. All authors approved the final version of the manuscript for submission.

## FUNDING

This work was supported by National Key R&D Program of China (Grant # 2018YFC1311600), Jilin Science and Technology Agency funding (20180520124JH, 20180519003JH, 20190701078GH and 20180414050GH) and Jilin Province medical and health talents (2019SCZT007).

## REFERENCES

Ahmadiankia, N., Moghaddam, H. K., Mishan, M. A., Bahrami, A. R., Naderi-Meshkin, H., Bidkhori, H. R., et al. (2016). Berberine suppresses migration of MCF-7 breast cancer cells through down-regulation of chemokine receptors. *Iranian J. Of Basic Med. Sci.* 19, 125–131.

Alolga, R. N., Fan, Y., Chen, Z., Liu, L. W., Zhao, Y. J., Li, J., et al. (2016). Significant pharmacokinetic differences of berberine are attributable to variations in gut microbiota between Africans and Chinese. *Sci. Rep.* 6 27671. doi: 10.1038/srep27671

Babiker, A. Y., Almatroudi, A., Allemailem, K. S., Husain, N. E. O. S., Alsammani, M. A., Alsahli, M. A., et al. (2018). Clinicopathologic aspects of squamous cell carcinoma of the uterine cervix: role of PTEN, BCL2 and P53. *Applied Sciences-Basel* 8 (11), 10. doi: 10.3390/app8112124

Barzegar, E., Fouladdel, S., Movahhed, T. K., Atashpour, S., Ghahremani, M. H., Ostad, S. N., et al. (2015). Effects of berberine on proliferation, cell cycle distribution and apoptosis of human breast cancer T47D and MCF7 cell lines. *Iranian J. Of Basic Med. Sci.* 18, 334–342.

Bauer, J. A., Frye, G., Bahr, A., Gieg, J., and Brofman, P. (2010). Anti-tumor effects of nitrosylcobalamin against spontaneous tumors in dogs. *Invest. New Drugs* 28 (5), 694–702. doi: 10.1007/s10637-009-9282-0

Belanova, A., Beseda, D., Chmykhalo, V., Stepanova, A., Belousova, M., Khrenkova, V., et al. (2019). Berberine Effects on NF kappa B, HIF1A and NFE2L2/AP-1 pathways in HeLa Cells. *Anti-Cancer Agents In Med. Chem.* 19, 487–501. doi: 10.2174/1871520619666181211121405

Cai, Y. C., Xia, Q., Luo, R. Z., Huang, P. Y., Sun, Y. L., Shi, Y. X., et al. (2014). Berberine inhibits the growth of human colorectal adenocarcinoma in vitro and in vivo. *J. Of Nat. Med.* 68, 53–62. doi: 10.1007/s11418-013-0766-z

Chen, W. H., Pang, J. Y., Qin, Y., Peng, Q., Cai, Z. W., and Jiang, Z. H. (2005). Synthesis of linked berberine dimers and their remarkably enhanced DNA-binding affinities. *Bioorg. Med. Chem. Lett.* 15, 2689–2692. doi: 10.1016/j.bmcl.2004.10.098

Chen, J., Wu, F. X., Luo, H. L., Liu, J. J., Luo, T., Bai, T., et al. (2016). Berberine upregulates miR-22-3p to suppress hepatocellular carcinoma cell proliferation by targeting Sp1. *Am. J. Of Trans. Res.* 8, 4932–4941.

Chiu, J. J., and Chien, S. (2011). Effects of disturbed flow on vascular endothelium: pathophysiological basis and clinical perspectives. *Physiol. Rev.* 91, 327–387. doi: 10.1152/physrev.00047.2009

Choi, M. S., Oh, J. H., Kim, S. M., Jung, H. Y., Yoo, H. S., Lee, Y. M., et al. (2009). Berberine inhibits p53-dependent cell growth through induction of apoptosis of prostate cancer cells. *Int. J. Oncol.* 34, 1221–1230.

Chrysovergis, A., Papanikolaou, V., Tsiambas, E., Stavraka, C., Ragos, V., Peschos, D., et al. (2019). P53/MDM2 Co-expression in laryngeal squamous cell carcinoma based on digital image analysis. *Anticancer Res.* 39, 4137–4142. doi: 10.21873/anticanres.13572

Cui, J. S., Xu, F., Pang, J. Y., Chen, W. H., and Jiang, Z. H. (2010). Synthesis and DNA-binding affinities of protoberberine-based multivalent agents. *Chem. Biodivers.* 7, 2908–2916. doi: 10.1002/cbdv.200900386

Dai, B. L., Ma, Y. J., Yang, T. F., Fan, M. Y., Yu, R. Z., Su, Q., et al. (2019). Synergistic effect of berberine and HMQ1611 impairs cell proliferation and migration by regulating Wnt signaling pathway in hepatocellular carcinoma. *Phytother. Res.* 33, 745–755. doi: 10.1002/ptr.6267

Draganov, A. B., Yang, X. X., Anifowose, A., De La Cruz, L. K. C., Dai, C. F., Ni, N. T., et al. (2019). Upregulation of p53 through induction of MDM2 degradation: Anthraquinone analogs. *Bioorg. Med. Chem.* 27, 3860–3865. doi: 10.1016/j.bmc.2019.07.019

Dzinic, S. H., Chen, K., Thakur, A., Kaplun, A., Bonfil, R. D., Li, X. H., et al. (2014). No Maspin expression in prostate tumor elicits host anti-tumor immunity. *Oncotarget* 5, 11225–11236. doi: 10.18632/oncotarget.2615

El-Zeftawy, M., Ghareeb, D., Elbealy, E. R., Saad, R., Mahmoud, S., Elguindy, N., et al. (2019). Berberine chloride ameliorated PI3K/Akt-p/SIRT-1/PTEN signaling pathway in insulin resistance syndrome induced in rats. *J. Food Biochem.* 11. doi: 10.1111/jfbc.13049

Eo, S. H., and Kim, S. J. (2014). Berberine cell cycle arrest at the G2/M phase via PI3K and p38 kinase in human chondrosarcoma cell line, HTB94 cells. *J. Of Biotechnol.* 185, S97–S97. doi: 10.1016/j.jbiotec.2014.07.331

Eom, K. S., Hong, J. M., Youn, M. J., So, H. S., Park, R., Kim, J. M., et al. (2008). Berberine induces G1 arrest and apoptosis in human glioblastoma T98G cells through mitochondrial/caspases pathway. *Biol. Pharm. Bull.* 31, 558–562. doi: 10.1248/bpb.31.558

Feng, A. W., Gao, W., Zhou, G. R., Yu, R., Li, N., Huang, X. L., et al. (2012). Berberine ameliorates COX-2 expression in rat small intestinal mucosa partially through PPAR gamma pathway during acute endotoxemia. *Int. Immunopharmacol.* 12, 182–188. doi: 10.1016/j.intimp.2011.11.009

Franceschin, M., Rossetti, L., D'ambrosio, A., Schirripa, S., Bianco, A., Ortaggi, G., et al. (2006). Natural and synthetic G-quadruplex interactive berberine derivatives. *Bioorg. Med. Chem. Lett.* 16, 1707–1711. doi: 10.1016/j.bmcl.2005.12.001

Fu, L. Y., Chen, W. B., Guo, W., Wang, J. S., Tian, Y., Shi, D. B., et al. (2013). Berberine Targets AP-2/hTERT, NF-kappa B/COX-2, HIF-1 alpha/VEGF and Cytochrome-c/Caspase signaling to suppress human cancer cell growth. *Plos One* 8 (7), e69240. doi: 10.1371/journal.pone.0069240

Ge, L., Bao, A. X., and Yang, K. D. (2016). Determination and correlation of the solubility for berberine chloride in pure imidazolium-based ionic liquids. *J. Chem. And Eng. Data* 61, 1829–1835. doi: 10.1021/acs.jced.5b01017

Gornall, K. C., Samosorn, S., Talib, J., Bremner, J. B., and Beck, J. L. (2007). Selectivity of an indolyl berberine derivative for tetrameric G-quadruplex DNA. *Rapid Commun. Mass Spectrom.* 21, 1759–1766. doi: 10.1002/rcm.3019

Gu, L. B., Shah, N., and Zhou, M. X. (2008). Berberine induces apoptosis in acute lymphoblastic leukemia cells through downregulation of the MDM2 Oncoprotein. *Blood* 112, 575–575.

Gu, M. M., Xu, J., Han, C. Y., Kang, Y. X., Liu, T. F., He, Y. F., et al. (2015). Effects of Berberine on cell cycle, DNA, reactive oxygen species, and apoptosis in L929 murine fibroblast cells. *Evidence-Based Complement. Alternat. Med.* 796306. doi: 10.1155/2015/796306

Ho, Y. T., Yang, J. S., Lu, C. C., Chiang, J. H., Li, T. C., Lin, J. J., et al. (2009). Berberine inhibits human tongue squamous carcinoma cancer tumor growth in a murine xenograft model. *Phytomedicine* 16, 887–890. doi: 10.1016/j.phymed.2009.02.015

Hou, Q., Tang, X., Liu, H. Q., Tang, J. Q., Yang, Y., Jing, X. H., et al. (2011). Berberine induces cell death in human hepatoma cells in vitro by downregulating CD147. *Cancer Sci.* 102, 1287–1292. doi: 10.1111/j.1349-7006.2011.01933.x

Huang, L., Luo, Z. H., He, F., Shi, A. D., Qin, F. F., and Li, X. S. (2010). Berberine derivatives, with substituted amino groups linked at the 9-position, as inhibitors of acetylcholinesterase/butyrylcholinesterase. *Bioorg. Med. Chem. Lett.* 20, 6649–6652. doi: 10.1016/j.bmcl.2010.09.013

Iwasa, K., Kamigauchi, M., Ueki, M., and Taniguchi, M. (1996). Antibacterial activity and structure-activity relationships of berberine analogs. *Eur. J. Of Med. Chem.* 31, 469–478. doi: 10.1016/0223-5234(96)85167-1

Jantova, S., Cipak, L., Cernakova, M., and Kost'alova, D. (2003). Effect of berberine on proliferation, cell cycle and apoptosis in HeLa and L1210 cells. *J. Of Pharm. And Pharmacol.* 55, 1143–1149. doi: 10.1211/002235703322277186

Jee, H. J., Kim, A. J., Song, N., Kim, H. J., Kim, M., Koh, H., et al. (2010). Nek6 overexpression antagonizes p53-induced senescence in human cancer cells. *Cell Cycle* 9, 4703–4710. doi: 10.4161/cc.9.23.14059

Ji, C., Yang, B., Yang, Y. L., He, S. H., Miao, D. S., He, L., et al. (2010). Exogenous cell-permeable C6 ceramide sensitizes multiple cancer cell lines to Doxorubicin-induced apoptosis by promoting AMPK activation and mTORC1 inhibition. *Oncogene* 29, 6557–6568. doi: 10.1038/onc.2010.379

Jiang, H., Song, J., Tang, Z., Gao, X., and Liu, J. (2019). Protective effect of Berberine on spermatogenesis and reproductive competence in STZ-induced diabetic rats via inhibiting ROS/NF kappa B/JAK2 pathway. *Bju Int.* 123, 10–10.

Jin, X., Yan, L., Li, H. J., Wang, R. L., Hu, Z. L., Jiang, Y. Y., et al. (2015). Novel triazolyl berberine derivatives prepared via CuAAC click chemistry: synthesis, anticancer activity and structure-activity relationships. *Anti-Cancer Agents Med. Chem.* 15, 89–98. doi: 10.2174/1871520614666141203142012

Kim, H. S., and Jung, G. (2012). p53 transactivation domain phosphorylation level is associated with poor clinicopathological features of wild-type p53 HCCs. *J. Gastroenterol. Hepatol.* 27, 345–345.

Kim, S., You, D., Jeong, Y., Yu, J., Kim, S. W., Nam, S. J., et al. (2018). Berberine down-regulates IL-8 expression through inhibition of the EGFR/MEK/ERK pathway in triple-negative breast cancer cells. *Phytomedicine* 50, 43–49. doi: 10.1016/j.phymed.2018.08.004

Krishnan, P., and Bastow, K. F. (2000). The 9-position in berberine analogs is an important determinant of DNA topoisomerase II inhibition. *Anti-Cancer Drug Design* 15, 255–264.

Kuang, Y. H., Chen, X., Su, J., Wu, L. S., Liao, L. Q., Li, D., et al. (2009). RNA interference targeting the CD147 induces apoptosis of multi-drug resistant cancer cells related to XIAP depletion. *Cancer Lett.* 276 (2), 189–195. doi: 10.1016/j.canlet.2008.11.010

Lan, T., Wu, T., Chen, C., Chen, X. L., Hao, J., Huang, J. Y., et al. (2014). Berberine attenuates high glucose-induced proliferation and extracellular matrix accumulation in mesangial cells: Involvement of suppression of cell cycle progression and NF-kappa B/AP-1 pathways. *Mol. Cell. Endocrinol.* 384, 109–116. doi: 10.1016/j.mce.2014.01.022

Li, Y. B., Zhao, W. L., Wang, Y. X., Zhang, C. X., Jiang, J. D., Bi, C. W., et al. (2013). Discovery, synthesis and biological evaluation of cycloprotoberberine derivatives as potential antitumor agents. *Eur. J. Of Med. Chem.* 68, 463–472. doi: 10.1016/j.ejmech.2013.07.026

Li, J., Li, O., Kan, M. J., Zhang, M., Shao, D., Pan, Y., et al. (2015). Berberine induces apoptosis by suppressing the arachidonic acid metabolic pathway in hepatocellular carcinoma. *Mol. Med. Rep.* 12, 4572–4577. doi: 10.3892/mmr.2015.3926

Li, D. D., Zhang, Y. Y., Liu, K., Zhao, Y. J., Xu, B. B., Xu, L., et al. (2017a). Berberine inhibits colitis-associated tumorigenesis via suppressing inflammatory responses and the consequent EGFR signaling-involved tumor cell growth. *Lab. Invest.* 97, 1343–1353. doi: 10.1038/labinvest.2017.71

Li, L., Wang, X. C., Sharvan, R., Gao, J. Y., and Qu, S. (2017b). Berberine could inhibit thyroid carcinoma cells by inducing mitochondrial apoptosis, G0/G1 cell cycle arrest and suppressing migration via PI3K-AKT and MAPK signaling pathways. *Biomed. Pharmacother.* 95, 1225–1231. doi: 10.1016/j.biopha.2017.09.010

Li, J., Liu, F., Jiang, S. L., Liu, J., Chen, X. H., Zhang, S. N. A., et al. (2018). Berberine hydrochloride inhibits cell proliferation and promotes apoptosis of non-small cell lung cancer via the suppression of the MMP2 and Bcl-2/Bax signaling pathways. *Oncol. Lett.* 15, 7409–7414. doi: 10.3892/ol.2018.8249

Li, T., Wang, P. L., Guo, W. B., Huang, X. M., Tian, X. H., Wu, G. R., et al. (2019). Natural berberine-based chinese herb medicine assembled nanostructures with modified antibacterial application. *Acs Nano* 13, 6770–6781. doi: 10.1021/acsnano.9b01346

Liao, S. L., Zhang, G. G., Cao, H., Chen, B. Y., Li, W. M., Wu, X., et al. (2018). Synthesis and Anti-tumor Activities against HepG2 Cell in vitro of the Conjugates of Honokiol, Quercetin and Berberine. *Chin. J. Org. Chem.* 38, 1549–1555. doi: 10.6023/cjoc201801023

Lin, C. C., Lin, S. Y., Chung, J. G., Lin, J. P., Chen, G. W., and Kao, S. T. (2006). Down-regulation of cyclin B1 and up-regulation of Wee1 by berberine promotes entry of leukemia cells into the G2/M-phase of the cell cycle. *Anticancer Res.* 26, 1097–1104.

Liu, J., Zhang, X. L., Liu, A. G., Liu, S. Y., Zhang, L. Q., Wu, B., et al. (2013). Berberine induces apoptosis in p53-Null leukemia cells by down-regulating XIAP at the post-transcriptional level. *Cell. Physiol. Biochem.* 32, 1213–1224. doi: 10.1159/000354520

Liu, Z. Y., Guo, L., Xiao, G., Dong, G. Y., Zhang, Y. X., Cheng, H., et al. (2018). Significance and expression of c-erBb-2, p53, and caspase-3 in breast cancer tissue in different age groups. *Eur. J. Of Gynaecol. Oncol.* 39, 430–432.

Liu, H. Q., Zheng, T. T., Zhou, Z. Q., Hu, A. Z., Li, M. H., Zhang, Z. X., et al. (2019a). Berberine nanoparticles for promising sonodynamic therapy of a HeLa xenograft tumour. *Rsc Adv.* 9, 10528–10535. doi: 10.1039/C8RA09172B

Liu, L., Fan, J. Y., Ai, G. H., Liu, J., Luo, N., Li, C. X., et al. (2019b). Berberine in combination with cisplatin induces necroptosis and apoptosis in ovarian cancer cells. *Biol. Res.* 52 (1), 37. doi: 10.1186/s40659-019-0243-6

Lo, C. Y., Hsu, L. C., Chen, M. S., Lin, Y. J., Chen, L. G., Kuo, C. D., et al. (2013). Synthesis and anticancer activity of a novel series of 9-O-substituted berberine derivatives: a lipophilic substitute role. *Bioorg. Med. Chem. Lett.* 23, 305–309. doi: 10.1016/j.bmcl.2012.10.098

Lu, Y. C., Lin, Q., Luo, G. S., and Dai, Y. Y. (2006). Solubility of berberine chloride in various solvents. *J. Of Chem. And Eng. Data* 51, 642–644. doi: 10.1021/je0504360

Ma, Y., Ou, T. M., Hou, J. Q., Lu, Y. J., Tan, J. H., Gu, L. Q., et al. (2008). 9-N-Substituted berberine derivatives: stabilization of G-quadruplex DNA and down-regulation of oncogene c-myc. *Bioorg. Med. Chem.* 16 (16), 7582–7591. doi: 10.1016/j.bmc.2008.07.029

Ma, C., Tang, K. L., Liu, Q., Zhu, R. X., and Cao, Z. W. (2013). Calmodulin as a potential target by which berberine induces cell cycle arrest in human hepatoma Bel7402 Cells. *Chem. Biol. Drug Design* 81, 775–783. doi: 10.1111/cbdd.12124

Ma, G. Y., Wang, C., Lv, B. Y., Jiang, Y. Z., and Wang, L. (2019). Proteinase-activated receptor-2 enhances Bcl2-like protein-12 expression in lung cancer cells to suppress p53 expression. *Arch. Med. Sci.* 15, 1147–1153. doi: 10.5114/aoms.2019.86980

Mahata, S., Bharti, A. C., Shukla, S., Tyagi, A., Husain, S. A., and Das, B. C. (2011). Berberine modulates AP-1 activity to suppress HPV transcription and downstream signaling to induce growth arrest and apoptosis in cervical cancer cells. *Mol. Cancer* 10, 39. doi: 10.1186/1476-4598-10-39

Mei, X., Wu, X., Zhang, T., Liang, M., and Fan, C. (2015). [18F-Berberine Derivatives: a Potential Molecular Imaging Agent for Tumor Targeting by PET/CT Tumor]. Sheng Wu Yi Xue Gong Cheng Xue Za Zhi 32 (2), 460–464. doi: 10.7507/1001-5515.20150083

Mistry, B., Patel, R. V., Keum, Y. S., and Kim, D. H. (2017). Evaluation of the biological potencies of newly synthesized berberine derivatives bearing benzothiazole moieties with substituted functionalities. *J. Of Saudi Chem. Soc.* 21, 210–219. doi: 10.1016/j.jscs.2015.11.002

Nechepurenko, I. V., Boyarskikh, U. A., Komarova, N. I., Polovinka, M. P., Filipenko, M. L., Lifshits, G. I., et al. (2011). LDLR Up-regulatory activity of berberine and its bromo and iodo derivatives in human liver HepG2 Cells. *Doklady Chem.* 439, 204–208. doi: 10.1134/S0012500811070093

Nkpaa, K. W., Awogbindin, I. O., Amadi, B. A., Abolaji, A. O., Adedara, I. A., Wegwu, M. O., et al. (2019). Ethanol exacerbates manganese-induced neurobehavioral deficits, striatal oxidative stress, and apoptosis via regulation of p53, caspase-3, and Bax/Bcl-2 ratio-dependent pathway. *Biol. Trace Elem. Res.* 191, 135–148. doi: 10.1007/s12011-018-1587-4

Ortiz, L. M. G., Tillhon, M., Parks, M., Dutto, I., Prosperi, E., Savio, M., et al. (2014). Multiple Effects of Berberine Derivatives on Colon Cancer Cells. *Biomed. Res. Int.* 2014, 924585. doi: 10.1155/2014/924585

Pang, J. Y., Qin, Y., Chen, W. H., Luo, G. A., and Jiang, Z. H. (2005). Synthesis and DNA-binding affinities of monomodified berberines. *Bioorg. Med. Chem.* 13, 5835–5840. doi: 10.1016/j.bmc.2005.05.048

Pang, J. Y., Long, Y. H., Chen, W. H., and Jiang, Z. H. (2007). Amplification of DNA-binding affinities of protoberberine alkaloids by appended polyamines. *Bioorg. Med. Chem. Lett.* 17, 1018–1021. doi: 10.1016/j.bmcl.2006.11.037

Park, K. D., Lee, J. H., Kim, S. H., Kang, T. H., Moon, J. S., and Kim, S. U. (2006). Synthesis of 13- (substituted benzyl) berberine and berberrubine derivatives as antifungal agents. *Bioorg. Med. Chem. Lett.* 16, 3913–3916. doi: 10.1016/j.bmcl.2006.05.033

Qin, Y., Pang, J. Y., Chen, W. H., Cai, Z., and Jiang, Z. H. (2006). Synthesis, DNA-binding affinities, and binding mode of berberine dimers. *Bioorg. Med. Chem.* 14 (1), 25–32. doi: 10.1016/j.bmc.2005.07.069

Refaat, A., Abdelhamed, S., Saiki, I., and Sakurai, H. (2015). Inhibition of p38 mitogen-activated protein kinase potentiates the apoptotic effect of berberine/tumor necrosis factor-related apoptosis-inducing ligand combination therapy. *Oncol. Lett.* 10, 1907–1911. doi: 10.3892/ol.2015.3494

Ruan, H., Zhan, Y. Y., Hou, J., Xu, B., Chen, B., Tian, Y., et al. (2017). Berberine binds RXR alpha to suppress beta-catenin signaling in colon cancer cells. *Oncogene* 36, 6906–6918. doi: 10.1038/onc.2017.296

Sagar, B. P. S., Panwar, R., Sangwan, A., Tyagi, K., and Zafar, R. (2006). In-vitro production of berberine in cultures of Berberis aristata and pharmacological investigation for anti-hepatotoxic activity. *J. Pharm. Pharmacol.* 58, A54–A54.

Serafim, T. L., Oliveira, P. J., Sardao, V. A., Perkins, E., Parke, D., and Holy, J. (2008). Different concentrations of berberine result in distinct cellular localization patterns and cell cycle effects in a melanoma cell line. *Cancer Chemother. Pharmacol.* 61, 1007–1018. doi: 10.1007/s00280-007-0558-9

Sheng, Z., Sun, Y., Zhu, R. X., Jiao, N., Tang, K. L., Cao, Z. W., et al. (2015). Functional cross-talking between differentially expressed and alternatively spliced genes in human liver cancer cells treated with berberine. *Plos One* 10 (11), e0143742. doi: 10.1371/journal.pone.0143742

Shi, A. D., Huang, L., Lu, C. J., He, F., and Li, X. S. (2011). Synthesis, biological evaluation and molecular modeling of novel triazole-containing berberine derivatives as acetylcholinesterase and beta-amyloid aggregation inhibitors. *Bioorg. Med. Chem.* 19, 2298–2305. doi: 10.1016/j.bmc.2011.02.025

Shukla, S., Sharma, A., Pandey, V. K., Raisuddin, S., and Kakkar, P. (2016). Concurrent acetylation of FoxO1/3a and p53 due to sirtuins inhibition elicit Bim/PUMA mediated mitochondrial dysfunction and apoptosis in berberine-treated HepG2 cells. *Toxicol. Applied Pharmacol.* 291, 70–83. doi: 10.1016/j.taap.2015.12.006

Su, K., Hu, P. C., Wang, X. L., Kuang, C. C., Xiang, Q. M., Yang, F., et al. (2016). Tumor suppressor berberine binds VASP to inhibit cell migration in basal-like breast cancer. *Oncotarget* 7, 45849–45862. doi: 10.18632/oncotarget.9968

Sujitha, S., Dinesh, P., and Rasool, M. (2018). Berberine modulates ASK1 signaling mediated through TLR4/TRAF2 via upregulation of miR-23a. *Toxicol. Applied Pharmacol.* 359, 34–46. doi: 10.1016/j.taap.2018.09.017

Sun, Y. Y., Xun, K. L., Wang, Y. T., and Chen, X. P. (2009). A systematic review of the anticancer properties of berberine, a natural product from Chinese herbs. *Anti-Cancer Drugs* 20, 757–769. doi: 10.1097/CAD.0b013e328330d95b

Van Der Stoep, D., Braunstahl, G. J., Van Zeben, J., and Wouters, J. (2009). Sarcoidosis during anti-tumor necrosis factor-alpha therapy: no relapse after rechallenge. *J. Rheumatol.* 36, 2847–2848. doi: 10.3899/jrheum.090307

Wang, X. N., Han, X., Xu, L. N., Yin, L. H., Xu, Y. W., Qi, Y., et al. (2008). Enhancement of apoptosis of human hepatocellular carcinoma SMMC-7721 cells through synergy of berberine and evodiamine. *Phytomedicine* 15, 1062–1068. doi: 10.1016/j.phymed.2008.05.002

Wang, N., Feng, Y. B., Zhu, M. F., Tsang, C. M., Man, K., Tong, Y., et al. (2010). Berberine induces autophagic cell death and mitochondrial apoptosis in liver cancer cells: the cellular mechanism. *J. Cell. Biochem.* 111, 1426–1436. doi: 10.1002/jcb.22869

Wang, K., Zhang, C., Bao, J., Jia, X., Liang, Y., Wang, X., et al. (2016). Synergistic chemopreventive effects of curcumin and berberine on human breast cancer cells through induction of apoptosis and autophagic cell death. *Sci. Rep.* 6, 26064. doi: 10.1038/srep26064

Wang, L. H., Liu, L. P., Shi, Y., Cao, H. W., Chaturvedi, R., Calcutt, M. W., et al. (2012). Berberine induces caspase-independent cell death in colon tumor cells through activation of apoptosis-inducing factor. *Plos One* 7 (5), e36418. doi: 10.1371/journal.pone.0036418

Wang, J. X., Zhang, B. H., Xu, D. D., Miao, G. Q., Wang, F., Guo, Q. L., et al. (2013). Synthesis and anti-tumor activity of NO-donating derivatives of gambogic acid. *Chin. J. Nat. Med.* 11, 87–96. doi: 10.1016/S1875-5364(13)60015-1

Wang, L., Wei, D. D., Han, X. J., Zhang, W., Fan, C. Z., Zhang, J., et al. (2014a). The combinational effect of vincristine and berberine on growth inhibition and apoptosis induction in hepatoma cells. *J. Cell. Biochem.* 115, 721–730. doi: 10.1002/jcb.24715

Wang, N., Zhu, M. F., Wang, X. B., Tan, H. Y., Tsao, S. W., and Feng, Y. B. (2014b). Berberine-induced tumor suppressor p53 up-regulation gets involved in the regulatory network of MIR-23a in hepatocellular carcinoma. *Biochim. Et Biophys. Acta-Gene Regul. Mech.* 1839, 849–857. doi: 10.1016/j.bbagrm.2014.05.027

Wang, H. Y., Yu, H. Z., Huang, S. M., and Zheng, Y. L. (2016). p53, Bcl-2 and cox-2 are involved in berberine hydrochloride-induced apoptosis of HeLa229 cells. *Mol. Med. Rep.* 14, 3855–3861. doi: 10.3892/mmr.2016.5696

Wang, Z., Liu, Y., Xue, Y., Hu, H., Ye, J., Li, X., et al. (2016). Berberine acts as a putative epigenetic modulator by affecting the histone code. *Toxicol In Vitro* 36, 10–17. doi: 10.1016/j.tiv.2016.06.004

Wen, C. J., Wu, L. X., Fu, L. J., Zhang, X., and Zhou, H. H. (2016). Berberine enhances the anti-tumor activity of tamoxifen in drug-sensitive MCF-7 and drug-resistant MCF-7/TAM cells. *Mol. Med. Rep.* 14, 2250–2256. doi: 10.3892/mmr.2016.5490

Wu, C. M., Li, T. M., Tan, T. W., Fong, Y. C., and Tang, C. H. (2013). Berberine reduces the metastasis of chondrosarcoma by modulating the alpha v beta 3 integrin and the PKC delta, c-Src, and AP-1 signaling pathways. *Evidence-Based Complement. Alternat. Med.* 2013, 423164. doi: 10.1155/2013/423164

Xiao, N., Chen, S., Ma, Y., Qiu, J., Tan, J. H., Ou, T. M., et al. (2012). Interaction of Berberine derivative with protein POT1 affect telomere function in cancer cells. *Biochem. Biophys. Res. Commun.* 419 (3), 567–572. doi: 10.1016/j.bbrc.2012.02.063

Xiao, D. P., Liu, Z. B., Zhang, S. S., Zhou, M., He, F., Zou, M., et al. (2018). Berberine derivatives with different pharmacological activities via structural modifications. *Mini-Rev. Med. Chem.* 18, 1424–1441. doi: 10.2174/1389557517666170321103139

Yan, S. W., and Asmah, R. (2017). Anti-proliferation of MDA-MB-231 Cells by Averrhoa bilimbi Extract is associated with G0/G1 Perturbation and Mitochondria-mediated Apoptosis Independent of p53. *Int. Food Res. J.* 24, 1331–1337.

Yang, X. L., and Huang, N. (2013). Berberine induces selective apoptosis through the AMPK-mediated mitochondrial/caspase pathway in hepatocellular carcinoma. *Mol. Med. Rep.* 8, 505–510. doi: 10.3892/mmr.2013.1506

Yang, P., Song, D. Q., Li, Y. H., Kong, W. J., Wang, Y. X., Gao, L. M., et al. (2008). Synthesis and structure-activity relationships of berberine analogues as a novel class of low-density-lipoprotein receptor up-regulators. *Bioorg. Med. Chem. Lett.* 18, 4675–4677. doi: 10.1016/j.bmcl.2008.07.005

Yang, Y. S., Lu, X., Zeng, Q. X., Pang, J., Fan, T. Y., You, X. F., et al. (2019). Synthesis and biological evaluation of 7-substituted cycloberberine derivatives as potent antibacterial agents against MRSA. *Eur. J. Med. Chem.* 168, 283–292. doi: 10.1016/j.ejmech.2019.02.058

Yu, F. S., Yang, J. S., Lin, H. J., Yu, C. S., Tan, T. W., Lin, Y. T., et al. (2007). Berberine inhibits WEHI-3 leukemia cells in vivo. *In Vivo* 21, 407–412.

Yu, R., Zhang, Z. Q., Wang, B., Jiang, H. X., Cheng, L., and Shen, L. M. (2014). Berberine-induced apoptotic and autophagic death of HepG2 cells requires AMPK activation. *Cancer Cell Int.* 14, 49. doi: 10.1186/1475-2867-14-49

Zhao, Y. W., Jing, Z. L., Li, Y., and Mao, W. F. (2016). Berberine in combination with cisplatin suppresses breast cancer cell growth through induction of DNA breaks and caspase-3-dependent apoptosis. *Oncol. Rep.* 36, 567–572. doi: 10.3892/or.2016.4785

Zhao, Y., Tian, X. F., Liu, G. F., Wang, K. J., Xie, Y. Y., and Qiu, Y. X. (2019). Berberine protects myocardial cells against anoxia-reoxygenation injury via p38 MAPK-mediated NF-B signaling pathways. *Exp. Ther. Med.* 17, 230–236. doi: 10.3892/etm.2018.6949

Zheng, F., Tang, Q., Wu, J. J., Zhao, S. Y., Liang, Z. Y., Li, L. N., et al. (2014). p38 alpha MAPK-mediated induction and interaction of FOXO3a and p53

contribute to the inhibited-growth and induced-apoptosis of human lung adenocarcinoma cells by berberine. *J. Exp. Clin. Cancer Res.* 33, 36. doi: 10.1186/1756-9966-33-36

Zhou, Y., Liu, S. Q., Yu, L., He, B., Wu, S. H., Zhao, Q., et al. (2015). Berberine prevents nitric oxide-induced rat chondrocyte apoptosis and cartilage degeneration in a rat osteoarthritis model via AMPK and p38 MAPK signaling. *Apoptosis* 20, 1187–1199. doi: 10.1007/s10495-015-1152-y

Zhu, X. H., Sun, Y. D., Zhang, C. G., and Liu, H. F. (2017). Effects of berberine on a rat model of chronic stress and depression via gastrointestinal tract pathology and gastrointestinal flora profile assays. *Mol. Med. Rep.* 15, 3161–3171. doi: 10.3892/mmr.2017.6353

Zou, K., Li, Z., Zhang, Y., Zhang, H. Y., Li, B., Zhu, W. L., et al. (2017). Advances in the study of berberine and its derivatives: a focus on anti-inflammatory and anti-tumor effects in the digestive system. *Acta Pharmacol. Sin.* 38, 157–167. doi: 10.1038/aps.2016.125

**Conflict of Interest:** The authors declare that the research was conducted in the absence of any commercial or financial relationships that could be construed as a potential conflict of interest.

frontiers in Pharmacology

ORIGINAL RESEARCH
published: 29 January 2020
doi: 10.3389/fphar.2019.01629

# Network Pharmacology-Based Strategy to Investigate the Pharmacologic Mechanisms of *Atractylodes macrocephala* Koidz. for the Treatment of Chronic Gastritis

*Songhong Yang[1†], Jinlian Zhang[1†], Yiqi Yan[2†], Ming Yang[1], Chao Li[1], Junmao Li[1], Lingyun Zhong[1*], Qianfeng Gong[1*] and Huan Yu[1*]*

[1] School of Pharmacy, Jiangxi University of Traditional Chinese Medicine, Nanchang, China, [2] Chinese Medicine Research Institute, Tianjin University of Traditional Chinese Medicine, Tianjin, China

OPEN ACCESS

**Edited by:**
Yonghua Wang,
Northwest A&F University,
China

**Reviewed by:**
Yinfeng Yang,
Anhui University of Chinese Medicine,
China
Wentzel Christoffel Gelderblom,
Cape Peninsula University of Technology,
South Africa

***Correspondence:**
Lingyun Zhong
ly1638163@163.com
Qianfeng Gong
gongqf2002@163.com
Huan Yu
yuhuanhebei@163.com

[†]These authors have contributed equally to this work and share first authorship

**Specialty section:**
This article was submitted to Ethnopharmacology, a section of the journal Frontiers in Pharmacology

**Received:** 18 June 2019
**Accepted:** 13 December 2019
**Published:** 29 January 2020

**Citation:**
Yang S, Zhang J, Yan Y, Yang M, Li C, Li J, Zhong L, Gong Q and Yu H (2020) Network Pharmacology-Based Strategy to Investigate the Pharmacologic Mechanisms of Atractylodes macrocephala Koidz. for the Treatment of Chronic Gastritis. Front. Pharmacol. 10:1629. doi: 10.3389/fphar.2019.01629

Chronic gastritis (CG) is an inflammatory disease. *Atractylodes macrocephala* Koidz (AMK) is employed in traditional Chinese medicine (TCM) to treat various disorders. AMK can be efficacious against CG, but the active ingredients, drug targets, and its exact molecular mechanism are not known. We employed network pharmacology to analyze the active ingredients, drug targets, and key pathways of AMK in CG treatment. Seventy-seven AMK candidate ingredients were selected from four databases, and 27 active ingredients were selected for CG treatment. Twenty-five overlapping gene symbols related to CG and drugs were obtained from GeneCards and OMIM databases. A protein–protein interaction (PPI) network and TCM comprehensive network (Drug–Ingredients–Gene symbols–Disease network) were constructed, and 528 Gene Ontology (GO) terms and 26 pathways were obtained by analyses of enrichment of GO pathways and Kyoto Encyclopedia of Genes and Genomes (KEGG) pathways. We suggest that the interleukin-17 signaling pathway, C-type lectin receptor signaling pathway, tumor necrosis factor signaling pathway, and AGE-RAGE signaling pathway in diabetic complications might serve as the key points and principal pathways for CG treatment. We also evaluated the reliability of some important active ingredients and targets by *in vitro* experiments. We showed that AMK probably influences the inflammatory response, amino acid synthesis, and energy metabolism when treating CG. This study provides novel insights for researchers to explore the mechanism of action of TCM systematically.

**Keywords: network pharmacology, *Atractylodes macrocephala* Koidz., chronic gastritis, bioactive ingredients, mechanism of action**

## INTRODUCTION

Chronic gastritis (CG) is an inflammatory disease in which the epithelium of the gastric mucosa is invaded by various pathogenic factors, which results in persistent and chronic inflammatory changes. CG can be divided into three categories: chronic non-atrophic, chronic atrophic, and "special." If not treated in a timely manner, CG can transform into gastric cancer (Ohata et al., 2004; Yue et al., 2018; Osaki et al., 2019; Han et al., 2019). Most patients with CG do not have obvious symptoms, and the main symptom is dyspepsia, which is nonspecific. Some CG patients can present with abdominal pain, bloating, and other symptoms of indigestion.

Traditional Chinese medicine (TCM) has been used to treat various diseases for thousands of years. In TCM theory, CG is divided into six types according to the pattern of: accumulation of damp heat in the spleen–stomach; dampness obstructing the spleen–stomach; spleen–stomach Qi deficiency; spleen–stomach deficiency cold; liver–Qi stagnation; stagnant heat in the liver–stomach (Zhu et al., 2014).

*Atractylodes macrocephala* Koidz. (AMK) can invigorate the spleen and Qi, reduce dampness and moisture, act as an antiperspirant, and stop fever developing. In TCM, it is often used to treat spleen deficiency, malnutrition, abdominal distension, diarrhea, dizziness, palpitations, edema, spontaneous sweating, and fetal restlessness (The State Commission of Chinese Pharmacopoeia, 2010; Tang et al., 2012; Zhao, 2013).

In recent years, network pharmacology has been used widely in TCM research. By using "web"-based approaches, network pharmacology can systematically determine the effects and mechanisms of drugs used to treat complex diseases at molecular, cellular, tissue, and biologic levels.

Danlu capsules, the Maxing Ganshi Decoction, Wei Pi Xiao Decoction and Xiaoyao powder have been adopted widely in TCM (Liu et al., 2016; Huang et al., 2017; Song et al., 2018; Yang et al., 2019). AMK can be efficacious for CG treatment, but the active ingredients, drug targets, and the exact molecular mechanism are not known.

We used network pharmacology to analyze the active ingredients, drug targets, and key pathways of AMK in CG treatment (**Figure 1**). Results suggested that AMK may have a therapeutic effect against CG because it can regulate key factors in the inflammatory pathway.

**Abbreviations:** ADME, absorption, distribution, metabolism, and excretion; AMK, *Atractylodes macrocephala* Koidz.; ATL-I, atractylenolide-I; CG, chronic gastritis; CHRM3, muscarinic acetylcholine receptor M3; DL, drug-likeness; GO, Gene Ontology; IL, interleukin; KEGG, Kyoto Encyclopedia of Genes and Genomes; LPS, lipopolysaccharide; OB, oral bioavailability; OMIM, Online Mendelian Inheritance in Man; PPI, protein–protein interaction; PTGS2, prostaglandin G/H synthase 2; STRING, Search Tool for the Retrieval of Interacting Genes/Proteins; TCM, traditional Chinese medicine; TCMSP, Traditional Chinese Medicine Systems Pharmacology Database.

## MATERIALS AND METHODS

### Screening of Active Ingredients

All ingredients contained in AMK were searched for in the Traditional Chinese Medicine Systems Pharmacology Database and Analysis Platform (TCMSP; http://lsp.nwu.edu.cn/tcmsp.php), Chinese Academy of Sciences Chemistry Database (www.organchem.csdb.cn), TCM Database@taiwan (http://tcm.cmu.edu.tw), and Traditional Chinese Medicine Integrated Database (https://omictools.com/tcmid-too). TCMSP is a special platform based on systems pharmacology for Chinese herbal medicines that includes the relationships between drugs, targets, and diseases. TCMSP has information on 500 drugs and >12,000 ingredients (Ru et al., 2014).

"Oral bioavailability" (OB) refers to the percentage of unmodified drugs that enters the circulatory system after oral administration (Xu et al., 2012; Liu et al., 2013). OB is also an important indicator for objective evaluation of the internal quality of drugs (Alam et al., 2014). The higher the OB of an ingredient, the higher is the likelihood that it can be used clinically. "Drug likeness" (DL) is a vague concept that refers to the similarity between ingredients and known drugs (Walters and Murcko, 2002; Tao et al., 2013). Ingredients with DL properties are not drugs, but can become drugs. This class of ingredient comprises drug-like molecules or drug analogs. The Tanimoto coefficient was used to evaluate the DL index of the molecules in AMK using the following formula:

$$T(\alpha, \beta) = \frac{\alpha \times \beta}{\alpha^2 + \beta^2 - \alpha \times \beta} \quad (1)$$

where $\alpha$ is the molecular property of the AMK ingredient on the basis of Dragon software (www.talete.mi.it/products/dragon_description.htm) and $\beta$ denotes the average molecular property for all drugs in the DrugBank database (www.drugbank.ca/) (Mauri et al., 2006).

Most ingredients in Chinese formulations have poor pharmacologic properties, so they cannot bind to specific protein targets on cells efficaciously. Therefore, several researchers have recommended that molecules with OB ≥ 30% or DL ≥ 0.18 are considered to have better pharmacologic effects, and are selected as candidate ingredients for further analyses (Liu et al., 2016; Huang et al., 2017; Yang et al., 2019). We used this principle to screen for active ingredients to be used in further analyses.

### Identification of the Related Targets and Gene Symbols of AMK Ingredients

Target forecasts and target-prediction methods can be divided into four categories based on: the predictions of a ligand (chemical similarity and pharmacophore model); the predictions of a receptor (molecular docking); machine learning (the molecules in a database must have a clear correspondence with the target, and the name of the target must be standardized); a combined forecast. Considering the limitations of the experimental conditions of molecular docking and machine learning and our previous experience, we chose a

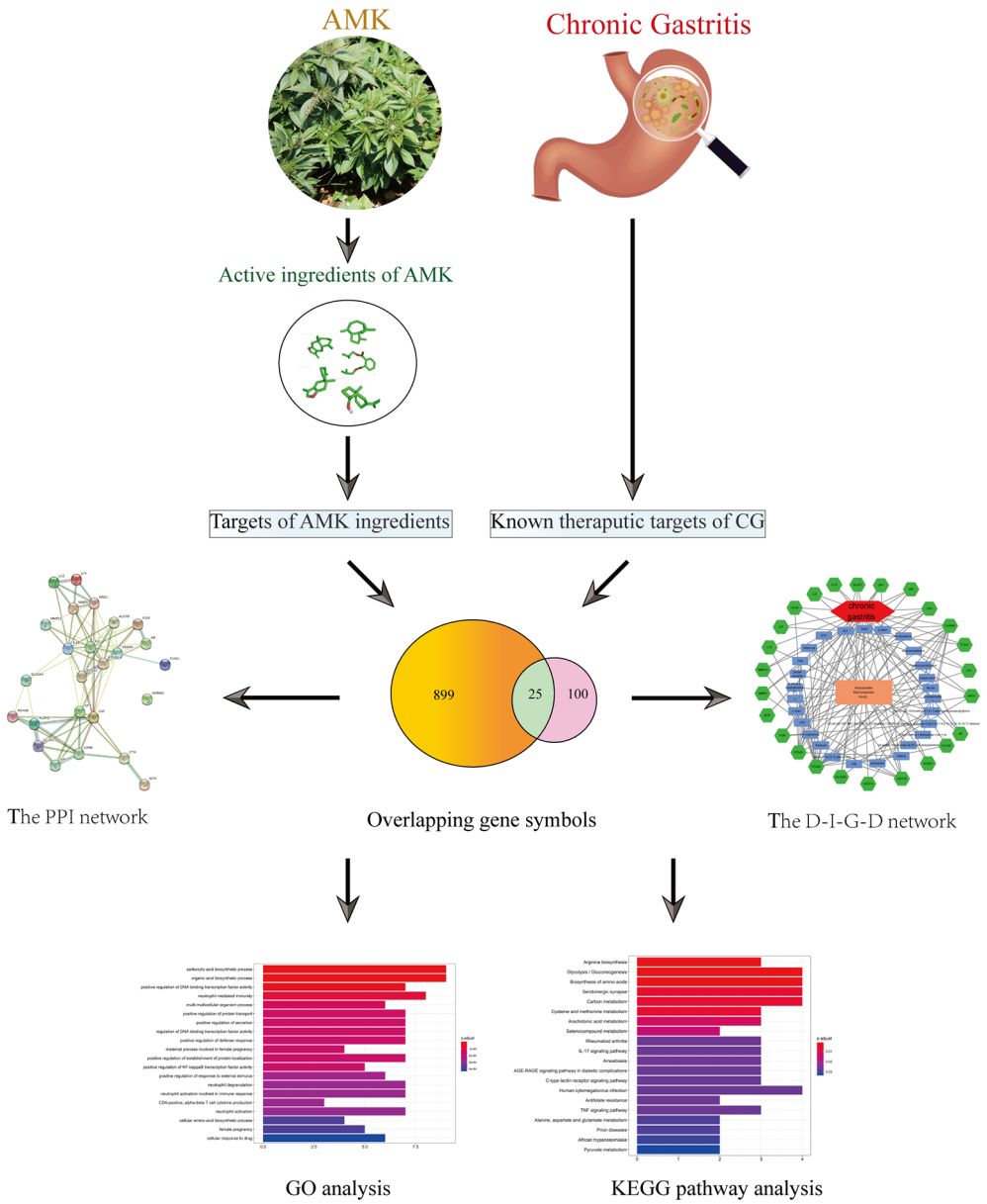


**FIGURE 1 |** Flowchart of a network pharmacology-based strategy to investigate the pharmacologic mechanisms of *Atractylodes macrocephala* Koidz. for treatment of chronic gastritis.

prediction method based on ligands for subsequent research (Yu et al., 2012; Wu et al., 2016; Wang et al., 2017).

All the protein targets of the ingredients in AMK were retrieved from TCMSP (http://lsp.nwu.edu.cn/tcmsp.php). We removed redundant information and retained only those targets that could interact directly with each of these ingredients in AMK. Then, the target was transformed using the UniProt knowledge database (www.uniprot.org) with the selected species as *Homo sapiens*. After deletion of redundant items, data were merged to obtain gene symbols.

## Acquisition of Gene Targets for CG

We collected gene targets for CG from two sources. The first source was the GeneCards v4.9.0 (www.genecards.org/). GeneCards is a searchable, comprehensive database that offers all comments and predicts human genetic information comprehensively in a user-friendly manner (Rebhan, 1997; Safran et al., 2010). We used the keyword "chronic gastritis" to search this database. The second source was the Online Mendelian Inheritance in Man (OMIM) database (www.omim.org/, updated on 28 February 2019) (Hamosh et al., 2005).

## Construction of a Drug–Ingredients–Gene Symbols–Disease (D–I–G–D) Network

First, we intersected the obtained drug targets with the genes associated with a disease and obtained a Venn diagram of the intersected gene symbols. Then, we built a network of complex information based on interactions between the drug (AMK), ingredients, gene symbols, and disease (CG). Next, we used Cytoscape v3.7.1 (www.cytoscape.org/) (Shannon, 2003; Su et al., 2014) to undertake visual analyses of the D–I–G–D network (which is a graphical display of network analyses and editing software).

## Construction of a Protein–Protein Interaction (PPI) Network

PPI data were obtained from the String v11.0) https://string-db.org/, updated on 19 January 2019) (Hsia et al., 2015). Then, the target was transformed using the UniProt knowledge database. After deletion of redundant items, data were merged to obtain gene symbols. Finally, we searched these gene symbols using the "multiple proteins" option while simultaneously setting the organism to *Homo sapiens*. Then, the PPI network of AMK active ingredients–target symbols and chronic gastritis-related target symbols was constructed.

## Enrichment of Gene Ontology (GO) Pathways

GO is an international standard classification system for gene function (Ashburner et al., 2000). We used Bioconductor (R) v3.8 (http://bioconductor.org/, released on 31 October 2018) for analyses.

## Enrichment of the Kyoto Encyclopedia of Genes and Genomes (KEGG) Pathway

The KEGG database analyzes the metabolic pathways of gene products in cells and the functions of these gene products (Kanehisa and Susumo, 2000). We used Bioconductor (R) v3.8 (http://bioconductor.org/, released on 31 October 2018) for analyses.

## Computational Validation of Ingredients–Targets Interactions

We wished to ascertain the interaction between active ingredients and their protein targets and explore their binding modes. Hence, we selected three active ingredients and three targets, a total of four ingredients–targets interactions for verification of molecular docking. We used GOLD v5.1 (a genetic algorithm-based docking program to dock protein–ligand complexes). We obtained the X-ray crystal structures of interleukin (IL)-6, IL-1β, and muscarinic acetylcholine receptor M3 (CHRM3) from the RCSB Protein Data Bank (PDB) (www.rcsb.org); the PDB entry code for these proteins is 1ALU, 2NVH, and 4DAJ, respectively. During molecular docking, we adopted the GOLD Score fitness function. The GOLD fitness function comprised three main terms: a hydrogen energy; a pairwise van der Waals steric energy between the protein and the ligand; and an internal energy term for the ligand.

## Experimental Validation

### Reagents

Atractylenolide-I (ATL-I; purity ≥98%) was purchased from Must Biotechnology (Chengdu, China). A stock solution of 100 mM ATL-I in dimethyl sulfoxide was prepared and stored at 4°C. Enzyme-linked immunosorbent assay (ELISA) kits for IL-6 and IL-1β were purchased from Elabscience Biotechnology (Wuhan, China).

### Cell Culture

RAW264.7 cells were obtained from the cell bank of the Chinese Academy of Sciences (Shanghai, China). RAW264.7 cells were cultured in Dulbecco's modified Eagle's medium (Gibco, Billings, MT, USA) with 10% fetal bovine serum (Gibco). Cells were cultured at 37°C in an atmosphere of 5% $CO_2$ for all experiments.

### Assay to Measure Cell Viability

RAW264.7 cells in the logarithmic phase were seeded at $8 \times 10^3$ cells/well in 96-well culture plates. After incubation for 24 h, Raw264.7 cells were exposed to ATL-I (0, 20, 40, 60, 80, or 100 μmol/L). After treatment for 24 h, 20 μL of Cell Counting Kit (CCK-8) assay solution (Biosharp, Hefei, China) was added to each well, and cells were incubated for 4 h at 37°C in an atmosphere of 5% $CO_2$. The absorbance at 450 nm was measured by a microplate reader. Cell survival was calculated as: absorbance/absorbance of control ×100%.

### Determination of Levels of IL-6 and IL-1β by ELISAs

RAW264.7 cells ($5 \times 10^3$ cells/well) were incubated with lipopolysaccharide (LPS; 1 μg/mL) for 24 h and then treated with ATL-I (20, 40, or 60 μM) for 24 h. Supernatants were harvested and the level of IL-6 and IL-1β determined by ELISA kits (Biosharp).

### Real-Time Quantitative Polymerase Chain Reaction (qRT-PCR)

Total RNA was extracted with TRIzol® Reagent (Thermo Scientific, Waltham, MA, USA), and reverse-transcribed with oligo-DT using HiScript™ Reverse Transcriptase (Vazyme, Beijing, China) according to manufacturer instructions. The primers used were synthesized by Tsingke (Beijing, China). The sequences were (forward and reverse, respectively) 5′-TCA GGCAGGCAGTATCACTC-3′ and 5′-AGCTCATATGGGTC CGACAG-3′ for IL-1β; 5′-CACAGAGGATACCACTCCCA ACAGA-3′ and 5′-ACAATCAGAATTGCCATTGCACAAC-3′ for IL-6; 5′-ATGGGTGTGAACCACGAGA-3′ and 5′-CAGGGATGATGTTCTGGGCA-3′ for the internal control glyceraldehyde 3-phosphate dehydrogenase (GAPDH).

qRT-PCR was done using SYBR™ Green Master Mix (Vazyme) in the QuantStudio 6 Flex system (Applied Biosystems, Foster City, CA, USA). The PCR cycling profile was: one cycle at 50°C for 2 min and 95°C for 10 min, 40 cycles at 95°C and 60°C for 30s. Fluorescence signals were detected using the QuantStudio 6 Flex system. Gene-expression data were normalized to that of the endogenous control GAPDH. The $2^{-\Delta\Delta CT}$ method was the basis for relative expression of genes.

## Statistical Analyses

Data are the mean ± SD. The significance of results was determined based on one-way analysis of variance using Prism 8.0.1 (Graphpad, San Diego, CA, USA). $p < 0.05$ was considered significant. All experiments were repeated at least three times.

# RESULTS

## Screening of Active Ingredients

Seventy-seven AMK candidate ingredients were selected from three databases (**Supplementary Table S1**). To identify the active ingredients of AMK, two classical absorption, distribution, metabolism, and excretion (ADME) parameters, OB and DL, were used for screening. Some ingredients were not in accordance with the standard of screening ingredients and were also likely to produce therapeutic effects in the human body. To study this issue more comprehensively, although they did not meet the screening criteria, these candidate ingredients were retained as active ingredients in our study. For example, ATL-I had a low DL, but it was retained as an active ingredient because it is the major constituent of AMK (Zhang et al., 1998; Li et al., 2007). We found that proliferation of human gastric cancer (mgc-803) cells was inhibited by ATL-I in a time-dependent and dose-dependent manner ($p < 0.05$). ATL-I inhibited expression of Notch-1, Hey-1, Jagged-1, and Hes-1 in the Notch signaling pathway. ATL-I inhibited expression of the mRNA of Notch-1, Hey-1, Jagged-1, and Hes-1 ($p < 0.05$). ATL-I has been shown to inhibit proliferation of mgc-803 cells in human gastric cancer by inhibiting the Notch signaling pathway (Ma et al., 2014). ATL-I could inhibit the increase in vascular permeability caused by acetic acid and can resist proliferation of granuloma tissue. AMK also has a therapeutic effect on acute or chronic inflammation (Chen, 1987; Li et al., 2007). It is important to note that although the pharmacokinetic values of several ingredients were relatively low, they had biologic activity, so they were also regarded as candidate ingredients. In addition, we expanded the criteria for screening beyond the ADME principle. We postulated that, as long as the candidate ingredients in AMK intersect with the targets of CG, they can be considered to be active ingredients.

In summary, 27 ingredients were selected as active ingredients in AMK (**Table 1**).

## Identification of the Related Targets and Gene Symbols of the Ingredients in AMK

After collection from the TCMSP database, conversion into the UniProt database, and deletion of redundant items, 27 ingredients in AMK and 100 known target symbols related to them were obtained (**Supplementary Table S2**).

## Acquisition of Known Therapeutic Gene Targets for CG

A total of 901 known therapeutic target symbols for CG were collected from the GeneCards database. In addition, 23 known therapeutic targets for CG were obtained from the OMIM database. After elimination of redundancies, 899 known therapeutic targets for CG were collected (**Supplementary Table S3**).

## Analyses of the D-I-G-D Network

**Figure 2A** shows that 899 gene symbols for disease and 100 gene symbols for drugs had 25 overlaps. That is, 25 gene symbols may be the key for CG treatment by AMK. The 25 overlapping gene symbols are detailed in **Supplementary Table S4**.

To clarify how AMK may act against CG, we used Ctyoscape to build a D–I–G–D network (**Figure 2B**); the orange node represents AMK and the red node represents CG. Also, the 27 blue nodes represent the active ingredients in AMK; the 25 green nodes represent the overlapping gene symbols between the disease and drug. The edges denote that nodes can interact with each other.

We conducted further network analyses by evaluating centralization and heterogeneity, which were 0.432 and 1.077, respectively. Hence, some nodes were more concentrated in the network than others. That is, the ingredient–target symbol space tended to veer toward certain ingredients and target symbols. Hence, the network included some ingredients with multiple target symbols, such as glycine (GLY; degree = 17), (L)-Alanine (LPG; degree = 12), (5E,9Z)-3,6,10-trimethyl-4,7,8,11-tetrahydrocyclodeca[b]furan (5), 3β-acetoxyatractylone (4), ATL-I (4), and atractylone (2). Moreover, it meant that AMK could act on multiple targets through the same active ingredient. For example, ATL-I could have an effect on vascular endothelial growth factor A (VEGFA), IL-6, and IL-1β if used for CG treatment. Wang and colleagues showed that ATL-I can achieve anti-inflammatory effects by inhibiting expression of IL-6 and IL-1β (Wang et al., 2009). Detailed information regarding active ingredients and gene symbols are described in **Supplementary Table S5**.

## Analyses of a PPI Network

We constructed a PPI network consisting of 25 nodes and 77 edges (**Figure 3A**). This was based on the premise that proteins have more interactions among themselves than would be expected for a random set of proteins of similar size, drawn from the genome. Such an enrichment indicates that the proteins are at least partially biologically connected, as a group.

The light-blue edges denote known interactions from curated databases. The pink edges denote that the known interactions were determined by experimental methods. The green edges denote that the predicted interactions arose from the neighborhood gene. The red edges denote that the predicted interactions arose from gene fusions. The dark-blue edges denote that the predicted interactions arose from gene co-occurrence. The yellow edges denote that the predicted interactions arose from text-mining. The black edges denote that the predicted interactions arose from co-expression. The lavender edges denote that the predicted interactions arose from protein homology. The details of the PPI network are described in **Supplementary Table S6**.

We took the first 20 proteins in the PPI network. As seen from **Figure 3B**, catalase (CAT), IL-6, IL-1β, and VEGFA could

**TABLE 1 |** A total of twenty-seven ingredients were selected as the details of the active ingredients of AMK in this study.

| No. | Mol ID | CAS No. | Molecule Name | OB | DL | Concentration: DW (mg/g) or The relative content = Volatile ingredient / total volatile oil×100% | Reference |
|---|---|---|---|---|---|---|---|
| 1 | MOL000050 | 56-40-6 | Glycine | 48.74 | 0.00 | 0.70 mg/g | C.-Y. Hu et al. "Nutritional components of wild plant Qibaizhu (Atractylodes macracephala Koidz)," Journal of Biology, 3 (2005). |
| 2 | MOL000054 | 74-79-3 | Arginin | 47.64 | 0.03 | 16.1 mg/g | C.-Y. Hu et al. "Nutritional components of wild plant Qibaizhu (Atractylodes macracephala Koidz)," Journal of Biology, 3 (2005). |
| 3 | MOL000056 | 60-18-4 | L-Tyrosine | 57.55 | 0.05 | 1.60 mg/g | C.-Y. Hu et al. "Nutritional components of wild plant Qibaizhu (Atractylodes macracephala Koidz)," Journal of Biology, 3 (2005). |
| 4 | MOL000061 | 147-85-3 | L-Proline | 77.57 | 0.01 | 2.30 mg/g | C.-Y. Hu et al. "Nutritional components of wild plant Qibaizhu (Atractylodes macracephala Koidz)," Journal of Biology, 3 (2005). |
| 5 | MOL000064 | 302-84-1 | DL-Serine | 83.59 | 0.01 | 1.80 mg/g | C.-Y. Hu et al. "Nutritional components of wild plant Qibaizhu (Atractylodes macracephala Koidz)," Journal of Biology, 3 (2005). |
| 6 | MOL000065 | 6899-03-2 | L-aspartic acid | 79.74 | 0.02 | 5.30 mg/g | C.-Y. Hu et al. "Nutritional components of wild plant Qibaizhu (Atractylodes macracephala Koidz)," Journal of Biology, 3 (2005). |
| 7 | MOL000067 | 7004-03-7 | Valine | 53.33 | 0.01 | 3.60 mg/g | C.-Y. Hu et al. "Nutritional components of wild plant Qibaizhu (Atractylodes macracephala Koidz)," Journal of Biology, 3 (2005). |
| 8 | MOL000071 | 30641-68-0 | 2-amino-3-(3H-imidazol-4-yl) propanoic acid | 53.18 | 0.03 | 0.40 mg/g | C.-Y. Hu et al. "Nutritional components of wild plant Qibaizhu (Atractylodes macracephala Koidz)," Journal of Biology, 3 (2005). |
| 9 | MOL000042 | 115967-49-2 | (2S)-2-aminopropanoic acid | 87.69 | 0.01 | 1.60 mg/g | C.-Y. Hu et al. "Nutritional components of wild plant Qibaizhu (Atractylodes macracephala Koidz)," Journal of Biology, 3 (2005). |
| 10 | MOL000041 | 5297-02-9 | (2S)-2-amino-3-phenylpropanoic acid | 41.62 | 0.04 | 0.70 mg/g | C.-Y. Hu et al. "Nutritional components of wild plant Qibaizhu (Atractylodes macracephala Koidz)," Journal of Biology, 3 (2005). |
| 11 | MOL000047 | 473-04-1 | juniper camphor | 33.30 | 0.10 | 0.66 % | LI, Ying. GC-MS analysis of the essential oil components in Atractylodis Macrocephalae Rhizoma and its stir-baked product. Chinese Journal of Pharmaceutical Analysis 33.7 (2013): 1210-1217. |
| 12 | MOL000038 | 260-94-6 | Akridin | 33.71 | 0.10 | 0.31 % | Q. Qiu,et al. Study on the chemical constituents of the volatile oil of atractylodes atractylodes by gc-ms. Chinese Traditional and Herbal Drugs. vol.11, pp.23-24+44, 2002. |
| 13 | MOL000025 | 1493692 | α-Longipinene | 53.26 | 0.12 | 0.15 % | LI, Ying. GC-MS analysis of the essential oil components in Atractylodis Macrocephalae Rhizoma and its stir-baked product. Chinese Journal of Pharmaceutical Analysis 33.7 (2013): 1210-1217. |
| 14 | MOL000019 | 5794-03-6 | D-Camphene | 34.98 | 0.04 | 0.02 % | Zhou J.J., Xie G.R., Yan X.J. Chemical composition of traditional Chinese medicine. Science Press, 2009 |
| 15 | MOL000018 | 124-76-5 | DL-Isoborneol | 86.98 | 0.05 | 6.71 % | X. D, Li. et al. Extraction process of the essential oil from Zingiber officinale Rosc. and Atractylodes macrocephala Koidz. Journal of Shenyang Pharmaceutical University 1 (2003). |
| 16 | MOL000022 | 113269-36-6 | 14-acetyl-12-senecioyl-2E,8Z,10E-atractylentriol | 63.37 | 0.3 | Identified | Yao, C.M., Yang, X.W. Bioactivity-guided isolation of polyacetylenes with inhibitory activity against NO production in LPS-activated RAW264.7 macrophages from the rhizomes of Atractylodes macrocephala. Ethnopharmacol. 151, pp. 791–799, 2014. |
| 17 | MOL000030 | 103729-80-2 | (±)-2-methyl-1-phenylprop-2-en-1-ol | 75.1 | 0.03 | Identified | Zhou J.J., Xie G.R., Yan X.J. Chemical composition of traditional Chinese medicine. Science Press, 2009 |
| 18 | MOL000072 | 113269-35-5 | 8β-ethoxy atractylenolide III | 35.95 | 0.21 | Identified | Z.-L. Chen, "The acetylenes from Atractylodes macrocephala," Planta Medica, 53, 5, pp. 493–494, 1987. |
| 19 | MOL000048 | 19912-61-9 | furanodiene | 43.17 | 0.1 | 0.314 % | Q. Zhang, Z. W. Li. Studies on chemical constituents of the essential of Atractylodes macrocephala Koidz. West china journal of pharmaceutical sciences.1997,2. |
| 20 | MOL000023 | 5989-27-5 | Limonene | 39.84 | 0.02 | 0.007 % | Zheng J. Analysis on Chemical Constituents of Essential Oils from Different Varieties of Atractylodes macrocephala by GC-MS. China Pharmacy 31 (2007). |
| 21 | MOL000033 | 64997-52-0 | Beta-sitosterol | 36.23 | 0.78 | Identified | Sun, Xue, et al. "Influence of sulfur fumigation on the chemical profiles of Atractylodes macrocephala Koidz. evaluated by UFLC–QTOF–MS combined with multivariate statistical analysis." Journal of pharmaceutical and biomedical analysis 141 (2017): 19-31. |
| 22 | MOL000066 | 25246-27-9 | Alloaromadendrene | 53.46 | 0.1 | 0.039 % | Zheng J. Analysis on Chemical Constituents of Essential Oils from Different Varieties of Atractylodes macrocephala by GC-MS. China Pharmacy 31 (2007). |

*(Continued)*

**TABLE 1** | Continued

| No. | Mol ID | CAS No. | Molecule Name | OB | DL | Concentration: DW (mg/g) or The relative content = Volatile ingredient / total volatile oil×100% | Reference |
|---|---|---|---|---|---|---|---|
| 23 | MOL000057 | 84-69-5 | DIBP | 49.63 | 0.13 | Identified | Zhou J.J., Xie G.R., Yan X.J. Chemical composition of traditional Chinese medicine. Science Press, 2009 |
| 24 | MOL000060 | 54707-47-0 | selina-4(14),7(11)-dien-8-one | 32.31 | 0.1 | Identified | Sun, Xue, et al. "Influence of sulfur fumigation on the chemical profiles of Atractylodes macrocephala Koidz. evaluated by UFLC–QTOF–MS combined with multivariate statistical analysis." Journal of pharmaceutical and biomedical analysis 141 (2017): 19-31. |
| 25 | MOL000043 | 73069-13-3 | atractylenolide I | 37.37 | 0.15 | 0.375 mg/g | Y.-H. Meng et al. "Determination of Atractylone and other four effective components in Atractylodes macrocephala and its processed products by HPLC," Chemical Engineer, 33, 08 pp.24-26, 2019. |
| 26 | MOL000046 | 6989-21-5 | atractylone | 41.1 | 0.13 | 46.05 % | LI, Ying. "GC-MS analysis of the essential oil components in Atractylodis Macrocephalae Rhizoma and its stir-baked product," Chinese Journal of Pharmaceutical Analysis, vol.33 no.7 pp. 1210-1217, 2013. |
| 27 | MOL000049 | 61206-10-8 | 3β-acetoxyatractylone | 54.07 | 0.22 | Identified | Shan, Guo-Shun, et al. "Metabolomic study of raw and processed Atractylodes macrocephala Koidz by LC–MS." *Journal of pharmaceutical and biomedical analysis* 98 (2014): 74-84. |

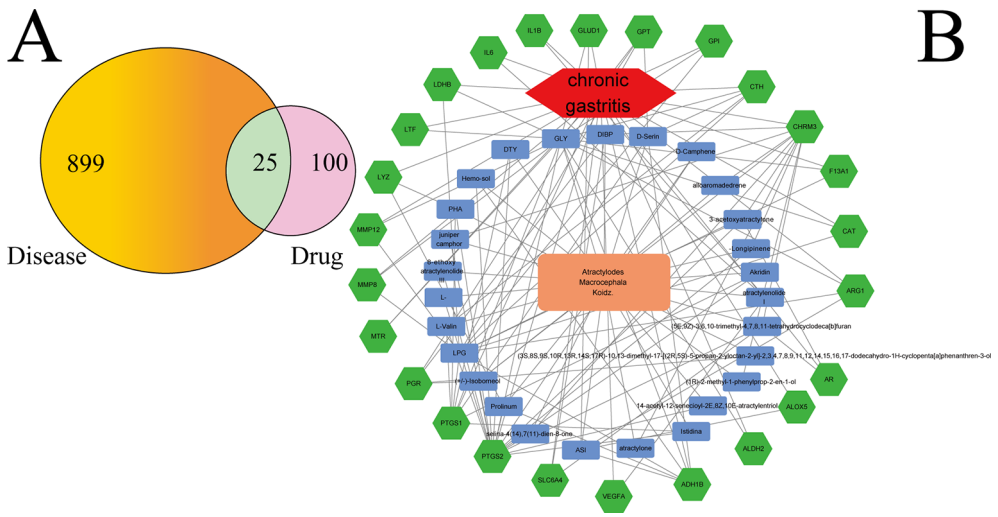


**FIGURE 2 | (A)** Twenty-five overlapping gene symbols between the disease and drug. **(B)** D-I-G-D network. The orange node represents AMK and the red node represents CG. The 27 blue nodes represent the active ingredients in AMK; The 25 green nodes represent the overlapping gene symbols between the disease and drug. The edges denote that nodes can interact with each other.

be related to the other 13 proteins. These results suggested that these four proteins would be the focus of our research of PPIs. Prostaglandin G/H synthase 2 (PTGS2) could be related to the other 11 proteins. CHRM3 was not associated with other proteins in this PPI network.

## Analyses of Enrichment of GO Pathways

To ascertain if the 25 gene symbols were related to CG, we conducted analyses of enrichment of GO pathways to clarify the relevant biologic processes ($p < 0.01$) (**Figure 4A**). The y-axis represents GO terms. The x-axis indicates the number of genes enriched in that term. The redder the color, the smaller the value of p.adjust (FDR); it also denotes greater credibility and greater importance. In contrast, the bluer the color, the greater is the value of p.adjust. For a brief demonstration, we intercepted the first 20 terms from small to large according to the p-value. The details of GO analyses are described in **Supplementary Table S7**. The results indicated that numerous biologic processes were involved in CG treatment, including carboxylic acid biosynthetic process (GO:0046394), organic acid biosynthetic

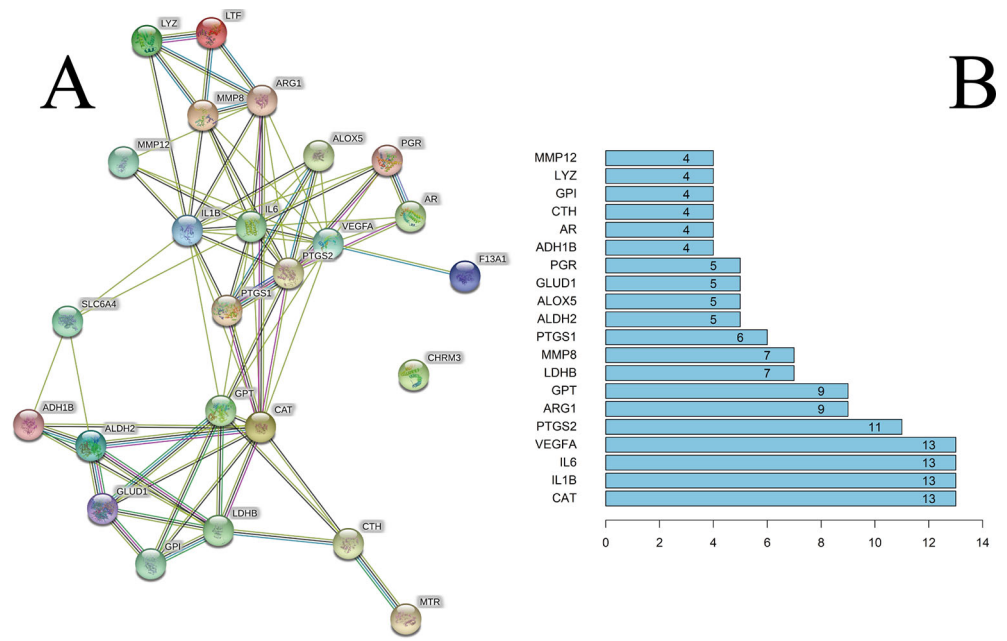


**FIGURE 3 | (A)** The PPI network. **(B)** The bar plot of the PPI network. The x-axis represents the number of neighboring proteins of the target protein. The y-axis represents the target protein.

process (GO:0016053), positive regulation of DNA binding transcription factor activity (GO:0051091), positive regulation of the defense response (GO:0031349), and neutrophil activation involved in the immune response (GO:0002283).

## Analyses of Enrichment of the KEGG Pathway

Analyses of enrichment of the KEGG pathway were carried out using Bioconductor (R) ($p < 0.01$) (**Figure 4B**). The y-axis represents the KEGG pathway. The x-axis indicates the number of genes enriched in that pathway. The redder the color, the smaller the value of p.adjust; it also denotes greater credibility and greater importance. In contrast, the bluer the color, the greater the value of p.adjust. The 25 overlapping gene symbols were mapped to 26 pathways after enrichment of the KEGG pathway. For a brief demonstration, we intercepted the first 20 pathways from small to large according to the p-value. The details of enrichment of the KEGG pathway are described in **Supplementary Table S8**.

Enrichment of the KEGG pathway could be divided approximately into modules of amino acid synthesis, energy metabolism, and inflammation. As shown in **Figure 4B**, the 25 overlapping gene symbols interacted closely with the pathways involved in the IL-17 signaling pathway (hsa04657), C-type lectin receptor signaling pathway (hsa04625), tumor necrosis factor (TNF) signaling pathway (hsa04668), and AGE-RAGE signaling pathway in diabetic complications (hsa04933). These pathways may be the key pathways responsible for CG treatment. Such analyses offer a new way to study CG treatment.

## Computational Validation of Selected Ingredients–Targets Interactions

In general, the number and strength of a ligand bound to a receptor is determined largely by the inhibitory efficiency (Wang et al., 2017). Therefore, we explored the interactions and binding modes between the inflammatory factors IL-6, IL-1β, and gastrointestinal regulatory target CHRM3 with their active ingredients by molecular docking.

ATL-I has special pharmacologic effects and high content in AMK. Hence, we first conducted molecular docking of ATL-I with IL-6 (**Figure 5A**). We can see clearly from **Figure 5A** that the O atoms in ATL-I and arginine (ARG)-179 (3.0 Å) and ARG-179 (3.2 Å) interact with each other between each N atom. In **Figure 5B**, the molecular-docking result of ATL-I with IL-1β shows that the O atoms on the lactone ring in ATL-I can interact with the N atoms on lysine (LYS)-92 (3.1Å) of IL-1β. The results of molecular docking were also consistent with our cell-experiment results, which demonstrated that ATL-I had a significant anti-inflammatory effect.

As another active ingredient with high content in AMK, atractylone was docked with CHRM3 (**Figure 5C**). The O atoms in atractylone interact with N and O atoms in isoleucine (ILE)-222 (3.2Å) and tyrosine (TYR)-148 (3.1Å), respectively, in CHRM3. This interaction also ensures a tight fit between atractylone and CHRM3. In **Figure 5D**, the carbonyl group in bis(2-methylpropyl) benzene-1,2-dicarboxylate (DIBP) is associated with the O atoms in TYR-148 (3.1Å) and TYR-506 (3.1Å) in CHRM3.

Based on these data, we can consider that the interaction between these active ingredients and targets is the basis of their

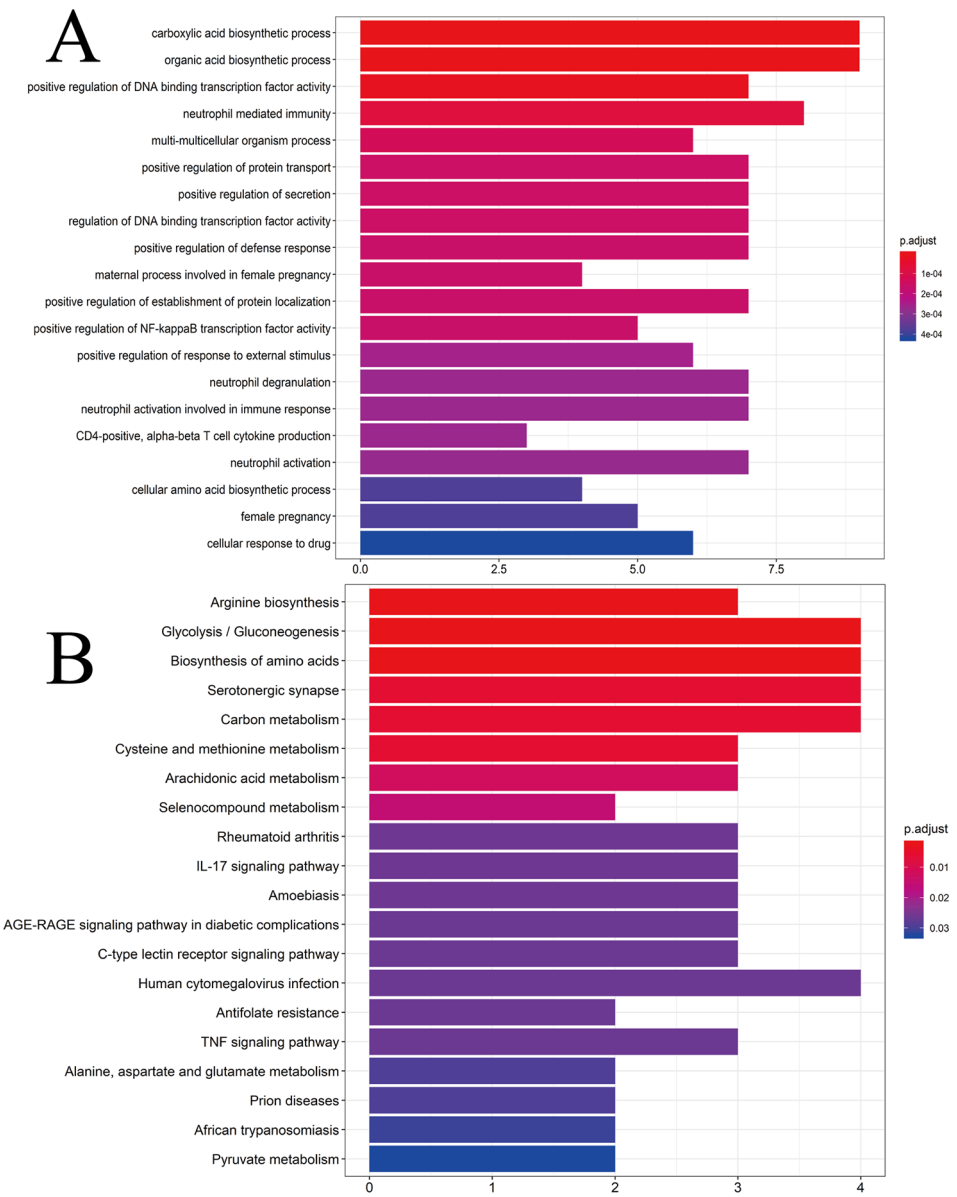


**FIGURE 4 | (A)** GO analyses of the 25 gene symbols associated with chronic gastritis. The x-axis represents significant enrichment in the counts of these terms. The y-axis represents the categories of "biological process" in the GO of the target genes ($p < 0.01$). **(B)** KEGG pathway enrichment analyses. The x-axis represents the counts of the target symbols in each pathway; the y-axis represents the main pathways ($p < 0.01$).

biologic activity. It also means that AMK has multiple ingredients and multiple targets.

## Experimental Validation *In Vitro*

### CCK-8 Assay

First, we determined the effects of different doses of ATL-I on the viability of RAW264.7 cells using the CCK-8 assay (**Figure 6A**). ATL-I at <60 μmol/L had high cell viability (>90%). Therefore, three concentrations were selected (20, 40, 60 μmol/L) for subsequent experiments.

### Validation of Targets

To further evaluate the results obtained in systematic pharmacologic analyses, ATL-I was selected from AMK to examine potential anti-inflammatory effects using LPS (1 μg/mL)-stimulated RAW264.7 cells. We undertook ELISAs and qRT-PCR for IL-6 and IL-1β to confirm the predicted anti-inflammatory effects of the ingredients. IL-6 production showed a significant decreasing trend with increasing ATL-I concentration (**Figure 6B**). Simultaneously, a significant decrease in IL-6 mRNA expression was observed (**Figure 6C**). Production and mRNA

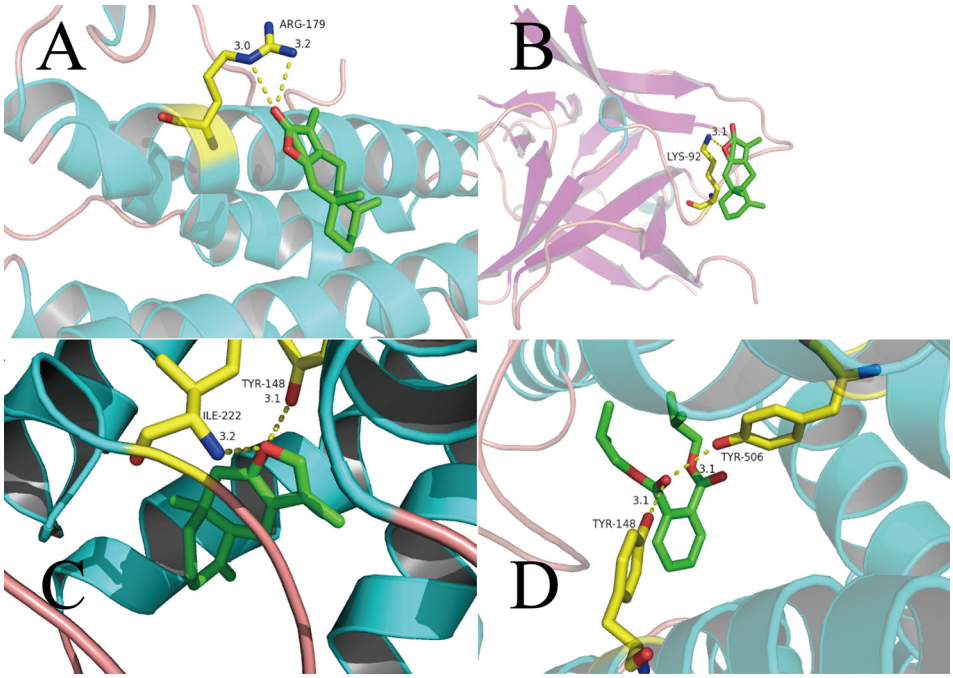


**FIGURE 5 |** Binding studies of selected ingredients–targets interactions. **(A)** ATL-I with IL-6; **(B)** ATL-I with IL-1β; **(C)** atractylone with CHRM3; **(D)** DIBP with CHRM3. Molecules are represented by a ball-and-stick model, the hydrogen bonds are represented by a dotted line, and the distance is in angstroms. Atoms C, O, and N are green, red, and blue, respectively.

expression of IL-1β also decreased significantly with increasing ATL-I concentration (**Figures 6D, E**).

To summarize, these data suggested that ATL-I from AMK may have a therapeutic effect against CG because it can regulate expression of IL-6 and IL-1β to inhibit inflammation. *In vitro* studies also provided additional information for screening ingredients with potential anti-inflammatory effects, and demonstrated the rationality of molecular-docking results and the reliability of a screening strategy based on systems pharmacology.

## DISCUSSION

Western medicine often uses antibacterial therapy and gastric-mucosa protection for CG. However, this strategy can lead to bacterial resistance and, increasingly, drugs cannot control CG efficaciously. Some scholars have suggested that TCM can achieve similar (or even better) curative effects than those of western medicine (Qian et al., 2007; Niu and Meng, 2013; Jia et al., 2017). A detailed study showed that traditional Chinese formulations, which include AMK, have biologic effects in patients with gastric diseases of spleen-deficiency and Qi-stagnation syndrome (Zhang et al., 2013). However, the specific pharmacologic mechanism is incompletely understood. Therefore, we explored the mechanism of action of AMK in CG treatment. We applied network pharmacology combined with screening of active ingredients, drug target symbols, and network/pathway analyses.

We showed that 27 active ingredients in AMK influence 25 overlapping gene symbols that have important roles in CG treatment. Thirty GO terms and 26 pathways were obtained by analyses of enrichment of GO pathways and KEGG pathways. We postulate that the IL-17 signaling pathway (hsa04657), C-type lectin receptor signaling pathway (hsa04625), TNF signaling pathway (hsa04668), and AGE-RAGE signaling pathway in diabetic complications (hsa04933) might serve as the key points and principal signaling pathways in CG treatment.

ATL-I and atractylone have been identified as bioactive ingredients by researchers (Chen, 1987; Hwang et al., 1996; Wang et al., 2006). In addition, in TCM theory, AMK is considered to replenish QI. Therefore, when we screened the active ingredients of AMK, although the DL of some amino acids was <0.18 (e.g., GLY, LPG), they were not removed. Our hypothesis was confirmed in analyses of enrichment of GO pathways and KEGG pathways. For example, ingredients such as GLY and LPG can affect alanine aminotransferase 1 (GPT), but GPT is enriched in carbon metabolism, arginine biosynthesis, glycolysis/gluconeogenesis, biosynthesis of amino acids, alanine, aspartate, and glutamate metabolism. Hence, AMK can act through synthetic or metabolic pathways involved in CG treatment.

In addition, the same target can be linked to multiple active ingredients, for example, PTGS2 can be associated with D-camphene, α-longipinene, akridin, and 14-acetyl-12-senecioyl -2E,8Z, 10E-atractylentriol. These data suggest that AMK can act on the same target through multiple active ingredients. ATL-I

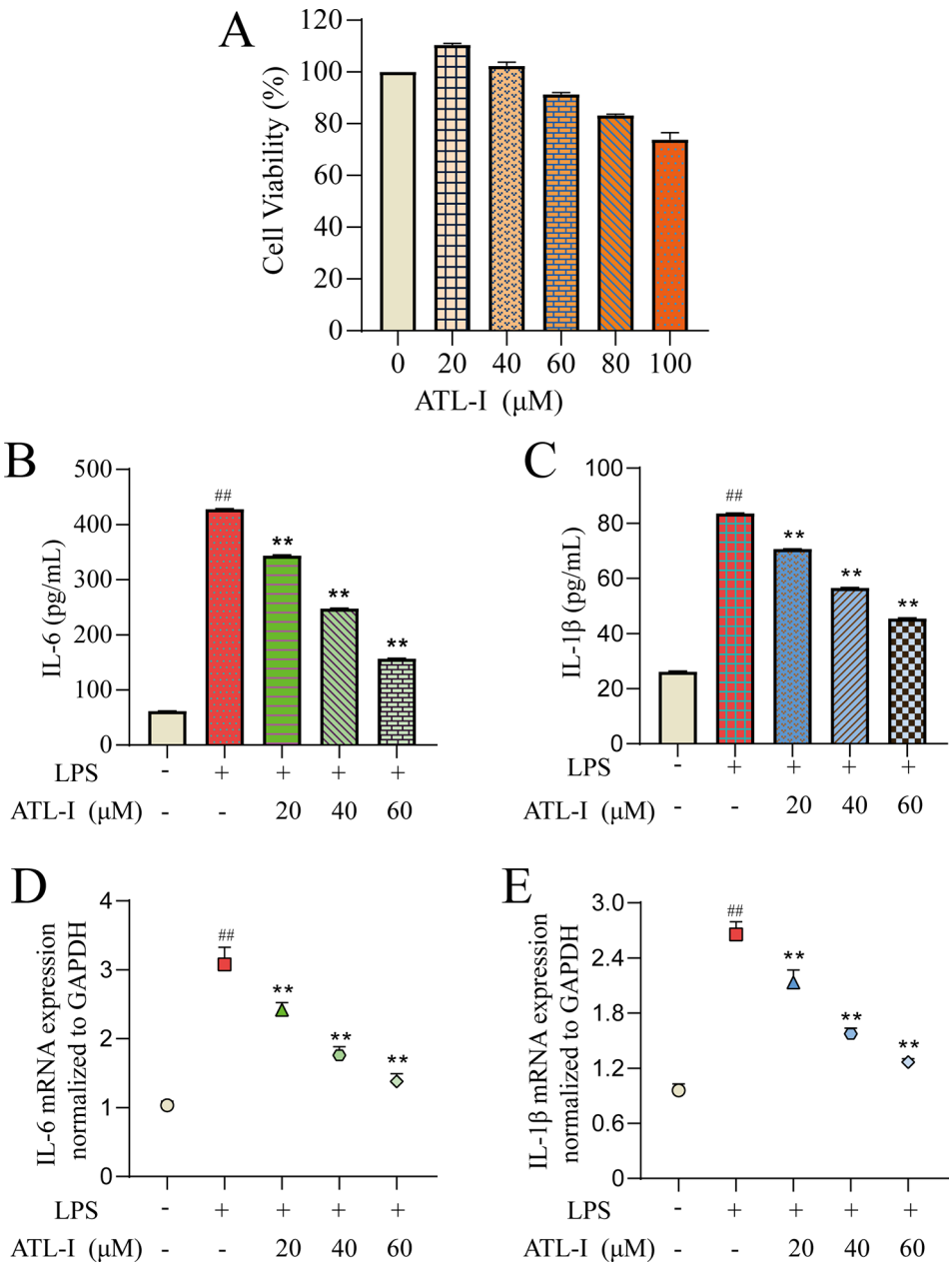


**FIGURE 6 |** Action of ATL-I on RAW264.7 cells. RAW264.7 cells were incubated with LPS (1 μg/mL) for 24 h and then treated with ATL-I (20, 40, or 60 μM) for 24 h. The effects of ATL-I **(A)** on the viability of RAW264.7 cells using the CCK-8 assay. Production of IL-6 **(B)** and IL-1β **(C)** was determined by ELISAs. Protein expression of IL-6 **(D)** and IL-1β **(E)** was determined by qRT-PCR. ##$p < 0.01$ *versus* blank control group. **$p < 0.01$ LPS-treated group.

can be associated with IL-6, IL-1β, and VEGFA, which also suggests that AMK can act on multiple targets through the same active ingredient.

Analyses of a PPI network showed that CAT, IL-6, IL-1β, and VEGFA were the most correlated proteins, followed by PTGS2. In combination with analyses of enrichment of GO pathways and KEGG pathways, we believe that the mechanism of action of AMK in CG treatment is closely related to inflammation regulation (Graham et al., 2000; Bartchewsky et al., 2009; Chen et al., 2018). For example, the target symbol PTGS2 (also named cyclo-oxygenase (COX)-2) can be associated with 18 active ingredients in AMK which can affect the IL-17 signaling pathway, TNF signaling pathway, and C-type lectin receptor signaling pathway and, thus, the regulation of inflammation. If not treated in a timely manner, CG can transform into gastric cancer. Studies have shown that COX-2 plays an important part in the pathogenesis of gastric cancer (Sheu et al., 2003; Bartchewsky et al., 2009). In addition, Zhang and colleagues

showed that a reduction in the COX-2 level is related to regression of precancerous lesions (Zhang et al., 2015).

To some extent, the data mentioned above also suggest that AMK has multiple ingredients, multiple targets, and multiple approaches. Such data provide the basis for multi-ingredient synergies in future research.

To summary, network pharmacology has been used widely in TCM research (Yang et al., 2017; Wang et al., 2017).

In China, AMK can be used to treat constipation, irritable bowel syndrome (IBS) and diarrhea (Pan et al., 2009; Xiao et al., 2015; Li and Li, 2015). In TCM theory, patients with spleen deficiency and dampness can suffer diarrhea after taking AMK. The interactions between the herbs in AMK merit investigation. Studies have shown that solute carrier family 6 member 4 (SLC6A4) can have an effect on IBS (Kim et al., 2004; Yuan et al., 2014). The target is associated with diarrhea and constipation. Therefore, we speculate that AMK may have side effects by affecting SLC6A4. But more proof is needed to verify this hypothesis.

We explored, systematically, how AMK may operate in terms of CG treatment. Our data may offer insights into how TCM can be employed in CG treatment.

## DATA AVAILABILITY STATEMENT

The data used to support the findings of our study are included within the article, or within the **Supplementary Material**.

## AUTHOR CONTRIBUTIONS

SY and HY conceived and designed the study. YY conceived and designed the experimental validation in vitro. All authors participated in drafting of the manuscript and revising it before final submission. These authors: SY, JZ and YY have contributed equally to this work and share first authorship.

## FUNDING

This work was supported by the National Key Research and Development Project of China (2018YFC1707206).

## ACKNOWLEDGMENTS

The authors are thankful to Jiangxi University of Traditional Chinese Medicine for the help in conducting this study.

## SUPPLEMENTARY MATERIAL

The Supplementary Material for this article can be found online at: https://www.frontiersin.org/articles/10.3389/fphar.2019.01629/full#supplementary-material

## REFERENCES

Alam, M., Al-Jenoobi, F., Al-Mohizea, A., and Ali, R. (2014). Understanding and managing oral bioavailability: physiological concepts and patents. *Recent Pat. Anti-Cancer Drug Discovery* 10 (1), 87–96. doi: 10.2174/15748928096661409171038 34

Ashburner, M., Ball, C. A., Blake, J. A., Botstein, D., Butler, H., Chery, J. M., et al. (2000). Gene ontology: tool for the unification of biology. *Nat. Genet.* 25 (1), 25–29. doi: 10.1038/75556

Bartchewsky, W. Jr., Martini, M. R., Masiero, M., Squassoni, A. C., Alvarez, M. C., Ladeira, M. S., et al. (2009). Effect of *helicobacter pylori* infection on IL-8, IL-1beta and COX-2 expression in patients with chronic gastritis and gastric cancer. *Scand. J. Gastroenterology* 44 (2), 153–161. doi: 10.1080/00365520802530853

Chen, Y., Wang, X., Yu, Y., Xiao, Y., Huang, J., Yao, Z., et al. (2018). Serum exosomes of chronic gastritis patients infected with Helicobacter pylori mediate IL-1α expression via IL-6 trans-signalling in gastric epithelial cells. *Clin. Exp. Immunol.* 194 (3), 339–349. doi: doi:10.1111/cei.13200

Chen, Z.-L. (1987). The acetylenes from *Atractylodes macrocephala*. *Planta Med.* 53 (5), 493–494.

Graham, D. Y., Gutierrez, G. O., Gomez, M., El-Zimaity, H. M., and Yamaoka, Y. (2000). Effect of antibiotic therapy on acid secretion H. pylori density, inflammation and mucosal interleukin-I (IL-1B levels in corpus gastritis. *Gastroenterology* 118 (4), A740. doi: 10.1016/s0016-5085(00)85096-9

Hamosh, A., Scott, A. F., Amberger, J. S., Bocchini, C. A., and Mckusick, V. A. (2005). Online mendelian inheritance in man (OMIM), a knowledgebase of human genes and genetic disorders. *Nucleic Acids Res.* 30 (1), 52–55. doi: 10.1093/nar/30.1.52

Han, T.-S., Voon, D. C.-C., Oshima, H., Nakayama, M., Echizen, K., Sakai, E., et al. (2019). Interleukin 1 up-regulates MicroRNA 135b to promote inflammation-associated gastric carcinogenesis in mice. *Gastroenterology* 156 (4), 1140–1155, e1144. doi: 10.1053/j.gastro.2018.11.059

Hsia, C.-W., Ho, M.-Y., Shui, H.-A., Tsai, C.-B., and Tseng, M.-J. (2015). Analysis of dermal papilla cell interactome using STRING database to profile the ex vivo hair growth inhibition effect of a vinca alkaloid drug, colchicine. *Int. J. Mol. Sci.* 16 (2), 3579–3598. doi: 10.3390/ijms16023579

Huang, J., Tang, H., Cao, S., et al. (2017). Molecular targets and associated potential pathways of danlu capsules in hyperplasia of mammary glands based on systems pharmacology. *Evidence-Based Complement. Altern. Med.* 2017 1–10. doi: 10.1155/2017/1930598

Hwang, J.-M., Tseng, T.-H., Hsieh, Y.-S., Chou, F.-P., Wang, C. J., and Chu, C.-Y. (1996). Inhibitory effect of atractylon on tert-butyl hydroperoxide induced DNA damage and hepatic toxicity in rat hepatocytes. *Arch. Toxicol.* 70 (10), 640–644. doi: 10.1007/s002040050323

Jia, Y., Liu, X., Jia, Q., Zhang, W., Sun, C., Yuan, D., et al. (2017). The anti-hyperplasia of mammary gland effect of protein extract HSS from *Tegillarca granosa*. *Biomed. Pharmacother.* 85, 1–6. doi: 10.1016/j.biopha.2016.11.109

Kanehisa, M., and Susumo, G. (2000). KEGG: kyoto encyclopedia of genes and genomes. *Nucleic Acids Res.* 27 (1), 27–30. doi: 10.1093/nar/28.1.27

Kim, H. J., Camilleri, M., Carlson, P. J., Cremonini, F., Ferber, I., and Stephens, D. (2004). Association of distinct α2 adrenoceptor and serotonin transporter polymorphisms with constipation and somatic symptoms in functional gastrointestinal disorders. *Gut* 53 (6), 829–837. doi: 10.1136/gut.2003.030882

Li, C. Y., and Li, S. C. (2015). "Treatment of irritable bowel syndrome in China: a review,". *World J. Gastroenterology: WJG* 21 (8), 2315. doi: 10.3748/wjg.v21.i8.2315

Li, C.-Q., He, L.-C., Dong, H.-Y., and Jin, J.-Q. (2007). Screening for the anti-inflammatory activity of fractions and compounds from *Atractylodes macrocephala* koidz. *J. Ethnopharmacology* 114 (2), 212–217. doi: 10.1016/j.jep.2007.08.002

Liu, H., Wang, J., Zhou, W., Wang, Y., and Yang, L. (2013). Systems approaches and polypharmacology for drug discovery from herbal medicines: an example using licorice. *J. Ethnopharmacology* 146 (3), 773–793. doi: 10.1016/j.jep.2013.02.004

Liu, H., Zeng, L., Yang, K., and Zhang, G. (2016). A network pharmacology approach to explore the pharmacological mechanism of Xiaoyao powder on

anovulatory infertility. *Evidence-Based Complement. Altern. Med.* 2016, 1–13. doi: 10.1155/2016/2960372

Ma, L., Mao, R., Shen, K., Zheng, Y., Li, Y., Liu, J., and Ni, L. (2014). Atractylenolide I-mediated Notch pathway inhibition attenuates gastric cancer stem cell traits. *Biochem. Biophys. Res. Commun.* 450 (1), 353–359. doi: 10.1016/j.bbrc.2014.05.110

Mauri, A., Consonni, V., Pavan, M., and Todeschini, R. (2006). DRAGON software: an easy approach to molecular descriptor calculations. *Match Commun. In Math. In Comput. Chem.* 56 (2), 237–248.

Niu, Y., and Meng, Q. -X. (2013). Chemical and preclinical studies on Hedyotis diffusawith anticancer potential. *J. Asian Natural Products Res.* 15 (5), 550–565. doi: 10.1080/10286020.2013.781589

Ohata, H., Kitauchi, S., Yoshimura, N., Mugitani, K., Iwane, M., Nakamura, H., et al. (2004). Progression of chronic atrophic gastritis associated with *Helicobacter pylori* infection increases risk of gastric cancer. *Int. J. Cancer* 109 (1), 138–143. doi: 10.1002/ijc.11680

Osaki, L. H., Bockerstett, K. A., Wong, C. F., Ford, E. L., Madison, B. B., DiPaolo, R. J., et al. (2019). Interferon-γ directly induces gastric epithelial cell death and is required for progression to metaplasia. *J. Pathol.* 247 (4), 513–523. doi: 10.1002/path.5214

Pan, F., Zhang, T., Zhang, Y., Xu, J., and Chen, F. (2009). Effect of Tongxie Yaofang granule in treating diarrhea-predominate irritable bowel syndrome. *Chin. J. Integr. Med.* 15 (3), 216–219. doi: 10.1007/s11655-009-0216-7

Qian, L.-Q., Pei, X.-H., Xu, Z.-Y., and Wang, C. (2007). Clinical observation on treatment of hyperplasia of mammary gland by lirukang granule. *Chin. J. Integr. Med.* 13 (2), 120–124. doi: 10.1007/s11655-007-0120-y

Rebhan, M. (1997). GeneCards: integrating information about genes, proteins and diseases. *Trends In Genet.* 13 (4), 163. doi: 10.1016/s0168-9525(97)01103-7

Ru, J., Li, P., Wang, J., Zhou, W., Li, B., Huang, C., et al. (2014). TCMSP: a database of systems pharmacology for drug discovery from herbal medicines. *J. Cheminform.* 6 (1), 13. doi: 10.1186/1758-2946-6-13

Safran, M., Dalah, I., Alexander, J., Rosen, N., Iny Stein, T., Shmoish, M., et al. (2010). GeneCards version 3: the human gene integrator. *Database (Oxford)* 2010, baq020. doi: 10.1093/database/baq020

Shannon, P. (2003). Cytoscape: a software environment for integrated models of biomolecular interaction networks. *Genome Res.* 13 (11), 2498–2504. doi: 10.1101/gr.1239303

Sheu, B. S., Yang, H. B., Sheu, S. M., Huang, A. H., and Wu, J. J. (2003). Higher gastric cycloxygenase-2 expression and precancerous change in *Helicobacter pylori*-infected relatives of gastric cancer patients. *Clin. Cancer Res.* 9 (1), 5245–5251.

Song, W., Ni, S., Fu, Y., and Wang, Y. (2018). Uncovering the mechanism of maxing ganshi decoction on asthma from a systematic perspective: a network pharmacology study. *Sci. Rep.* 8 (1). doi: 10.1038/s41598-018-35791-9

Su, G., Morris, J. H., Demchak, B., and Bader, G. D. (2014). Biological network exploration with cytoscape 3. *Curr. Protoc. In Bioinf.* 47 (1), 8.13.11–18.13.24. doi: 10.1002/0471250953.bi0813s47

Tang, X.-D., Liu, B., Zhou, L.-Y., Zhan, S., Li, Z., Li, B., et al. (2012). "Clinical practice guideline of Chinese medicine for chronic gastritis,". *Chin. J. Integr. Med.* 18 (1), pp.57–pp.71. doi: 10.1007/s11655-012-0960-y

Tao, W., Xu, X., Wang, X., Li, B., Wang, Y., Li, Y., et al. (2013). Network pharmacology-based prediction of the active ingredients and potential targets of Chinese herbal radix curcumae formula for application to cardiovascular disease. *J. Ethnopharmacology* 145 (1), 1–10. doi: 10.1016/j.jep.2012.09.051

The State Commission of Chinese Pharmacopoeia (2010). *Pharmacopoeia of People's Republic of China, Part I* (Beijing, China: Chemical Industry Press).

Walters, W. P., and Murcko, M. A. (2002). Prediction of 'drug-likeness'. *Adv. Drug Deliv. Rev.* 54 (3), 255–271. doi: 10.1016/S0169-409X(02)00003-0

Wang, C.-C., Lin, S.-Y., Cheng, H.-C., and Hou, W.-C. (2006). Pro-oxidant and cytotoxic activities of atractylenolide I in human promyeloleukemic HL-60 cells. *Food Chem. Toxicol.* 44 (8), 1308–1315. doi: 10.1016/j.fct.2006.02.008

Wang, C., Duan, H., and He, L. (2009). Inhibitory effect of atractylenolide I on angiogenesis in chronic inflammation in vivo and in vitro. *Eur. J. Pharmacol.* 612 (1-3), 143–152. doi: 10.1016/j.ejphar.2009.04.001

Wang, S., Wang, H., and Lu, Y. (2017). Tianfoshen oral liquid: a CFDA approved clinical traditional Chinese medicine, normalizes major cellular pathways disordered during colorectal carcinogenesis. *Oncotarget* 8 (9), 14549–14569. doi: 10.18632/oncotarget.14675

Wang, J., Li, Y., Yang, Y., Chen, X., Du, J., Zeng, Q., Liang, Z., et al. (2017). A new strategy for deleting animal drugs from traditional chinese medicines based on modified yimusake formula. *Sci. Rep.* 7 (1), pp.1504–1526. doi: 10.1038/s41598-017-01613-7

Wang, J. H., Li, Y., Yang, Y. F., Du, J., Zhao, M., Lin, F., et al. (2017). Systems pharmacology dissection of multiscale mechanisms of action for herbal medicines in treating rheumatoid arthritis. *Mol. Pharmaceutics* 14 (9), 3201–3217. doi: 10.1021/acs.molpharmaceut.7b00505

Wu, C. W., Lu, L., Liang, S. W., Chen, C., and Wang, S. M. (2016). Application of drug-target prediction technology in network pharmacology of traditional Chinese medicine. *Zhongguo Zhong Yao Za Zhi* 41 (3), 377–382. doi: 10.4268/cjcmm20160303

Xiao, H. T., Zhong, L., Tsang, S. W., Lin, Z. -S., and Bian, Z. -X. (2015). Traditional Chinese medicine formulas for irritable bowel syndrome: from ancient wisdoms to scientific understandings. *Am. J. Chin. Med.* 43 (1), 1–23. doi: 10.1142/s0192415x15500019

Xu, X., Zhang, W., Huang, C., Li, Y., Yu, H., Wang, Y., et al. (2012). A novel chemometric method for the prediction of human oral bioavailability. *Int. J. Mol. Sci.* 13 (6), 6964–6982. doi: 10.3390/ijms13066964

Yang, Y., Li, Y., Wang, J., Sun, K., Tao, W., Wang, Z., et al. (2017). Systematic investigation of Ginkgo biloba leaves for treating cardio-cerebrovascular diseases in an animal model. *ACS Chem. Biol.* 12 (5), pp.1363–1372. doi: 10.1021/acschembio.6b00762

Yang, L., Liu, W., Hu, Z., Yang, M., Li, J., Fan, X., et al. (2019). A systems pharmacology approach for identifying the multiple mechanisms of action of the Wei Pi Xiao decoction for the treatment of gastric precancerous lesions. *Evidence-Based Complement. Altern. Med.* 2019, 1–15. doi: 10.1155/2019/1562707

Yu, H., Chen, J., Xu, X., Li, Y., Zhao, H., Fang, Y., et al. (2012). A systematic prediction of multiple drug-target interactions from chemical, genomic, and pharmacological data. *PloS One* 7 (5), e37608. doi: 10.1371/journal.pone.0037608

Yuan, J., Kang, C. Y., Wang, M. Wang, Q. Li, P. Liu, H., et al. (2014). Association study of serotonin transporter SLC6A4 gene with Chinese Han irritable bowel syndrome. *PloS One* 9 (1), e84414. doi: 10.1371/journal.pone.0084414

Yue, H., Shan, L., and Bin, L. (2018). The significance of OLGA and OLGIM staging systems in the risk assessment of gastric cancer: a systematic review and meta-analysis. *Gastric. Cancer* 21 (4), 579–587. doi: 10.1007/s10120-018-0812-3

Zhang, Q. F., Luo, S. D., and Wang, H. Y. (1998). Two new sesquiterpenes from *Atractylodes macrocehpala*. *Chin. Chem. Lett.* 9 (12), 1097–1100.

Zhang, S., Zhao, L., Wang, H., Wang, C., Huang, S., Shen, H., et al. (2013). Efficacy of modified LiuJunZi decoction on functional dyspepsia of spleen-deficiency and qi-stagnation syndrome: a randomized controlled trial. *BMC Complement. Altern. Med.* 13 (1), 54. doi: 10.1186/1472-6882-13-54

Zhang, Y., Pan, K. F., Zhang, L., Ma, J., Zhou, T., Li, J., et al. (2015). *Helicobacter pylori*, cyclooxygenase-2 and evolution of gastric lesions: results from an intervention trial in China. *Carcinogenesis* 36 (12), 1572–1579. doi: 10.1093/carcin/bgv147

Zhao, Z.-H. (2013). Review of pharmacological study and clinical application of Xiangsha Liujunzi Decoction. *J. Liaoning Univ. Tradit. Chin. Med.* 15 (5), 245–247. doi: 10.13194/j.jlunivtcm.2013.05.247.zhangzhh.089

Zhu, W., Fan, Z., Liu, G., Yan, J., Zhong, T., Wang, C., et al. (2014). Symptom clustering in chronic gastritis based on spectral clustering. *J. Tradit. Chin. Med.* 34 (4), 504–510. doi: 10.1016/s0254-6272(15)30054-6

**Conflict of Interest:** The authors declare that the research was conducted in the absence of any commercial or financial relationships that could be construed as a potential conflict of interest.

frontiers in Pharmacology

ORIGINAL RESEARCH
published: 29 January 2020
doi: 10.3389/fphar.2019.01623

# Identification of the Perturbed Metabolic Pathways Associating With Renal Fibrosis and Evaluating Metabolome Changes of Pretreatment With Astragalus polysaccharide Through Liquid Chromatography Quadrupole Time-Of-Flight Mass Spectrometry

*Lei Ren[1†*], Xiao-Ying Guo[2†], Fei Gao[3], Mei-Li Jin[3] and Xiang-Nan Song[3]*

*[1] Department of Clinical Laboratory, Affiliated Hospital, Guilin Medical University, Guilin, China, [2] Department of Clinical Laboratory, Daqing Oilfield General Hospital, Daqing, China, [3] Department of Clinical Laboratory, The Second Affiliated Hospital of Harbin Medical University, Harbin, China*

OPEN ACCESS

***Edited by:***
*Aiping Lu,*
*Hong Kong Baptist University, Hong Kong*

***Reviewed by:***
*Xijun Wang,*
*Heilongjiang University of Chinese Medicine, China*
*Qun Liang,*
*First Affiliated Hospital of Heilongjiang University of Chinese Medicine, China*

****Correspondence:***
*Lei Ren*
*effect802@163.com;*
*rla_2000@126.com*

*†These authors have contributed equally to this work*

***Specialty section:***
*This article was submitted to Ethnopharmacology, a section of the journal Frontiers in Pharmacology*

***Received:*** *28 July 2019*
***Accepted:*** *13 December 2019*
***Published:*** *29 January 2020*

***Citation:***
*Ren L, Guo X-Y, Gao F, Jin M-L and Song X-N (2020) Identification of the Perturbed Metabolic Pathways Associating With Renal Fibrosis and Evaluating Metabolome Changes of Pretreatment With Astragalus polysaccharide Through Liquid Chromatography Quadrupole Time-Of-Flight Mass Spectrometry. Front. Pharmacol. 10:1623. doi: 10.3389/fphar.2019.01623*

Renal fibrosis is glomerulosclerosis and renal tubulointerstitial fibrosis caused by the increase of interstitial cells and intercellular substances and the accumulation of extracellular matrix, and is a common pathological manifestation of renal disease progressing to end-stage renal failure. It has proved that Astragalus polysaccharide (AP) has curative effect on renal disease; however, its therapeutic mechanism on renal fibrosis is still unclear. Metabolomics approach provides an opportunity to identify novel molecular biomarkers. The purpose of this study is to study the changes of serum metabolic profile of rats with unilateral tubal ligation and replication of renal fibrosis model and the therapeutic effect of AP on it. The blood samples of rats in the control group, renal fibrosis model group, and AP treatment group collected on the 21st day were analyzed by metabolomics method based on UPLC-Q-TOF-MS. Principal component analysis (PCA) showed that clustering was obvious and significantly separated, and paired partial least squares discriminant analysis (OPLS-DA) was used for further analysis. Combined with the network databases such as HMDB and KEGG and a large number of literatures, 32 potential biomarkers related to renal fibrosis were preliminarily screened out and further verified by MS/MS secondary debris information. After pretreatment with AP, 20 biomarkers were significantly regulated, and correlated with phenylalanine, tyrosine, and tryptophan biosynthesis, phenylalanine metabolism, arachidonic acid metabolism, etc. It also revealed the metabolic changes of renal fibrosis and intervention effect of AP. These data uncover a link between metabolism and the molecular mechanism with potential implications in the understanding of the intervention effect of AP. Conclusively, UPLC-Q-

TOF-MS–based metabolomics can be valuable and promising strategy to understand the disease mechanism and natural drug pretreatment.

**Keywords: metabolomics, biomarker, metabolic pathway, liquid chromatography quadrupole time-of-flight mass spectrometry, metabolome**

## INTRODUCTION

Renal fibrosis refers to glomerulosclerosis and tubulointerstitial fibrosis caused by the increase of interstitial cells and interstitial cells under the action of various pathogenic factors such as inflammation, injury, drugs, etc., especially the increase of matrix protein synthesis and the inhibition of matrix degradation resulting in a large accumulation of extracellular matrix (Zeisberg et al., 2002). It is a common pathological manifestation of renal disease progression to end-stage renal failure (Qin et al., 2011). In recent years, with the deepening of research, it has been found that renal tubulointerstitial fibrosis is related to the conversion or transdifferentiation of various cells (such as interstitial fibroblasts, renal tubular epithelial cells, etc.) into myofibroblasts (MFBs), and the transdifferentiation mechanism is also an important mechanism of fibrosis (Liu, 2006; Min, 2010). Fibroblasts are one of the main intrinsic renal cells in the stroma and the most important extracellular matrix secreting cells in the process of renal interstitial fibrosis, thus playing an important role in the process of disease. At present, it is believed that the molecular mechanism of renal fibrosis is mainly divided into four stages: 1) Activation and damage of cells. Inflammatory injury causes activation of renal tubular epithelial cells and infiltration of monocytes and macrophages in renal interstitium. 2) Release of fibrogenic factors. It includes cytokines, growth factors, vasoactive factors, chemotactic adhesion factors, etc (Zeisberg and Kalluri, 2004). 3) Formation of fibrosis. The main manifestation is that matrix protein synthesis increases and degradation decreases, resulting in matrix protein deposition in renal interstitium. The degradation of matrix protein is mainly affected by some protease inhibitors, which can inactivate renal protease (Vasko, 2016). 4) Renal structure and function are damaged. The structural and functional damage of kidney is mainly caused by ECM deposition in kidney (Eddy, 1996; Liu and Youhua, 2011). However, most of the existing researches on renal fibrosis focus on molecular mechanisms, and there are few reports on changes in metabolic levels. Changes in endogenous metabolites may provide basis for revealing the pathogenesis and early diagnosis.

Metabolomics has the comprehensive qualitative and quantitative analysis of metabolites in the body, the dynamic changes in different environments such as normal living conditions and internal and external environmental changes are described (Weckwerth, 2003). Living organisms are affected by diseases, toxicity, genes, or environmental factors, and the content of endogenous small molecules in the body will be correspondingly upregulated or downregulated. The purpose of metabolomics is to find the affected small molecules and finally apply them to the diagnosis and drug screening of some related diseases (Fiehn, 2002). As an application-driven emerging science, it has been widely used in medicine-related fields (Wang et al., 2013; Qiu et al., 2017). Non-targeted metabolomics refers to non-biased detection of the dynamic changes of all small molecule metabolites before and after stimulation or disturbance in cells, tissues, organs, or organisms, and screening of differential metabolites through bioinformatics analysis, and pathway analysis of differential metabolites to reveal the physiological mechanism of their changes (Dettmer et al., 2010; Zhang et al., 2014; Zhang et al., 2017). Targeted metabolomics focuses on a specific metabolic pathway or a specific metabolic pathway, and analyzes these specific components to confirm whether these components are different substances (Zhang et al., 2018). Metabolomics is not only applied to diseases and general health, but also has great application space in agronomy, environment, and nutrition. In recent years, with its high throughput, high resolution, high accuracy, and other characteristics, it has provided new ideas and methodological guarantees for the development and improvement of modern research of traditional Chinese medicine (TCM) and the diagnosis of chronic diseases (Zhang et al., 2010; Sun et al., 2013; Song et al., 2017).

Astragalus membranaceus (AM) has a long history of medicinal use and is an important qi-invigorating drug. Li Shizhen describes it as the "longest tonic" in the *Compendium of Materia Medica*. It is one of the most commonly used TCMs in past dynasties (Shao, 2004). There are many reports that AM or TCMs with AM as the main drug can improve renal function of patients with chronic renal failure (Chang et al., 2012). Recent studies have shown that the main chemical components of AM include Astragalus polysaccharides (AP) (Liu et al., 2010), saponins, flavonoids, and amino acids (Shao, 2004). Modern pharmacological research shows that AM can enhance and regulate the body's immune function (Adesso et al., 2018), and has the effects of dilating blood vessels, improving microcirculation, reducing plasma osmotic pressure and blood viscosity, regulating lipid metabolism, etc (Cho and Leung., 2007). In addition, it can also increase renal blood flow, which is conducive to the elimination of harmful substances such as lipid peroxide, and reduce the deposition of lipid in glomeruli and renal interstitium and the formation of microthrombi, thus protecting the kidney (Song et al., 2009; Li et al., 2011). Renal fibrosis is the terminal end of the development of various renal diseases, which will lead to irreversible damage to renal function. However, there is still a lack of therapeutic drugs that can inhibit or even reverse renal fibrosis. In recent years, TCM has shown its unique advantages with multi-channel and multi-target treatment strategies. AP is the active ingredient with the highest content in AM, which has the effects of lowering blood

sugar, reducing proteinuria, regulating lipid metabolism, and improving renal function in patients with nephropathy (Lian et al., 2014). Therefore, this study uses high-throughput metabolomics to study the effect of AP on endogenous metabolites in renal fibrosis rats and to find potential biomarkers, providing a method for clinical diagnosis of metabolic level of renal fibrosis, and further providing a basis for studying the mechanism of improvement of AP on renal fibrosis.

# EXPERIMENTS

## Drugs and Reagents

AP (80%): Nanjing Zelang Pharmaceutical Technology Co., Ltd. (Nanjing, China) batch number: ZL120513. Acetonitrile was purchased from Merck Corporation (Merck, Germany). Methanol was purchased from Fisher Scientific Corporation (Loughborough, UK). Leucineenkephalin was obtained from Sigma-Aldrich (St. Louis, MO, USA).

## Animal Grouping and Model Replication

Animal experiments were conducted in accordance with the guidelines for animal experiments of Affiliated Hospital of Guilin Medical University and approved by the Animal Ethics Committee. Thirty SPF healthy female SD rats (weighing 200–220 g) were purchase by the Experimental Animal Center of Affiliated Hospital of Guilin Medical University. Rats were raised in a standard environment (temperature: 18–25°C, humidity: 45–60%, light/dark cycle alternating every 12 h). During the whole experiment, rats were allowed to eat freely and take water. Before the start of the formal experiment, all animals adapted to the environment for 1 week, and then the model was reproduced by unilateral ureteral ligation. All rats were randomly divided into sham operation group (control group) with 10 rats and operation group (model group and treatment group with 10 rats each). After anesthesia, rats were shaved locally by intraperitoneal injection of 5% chloral hydrate. After routine disinfection, abdominal midline incision was selected. Open skin to abdominal cavity, free kidney and ureter in turn. Left ureter was held up at the middle part with tissue forceps, hemostatic forceps was clamped. Left ureter was ligated twice at both ends with 4-0 silk thread near renal pelvis. Ureter was cut off, and skin was continuously sutured. The surgical approach of the control group was the same as that of the operation group. After entering the abdominal cavity, the left ureter was separated but the ureter was not ligated, and then the skin was sutured. The administration group was given AP aqueous solution (1,000 $mg{\cdot}kg^{-1}{\cdot}d^{-1}$, 2 ml/d) by gavage, while the other groups were given the same amount of normal saline for 21 days.

## Collection and Preparation of Samples

Twenty-four hours after the last administration, weigh and record the weight of each group of rats, inject 0.5 ml/100 g of 4% chloral hydrate solution intraperitoneally to anesthetize the rats, blood was taken from abdominal aorta quickly, left to stand for 30 min, centrifuged at 4,000 rmp for 15 min at 4°C, supernatant was taken and split into five parts, 1 ml for each part, for detection of serum creatinine (SCr), blood urea nitrogen (BUN), and blood metabolomics, and freeze-store at −80°C till analysis. Double kidneys were weighed, and the kidney–body ratio (2 × left kidney/body weight) was calculated.

The unfreeze the serum sample in an ice bath, take 200 μl of serum sample, add 800 μl of acetonitrile to precipitate protein, vortex for 30 s, 4°C, 13,000 rmp for 15 min, remove supernatant, blow-dry in a 40°C water bath under nitrogen, add 200 μl of methanol:water (9:1, v/v) mixed solution to the residue, vortex for 60 s, centrifuge at 4°C, 13,000 rmp for 10 min, take supernatant through a 0.22 μm filter membrane, and take 5 μl of filtrate for UPLC-MS/MS analysis.

## Mass Spectrum Conditions

The UPLC-MS/MS analysis was carried out using a Waters ACQUITY™ ultra performance liquid chromatography system (Waters Corp., Milford, USA) coupled with a Waters Synapt™ Q-TOF Mass system (Waters Corporation) equipped with an ESI ion source and hybrid Q-TOF mass spectrometer in both ESI− and ESI+ ion mode. The UPLC column was a Waters BEH C18 (2.1 × 100 mm, 1.7 μm), and flow rate is 0.4 ml/min with 40°C temperature. The mobile phases A and B are respectively acetonitrile with 0.1% formic acid and water with 0.1% formic acid and optimal linear elution gradient procedure as followed: 0–1 min, 2–20% A; 1–3 min, 20–40% A; 3–10 min, 40–80% A; 10.0–13.0 min, 80–90% A; 13.0–14.0 min, 90–98% A; 14–15 min, 98–2% A; 15–17 min, 2% A. All samples were kept in a refrigerator at 4°C during analysis.

Mass spectrometry conditions: ESI− and ESI+ ion scanning mode capillary voltage respectively 1,500 and 1,300 V. All other parameters are the identical, respectively sample cone voltage: 60 V; ion source temperature: 110°C; desolvation gas temperature: 350°C; desolvation gas flow: 800 L/h; the flow rate: 20 L/h. The calibration solution is leucine enkephalin ([M+H]+ = 556.2771; [M+H] − = 554.2615), injected at an injection amount of 100 μl/min every 15 s, and the collection range is 100–2,000 Da. All samples were collected and collected under the control of Masslynx 4.1 software.

## Multivariate Data Processing

The established analysis method is used to carry out full scanning of ESI+ and ESI− of the sample to obtain the metabolic profile map containing three-dimensional information of individual samples of the sample group. Peak identification and matching are carried out by MassLynx V4.1 software. After data extraction and standardization, principal component analysis (PCA) of unsupervised mode is firstly carried out by EZinfo 3.0.3 software, and PCA score chart and 3D-PCA score chart reflecting aggregation and dispersion degree between groups are drawn. In order to find endogenous metabolites that play a key role in metabolic profile, paired partial least squares discriminant analysis (OPLS-DA) was performed on metabolic profile data between control group and model group to obtain VIP plot and loading plot. The further away from the center the ion pair contributes to its grouping. According to the variable

weight value (VIP) of the relevant reactive ion contribution degree, in the VIP scatter plot, the ion fragments are arranged in a V-shape, the bottom ions (VIP value is small), the contribution to differential metabolism is smaller; top ions (VIP value is large) contribute a lot to the changes of metabolic profile trajectory. In loading plot, the farther away from the distant point in the load map, the greater the contribution of ions to the change of metabolic profile trajectory. In order to verify whether the differences found in multi-dimensional statistics are statistically significant, T-Test was used to screen metabolites with greater difference between groups. Finally, VIP > 1 and $p < 0.05$ were selected as screening conditions as potential biomarker sets. According to the accurate retention time and mass–core ratio of the obtained potential biomarkers, the result of matching metabolite database under the metabolite identification module of Progenesis QI software is fitted. The higher the score is, the greater the accuracy of structural identification. The obtained results are marked, and then retrieved by HMDB (http://www.hmdb.ca/), KEGG, (http://www.genome.jp/kegg/), and other databases for secondary matching. Finally, the structure analysis and verification are carried out by MS/MS data to determine the name and chemical structure of the biomarker. The mass fragment module in Masslynx V4.1 software was used to determine the possible cleavage information of the marker. Then, the identified biomarker information is input to the MetaboAnalyst for relevant metabolic pathway matching to obtain the blood metabolic pathway related to the renal fibrosis model.

## Statistical Methods

Statistical analysis was performed on each group of data using the SPSS v19.0 data package. Results were expressed as mean ± standard deviation; $P < 0.05$ was considered statistically significant.

# RESULTS

## Biochemical Index Analysis

The changes of body weight, kidney–body ratio, SCr, and BUN content after 21 days of rat modeling are shown in **Table S1**. The body weight of the rats in the model group and the treatment group on the 21st day are significantly lower than those in the control group ($p < 0.05$), and the treatment group has an increasing trend compared with the control group, but there is no significant difference ($p > 0.05$). The kidney–body ratio is significantly higher than those in the control group ($p < 0.05$), and the treatment group has a reduced trend compared with the control group, but there is no significant difference ($p > 0.05$).The serum of rats was taken and the SCr and BUN contents were determined by a full-automatic biochemical analyzer (model KONELAB301). The results showed that the SCr and BUN contents in the model group and the treatment group were significantly higher than those in the control group. Compared with the model group, the contents of SCr and BUN in the drug administration group were both decreased, and were recalled to the control group, but there was no significant difference in SCr, and BUN showed significant difference ($p < 0.01$). This indicates that the rat model was successfully replicated.

## Methodological Verification

Before the formal analysis of serum samples, the conditions of UPLC-Q-TOF-MS/MS system were investigated for methodology. Forty microliters of each sample was extracted and mixed evenly to prepare quality control (QC) samples. The same QC sample was injected repeatedly for six times in succession. The results showed that the RSD% of the retention time and peak area of precision were lower than 0.25% and 3.56% respectively. QC solutions of six different samples were prepared by the same preparation method and injected into the detection system. The results showed that RSD% of retention time and peak area was lower than 0.14% and 3.79%, respectively. By comparing the six QC samples kept for 24 h in the autosampler (4°C) with the six same QC samples newly prepared, the stability of the samples was tested, and the RSD% of retention time and peak area were lower than 0.78% and 5.40%, respectively. According to the above, this method meets the requirements of this study. During the whole experiment, one QC sample was run in the middle of every 10 samples to maintain the stability of the system.

## Serum Metabolic Profile

In this study, all serum samples were scanned in ESI+ and ESI– ion mode under the stable UPLC-Q-TOF-MS/MS system. MassLynx V4.1 software (Waters, USA) integrates data analyzed by UPLC-MS/MS platform to obtain representative BPI metabolic profiles (**Figures S1A–C** and **Figures S2A–C**) in different groups of samples. It was found that the serum metabolic profile expression of each group was similar, but there were obvious content differences in many places. In order to further find metabolites with different content expressions, this study conducted non-targeted metabolomics analysis on renal fibrosis model rats based on UPLC-MS/MS technology, and imported all the original data into Progenesis QI software for peak alignment, peak extraction, and normalization. Then the ion information was transferred to Ezinfo3.0.3 software for multivariate data analysis. The PCA score chart (**Figure 1**) of PCA showed that the metabolic profiles in each group were clustered clearly and separated obviously; the treatment group was also far away from the model group and approached to the control group. 3D plot (**Figures S1D** and **S2D**) could also clearly observe the obvious spatial separation of each group, indicating that the serum metabolic level of the model rats had obvious changes and showed certain effects after AP treatment. This indicates that the rat model of renal fibrosis has been successfully replicated at the level of serum metabolism.

## Screening and Identification of Potential Biomarkers

In order to find out the different metabolites that affect the metabolic profile changes, the serum metabolic profile data of rats in the control group and the model group were further analyzed by OPLS-DA, and OPLS-DA plot (**Figures 2A, B**) and 3D plot (**Figures 2C, D**) between the control group and the

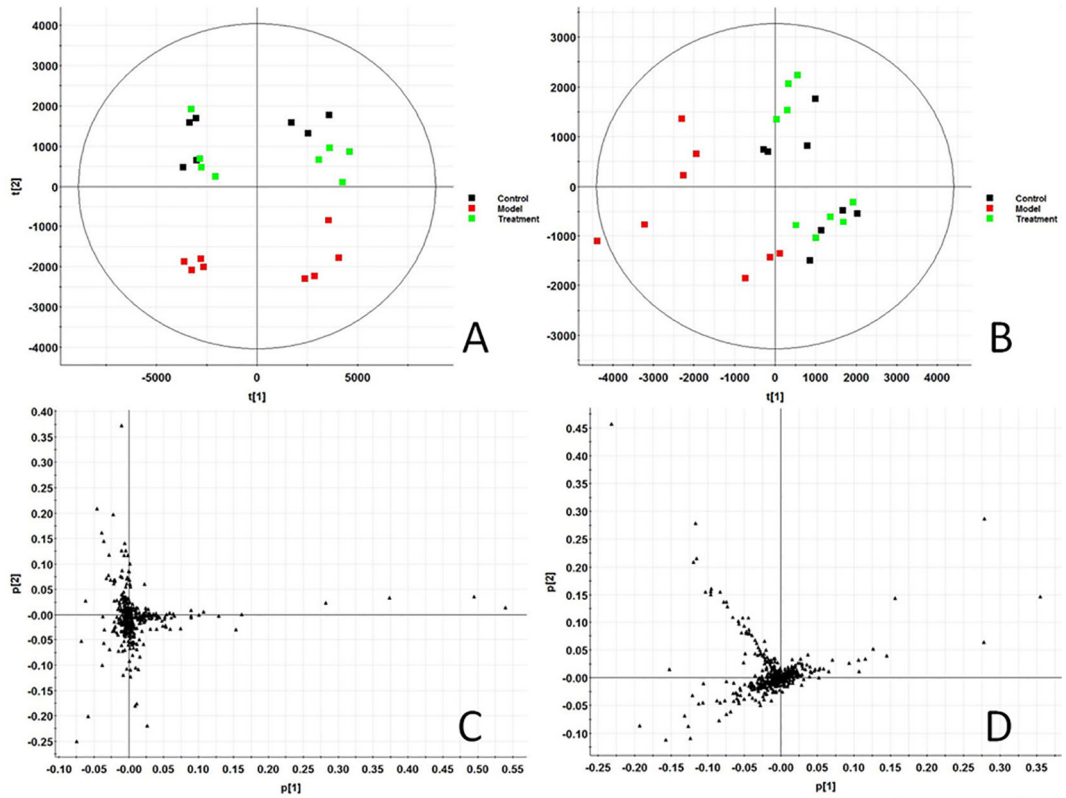


**FIGURE 1 |** Score plot of serum profile of Control group, model group and treatment group scanned by PCA analysis. **(A)** PCA score in positive ion mode. **(B)** PCA score in negative ion mode. **(C)** Loading score in positive ion mode. **(D)** Loading score in negative ion mode.

model group were obtained. The Figure shows that the two groups are significantly separated. Furthermore, VIP plot diagrams (**Figures 3A, B**) and s-plot diagrams (**Figures 3C, D**) which can reflect the contribution rate between groups are obtained. In VIP plot, the farther ions are from the origin, the greater the contribution to the difference between the two groups. Carry out independent sample T-Test on the obtained data, screen potential endogenous biomarkers with $p < 0.05$ and VIP value greater than 1, and provide information including retention time, accurate quality, and MS/MS data according to the UPLC-MS platform. The precise molecular weight of the compound was determined by Q-TOF method within a reasonable measurement error range, and the element composition, unsaturation, and other information of the compound were obtained. By referring to literatures and data retrieval platforms such as HMDB and KEGG, the structure of potential endogenous marker MS/MS data is analyzed to determine the possible chemical structure. Combining the secondary fragment information provided by Masslynx V4.1, matching is carried out to obtain accurate structure and cracking information. Taking 6.91-319.2239 5,6-epoxy-8,11,14-eicosanoic acid as an example, the matching and cracking rules of secondary fragment information are shown in **Figure 4**. Finally, we identified and characterized 32 potential biomarkers, 16 in positive and 16 in negative ion mode. See **Table S2** for specific information. Compared with the control group, the 17 metabolite content expression in the model group was significantly increased. The levels of 15 metabolites were significantly decreased. Among them, 25 biomarkers showed extremely significant differences.

## Related Metabolic Pathways

Based on the identified endogenous biomarkers, MetaboAnalyst and KEGG and other network databases were used for enrichment analysis of relevant metabolic pathways to explore the metabolic pathways affected in serum metabolism of renal fibrosis rats (**Figure 5**). Twelve metabolic pathways including biosynthesis of unsaturated fatty acids were characterized. Phenylalanine, tyrosine, and tryptophan biosynthesis, phenylalanine metabolism, arachidonic acid metabolism, pyrimidine metabolism, fatty acid biosynthesis, ether lipid metabolism, fatty acid elongation in mitochondria, steroid hormone biosynthesis, glycerophospholipid metabolism, fatty acid metabolism, aminoacyl-tRNA biosynthesis. Among them, phenylalanine, tyrosine, and tryptophan biosynthesis, phenylalanine metabolism, and arachidonic acid metabolism pathway impact is greater than 0.3. It may be the most important metabolic pathway in the pathogenesis and development of renal fibrosis model rats. **Figure 6** is a correlation network diagram of potential biomarkers related to renal fibrosis models based on KEGG network. In the Figure, red is

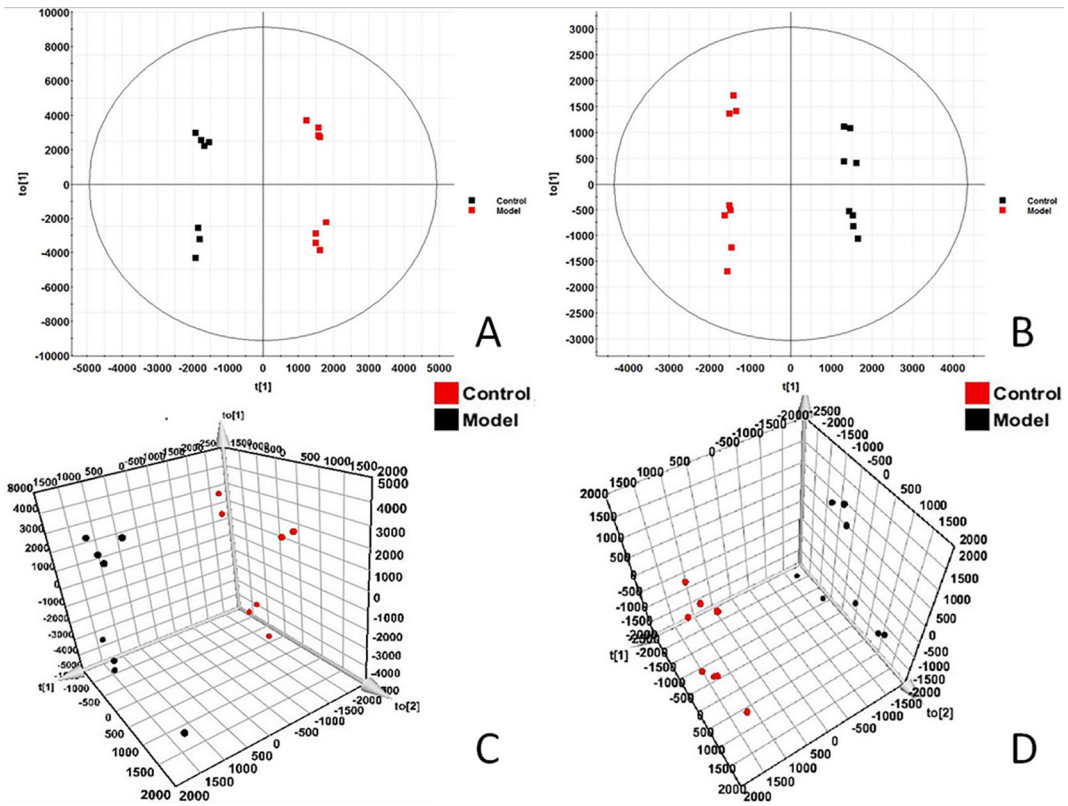


**FIGURE 2 |** OPLS-DAscore and 3D-score plot of serum profile of control group and model group scanned by OPLS-DA analysis. **(A)** OPLS-DAscore inpositive ion mode. **(B)** OPLS-DAscore innegative ion mode. **(C)** 3D-Plotscore inpositive ion mode. **(D)** 3D-Plotscore in negative ion mode.

a potential biomarker with high expression after modeling, green is a potential biomarker with low expression, metabolites in the orange box belong to the same metabolic pathway, and blue is the name of the relevant metabolic pathway; it can be seen that the metabolic pathway in rats changes after the model is established.

## Effect of AP on Metabolic Profile

In order to evaluate the effect of AP on metabolic profile of renal fibrosis rat model, PCA was carried out on the blood metabolic profile of three groups of rats, the results manifest the blood metabolism spectrum of the treatment group was far away from the model group and close to the control group. The results manifest AP can significantly reverse the metabolic profile of renal fibrosis model rats and make them approach a healthy state, further indicating that AP plays a certain intervention role in the occurrence and development of renal fibrosis model rats. In addition, by analyzing the change trend of potential biomarker content of AP on renal fibrosis model rats, it is found that AP intervention can affect the content of potential biomarkers and make them regulate to the direction of control group. The specific information is shown in **Table S2**. And in the bar graph (**Figure 7**), we can see that among the 32 potential biomarkers identified, compared with model group, AP treatment group can regulate 30, of which 4 have significant difference ($p < 0.05$) and 16 have extremely significant differences ($p < 0.01$). In order to further study the differences of potential biomarkers between different groups, cluster thermal analysis of 32 metabolites, such as **Figure 8**, reveals the changes in the relative content of potential biomarkers between the two groups. Studies on biomarkers of AP callback show that its main metabolic pathways involved in regulation are phenylalanine, tyrosine and tryptophan biosynthesis; phenylalanine metabolism; arachidonic acid metabolism; glycerophospholipid metabolism, etc. This indicates that AP may play a role in preventing and treating renal fibrosis by interfering with the above metabolic pathways.

# DISCUSSION

Renal fibrosis is a pathological repair reaction of kidney to chronic injury. It is characterized by excessive proliferation and deposition of extracellular matrix components in kidney which is the common pathological basis of various chronic kidney diseases and an important way for chronic kidney diseases to progress to end-stage renal failure. Therefore, early prevention or even reversal of renal fibrosis is of great significance for the prevention and treatment of end-stage renal failure. TGF-β has been the focus of attention in renal fibrosis and anti-renal fibrosis treatment (Wang et al., 2012). Renal fibrosis caused by TGF-β1 is mainly manifested in the following aspects: it can stimulate

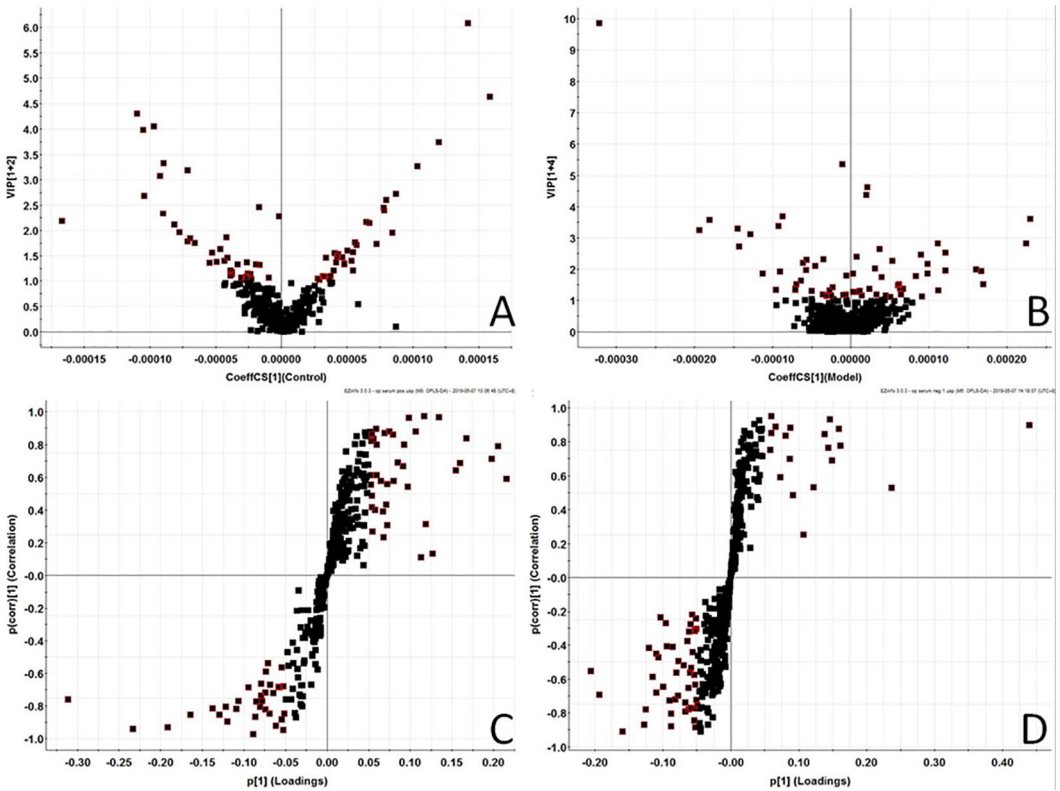


**FIGURE 3 |** Metabolomics profiling of the control group and model group. VIP-plot of serum profile of control group and model group scanned by OPLS-DA analysis inpositive ion mode. **(B)** VIP-plot of serum profile of control group and model group scanned by OPLS-DA analysis innegative ion mode. **(C)** S-plot of serum profile of control group and model group scanned by OPLS-DA analysis in positive ion mode. **(D)** S-plot of serum profile of control group and model group scanned by OPLS-DA analysis in negative ion mode.

fibroblasts and other factors to increase ECM component synthesis; by inhibiting the activities of various ECM degrading enzymes (MMPs) and plasminogen activator, and stimulating the activities of tissue inhibitor of metalloproteinase-1 (TIMPS) and plasminogen activator-1 (PAI-1), ECM degradation is inhibited. Stimulating renal tubular epithelial cells to transdifferentiate into MFBs; increase the expression of ECM receptors such as integrins, thus increasing the interaction between ECM and cells, etc. Overexpression of collagen is an important link in the formation of renal interstitial fibrosis, and TGF-β1 is the most important regulator of type I collagen (Jiang et al., 2016). Anti-TGF-β is considered as one of the promising methods for anti-fibrosis treatment (Doi et al., 2011). However, the pathological mechanism of organ fibrosis is complex, and there are often multiple links and targets. The intervention effect of a single target may not be good (Zeisberg et al., 2002). However, TCM has the characteristics of multi-component and multi-link action, and often has comprehensive advantages in diseases with complicated pathological changes such as renal fibrosis. In this study, a rat model of renal fibrosis was established by unilateral ureteral ligation. The serum of control group, model group, and AP treatment group were analyzed based on high-throughput metabolomics combined with quadrupole time-of-flight mass spectrometry technology. The differences of metabolic profiles of endogenous metabolites in serum of rats between different groups were studied. The results showed that on the 21st day of model replication, the model group and control group were clustered obviously. Through searching HMDB, MetPA, KEGG, and other databases, 32 potential biomarkers that have significant impact on clustering grouping were finally locked, 16 in positive and negative ion mode respectively, and a total of 12 related metabolic pathways were characterized by metabolic pathway enrichment analysis, of which the most relevant are phenylalanine, tyrosine, and tryptophan biosynthesis; phenylalanine metabolism; and arachidonic acid metabolism, which indicates that these metabolic pathways may be the pathological mechanism in the process of renal fibrosis. After 21 days of gastric administration of AP solution, 30 potential biomarkers can be recalled, of which 20 have significant differences, which indicates that AP can achieve the effect of treating renal fibrosis by adjusting the metabolic level of these markers. The metabolic pathways most related to this change are arachidonic acid metabolism and glycerophospholipid metabolism.

Previous studies have shown that AP has a significant effect on the treatment of kidney diseases (Jiang et al., 2016). Studies have found that APS can effectively reduce diabetic glomerular fibrosis induced by high fat plus low dose STZ in rats and inhibit the overexpression of TGF-β1 in damaged renal tubular epithelial cells (Zhang et al., 2007). In the kidney yang deficiency diabetic rat

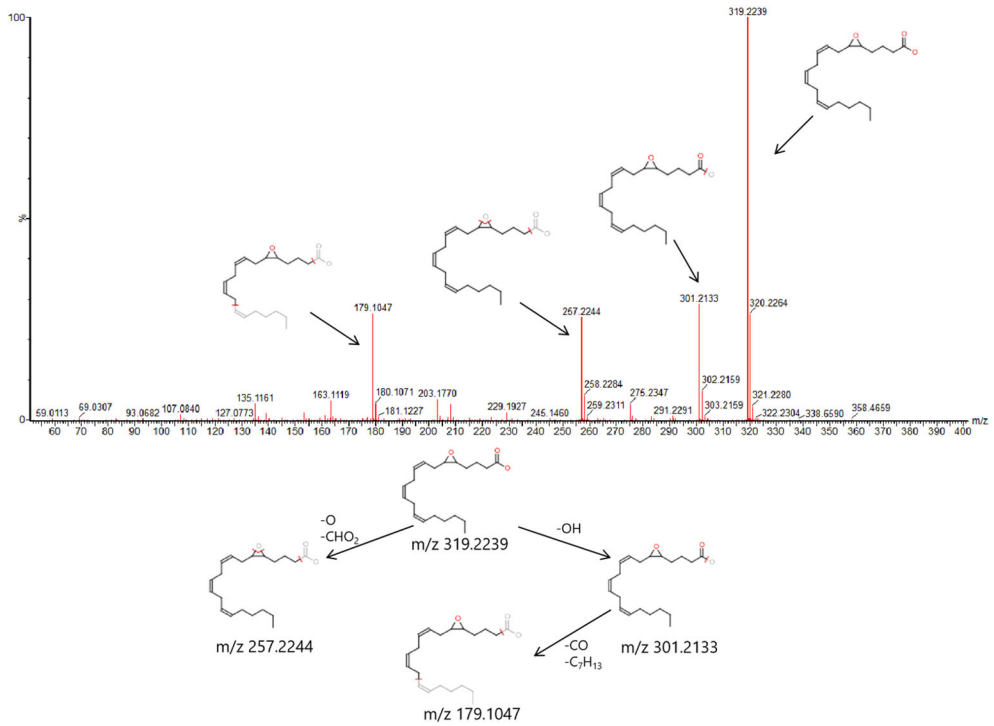


**FIGURE 4 |** 6.91-319.2239 (tR-m/z) compound secondary mass spectrometry fragment attribution and cracking process based on UPLC-Q-TOF-MS/MS .

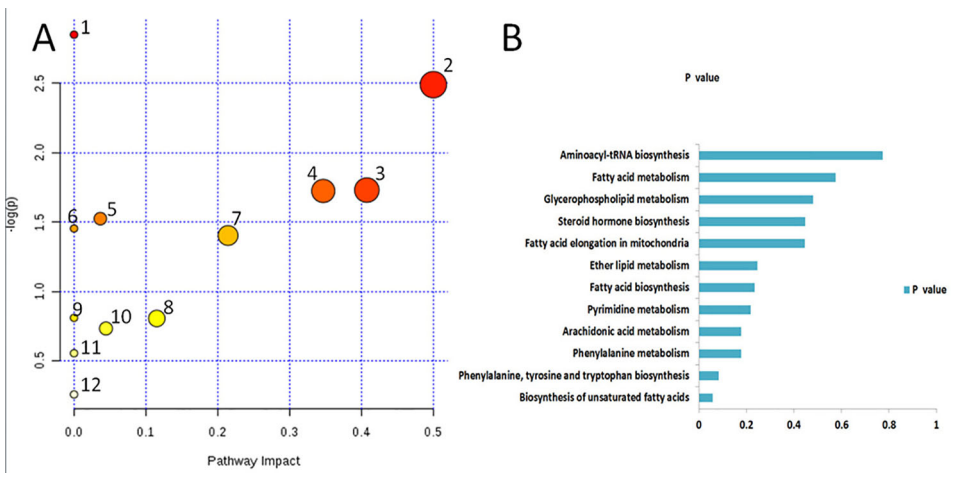


**FIGURE 5 |** Metabolic pathways associated with potential biomarkers in rat serum. **(A)** The map was generated using MetaboAnalyst. 1. Biosynthesis of unsaturated fatty acids. 2. Phenylalanine, tyrosine and tryptophan biosynthesis. 3. Phenylalanine metabolism. 4. Arachidonic acid metabolism. 5. Pyrimidine metabolism. 6. Fatty acid biosynthesis. 7. Ether lipid metabolism. 8. Fatty acid elongation in mitochondria. 9. Steroid hormone biosynthesis. 10. Glycerophospholipid metabolism. 11. Fatty acid metabolism. 12. Aminoacyl-tRNA biosynthesis. **(B)** P values of 12relatedmetabolic pathways.

model, AP can also inhibit the overexpression of TGF-β1 mRNA, thus delaying the progress of diabetic nephropathy. Some studies have confirmed that renal tissue fibrosis can occur in rats with left renal vein stenosis. AM can reduce renal tissue fibrosis damage by reducing the expression of TGF-β1 (Lan, 2011; Qin et al., 2011). In this study, AP interferes with the content and activity of serum metabolites in rats with renal fibrosis induced by left ureter ligation. It can be seen that the changes of serum metabolites in rats with AP interference are mainly related to renal tubular fibrosis, glomerular mesangial cell accumulation, inflammation,

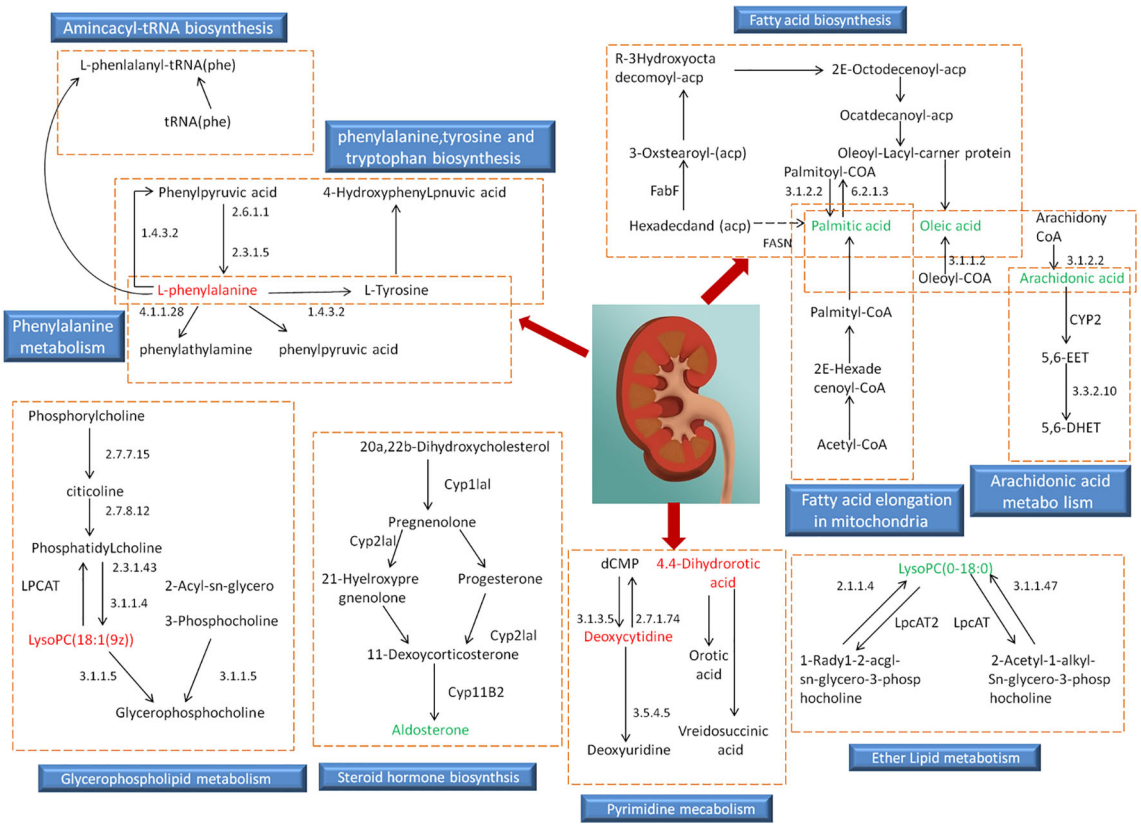


**FIGURE 6 |** Relevant network diagram of potential biomarkers related to renal fibrosis model based on KEGG. Red is the potential biomarker of high expression after modeling, green is the potential biomarker of low expression, metabolites in orange frame belong to the same metabolic pathway, and blue is the name of the relevant metabolic pathway.

oxidative stress, lipid metabolism, etc. Among the 32 metabolic biomarkers characterized by the model group, 2 important substances: arachidonic acid and 5-EET are involved in arachidonic acid metabolism; involved in unsaturated fatty acid metabolism are palmitic acid, oleic acid, and arachidonic acid; glycerol phospholipid metabolism: LysoPC [18:1(9z)]; biosynthesis of steroid hormone matches pregnenolone, aldosterone; phenylalanine metabolic pathway: L-phenylalanine.

Fatty acid biosynthetic pathways include palmitic acid, oleic acid, and arachidonic acid; palmitic acid is a free fatty acid component, a donor of cell membrane lipid structure and prostaglandin synthesis, and an intermediate product of fatty acid metabolism. It participates in the β-oxidation process of fatty acid and plays a role in energy metabolism and fatty acid digestion (Lu et al., 2003). Oleic acid is a monounsaturated ω-9 fatty acid, which is the most widely distributed fatty acid with the highest fat content in nature. Both can induce apoptosis of interstitial cells by producing ceramide (Mu et al., 2001). Studies have shown that palmitic acid can induce apoptosis of renal tubular epithelial cells, upregulate cPLA2, produce bioactive components such as free fatty acid and lysolecithin, which are mainly arachidonic acid, and participate in the occurrence and development of tissue fibrosis (Baggio et al., 2005; Allison, 2015).

LysoPCs is a lysophosphate compound, which can promote epithelial cell apoptosis, increase vascular permeability, promote fibroblast migration and anti-apoptosis ability, activate the activity of potential TGF-β1, increase the secretion of fibrogenic factors PDGF-β and CTGF by proximal tubule cells, mediate the role of lysophosphatidic acid and sphingosine 1-phosphate in fibrosis, and accelerate the process of fibrosis. In addition, LysoPC can promote oxidative stress, inhibit glucose transport and insulin-mediated glucose metabolism, and inhibit the activity of $Na^+$–$K^+$–ATP enzyme, thus causing abnormalities in cell structure and function. The changes of LysoPCs are closely related to the renal fibrosis process and oxidative stress reaction in rats with renal fibrosis (Kang et al., 2015; Zeng et al., 2017; Sun et al., 2018;).

The metabolic pathway of arachidonic acid includes 5,6-epoxy-8,11,14-eicosanoic acid; arachidonic acid has two kinds of metabolism, among which arachidonic acid has the effects of esterifying cholesterol, increasing vascular elasticity, reducing vascular viscosity, regulating blood cell function, etc. Peanut-like acids, such as 20-HETE and EETs, which have the function of regulating the transport of renal tubular epithelial cells, can be produced by cytochrome P450 cyclooxygenase, which is of great significance for maintaining renal function of patients with nephropathy (Maier and Roman, 2001). In addition,

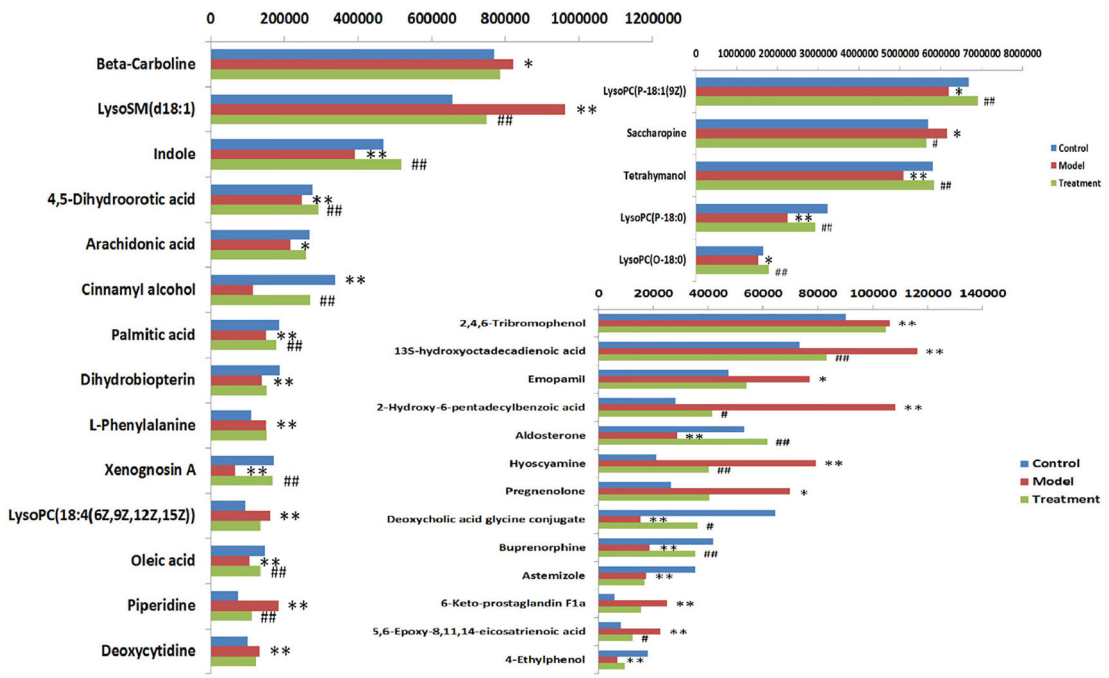


**FIGURE 7 |** Heat map analysis of 32 differential metabolites in control group, model group and treatment group rats. Different color marks represent the change degree of relative content and the darker the color, the higher the relative content. Each row represents a metabolite, and each column represents a single sample. *model vs control, $p < 0.05$; **model vs control, $p < 0.01$. #Treament vs model, $p < 0.05$; ##Treament vs model, $p < 0.01$.

arachidonic acid is the direct premise of prostaglandins, leukotrienes, and other substances, and has important regulatory effects on lipid protein metabolism, vascular rheology, vascular elasticity, inflammatory response, and so on (Skibba et al., 2017). 5,6-epoxy-8,11,14-eicosartienoic acid is a metabolite produced by arachidonic acid through cytochrome P450 cyclooxygenase, and the changes of the contents of the two are closely related to the inflammatory reaction, high blood viscosity, and the characterization of dyslipidemia in renal fibrosis rats (Xiang et al., 2016). The influence of these pathways explains from a certain angle that renal fibrosis may be a comprehensive disease, and it is also an explanation that renal fibrosis is difficult to be completely controlled by a single drug. However, the complex and diverse components of TCM may realize multi-target synergistic effect and treat comprehensive kidney diseases.

Metabolomics is an important branch of system biology. It mainly studies the changes of all metabolites produced by external stimuli. Metabolomics takes metabolic product groups in organisms as analysis targets, adopts high-throughput detection as technical means (chromatography, mass spectrometry, nuclear magnetic resonance, spectrum, etc.) (Wang et al., 2019), uses data processing for systematic integration, combines qualitative detection technology and quantitative characterization methods to discover possible small molecular compounds, interprets the biological significance contained in the data by means of bioinformatics platform, and excavates potential biomarkers (Zhang et al., 2019). So as to further explore the internal metabolic circulation pathway and signal pathway of the disease and provide possibility for exploring the development process and mechanism of the disease (Sun et al., 2015).

The occurrence and development of renal diseases involve changes in the expression levels of many functional genes and proteins, and minor changes in gene and protein expression can be amplified in small molecule metabolism, so high-throughput metabolomics can be used for accurate identification. Therefore, this study is based on the research method of high-throughput metabolomics. With the help of UPLC-Q-TOF/MS and other advanced instruments and equipment, the blood of renal fibrosis model rats established by unilateral tubal ligation operation is analyzed, and the metabolic fingerprint of serum of renal fibrosis rats is established. Combined with PCA and OPLS-DA analysis, potential biomarkers and metabolic pathways related to renal fibrosis are found, and 32 biomarkers and 12 metabolic pathways related to renal fibrosis are finally determined. It is also found that 20 potential biomarkers can be recalled after AP treatment, and there is a statistical difference compared with the model group. These biomarkers mainly involve changes in metabolic pathways such as arachidonic acid metabolism and glycerophospholipid metabolism, thus providing a basis for exploring the pathogenesis of renal fibrosis model rats and the therapeutic effect of AP. This study is the first time to explain the preventive and therapeutic effects of oral AP on renal fibrosis from the perspective of metabolic pathway, and to prove the effectiveness and time potential of metabolomics in the study of intervention effects of TCM.

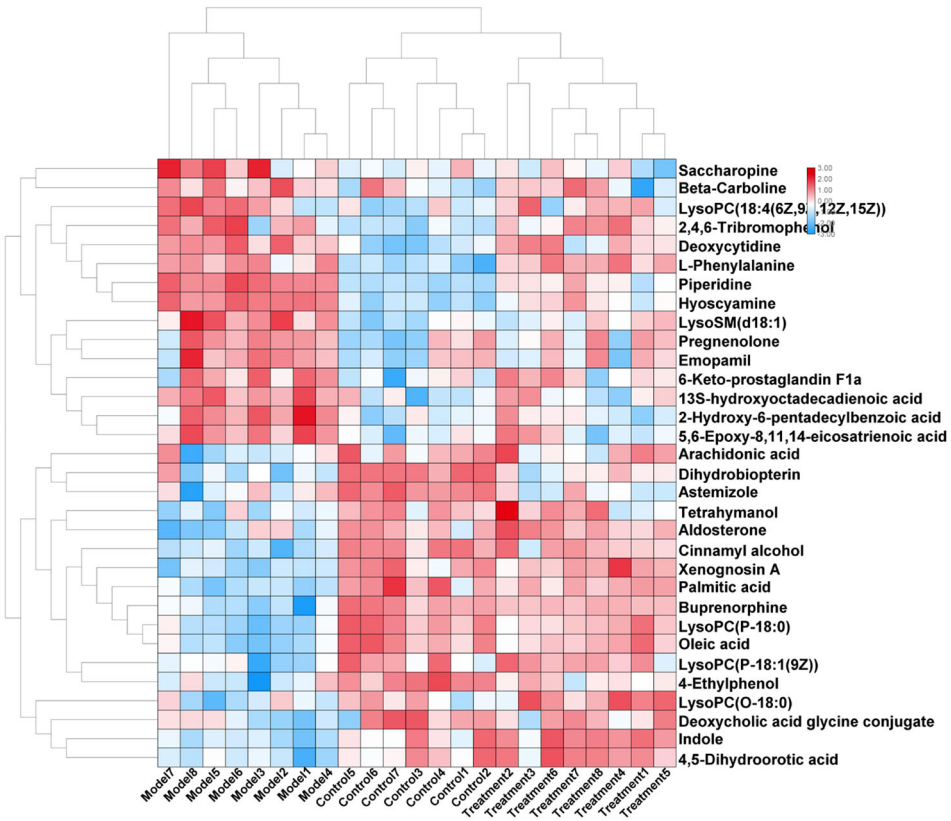


**FIGURE 8 |** Changes in serum relative content of potential biomarkers after AP treament. The depth of the color represents the change of the content of the corresponding marker.

## CONCLUSION

In this study, a rat model of renal fibrosis was established by unilateral tubal ligation. Based on UPLC-Q-TOF/MS and multivariate data analysis, 32 potential biomarkers related to renal fibrosis and 12 related metabolic pathways were revealed from the level of serum metabolomics. AP can recall 30 potential markers, 16 of which have significant difference ($p < 0.01$). Compared with the model group, four have significant differences, mainly regulating three metabolic pathways. Furthermore, it will affect the metabolic level of renal fibrosis model rats and make them develop towards remission, thus providing support for further research on AP treatment of renal fibrosis.

## DATA AVAILABILITY STATEMENT

The raw data supporting the conclusions of this article will be made available by the authors, without undue reservation, to any qualified researcher.

## ETHICS STATEMENT

The animal study was reviewed and approved by Guilin Medical University.

## AUTHOR CONTRIBUTIONS

LR conceived and designed the experiments. LR, X-YG, FG, M-LJ, and X-NS performed the experiment. X-YG analyzed the data. FG guided the experiment. LR wrote the paper. All authors read and approved the final manuscript.

## SUPPLEMENTARY MATERIAL

The Supplementary Material for this article can be found online at: https://www.frontiersin.org/articles/10.3389/fphar.2019.01623/full#supplementary-material

## REFERENCES


Adesso, S., Russo, R., Quaroni, A., Autore, G., and Marzocco, S. (2018). Astragalus membranaceus extract attenuates inflammation and oxidative stress in intestinal epithelial cells *via* NF-κB activation and Nrf2 response. *Int. J. Mol. Sci.* 19 (3), 800. doi: 10.3390/ijms19030800

Allison, S. J. (2015). Fibrosis: dysfunctional fatty acid oxidation in renal fibrosis. *Nat. Rev. Nephrol.* 11 (2), 64. doi: 10.1038/nrneph.2014.244

Baggio, B., Musacchio, E., and Priante, G. (2005). Polyunsaturated fatty acids and renal fibrosis: Pathophysiologic link and potential clinical implications. *J. Nephrol.* 18.4, 362–367.

Chang, Y. X., Sun, Y. G., Li, J., Zhang, Q. H., Guo, X. R., Zhang, B. L., et al. (2012). The experimental study of astragalus membranaceus on meridian tropsim: the distribution study of astragaloside iv in rat tissues. *J. chromatography. B Analytical Technol. Biomed. Life Sci.* 911. 23, 71–75. doi: 10.1016/j.jchromb.2012.10.024

Cho, W. C., and Leung., K. N. (2007). In vitro and in vivo anti-tumor effects of Astragalus membranaceus. *Cancer Lett.* 252.1, 43–54. doi: 10.1016/j.canlet.2006.12.001

Dettmer, K., Aronov, P. A., and Hammock., B. D. (2010). Mass spectrometry-based metabolomics. *Mass Spectrometry Rev.* 26.1, 51–78. doi: 10.1002/mas.20108

Doi, S., Zou, Y., Togao, O., Pastor, J. V., John, G. B., Wang, L., et al. (2011). Klotho inhibits transforming growth factor-β1 (tgf-β1) signaling and suppresses renal fibrosis and cancer metastasis in mice. *J. Biol. Chem.* 286. 10, 8655. doi: 10.3389/fphar.2017.00406

Eddy, A. A. (1996). Molecular insights into renal interstitial fibrosis. *J. Am. Soc. Nephrol.* 7 (12), 2495–2508. doi: 10.1089/end.1996.10.565

Fiehn, O. (2002). Metabolomics – the link between genotypes and phenotypes. *Plant Mol. Biol.* 48 (1-2), 155–171. doi: 10.1023/a:1013713905833

Jiang, Y., Qi, X., Gao, K., Liu, W., Li, N., Cheng, N., et al. (2016). Relationship between molecular weight, monosaccharide composition and immunobiologic activity ofastragaluspolysaccharides. *Glycoconjugate J.* 33 (5), 755–761. doi: 10.1007/s10719-016-9669-z

Kang, H. M., Ahn, S. H., Choi, P., Ko, Y. A., and Susztak, K. (2015). Defective fatty acid oxidation in renal tubular epithelial cells has a key role in kidney fibrosis development. *Nat. Med.* 21 (1), 37. doi: 10.1038/nm.3762

Lan, H. Y. (2011). Diverse Roles of TGF-β/Smads in Renal Fibrosis and Inflammation. *Int. J. Biol. Sci.* 7.7, 1056–1067. doi: 10.7150/ijbs.7.1056

Li, M., Wang, W., Xue, J., Gu, Y., and Lin, S. (2011). Meta-analysis of the clinical value of astragalus membranaceus in diabetic nephropathy. *J. Ethnopharmacol.* 133 (2), 412–419. doi: 10.1016/j.jep.2010.10.012

Lian, Y., Xie, L., Chen, M., and Chen, L. (2014). Effects of an astragalus polysaccharide and rhein combination on apoptosis in rats with chronic renal failure. *Evid. Based Compl. Altern. Med.* 2014, 1–7. doi: 10.1155/2014/271862

Liu,, and Youhua, (2011). Cellular and molecular mechanisms of renal fibrosis. *Nat. Rev. Nephrol.* 7 (12), 684–696. doi: 10.1038/nrneph.2011.149

Liu, M., Wu, K., Mao, X., Wu, Y., and Ouyang, J. (2010). Astragalus polysaccharide improves insulin sensitivity in kkay mice: regulation of pkb/glut4 signaling in skeletal muscle. *J. Ethnopharmacol.* 127 (1), 0–37. doi: 10.1016/j.jep.2009.09.055

Liu, Y. (2006). Renal fibrosis: new insights into the pathogenesis and therapeutics. *Kidney Int.* 69.2, 213–217. doi: 10.1038/sj.ki.5000054

Lu, Z.-H., Mu, Y.-M., Wang, B.-A., Li, X.-L., Lu, J.-M., Li, J.-Y., et al. (2003). Saturated free fatty acids, palmitic acid and stearic acid, induce apoptosis by stimulation of ceramide generation in rat testicular Leydig cell. *Biochem. Biophys. Res. Commun.* 303 (4), 1002–1007. doi: 10.1016/s0006-291x(03)00449-2

Maier, K. G., and Roman, R. J. (2001). Cytochrome p450 metabolites of arachidonic acid in the control of renal function. *Curr. Opin. In Nephrol. Hypertension* 10 (1), 81–87. doi: 10.1097/00041552-200101000-00013

Min, H. C. (2010). Renal fibrosis. *Korean J. Pediatr.* 53.7, 735–740. doi: 10.3345/kjp.2010.53.7.735

Mu, Y. M., Yanase, T., Nishi, Y., Tanaka, A., Saito, M., Jin, C. H., et al (2001). Saturated FFAs, palmitic acid and stearic acid, induce apoptosis in human granulosa cells. *Endocrinology* 142 (8), 3590–3597. doi: 10.1210/endo.142.8.8293

Qin, W., Chung, A. C. K., Huang, X. R., Meng, X. M., Hui, D. S. C., and Yu, C. M. (2011). TGF-β/Smad3 signaling promotes renal fibrosis by inhibiting miR-29. *J. Am. Soc. Nephrol.* 22 (8), 1462–1474. doi: 10.1681/ASN.2010121308

Qiu, S., Zhang, A., Zhang, T., Sun, H., and Wang, X. (2017). Dissect new mechanistic insights for geniposide efficacy on the hepatoprotection using multiomics approach. *Oncotarget* 8 (65), 108760–108770. doi: 10.18632/oncotarget.21897

Shao, B. M. (2004). A study on the immune receptors for polysaccharides from the roots of AM, a Chinese medicinal herb. *Biochem. Biophys. Res. Commun.* 320.4, 1103–1111. doi: 10.1016/j.bbrc.2004.06.065

Skibba, M., Hye Khan, Md A., Kolb, L. L., Yeboah, M. M., Falck, J. R., Amaradhi, R., et al. (2017). Epoxyeicosatrienoic acid analog decreases renal fibrosis by reducing epithelial-to-mesenchymal transition. *Front. Pharmacol.* 8, 406. doi: 10.3389/fphar.2017.00406

Song, J., Meng, L., Li, S., Qu, L., and Li, X. (2009). A combination of chinese herbs, astragalus membranaceus var. mongholicus and angelica sinensis, improved renal microvascular insufficiency in 5/6 nephrectomized rats. *Vasc. Pharmacol.* 50 (5-6), 185–193. doi: 10.1016/j.vph.2009.01.005

Song, Qi, Zhang, A. H., Yan, G. L., Liu, L., and Wang, X. J. (2017). Technological advances in current metabolomics and its application in tradition Chinese medicine. *Rsc Adv.* 7 (84), 53516–53524. doi: 10.1039/c7ra02056b

Sun, H., Zhang, A., Yan, G., Piao, C., Li, W., Sun, C., et al. (2013). Metabolomic analysis of key regulatory metabolites in hepatitis C virus–infected tree shrews. *Mol. Cell. Proteomics* 12 (3), 710–719. doi: 10.1074/mcp.M112.019141

Sun, H., Wang, H., Zhang, A., Yan, G., Zhang, Y., An, N., et al. (2015). Berberine ameliorates nonbacterial prostatitis via multi-target metabolic network regulation. *Omics: J. Integr. Biol.* 19 (3), 186–195. doi: 10.1089/omi.2014.0112

Sun, H., Zhang, A. H., Song, Q., Fang, H., Liu, X. Y., Su, J., et al. (2018). Functional metabolomics discover pentose and glucuronate interconversion pathways as promising targets for Yang Huang syndrome treatment with Yinchenhao Tang. *RSC Adv.* 8 (64), 36831–36839. doi: 10.1039/c8ra06553e

Vasko, R. (2016). Peroxisomes and Kidney Injury. *Antioxid. Redox Signal.* 25, 217–231. doi: 10.1089/ars.2016.6666

Wang, B., Komers, R., Carew, R., Winbanks, C. E., Xu, B., Herman-Edelstein, M., et al. (2012). Suppression of microrna-29 expression by TGF-β1 promotes collagen expression and renal fibrosis. *J. Am. Soc. Nephrol.* 23 (2), 252–265. doi: 10.1681/ASN.2011010055

Wang, X., Zhang, A., Wang, P., Sun, H., and Meng, X. (2013). Metabolomics coupled with proteomics advancing drug discovery toward more agile development of targeted combination therapies. *Mol. Cell. Proteomics* 12.5, 1226–1238. doi: 10.1074/mcp.M112.021683

Wang, X. J., Ren, J. L., Zhang, A. H., Sun, H., Yan, G. L., Han, Y., et al. (2019). Novel applications of mass spectrometry-based metabolomics in herbal medicines and its active ingredients: current evidence. *Mass Spectrom Rev.* 38 (4-5), 380–402.

Weckwerth, W. (2003). Metabolomics in systems biology. *Annu. Rev. Plant Biol.* 54 (54), 669–689. doi: 10.1146/annurev.arplant.54.031902.135014

Xiang, Z., Sun, H., Cai, X., and Chen, D. (2016). The study on serum and urine of renal interstitial fibrosis rats induced by unilateral ureteral obstruction based on metabonomics and network analysis methods. *Analytical Bioanalytical Chem.* 408 (10), 2607–2619. doi: 10.1007/s00216-016-9368-4

Xiong, H., Zhang, A. H., Zhao, Q. Q., Yan, G. L., Sun, H., and Wang, X. J. (2019). Discovery and screening quality-marker ingredients of Panax quinquefolius using chinmedomics approach. *Phytomedicine*. 0944-7113(19)30097-2. doi: 10.1016/j.phymed.2019.152928

Zeisberg, M., Bonner, G., Maeshima, Y., Colorado, P., Müller, G. A., Strutz, F., et al. (2002). Renal Fibrosis. collagen composition and assembly regulates epithelial-mesenchymal transdifferentiation. *Am. J. Pathol.* 159.4, 1313–1321. doi: 10.1016/S0002-9440(10)62518-7

Zeisberg, M., and Kalluri, R. (2004). The role of epithelial-to-mesenchymal transition in renal fibrosis. *J. Mol. Med.* 82.3, 175–181. doi: 10.1007/s00109-003-0517-9

Zeisberg, M., Maeshima, Y., Mosterman, B., and Kalluri, R. (2002). Renal fibrosis: extracellular matrix microenvironment regulates migratory behavior of activated tubular epithelial cells. *Am. J. Pathol.* 160 (6), 2001–2008. doi: 10.1016/s0002-9440(10)61150-9

Zeng, Z., Yang, H., Wang, Y., Ren, J., Dai, Y., and Dai, C. (2017). Omega-3 polyunsaturated fatty acids attenuate fibroblast activation and kidney fibrosis involving mtorc2 signaling suppression. *Sci. Rep.* 7, 46146. doi: 10.1038/srep46146

Zhang, Y. W., Wu, C. Y., and Cheng, J. T. (2007). Merit of Astragalus polysaccharide in the improvement of early diabetic nephropathy with an effect on mRNA expressions of NF-κB and IκB in renal cortex of streptozotoxin-induced diabetic rats. *J. Ethnopharmacol.* 114.3, 387–392. doi: 10.1016/j.jep.2007.08.024

Zhang, A., Sun, H., Wang, Z., Sun, W., Wang, P., and Wang, X. (2010). Metabolomics: towards understanding traditional chinese medicine. *Planta Med.* 76 (17), 2026–2035. doi: 10.1055/s-0030-1250542

Zhang, A., Sun, H., Yan, G., Wang, P., and Wang, X. (2014). Mass spectrometry-based metabolomics: applications to biomarker and metabolic pathway research. *Biomed. Chromatography* 30 (1), 7–12. doi: 10.1002/bmc.3453

Zhang, T., Zhang, A., Qiu, S., Yang, S., and Wang, X. (2016). Current trends and innovations in bioanalytical techniques of metabolomics. *Crit. Rev. Anal. Chem.* 46 (4), 342–351. doi: 10.1080/10408347.2015.1079475

Zhang, A., Sun, H., and Wang, X. (2017). Emerging role and recent applications of metabolomics biomarkers in obesity disease research. *RSC Adv.* 7 (25), 14966–14973. doi: 10.1039/c6ra28715h

Zhang, A. H., Yu, J. B., Sun, H., Kong, L., Wang, X. Q., Zhang, Q. Y., et al. (2018). Identifying quality-markers from Shengmai San protects against transgenic mouse model of Alzheimer's disease using chinmedomics approach. *Phytomedicine* 45, 84–92. doi: 10.1016/j.phymed.2018.04.004

Zhang, A. H., Sun, H., Yan, G. L., Han, Y., Zhao, Q. Q., and Wang, X. J. (2019). Chinmedomics: a powerful approach integrating metabolomics with serum pharmacochemistry to evaluate the efficacy of traditional Chinese medicine. *Engineering* 5, 60–68. doi: 10.1016/j.eng.2018.11.008

**Conflict of Interest:** The authors declare that the research was conducted in the absence of any commercial or financial relationships that could be construed as a potential conflict of interest.

frontiers in Pharmacology

REVIEW
published: 18 March 2020
doi: 10.3389/fphar.2020.00335

# Traditional Chinese Medicine of Angelicae Pubescentis Radix: A Review of Phytochemistry, Pharmacology and Pharmacokinetics

*Yaqi Lu[1,2†], Hongwei Wu[1†], Xiankuo Yu[1], Xiao Zhang[1,2], Hanyan Luo[1], Liying Tang[1*] and Zhuju Wang[1*]*

*[1] Institute of Chinese Materia Medica, China Academy of Chinese Medical Science, Beijing, China, [2] College of Pharmacy, Henan University of Chinese Medicine, Zhengzhou, China*

Angelicae Pubescentis Radix (APR) is a widely used antirheumatic Chinese medicinal herb known as "Duhuo" in China. It has the effects of dispelling wind and removing dampness, diffusing impediment, and relieving pain, and is mainly indicated for rheumatic arthritis with pain in the lower back and knees, and headache. To the best of our knowledge, an attempt is made to provide an up-to-date review on these aspects based on published materials, including ancient and modern books; Master's and doctoral theses; monographs on medicinal plants; the pharmacopoeia of different countries, websites for publication of patent and electronic databases, such as SCI finder, PubMed, Web of Science, ACS, Science Direct, Wiley, Springer, Taylor, CNKI, and Google Scholar. APR, which has a good clinical effect, has been used for traditional Chinese medicine more than 2000 years. Since 1957, a variety of chemical constituents have been reported from the medicinal plants of this herb, mostly coumarins and volatile oil. In the past 30 years, numerous studies have shown that the extracts and compounds isolated from APR showed effective analgesic and anti-inflammatory actions, also showing well effects on central nervous system, effects on cardiovascular system and deworming activity. In addition, we also present and discuss the botany, traditional medicinal use, pharmacokinetics, toxicity, quality control, future trends and prospects of APR. All this information suggest that future research of APR should be supplemented in the area of pharmacology and toxicology to provide further insight on the clinical use and quality control.

**Keywords: Angelicae Pubescentis Radix, phytochemistry, pharmacology, pharmacokinetics, botany, traditional medicinal use, toxicity, quality**

OPEN ACCESS

***Edited by:***
*Wei Zhou,*
*Hospital of Shenzhen University, China*

***Reviewed by:***
*Yi Ding,*
*Fourth Military Medical University, China*
*Tao Yi,*
*Hong Kong Baptist University, Hong Kong*

****Correspondence:***
*Liying Tang*
*bjtangliying@163.com*
*Zhuju Wang*
*wangzhuju@sina.com*

*[†]These authors have contributed equally to this work and share first authorship*

***Specialty section:***
*This article was submitted to Ethnopharmacology, a section of the journal Frontiers in Pharmacology*

***Received:*** *02 August 2019*
***Accepted:*** *06 March 2020*
***Published:*** *18 March 2020*

***Citation:***
*Lu Y, Wu H, Yu X, Zhang X, Luo H, Tang L and Wang Z (2020) Traditional Chinese Medicine of Angelicae Pubescentis Radix: A Review of Phytochemistry, Pharmacology and Pharmacokinetics. Front. Pharmacol. 11:335. doi: 10.3389/fphar.2020.00335*

## INTRODUCTION

Angelicae Pubescentis Radix (equivalent to Angelica Pubescens Root, known as "Duhuo" in China, "Dokwhal" in Korea, "Dokkatsu" in Japan) has been used as herbal medicine extensively since ancient times in Asian countries, including China, Korea and Japan. Due to its effective medicinal value, it has been included in Chinese Pharmacopoeia, British Pharmacopoeia, European Pharmacopoeia, and so on. As an antirheumatic and analgesic agent, it is commonly used as a traditional Chinese medicine (TCM) to treat rheumatic arthralgia and headache. Rheumatic arthralgia is the professional description of TCM syndrome, and includes clinical symptoms such as muscle and joint pain, joint deformities, and dysfunction, with resulting exhaustion and lack of strength. These symptoms are common in rheumatic diseases such as rheumatism and rheumatoid arthritis (RA), with modern medicine ascribing them to an immune deficiency (Wang et al., 2009). In addition, APR is also used in the field of health-care products and cosmetics.

From the Chinese Pharmacopoeia (version 1977), Angelicae Pubescentis Radix (APR) is the dried roots of *Angelica biserrata* (R.H.Shan & C.Q.Yuan) C.Q.Yuan & R.H.Shan (a synonym for *Angelica pubescens* f. *biserrata* R.H. Shan & C.Q. Yuan in Chinese Pharmacopoeia). Besides, *Angelica pubescens* Maxim used to be a plant source of APR in China, and it is still a medicinal plant in Japan. In this review, *A. biserrata* and *A. pubescens* will be reviewed collectively.

APR is mainly produced in Sichuan, Hubei, Anhui and other provinces in China. Usually, its excavation takes place in early spring or late fall. It is common to remove the fibrous roots and sediment, half dried above the heated mud. They were piled for 2 to 3 days, then heated to dry absolutely when they become soft. To date, 87 compounds, including coumarins, polyene-alkynes, phenolic acids, steroids, nucleoside elements have been isolated and identified from APR. What's more, nearly 100 volatile oil compounds have been analyzed by GC-MS. In modern clinical practice, APR plays an important role in treating RA, osteoarthritis pain, vascular dementia (VD), Alzheimer's disease (AD) and headache (Wang et al., 2011a; Jia et al., 2015; Zheng et al., 2017).

In this review, we discussed the botany, traditional medicinal use, phytochemistry, pharmacology, pharmacokinetic, toxicology and quality control of APR as comprehensively as possible, to obtain a comprehensive understanding of the effects of APR and also provide a basis for further research and development of new drugs.

## BOTANY

*Angelica biserrata* (R.H.Shan & C.Q.Yuan) C.Q.Yuan & R.H.Shan (*A. biserrata*, Chinese name: Chongchi Maodanggui) and *Angelica pubescens* Maxim (*A. pubescens*, Chinese name: Maodanggui) used to be or still be medicinal plants of APR. At present, *A. biserrata* is the plant source of APR recorded in multi-national pharmacopoeia, including Chinese, British, the European. *A. pubescens*, which used to be a medicinal plant for APR in China, is mainly produced in Japan and is used medically in that country at present (Zhengkang, 2006; Rao et al., 1994). In the following discussion, *A. biserrata* and *A. pubescens* will be reviewed collectively.

*A. biserrata* and *A. pubescens* both belong to the genus *Angelica* of the family *Apiaceae*, and the former is a variant of the latter. Due to too much similarity of the plants and constant errors in the study of the resources, some of the *A. biserrata* were once mistaken for *A. pubescens* before the 1990s. According to the resource survey, there is no such a species as *A. pubescens* in China (Institute of Materia Medica, Chinese Academy of Medical Sciences, 1959; Shan et al., 2014). It has been concluded that *A. biserrata* is primarily distributed in China South-Central, China Southeast, and Vietnam, while *A. pubescens* is primarily distributed in Japan and Vietnam (http://www.plantsoftheworldonline.org/).

*A. biserrata* primarily grows on wet and damp slopes, under the forest grass, or in sparse shrubs in Sichuan, Hubei, Jiangxi, Anhui, and Zhejiang provinces, among other selected regions. It is also cultivated in the high mountains of the Sichuan, Hubei, and Shanxi provinces, and breeding methods include seed breeding, direct seeding, and the transplanting of seedlings. In terms of *A. biserrata*, the medicinal material shape of the cultivated variety is similar to the wild product, but the root of the cultivated product is large and soft, with a length of 10–20 cm, and a strong fragrance (http://frps.iplant.cn/; Xiong, 2014).

The description of *A. biserrata* and *A. pubescens* plants morphology as referenced by the Flora of China (FOC) and Flora of Japan (FOJ) is presented in **Table 1**. The whole plant of *A. biserrata* (**Figure 1A**), medicinal parts of APR (**Figure 1B**), and the processed of APR (**Figure 1C**) are shown in **Figure 1**. To further distinguish the two plants, the comparison between them were performed based on scientific synonyms included in Kew's taxonomic resources and names published in medicinal references, and the results are shown in **Table 2**.

## TRADITIONAL MEDICINAL USE

APR is widely used as the important traditional Chinese medicine to treat rheumatic arthralgia and headache for nearly 2000 years. In the Chinese Pharmacopoeia (version 2015), it has been used to treat conditions such as wind-cold-dampness arthralgia, lumbar and knee pain, wind-cold dampness headache, and its recommended dosage is 3–10 g (Committee for the Pharmacopoeia of PR China., 2015).

According to TCM records, APR was initially recorded in "Shen Nong Ben Cao Jing" during the Eastern Han Dynasty (perhaps earlier), which is deemed as the earliest treatise for medicine in China. In this monograph, APR was described as a treatment for wind-cold blows, gold sore pain and hernia mass in

**TABLE 1** | The Characteristics and Distribution of medicinal plants as APR.

| Scientific name | Chinese name | Characteristics | Distribute | Reference |
|---|---|---|---|---|
| *Angelica biserrata* (R.H. Shan & C.Q. Yuan) C.Q. Yuan & R.H. Shan/ *Angelica pubescens* f. *biserrata* R.H. Shan & C.Q. Yuan | Chongchi Maodanggui 重齿毛当归 | Plants perennial, 1-2 m, stout. Root cylindric, brown, up to 15 × 1–2.5 cm, aromatic. Stem purplish green, up to 1.5 cm thick, thinly ribbed, hispid above. Basal and lower leaves petiolate, sheaths oblong, inflated, glabrous or slightly pubescent abaxially; blade broad-ovate, 2-ternate-pinnate; leaflets ovate-long-elliptic, base often decurrent along rachis, margin irregularly cuspidate-biserrate, apex acuminate, pubescent along nerves and margin. Peduncles, densely hispidulous; bracts 1, long-subulate, ciliate, deciduous; bracteoles 5–10, broad-lanceolate, apex long-cuspidate, ciliate, pubescent abaxially; umbellules flowered. Calyx teeth obsolete. Petals white, obovate. | Sparse shrubby thickets, damp slopes; Sichuan, Hubei, Jiangxi, Anhui, Zhejiang, Shanxi, Chongqing, Gansu. | FOC[a] (version 2004) |
| *Angelica pubescens* Maxim. | Maodanggui 毛当归 | Stems stout, green, terete, 1–2 m. long, sparingly pubescent; leaves large, about thrice ternately pinnate, the leaflets ovate to elliptic, 5–10 cm. long, sometimes oblong, abrupdy acuminate, often decurrent at base, acutely dentate, pale green beneath, the upper leaves much reduced, with obovate, inflated sheaths; umbels rather numerous, the bracts and bractlets lacking, the rays numerous, 3–16 cm. long, puberulent, the pedicels 25–40, slender. long, puberulent; 2–6 on the commissure, the styles short, shorter than the stylopodium. | Hills and low mountains; Honshu, Shikoku, Kyushu; rather variable. | FOJ[b] (version 1965) |

[a]*Cited from the website: http://foc.iplant.cn/.*
[b]*Cited from the website: https://www.ndl.go.jp/.*
*APR, Angelicae Pubescentis Radix.*

women. In "Ben Cao Gang Mu", another monograph of TCM, APR was described as a treatment to resist stroke, joint pain, tooth swelling and pain by wind. In ancient times, the long-term clinical application was primarily the function of expelling wind and removing dampness, thus relieving pain and exterior syndrome, acting as an antispasmodic, suppressing the hyperactive liver for calming endogenous wind, flattening the Qi, and lowering the inverse to stop vomiting, relieving itching, detoxifying, and inducing hemostasis (Zhang and Liang, 2018).

In addition, APR also has been used with other herbs to treat wind-cold exterior syndrome (TCM term: Fenghan Biaozheng, also can be interpreted as superficial syndrome due to wind-cold), and wind-cold-damp bi-syndromes (TCM term: Fenghanshi Bizheng, also can be interpreted as painful obstructions from wind, damp, and cool environments) in China since ancient times. For example, Duhuo Tang consists of APR together with Angelicae Sinensis Radix, Atractylodis Macrocephalae Rhizoma, Astragali Radix, Cinnamomi


**FIGURE 1** | The whole plant of *A. biserrata* **(A)**, medicinal parts of APR **(B)**, the processed of APR **(C)**.

**TABLE 2 |** Scientific synonyms and names published in medicinal references of medicinal plants as APR.

| Scientific name | No. | Scientific synonyms | No. | Names published in medicinal references |
|---|---|---|---|---|
| *Angelica biserrata* (R.H. Shan & C.Q. Yuan) C.Q. Yuan & R.H. Shan | 1 | *Angelica pubescens* f. *biserrata* R.H. Shan & C.Q. Yuan | 1 | *Angelica biserrata (*R.H. Shan & C.Q. Yuan) C.Q. Yuan & R.H. Shan |
| | | | 2 | *Angelica biserrata* (Shan et Yuan) Yuan et Shan |
| | | | 3 | *Angelica pubescens* Maxim. f. *biserrata* R.H.Shan et C.Q.Yuan |
| | | | 4 | *Angelica pubescens* Maxim. f. *biserrata* Shan et Yuan |
| *Angelica pubescens* Maxim. | 1 | *Angelica myriostachys* Koidz. | 1 | *Angelica pubescens* Maxim. |
| | 2 | *Angelica polyclada* Franch. | 2 | *Angelica pubescens* |
| | 3 | *Angelica schishiudo* Koidz. | 3 | *Angelica polyclada* Franchet |
| | | | 4 | *Angelica pubescens* Maximowicz |

*Cited from the website: https://mpns.science.kew.org/mpns-portal/.*
*APR, Angelicae Pubescentis Radix.*

Cortex, Achyranthis Bidentatae Radix, and Glycyrrhizae Radix et Rhizoma and can be used to treat rheumatic arthralgia (Gao, 2007). In addition, it was reported that Duhuo Jisheng Tang was effective in treating arthralgia syndrome in the 1990s in Germany (Zuo, 1998). Many classic prescriptions had been created by the ancient famous doctors and have been handed down from generation to generation through repeated clinical verification for thousands of years. Due to its definite clinical effects, TCM prescriptions are the main form of TCM used in clinics. The combination of several different types of TCM can enhance efficacy and reduce adverse reactions.

The application of APR in the field of health care has a long history. Early in "Shen Nong Ben Cao Jing", there is a record that it can make the body light and slow down your aging. There are also a variety of ways to eat APR, such as Duhuo tea recorded in "Yao Cha Zhi Bai Bing", Duhuo Renshen wine recorded in "Tai Ping Sheng Hui Fang", and Duhuo Danggui wine recorded in "Sheng Ji Zong Lu". In recent years, the application of APR to the field of health care has been further developed, and there have been multiple patent authorizations for inventions, such as a types of APR to dispel wind and dehumidify hot pot material, types of production methods (Wang, 2014), treating a kind of internal injury fever, and APR health wine (Qian, 2014).

In addition to the above application areas, APR has entered the field of beauty and makeup, and has been granted a number of invention patents, such as APR grass oil emollient water (Wang, 2013), and the preparation methods for APR oil tea emulsion (Li, 2013).

## PHYTOCHEMISTRY

At present, many chemical compounds, including coumarins, polyene-alkynes, phenolic acids, steroids, nucleoside elements, and others, have been isolated and identified from *A. biserrata* and *A. pubescens*. Among these, Coumarins are believed to be the principle non-volatile ingredients with important biological properties. In addition, nearly 100 volatile oil compounds, consisting of terpenoids, small molecular aliphatic and aromatic compounds, have been analyzed by GC-MS (Yang et al., 2006; Wang et al., 2011b). The name, molecular formula, precise mass, and the source of these compounds are listed in **Table 3**. The relevant structures of these compounds are shown in **Figures 2** and **3**.

### Coumarins

Coumarins are phenolic compounds characterized by a benzene ring attached to an alpha-pyrone ring, which can be regarded as a lactone formed by the dehydration of o-hydroxy cinnamic acid. Coumarins have a fragrant smell and occur naturally in many plants. In addition, they are known to possess a myriad of pharmacological activities, including antioxidant, anti-cancer, and anticoagulant effects. They are also known to be fluorophores with their fluorescence changing drastically with varying substituents and newly introduced positions. Therefore, coumarins can be identified using fluorescence detection (Murata et al., 2005). So far, the coumarins separated from APR are mainly composed of simple coumarin as the parent nucleus, linear furocoumarin formed by substitution of seven and six positions, and flavonocoumarin formed by substitution of seven and eight positions. Simple coumarins, angular furocoumarins, psoralen furocoumarins, and nodakenetin furocoumarins have been isolated and identified, with the chemical structures of these coumarins shown in **Table 3** and **Figure 2**.

Simple coumarins (**1**–**39**) have one or more substituents at five, six, seven, eight sites in the mother nucleus of coumarin, which are replaced by -OH, -$OCH_3$, etc. Some (**25**–**27**) can be glycosylated with sugar. Structures of the simple coumarins are shown in **Figure 2**.

At present, there are 11 angular furocoumarin (**40**–**50**, **65**) compounds that have been reported. They can be divided into two types, with one type (**40**–**49**, **65**) having a single bond at the position of 1' and 2', while the other type (**50**) has a double bond. Two (**44**, **45**) of them are glycosylated. Their structures are shown in **Figure 2**.

Currently, 15 psoralen furocoumarins (**51**–**64**, **66, 67**) have been reported, all of which have the skeleton characteristics of psoralen. The side chains of two compounds (**62**, **64**) have an epoxy structure, the other two (**63**, **64**) are glycosylated, and the remaining 11 compounds are typical psoralen furocoumarins. Their structures are shown in **Figure 2**.

**TABLE 3 |** Chemical constituents isolated from medicinal plants as APR.

| No. | Compound | Molecular Formula | Precise Mass | Source | References |
|---|---|---|---|---|---|
| **COUMARINS** | | | | | |
| **1** | Angelitriol | $C_{15}H_{18}O_6$ | 294.1103 | Root & rhizome of *A. biserrata* | Liu et al., 1995a; Liu et al., 1996a |
| **2** | Anpubesol | $C_{20}H_{26}O_7$ | 378.1679 | Root of *A. biserrata* | Pan et al., 1987 |
| **3** | Angelol A (Angelol) | $C_{20}H_{24}O_7$ | 376.1522 | Root of *A. pubescens*; Root & rhizome of *A. biserrata* | Hata and Kozawa, 1965; Liu et al., 1996b |
| **4** | Angelol B | $C_{20}H_{24}O_7$ | 376.1522 | Root of *A. pubescens*; Root & rhizome of *A. biserrata* | Baba et al., 1982; Liu et al., 1996b |
| **5** | Angelol C | $C_{20}H_{26}O_7$ | 378.1679 | Root of *A. pubescens*; Root & rhizome of *A. biserrata* | Baba et al., 1982; Liu et al., 1996b |
| **6** | Angelol D | $C_{20}H_{24}O_7$ | 376.1522 | Root of *A. pubescens*; Root & rhizome of *A. biserrata* | Baba et al., 1982; Liu et al., 1996b |
| **7** | Angelol E | $C_{20}H_{26}O_7$ | 378.1679 | Root of *A. pubescens*; Root & rhizome of *A. biserrata* | Baba et al., 1982; Liu et al., 1996b |
| **8** | Angelol F | $C_{20}H_{26}O_7$ | 378.1679 | Root of *A. pubescens*; Root & rhizome of *A. biserrata* | Baba et al., 1982; Liu et al., 1996b |
| **9** | Angelol G | $C_{20}H_{24}O_7$ | 376.1522 | Root of *A. pubescens*; Root & rhizome of *A. biserrata* | Baba et al., 1982; Liu et al., 1996b |
| **10** | Angelol H | $C_{20}H_{26}O_7$ | 378.1679 | Root of *A. pubescens* | Baba et al., 1982 |
| **11** | Angelol I | $C_{20}H_{26}O_7$ | 378.1679 | Root & rhizome of *A. biserrata* | Liu et al., 1996b |
| **12** | Angelol J | $C_{17}H_{22}O_6$ | 322.1416 | Root & rhizome of *A. biserrata* | Liu et al., 1995a; Liu et al., 1996b |
| **13** | Angelol K | $C_{20}H_{24}O_7$ | 376.1522 | Root of *A. biserrata* | Liu et al., 1995b; Liu et al., 1996b |
| **14** | Angelol L | $C_{20}H_{26}O_7$ | 378.1679 | Root of *A. biserrata* | Liu et al., 1995b; Liu et al., 1996b |
| **15** | Isoangelol | $C_{24}H_{24}O_7$ | 376.1522 | Root of *A. biserrata* | Pan et al., 1987 |
| **16** | Umbelliferone | $C_9H_6O_3$ | 162.0317 | Fruit of *A. pubescens*; Root & rhizome of *A. biserrata* | Hata et al., 1981; Liu et al., 1994 |
| **17** | Osthole (Osthol) | $C_{15}H_{16}O_3$ | 244.1099 | Fruit of *A. pubescens*; Root of *A. pubescens* | Hata and Kozawa, 1965; Hata et al., 1981 |
| **18** | Osthenol | $C_{14}H_{14}O_3$ | 230.0943 | No mentioned | Wang et al., 2014 |
| **19** | 2'-deoxymeranzin hydrate | $C_{15}H_{18}O_4$ | 262.1205 | Root of *A. biserrata* | Zhang et al., 2007 |
| **20** | Meranzin hydrate | $C_{15}H_{18}O_5$ | 278.1154 | Root & rhizome of *A. biserrata* | Liu et al., 1996a |
| **21** | Scopoletin | $C_{10}H_8O_4$ | 192.0423 | Fruit of *A. pubescens* | Hata et al., 1981 |
| **22** | 7-methoxy-6-coumarinaldehyde (Angelical) | $C_{11}H_8O_4$ | 204.0423 | Root of *A. pubescens* | Hata and Tanaka, 1957 |
| **23** | Ulopterol | $C_{15}H_{18}O_5$ | 278.1154 | Root & rhizome of *A. biserrata* | Liu et al., 1994 |
| **24** | Peucedanol | $C_{14}H_{16}O_5$ | 264.0988 | Root & rhizome of *A. biserrata* | Liu et al., 1994 |
| **25** | 7-*O*-$\beta$-D-glucopyranosyl-umbelliferone | $C_{15}H_{16}O_8$ | 324.0845 | Root & rhizome of *A. biserrata* | Ding et al., 2009 |
| **26** | 7-*O*-$\beta$-D-apiofuranosyl-(1→6)-$\beta$-D-glucopyranosyl-umbelliferone | $C_{20}H_{24}O_{12}$ | 456.1268 | Root & rhizome of *A. biserrata* | Ding et al., 2009 |
| **27** | 6-*O*-$\beta$-D-apiofuranosyl-(1→6)-$\beta$-D-glucopyranosyl-scopoletin | $C_{20}H_{24}O_{13}$ | 472.1217 | Root & rhizome of *A. biserrata* | Ding et al., 2009 |
| **28** | 5-isopentenyloxy-7-methoxy-8-senecioylcoumarin (Angelin) | $C_{20}H_{22}O_5$ | 342.1467 | Root of *A. pubescens* | Kozawa et al., 1980 |
| **29** | Coumurrayin | $C_{16}H_{18}O_4$ | 274.1205 | Root of *A. pubescens* | Kozawa et al., 1980 |
| **30** | 7-methoxy-8-senecioylcoumarin | $C_{15}H_{14}O_4$ | 258.0892 | Root of *A. pubescens* | Kozawa et al., 1980 |
| **31** | 8-(3-hydroxyisovaleroyl)-5,7-dimethoxycoumarin | $C_{16}H_{18}O_6$ | 306.1103 | Root of *A. pubescens* | Kozawa et al., 1980 |
| **32** | Glabra-lactone | $C_{16}H_{16}O_5$ | 288.0998 | Fruit of *A. pubescens;* Root of *A. pubescens* | Hata and Kozawa, 1965; Hata et al., 1981 |
| **33** | Umbelliprenin | $C_{24}H_{30}O_3$ | 366.2195 | Fruit of *A. pubescens* | Hata et al., 1981 |
| **34** | Apiosylskimmin | $C_{20}H_{24}O_{12}$ | 456.1268 | Root & rhizome of *A. biserrata* | Liu et al., 1994 |
| **35** | Angepubebisin | $C_{23}H_{28}O_7$ | 416.1835 | Root of *A. biserrata* | Yang et al., 2009 |
| **36** | Isoangelol dehydration | $C_{20}H_{22}O_6$ | 358.1416 | Not mentioned | Wang et al., 2014 |
| **37** | Angelol A dehydration | $C_{20}H_{22}O_6$ | 358.1416 | Not mentioned | Wang et al., 2014 |
| **38** | Anpubesol dehydration | $C_{20}H_{24}O_6$ | 360.1573 | Not mentioned | Wang et al., 2014 |
| **39** | Angelol C dehydration | $C_{20}H_{24}O_6$ | 360.1573 | Not mentioned | Wang et al., 2014 |
| **40** | Columbianadin | $C_{19}H_{20}O_5$ | 328.1311 | Root of *A. biserrata* | Wang et al., 1988 |
| **41** | Columbianetin acetate | $C_{16}H_{16}O_5$ | 288.0998 | Root of *A. biserrata* | Wang et al., 1988 |
| **42** | Columbianetin propionate | $C_{17}H_8O_5$ | 302.1154 | Root of *A. biserrata* | Liu et al., 1998a |
| **43** | Columbianetin | $C_{14}H_{14}0_4$ | 246.0892 | Root of *A. biserrata* | Wang et al., 1988 |
| **44** | Columbianetin-$\beta$-D-glucopyranoside | $C_{20}H_{24}O_9$ | 394.1264 | Root & rhizome of *A. biserrata* | Li et al., 1989b; Wu and Li, 1993 |
| **45** | Columbianin | $C_{26}H_{34}O_{14}$ | 570.1949 | Root & rhizome of *A. biserrata* | Liu et al., 1996a |
| **46** | 2'-(1", 2", 3"-three hydroxyl)-isoamyl Angelica lactone | $C_{16}H_{18}O_7$ | 322.1053 | Root of *A. biserrata* | Wu and Li, 1993 |

*(Continued)*

**TABLE 3** | Continued

| No. | Compound | Molecular Formula | Precise Mass | Source | References |
|---|---|---|---|---|---|
| **47** | Angelidiol(heramandiol) | $C_{14}H_{14}O_5$ | 262.0841 | Root & rhizome of *A. biserrata* | Liu and Yao, 1995; Liu et al., 1996a |
| **48** | Angenomalin | $C_{14}H_{12}O_3$ | 228.0786 | Root of *A. biserrata* | Yang et al., 2008 |
| **49** | Dihydrocolumbianadin | $C_{19}H_{22}O_5$ | 330.1467 | Root of *A. biserrata* | Wang et al., 2014 |
| **50** | Isobergapten | $C_{12}H_8O_4$ | 216.0423 | Root of *A. biserrata* | Sun et al., 2014 |
| **51** | Psoralen | $C_{11}H_6O_3$ | 186.0317 | Fruit of *A. pubescens*; Root of *A. biserrata* | Hata et al., 1981; Zhang et al., 2007 |
| **52** | Bergapten | $C_{12}H_8O_4$ | 216.0423 | Fruit & root of *A. pubescens* | Hata and Kozawa, 1965; Hata et al., 1981 |
| **53** | Bergaptol | $C_{11}H_6O_4$ | 202.0266 | Root of *A. biserrata* | Zhang et al., 2007 |
| **54** | Imperatorin | $C_{16}H_{14}O_4$ | 270.0892 | Root of *A. biserrata*; Fruit of *A. pubescens* | Hata et al., 1981; Sun et al., 2014 |
| **55** | Isoimperatorin | $C_{16}H_{14}O_4$ | 270.0892 | Root of *A. biserrata* | Pan et al., 1987; Wang et al., 2014 |
| **56** | Oxypeucedanin hydrate | $C_{16}H_{16}O_6$ | 304.0947 | Root & rhizome of *A. biserrata* | Liu et al., 1994 |
| **57** | Xanthotoxin | $C_{12}H_8O_4$ | 216.0423 | Fruit of *A. pubescens*; Root of *A. biserrata* | Hata et al., 1981; Pan et al., 1987 |
| **58** | Isopimpinellin | $C_{13}H_{10}O_5$ | 246.0528 | Root of *A. pubescens* | Kozawa et al., 1980 |
| **59** | Byak-angelicin | $C_{17}H_{18}O_7$ | 334.1053 | Root of *A. pubescens* | Kozawa et al., 1980 |
| **60** | 5-methoxy-8-(2-acethoxy-3-hydroxy-3-methylbutoxy) psoralen [sec-*O*-acetylbyakangelicin] | $C_{19}H_{20}O_8$ | 376.1158 | Fruit of *A. pubescens* | Hata et al., 1981 |
| **61** | Neobyakangelicol | $C_{17}H_{16}O_6$ | 316.0947 | Fruit of *A. pubescens* | Hata et al., 1981 |
| **62** | Cnidilin | $C_{17}H_{16}O_5$ | 300.0998 | Root of *A. biserrata* | Zaugg et al., 2011 |
| **63** | Oxypeucedanin | $C_{16}H_{14}O_5$ | 286.0841 | Fruit of *A. pubescens* | Hata et al., 1981 |
| **64** | Ferulin | $C_{17}H_{16}O_6$ | 316.0947 | Fruit of *A. pubescens* | Hata et al., 1981 |
| **65** | Angelmarin | $C_{23}H_{20}O_6$ | 392.1260 | Rhizome of *A. biserrata* | Awale et al., 2006 |
| **66** | *Sec*-*O*-$\beta$-D-glucopyranosyl-(R)-byakangelicin | $C_{23}H_{28}O_{12}$ | 496.1581 | Root of *A. biserrata* | Ding et al., 2008 |
| **67** | *Tert*-*O*-$\beta$-D-glucopyranosyl-(R)-byakangelicin | $C_{23}H_{28}O_{12}$ | 496.1581 | Root of *A. biserrata* | Ding et al., 2008 |
| **68** | Marmesinin | $C_{20}H_{24}O_9$ | 408.1420 | Root & rhizome of *A. biserrata* | Liu et al., 1996a |
| **69** | Nodakenetin | $C_{14}H_{14}O_4$ | 246.0892 | Root & rhizome of *A. biserrata* | Liu et al., 1996a |
| **70** | Nodakenin | $C_{20}H_{24}O_9$ | 408.1420 | Root & rhizome of *A. biserrata* | Liu et al., 1994 |
| **POLYENE-ALKYNES** | | | | | |
| **71** | Falcarindiol | $C_{17}H_{24}O_2$ | 260.1776 | Root of *A. biserrata* | Liu et al., 1998a |
| **72** | 11(S),16(R)-dihydroxy-octadeca-9Z,17-dien-12,14-diyn-1-yl acetate | $C_{20}H_{28}O_4$ | 322.1988 | Root of *A. biserrata* | Liu et al., 1998a |
| **PHENOLIC ACIDS** | | | | | |
| **73** | 3-*O*-*trans*-coumaroylquinic acid | $C_{16}H_{18}O_8$ | 338.1002 | Root of *A. biserrata* | Yang et al., 2008 |
| **74** | 3-*O*-*trans*-feruloylquinic acid | $C_{17}H_{20}O_9$ | 368.1107 | Root of *A. biserrata* | Yang et al., 2008 |
| **75** | Ferulic acid | $C_{10}H_{10}O_4$ | 194.0579 | Root of *A. biserrata* | Sun et al., 2014 |
| **STEROIDS** | | | | | |
| **76** | Daucosterol | $C_{35}H_{60}O_6$ | 576.4390 | Root & rhizome of *A. biserrata* | Liu et al., 1994 |
| **77** | $\beta$-sitosterol | $C_{29}H_{50}O$ | 414.3862 | Root & rhizome of *A. biserrata* | Liu and Yao, 1995 |
| **OTHERS** | | | | | |
| **78** | Adenosine | $C_{10}H_{13}N_5O_4$ | 267.0968 | Root & rhizome of *A. biserrata* | Liu et al., 1994; Sun et al., 2014 |
| **79** | Uridine | $C_9H_{12}N_2O_6$ | 243.0632 | Root of *A. biserrata* | Sun et al., 2014 |
| **80** | Bisabolangelone | $C_{15}H_{20}O_3$ | 248.1412 | Root of *A. biserrata & A. pubescens* | Liu et al., 1998a |
| **81** | 2,3,4,9-Tetrahydro-1H-pyrido[3,4-b] indole-3-carboxylic acid | $C_{12}H_{12}N_2O_2$ | 216.0899 | Root & rhizome of *A. biserrata* | Liu et al., 1994 |
| **82** | Sucrose | $C_{12}H_{22}O_{11}$ | 342.1162 | Root & rhizome of *A. biserrata* | Liu et al., 1994 |
| **83** | Angepubefurin | $C_{19}H_{30}O_4$ | 322.2144 | Root of *A. biserrata* | Yang et al., 2009 |
| **84** | Rutin | $C_{27}H_{30}O_{16}$ | 610.1534 | Root of *A. biserrata* | Yang, 2007 |
| **85** | $\gamma$-aminobutyric acid | $C_4H_9NO_2$ | 103.0633 | Root & rhizome of *A. biserrata* | Li et al., 1989a |
| **86** | Angesesquid A | $C_{15}H_{22}O_5$ | 280.1675 | Root of *A. biserrata* | Li et al., 2019 |
| **87** | Angesesquid B | $C_{15}H_{22}O_5$ | 280.1675 | Root of *A. biserrata* | Li et al., 2019 |

*APR, Angelicae Pubescentis Radix.*

There are reported 3 nodakenetin furocoumarins (**68–70**) currently. The difference in these compounds from the psoralen structure is the hydrogenation of the double bonds on the furan ring. Their structures are shown in **Figure 2**.

## Polyene-Alkynes

Two long chain polyene-alkynes (**71**, **72**) have been isolated from the root of *A. biserrata*, and they have conjugated systems with multiple double bonds and alkyne bonds. Falcarindiol (**71**) has

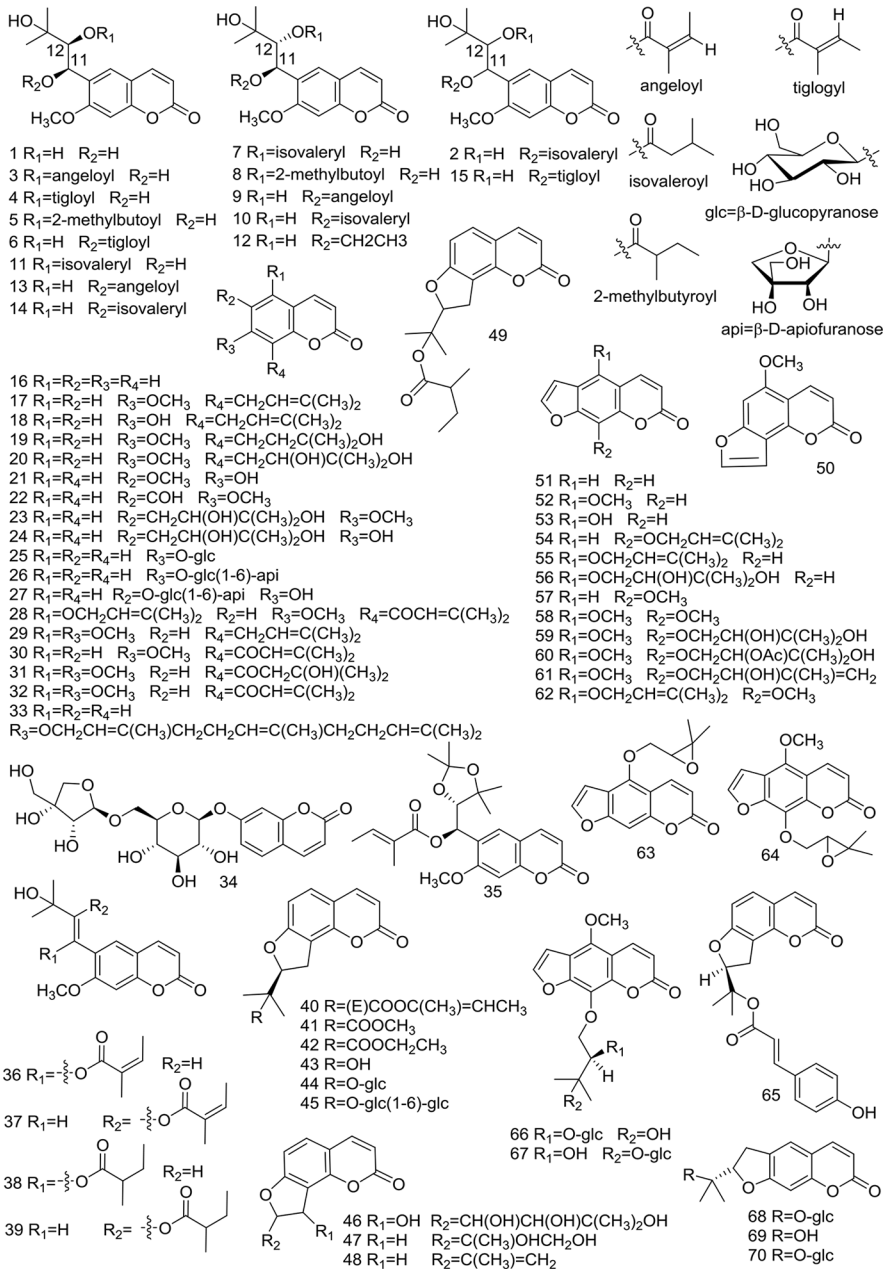


**FIGURE 2 |** Structures of coumarins **(1–70)** isolated from medicinal plants as APR.

been reported to be an anesthetic with antifungal activity. It also exhibits prominently inhibitory effects on 5-LO with an $IC_{50}$ value of 9.4 μM, and moderate inhibitory activity on COX-1 with an $IC_{50}$ value of 66 μM (Liu et al., 1998a). The chemical structures of the polyene-alkynes are shown in **Figure 3**.

## Phenolic Acids

Three phenolic acids (**73–75**) have been isolated from the root of *A. biserrata*. Since phenolic hydroxyl groups replace their structure, these compounds are unstable and thus easily transformed by water, temperature, light, enzymes, acids, and alkalis (Lin et al., 2017). The chemical structures of the phenolic acids are shown in **Figure 3**.

## Steroids

Two steroids (**76**, **77**) have been isolated from the root and rhizome of *A. biserrata*. They represent fused tetracyclic compounds composed of three hexacyclohexane (A, B, C) and

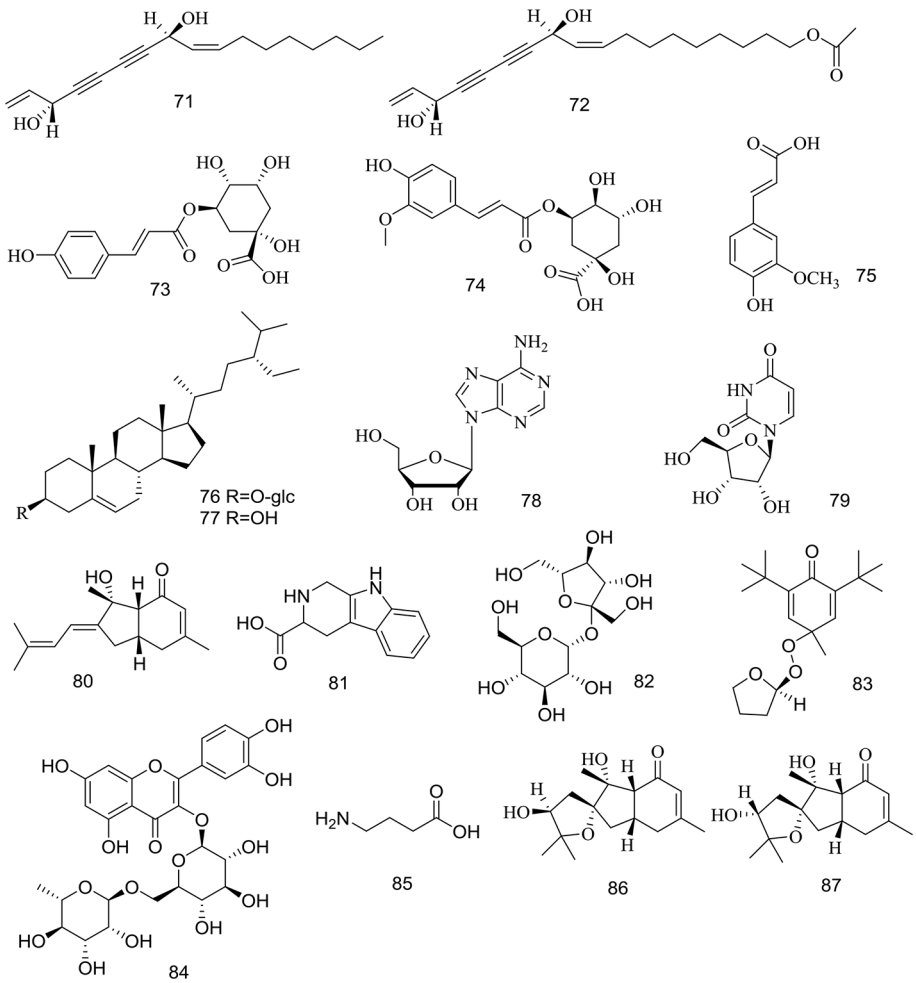


**FIGURE 3 |** Structures of polyene-alkynes **(71, 72)**, phenolic acids **(73–75)**, steroids **(76–77)** and others **(78–87)** isolated from medicinal plants as APR.

a five-carbon ring (D). In addition, $\beta$-sitosterol (**77**) is a phytosterol that is common in higher plants. The chemical structures of the steroids are shown in **Figure 3**.

## Other Compounds

Apart from the ingredients above, other compounds have been isolated and identified from *A. biserrata* and *A. pubescens*. Two nucleosides, including adenosine (**78**) and uridine (**79**), have been isolated from the root or rhizome of *A. biserrata*. Bisabolangelone (**80**) has been isolated from *A. pubescens* for the first time with strong anti-feeding properties against insects but it's been reported to be unstable in both basic and acidic media (Liu et al., 1998a). In addition, 2, 3, 4, 9-Tetrahydro-1H-pyrido [3, 4-b] indole-3-carboxylic acid (**81**) and Sucrose (**82**) were isolated from the plant for the first time in 1994 (Liu et al., 1994). A new furan, angepubefurin (**83**), was determined by HR-FTICR-MS and X-ray diffraction analyses (Yang et al., 2009). Rutin (**84**) and $\gamma$-aminobutyric acid (**85**) have also been isolated and identified in succession (Li et al., 1989a; Yang, 2007). Both new sesquiterpenoid derivatives (**86**) and (**87**) could moderately inhibit the inflammatory reaction. The beneficial elements Ca, Mg, and K in APR have been determined by LIBS spectra and the artificial neural network method (Wang et al., 2018a). The chemical structures of other compounds are shown in **Figure 3**.

# PHARMACOLOGY

The study of pharmacological activities has indicated that APR has proven to have positive effects as an analgesic and anti-inflammatory agent, which are important for RA treatment strategies. Other reported functions of APR include effects on the central nervous system, effects on the cardiovascular system, deworming activity. The main pharmacological activities of the extracts or isolated compounds from APR that have been reported in animal and *in vitro* studies are summarized in **Table 4**.

**TABLE 4 |** The pharmacological activities of APR extracts or certain ingredients.

| Compounds or extracts | Assay | Effect | Reference |
|---|---|---|---|
| **ANALGESIC AND ANTI-INFLAMMATORY ACTIONS** | | | |
| CRAB (1.10 g/ml) | Male SD rats; SNI model of neuropathic pain; 20 mg/kg/d *i.g.*, 14 d | Levels of TNF-$\alpha$, IL-1$\beta$ and IL-6↓, expression of TRPV1 and pERK↓; $ID_{50}$: 10.28 mg/kg | Li et al., 2017 |
| Columbianetin | LPS-stimulated human peripheral blood mononuclear cell model, *in vitro*; 0, 10, 20, 40 μg/ml, 4 h | TNF-$\alpha$, IL-6, MCP-1, and IL-1$\beta$↓, activity of NOD1, RIP2, and NF-$\kappa\beta$↓, NOD1/NF-$\kappa\beta$ pathways were blocked by ML130 | Lu et al., 2018 |
| ERAB (0.82 g/ml) | LPS-induced inflammation model, *in vitro*; 1, 5, 25 mg/L, 6 h | Activity of NAAA↓, PEA↑, TNF-$\alpha$, iNOS and IL-6↓, TNF-$\alpha$, NO↓ | Sun et al., 2011 |
| **EFFECTS ON THE CENTRAL NERVOUS SYSTEM** | | | |
| WRAB (0.365 g/ml) | Male Wister rats; Rat model of AD induced by intracerebral injection of A$\beta_{1\text{-}40}$; 2 ml/d *i.g.*, 28 d | IL-4↑, TNF-$\alpha$↓ | Zhu et al., 2009 |
| WRAB | Male Wister rats; Rat model of AD induced by intracerebral injection of A$\beta_{1\text{-}40}$; 2 ml/d *i.g.*, 28 d | Expression of p38 mitogen-activated protein kinases↓ | Zhang and Du, 2010 |
| WRAB and ARAB (1.10 g/ml) | Male and female Kunming mice; D-galactose brain aging model; 2.7, 8.1, 24.3 g/kg/d *i.g.*, 8 w | Phosphatidylcholine (PC)↑, sphingomyelin (SM)↓, SM/PC↓, IL-2↑ | Jin et al., 2003 |
| CRAB (purity 95.8%) | C57BL/6 mice; A$\beta$-induced neurons damage; 10, 50, 100, 150, 250 mg/ml, 24 h | Expressions of Phosphorylation of CREB and brain-derived neurotrophic factor (BDNF)↑; The optimal dose: 100 mg/ml | Yan et al., 2016 |
| WRAB (1 g/ml) | Male Wister rats; Rat model of VD; 0.3125 ml/100g/d, 28 d | Expressions of MDA↓, SOD↑ | Weng et al., 2012 |
| WRAB | Male Wister rats; AD model induced by A$\beta_{1\text{-}40}$ protein and VD model of persistent bilateral ligation of bilateral common carotid arteries; 3.125 g/kg/d, 28 d | IL-4↑, TNF-$\alpha$↓ | Wang et al., 2011a |
| RAB extracts of 95% ethanol, petroleum ether, ethyl acetate and petroleum ether-ethyl acetate | SH-SY5Y cells injury induced by hydrogen peroxide, *in vitro*; 10, 50, 100, 250, 500 mg/L, 24 h | SOD↑, MDA↓, level of BDNF and nerve factor-3↑; The optimal dose of APR 95% ethanol and petroleum ether extracts: 500 mg/L, the optimal dose of APR ethyl acetate and petroleum ether-ethyl acetate extracts: 250 mg/L | Hu et al., 2013a |
| Osthole (> 98% purity) | BM-NSCs against injury induced by hydrogen peroxide lactate dehydrogenase leakage, *in vitro*; 0, 10, 50, and 100 μM, 24h | The expression ratio of Bcl2-associated X/B-cell lymphoma-2 mRNA↓, increase phosphorylation of CREB and PI3K↑ | Yan et al., 2017 |
| **THE EFFECT ON THE CARDIOVASCULAR SYSTEM** | | | |
| ARAB | MTT, *in vitro*; 3.75, 7.5, 15, 30 μg/ml, 48 h | HUVEC proliferation, migration and tubule formation↓, HUVEC apoptosis↑ | Hu et al., 2013b |
| Osthole | MTT, *in vitro*; 3.75, 7.5, 15, 30 μg/ml, 24 h | HUVEC proliferation, migration and tubule formation↓, HUVEC apoptosis↑ | Hu et al., 2013b |
| Osthole (> 99% purity) | Male Wister rats, *in vitro*; Isolated pulmonary arteries model; $10^{-9}$ M to $10^{-5}$ M | NO↑, Akt and eNOS↑, phosphorylations of Akt at Phospho-Akt and eNOS at Phospho-eNOS in endothelial cells↑ | Yao et al., 2013 |

*APR, Angelicae Pubescentis Radix.*

## Analgesic and Anti-Inflammatory Actions

APR is a high-frequency drug for the treatment of RA, which is an autoimmune disease requiring the use of analgesics and anti-inflammatory medicines to alleviate the associated pain. Some molecules, including extracellular signal-regulated kinase 1/2, arylhydrocarbon receptor, Histone h3, prostaglandin E receptor 2, nuclear factor κappa $\beta$ (NF-$\kappa\beta$), programmed cell death 5, interleukin (IL)-36, IL-10, IL-4, Hypoxia Inducible Factor 1A, and arachidonate 15-lipoxygenase, are common molecular targets related to APR and RA, with the Eicosanoid signaling pathway the common pathway of APR and RA (Jia et al., 2015).

In TCM, the crude water extract of the root of *A. biserrata* (RAB) is considered a selective and effective herbal agent in attenuating persistent hindpaw inflammation and hyperalgesia in rats (Wei et al., 1999). RAB consisting of 60% ethanol extract (1.5 g/kg, *i.g.*) significantly inhibits inflammation in three models, including xylene-induced mouse ear edema test, the mice pettitoes swelling by egg white test and mouse tampon granulation swelling test (Li et al., 2013). However, the methanol-, chloroform-, and ethyl acetate extracts from the root of *A. pubescens* not only effectively reduced pain that was induced by 1% acetic acid and a hot plate, but also reduced the edema that was induced by 3% formalin or 1.5% carrageenan (Chen et al., 1995).

The analgesic effect of coumarins isolated from RAB (CRAB, 20 mg/kg, *i.g.*) is mediated by inflammatory factors and transient receptor potential cation channel 1 (TRPV1) as evidenced by a spared nerve injury (SNI) model of neuropathic pain. Molecular profiling has revealed that CRAP reduces levels of the proinflammatory cytokines tumor necrosis factor-$\alpha$ (TNF-$\alpha$), IL-1$\beta$, and IL-6 and significantly attenuates the expressions of TRPV1 and phosphorylated extracellular regulated protein kinases (pERK) in damaged dorsal root ganglion neurons (Li et al., 2017).

Four coumarins (10 mg/kg, *i.p.*), including columbianadin (**40**), columbianetin acetate (**41**), bergapten (**52**) and umbelliferone (**16**), have been demonstrated to have significant anti-inflammatory and analgesic activities. While the coumarins osthole (**17**) and xanthotoxin (**57**) appear to only have anti-inflammatory activity, isoimperatorin (**55**) demonstrates only an

analgesic effect. Columbianetin (**43**) inhibits the production of inflammatory cytokines induced by lipopolysaccharide (LPS), which is involved in the downregulation of nucleotide-binding and oligomerization domain 1 (NOD1)/NF-$\kappa\beta$ pathways (Lu et al., 2018). The methanol extract from the root of *A. pubescens* have inhibitory activities on rat hind paw edema induced by carrageenan and on writhing induced by acetic acid in mouse, and the active principle was isolated and identified as osthol (Kosuge et al., 1985). The anti-inflammatory and analgesic constituents from *A. pubescens* appear to be related to the peripheral inhibition of inflammatory substances and to have influences on the central nervous system (Chen et al., 1995).

The essential oil from RAB (ERAB) has anti-inflammatory and analgesic effects (Fan et al., 2009). The effect of EAPR on inflammation is mediated by the inhibition of N-acylethanolamine-hydrolyzing acid amidase (NAAA) activity, which increases cellular endobioactor N-palmitoylethanolamine (PEA) levels while decreasing proinflammatory factor (Sun et al., 2011).

## Effects on the Central Nervous System

Brain aging is a neurodegenerative disease, which is incurable debilitating disorders characterized by structural and functional neuronal loss. The primary disease of brain aging is dementia, which includes VD, AD, and a mixed type of both (Wang et al., 2011a). Free radical damage and immune inflammatory mechanisms have been recognized in current research regarding the mechanisms of brain aging. Because of its large oxygen load, the brain becomes the most vulnerable target of oxygen free radicals, which can damage the central nervous system through a variety of processes, including causing the necrosis or apoptosis of nerve cells (Jin et al., 2003).

A water maze test on mice of a D-galactose-induced brain aging model was performed to study the ability of learning and memory (Jin et al., 2003). The authors found that RAB and its alcohol extract at 18 mg/kg/d can repair the membrane phospholipid structure in different parts of the mouse cerebral cortex and striatum, as well as improve the IL-2 content of aging model mice and resist free radicals and inflammatory damage, thereby improving the learning and memory ability of mice (Pei et al., 2005). From the perspective of inhibiting the apoptotic rate of brain tissue cells, the mechanism of RAB water decoction and its alcohol extract in retarding brain aging was revealed.

RAB and/or its water decoction (2 ml/d, *i.g.*) have an inhibitory effect on the inflammatory response of AD model rats induced by Human amyloid beta peptide 1–40 ($A\beta_{1\text{-}40}$), thus improving the learning and memory ability of AD model rats (Zhu et al., 2009; Zhang and Du, 2010). The water decoction of RAB (1.08 mg/ml, *i.g.*) can improve the positioning and learning and memory ability of model rats, shortening the time to navigate the water maze (Du et al., 2009). CRAB (purity 95.8%) possess neuroprotective effects in A$\beta$ damaging neuron (Yan et al., 2016). In addition, CRAB (purity 72.4%, 14.4 mg/kg, *i.g.*) can significantly protect amyloid precursor protein/presenilin-1 (APP/PS1) mice from neural damage, likely through improving Neurofilament tirplet M expression and reducing apoptotic cells in the brain of APP/PS1 transgenic mice (Jiao et al., 2014). Moreover, the water decoction of RAB (3.125 g/kg, *i.g.*) can inhibit the expression of malondialdehyde (MDA) in rat serum and increase the activity of Superoxide dismutase (SOD) in order to inhibit free radical damage in VD model rats (Weng et al., 2012). Finally, APR has a regulating effect on immune inflammatory injury in AD and VD rats, particularly for the treatment of VD (Wang et al., 2011a). Extracts, including 95% ethanol, petroleum ether, ethyl acetate, and petroleum ether-ethyl acetate extracts of RAB do not appear to be toxic to SH-SY5Y cells. All of these may increase cell viability and exert antioxidant activity induced by $H_2O_2$ in SH-SY5Y cells, whereas the neuroprotective effects of the petroleum ether-ethyl acetate extract have been shown to be the strongest (Hu et al., 2013a). Osthole (**17**) protects bone marrow-derived neural stem cells (BM-NSCs) from oxidative damage through the phosphatidylinositol 3 kinase (PI3K)/protein kinase B (Akt-1) pathway, and it has been shown to improve the inflammatory environment of neurodegenerative diseases and promote the survival rate of transplanted NSCs (Yan et al., 2017).

## Effects on the Cardiovascular System

$\gamma$-aminobutyric acid (**85**) (10 mg/kg, *i.v.*) isolated from the water extract of RAB (WRAB) showed that it can treat a variety of empirical cardiac arrhythmias, with effects on the action potential of rat neoventricular muscle (Li et al., 1989a). The alcohol extract of RAB (ARAB) and WRAB both have anti-angiogenic effects (Zou et al., 2008; Hu et al., 2013b). Osthole (**17**) isolated from ARAB inhibits angiogenesis *in vitro* more strongly than that in the ARAP, indicating that it may be the main antiangiogenic component of ARAB, and its mechanism may be related to the inhibition of human umbilical vein endothelial cell (HUVEC) proliferation, migration and tubule formation, the induction of HUVEC apoptosis, and the arrest of HUVEC cell cycle (Hu et al., 2013b). ARAB inhibits platelet aggregation and platelet thrombosis in circulating blood (Meng et al., 1988; Li et al., 1989b). Columbianetin (**43**), columbianetin acetate (**41**), columbianadin (**40**), osthol and columbianetin-$\beta$-D-glucopyranoside (**44**) also have inhibitory effects on rat platelet aggregation induced by ADP *in vitro* (Li et al., 1989b).

Pulmonary arterial hypertension (PAH) is a progressive cardiovascular-disease with high mortality lacking high-efficiency drug. Excitingly, osthole (**17**) extracted from RAB was observed to significantly restore 98 of 315 differential proteins significantly modified by PAH progression (Yao et al., 2018). What's more, osthole (**17**) extracted from the root of *A. pubescens* has been shown to suppress tracheal smooth muscle contraction, exerting a non-specific relaxant effect on the trachealis by inhibiting cAMP and cGMP phosphodiesterases (Teng et al., 1994). However, its dilative effect is dependent on endothelial integrity and NO production, and is mediated by the endothelial PI3K/Akt- endothelial NO synthase (eNOS)-NO pathway (Yao et al., 2013). These findings may provide candidates for a new pulmonary vasodilator for the therapy of PAH.

## Deworming Activity

RAB extracts using different solvents have quite different effects on treating ring worm. ARAB exhibited the best anthelmintic

efficacy with 100% mortality of dactylogyrus and no death of the fish at the optimal anthelminthic concentration of 120 mg/L (Wang et al., 2011c; Xie et al., 2016). Osthole (**17**) can reach the 100% parasiticidal rate when the concentration was 1.6 mg/L, with no toxicity to fish at a dose up to 6.2 mg/L. As for scopoletin (**21**), 5 mg/L appears to represent a parasiticidal rate of 74.9% (Wang et al., 2011c; Wang et al., 2012).

### Others

Osthole (**17**) also shows osteopromotive effects on osteoblasts both *in vitro* and *in vivo*. Osthole (**17**) -mediated osteogenesis is related to the activation of the cAMP/cAMP response element-binding protein (CREB) signaling pathway and downstream osterix expression (Zhang et al., 2017). N-hexane and dichloromethane extracts of RAB show inhibitory effects on COX-1 and 5-LO. Linoleic acid appears to be the most active constituent in the extract, exerting COX-1 inhibition, and also has strong inhibitory activity on 5-LO, which is similar to osthole (**17**) (Liu et al., 1998b).

## PHARMACOKINETIC

So far, few pharmacokinetic studies on APR have been done, which mainly focus on coumarins. What's more, only medicinal plants *A. biserrata* have been studied. The main pharmacokinetic researches of the extracts or isolated compounds from APR that have been reported studies in animal are discussed below.

Four of the coumarins [columbianetin acetate (**41**), imperatorin (**54**), isoimperatorin (**55**), and osthole (**17**)] were rapidly absorbed, while the remaining three coumarins [psoralen (**51**), bergapten (**52**), and xanthotoxin (**57**)] were slowly absorbed in rat plasma after oral administration of APR extract (6.0 g/kg) (Chang et al., 2013). To assess the brain distributions and blood-brain barrier permeabilities of APR, a UPLC-MS/MS method was applied to the simultaneous determinations of the main coumarins in the rat cerebrospinal fluid (CSF) and brain after oral administration of APR extract (4 g/kg), including psoralen (**51**), xanthotoxin (**57**), bergapten (**52**), isoimperatorin (**55**), columbianetin (**43**), columbianetin acetate (**41**), columbianadin (**40**), oxypeucedanin hydrate (**56**), angelol B (**4**), osthole (**17**), meranzin hydrate (**20**), and nodakenetin (**69**). Most of the tested coumarins entered the rat CSF and brain quickly, and double-peak phenomena in concentration-time curves were similar to those of their plasma pharmacokinetics. Columbianetin (**43**) had the highest concentration in the CSF ($C_{max}$: 485.36 ± 91.40 μg/L, $AUC_{0\rightarrow\infty}$: 4142.82 ± 602.33 μg/L/h) and brain, while psoralen (**51**) and columbianetin acetate (**41**) had the largest percent of CSF/plasma and brain/plasma. (Yang et al., 2018). Under the administration mode and dose as above, columbianetin (**43**) was also easier to absorbed compound across caco-2 cell, and also had extremely highest plasma concentration (2000 ng/ml) *in vivo* (Yang et al., 2017). The pharmacokinetic properties of columbianetin (**43**) in rat after oral administration were characterized as rapid oral absorption, quick clearance and good absolute bioavailability. Columbianetin (**43**) showed dose proportionality over the dose range 5–20 mg/kg. The bioavailability of columbianetin (**43**) is independent of the doses studied (Luo et al., 2013).

The tissues distributions research after oral administration of APR extract (6.0 g/kg) to rat, four coumarins [columbianetin (**43**), columbianetin acetate, (**41**) osthole (**17**), columbianadin (**40**)] were in the liver, followed by the ovary, uterus, kidney, lung, heart, spleen, and muscle (Ge et al., 2019). The AUC and $C_{max}$ of bisabolangelone (**80**) after oral administrated pure bisabolangelone (**80**) are higher than those after oral administrated APR extract. Among them, there are significant differences on AUC between pure bisabolangelone (**80**) (7.5 mg/kg *i.g.*) and APR extract (equivalent to bisabolangelone (**80**) at dose of 7.5 mg/kg, *i.g.*). For tissue distribution, the amount of bisabolangelone (**80**) mainly appeared in heart, liver and spleen. Bisabolangelone (**80**) appearance in the brain also revealed that bisabolangelone (**80**) could pass the blood-brain barrier. (Ge et al., 2018).

A sensitive LC-MS/MS method has been validated to determine the concentration of columbianadin (**40**) in rat plasma after intravenous administration of columbianadin (**40**) (1, 2.5 and 5 mg/kg). The results show that the distribution half-life ($T_{1/2\alpha}$) were 0.027 0.016, 0.060 0.065, and 0.028 0.023 h, and the elimination half-lives ($T_{1/2\beta}$) were 0.58 0.20, 0.52 0.25, and 0.52 0.22 h (Chang et al., 2014). After oral administration of pure columbianadin (**40**), approximately 0.12% columbianadin (**40**) was transformed into columbianetin (**43**). Oral administration of pure columbianadin (**40**) may be more beneficial for the clinical efficacy of columbianadin (**40**) (25 mg/kg) than APR extract (3.74 g/kg). Pure columbianadin (**40**) group: $T_{max}$: 3.03 ± 1.87 h, $C_{max}$: 1.82 ± 0.64 ng/ml, $AUC_{(0\text{-}tn)}$: 1.05 ± 1.02 ng/ml/h; APR extract group: $T_{max}$: 0.55 ± 0.33 h, $C_{max}$: 13.33 ± 25.37 ng/ml, $AUC_{(0\text{-}tn)}$: 28.80 ± 41.46 ng/ml/h (Li et al., 2018).

Columbianetin acetate (**41**) and columbianetin-$\beta$-D-glucopyranoside (**44**, CBG) were rapidly and widely distributed in rats, and eliminated rapidly from plasma. Columbianetin acetate (**41**) could be metabolized into columbianetin (**43**) *in vivo*. Absolute bioavailability of pure columbianetin acetate (**41**) is 7.0 ± 4.3%. Other co-existing ingredients in APR extract could increase the concentration of its metabolite columbianetin (**43**) in plasma and this was caused by CBG (**44**). Cumulative excretion of columbianetin acetate (**41**) in urine accounted for 0.0109 ± 0.0067% of total dosage. The cumulative amounts of columbianetin acetate (**41**) in the feces present 9.32 ± 6.63% of the total dose. Columbianetin acetate (**41**) was mainly excreted in the feces (Jiao et al., 2015). Besides, CBG (**44**) also could be catabolized into its active metabolite columbianetin (**43**) *in vivo*. The absolute bioavailability of CBG (**44**) was 5.63 ± 4.42%. The other co-existing constituents from the APR ethanol extract could enhance the absorption of CBG (**44**). CBG (**44**) and columbianetin (**43**) were rapidly and broadly distributed in the stomach, ovary, kidney, liver, spleen, lung, muscles, heart and

brain. Higher levels of accumulation of CBG (**44**) and columbianetin (**43**) were detected in the ovary and kidney tissues. Eight metabolites of CBG (**44**) were tentatively identified in blood, urine, bile and faeces of rats after oral administration of pure CBG (**44**). It was also found that CBG (**44**) and columbianetin (**43**) were mainly excreted through the faecal route (Zhang et al., 2018).

## TOXICOLOGY

In ancient and modern books of traditional Chinese medicine including with APR, there was no record of toxicity. The records of toxicity also have not been reported in clinical applications. So far, only a few toxicity tests have been conducted in animals.

In acute toxicity experiments through oral administration, mice of the Kunming species appeared to have cyanosis, agitated activity, and a quickened respiration after 10 min of taking water decoction of APR, and several mice died because of respiratory failure in serious cases. The $LD_{50}$ of mice (*i.g.*) was determined to be 7.35 ± 0.62g/kg (Duan et al., 2002). In subacute toxicity testing, WAPR has a certain nephrotoxicity, potentially inducing kidney injury through inhibiting organic anion transporters 1 (Oats1), Oat2, Oat3 (Chen et al., 2015). WAPR also can cause obvious organ toxicity to juvenile zebrafish, such as yolk sac swelling, deformation, black, pericardial edema, and bleeding, with a minimum lethal dose of 100 μg/ml at 3 days after fertilization in healthy zebrafish embryos (Chen et al., 2016). In a 90-days toxicity experiment by mouth, Wistar rats and hybrid dogs were selected. Among them, rats appeared to have cyanosis, agitated activity, and quicken respiration after 10 min of taking APR capsule; however, toxicity symptoms in the rats disappeared after 30 days of taking WAPR. At higher doses of WAPR, the rats grew slower, and pathology inspection revealed gaseous distention in the stomach and edema of mucous membrane. While there were myeline bodies in the liver cells of some rats and dogs, it appeared to be reversible. No differences in the blood and biochemistry indexes of rats and dogs were observed (Duan et al., 2002).

## QUALITY CONTROL

APR has special aromatous smell, bitter and spicy taste, and makes feeling slightly numbness of tongue. It is traditionally thought that APR with thick and fat branches, strong aroma is of good quality. From the phytochemistry and the pharmacological activity discussed above, coumarins are considered the most important constituents, demonstrating a wide range of pharmacological activities. In Chinese Pharmacopoeia (2015 edition), APR is calculated by dry product, containing osthole (**17**) at not less than 0.50% and columbianadin (**40**) at not less than 0.080%. What's more, quality control items for APR in multi-national Pharmacopoeias are listed in **Table 5**.

APR primarily contains coumarins and volatile oils as the active ingredients (Zhang et al., 2007). Near IR spectroscopy (NIRs) became a new analysis technique for the quantitative analysis of Chinese medicinal materials because of its rapid analysis speed and no need for sample pretreatment. NIRs also can achieve quantitative analysis for the quality control of osthole (**17**) and columbianadin (**40**) as indicators in APR, except for HPLC (Zhan et al., 2017). Modern pharmacological research has shown that ferulic acid (**75**) is also the main effective component, providing the effect of activating the blood. However, its content has not been used as an index in Chinese Pharmacopoeia, which is not conducive to the quality control of APR. Therefore, the method for the determination of ferulic acid (**75**) content in APR was established by reverse HPLC (Fang, 2013). Bisabolangelone (**80**), adenosine (**78**), and 30 coumarins in APR were identified by UPLC-PAD-Q-TOF-MS. The developed method could successfully be used to differentiate samples from different regions and could be a helpful tool for detection and confirmation of the quality of TCM (Ge et al., 2014). However, one or several chemical constituents are not the only effective parts of APR. The HPLC fingerprint of APR from

**TABLE 5** | Quality control items for APR in multi-national Pharmacopoeias.

| Pharmacopoeia | Identification | Water detection or Loss on drying | Ash detection | | Determination of content | |
|---|---|---|---|---|---|---|
| | | | Total ash | Acid insoluble ash | Marker components | Content requirements |
| Chinese Pharmacopoeia (version 2015) | Fragments identification and TLC | ≤10% | ≤8% | ≤3% | Osthole and columbianadin | The total content≥0.080% (dried drug). |
| British Pharmacopoeia (version BP2017) | Microscopic examination and TLC (Reference solution: (Z)-Ligustilide, Osthole and Imperatorin) | ≤10% | ≤8.0% | ≤3.0% | Osthole | The total content≥0.50% (dried drug). |
| European Pharmacopoeia (version EP9.3) | Microscopic examination and TLC (Reference solution: (Z)-Ligustilide, Osthole and Imperatorin) | ≤10% | ≤8.0% | ≤3.0% | Osthole | The total content≥0.50% (dried drug). |

*APR, Angelicae Pubescentis Radix.*

different producing areas was constructed with 21 common chromatographic peaks, and the content of columbianetin (**43**), osthole (**17**), isoimperatorin (**55**), and columbianadin (**40**) were determined in APR simultaneously (Wang et al., 2018b). The GC fingerprint of APR was also established (Jin et al., 2009).

## CONCLUSION AND FUTURE PERSPECTIVES

A significant breakthrough has been made in the last several decades in the areas of phytochemistry and pharmacology of APR. Research on phytochemistry indicated that coumarins and essential oil compounds might be the major active constituents. Crude extracts and pure compounds from the root have been shown to possess multiple biological activities, particularly analgesic and anti-inflammatory actions, as well as effects on the central nervous system. However, further study is still urgently needed to gain a better understanding of APR and its clinical use.

Firstly, 87 compounds, mainly coumarins, have been separated and identified, and more than 100 volatile components have been analyzed by GC-MS, but they were mainly separated from root of *A. biserrata*. Therefore, in further research on the phytochemistry of this plant, more attention should be focused on the others parts, such as rhizome, fruit. Besides, the water-soluble part of APR should be a major focus, because decoction is the main method of administration in the TCM clinic. The majority of pharmacological studies of APR have been conducted using crude and poorly characterized extracts. Thus, bioactivity-guided isolation strategies could be used to study the chemicals underlying the pharmacological activity. To illustrate the scientific significance of medicines' using, network pharmacology should be used to predict drug targets and the possible molecular mechanisms involved. Then experiments should be further conducted to prove whether the targets and signal path works.

Secondly, studies on pharmacological effects and its mechanisms mainly focus on several coumarins, and the inherent relations between them and the mechanism of treatment of disease have not been explicit enough. More relationships between the chemical composition and pharmacological activity should be established to further explain the principle of disease treatment. Moreover, the pathways of their distribution, absorption, metabolism, and excretion need to be further clarified with pharmacokinetic studies.

Thirdly, records of toxicity were rarely recorded in ancient clinical applications; however, modern pharmacological research has related acute toxicity in animal experiments. Meanwhile, it should be noticed that most pharmacological studies on APR have only been conducted in animal models, cell models, and other *in vitro* experiments. Therefore, comprehensive placebo-controlled and double-blind clinical trials should be undertaken to provide remarkable evidence for these positive findings on the efficacy of APR in the future. In addition, the exact mechanisms of many medicinal properties of this herb still remain vague to date; thus, additional studies to better identify the functions and molecular targets seem to be necessary.

Next, the result of the research on plant resources found that *A. biserrata* had been mistaken as *A. pubescens* in China. At present, *A. pubescens* is only a medicinal plant for local use with a few researches, and the specific difference between the two medicinal plants in clinical use have not been mentioned. In order to standardize the use of traditional Chinese medicine, it is necessary to study the specific differences in the clinical use and pharmacological effect of the two medicinal plants.

Lastly, the natural resources of APR are limited, and the demand is increasing year by year. Since April 2018, the State Administration of Traditional Chinese Medicine of the People's Republic of China issued a list of Chinese classical prescriptions (first batch), in which six prescriptions contain APR. This means that the needs of APR will continue to grow. In the course of the determination of the content, our laboratory collected some unqualified cultivation products, so we considered that it might be caused by irregular planting methods. So, the safe, high quality and high efficiency planting technology of this unique living plant needs to be further studied in order to guide the production of TCM.

In summary, APR has been successfully used in clinical practice to treat rheumatic disease as an anodyne for thousands of years. Indeed, modern pharmacological studies have shown that it has effective analgesic and anti-inflammatory actions, as well as effects on the central nervous system. The linkage between traditional uses and modern scientific studies, safety, and efficacy were done on this herb ensuring its clinical use and application.

## AUTHOR CONTRIBUTIONS

YL and HW searched the literature, collected the data, and drafted the manuscript. YL and ZW contributed to analysis and manuscript preparation. XY, XZ, and HL helped in checking the chemical structures and formula. YL and LT downloaded the documents and made classification. ZW and LT contributed comments for a version of the manuscript. All authors read and approved the final manuscript.

## FUNDING

The work was supported by grants from the National Key Research and Development Plan (2018YFC1707106), the Key Research and Development Plan of Shandong Province in 2018 (No. 2018CXGC1305) and National Science and Technology Major Projects for "Major New Drugs Innovation and Development" (2019ZX09201005). Basic scientific research project of the Institute of Chinese Materia Medica, China Academy of Chinese Medical Science (ZXKT17014).

## ACKNOWLEDGMENTS

We acknowledge the Institute of Chinese Materia Medica, China Academy of Chinese Medical Science for providing support and assistance for this review article. And the authors are grateful to Enago for providing language assistance and grammar check.

## REFERENCES


Awale, S., Nakashima, E. M., Kalauni, S. K., Tezuka, Y., Kurashima, Y., Lu, J., et al. (2006). Angelmarin, a novel anti-cancer agent able to eliminate the tolerance of cancer cells to nutrient starvation. *Bioorg. Med. Chem. Lett.* 37, 581–583. doi: 10.1016/j.bmcl.2005.10.046

Baba, K., Matsuyama, Y., Ishida, T., Inoue, M., and Kozawa, M. (1982). Studies on coumarins from the root of *Angelica pubescens* Maxim. V. Stereochemistry of angelols A-H. *Chem. Pharm. Bull.* 30, 2036–2044. doi: 10.1248/cpb.30.2036

Chang, Y., Zhang, Q., Li, J., Zhang, L., Guo, X., He, J., et al. (2013). Simultaneous determination of scopoletin, psoralen, bergapten, xanthotoxin, columbianetin acetate, imperatorin, osthole and isoimperatorin in rat plasma by LC-MS/MS for pharmacokinetic studies following oral administration of Radix Angelicae Pubescentis extract. *J. Pharm. Biomed.* 77, 71–75. doi: 10.1016/j.jpba.2012.12.031

Chang, Y., Wang, C., Li, J., Bai, Y., Luo, Q., He, J., et al. (2014). LC–MS/MS determination and pharmacokinetic study of columbianadin in rat plasma after intravenous administration of pure columbianadin. *Chem. Cent. J.* 8 (1), 64. doi: 10.1186/s13065-014-0064-1

Chen, Y. F., Tsai, H. Y., and Wu, T. S. (1995). Anti-inflammatory and analgesic activities from roots of *Angelica pubescens*. *Planta Med.* 61, 2–8. doi: 10.1055/s-2006-957987

Chen, S., Qi, J., Yu, W., Wang, Y., Lin, M., and Zhang, N. (2015). Effects of 10 kinds of nephrotoxic TCM on kidney organic anion transporter in mice. *China Pharm.* 26, 2673–2676. doi: 10.6039/j.issn.1001-0408.2015.19.25

Chen, Y., Wang, J., Chen, S., Jing, L., and Wei, Y. (2016). Screening on toxicity of 26 kinds of common orthopedic herbal medicine using Zebrafish model. *J. Nanjing Univ. Tradit. Chin. Med.* 32, 465–469. doi: 10.14148/j.issn.1672-0482.2016.0465

Committee for the Pharmacopoeia of PR China (2015). *Pharmacopoeia of the People"s Republic of China, Part1* (Beijing, China: China Medical Science Press), 263.

Ding, X., Feng, X., Dong, Y., Zhao, X., Chen, Y., and Wang, M. (2008). Studies on chemical constituents of the roots of *Angelica pubescens*. *Chin. Med. Mat.* 31, 516–518. doi: 10.3321/j.issn:1001-4454.2008.04.017

Ding, X., Feng, X., Dong, Y., Zhao, X., Chen, Y., and Liang, Y. (2009). Studies on the constituents of coumarins from Duhuo. *Chin. Tradit. Pat. Med.* 31, 1102–1104. doi: 10.3969/j.issn.1001-1528.2009.07.036

Du, J., Gao, S., Wang, C., Yang, X., Liu, Y., and Wang, B. (2009). Duhuo's effect on the positioning navigation ethology of the AD model rat. *J. Liaoning Univ. Tradit. Chin. Med.* 36, 144–145. doi: 10.13192/j.ljtcm.2009.01.148.dujg.064

Duan, Z., Zhang, Y., Li, H., Wang, J., Zhang, L., and Sheng, W. (2002). The research on acute and long-time toxicity of Angelicaroot Capsule. *J. Shenyang Pharm. Univ.* 4, 4–9. doi: 10.3969/j.issn.1008-2344.2002.01.002

Fan, L., Li, L., and He, H. (2009). Pharmacological studies on anti-inflammatory and analgesic effects of Radix Angelicae Pubeascentis' s volatile oil. *Anhui Med. Pharm. J.* 13, 133–134. doi: 10.3969/j.issn.1009-6469.2009.02.007

Fang, Y. (2013). Ferulic acid content of *Angelica pubescens* in Three Gorges Reservoir area. *Med. Plant* 4, 38–40.

Gao, X. M. (2007). *Science of Chinese materia medica*. (Beijing, China: China Press of Traditional Chinese Medicine), 651–653.

Ge, A., Ma, W., Wang, C., Li, J., He, J., Liu, E., et al. (2014). Ultra-high-performance-liquid chromatography with photodiode array detector and quadrupole time-of-flight tandem mass spectrometry coupled with discriminant analysis to evaluate Angelicae Pubescentis Radix from different regions. *J. Sep. Sci.* 37, 2523–2534. doi: 10.1002/jssc.201400289

Ge, Y., Li, Z., Zhang, L., Li, J., He, J., Hao, J., et al. (2018). Pharmacokinetics and tissue distribution study of bisabolangelone from Angelicae Pubescentis Radix in rat using LC–MS/MS. *BioMed. Chromatogr.* 33, e4433. doi: 10.1002/bmc.4433

Ge, Y., Chen, S., Luo, Q., Wang, C., Hao, J., He, J., et al. (2019). The tissue distribution of four major coumarins after oral administration of Angelicae Pubescentis Radix extract to rats using ultra-high-performance liquid chromatography. *Evid.-Based Complementary Altern. Med.* 2019, 8. doi: 10.1155/2019/2365697

Hata, K., and Kozawa, M. (1965). The constitution of angelol, a new coumarin isolated from the root of *Angelica pubescens* Maxim (umbelliferae). *Tetrahedron Lett.* 6 (50), 4557–4562. doi: 10.1016/S0040-4039(01)89063-8

Hata, K., and Tanaka, Y. (1957). Study on the chemical components of umbelliferous plants. III. Components of the root of *Angelica pubescens* Maxim (1). *Yakugaku Zasshi J. Pharm. Soc. Japan* 77, 937–940. doi: 10.1248/yakushi1947.77.9_937

Hata, K., Nishino, T., Hirai, Y., Wada, Y., and Kozawa, M. (1981). On Coumarins from the fruits of *Angelica pubescens* Maxim. *Yakugaku Zasshi J. Pharm. Soc. Japan* 101, 67–71. doi: 10.1248/yakushi1947.101.1_67

Hu, Y., Zhao, D., Zhang, X., Sun, D., Hao, H., and Yang, J. (2013a). Different extracts of *Angelica pubescens* inhibit $H_2O_2$-induced SH-SY5Y cells injury. *Chin. J. Exp. Tradit. Med. Form.* 19, 184–188. doi: 10.11653/syfj2013240184

Hu, J., Lin, L., Qian, X., Liu, B., Zhang, G., Hu, W., et al. (2013b). Experimental study of *Angelica pubescens* and osthole isolated from *Angelica pubescens* inhibiting angiogenesis *in vitro*. *J. Mod. Oncol.* 21, 1945–1949. doi: 10.3969/j.issn.1672-4992.2013.09.11

Institute of Materia Medica, Chinese Academy of Medical Sciences (1959). *Chinese medicinal records, Volume II* (Beijing, China: People's Medical Publishing House), 345–352.

Jia, D., He, X., Jiang, M., Yi, X., Zhao, N., Tan, Y., et al. (2015). Prediction of molecular mechanism of Radix Angelicae Pubescentis in treatment of rheumatoid arthritis by network pharmacology. *J. Liaoning Univ. Tradit. Chin. Med.* 42, 1838–1841. doi: 10.13192/j.issn.1000-1719.2015.10.005

Jiao, Y., Hu, Y., Zhao, D., Sun, D., Hao, H., and Yang, J. (2014). The neuroprotective effect of total coumarins of Angelica Pubescentis on APP/PS1 double transgenic AD model mouse. *Chin. Med. Pharmaco Clinic.* 30, 67–70. doi: 10.13412/j.cnki.zyyl.2014.05.022

Jiao, X., Li, J., Yu, X., Liu, W., Tian, J., He, J., et al. (2015). The pharmacokinetics, bioavailability and excretion of columbianetin acetate and its metabolite columbianetin were analysed in rat plasma by LC-MS/MS after administration of columbianetin acetate and Angelicae Pubescentis Radix extract. *RSC Adv.* 5, 95882–95893. doi: 10.1039/C5RA13961A

Jin, H., Li, D., and Sun, S. (2003). Experimental research into the mechanism in delaying brain aging process by *Angelica pubescens* and its alcohol extractive. *Shanghai J. Tradit. Chin. Med.* 37, 54–56. doi: 10.3969/j.issn.1007-1334.2003.11.025

Jin, H., Chen, X., Zhang, S., Li, Q., and Bi, K. (2009). Establishment of chromatographic fingerprint and dentification of Rhizoma et Radix Notopterygii and Radix Angelicae Pubescentis by GC. *J. Shenyang Pharm. Univ.* 26, 369–375. doi: 10.14066/j.cnki.cn21-1349/r.2009.05.007

Kosuge, T., Yokota, M., Sugiyama, K., Yamamoto, T., Mure, T., and Yamazawa, H. (1985). Studies on Bioactive Substances in Crude Drugs Used for Arthritic Diseases in Traditional Chinese Medicine. II. Isolation and Identification of an Anti-inflammatory and Analgesic Principle from the Root of *Angelica Pubescens* Maxim. *Chem. Pharm. Bull.* 33, 5351–5354. doi: 10.1248/cpb.33.5351

Kozawa, M., Baba, K., Matsuyama, Y., and Hata, K. (1980). Studies on coumarins from the root of *Angelica pubescens* Maxim. III. Structures of various coumarins including angelin, a new prenylcoumarin. *Chem. Pharm. Bull.* 28, 1782–1787. doi: 10.1248/cpb.28.1782

Li, R., He, Y., Zhang, Q., Meng, J., Wang, L., and Gu, Y. (1989a). Study on γ-aminobutyric acid, an antiarrhythmic active component of traditional Chinese medicine Duhuo. *J. Beijing Med. Univ.* 21, 376.

Li, R., He, Y., Qiao, M., Xu, Y., Zhang, Q., Meng, J., et al. (1989b). Studies of the active constituents of the Chinese drug Duhuo *Angelica pubescens*. *Acta Pharm. Sin.* 24, 546–551.

Li, X., Wang, J., and Gao, L. (2013). Anti-inflammatory and analgesic activity of R.A.P. (Radix Angelicae Pubescentis) ethanol extracts. *Afr J. Tradit. Complem.* 10, 422–426. doi: 10.4314/ajtcam.v10i3.6

Li, R., Zhao, C., Yao, M., Wu, Y., Song, Y., and Wen, A. (2017). Analgesic effect of coumarins from Radix Angelicae Pubescentis is mediated by inflammatory factors and TRPV1 in a spared nerve injury model of neuropathic pain. *J. Ethnopharmacol.* 195, 81–88. doi: 10.1016/j.jep.2016.11.046

Li, J., Li, Z., Luo, Q., Wang, C., He, J., Pang, X., et al. (2018). Simultaneous determination of columbianadin and its metabolite columbianetin in rat plasma by LC-MS/MS: application to pharmacokinetics of columbianadin after oral administration. *Evid.-Based Complementary Altern. Med.* 2018, 8. doi: 10.1155/2018/8568303

Li, M., Wen, J., Ni, F., Xue, X., Wu, Y., Wang, Z., et al. (2019). Anti-inflammatory activity of two new sesquiterpenoids from Radix Angelicae Pubescentis. *Acta Pharm. Sin.* 54 (02), 173–177. doi: 10.16438/j.0513-4870.2018-0960

Li, J. (2013). *Preparation method of oil tea emulsion from Angelica pubescens Maxim*. (China, CN103271846A: State Intellectual Property Office).

Lin, P., Jia, X., Qi, Y., and Liao, S. (2017). Advances in study on phenolic acids. *Guangdong Chem. Ind.* 44, 50–52. doi: 10.3969/j.issn.1007-1865.2017.01.025

Liu, J., and Yao, X. (1995). Studies on the chemical constituents of *Angelica pubescens* f. *biserrata* and its Anti-human platelet and Anti-inflammatory effects. *J. Shenyang Pharm. Univ.* 12, 116. doi: 10.14066/j.cnki.cn21-1349/r.1995.02.010

Liu, J., Tan, Y., Chen, Y., Xu, S., and Yao, X. (1994). Studies on the chemical constituents of *Angelica pubescence* f. *biserrata*. *Chin. Tradit. Herbal Drugs* 25, 288–291.

Liu, J., Xu, S., Yao, X., and Kobayashi, H. (1995a). Two new 6-Alkylcoumarins from *Angelica pubescens* f. *biserrata*. *Planta Med.* 61, 482–484. doi: 10.1055/s-2006-958145

Liu, J., Xu, S., Yao, X., and Kobayashi, H. (1995b). Angelol-type coumarins from *Angelica pubescence* f. *biserrata* and their inhibitory effect on platelet aggergation. *Phytochemistry.* 39, 1099–1101. doi: 10.1016/0031-9422(95)00045-9

Liu, J., Xu, S., Yao, X., and Kobayashi, H. (1996a). Studies of NMR and MS on 6- or 8-alkyl-7-oxycoumarins and dihydrofuranocoumarins. *Chin. J. Magn. Reson.* 13, 35–46. doi: 10.1007/BF02943147

Liu, J., Xu, S., Yao, X., and Wu, Y. (1996b). Further studies on chemical constituents of *Angelica pubescens* f. *biserrata*. *Acta Pharm. Sin.* 31, 63–67. doi: 10.16438/j.0513-4870.1996.01.014

Liu, J., Zschocke, S., and Bauer, R. (1998a). A polyacetylenic acetate and a coumarin from *Angelica pubescens* f. *biserrata*. *Phytochemistry.* 49, 211–213. doi: 10.1016/S0031-9422(97)00951-5

Liu, J. H., Zschocke, S., Reininger, E., and Bauer, R. (1998b). Comparison of Radix Angelicae Pubescentis and substitutes. constituents and inhibitory effect on 5-lipoxygenase and cyclooxygenase. *Pharm. Biol. (Lisse Netherlands)* 36, 207–216. doi: 10.1076/phbi.36.3.207.6343

Lu, J., Fang, K., Xiong, L., Zhang, C., Guan, X., Zheng, R., et al. (2018). Anti-Inflammatory effect of columbianetin on Lipopolysaccharide-stimulated human peripheral blood mononuclear cells. *Mediat. Inflamm.* 2018, 1–8. doi: 10.1155/2018/9191743

Luo, Q., Wang, C., Li, J., Ma, W., Bai, Y., Ma, L., et al. (2013). The pharmacokinetics and oral bioavailability studies of columbianetin in rats after oral and intravenous administration. *J. Ethnopharmacol.* 150, 175–180. doi: 10.1016/j.jep.2013.08.030

Meng, J., Gu, Y., Ge, L., Li, R., and He, Y. (1988). Effect of alcohol extract (H6F4) on platelet aggregation and experimental thrombosis. *Chin. Tradit. Herbal Drugs* 19, 23–25.

Murata, C., Masuda, T., Kamochi, Y., Todoroki, K., Yoshida, H., Nohta, H., et al. (2005). Improvement of fluorescence characteristics of coumarins: Syntheses and fluorescence properties of 6-methoxycoumarin and benzocoumarin derivatives as novel fluorophores emitting in the longer wavelength region and their application to analytical reagents. *Chem. Pharm. Bull.* 53, 750–758. doi: 10.1002/chin.200549022

Pan, J., Lamy, K., Arison, B., Smith, J., and Han, G. (1987). Isolation and identification of isoangelol, anpubesol and other coumarins from *Angelica Pubescens* Maxin. *Acta Pharm. Sin.* 22, 380–384. doi: 10.16438/j.0513-4870.1987.05.013

Pei, Y., Li, D., and Sun, S. (2005). Effects of Duhuo and its alcohol extracts on apoptosis of brain tissue in natural aging mice. *Chin. J. Gerontol.* 25 (8), 959. doi: 10.3969/j.issn.1005-9202.2005.08.044

Qian, B. (2014). *A kind of internal injury fever and Angelica pubescens Maxim health wine.* (China, CN103720991A: State Intellectual Property Office).

Rao, G., Yang, Q., and Dai, W. (1994). Herb evolution and plant origin of Chinese medicine Duhuo and Qianghuo. *J. Yunnan Univ. Tradit. Chin. Med.* 17 (4), 11–16. doi: 10.19288/j.cnki.issn.1000-2723.1994.04.003

Shan, F., Yuan, Y., Hao, J., and Huang, L. (2014). Herbal textual research on origin and development of traditional Chinese medicine Duhuo and Qianghuo. *Chin. J. Chin. Mater. Med.* 39, 3399–3403. doi: 10.4268/cjcmm20141740

Sun, W., Yang, L., Qiu, Y., Ren, J., Huang, R., and Fu, J. (2011). Identify nature N-acylethanolamide-hydrolyzing acid amide (NAAA) inhibitor: effect of Angelicae Pubescentis Radix on anti-inflammation. *Chin. J. Chin. Mater. Med.* 36, 3161–3166. doi: 10.4268/cjcmm20112221

Sun, D., Xu, X., Yan, S., Song, X., and Li, X. (2014). Analysis on chemical components from water extract of Angelicae Pubescentis Radix by high performance liquid chromatography-electrospray Ionization-quadrupole-time of flight-mass spectrometry. *Nat. Prod. Res. Dev.* 23, 69–76. doi: 10.16333/j.1001-6880.2014.01.019

Teng, C., Lin, C., Ko, F., Wu, T., and Huang, T. (1994). The relaxant action of osthole isolated from *Angelica pubescens* in guinea-pig trachea. *Naunyn-Schmiedeberg's Arch. Pharmacol.* 349, 202–208. doi: 10.1007/BF00169838

Wang, C., Shen, P., and Hu, Y. (2009). *Symptoms of rheumatism.* (Beijing, China: People's Medical Publishing House), 22–33.

Wang, Z., Shen, Y., Chen, Y., and Yao, X. (1988). Studies on the active principles of *Angelica pubescens* Maxim. *J. Shenyang Pharm. Univ.* 5 (3), 183–188. doi: 10.14066/j.cnki.cn21-1349/r. 1988.03.005.

Wang, C., Cui, J., Zhu, M., Weng, J., and Yu, M. (2011a). Experimental study on the regulation of IL-4 and TNF-$\alpha$ in rats with AD and VD by Chinese medicine Duhuo. *J. Liaoning Univ. Tradit. Chin. Med.* 38, 1701–1702. doi: 10.13192/j.ljtcm.2011.09.8.wangcx.070

Wang, X., Qiu, J., and Li, S. (2011b). Rapid GC-MS analysis of essential oils in Radix Angelicae Biseratae. *J. Yanbian Univ. (Nat. Sci.)* 37, 128–131. doi: 10.3969/j.issn.1004-4353.2011.02.008

Wang, K., Yao, L., Du, Y., Xie, J., Huang, J., and Yin, Z. (2011c). Anthelmintic activity of the crude extracts, fractions, and osthole from Radix Angelicae Pubescentis against Dactylogyrus intermedius in goldfish (Carassius auratus) *in vivo*. *Parasitol. Res.* 108, 195–200. doi: 10.1007/s00436-010-2058-9

Wang, K., Yao, L., Xie, J., Huang, J., and Miao, C. (2012). Effect of active monomer from Radix Angelicae Pubescentis on killing Dactylogyrus intermedius and its active component identification. *Acta Hydrobiol. Sinica* 36, 93–101. doi: 10.3724/SP.J.1035.2012.00093

Wang, B., Liu, X., Zhou, A., Meng, M., and Li, Q. (2014). Simultaneous analysis of coumarin derivatives in extracts of Radix Angelicae Pubescentis (Duhuo) by HPLC-DAD-ESI-$MS^n$ technique. *Anali. Methods* 6, 7996–8002. doi: 10.1039/C4AY01468E

Wang, J., Shi, M., Zheng, P., Xue, S., and Peng, R. (2018a). Quantitative Analysis of Ca, Mg, and K in the roots of *Angelica pubescens* f. *biserrata* by Laser-induced breakdown spectroscopy combined with artificial neural networks. *J. Appl. Spectrosc.* 85, 190–196. doi: 10.1007/s10812-018-0631-7

Wang, J., Tan, J., Li, L., Liu, J., and Zhang, J. (2018b). HPLC fingerprint of Angelica Pubescens Radix and determination of four kinds of coumarin. *Chin. J. Pharm. Anal.* 6, 955–963. doi: 10.16155/j.0254-1793.2018.06.06

Wang, F. (2013). *Grass oil emollient water from Angelica pubescens Maxim.* (China, CN103340784A: State Intellectual Property Office).

Wang, L. (2014). *A kind of material for removing wind and dehumidifying hot pot and its production method of Angelica pubescens Maxim.* (China, CN103798715A: State Intellectual Property Office).

Wei, F., Zou, S., Young, A., Dubner, R., and Ren, K. (1999). Effects of four herbal extracts on adjuvant-induced inflammation and hyperalgesia in rats. *J. Altern. Complem. Med. (New York N.Y.)* 5, 429–436. doi: 10.1089/acm.1999.5.429

Weng, J., Wang, C., and Yang, W. (2012). Experiment research on protective effect of Duhuo on free radical of rats with Vascular Dementia. *Chin. Arch. Tradit. Chin. Med.* 30, 899–900. doi: 10.13193/j.archtcm.2012.04.229.wengj.065

Wu, Q., and Li, R. (1993). Studies on the chemical constituents of Duhuo. *Chin. Tradit. Herbal Drugs* 24, 3. 48.

Xie, J., Yao, L., Li, C., Chen, D., and Liang, L. (2016). Study on the active site and extraction method of Duhuo in killing Dioscorea japonicus. *Veter. Orientat.* 39 (12), 211–212. doi: 10.3969/j.issn.1673-8586.2016.12.202

Xiong, F. (2014). High-yield cultivation techniques for Angelicae Pubescentis Radix seedling transplanting. *Sci. Breed.* 4, 17–18. doi: 10.3969/j.issn.1673-3339.2014.04.011

Yan, Y., Li, S., Kong, L., Jiao, Y., Yao, Y., Tao, Z., et al. (2016). Neuroprotective effects of total coumarins in *Angelica pubescens* against A$\beta$-Induced neurons damage. *J. Liaoning Univ. Tradit. Chin. Med.* 43, 1714–1717. doi: 10.13192/j.issn.1000-1719.2016.08.052

Yan, Y., Li, S., Li, H., Lin, Y., and Yang, J. (2017). Osthole protects bone Marrow-Derived neural stem cells from oxidative damage through PI3K/Akt-1 pathway. *Neurochem. Res.* 42, 398–405. doi: 10.1007/s11064-016-2082-y

Yang, X., Liu, Y., Tao, H., Yang, Z., and Xiao, S. (2006). GC-MS analysis of essential oils from Radix Angelicae Pubescentis. *Chin. J. Chin. Mater. Med.* 31, 663–666. doi: 10.3321/j.issn:1001-5302.2006.08.012

Yang, X., Guo, Q., Zhang, C., and Zhang, B. (2008). Further studies on the chemical constituents of the root of *Angelica pubescens* f. *biserrata*. *Pharm. J. Chin. Pla.* 24, 389–392. doi: CNKI:SUN:JFJN.0.2008-05-005

Yang, X. W., Zhang, C. Y., Zhang, B. G., Lu, Y., Luan, J. W., and Zheng, Q. T. (2009). Novel coumarin and furan from the roots of *Angelica pubescens* f.

*biserrata*. *J. Asian Nat. Prod. Res.* 11, 698–703. doi: 10.1080/10286020802619140

Yang, Y., Zhang, L., Zhang, Y., and Yang, X. (2017). Simultaneous assessment of absorption characteristics of coumarins from Angelicae Pubescentis Radix: *In vitro* transport across Caco-2 cell and *in vivo* pharmacokinetics in rats after oral administration. *J. Chromatogr. B.* 1060, 308–315. doi: 10.1016/j.jchromb.2017.06.020

Yang, Y., Zhang, L., and Yang, X. (2018). Distribution assessments of coumarins from Angelicae Pubescentis Radix in rat cerebrospinal fluid and brain by Liquid Chromatography Tandem Mass Spectrometry analysis. *Molecules.* 23, 225–236. doi: 10.3390/molecules23010225

Yang, W. (2007). Divide the light intensity of light method to measurese Radix Angelcae Pubesentis inside the flavonoid's research. *Sci. Technol. Inf.* 23 (36), 391. 200. doi: CNKI:SUN:KJXX.0.2007-36-299

Yao, L., Lu, P., Li, Y., Yang, L., Feng, H., Huang, Y., et al. (2013). Osthole relaxes pulmonary arteries through endothelial phosphatidylinositol 3-kinase/Akt-eNOS-NO signaling pathway in rats. *Eur. J. Pharmacol.* 699, 23–32. doi: 10.1016/j.ejphar.2012.11.056

Yao, L., Yang, Y., He, G., Ou, C., Wang, L., and Liu, K. (2018). Global Proteomics Deciphered Novel-Function of Osthole Against Pulmonary Arterial Hypertension. *Sci. Rep.-UK* 8 (1), 5556. doi: 10.1038/s41598-018-23775-8

Zaugg, J., Eickmeier, E., Rueda, D. C., Hering, S., and Hamburger, M. (2011). HPLC-based activity profiling of Angelica pubescens roots for new positive GABA A receptor modulators in Xenopus oocytes. *Fitoterapia* 82, 434–440. doi: 10.1016/j.fitote.2010.12.001

Zhan, H., Fang, J., Yang, B., Fu, M., Liu, M., Li, H., et al. (2017). Determination of osthole and columbianadin in Radix Angelicae Pubescentis with near infrared spectroscopy. *Spectrosc. Spect. Anal. (Beijing)* 37, 1110–1113. doi: 10.3964/j.issn.1000-0593(2017)04-1110-04

Zhang, J., and Du, W. (2010). Effect of Duhuo on p38MAPK signal transduction pathway in brain of Dementia rats. *Chin. J. Gerontol.* 30, 1514–1515. doi: 10.3969/j.issn.1005-9202.2010.11.020

Zhang, L., and Liang, M. (2018). Exploration and analysis on the potential function of Radix Angelicae Pubescentis. *Chin. J. Tradit. Chin. Med. Pharm.* 33, 46–49. doi: 10.1016/S0254-6272(13)60099-0

Zhang, C., Zhang, B., and Yang, X. (2007). Studies on chemical consituents of the root of *Angelica pubescens* f. *biserrata*. *Med. Pharm. J. Chin. Pla.* 23, 241–245. doi: 10.3969/j.issn.1008-9926.2007.04.001

Zhang, Z., Leung, W., Li, G., Kong, S., Lu, X., Wong, Y., et al. (2017). Osthole enhances osteogenesis in osteoblasts by elevating transcription factor osterix via cAMP/CREB signaling *in vitro* and *in vivo*. *Nutrients.* 9, 588. doi: 10.3390/nu9060588

Zhang, L., Ge, Y., Li, J., Hao, J., Wang, H., He, J., et al. (2018). Simultaneous determination of columbianetin-$\beta$-D-glucopyranoside and columbianetin in a biological sample by High-performance liquid chromatography with fluorescence detection and identification of other columbianetin-$\beta$-D-glucopyranoside metabolites by ultra-high-performance-liquid-chromatography coupled with quadrupole-time of flight mass spectrometry. *J. Pharm. Biomed.* 153, 221–231. doi: 10.1016/j.jpba.2018.02.055

Zheng, C., Fu, C., Ye, J., Wu, G., Li, X., Ye, H., et al. (2017). A computer simulation study of heracleum for treatment of osteoarthritis pain. *J. Trad. Chin. Orthop. Trauma* 29, 1–4. doi: 10.3969/j.issn.1001-6015.2017.07.001

Zhengkang, M. (2006). *Chinese pharmacology* (Beijing, China: China Medical Science Press), 122–124.

Zhu, M., Cui, J., and Wang, C. (2009). The experimental study of the intervention effect of Duhuo on immune damage of model rats suffering from Alzheimer. *J. Liaoning Univ. Tradit. Chin. Med.* 38, 2085–2086. doi: 10.13192/j.ljtcm.2011.10.168.zhumd.063

Zou, X., Wang, R., Dai, H., and Hu, Y. (2008). Experimental study on antiangiogenic effect of Duhuo. *J. Nanjing Univ. Tradit. Chin. Med.* 24, 194–196. doi: 10.14148/j.issn.1672-0482.2008.03.020

Zuo, Y. (1998). *Overview of foreign traditional Chinese medicine*. (Beijing, China: People's Medical Publishing House), 203.

**Conflict of Interest:** The authors declare that the research was conducted in the absence of any commercial or financial relationships that could be construed as a potential conflict of interest.

frontiers in Pharmacology

ORIGINAL RESEARCH
published: 20 March 2020
doi: 10.3389/fphar.2020.00347

# Network Pharmacology-Based Dissection of the Anti-diabetic Mechanism of *Lobelia chinensis*

*Qi Ge[1,2], Liang Chen[2], Yi Yuan[2,3], Lanlan Liu[2], Fan Feng[4], Peng Lv[2], Shangshang Ma[2,3], Keping Chen[2]* and Qin Yao[1,2]**

[1] School of the Environment and Safety Engineering, Jiangsu University, Zhenjiang, China, [2] Institute of Life Sciences, Jiangsu University, Zhenjiang, China, [3] School of Food and Biological Engineering, Jiangsu University, Zhenjiang, China, [4] School of Biological and Food Engineering, Suzhou University, Suzhou, China

Diabetes mellitus (DM) is a chronic inflammatory disease, and the rapidly increasing DM is becoming a major problem of global public health. Traditional Chinese medicine (TCM) has a long history of treating diabetes. It has been developed and utilized because of its good efficacy and no toxic side effects. *Lobelia chinensis* is a traditional whole grass herbal. With the continuous deepening of pharmacological research on TCM, the active ingredients of *L. chinensis* are continuously revealed, which contained the alkaloids, flavonoids, flavonoid glycosides and amino acids that have the good effects of anti-inflammatory, anti-viral and anti-diabetic. In order to further explore the targets of active ingredients and its anti-diabetic mechanism, a feasible network pharmacology analysis model based on chemical, pharmacokinetic and pharmacological data was developed by network construction method to clarify the anti-diabetic mechanism of *L. chinensis*. The present study conducted by gas chromatography–mass spectrometer (GC/MS), which identified 208 metabolites of *L. chinensis*, of which 23 ingredients may have effective pharmacological effects after absorption, distribution, metabolism, and excretion (ADME) screening. Network pharmacological analysis on the active ingredients revealed that 5-hydroxymethylfurfural in *L. chinensis* affects the insulin resistance signaling pathway by acting on GSK3B, TNF, and MAPK1, acacetin affects the diabetic pathway by acting on INSR, DPP4, and GSK3B, that regulate type 2 diabetes, non-insulin-dependent DM, and inflammatory diseases. These results successfully indicated the potential anti-diabetic mechanism of the active ingredients of *L. chinensis*.

**Keywords:** ***Lobelia chinensis*, active ingredients, network pharmacology, anti-diabetic, anti-inflammatory**

OPEN ACCESS

***Edited by:***
*Wei Zhou,*
*The Affiliated Hospital of Shenzhen University, China*

***Reviewed by:***
*Haolong Liu,*
*Peking University Health Science Centre, China*
*Hongbin Xiao,*
*Beijing University of Chinese Medicine, China*

****Correspondence:***
*Keping Chen*
*kpchen@ujs.edu.cn*
*Qin Yao*
*yaoqin@ujs.edu.cn*

***Specialty section:***
*This article was submitted to Ethnopharmacology, a section of the journal Frontiers in Pharmacology*

***Received:*** *04 August 2019*
***Accepted:*** *09 March 2020*
***Published:*** *20 March 2020*

***Citation:***
*Ge Q, Chen L, Yuan Y, Liu L, Feng F, Lv P, Ma S, Chen K and Yao Q (2020) Network Pharmacology-Based Dissection of the Anti-diabetic Mechanism of Lobelia chinensis. Front. Pharmacol. 11:347. doi: 10.3389/fphar.2020.00347*

## INTRODUCTION

Diabetes mellitus (DM) is a chronic inflammatory disease that seriously threatens human health, and is affected by the interaction between genetic and environmental factors (Yue et al., 2017a). DM is caused by a metabolic disorder of the endocrine system, and a long-term illness can lead to tissues and organs damage to the cardiovascular, endocrine, nervous, and urinary systems (Ge et al., 2017). Beta cell (β cell) failure plays an important role in the development of type 2 DM (T2DM). The dysregulation of

metabolic and inflammatory process caused by the onset of DM contributes to the loss of islet function and impaired insulin secretion of β cells, and then affect the body's immune system, leading to various complications of DM (Macdougall et al., 2019).

Traditional Chinese medicine (TCM) has been used for treating DM for more than 2000 years. Relevant studies have shown that TCM can significantly improve blood sugar and clinical indicators of diabetic patients, and effectively delay the progress of DM. (Tian et al., 2019). *Lobelia chinensis* (*L. chinensis* Lour.) is an annual dwarf herb, belonging to the family Campanulaceae, and is widely distributed in East Asian countries including China, Korea, and Japan (Yang et al., 2014). Modern pharmacology research indicates that the whole herb of *L. chinensis* contains a variety of alkaloids, which has medicinal functions of clearing heat-toxin, promoting diuresis, and diminishing inflammatory (Li et al., 2009). According to preliminary literature reports, *L. chinensis* contains flavonoids (Yang et al., 2014), terpenoids (Chen et al., 2014), lignans (Shibano et al., 2001), alkaloids (Kuo et al., 2011), and some other active ingredients. Although the active ingredients in *L. chinensis* are known, it is still unclear how the active ingredients act on target proteins and regulate signaling pathways to achieve the pharmacological effects of anti-inflammatory and anti-diabetic.

In order to comprehensively evaluate the pharmacological effects of TCM, network pharmacology has been introduced to explore the molecular mechanism of TCM in recent years (Hong et al., 2017a; Hong et al., 2017b). The development of systematic pharmacological studies on the relationship between biological processes and the treatment of TCM has attracted considerable interest. Therefore, by integrating systematic information with the overall characteristics of TCM to achieve a comprehensive analysis, and turning the idea of "one drug, one target and one disease" to multi-target combination (Pujol et al., 2010). Based on network interaction to study the basic biological knowledge of TCM can provide a deep insight or scientific evidence for the discovery of TCM, and help us to clarify the pharmacological mechanism of active ingredients of TCM at the level of biomolecule (Yang et al., 2018). Network pharmacology is gradually becoming a holistic and efficient tool to describe the complex interactions between drugs and biological systems including the human organs, diseases, metabolic pathways, and target proteins from a network perspective(Zhang et al., 2016). Combined with pharmacology and pharmacodynamics, it has been successfully applied to explain the mechanism of TCM at the molecular network level (Yue et al., 2017b). In this study, we first identified the active ingredients in *L. chinensis* by metabolomics analysis. Based on the pharmacokinetic and pharmacological data of components, we constructed a network pharmacological model of active ingredients, and systematically analyzed the potential anti-diabetes mechanism of active ingredients in *L. chinensis*. The detailed procedures can be seen in **Figure 1**.

# MATERIALS AND METHODS

## Description of the Study Material

*L. chinensis* is a plant, commonly called Chinese lobelia, creeping lobelia, or Banbianlian, is a low-growing, tiny-leaved, herbaceous perennial that typically forms an attractive ground cover rising to only 2–3″ tall but spreading rapidly by creeping decumbent stems to 36″ wide. Creeping stems are clad with narrow, lanceolate, green leaves (to 3/4″ long). Pale pink to white, usually solitary flowers (1 1/4″across) bloom from the leaf axils from July to October. Each lobelia-like flower features two lanceolate to oblanceolate lateral lobes and three more prominent central elliptic lobes in a flattened plane. *L. chinensis* is 1 of the 50 fundamental herbs used in TCM (**Supplementary Figure 3**). Voucher specimen accession number NAS00276292 was deposited in Institute of Botany, Jiangsu Province and Chinese Academy of Sciences (**Supplementary Figure 1**).

## Determination of Active Ingredients From *L. chinensis*

*L. chinensis* was collected in Quanjiao, Anhui Province, and now is preserved in the Institute of Life Sciences, Jiangsu University. The whole plants were dried and ground to a fine powder in an electric grinder. All chemicals and reagents were analytical or HPLC grade. The 60 mg accurately weighted *L. chinensis* powder was transferred to a 2.0-ml Eppendorf tube. Two small steel balls were added to the tube, 360 μl of cold methanol and 40 μl of internal standard (0.3 mg/ml 2-chloro-L-phenylalanine, dissolved in methanol) were added to the tube, and then placed at −80°C for 2 min, ground at 60 Hz for 2 min, and sonicated for 30 min. After that, 200 μl of chloroform was added to the tube and the mixtures were mixed thoroughly at ambient temperature, then 400 μl of water was added. The samples were centrifuged at 12,000*g* for 10 min at 4°C. An aliquot of the 200 μl supernatant was transferred to a glass sampling vial for desiccation at room temperature. Eighty microliters of methoxyamine hydrochloride in pyridine (15 mg/ml) was subsequently added. The resultant mixture was vortexed vigorously for 2 min and incubated at 37°C for 90 min, then 80 μl of BSTFA (with 1% TMCS) and 20 μl n-hexane was added into the mixture, which was vortexed vigorously for 2 min and incubated at 70°C for 60 min. All the samples were placed at ambient temperature for 30 min before gas chromatography–mass spectrometry (GC-MS) analysis. And all the samples were tested in triplicate.

## GC-MS Experiments

The derivatized samples were analyzed on an Agilent 7890B gas chromatography system coupled to an Agilent 5977A MSD system (Agilent Technologies Inc., CA, USA). DB-5MS fused-silica capillary columns (30 m × 0.25 mm × 0.25 μm, Agilent J & W Scientific, Folsom, CA, USA) with highly pure helium (purity not less than 99.999%) at a constant flow rate of 1.0 ml/min were utilized to separate the derivatives. The injector temperature was maintained at 260°C. Injection volume was 1 μl, and the split ratio was 10:1. The initial temperature of the column oven was 60°C, ramped to 125°C at a rate of 8°C/min, to 210°C at a rate of 4°C/min, to 270°C at a rate of 5°Cmin, to 305°C at a rate of 10°C/min, and finally held at 305°C for 3 min. The temperature of MS quadrupole and ion source (electron impact) was set to 150°C and 230°C, respectively. The collision energy was 70 eV. Scan

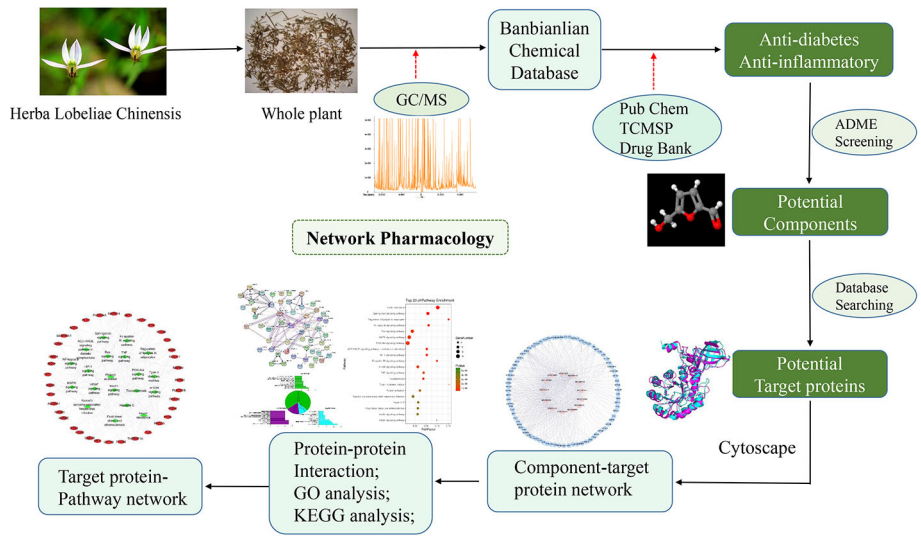


**FIGURE 1 |** The flowchart of the network pharmacological analysis approach.

mode was Full Scan mode (SCAN) and mass scan range was m/z 50–500.

## Chemical Ingredients Database Building and Screening

All of the constituent data of *L. chinensis* were obtained from Traditional Chinese Medicine Systems Pharmacology Database and Analysis Platform (TCMSP, http://lsp.nwu.edu.cn/tcmsp.php) (Ru et al., 2014). The active ingredients obtained from GC-MS and supplemented through a wide-scale text-mining method were input into TCMSP website to screen the chemical ingredients that interact with DM and inflammation. The effective ingredients of *L. chinensis* are mainly filtered by oral bioavailability (OB) and blood–brain barrier (BBB) permeability. OB is one of the most important pharmacokinetic parameters in the characteristics of absorption, distribution, metabolism, and excretion (ADME) characteristics of drugs, indicating the ratio of the oral drug to the oral dosage of the blood circulatory system (Fang et al., 2017). The ADME parameter-based virtual screening of the ingredients was utilized to further identify anti-diabetic ingredients using an OB threshold OB ≥ 30% and barrier permeability (BBB) ≥ −0.30 as parameters (Tsaioun et al., 2016). Meanwhile, the chemical information of these ingredients (structure, specification name, and CID number) for computational analysis were also collected according to the Pub Chem (https://pubchem.ncbi.nlm.nih.gov/) and Drug Bank (https://www.drugbank.ca/drugs).

## Ingredient–Target Network Construction

In order to identify the corresponding targets of the active ingredients of *L. chinensis*, a method combined with information integration and data mining was implemented. First of all, the active ingredients and interact targets were submitted to Cytoscape 3.2.1 software to construct an ingredient–target network to explore the pharmacological mechanism of the active ingredients of *L. chinensis*. The input data with Excel format file can be seen in the **Supplementary Tables 3 and 4**.

## Protein-Protein Interaction Network Construction

To explain the interaction between target proteins, the target proteins of related ingredients of *L. chinensis* were uploaded to STRING (http://string-db.org) online website to obtain the information of protein-protein interaction (PPI). The website generated a score for each protein mutual information. The higher the score, the higher the confidence in the interaction between target proteins. Therefore, we selected high confidence data >0.7 to ensure the reliability of this analysis. The obtained protein interaction data were imported into Cytoscape 3.2.1 software to construct a PPI protein interaction network.

## Gene Ontology and KEGG Enrichment Analysis of Target Proteins

To elucidate the role of target proteins that interact with the active ingredients of *L. chinensis* in gene function and signaling pathway, the Database for Annotation, Visualization and Integrated Discovery (DAVID, https://david.ncifcrf.gov/) v6.8 was used to analyze the Gene Ontology (GO) function and KEGG pathway enrichment of proteins involved in PPI network. The target proteins involved in the cellular components (CC), molecular function (MF), biological process (BP), and the pathways were also described.

## Ingredient–Target–Pathway Network Construction

After getting the interaction information of the active ingredient compounds, target proteins, and the pathways, the "Ingredient–Target–Pathway" network was established by Cystoscope 3.2.1

software. In the network, nodes represent components, targets, and pathways, edges represent the interaction of each other. Then a hypothesized schematic diagram of the target proteins involved in the pathways was drawn. Based on the network model map, the pathway of active ingredients and targets in the disease is initially explored to provide a preliminary theoretical basis for the design of subsequent targeted drugs.

# RESULTS

## GC/MS Determination of Active Ingredients in *L. chinensis*

To demonstrate the ability of the GC/MS method to accurately separate and identify ingredients, the sample of *L. chinensis* powder was analyzed triple times by GC/MS. The results showed strong signals, high peak capacity, and well reproducibility. The typical total ion current (TIC) was shown in **Supplementary Figure 2**. The detected ingredients contained acacetin (4.78 mg/g), norlobelanine (6.05 mg/g), 5-hydroxymethylfurfural (1.26 mg/g), and other bioactive ingredients. The concentration of the active ingredients of *L. chinensis* are shown in **Table 1**. A total of 208 chemical ingredients were identified and shown in **Supplementary Table 1**.

## Screening of Effective Anti-Diabetic Ingredients in *L. chinensis*

Early assessment of the ADME properties of candidate active ingredients has become an important process in modern drug discovery. And the correct use of ADME identifies candidates that are more likely to have good pharmacokinetic properties. Currently, OB and BBB are considered as a key parameter in drugs discovery. TCMs are often administered orally, and its OB is determined by body absorption, distribution, and liver metabolism. It is important to identify the active ingredients of medicinal herbs. In this research, OB and BBB indicators were used to screen for *L. chinensis* ingredients with favorable pharmacokinetic properties. Therefore, all chemicals that meet the screening criteria: OB (> 30%) and BBB (>-0.3) are considered as candidate ingredients. Twenty-three differentiated ingredients with effective pharmacological activities were identified after screening ADME parameters (**Table 2**).

**TABLE 1** | The concentration of the active ingredients of *Lobelia chinensis*.

| MOL ID | Ingredients | Concentration |
|---|---|---|
| MOL012231 | Leptodactylone | 23.58 mg/g |
| MOL012207 | Lobelanidine | 12.62 mg/g |
| MOL001689 | Acacetin | 4.78 mg/g |
| MOL012216 | Norlobelanine | 6.05 mg/g |
| MOL001999 | Scoparone | 0.13 mg/g |
| MOL005928 | Isoferulic acid | 22.77 mg/g |
| MOL012209 | 2-[(2R,6S)-6-[(2R)-2-hydroxy-2-phenylethyl]-1-methylpiperidin-2-yl]-1-phenylethanone (Lobelin) | 46.60 mg/g |
| MOL009009 | (+)-Medioresinol | 0.84 mg/g |
| MOL004678 | Limetin | 2.51 mg/g |
| MOL012208 | Lobelanine | 27.88 mg/g |
| MOL002341 | Hesperetin | 3.27 mg/g |
| MOL000748 | 5-Hydroxymethylfurfural (HMF) | 1.26 mg/g |
| MOL000103 | 4-Oxoniobenzoate (PHB) | 5.49 mg/g |

## Interactions Analysis of Active Ingredients and Target Proteins

According to the analysis, the active ingredients of *L. chinensis* have good pharmacological effects on anti-inflammatory and anti-diabetic in a synergistic way. To further study the mechanism of anti-diabetes, it is of paramount important to understand the target proteins on which these ingredients act. With the development of network pharmacology, it provides an effective tool for the study of TCM pharmacology. Using TCMSP, the active ingredients of *L. chinensis* and the target proteins related to inflammation and DM were searched. Cytoscape 3.2.1 was used to analyze the interaction between 23 active ingredients and target proteins. The results are shown in **Figure 2**. The analysis ingredients–targets network consisted a total of 93 nodes and 581 edges, of which 13 are anti-inflammatory and anti-diabetic active ingredients, and the other 80 are target protein nodes. The result shows that MOL001689 (acacetin), MOL012216 (norlobelanine), MOL000748 (5-hydroxymethylfurfural) have more target proteins play a key role in the interaction network, which may be the key ingredients or target proteins that play an anti-inflammation and anti-diabetic role in *L. chinensis*. **Supplementary Table 2** lists the ingredients and the related target proteins. Based on the number of ingredients–targets relationships, the number of target proteins acting on average per ingredients is about 6.15. These results indicate that muti-ingredients muti-targets interactions occur in *L. chinensis*.

## Construction and Analysis of Target Proteins PPI Network

The target proteins that act with its corresponding ingredients were submitted to STRING version 10.5 (http://string-db.org/) for PPI network construction, and high confidence of protein interaction data with a score >0.7 was selected (**Figure 3**). The results include a total of 75 nodes, 107edges, of which nodes represent the target proteins and the edges represent the interactions between the proteins. In this network interaction, the larger the degree, the stronger relationship between the proteins corresponding to the node in this network, which indicates that the target proteins play a key role in the whole interaction network, which is the important target protein. **Figure 3** shows that PIK3CA, PDPK1, AKT1, and TNF are centrally located in the PPI network, indicating that these proteins are involved in the pathogenesis of DM and inflammation.

## GO Analysis of Target Proteins

GO enrichment analysis of target proteins that act with its corresponding ingredients was performed by DAVID. The top 10 significantly enriched terms in BP, MF, and CC categories were selected, according to $P < 0.05$, P-values were corrected using the Benjamini–Hochberg procedure. As shown in **Figure 4**, BP (198 records), MF (40 records), and CC (32 records) accounted for 71.74%, 16.67%, and 11.59%, respectively. In the

**TABLE 2 |** Ingredients information of *Lobelia chinensis*.

| MOL ID | Name | Molecular Formula | CAS No. | MW (g/mol) | OB% | BBB | DL | HL | Structural Formula |
|---|---|---|---|---|---|---|---|---|---|
| MOL012207 | Lobelanidine | N/A | 552-72-7 | 339.52 | 60.53 | 0.31 | 0.32 | 5.78 | 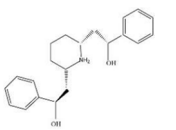 |
| MOL012208 | Lobelanine | C22H25NO2 | 579-21-5 | 335.48 | 54.13 | 0.46 | 0.32 | 31.96 | 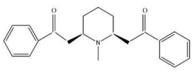 |
| MOL000103 | 4-Oxoniobenzoate (PHB) | C7H6O3 | 99-96-7 | 138.13 | 30.15 | 0.21 | 0.03 | 11.77 | 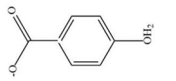 |
| MOL012209 | 2-[(2R,6S)-6-[(2R)-2-hydroxy-2-phenylethyl]-1-methylpiperidin-2-yl]-1-phenylethanone (Lobelin) | C22H27NO2 | 90-69-7 | 337.50 | 45.53 | 0.22 | 0.32 | 19.19 | 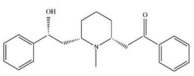 |
| MOL011678 | (3S,8S,9S,10R,13R,14S,17R)-17-[(1S,4R)-4-ethyl-1,5-dimethylhexyl]-10,13-dimethyl-2,3,4,7,8,9,11,12,14,15,16,17-dodecahydro-1H-cyclopenta[a]phenanthren-3-ol | C29H50O | 474-58-8 | 414.79 | 36.91 | 1.15 | 0.75 | 4.93 | 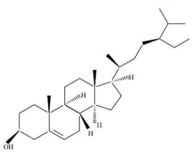 |
| MOL012215 | Propanol (POL) | C3H8O | 71-23-8 | 60.11 | 72.69 | 0.97 | 0.00 | 11.62 |  |
| MOL012216 | Norlobelanine | C21H23NO2 | 6035-31-0 | 321.45 | 64.08 | 0.33 | 0.30 | 35.32 | 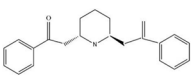 |
| MOL012217 | Phytenal | N/A | 13754-69-3 | 294.58 | 35.22 | 1.41 | 0.14 | 3.96 | 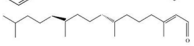 |
| MOL012221 | Trans-10-ethyl-8-methyl-lobelidiol | N/A | N/A | 229.41 | 33.93 | -0.04 | 0.07 | 2.73 | 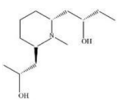 |
| MOL012223 | Trans-N-methyl-2,6-bis(2-hydroxybutyl)-△3-piperideine | N/A | N/A | 243.44 | 42.40 | -0.19 | 0.08 | 4.73 | 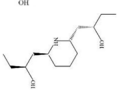 |
| MOL012231 | Leptodactylone | C11H10O5 | 61899-44-3 | 222.21 | 37.56 | 0.22 | 0.10 | 2.68 | 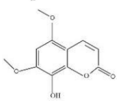 |
| MOL001999 | Scoparone | C11H10O4 | 120-08-1 | 206.21 | 74.75 | 0.46 | 0.09 | 0.73 | 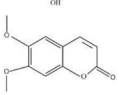 |
| MOL002341 | Hesperetin | C16H14O6 | 520-33-2 | 302.30 | 70.31 | -0.25 | 0.27 | 15.78 | 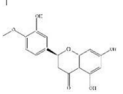 |
| MOL004678 | Limetin | C11H10O4 | 487-06-9 | 206.21 | 36.63 | 0.47 | 0.09 | 1.33 | 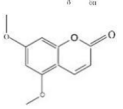 |
| MOL005928 | Isoferulic acid | C10H10O4 | 537-73-5 | 194.20 | 50.83 | 0.01 | 0.06 | 2.45 | 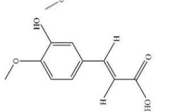 |
| MOL007170 | Cirsiumaldehyde | C12H10O5 | 7389-38-0 | 234.22 | 41.38 | 0.03 | 0.11 | 7.81 | 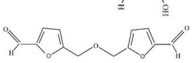 |
| MOL000748 | 5-Hydroxymethylfurfural (HMF) | C6H6O3 | 76330-16-0 | 126.12 | 45.07 | -0.27 | 0.02 | 11.73 | 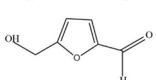 |
| MOL009009 | (+)-Medioresinol | N/A | 40957-99-1 | 388.45 | 87.19 | -0.29 | 0.62 | 1.39 | 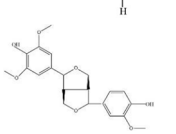 |

*(Continued)*

**TABLE 2** | Continued

| MOL ID | Name | Molecular Formula | CAS No. | MW (g/mol) | OB% | BBB | DL | HL | Structural Formula |
|---|---|---|---|---|---|---|---|---|---|
| MOL012232 | 5-Hydroxy-6,7-dimethoxycoumarin | C11H10O5 | 28449-62-9 | 222.21 | 67.31 | 0.20 | 0.10 | 1.83 | 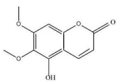 |
| MOL009653 | Cycloeucalenol | N/A | 469-39-6 | 426.80 | 39.73 | 1.04 | 0.79 | 5.01 | 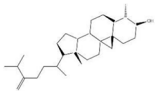 |
| MOL001504 | (E,7R,11S)-3,7,11,15-tetramethylhexadec-2-en-1-ol | C20H40O | 150-86-7 | 296.60 | 33.82 | 0.90 | 0.13 | 3.46 | 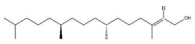 |
| MOL001689 | Acacetin | C16H12O5 | 480-44-4 | 284.28 | 34.97 | -0.05 | 0.24 | 17.25 | 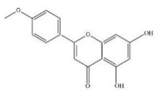 |
| MOL004688 | Cumic acid | C10H12O2 | 536-66-3 | 164.22 | 45.78 | 1.10 | 0.04 | -3.13 | 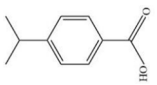 |

BP category, the target proteins were mainly involved in inflammatory response, participate in leukocyte migration, and glucose metabolic process. In the MF category, the target proteins were mainly involved in protein homodimerization activity and ATP binding. In the CC category, the target proteins were classified into plasma membrane and cell surface. The GO enrichment analysis results showed that the active ingredients of *L. chinensis* could bind kinase in cell membrane and plasma membrane in the process of inflammation, so as to exert anti-inflammatory and anti-diabetic potential.

## KEGG Classification of Target Proteins

To further clarify the relationship between target proteins and the pathways, we constructed a target–pathway interaction network using the data extracted from DAVID database (**Figure 5A**), and the top 20 pathways involving 33 target proteins were screened according to the KEGG analysis with BH-corrected P-values < 0.05 (**Figure 5B**). The results showed that these target proteins were mainly involved in insulin resistance, sphingolipid signaling pathway, regulation of lipolysis in adipolysis, NF-kappa B signaling pathway, MAPK signaling pathway, PI3K–AKT signaling pathway, and so on. The target proteins involved in insulin resistance included RAC-alpha serine/threonine-protein kinase (AKT1), carnitine palmitoyltransferase 1B (CPT1B), glycogen synthase kinase 3 beta (GSK3B), inhibitor of nuclear factor kappa B kinase subunit beta (IKBKB), INSR, mitogen-activated protein kinase 9 (MAPK9), nitric oxide synthase 3 (NOS3), phosphoinositide-dependent kinase-1 (PDPK1), phosphatidylinositol 4,5-bisphosphate 3-kinase catalytic subunit alpha isoform (PIK3CA), protein kinase C beta (PRKCB), glycogen phosphorylase (PYGL), tumor necrosis factor (TNF), and tumor necrosis factor receptor superfamily member 1A (TNFRSF1A); the target proteins involved in sphingolipid signaling pathway were adenosine A1 receptor (ADORA1), AKT1, mitogen-activated protein kinase 14 (MAPK14), MAPK9, NOS3, PDPK1, PIK3CA, phospholipase D1 (PLD1), protein kinase C beta (PRKCB), TNF, and TNFRSF1A; the target proteins involved in MAPK signaling pathway were AKT1, insulin-like growth factor 1 receptor (IGF1R), IKBKB, INSR, interleukin-1 receptor-associated kinase 4 (IRAK4), mast/stem cell growth factor receptor Kit (KIT), MAPK14, MAPK9, phospholipase A2 group IVA (PLA2G4A), PRKCB, angiopoietin-1 receptor (TEK), TNF, and TNFRSF1A. Therefore, there are multiple target proteins in one pathway, and the same target protein exists in multiple pathways. Essentially, a pathway involving multiple target proteins is more important than the interaction between one target protein and multiple pathways. These results suggest that the effective pharmacological active ingredients in *L. chinensis* may act on these signaling pathways to alleviate inflammation, including some chronic inflammation, such as type 2 diabetes and other diseases.

## Network Analysis of Target Proteins Involved in Signaling Pathways

As an important part of systemic pharmacology, signaling pathways can link receptor–ligand interactions with pharmacodynamics pathways. All target proteins interacting with the active ingredients of *L. chinensis* were located in the top 20 KEGG pathways and then generated a target–pathway signaling network. Among them, there are lots of target proteins involved in the PI3K–AKT signaling pathway, insulin signaling pathway, and TNF signaling pathway, which play an explicit role in maintaining insulin secretion, glucose homeostasis, and inflammation (Taniguchi et al., 2006). TNF is associated with a variety of inflammatory, infectious and malignant diseases (Bradley, 2008). In addition, the vascular endothelial growth factor signaling pathway that involving many target proteins, such as INSR, NOS3, PTGS2, and vascular endothelial growth factor A (VEGFA), plays a key regulatory role in diabetic retinopathy (Antonetti et al., 2012). VEGF can cause injury of vascular endothelial cells (ECs), inflammation, and oxidative stress, which can lead to an abnormal metabolism of blood glucose caused by diabetes, and also cause the insulin secretion from islet cells due to elevation of blood glucose, that aggravates

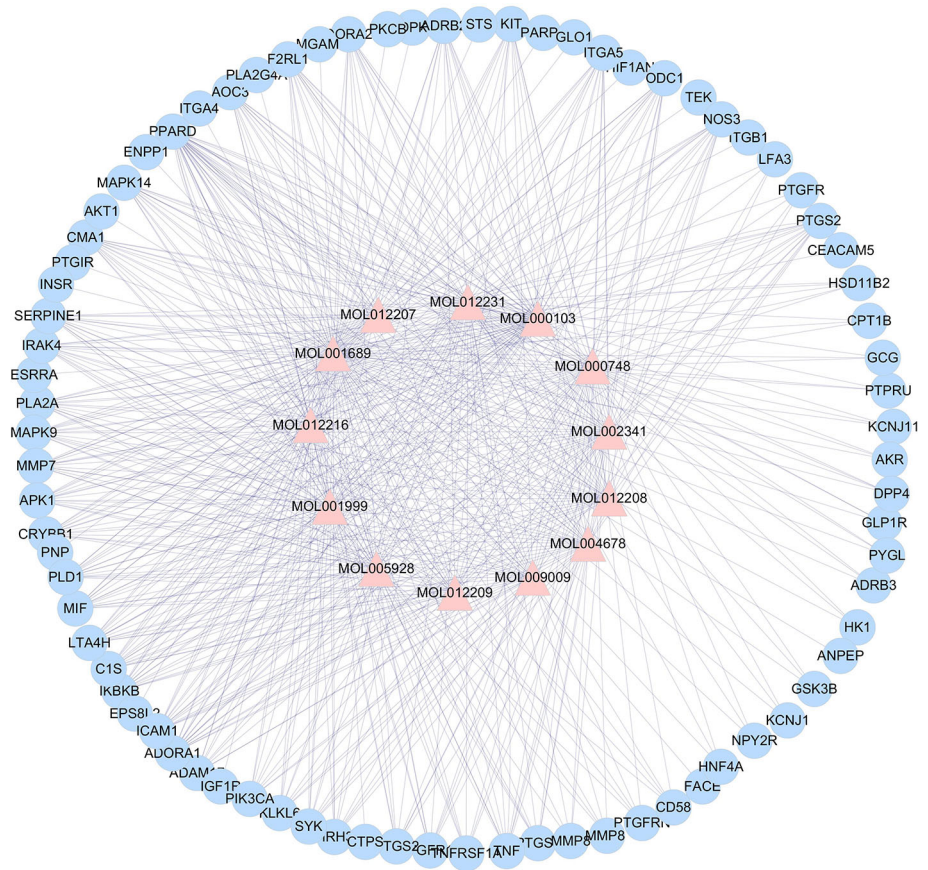


**FIGURE 2 |** *Lobelia chinensis* ingredients–target interaction network. The pink triangle represent the 13 bioactive ingredients, and the blue circle represent the 80 target proteins.

the symptoms of insulin resistance (Zhang et al., 2006). mTOR is a serine/threonine-protein kinase whose signal transduction regulates protein synthesis and cell growth, especially hypertrophy. Therefore, activation of the mTOR signaling pathway is a potential reason for early renal hypertrophy in DM (Sakaguchi et al., 2006). Interestingly, after network construction, we also found that active ingredients can play a therapeutic role in type 2 diabetes by activating the VEGFA to regulate the expression of PI3R1 and decreasing insulin resistance. As shown in **Figure 6**, the anti-inflammatory and anti-diabetic active ingredients present in *L. chinensis*, which can synergize with multiple target proteins in these pathways to form a multi-ingredients-multi-targets-multi-pathways mechanism.

## DISCUSSION

Medicinal plants have a long history in the treatment of chronic inflammatory diseases such as DM and various complications. In the pharmacological study of active ingredients, research methods based on network interaction are expected to highlight the understanding of drug action across multiple layers of information. The network model of active ingredients and target proteins is an important way to characterize the pharmacological mechanism of active ingredients, which can provide a theoretical basis for future drug development and design (Boezio et al., 2017). The research ideas of network pharmacology provide a unique and innovative way for the study of active ingredients in TCM, in order to understand the mechanism of the multi-ingredients-multi-targets mode of TCM (Ge et al., 2018a).

In this study, 208 metabolites of active ingredients in *L. chinensis* were determined by GC/MS metabonomics analysis. Among them, 23 active ingredients such as lobelanidine, 5-hydroxymethylfural, acacetin, and hesperetin possess the pharmacological activities (**Table 2**), of which 13 ingredients have anti-inflammatory and anti-diabetic effects (**Figure 2**). Subsequently, according to the analysis of network pharmacology, we found that these ingredient compounds which have therapeutic effects on inflammation and diabetes-related symptoms can treat or alleviate the symptoms of inflammation and diabetes, through the role of related target proteins in metabolic pathways caused by the occurrence of diseases. GO and KEGG analysis results showed that the target

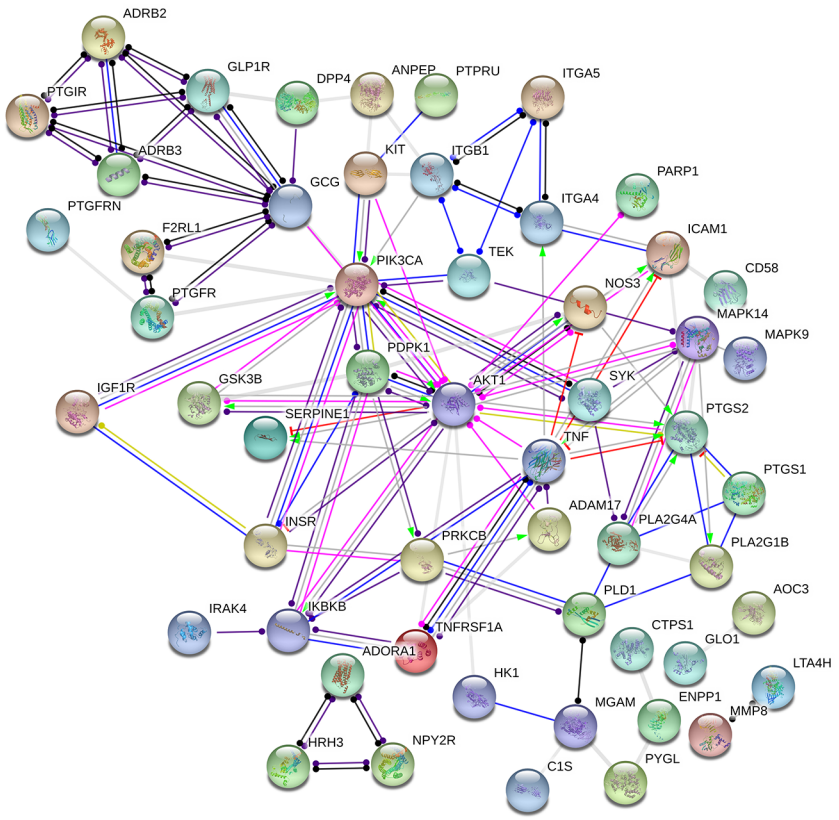


**FIGURE 3 |** Protein–protein interaction (PPI) network analysis.

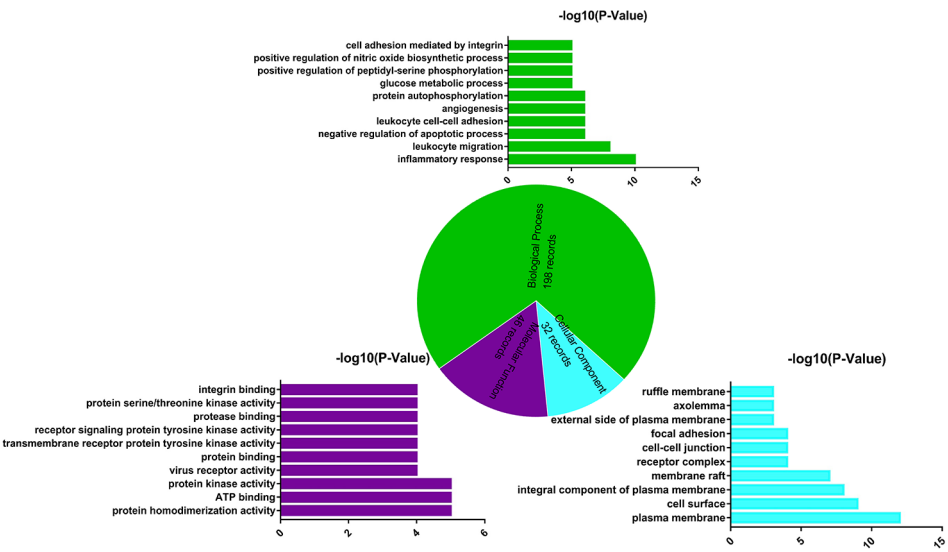


**FIGURE 4 |** Gene Ontology (GO) enrichment analysis of the target proteins. Biological process (green), molecular function (purple), and cellular component (blue) accounted for 71.47%, 16.67%, and 11.59%, respectively.

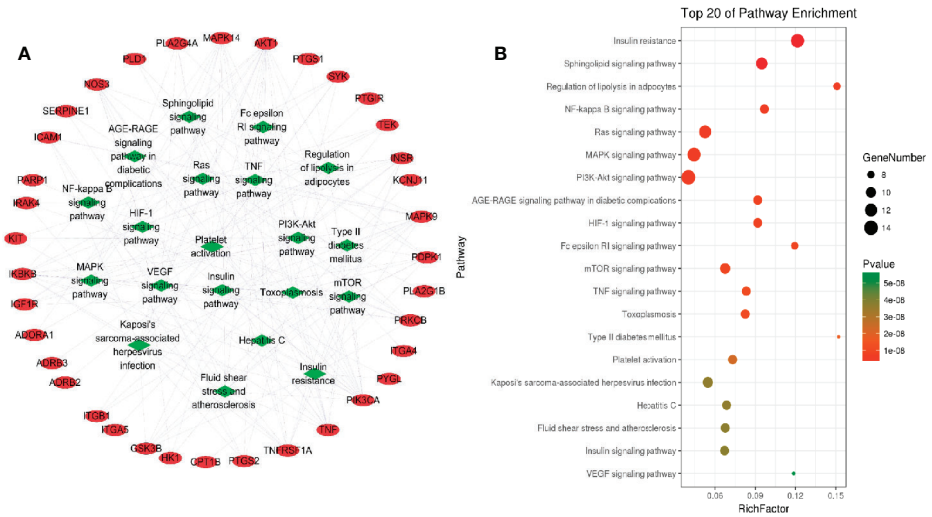


**FIGURE 5 |** Targets–pathway interaction analysis **(A)** and KEGG analysis of target proteins **(B)**. The red ellipse represent the target proteins, and the green diamond represent the pathways.

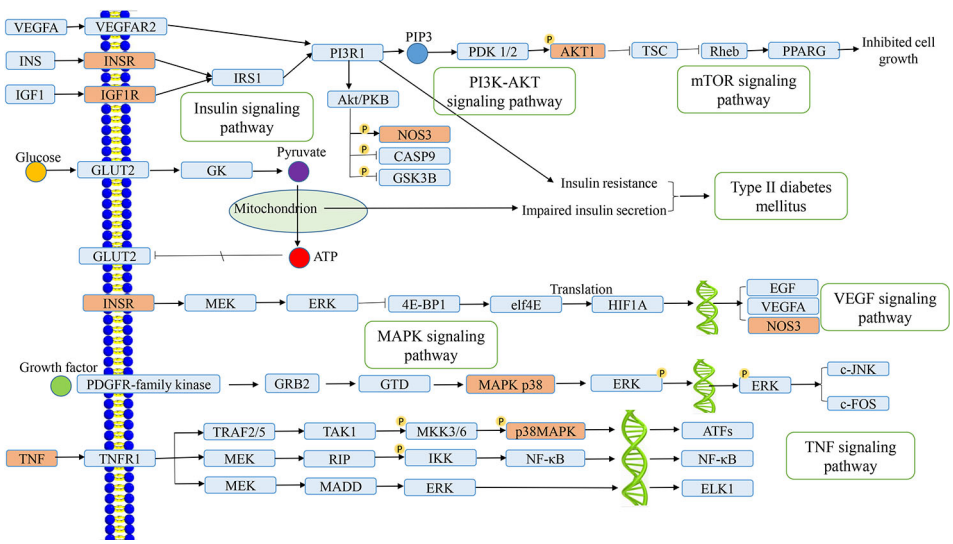


**FIGURE 6 |** Distribution of the target proteins of *Lobelia chinensis* on the predicted pathway. The orange nodes are potential target proteins of *L. chinensis*, while the blue nodes are relevant targets in the pathway.

proteins involved in main pathways were inflammation, non-insulin dependent pathway, MAPK signaling pathway, PI3K–AKT signaling pathway, TNF signaling pathway, and DM signaling pathway (**Figure 5**). The systematic pharmacological analysis showed that the active ingredients of 5-hydroxymethylfural and acacetin in *L. chinensis* could stimulate insulin secretion, improve insulin resistance, and promote glucose utilization by acting on GSK3B, MAPK, INR, and dipeptidyl peptidase-4 (DPP4). Meanwhile, they could also regulate inflammatory cytokines, promote endocrine and metabolism, and achieve the therapeutic effect in the treatment of diabetes.

GSK3B is a serine-threonine kinase in glycogen synthase subfamily, and it is also a negative regulator of glycometabolism balance that participates in energy metabolism, inflammatory response, endoplasmic reticulum stress, mitochondrial dysfunction, and apoptotic pathway (MacAulay and Woodgett, 2008). Selective inhibition of GSK3B in insulin resistance pathway can improve insulin-stimulated glucose transport activity, which may be due to

enhanced insulin signal transduction and GLUT-4 translocation (Henriksen and Dokken, 2006). Therefore, inhibition of GSK3B may have the potential to treat DM and insulin resistance. DPP4 is capable of rapidly degrading endogenous GLP-1, which plays a crucial role in glucose metabolism (Barnett, 2006). At present, GLP-1 is the only known protein to reduce blood glucose levels by increasing insulin secretion (MacDonald et al., 2002). The hypoglycemic mechanism of two diabetic drugs such as sitagliptin and vildagliptin is also based on DPP4 inhibitors (Karasik et al., 2008; Forst and Bramlage, 2014). Therefore, it is important to evaluate the inhibitory effect of active ingredients of *L. chinensis* on DPP-4.

According to the results of pathway analysis, mitogen-activated protein kinases (MAPKs), including extracellular signal-regulated kinase (ERK), c-Jun N-terminal kinase (JNK), and p38 MAPK, may also play a crucial role in regulating diabetes and inflammation through the MAPK signaling pathway. The MAPKs are extracellular signal-regulated protein kinases, increasing cellular proliferation and involving in the cell survival regulation (Chen and Jiang, 2018). MAPK can also be inactivated by protein phosphatases, which counteract many kinase-driven intracellular signaling pathways through dephosphorylating key proteins (Perrotti and Neviani, 2013). The liver is the main important organ to control metabolism in the human body (Ge et al., 2018b). MAPKs can regulate inflammatory response along with a wide range of cellular processes including cell metabolism, proliferation, motility, apoptosis, survival, differentiation, and survival in physiological and pathological processes (Li et al., 2020). Previous studies have shown that p38 MAPK controls cellular responses to cytokines and stress (Zielinski and Krueger, 2012). Thus, MAPK p38 inhibitors inhibit the production of many proinflammatory cytokines, including IL-1β and TNF-α, and inducible nitric oxide synthase (iNOS) (Sun et al., 2017). These findings further confirm that the pharmacological activation of MAPK may be mediated by signal transduction, metabolism, and gene expression, while changes in liver metabolism may lead to the occurrence of insulin resistance, type 2 diabetes, and obesity. Therefore, we think that MAPK may be associated with metabolic diseases, which also provides a new strategy for the treatment of metabolic diseases such as type 2 diabetes and obesity.

Additionally, TNF signaling pathway can induce multiple cascade reactions, including activation of the transcription factor NF-kappa B and programmed cell death (Van Antwerp et al., 1996). TNF activates the pro-inflammatory function of vascular ECs by binding to cytokines such as TNFRSF1A/TNFR1 and TNFRSF1B/TNFBR expressed on the cell surface and is a potent pyrogen (Wang et al., 2003). It is mainly secreted by macrophages and can induce cell death in some cancer cell lines (Wang et al., 1996). Previous researches on TNF signaling have indicated that TNF signaling pathway is a negative feedback mechanism, and the activation of NF-kappa B inhibits the signal of cell death (Ge et al., 2018a). Mavrogonatou and Ji *et al.* have shown that TNF-alpha is an inflammatory mediator, and its overexpression can lead to the rapid activation of p38MAPK under the external or internal stimulation, which promotes the production of IL-6 and induces the body's inflammatory response (Ji et al., 2016; Mavrogonatou et al., 2018).

T2DM is caused by insulin resistance and loss of islet beta-cell function. Insulin signaling occurs through the INSR, which is selectively spliced into two isomers: INSR-A and INSR-B (Besic et al., 2015). Malakar *et al.* showed that insulin could regulate selective splicing of INSR through Ras-MAPK/ERK signaling pathway and that INSR-B had a protective effect in β cells, while the expression of INSR-A made β cells sensitive to programmed cell death (Malakar et al., 2016). Previous studies have also shown that insulin signal transduction pathway plays a crucial role in the pathogenesis of diabetes, which is of great significance for the study of insulin signal transduction in type 2 diabetes (Ge et al., 2018a). Insulin binding to INSR on cell membranes will induce signal transduction, and the insulin receptor substrate (IRS) plays a key role in insulin signaling system (Cai et al., 2016). It mediates multidirectional cell signal transduction effects such as IRS and insulin-like growth factor (IGF), thereby exercising the connection and functional regulation with other cytokines (Moon et al., 2015).

This enrichment pathway analysis result indicates that insulins can bind to INSR on the cell membrane, and affect the occurrence of diabetes and inflammation through PI3K–AKT signal transduction pathway. After release of insulin into the blood, insulin could bind to insulin receptor (INSR) on the surface of liver cell membrane and then activates insulin receptor phosphorylates tyrosine site of IRS-1/2, regulating the PI3K/AKT signal pathway, of which IRS2 is the main target in the insulin metabolism effects in liver (Wang et al., 2013). The activated PI3K can catalyze 4, 5-2 phosphatidyl inositol phosphate (PIP2) and generate PIP3, which may act the second messenger to activate AKT, and the activated AKT has an effect on the biological metabolism by regulating downstream molecules (Dai et al., 2016). Therefore, any abnormality in the PI3K–AKT signaling pathway will affect insulin signal transduction, thereby promoting the occurrence and development of insulin resistance and type 2 diabetes.

In summary, the pathogenesis of DM is more complex, and the signal pathways are cross-linked and mutually modulated, presenting a multi-pathway and multi-target pattern. The active ingredients of *L. chinensis* can regulate target proteins involved in signal pathways and play a role in stabilizing signal pathway, revealing the multi-ingredient–multi-target–multi-pathway action mode of TCM. Deep analysis of anti-diabetic and anti-inflammatory pharmacological effects of *L. chinensis*, as well as the target and pathway acting with the active ingredients still need to be further validated.

## DATA AVAILABILITY STATEMENT

All datasets generated for this study are included in the article/ **Supplementary Material**.

## AUTHOR CONTRIBUTIONS

QG is the major contributor to this manuscript. QG conducted the analytical part, wrote the first version of the manuscript, and

finalized the manuscript. LC and YY downloaded the reference and processed the graph and the table in the manuscript. LL, FF, PL, and SM collected the data. KC (corresponding author) and QY (corresponding author) conceived and coordinated the study, and critically evaluated the data. All authors read and approved the final manuscript.

## FUNDING

This work was supported by the National Natural Science Foundation of China (No. 31861143051, 31872425, 31802140, and 81672913) and the Maternal and Child Health Research Project of Jiangsu Province (F201604).

## ACKNOWLEDGMENTS

All authors are thankful to Institute of Life Sciences, Jiangsu University for the help in conducting this study. And we are very grateful to Shanghai Luming Biotech CO. for providing GC/MS analysis.

## SUPPLEMENTARY MATERIAL

The Supplementary Material for this article can be found online at: https://www.frontiersin.org/articles/10.3389/fphar.2020.00347/full#supplementary-material.

## REFERENCES

Antonetti, D. A., Klein, R., and Gardner, T. W. (2012). Diabetic retinopathy. *N Engl. J. Med.* 366 (13), 1227–1239. doi: 10.1056/NEJMra1005073

Barnett, A. (2006). DPP-4 inhibitors and their potential role in the management of type 2 diabetes. *Int. J. Clin. Pract.* 60 (11), 1454–1470. doi: 10.1111/j.1742-1241.2006.01178.x

Besic, V., Shi, H., Stubbs, R. S., and Hayes, M. T. (2015). Aberrant liver insulin receptor isoform a expression normalises with remission of type 2 diabetes after gastric bypass surgery. *PloS One* 10 (3), e0119270. doi: 10.1371/journal.pone.0119270

Boezio, B., Audouze, K., Ducrot, P., and Taboureau, O. (2017). Network-based Approaches in Pharmacology. *Mol. Inform.* 36 (10), 1700048. doi: 10.1002/minf.201700048

Bradley, J. R. (2008). TNF-mediated inflammatory disease. *J. Pathol.* 214 (2), 149–160. doi: 10.1002/path.2287

Cai, S., Sun, W., Fan, Y., Guo, X., Xu, G., Xu, T., et al. (2016). Effect of mulberry leaf (Folium Mori) on insulin resistance *via* IRS-1/PI3K/Glut-4 signalling pathway in type 2 diabetes mellitus rats. *Pharm. Biol.* 54 (11), 2685–2691. doi: 10.1080/13880209.2016.1178779

Chen, X., and Jiang, S. (2018). Maduramicin-activated protein phosphatase 2A results in extracellular signal-regulated kinase 1/2 inhibition, leading to cytotoxicity in myocardial H9c2 cells. *Toxicol. Lett.* 284, 96–102. doi: 10.1016/j.toxlet.2017.12.003

Chen, M. W., Chen, W. R., Zhang, J. M., Long, X. Y., and Wang, Y. T. (2014). Lobelia chinensis: chemical constituents and anticancer activity perspective. *Chin. J. Nat. Med.* 12 (2), 103–107. doi: 10.1016/s1875-5364(14)60016-9

Dai, B., Wu, Q., Zeng, C., Zhang, J., Cao, L., Xiao, Z., et al. (2016). The effect of Liuwei Dihuang decoction on PI3K/Akt signaling pathway in liver of type 2 diabetes mellitus (T2DM) rats with insulin resistance. *J. Ethnopharmacol* 192, 382–389. doi: 10.1016/j.jep.2016.07.024

Fang, J., Wang, L., Wu, T., Yang, C., Gao, L., Cai, H., et al. (2017). Network pharmacology-based study on the mechanism of action for herbal medicines in Alzheimer treatment. *J. Ethnopharmacol* 196, 281–292. doi: 10.1016/j.jep.2016.11.034

Forst, T., and Bramlage, P. (2014). Vildagliptin, a DPP-4 inhibitor for the twice-daily treatment of type 2 diabetes mellitus with or without metformin. *Expert Opin. Pharmacother.* 15 (9), 1299–1313. doi: 10.1517/14656566.2014.920009

Ge, Q., Chen, L., and Chen, K. (2017). Treatment of Diabetes Mellitus Using iPS Cells and Spice Polyphenols. *J. Diabetes Res. 2017,(2017-7-3)* 2017 (1), 5837804. doi: 10.1155/2017/5837804

Ge, Q., Chen, L., Tang, M., Zhang, S., Gao, L., Ma, S., et al. (2018a). Analysis of mulberry leaf components in the treatment of diabetes using network pharmacology. *Eur. J. Pharmacol.* 833 (2018), 50–62. doi: 10.1016/j.ejphar.2018.05.021

Ge, Q., Zhang, S., Chen, L., Tang, M., Liu, L., Kang, M., et al. (2018b). Mulberry Leaf Regulates Differentially Expressed Genes in Diabetic Mice Liver Based on RNA-Seq Analysis. *Front. Physiol.* 9 (2018), 1051. doi: 10.3389/fphys.2018.01051

Henriksen, E. J., and Dokken, B. B. (2006). Role of glycogen synthase kinase-3 in insulin resistance and type 2 diabetes. *Curr. Drug Targets* 7 (11), 1435–1441. doi: 10.2174/1389450110607011435

Hong, M., Li, S., Tan, H. Y., Cheung, F., Wang, N., Huang, J., et al. (2017a). A Network-Based Pharmacology Study of the Herb-Induced Liver Injury Potential of Traditional Hepatoprotective Chinese Herbal Medicines. *Molecules* 22 (4), 632. doi: 10.3390/molecules22040632

Hong, M., Li, S., Wang, N., Tan, H. Y., Cheung, F., and Feng, Y. (2017b). A Biomedical Investigation of the Hepatoprotective Effect of Radix salviae miltiorrhizae and Network Pharmacology-Based Prediction of the Active Compounds and Molecular Targets. *Int. J. Mol. Sci.* 18 (3), 620. doi: 10.3390/ijms18030620

Ji, M., Lu, Y., Zhao, C., Gao, W., He, F., Zhang, J., et al. (2016). C5a Induces the Synthesis of IL-6 and TNF-alpha in Rat Glomerular Mesangial Cells through MAPK Signaling Pathways. *PloS One* 11 (9), e0161867. doi: 10.1371/journal.pone.0161867

Karasik, A., Aschner, P., Katzeff, H., Davies, M. J., and Stein, P. P. (2008). Sitagliptin, a DPP-4 inhibitor for the treatment of patients with type 2 diabetes: a review of recent clinical trials. *Curr. Med. Res. Opin.* 24 (2), 489–496. doi: 10.1185/030079908x261069

Kuo, P. C., Hwang, T. L., Lin, Y. T., Kuo, Y. C., and Leu, Y. L. (2011). Chemical constituents from Lobelia chinensis and their anti-virus and anti-inflammatory bioactivities. *Arch. Pharm. Res.* 34 (5), 715–722. doi: 10.1007/s12272-011-0503-7

Li, J., Chen, K., Yang, B., and Yu, X. (2009). Comparison for Antitumor Activities of Some Chinese Medicinal Herb Extracts. *3rd International Conference on Bioinformatics and Biomedical Engineering, iCBBE 2009*. doi: 10.1109/ICBBE.2009.5162537

Li, Z., Liu, F. Y., and Kirkwood, K. L. (2020). The p38/MKP-1 signaling axis in oral cancer: Impact of tumor-associated macrophages. *Oncol.* 103, 104591. doi: 10.1016/j.oraloncology.2020.104591

MacAulay, K., and Woodgett, J. R. (2008). Targeting glycogen synthase kinase-3 (GSK-3) in the treatment of Type 2 diabetes. *Expert Opin. Ther. Targets* 12 (10), 1265–1274. doi: 10.1517/14728222.12.10.1265

MacDonald, P. E., El-Kholy, W., Riedel, M. J., Salapatek, A. M., Light, P. E., and Wheeler, M. B. (2002). The multiple actions of GLP-1 on the process of glucose-stimulated insulin secretion. *Diabetes* 51 Suppl 3, S434–S442. doi: 10.2337/diabetes.51.2007.S434

Macdougall, C. E., Wood, E. G., Solomou, A., Scagliotti, V., Taketo, M. M., Gaston-Massuet, C., et al. (2019). Constitutive Activation of β-Catenin in Conventional Dendritic Cells Increases the Insulin Reserve to Ameliorate the Development of Type 2 Diabetes in Mice. *Diabetes* 68 (7), 1473–1484. doi: 10.2337/db18-1243

Malakar, P., Chartarifsky, L., Hija, A., Leibowitz, G., Glaser, B., Dor, Y., et al. (2016). Insulin receptor alternative splicing is regulated by insulin signaling and modulates beta cell survival. *Sci. Rep.* 6, 31222. doi: 10.1038/srep31222

Mavrogonatou, E., Konstantinou, A., and Kletsas, D. (2018). Long-term exposure to TNF-alpha leads human skin fibroblasts to a p38 MAPK- and ROS-mediated premature senescence. *Biogerontology* 19 (3-4), 237–249. doi: 10.1007/s10522-018-9753-9

Moon, J. S., Lee, S., Park, M. A., Siempos, I. I., Haslip, M., Lee, P. J., et al. (2015). UCP2-induced fatty acid synthase promotes NLRP3 inflammasome activation during sepsis. *J. Clin. Invest.* 125 (2), 665–680. doi: 10.1172/jci78253

Perrotti, D. D., and Neviani, P. (2013). Protein phosphatase 2A: A target for anticancer therapy. *Lancet Oncol.* 14 (6), e229–e238. doi: 10.1016/S1470-2045(12)70558-2

Pujol, A., Mosca, R., Farres, J., and Aloy, P. (2010). Unveiling the role of network and systems biology in drug discovery. *Trends Pharmacol. Sci.* 31 (3), 115–123. doi: 10.1016/j.tips.2009.11.006

Ru, J., Li, P., Wang, J., Zhou, W., Li, B., Huang, C., et al. (2014). TCMSP: a database of systems pharmacology for drug discovery from herbal medicines. *J. Cheminform.* 6, 13. doi: 10.1186/1758-2946-6-13

Sakaguchi, M., Isono, M., Isshiki, K., Sugimoto, T., Koya, D., and Kashiwagi, A. (2006). Inhibition of mTOR signaling with rapamycin attenuates renal hypertrophy in the early diabetic mice. *Biochem. Biophys. Res. Commun.* 340 (1), 296–301. doi: 10.1016/j.bbrc.2005.12.012

Shibano, M., Tsukamoto, D., Masuda, A., Tanaka, Y., and Kusano, G. (2001). Two new pyrrolidine alkaloids, radicamines A and B, as inhibitors of alpha-glucosidase from Lobelia chinensis Lour. *Chem. Pharm. Bull. (Tokyo)* 49 (10), 1362–1365. doi: 10.1248/cpb.49.1362

Sun, H. Y., Hu, K. Z., and Yin, Z. S. (2017). Inhibition of the p38-MAPK signaling pathway suppresses the apoptosis and expression of proinflammatory cytokines in human osteoarthritis chondrocytes. *Cytokine* 90, 135–143. doi: 10.1016/j.cyto.2016.11.002

Taniguchi, C. M., Emanuelli, B., and Kahn, C. R. (2006). Critical nodes in signalling pathways: insights into insulin action. *Nat. Rev. Mol. Cell Biol.* 7 (2), 85–96. doi: 10.1038/nrm1837

Tian, J., Jin, D., Bao, Q., Ding, Q., Zhang, H., Gao, Z., et al. (2019). Evidence and Potential Mechanisms of Traditional Chinese Medicine for the Treatment of Type 2 Diabetes: A Systematic Review and Meta-analysis. *Diabetes Obes. Metab.* 21(8), 1801–1816. doi: 10.1111/dom.13760

Tsaioun, K., Blaauboer, B. J., and Hartung, T. (2016). Evidence-based absorption, distribution, metabolism, excretion (ADME) and its interplay with alternative toxicity methods. *Altex* 33 (4), 343–358. doi: 10.14573/altex.1610101

Van Antwerp, D. J., Martin, S. J., Kafri, T., Green, D. R., and Verma, I. M. (1996). Suppression of TNF-alpha-induced apoptosis by NF-kappaB. *Science* 274 (5288), 787–789. doi: 10.1126/science.274.5288.787

Wang, C. Y., Mayo, M. W., and Baldwin, A. S.Jr. (1996). TNF- and cancer therapy-induced apoptosis: potentiation by inhibition of NF-kappaB. *Science* 274 (5288), 784–787. doi: 10.1126/science.274.5288.784

Wang, J., Al-Lamki, R. S., Zhang, H., Kirkiles-Smith, N., Gaeta, M. L., Thiru, S., et al. (2003). Histamine antagonizes tumor necrosis factor (TNF) signaling by stimulating TNF receptor shedding from the cell surface and Golgi storage pool. *J. Biol. Chem.* 278 (24), 21751–21760. doi: 10.1074/jbc.M212662200

Wang, X., Wang, Z. Z., and Chen, Y. (2013). The functions of PI3K/AKT signaling pathway in glucose homeostasis. *Chin. Bull. Life Sci.* 25 (2013), 133–137. doi: 10.13376/j.cbls/2013.02.001

Yang, S., Shen, T., Zhao, L., Li, C., Zhang, Y., Lou, H., et al. (2014). Chemical constituents of Lobelia chinensis. *Fitoterapia* 93, 168–174. doi: 10.1016/j.fitote.2014.01.007

Yang, M., Chen, J., Xu, L., Shi, X., Zhou, X., An, R., et al. (2018). A Network Pharmacology Approach to Uncover the Molecular Mechanisms of Herbal Formula Ban-Xia-Xie-Xin-Tang. *Evid Based Complement Alternat. Med.* 2018, 4050714. doi: 10.1155/2018/4050714

Yue, S. J., Liu, J., Feng, W. W., Zhang, F. L., Chen, J. X., Xin, L. T., et al. (2017a). System Pharmacology-Based Dissection of the Synergistic Mechanism of Huangqi and Huanglian for Diabetes Mellitus. *Front. Pharmacol.* 8, 694. doi: 10.3389/fphar.2017.00694

Yue, S. J., Xin, L. T., Fan, Y. C., Li, S. J., Tang, Y. P., Duan, J. A., et al. (2017b). Herb pair Danggui-Honghua: mechanisms underlying blood stasis syndrome by system pharmacology approach. *Sci. Rep.* 7, 40318. doi: 10.1038/srep40318

Zhang, S. X., Wang, J. J., Gao, G., Parke, K., and Ma, J. X. (2006). Pigment epithelium-derived factor downregulates vascular endothelial growth factor (VEGF) expression and inhibits VEGF-VEGF receptor 2 binding in diabetic retinopathy. *J. Mol. Endocrinol.* 37 (1), 1–12. doi: 10.1677/jme.1.02008

Zhang, Y. Q., Mao, X., Guo, Q. Y., Lin, N., and Li, S. (2016). Network Pharmacology-based Approaches Capture Essence of Chinese Herbal Medicines. *Chin. Herbal Medicines* 8 (2), 107–116. doi: 10.1016/S1674-6384(16)60018-7

Zielinski, M. R., and Krueger, J. M. (2012). "Chapter 48 - Inflammation and Sleep," in *Therapy in Sleep Medicine*. Eds. T. J. Barkoukis, J. K. Matheson, R. Ferber and K. Doghramji (Philadelphia: W.B. Saunders), 607–616.

**Conflict of Interest:** The authors declare that the research was conducted in the absence of any commercial or financial relationships that could be construed as a potential conflict of interest.

frontiers in Pharmacology

ORIGINAL RESEARCH
published: 20 March 2020
doi: 10.3389/fphar.2020.00292

# Antitumor Effects and the Compatibility Mechanisms of Herb Pair *Scleromitrion diffusum* (Willd.) R. J. Wang–*Sculellaria barbata* D. Don

*Li Lu*[1], *Sheng Zhan*[1], *Xiaohui Liu*[1], *Xin Zhao*[2], *Xiukun Lin*[1] *and Huanli Xu*[1]*

[1] Department of Pharmacology, School of Basic Medical Sciences, Capital Medical University, Beijing, China, [2] The Second Affiliated Hospital of Southern University of Science and Technology, Shenzhen, China

OPEN ACCESS

**Edited by:**
*Aiping Lu,*
*Hong Kong Baptist University, Hong Kong*

**Reviewed by:**
*William Chi-Shing Tai,*
*Hong Kong Polytechnic University, Hong Kong*
*Jiumao Lin,*
*Fujian University of Traditional Chinese Medicine, China*
*Zhong Liu,*
*Jinan University, China*

***Correspondence:**
*Huanli Xu*
*13301261635@163.com*

**Specialty section:**
*This article was submitted to Ethnopharmacology, a section of the journal Frontiers in Pharmacology*

**Received:** *27 September 2019*
**Accepted:** *27 February 2020*
**Published:** *20 March 2020*

**Citation:**
*Lu L, Zhan S, Liu X, Zhao X, Lin X and Xu H (2020) Antitumor Effects and the Compatibility Mechanisms of Herb Pair Scleromitrion diffusum (Willd.) R. J. Wang–Sculellaria barbata D. Don. Front. Pharmacol. 11:292. doi: 10.3389/fphar.2020.00292*

Herb pair *Scleromitrion diffusum* (Willd.) R. J. Wang (HD) and *Scutellaria barbata* D. Don (SB) has been most frequently used for cancer treatment in traditional Chinese medicine. This study aimed to explore the *in vitro* and *in vivo* antitumor effects of HD-SB extract and to elucidate the underlying compatibility mechanisms. HD, SB, and HD-SB extracts were prepared, and the components were detected by ultraperformance liquid chromatography coupled with quadrupole time-of-flight mass spectrometry method. The *in vitro* antitumor effects of various concentrations of these extract were detected on several tumor cell lines using MTS assay. The *in vivo* antitumor effects were evaluated in Panc28 cells–bearing nude mice model. The compatibility mechanisms of herb pair HD-SB were evaluated based on the systems pharmacology strategy and then validated by cellular experiments. HD-SB extract was demonstrated to inhibit the proliferation of the cancer cell lines dose dependently by MTS assay. *In vivo* antitumor effects of HD-SB were much more potent than either of the two single herbs in Panc28 xenograft mice model. A total 29 active ingredients involved in antitumor effects were selected from HD and SB, and the "herb–composition–target–disease" network was constructed. Then, 58 cancer-related targets and 66 KEGG pathways were identified, and PTGS2-, HSP90-, EGFR-, MMP2-, PPARγ-, and GSTP-mediated pathways were predicted to be the antitumor mechanisms of HD-SB. The cellular experiments showed that HD-SB significantly induced cancer cell apoptosis, decreased p-EGFR, HSP90 and bcl-2 expressions, and increased PPARγ, bax, cleaved caspase 3, cleaved PARP, p-AKT, and p-PI3K expressions compared with HD or SB treatment. Our study showed that HD-SB inhibited tumor growth both *in vitro* and *in vivo*, which might be related with apoptosis induction *via* the EGFR/PPARγ/PI3K/AKT pathway.

**Keywords: *Scleromitrion diffusum* (Willd.) R. J. Wang (HD), *Scutellaria barbata* D. Don (SB), network pharmacology, antitumor, apoptosis**

## INTRODUCTION

Despite the wide use of herb formulas in China and other countries, its modernization faced many obstacles due to its multiherb prescription and complexity. Herb pairs, the most basic composition units of multiherb formulas, are a centralized representative of Chinese herbal compatibility. Because of their simplicity and the basic characteristics of complex formulas, herb pairs are thought to play key roles in the investigation of herb compatibility (Wang et al., 2012; Zhou et al., 2019).

In the clinical practices of traditional Chinese medicine (TCM), herb pair *Scleromitrion diffusum* (Willd.) R. J. Wang (also named *Hedyotis diffusa* Willd., HD, Baihuasheshecao in Chinese) and *Scutellaria barbata* D. Don (SB, Banzhilian in Chinese) is frequently used in numerous classic formulas such as *Erbanerbai Tang*, *Zhongliuhefang*, *Fuzhenghuadu Tang*, *Yupengqianbailian Heji*, and so on (Pan et al., 2016; Yang et al., 2018).

HD, belonging to the Rubiaceae family, is a well-known traditional Chinese medicinal herb. It has long been utilized as a critical ingredient of several TCM formulations for clinical cancer treatment. Previous study showed that HD extract could induce apoptosis and inhibit the proliferation by affecting multiple intracellular targets (Lin et al., 2013; Lin et al., 2015; Sun et al., 2016). Lin et al. (2013) showed HD extract inhibits the growth of colorectal cancer *via* inhibiting tumor angiogenesis by Hedgehog signaling pathway. It also induced the cell apoptosis *via* the interleukin 6–inducible STAT3 pathway (Lin et al., 2015). It was also shown that HD inhibited proliferation and induced apoptosis in colorectal cancer cells *via* regulating PI3K/AKT pathway (Li et al., 2018). SB has long been used in TCM to treat bacterial infections, hepatitis, and tumors along with other herbs (Zhang et al., 2017). SB extract was reported to have anticancer activities in many tumor cell lines, including breast cancer, colorectal cancer, and hepatocarcinoma (Tao and Balunas, 2016; Liu et al., 2018; Wang et al., 2019). SB extract treatment significantly suppressed the activation of several colorectal cancer-related pathways, including STAT3, Erk, and p38 signalings in tumor tissues, and altered the expression of multiple critical target genes such as Bcl-2, Bax, cyclin D1, CDK4, and p21 (Lin et al., 2014). It was also shown that SD inhibited colorectal cancer growth *via* suppression of Wnt/β-catenin signaling pathway (Wei et al., 2017). HD-SB combination has long been used as a classic herb pair for cancer treatment, and clinical practices show that HD-SB combination exhibits better therapeutic effects than the two single individuals (Yeh et al., 2014). However, the compatibility mechanisms of paired HD-SB remain unknown. In this study, the *in vitro* and *in vivo* antitumor effects of HD-SB extract were evaluated, and the compatibility mechanisms were investigated.

## MATERIALS AND METHODS

### Reagents

Human Bel7402, Panc28 cells were obtained from the cell bank of Chinese Academy of Sciences Shanghai (Shanghai, China). Female C57BL/6 mice (6–8 weeks old) were purchased from the Beijing Vital River Laboratory Animal Technology Co. (Beijing, China). Asperulosidic acid methyl ester, kaempferol, rutin, quercetin, apigenin, scutellarin, luteolin, quercetin, and scutebarbatine B were bought from Chroma Biotechnology Co. Ltd. (Chengdu, China). 3-(4,5-Dimethylthiazol-2-yl)-5-(3-carboxymethoxyphenyl)-2-(4-sulfophenyl)- 2H- tetrazolium (MTS) assay kit, RIPA lysis buffer, and Annex V/PI apoptosis kit were purchased from Promega (Madison, WI, USA). Antibodies against prostaglandin G/H synthase 2 (PTGS2), phosphorylated epidermal growth factor receptor (p-EGFR), EGFR, p-AKT, p-PI3K, peroxisome proliferator-activated receptor γ (PPARγ), glutathione S–transferase P (GSTP), and GAPDH were purchased from Abcam (Cambridge, MA, USA). Antibodies for Bcl-2, bax, cleaved caspase 3, cleaved PARP, heat shock protein 90 (HSP90), and 72-kDa type IV collagenase (MMP2) were purchased from Santa Cruz (Dallas, TX, USA). Dulbecco modified Eagle medium, RPMI1640 medium, and fetal bovine serum were purchased from HyClone (Logan, UT, USA). Mammalian whole-cell protein extraction kit and BCA protein assay kit were bought from Thermo Fisher Scientific (Rockford, IL, USA).

### Preparation of HD-SB

HD and SB herb were purchased from Beijing Tongren Co., Ltd. (batch no. 1711046, 1704050, Beijing, China) and identified by Dr. Rui He (School of Traditional Chinese Medicine, Capital Medical University). Voucher specimens (ID: 2018-EJ024, 2018-EJ025, 2018-EJ026) were deposited in the Department of Materia Medica, School of Chinese Medicine, Capital Medical University, China. The dried HD and SB were washed and pulverized into powder. HD, SB, and HD-SB (1:1 wt/wt) were weighed and extracted with 10× volume 70% ethanol for 2 h using heating reflux at 100°C and repeated for three times. The extract solution was filtered and concentrated using vacuum evaporation, and the residual solution was then freeze dried and stored at 4°C. Because the major components of SB and HD are flavonoids, total contents of flavonoids were used as the quality assessment of the extract using the method in Pharmacopoeia of the People's Republic of China (Chinese Pharmacopoeia Commission, 2015). Total flavonoids in SB were expressed as microgram scutellarin equivalents/100 g. Total flavonoids in HD were expressed as microgram quercetin equivalents/100 g.

### Ultraperformance Liquid Chromatography/MS Analysis

Component analysis of the extracts of HD, SB, and HD-SB was performed on ultraperformance liquid chromatography (UPLC) coupled with quadrupole time-of-flight mass spectrometry (MS) system (Waters Corporation, Milford, MA, USA). HD, SB, and HD-SB extract were weighed accurately and dissolved into 10 mg/mL in methanol for analysis. Asperulosidic acid methyl ester, kaempferol, rutin, quercetin, apigenin, scutellarin, luteolin, quercetin, and scutebarbatine B were used as chemical standard compounds. Standard solutions were prepared by dissolving to 1 mg/mL in methanol. The samples were separated by a Waters ACQUITY UPLC HSS T3 Column (2.1 × 100 mm, 1.8 μm; Waters Corporation). The mobile phase

consisted of gradient mixture of acetonitrile (A) and 0.1% formic acid in water (B): 0 to 15 min, 95% to 80% A (vol/vol); 15 to 25 min, 80% to 50% A (v/v); 25 to 30 min, 50% to 20% A (vol/vol). The flow rate was 0.3 mL/min, and the detector scanned from 200 to 400 nm. The full-scan LC-MS data were acquired in both positive and negative ion modes from 30 to 1,300 Da with a 0.4-s scan time. The data were collected, and chromatogram was processed with MassLynx V4.1 software (Waters Corp). Molecular formula speculations of the compounds were determined with Elemental Composition software (Waters Corporation, Milford, MA, USA). Structural identification of the main compounds was determined with Mass Fragment software (Waters Corporation, Milford, MA, USA).

## MTS Assay

The effects of HD, SB, and HD-SB extracts on the growth of different cancer cell lines were detected by MTS assay. Briefly, cells were seeded in 96-well plates and incubated with various concentrations of HD, SB, and HD-SB extracts (0, 12.5, 25, 50, 100, 200 μg/mL). After 48-h incubation, the medium was replaced with new medium containing MTS and incubated for 2 h at 37°C. Then, the Optical Density (OD) value was measured at 490 nm using a microplate reader (EXL800; BioTek, Winooski, VT, USA). The $IC_{50}$ value (the half maximal inhibitory concentration) was defined as the concentration of drug inhibiting 50% of cells.

## *In Vivo* Antitumor Evaluation in Tumor-Bearing Nude Mice Model

The animal experiments were approved by the Committee of Animal Experiments and Experimental Animal Welfare of Capital Medical University in Beijing, China (no. AEEI-2019-078), and performed in accordance with the local institutional guidelines and ethics.

Panc28 cells in logarithmic growth phase were harvested and adjusted into the concentration of $1 \times 10^7$cells/mL. Female BALB/c nude mice (4–6 weeks, 18–20 g) were inoculated with 0.2 mL of the cell suspension subcutaneously. When the tumor grew up to approximately 100 $mm^3$, the mice were randomly divided into the following groups (n = 5): negative control group (0.9% normal saline), 150 mg/kg HD group, 150 mg/kg SB group, 150 mg/kg HD-SB group, or positive control group [50 mg/kg, cyclophosphamide (CTX)], respectively. The drugs were given intragastrically for three times a week. Tumor sizes and body weights were measured every day for 2 weeks. The tumor volumes were calculated according to the following formula: tumor volume = length × $width^2 \times 0.5$. All mice were sacrificed at the end of the experiment, and tissues were collected for analysis.

The excised tumor tissues were fixed with 4% paraformaldehyde and cut into 4- to 6-mm-thick sections. Then the tissue sections were stained with hematoxylin and eosin. Images were taken with a high-capacity digital slide scanner system (3DHISTECH Ltd., Budapest, Hungary).

## Network Pharmacology Analyses

### Chemical Ingredients Database Building and Target Prediction

Information on 124 active components related to HD and SB was collected from the Traditional Chinese Medicine Systems Pharmacology Database and Analysis Platform (TCMSP, http://tcmspw.com/tcmsp.php). Considering HD and SB are orally administrated in cancer treatment, the principle for screening potential active ingredients was defined as follows: oral bioavailability (OB) ≥30% and drug-likeness (DL) ≥ 0.18.

Then, ingredients and targets interactions were obtained from TCMSP, and only the proteins that had direct interactions with each chemical in HD and SB were selected as the putative targets.

### Network Construction and Pathway Analysis

To investigate the action mechanism of active compounds of HD and SB against cancer, the Cytoscape 3.6.1 software package (Boston, MA, USA) was used to construct the "herb–composition–target–disease" network. Two important parameters, degree (the number of edges connected to the node) and betweenness (the number of times a node acts as a bridge along the shortest path between two other nodes), were calculated by Network Analyzer of Cytoscape 3.6.1.

Gene Ontology (GO) enrichment analysis was performed using BiNGO of Cytoscape 3.6.1. The false discovery rate (FDR) was introduced to reveal a multiple-hypothesis testing faulty measure of $p$ values, and only GO terms with $p < 0.01$ were chosen. FDR ($p < 0.05$) was employed as an important cutoff in the analysis.

Pathway enrichment analyses using Kyoto Encyclopedia of Genes and Genomes (KEGG, http://www.genome.jp/kegg/) were performed, and significant pathways were evaluated using the Database Visualization and Integrated Discovery system (DAVID, http://david.abcc.ncifcrf.gov/home.jsp, version 6.8) (Yu et al., 2018). The threshold parameters were set at ease = 0.05, count = 5.

## Apoptosis Analysis

Annexin V–fluorescein isothiocyanate (FITC)/propidium iodide (PI) staining kit was used for detecting apoptosis rates induced by HD, SB, and HD-SB according to the manufacturer's instruction. Briefly, after treatment with HD, SB, and HD-SB for 48 h, the cells were collected and washed three times with washing buffer. Then, approximately $1 \times 10^5$ cells were resuspended in 500 μL detection buffer. Finally, 5 μL of PI and 5 μL of annexin V-FITC were added and analyzed using a flow cytometry (BD FACSCanto™, San Diego, CA, USA).

## Western Blot

After treatment with HD, SB, and HD-SB for 48 h, cells were collected by centrifugation at 3,000 rpm for 10 min. Whole-cell proteins were extracted using mammalian whole-cell protein extraction kit (Promega, Beijing, China). Supernatant protein concentrations were determined using BCA protein assay. Equal amount of protein was loaded and separated on 10% sodium dodecyl sulfate–polyacrylamide gel electrophoresis before being transferred to polyvinylidene fluoride membranes. The membranes were then incubated with 5% nonfat milk for 2 h. After overnight incubations with primary antibodies at 4°C, the membranes were incubated with goat anti–rabbit or goat anti–mouse alkaline phosphatase–conjugated secondary antibodies (1:3,000; Promega). The membranes were detected by

enhanced chemiluminescence Western blot detection regents. The immunoreactive bands were analyzed with Image J 1.43 software (National Institutes of Health, Bethesda, MD, USA).

## Statistical Analysis

All data are presented as the mean ± SD of three independent experiments. Two-tailed Student *t* test or analysis of variance by GraphPad Prism 5.0 (GraphPad Software, San Diego, CA, USA) was used for statistical analysis. Differences were considered statistically significant when $p < 0.05$.

# RESULTS

## Components Analysis for HD-SB

Because the main active components of SB and HD were reported to be flavonoids (Wang et al., 2008; Yang et al., 2018), total contents of flavonoids were determined. The total flavonoids in SB are approximately 1.84 g scutellarin equivalents/100 g and that in HD is approximately 2.01 g quercetin equivalents/100 g. The total flavonoids in HD-SB are approximately 2.53 g scutellarin equivalents/100 g and 1.97 quercetin equivalents/100 g.

The main components in HD, SB, and HD-SB were also determined by UPLC-MS. Representative chromatograms by UPLC-MS of SB, HD, and HD-SB are shown in **Figure 1**. Using the standards of main components in SB and HD, we identified that the ingredients in HD were asperulosidic acid methyl ester (retention time, 19.74 min), kaempferol (retention time:24.39 min), rutin (retention time, 29.88), and quercetin (retention time, 32.74 min) (**Figure 1A**), and the main ingredients in SB were apigenin (retention time, 13.98 min), scutellarin (retention time, 17.42 min), luteolin (retention time, 19.31 min), quercetin (retention time, 32.74 min), and scutebarbatine B (retention time, 33.98 min) (**Figure 1B**). All these ingredients can be found in the chromatogram of HD-SB (**Figure 1C**).

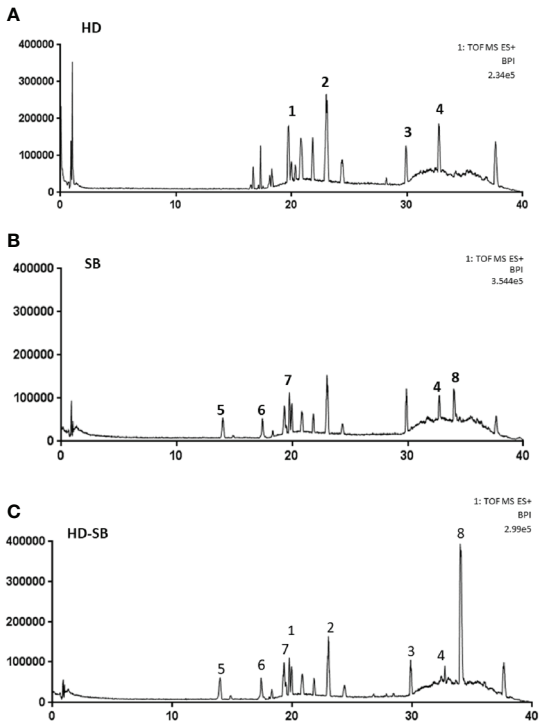


**FIGURE 1 |** Representative chromatogram by UPLC-MS of *Scleromitrion diffusum* (Willd.) R. J. Wang (HD), *Scutellaria barbata* D. Don (SB), and HD-SB. Results are shown with matching standards of asperulosidic acid methyl ester, kaempferol, rutin, quercetin, apigenin, scutellarin, luteolin, quercetin, and scutebarbatine B. **(A)** HD, **(B)** SB, **(C)** HD-SB.

## HD-SB Significantly Inhibited Cancer Cell Growth

The inhibitory effects of SB, HD, and HD-SB on the growth of tumor cell lines (Panc28, Bel7402, and HepG2 cells) and human normal liver cells (L02 cells) were evaluated by MTS assay. As shown in **Figure 2**, SB, HD, and HD-SB inhibited the growth of Panc28, Bel7402, and HepG2 cells dose dependently, and HD-SB showed more obvious inhibitory effects than SB or HD treatment. The $IC_{50}$ of HD-SB on Panc28, Bel7402, and HepG2 cells were 110.50 ± 7.10, 89.48 ± 10.24, and 105.45 ± 9.47 μg/mL, respectively. The $IC_{50}$ of HD on Panc28, Bel7402, and HepG2 cells were 207.14 ± 10.12, 179.35 ± 9.14, and 205.54 ± 9.74 μg/mL, respectively. The $IC_{50}$ of SB on Panc28, Bel7402, and HepG2 cells were all >200 μg/mL. Also, the inhibitory effects of SB, HD, and HD-SB on L02 cells were much weaker than that on cancer cells, with all the $IC_{50}$ > 200 μg/ml.

## HD-SB Significantly Inhibited Cancer Growth *In Vivo*

Panc28 cells xenograft tumors in BALB/c nude mice were established and treated with SB, HD, and HD-SB intragastrically. As shown in **Figure 3**, HD-SB treatment displayed more obvious inhibitory effects on tumor growth as compared to HD or SB treatment; the final inhibitory rates of tumor growth were 28.32%, 39.95%, and 52.28%, respectively, in mice treated with SB, HD, or HD-SB. Importantly, the body weight of the mice was less affected in mice treated with SB, HD, or HD-SB, compared with those treated with CTX (**Figure 3B**). Hematoxylin and eosin staining was performed to further evaluate the toxicity of SB, HD, or HD-SB (**Figure 3C**). As shown in **Figure 3D**, no obvious lesions were found in the main organs of mice treated with SB, HD, or HD-SB. These results suggested that HD-SB displayed potent antitumor effect *in vivo* with low toxicity.

## Network Pharmacology Analyses for HD-SB

### Active *Ingredients* Screening

A total of 131 chemical ingredients of HD and SB were retrieved from TCMSP. The compounds' ADME properties including OB (≥30%) and DL (≥0.18) were used to select active ingredients. As a result, 37 active ingredients were selected. According to the target-disease prediction system in TCMSP, 29 active ingredients were found to have potential anticancer effects among the 37 active ingredients selected. The information of the 29 active components in HD-SB is shown in **Supplementary Table 1**.

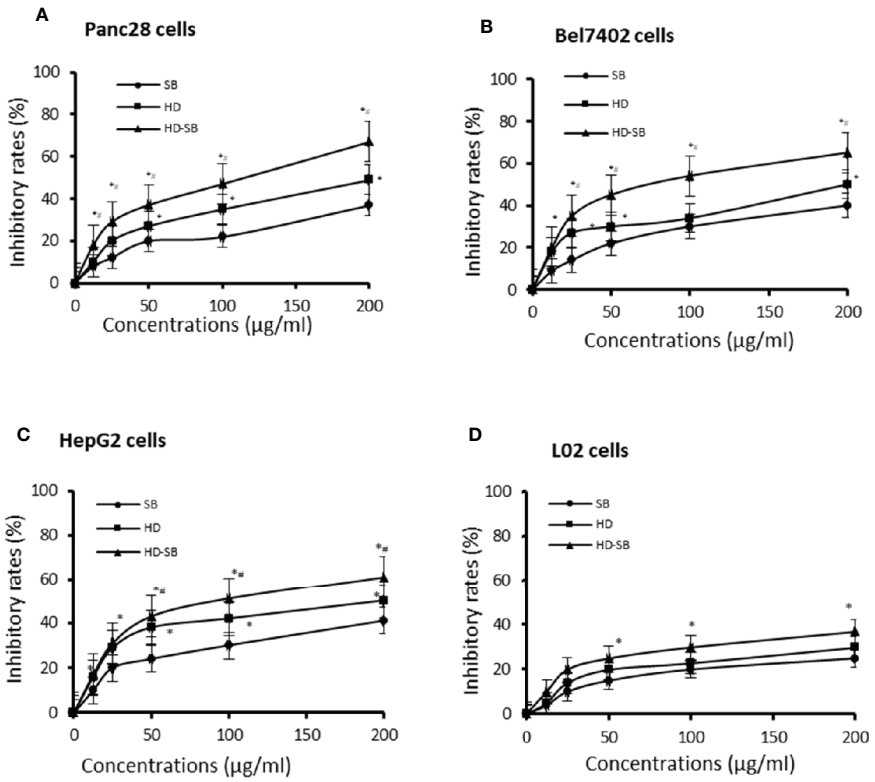


**FIGURE 2 |** *Scleromitrion diffusum* (Willd.) R. J. Wang (HD), *Scutellaria barbata* D. Don (SB), and HD-SB extract inhibited the cancer cell growth. Panc28 **(A)**, Bel7402 **(B)**, HepG2 **(C)**, and L02 **(D)** cells were treated with different concentrations of HD, SB, and HD-SB for 48 h, and the cell viability was determined by MTS assay. $^{*}P < 0.05$, compared with the SB group; $^{\#}P < 0.05$, compared with the HD group.

## Target and Function Analysis

To obtain the tumor-related targets of the 29 active components, components-related targets and targets-related disease were further screened using TCMSP. The proteins that had direct interactions with each chemical in HD and SB were selected as the putative targets. After comparison with UniProt Knowledgebase, 54 tumor-related targets were finally retrieved (**Supplementary Table 2**).

## Network and Pathway Analysis

To investigate the action mechanism of active compounds of HD and SB against cancer, "herb–composition–target–disease" network was constructed using the Cytoscape 3.6.1 software package. As shown in **Figure 4A**, 172 nodes (2 herbs, 29 compounds, 54 targets, and 87 pathways) and 612 edges (relationship between the nodes) were included in the "herb-composition-target-disease." Detailed information about nodes and parameters of the network are shown in **Supplementary Table 3**. The node degree and betweenness distribution (shortest path length distribution) are shown in **Figures 4B, C**. In the network, nodes and parameters of targets with the degree value ≥10 are shown in **Supplementary Table 4**. And nodes and parameters of diseases with the degree value ≥5 are shown in **Supplementary Table 5**.

The above information suggests that (1) quercetin, luteolin, wogonin, and cesterol (with higher degree) might be the material basis of the antitumor effects of HD-SB; (2) among targets with the degree value ≥10, the top six targets were PTGS2, HSP90, EGFR, MMP2, PPARγ, and GSTP, with the degree values of 50, 45, 27, 25, 22, and 21, respectively, indicating that these targets might be the antitumor targets of HD-SB; (3) among the tumor-related diseases with the degree value ≥5, the top six tumor-related diseases were cancer (unspecific), breast cancer, pancreatic cancer, prostate cancer, non–small cell lung cancer, and solid tumors.

The GO enrichment analysis included 1,732 GO items, among which 1,450 were related to biological processes, 177 were related to molecular functions, and 105 were related to cell composition (**Figure 5A**). GO classified cellular compositions of HD-SB–related genes, mainly including perikarya, muscle fiber membrane, postsynaptic membrane, mitochondrial outer membrane, vesicles, spindle apparatus, and so on. GO classified molecular function of HD-SB–related genes, mainly including protein kinases binding, protease binding, lipid binding, HSP90 binding, steroid binding, transcriptional factors activation, acetylcholine receptor activity, adrenergic receptor activity, and so on. GO classified biological process of HD-SB–related genes, mainly including cellular process

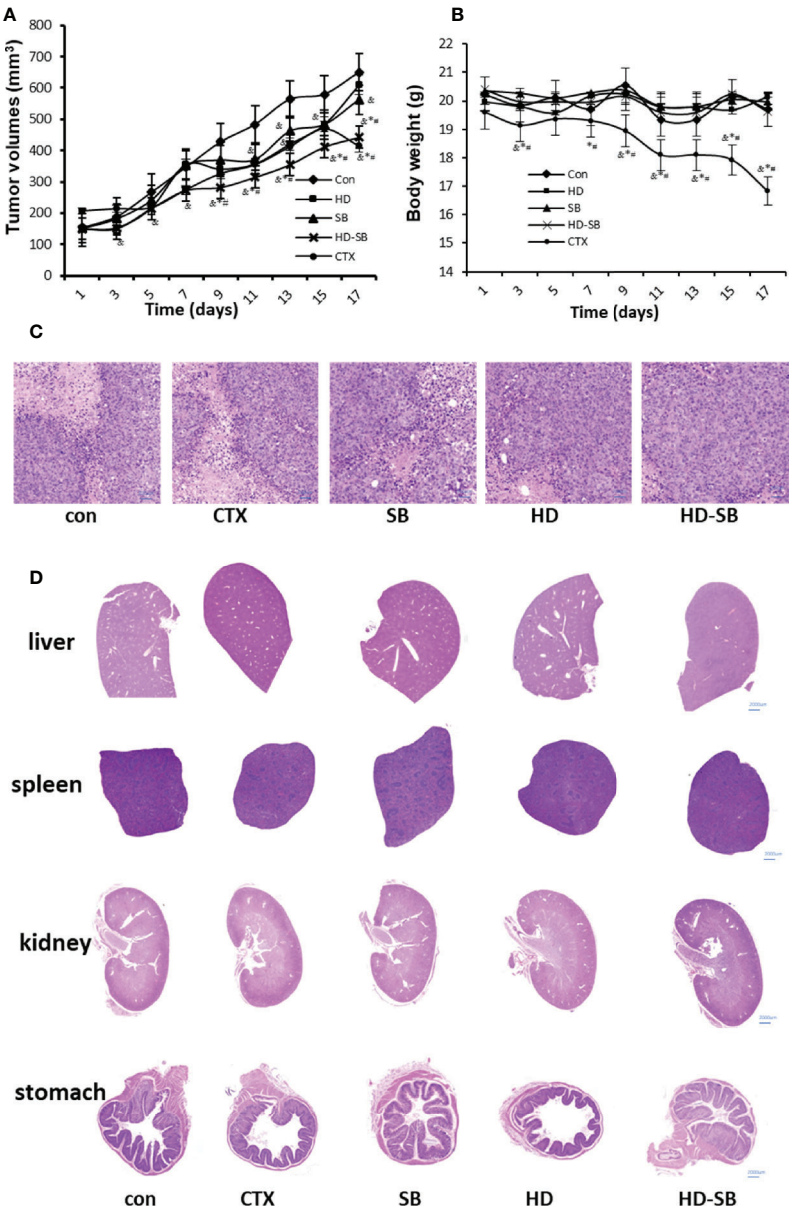


**FIGURE 3 |** *Scleromitrion diffusum* (Willd.) R. J. Wang (HD)-*Scutellaria barbata* D. Don (SB) extract inhibited tumor growth in the xenograft model. Mice bearing Panc28 cancer cells were treated with HD (150 mg/kg), SB (150 mg/kg), and HD-SB (150 mg/kg). **(A)** Tumor volume measured every 2 days. **(B)** Mouse body weight measured every 2 days. $^{\&}P < 0.05$, compared with the control group; $^{*}P < 0.05$, compared with the SB group; $^{\#}P < 0.05$, compared with the HD group. **(C)** Hematoxylin and eosin staining for tumor tissues excised. Scale bar, 200 μm. **(D)** Histological analysis of organs excised from Panc28 tumor-bearing mice, Scale bar, 2,000 μm.

regulation, polymer metabolism regulation, intracellular metabolism regulation, signal transduction, esterase activity regulation, cell proliferation regulation, cell apoptosis regulation, programmed cell death, and so on.

The enrichment analysis of KEGG pathways included 66 KEGG pathways. The top 20 pathways with ease <0.05, count ≥10, FDR <0.01 are shown in **Figure 5B**.

## HD-SB Induced Apoptosis by Targeting EFGR or PPARγ-Mediated Pathways

To validate the obtained results in systems pharmacology analysis, further experiment was performed to delineate the molecular mechanism. The expressions of predicted targets were determined by Western blot analysis. As shown in **Figure 6**, p-EGFR and HSP90 were significantly down-regulated, whereas PPARγ and GSTP were significantly up-

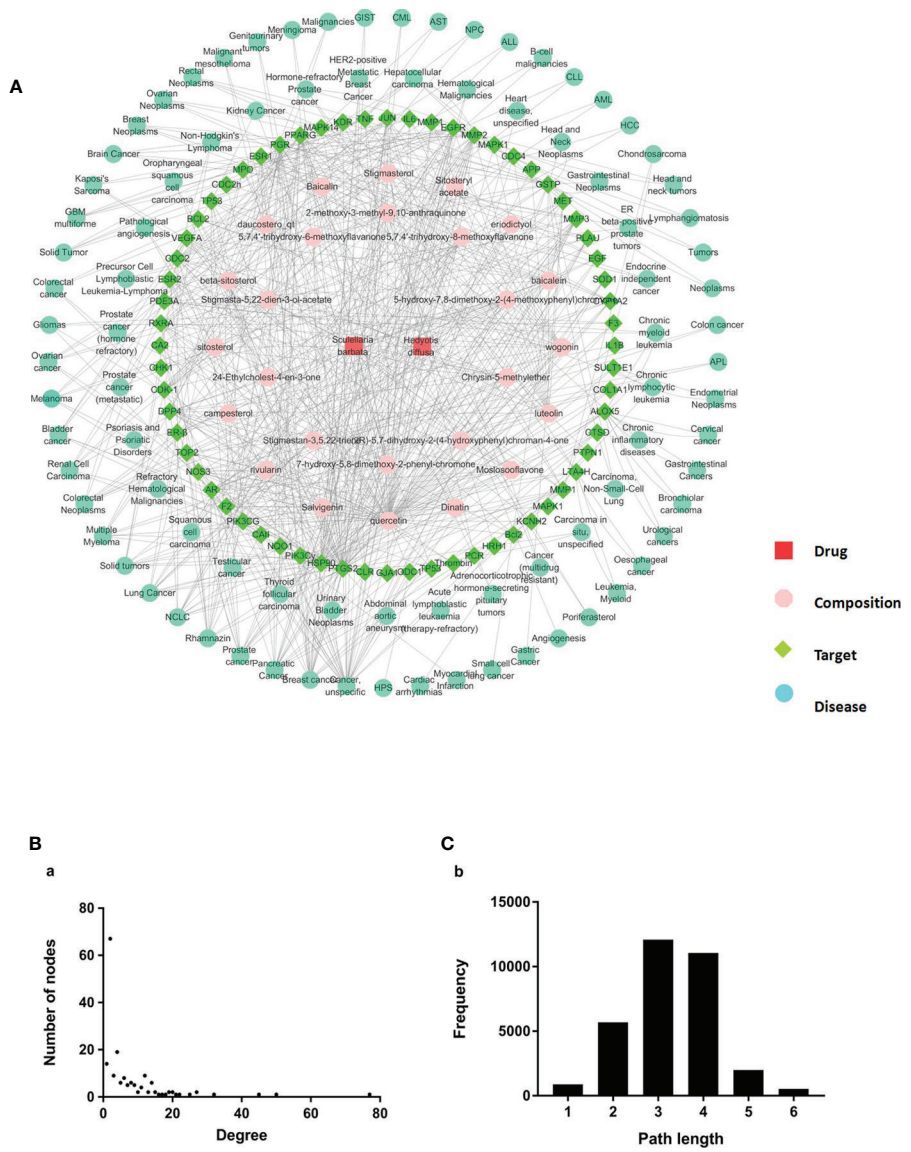


**FIGURE 4 |** Construction and properties analysis of "herb–composition–target–disease" network of *Scleromitrion diffusum* (Willd.) R. J. Wang (HD) and *Scutellaria barbata* D. Don (SB). **(A)** Herb-composition-target-disease network of HD and SB. **(B)** node degree; **(C)** betweenness distribution (shortest path length distribution).

regulated after HD-SB treatment, compared with HD or SB treatment.

The effects of HD-SB treatment on apoptosis and the proteins involved in apoptosis were also determined. As shown in **Figure 7A**, HD-SB treatment significantly induced apoptosis of both cell lines compared with HD or SB treatment. The apoptosis rates of Bel7402 cells treated with SB, HD, or HD-SB were 7.0%, 12.5%, and 22.9%, respectively, and those of panc28 cells were 10.6%, 15.5%, and 34.7%, respectively. The expressions of apoptosis-related proteins were also determined (**Figure 7B**). The result showed that Bcl-2 expression was obviously decreased, and bax, cleaved caspase 3, and cleaved PARP were obviously increased in the HD-SB treatment group compared with the HD or SB treatment groups. Also, p-AKT and p-PI3K were obviously increased in the HD-SB group compared with HD or SB treatment groups. These results showed that HD-SB inhibited cancer proliferation through induction of apoptosis and suppressed EGFR or PPARγ-related pathways.

## DISCUSSION

Herb pair HD-SB was the core couplet in TCM commonly used for anti-inflammation and anticancer treatments (Pan et al., 2016; Yang et al., 2018). Although HD-SB combination has long been used as a classic herb pair, the bioactive compounds, the potential targets, and compatibility mechanisms of HD-SB

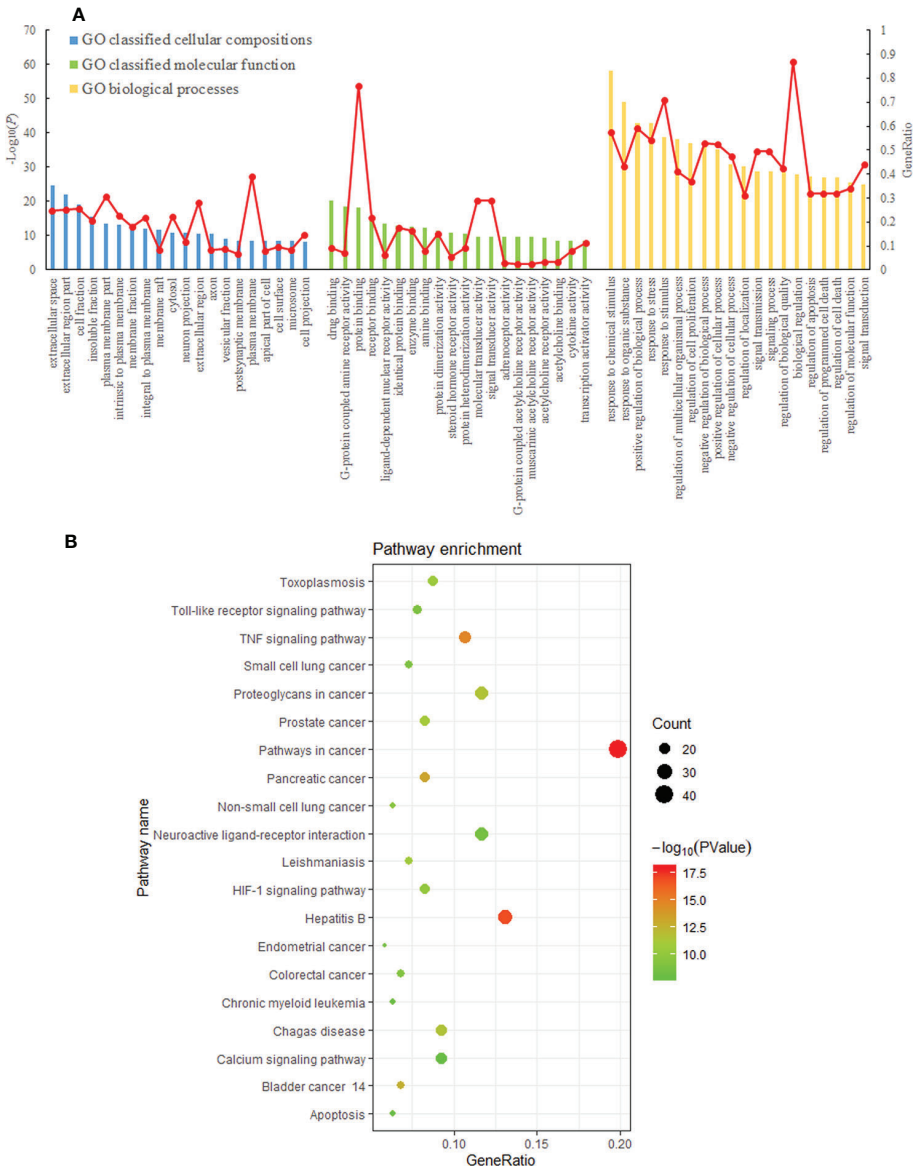


**FIGURE 5 |** Results of gene ontology (GO) and Kyoto Encyclopedia of Genes and Genomes (KEGG) pathway enrichment analysis. **(A)** Result of GO classified cellular compositions, molecular function, and biological process of *Scleromitrion diffusum* (Willd.) R. J. Wang (HD) and *Scutellaria barbata* D. Don (SB)–related genes. **(B)** KEGG pathway enrichment analysis of *Hedyotis diffusa–Sculellaria barbata*–related genes (the first 20 pathways with ease < 0.05, count ≥ 10, and FDR < 0.01).

remain unknown. In this study, ethanol extract of HD, SB, and equal ratio of HD-SB were prepared. The main components of these extract were determined with the aid of UPLC-MS. The *in vitro* and *in vivo* anti–pancreatic cancer effects of HD-SB extract were evaluated. And the results showed that HD-SB displayed much more potent inhibitory effects on tumor growth compared with HD or SB.

In recent years, network pharmacology analysis was successfully used to predict the underlying function mechanisms of TCM formulas for cancer, depression, and cardiovascular disease treatment (Zhao et al., 2019). Network pharmacology is a systems biology–based methodology for evaluating pharmacokinetics (ADME properties of drugs) and target prediction, as well as investigating the multipharmacological effects of traditional medicines at the molecular level (Di et al., 2018; Gong et al., 2018).

In the current study, network pharmacology was conducted to predict the potential targets and pathways of HD-SB in cancer

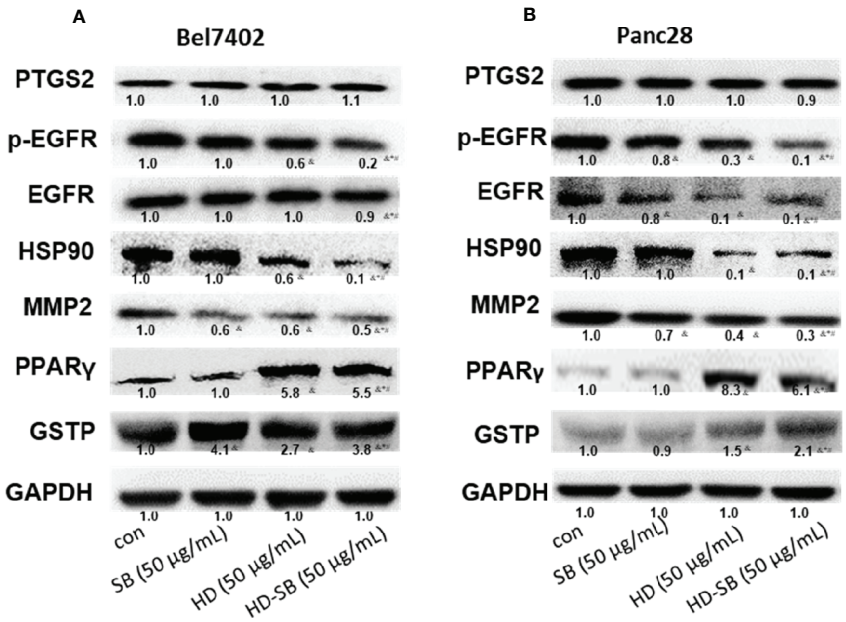


**FIGURE 6 |** Western blot analysis for the expressions of predicted targets of *Scleromitrion diffusum* (Willd.) R. J. Wang (HD) and *Scutellaria barbata* D. Don (SB) by systems pharmacology. **(A)** Bel7402 cells; **(B)** Panc28 cells.

treatment. The diagram of this study is shown in **Figure 8**. First, using target-disease prediction system in TCMSP and the screening principle of OB ≥30% and DL ≥0.18, 29 active compounds with potential anticancer effects were obtained. Then "herb–composition–target–disease" network was constructed using Cytoscape 3.6.1 software package, and GO and KEGG pathway enrichment analysis was done. The result showed that (1) quercetin, luteolin, wogonin, and cesterol might be the material basis of the antitumor effects of HD-SB; and (2) PTGS2-, HSP90-, EGFR-, MMP2-, PPARγ-, and GSTP-mediated pathways might be the antitumor mechanism of HD-SB.

To validate the prediction results by network pharmacology analysis, Western blot was conducted to detect the expressions of PTGS2, HSP90, EGFR, MMP2, PPARγ, and GSTP after HD-SB treatment. The result showed that p-EGFR and HSP90 were significantly down-regulated, whereas PPARγ was significantly up-regulated after HD-SB treatment, compared with HD or SB treatment. Because p-EGFR and PPARγ are related with cell apoptosis (Shi et al., 2016; Jackson and Ceresa, 2017), apoptosis rates and apoptosis-related proteins were also determined in cells treated with HD, SB, and HD-SB. It was found that HD-SB treatment significantly decreased bcl-2 expression; increased bax, cleaved caspase 3, cleaved PARP, p-AKT, and p-PI3K; and finally induced cancer cell apoptosis (**Figure 7**).

EGFR is a known oncoprotein, and EGFR ligands activate downstream signaling such as PI3K/AKT, PLCγ/PKC, and STATs signaling cascades, leading to cell proliferation, migration, metastasis, and adhesion (Ni et al., 2017). The PI3K/Akt signaling pathway is a major pathway in regulating cell survival signals. It was reported that PPARγ agonist exhibited antiproliferative activity and induction of apoptosis by inhibiting the PI3K/Akt survival pathway (Hyun et al., 2015). Our present result showed that HD-SB induced apoptosis by activating PPARγ and inhibiting EGFR and PI3K/AKT pathway (**Figure 8**). It was shown that EGFR activation can induce ubiquitination and degradation of PPARγ (Xu et al., 2016). Although several reports show that PPARγ agonists regulate EGFR signaling, almost all of these studies suggest that these effects on EGFR signaling are independent of PPARγ activation (Mansure et al., 2013; Shi et al., 2016). The relationship between EGFR inhibition and PPARγ activation regulated by HD-SB needs further investigation. Also, the mechanisms of EGFR inhibition and PPARγ activation regulated by HD-SB will be further studied.

In summary, our study systematically verified the antitumor effect of HD-SB *in vitro* and *in vivo*. Also, our study showed that HD-SB induced cancer cell apoptosis *via* EGFR/PPARγ/PI3K/AKT pathway and lays a solid foundation for further studies of the herb pair in cancer treatment.

## DATA AVAILABILITY STATEMENT

The raw data supporting the conclusions of this article will be made available by the authors, without undue reservation, to any qualified researcher.

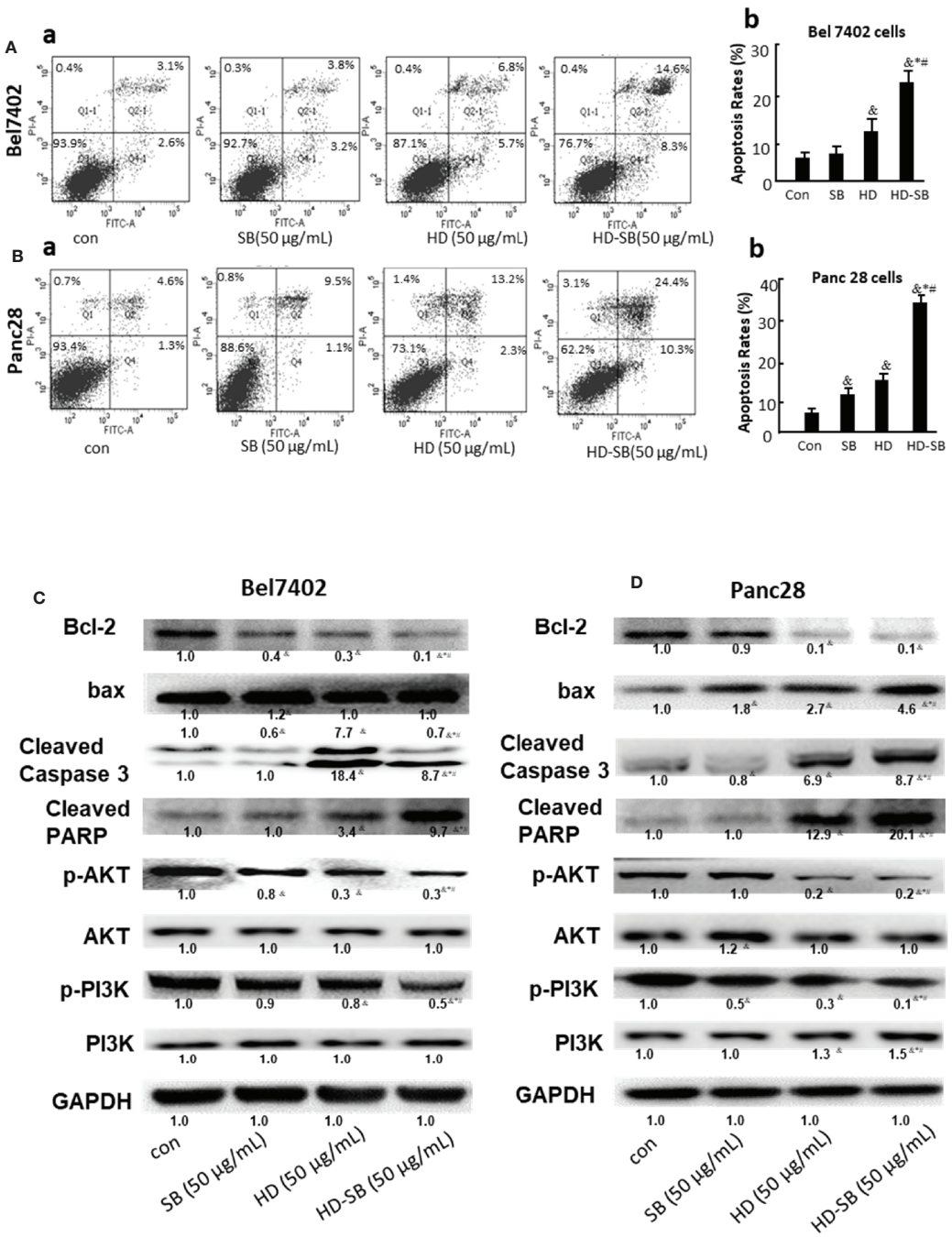


**FIGURE 7 |** Effects of *Scleromitrion diffusum* (Willd.) R. J. Wang (HD), *Scutellaria barbata* D. Don (SB), and HD-SB extract on apoptosis and expressions of apoptosis-related proteins. Apoptosis was detected by flow cytometry for **(Aa)** Bel7402 cells and **(Ba)** Panc28 cells treated by HD, SB, and HD-SB. Quantification of apoptosis in **(Ab)** Bel7402 cells and **(Bb)** Panc28 cells was shown. $^{\&}P < 0.05$, compared with the control group; $^{*}P < 0.05$, compared with the SB group; $^{\#}P < 0.05$, compared with the HD group. Expressions of apoptosis-related proteins in **(C)** Bel7402 cells and **(D)** Panc28 cells treated by HD, SB, and HD-SB were detected by Western blot.

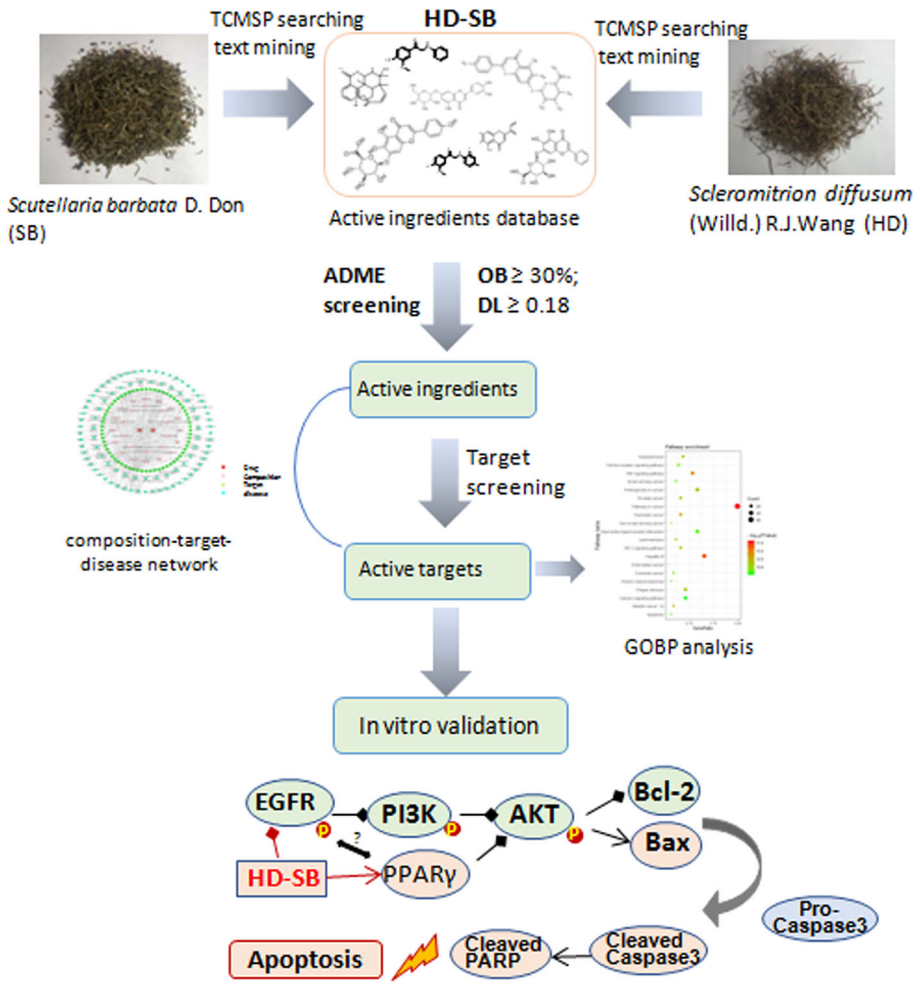


**FIGURE 8 |** The diagram for studying the compatibility mechanisms of *Scleromitrion diffusum* (Willd.) R. J. Wang (HD), *Scutellaria barbata* D. Don (SB), and (HD-SB).

## ETHICS STATEMENT

The animal experiments were approved by the Committee of Animal Experiments and Experimental Animal Welfare of Capital Medical University in Beijing, China (No.AEEI-2019-078).

## AUTHOR CONTRIBUTIONS

LL, XkL, and HX contributed conception and design of the study. LL, SZ, XhL, and XZ performed the study. XZ performed the statistical analysis. HX wrote the first draft of the manuscript. All authors contributed to manuscript revision, read and approved the submitted version.

## FUNDING

This work was supported by the Natural Science Foundation of China (#81774191), the Beijing Natural Science Foundation (#7172031 and 7172029). This work was also supported by Project of High-level Teachers in Beijing Municipal Universities in the Period of 13th 5-year Plan (#CIT&TCD201804086).

## ACKNOWLEDGMENTS

We thank Dr. Xuelin Zhou, Yi Ma, and Yi Wu in Capital Medical University for their assistance in the herb components analysis.

## SUPPLEMENTARY MATERIAL

The Supplementary Material for this article can be found online at: https://www.frontiersin.org/articles/10.3389/fphar.2020.00292/full#supplementary-material

## REFERENCES


Chinese Pharmacopoeia Commission (2015). *Pharmacopoeia of the People's Republic of China (Volume 1)* (Beijing: China Medical Science Press), p118.

Di, S., Han, L., Wang, Q., Liu, X., Yang, Y., Li, F., et al. (2018). A Network Pharmacology approach to uncover the mechanisms of Shen-Qi-Di-Huang decoction against diabetic nephropathy. *Evid. Based Complement Alternat. Med.* 2018, 7043402. doi: 10.1155/2018/7043402

Gong, B., Kao, Y., Zhang, C., Sun, F., and Zhao, H. (2018). Systematic investigation of Scutellariae barbatae herba for treating hepatocellular carcinoma based on network pharmacology. *Evid. Based Complement Alternat. Med.* 2018, 4365739. doi: 10.1155/2018/4365739.

Hyun, S., Kim, M. S., Song, Y. S., Bak, Y., Ham, S. Y., Lee, D. H., et al. (2015). Peroxisome proliferator-activated receptor-gamma agonist 4-O-methylhonokiol induces apoptosis by triggering the intrinsic apoptosis pathway and inhibiting the PI3K/Akt survival pathway in SiHa human cervical cancer cells. *J. Microbiol. Biotechnol.* 25 (3), 334–342. doi: 10.4014/jmb.1411.11073

Jackson, N. M., and Ceresa, B. P. (2017). EGFR-mediated apoptosis via STAT3. *Exp. Cell. Res.* 356 (1), 93–103. doi: 10.1016/j.yexcr.2017.04.016

Li, Q., Lai, Z., Yan, Z., Peng, J., Jin, Y., Wei, L., et al. (2018). Hedyotis diffusa Willd inhibits proliferation and induces apoptosis of 5-FU resistant colorectal cancer cells by regulating the PI3K/AKT signaling pathway. *Mol. Med. Rep.* 17 (1), 358–365. doi: 10.3892/mmr.2017.7903

Lin, J., Wei, L., Shen, A., Cai, Q., Xu, W., Li, H., et al. (2013). Hedyotis diffusa Willd extract suppresses Sonic hedgehog signaling leading to the inhibition of colorectal cancer angiogenesis. *Int. J. Oncol.* 42, 651–656. doi: 10.3892/ijo.2012.1753

Lin, J., Chen, Y., Cai, Q., Wei, L., Zhan, Y., Shen, A., et al. (2014). Scutellaria Barbata D Don Inhibits Colorectal Cancer Growth via Suppression of Multiple Signaling Pathways. *Integr. Cancer Ther.* 13 (3), 240–248. doi: 10.1177/1534735413508811

Lin, J., Li, Q., Chen, H., Lin, H., Lai, Z., and Peng, J. (2015). Hedyotis diffusa Willd. extract suppresses proliferation and induces apoptosis via IL-6-inducible STAT3 pathway inactivation in human colorectal cancer cells. *Oncol. Lett.* 9 (4), 1962–1970. doi: 10.3892/ol.2015.2956

Liu, J., Jiang, M., Li, Z., Zhang, X., Li, X., Hao, Y., et al. (2018). A novel systems pharmacology method to investigate molecular mechanisms of Scutellaria barbata D. Don for non-small cell lung cancer. *Front. Pharmacol.* 9,1473. doi: 10.3389/fphar.2018.01473

Mansure, J. J., Nassim, R., Chevalier, S., Szymanski, K., Rocha, J., Aldousari, S., et al. (2013). A novel mechanism of PPAR gamma induction via EGFR signalling constitutes rational for combination therapy in bladder cancer. *PloS One* 8 (2), e55997. doi: 10.1371/journal.pone.0055997

Ni, J., Zhou, L. L., Ding, L., Zhao, X., Cao, H., Fan, F., et al. (2017). PPARγ agonist efatutazone and gefitinib synergistically inhibit the proliferation of EGFR-TKI-resistant lung adenocarcinoma cells via the PPARγ/PTEN/Akt pathway. *Exp. Cell. Res.* 361 (2), 246–256. doi: 10.1016/j.yexcr.2017.10.024

Pan, L. T., Sheung, Y., Guo, W. P., Rong, Z. B., and Cai, Z. M. (2016). Hedyotis diffusa plus Scutellaria barbata induce bladder cancer cell apoptosis by inhibiting akt signaling pathway through downregulating miR-155 expression. *Evid. Based Complement Alternat. Med.* 2016, 9174903. doi: 10.1155/2016/9174903.

Shi, J., Zhang, W., You, M., Xu, Y., Hou, Y., and Jin, J. (2016). Pioglitazone inhibits EGFR/MDM2 signaling-mediated PPARγ degradation. *Eur. J. Pharmacol.* 791, 316–321. doi: 10.1016/j.ejphar.2016.09.010

Sun, G., Wei, L., Feng, J., Lin, J., and Peng, J. (2016). Inhibitory effects of Hedyotis diffusa Willd. on colorectal cancer stem cells. *Oncol. Lett.* 11 (6), 3875–3881. doi: 10.3892/ol.2016.4431

Tao, G., and Balunas, M. J. (2016). Current therapeutic role and medicinal potential of Scutellaria barbata in Traditional Chinese Medicine and Western research. *J. Ethnopharmacol.* 182, 170–180. doi: 10.1016/j.jep.2016.02.012

Wang, Y., Xue, X., Xiao, Y., Zhang, F., Xu, Q., and Liang, X. (2008). Purification and preparation of compounds from an extract of Scutellaria barbata D. Don using preparative parallel high performance liquid chromatography. *J. Sep. Sci.* 31 (10), 1669–1676. doi: 10.1002/jssc.200700609

Wang, S. P., Hu, Y. Y., Tan, W., Wu, X., Chen, R. E., Cao, J. L., et al. (2012). Compatibility art of traditional Chinese medicine: from the perspective of herb pairs. *J. Ethnopharmacol.* 143, 412–423. doi: 10.1016/j.jep.2012.07.033

Wang, L., Xu, J., Yan, Y., Liu, H., Karunakaran, T., and Li, F. (2019). Green synthesis of gold nanoparticles from Scutellaria barbata and its anticancer activity in pancreatic cancer cell (PANC-1). *Artif. Cells Nanomed. Biotechnol.* 47 (1), 1617–1627. doi: 10.1080/21691401.2019.1594862

Wei, L. H., Lin, J. M., Chu, J. F., Chen, H. W., Li, Q. Y., and Peng, J. (2017). Scutellaria barbata D. Don inhibits colorectal cancer growth via suppression of Wnt/β-catenin signaling pathway. *Chin. J. Integr. Med.* 23 (11), 858–863. doi: 10.1007/s11655-017-2775-3

Xu, Y., Jin, J., Zhang, W., Zhang, Z., Gao, J., Liu, Q., et al. (2016). EGFR/MDM2 signaling promotes NF-κB activation via PPARγ degradation. *Carcinogenesis* 37 (2), 215–222. doi: 10.1093/carcin/bgv252

Yang, W., He, S., Xiao, N., Qiao, Y., Sui, H., Liang, L., et al. (2018). Simultaneous determination of 15 flavonoids in Scutellaria barbata-Hedyotis diffusa herb pair by HPLC Q-TOF MS. *J. AOAC. Int.* 2018. doi: 10.5740/jaoacint.17-0469

Yeh, Y. C., Chen, H. Y., Yang, S. H., Lin, Y. H., Chiu, J. H., Lin, Y. H., et al. (2014). Hedyotis diffusa combined with Scutellaria barbata are the core treatment of Chinese herbal medicine used for breast cancer patients: a population-based study. *Evid. Based Complement Alternat. Med.* 2014, 1–9. doi: 10.1155/2014/202378.

Yu, G., Wang, W., Wang, X., Xu, M., Zhang, L., Ding, L., et al. (2018). Network pharmacology-based strategy to investigate pharmacological mechanisms of Zuojinwan for treatment of gastritis. *BMC. Complement Altern. Med.* 18 (1), 292. doi: 10.1186/s12906-018-2356-9

Zhang, L., Ren, B., Zhang, J., Liu, L., Liu, J., Jiang, G., et al. (2017). Anti-tumor effect of Scutellaria barbata D. Don extracts on ovarian cancer and its phytochemicals characterisation. *J. Ethnopharmacol.* 206, 184–192. doi: 10.1016/j.jep.2017.05.032

Zhao, M., Chen, Y., Wang, C., Xiao, W., Chen, S., Zhang, S., et al. (2019). Systems pharmacology dissection of multi-scale mechanisms of action of Huo-Xiang-Zheng-Qi formula for the treatment of gastrointestinal diseases. *Front. Pharmacol.* 9, 1448. doi: 10.3389/fphar.2018.01448

Zhou, Y., Tao, H., Wang, A., Zhong, Z., Wu, X., Wang, M., et al. (2019). Chinese herb pair Paeoniae Radix Alba and Atractylodis Macrocephalae Rhizoma suppresses LPS-induced inflammatory response through inhibiting MAPK and NF-κB pathway. *Chin. Med.* 14, 2. doi: 10.1186/s13020-019-0224-2


**Conflict of Interest:** The authors declare that the research was conducted in the absence of any commercial or financial relationships that could be construed as a potential conflict of interest.

frontiers in Pharmacology

ORIGINAL RESEARCH
published: 24 March 2020
doi: 10.3389/fphar.2020.00345

# Systems Pharmacology-Based Strategy to Investigate Pharmacological Mechanisms of Radix Puerariae for Treatment of Hypertension

*Wenting Wu*[†], *Songhong Yang*[†], *Peng Liu*[†], *Li Yin*, *Qianfeng Gong*[*] *and Weifeng Zhu*[*]

*School of Pharmacy, Jiangxi University of Traditional Chinese Medicine, Nanchang, China*

Hypertension is a clinical cardiovascular syndrome characterized by elevated systemic arterial pressure with or without multiple cardiovascular risk factors. Radix Pueraria (RP) has the effects of anti-myocardial ischemia, anti-arrhythmia, vasodilatation, blood pressure reduction, anti-inflammation, and attenuating insulin resistance. Although RP can be effective for the treatment of hypertension, its active compounds, drug targets, and exact molecular mechanism are still unclear. In this study, systems pharmacology was used to analyze the active compounds, drug target genes, and key pathways of RP in the treatment of hypertension. Thirteen active compounds and related information on RP were obtained from the TCMSP database, and 140 overlapping genes related to hypertension and drugs were obtained from the GeneCards and OMIM databases. A PPI network and a traditional Chinese medicine (TCM) comprehensive network (Drug-Compounds-Genes-Disease network) were constructed, and 2,246 GO terms and 157 pathways were obtained by GO enrichment analysis and KEGG pathway enrichment analysis. Some important active compounds and targets were evaluated by *in vitro* experiments. This study shows that RP probably acts by influencing the proliferation module, apoptosis module, inflammation module, and others when treating hypertension. This study provides novel insights for researchers to systematically explore the mechanism of action of TCM.

**Keywords: Radix puerariae, hypertension, bioactive ingredients, mechanism of action, systems pharmacology**

**Abbreviations:** ADME, absorption, distribution, metabolism, and excretion; BCL2, Apoptosis regulator Bcl-2;DL, drug-likeness; GO, Gene Ontology; IL-1β, interleukin-1 beta; IL-4, interleukin-4; IL-6, interleukin-6; KEGG, Kyoto Encyclopedia of Genes and Genomes; LPS, lipopolysaccharide; NF-κBIA, scoparoneNF-kappa-B inhibitor alpha; OB, oral bioavailability; OMIM, Online Mendelian Inheritance in Man; PPI, protein-protein interaction; PTGS2, prostaglandin G/H synthase 2; RP, Radix Puerariae; STRING, Search Tool for the Retrieval of Interacting Genes/Proteins; TCM, traditional Chinese medicine; TCMSP, Traditional Chinese Medicine Systems Pharmacology Database.

OPEN ACCESS

***Edited by:***
*Yonghua Wang, Northwest A&F University, China*

***Reviewed by:***
*Simone Carradori, University "G. d'Annunzio" of Chieti-Pescara, Italy*
*Simon W. Rabkin, University of British Columbia, Canada*

***Correspondence:**
*Qianfeng Gong*
*gongqf2002@163.com*
*Weifeng Zhu*
*zwf0322@126.com*

[†]*These authors contributed to the work equally and should be regarded as co-first authors.*

***Specialty section:***
*This article was submitted to Ethnopharmacology, a section of the journal Frontiers in Pharmacology*

***Received:*** *19 June 2019*
***Accepted:*** *09 March 2020*
***Published:*** *24 March 2020*

***Citation:***
*Wu W, Yang S, Liu P, Yin L, Gong Q and Zhu W (2020) Systems Pharmacology-Based Strategy to Investigate Pharmacological Mechanisms of Radix Puerariae for Treatment of Hypertension. Front. Pharmacol. 11:345. doi: 10.3389/fphar.2020.00345*

## INTRODUCTION

Hypertension is a clinical cardiovascular syndrome characterized by elevated systemic arterial pressure with or without multiple cardiovascular risk factors. It is also an important cause of and risk factor for a variety of cardiovascular and cerebrovascular diseases, affecting the structure and function of the heart, brain, kidney, and other important organs, eventually leading to organ failure (National Clinical Guideline Centre (UK), 2011; Moran et al., 2015).

Traditional Chinese medicine (TCM) has been used in clinical treatment in China for more than 2,500 years (Robinson, 2011). Compared with western medicine, TCM has different antihypertensive targets (Zhao et al., 2010). Traditional Chinese medicine has accumulated much experience in the treatment of hypertension, obesity hypertension, refractory hypertension, and other aspects (Xu and Chen, 2008; Wang and Xiong, 2012; Xiong et al., 2013). In TCM theory, hypertension belongs to the categories of "headache", "vertigo", and "true pain". The main etiology of hypertension can be divided into emotional disorders, eating disorders, long-term illness, labor injury, congenital endowment, and so on. The main pathological links are wind, fire, phlegm, blood stasis, and deficiency, which are closely related to liver, spleen, kidney, and other viscera. The pathogenesis is based on deficiency of liver and kidney, Yin deficiency of liver and kidney, hyperactivity of liver Yang, and turbid sputum. Pathogenesis can be divided into liver-yang hyperactivity, phlegm-dampness, blood stasis, liver-kidney Yin deficiency, kidney-yang deficiency. Radix Puerariae (RP) not only has the effects of anti-myocardial ischemia, anti-arrhythmia, vasodilatation, blood pressure reduction, anti-inflammation, and attenuating insulin resistance (Zhang et al., 2010; Hwang et al., 2011; Yuan et al., 2014; Zhou et al., 2014; Wang et al., 2016; Yuan et al., 2016), but also can be used to treat hypertension. Especially Puerarin, a major compound in RP, can attenuate angiotensin II–induced cardiac hypertrophy by inhibiting the activation of the redox-sensitive ERK1/2, p38, and the NF-κB signaling pathways (Chen G. et al., 2014).

Although RP can be effective for the treatment of hypertension, its active compounds, drug targets, and exact molecular mechanism are still unclear. Each formula consists of a variety of Chinese medicines, each containing dozens to hundreds of compounds. Due to a variety of compounds can play a role of synergistic treatment on multiple targets, so the analysis of the mechanism of the formula is a time consuming and resource intensive process. Fortunately, systems-pharmacology has become a recent academic field, which incorporates a variety of disciplines and technologies, including biological chemistry, physiology, genetics, and computer science system pharmacology, provides a holistic approach to explore and understand the nature of the traditional medicine and its formula. Systems-pharmacology is able to identify compound-compound, compound-target, and target-disease interactions in computer models and understand the effects of herbs on biological networks based on system theory. At present, there are many methods based on systematic pharmacology to study the effect of traditional Chinese medicine on hypertension. The study shows that the potential mechanism of the therapeutic effect of traditional Chinese medicine on hypertension can be predicted through systematic pharmacology, so as to verify its therapeutic potential. According to systems pharmacology studies, San Cao Decoction can lower hypertension through regulating the pathway of PI3K-Akt-eNOS. And Oryeong-san formula may suppress hypertension by controlling the renin-angiotensin-aldosterone system (RAAS) (Kim et al., 2019; Ma et al., 2019). By using web-based approaches, systems pharmacology can systematically determine the effects and mechanisms of drugs used to treat complex diseases at the molecular, cellular, tissue, and biological levels. This research strategy for Danlu capsules, the Maxing Ganshi Decoction, the Wei Pi Xiao Decoction, Zuojinwan, and other capsules from traditional Chinese medicine has been widely adopted (Huang et al., 2017; Song et al., 2018; Yu et al., 2018; Yang et al., 2019).

In this study, systems pharmacology was used to analyze the active compounds, drug targets and key pathways of RP in the treatment of hypertension, as shown in **Figure 1**. This study attempts to provide a potential novel insight for researchers to systematically explore the mechanism of action of RP.

## METHODS

### Screening of Active Compounds

All compounds contained in Radix Puerariae (RP) were searched from the Traditional Chinese Medicine Systems Pharmacology Database and Analysis Platform (TCMSP, http://tcmspw.com). TCMSP is a special systems pharmacology platform about Chinese traditional herbal medicines that includes the relationships between drugs, targets, and diseases. TCMSP has a wide range of 500 drugs and more than 12,000 compounds (Ru et al., 2014). It has a large number of chemical substances, targets, and drug target networks, as well as the corresponding drug target-disease network. It also includes the pharmacokinetic properties of natural compounds such as oral bioavailability, drug-likeness, intestinal epithelial permeability, etc.

Oral bioavailability (OB) refers to the percentage of unmodified drugs that enter the circulatory system after oral administration (Xu et al., 2012; Liu et al., 2013). OB is also an important indicator for objectively evaluating the internal quality of drugs (Alam et al., 2015). The higher the OB-value of a compound, the higher the likelihood that it can be used clinically. The drug-likeness (DL) is a vague concept that refers to the similarity between compounds and known drugs (Walters and Murcko, 2002; Tao et al., 2013). Compounds with drug-likeness properties are not drugs, but they have the possibility of becoming drugs. This class of compounds is called drug-like molecules or drug analogs. Therefore, the Tanimoto coefficient was used to evaluate the DL index of the molecule in RP. The formula is as follows:

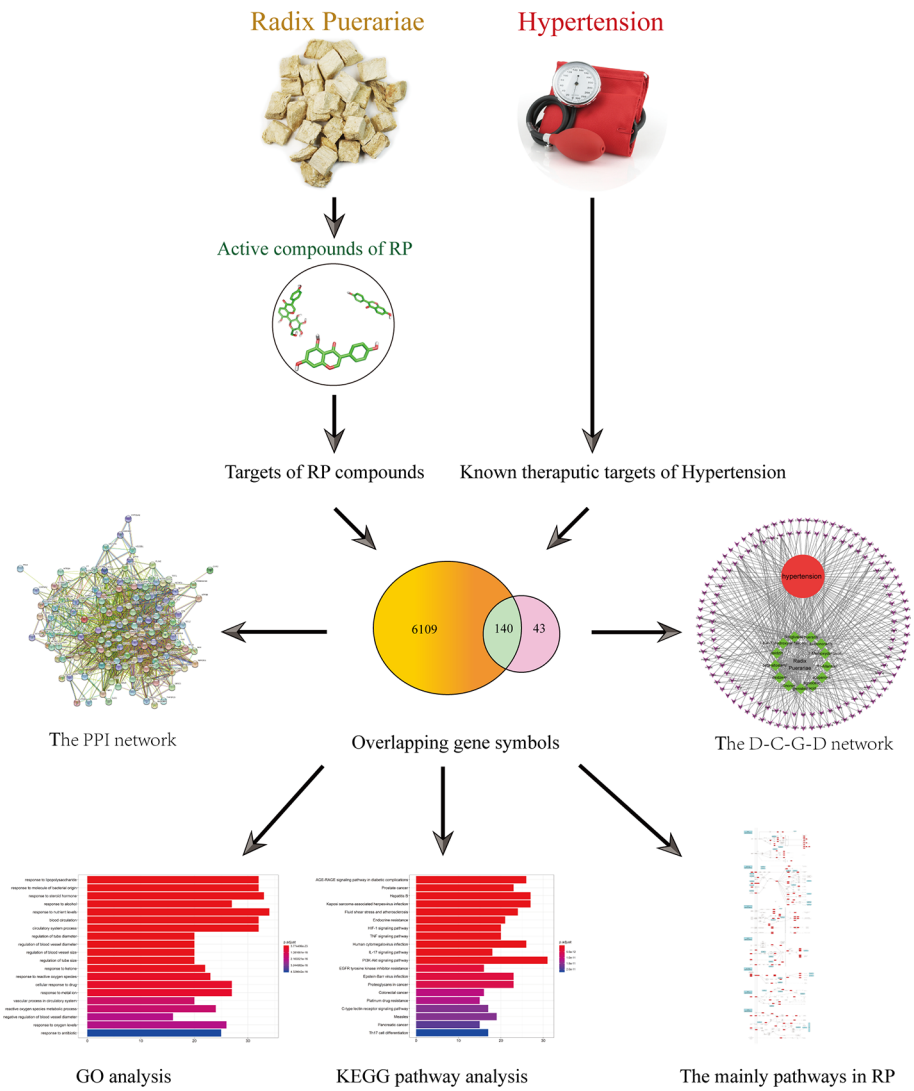


**FIGURE 1 |** The flowchart of a systems pharmacology-based strategy to investigate the pharmacological mechanisms of Radix Puerariae for the treatment of hypertension.

$$T(\alpha,\beta) = \frac{\alpha \times \beta}{\alpha^2 + \beta^2 - \alpha \times \beta} \quad (1)$$

In this formula, α is the molecular property of the RP compound on the basis of Dragon software (http://www.talete.mi.it/products/dragon_description.htm). β means the average molecular property for all drugs in the DrugBank database (Mauri et al., 2006).

Because most compounds in Chinese medicine have poor pharmacological properties, they cannot effectively bind to specific cell protein targets. Thus, many researchers have recommended that the OB ≥ 30% and DL ≥ 0.18 molecules be considered to have better pharmacological effects and be selected as candidate compounds for further analysis (Chen G. et al., 2014; Song et al., 2018; Yu et al., 2018; Kim et al., 2019; Ma et al., 2019; Yang et al., 2019). This study also used this principle to screen compounds for further analyses.

## Identification of the Related Targets and Gene Symbols of the Compounds in RP

According to the principle of different compounds-target forecast, target prediction techniques and methods can be divided into four categories: Based on the predictions of a ligand (chemical similarity search and pharmacophore model); Based on the predictions of a receptor (molecular docking); Machine learning to predict (the molecules of a database must have a clear correspondence between with the targets, and the name of the target must be standardized); and Combination forecast. But different technologies have their limitations. For example, the defect of molecular docking method is that it is

difficult to obtain target proteins with three-dimensional structure through experimental means or homologous modeling. However, the modeling process of machine learning prediction is blind and implicit, so the binding pattern between target proteins and compounds cannot be found directly. The data set used in the training model must contain accurate annotation information, which means that the small molecule must have a clear correspondence with the target and the target naming needs to be standardized, so the common compound database is not applicable. In addition, such methods may only focus on the receptor space of some protein families or are limited to the compound space of specific drugs, which is not ideal for the prediction of drugs and targets that are not in this space. Considering the limitations of the experimental conditions of molecular docking and machine learning prediction and combining that with previous experience, we finally chose the prediction method based on ligands for subsequent research (Yu et al., 2012; Wu et al., 2016; Wang S. et al., 2017).

All of the protein targets of the active compounds in RP were retrieved from TCMSP (http://lsp.nwu.edu.cn/tcmsp.php), removing redundant information and keeping only those that can interact directly with each of these compounds in RP as a presumption of targets. The target is then transformed using the UniProt knowledge database, and the selected species is *Homo sapiens* (Human). After deleting the redundant items, the data were merged to obtain the gene targets. UniProt is the most informative and well-resourced protein database. It is composed of data from three major databases: swiss-prot, TrEMBL, and pir-psd. The data come mainly from protein sequences obtained after the genome sequencing project was completed. It contains a wealth of information about the biological functions of proteins from the literature.

## The Acquisition of Gene Targets for Hypertension

This study collected gene targets for hypertension from two sources. The first one is the Gene Cards database (https://www.genecards.org/, version 4.9.0). Gene Cards is a searchable, comprehensive database that offers all comments and predicts human genetic information comprehensively in a user-friendly manner. It automatically integrates data from 150 web sources for the gene, including genome, transcriptome and proteome, genetics, and clinical and functional information (Rebhan et al., 1997; Safran et al., 2010). This study used the keyword "hypertension" to search this database. The second source is the Online Mendelian Inheritance in Man (OMIM) database. (http://www.omim.org/, updated on February 28, 2019) (Hamosh et al., 2005). It is a continuously updated database of human genes and genetic disorders. It focuses on genetic or inherited genetic diseases, including text information and relevant reference information, the sequence record, mapping, and other related databases. In this study, the keyword "hypertension" was searched by using the Gene map option in the advanced search field of this database. Eventually, we obtained genes for diseases associated with hypertension.

## Drug-Compounds-Genes-Disease (D-C-G-D) Network Construction

First, we intersected the obtained drug targets with the disease genes and obtained the Venn diagram of the intersected genes. Then, we built a network of complex information based on interactions between the drug (RP), compounds, genes and the disease (hypertension). Next, we used Cytoscape software (Shannon et al., 2003; Su et al., 2014) (version 3.7.1), which is a graphical display and network analysis and editing software, to perform a visual analysis of the "D-C-G-D network".

## PPI Network Construction

Protein-protein interaction data were obtained from the String database (https://string-db.org/, version 11.0, updated on January 19, 2019) (Hsia et al., 2015). This is a database that searches for known proteins and predicts interactions between proteins, which is available for 5,090 species and contains interactions between 24,584,628 proteins and 3,123,056,667 proteins. The target is then transformed using the UniProt knowledge database. After deleting the redundant items, the data were merged to obtain the genes. At last, we searched for these genes in the database using the multiple proteins option, and at the same time, we set the organism to *Homo sapiens* (Human). A PPI network of RP active compounds-targets and hypertension-related targets was then constructed.

## Gene Ontology Enrichment Analysis

Gene Ontology (GO) is an international standard classification system for gene function. It is a standard of language vocabulary that can be used in all species. It can define and describe the functions of genes and proteins, and it can be regularly updated with new research. It can help researchers to focus on the biological functions of different genes from the perspective of gene function (Ashburner et al., 2000). This study used the bioconductor (R) software (http://bioconductor.org/, version 3.8, released on October 31, 2018) for analysis.

## KEGG Pathway Enrichment Analysis

The KEGG (Kyoto Encyclopedia of Genes and Genomes) database is a database systematically analyzing the metabolic pathways of gene products in cells and the functions of these gene products. The database is useful for studying genes and expressed information as a whole network. KEGG integrates data from the genome, chemical molecules and biochemical systems, including metabolic pathways, drugs, diseases, and gene sequences (Ogata et al., 1999). *In vivo*, different gene products coordinate with each other to perform biological functions, and pathway annotation analysis of differentially expressed genes helps further interpret gene functions. Overrepresentation of differentially expressed proteins on a given pathway shows the pathway enrichment analysis of differentially expressed proteins. This study also used the Bioconductor (R) software (http://bioconductor.org/, version 3.8, released on October 31, 2018) for analysis.

## Computational Validation of Compounds-Targets Interactions

We wished to ascertain the interaction between active compounds and their protein targets and explore their binding modes. Hence, we selected three active compounds and four targets, a total of six compounds-targets interactions for verification of molecular docking. We used GOLD v5.1 (a genetic algorithm-based docking program to dock protein-ligand complexes). We obtained the X-ray crystal structures of IL-6, IL-1β, IL-4, and Prostaglandin G/H synthase 2 (PTGS2) from the RCSB Protein Data Bank (PDB) (www.rcsb.org); the PDB entry code for these proteins is 1ALU, 2NVH, 2D48, and 5F19, respectively. During molecular docking, we adopted the GOLD Score fitness function.

## Experimental Validation

### Reagents

Puerarin (purity ≥ 98%) and Daidzein (purity ≥ 98%) was purchased from Must Biotechnology (Chengdu, China). A stock solution of 100 mM puerarin or daidzein in dimethyl sulfoxide was prepared and stored at 4°C. Enzyme-linked immunosorbent assay (ELISA) kits for IL-6 and IL-4 were purchased from MultiSciences Biotech (Hangzhou, China).

### Cell Culture

RAW264.7 cells were obtained from the cell bank of the Chinese Academy of Sciences (Shanghai, China). RAW264.7 cells were cultured in Dulbecco's modified Eagle's medium (Gibco, Billings, MT, USA) with 10% fetal bovine serum (Gibco). Cells were cultured at 37°C in an atmosphere of 5% CO2 for all experiments.

### Assay to Measure Cell Viability

RAW264.7 cells in the logarithmic phase were seeded at $8 \times 10^4$ cells/well in 96-well culture plates. After incubation for 24 h, Raw264.7 cells were exposed to puerarin or daidzein (0, 5, 25, 50, 75, or 100 μmol/L). After treatment for 24 h, 20 μl of Cell Counting Kit (CCK-8) assay solution (Biosharp, Hefei, China) were added to each well, and cells were incubated for 4 h at 37°C in an atmosphere of 5% CO2. The absorbance at 450 nm was measured by a microplate reader. Cell survival was calculated as: absorbance/absorbance of control ×100%.

### Determination of Levels of IL-6 and IL-4 by ELISAs

RAW264.7 cells ($1\times10^6$ cells/well) were incubated with lipopolysaccharide (LPS; 1 μg/ml) for 24 h and then treated with daidzein (50, 75, or 100 μM) for 24 h. Supernatants were harvested and the level of IL-6 and IL-4 determined by ELISA kits (Biosharp).

### mRNA Expressions of NF–κBIA, BCl2, and PTGS2 Treat With Puerarin by qRT-PCR

RAW264.7 cells ($2\times10^6$ cells/well) were incubated with lipopolysaccharide (LPS; 1 μg/ml) for 24 h and then treated with puerarin (50, 75, or 100 μM) for 24 h.

Total RNA was extracted with TRIzol® Reagent (Thermo Scientific, Waltham, MA, USA), and reverse-transcribed with oligo-DT using HiScript™ Reverse Transcriptase (Vazyme, Beijing, China) according to manufacturer instructions. The primers used were synthesized by Genscript (Nanjing, China). The sequences were (forward and reverse, respectively) 5′-TTGGTCAGGTGAAGGGAGAC-3′ and 5′-GGATCACAGCCAGCTTTCAG-3′ for NF-κBIA; 5′-TTGCGTGAAGGCTTGAGATG-3′ and 5′-CTGGACAGGATGGAGGGTTT-3′ for BCL2; 5′-AAGCCTTCTCCAACCTCTCC-3′ and 5′-GCTGGGCAAAGAATGCAAAC-3′ for PTGS2; 5′-AACGGATTTGGCCGTATTGG-3′ and 5′-CATTCTCGGCCTTGACTGTG-3′ for the internal control glyceraldehyde 3-phosphate dehydrogenase (GAPDH).

qRT-PCR was done using SYBR™ Green Master Mix (Vazyme) in the QuantStudio 6 Flex system (Applied Biosystems, Foster City, CA, USA). The PCR cycling profile was: one cycle at 50°C for 2 min and 95°C for 10 min, 40 cycles at 95°C and 60°C for 30s. Fluorescence signals were detected using the QuantStudio 6 Flex system. Gene-expression data were normalized to that of the endogenous control GAPDH. The $2^{-\Delta\Delta CT}$ method was the basis for relative expression of genes.

## Statistical Analyses

Data are the mean ± SD. The significance of results was determined based on one-way analysis of variance using Prism 8.0.1 (Graphpad, San Diego, CA, USA). $p < 0.05$ was considered significant. All experiments were repeated at least three times.

# RESULTS

## Screening for Active Compounds

To identify the active compounds of RP, two classical ADME parameters, OB and DL, were used for screening. Some did not agree with the standard of screening compounds that are also likely to produce therapeutic effects on the human body. To study this issue more comprehensively, although they do not meet the screening criteria, the compounds were still retained as active compounds in this study. In the TCMSP database, there are 18 listed compounds of RP. Among them, only 4 compounds had an OB greater than 30.0% and a DL greater than 0.18. The DL of 16 compounds was greater than 0.18 and the OB of 6 compounds was greater than 30.0%. However, we found that puerarin, with an OB of 24.03%, is a well-known active compound in RP (Chen G. et al., 2014; Li et al., 2016; Tao et al., 2016; Li et al., 2017; Mocan et al., 2018). These studies showed that puerarin may be used as a new potential antihypertensive drug. It can improve the vascular insulin effect of patients with salt-sensitive hypertension and is beneficial against cardiovascular disease (Tan et al., 2017).

Similarly, the DL of allantoin is 0.03, which is far less than 0.18. However, studies have shown that allantoin has potential as a novel antihypertensive drug in the future (Chen M. et al., 2014). In addition, allantoin can also play a therapeutic role in diabetes through its antioxidant effect (Go et al., 2015). All these studies

**TABLE 1 |** Showing the thirteen active compounds from Radix Pueraria (RP) and their corresponding predicted oral bioavailability (OB), drug-likeliness (DL), and structure.

| No. | Mol ID | Molecule Nmae | OB | DL | Structure |
|---|---|---|---|---|---|
| 1 | MOL000392 | Formononetin | 69.67 | 0.21 | 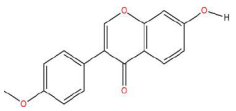 |
| 2 | MOL000357 | Sitogluside | 20.63 | 0.62 | 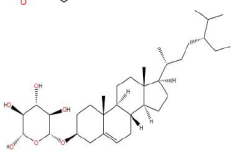 |
| 3 | MOL000358 | Beta-sitosterol | 36.91 | 0.75 | 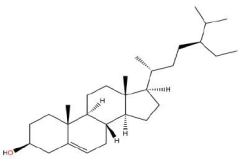 |
| 4 | MOL000390 | Daidzein | 19.44 | 0.19 | 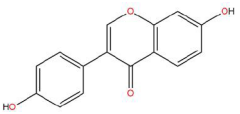 |
| 5 | MOL000391 | Ononin | 11.52 | 0.78 | 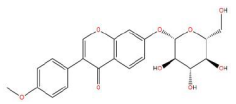 |
| 6 | MOL000481 | Genistein | 17.93 | 0.21 | 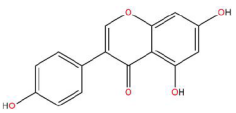 |
| 7 | MOL000663 | Lignoceric acid | 14.90 | 0.33 |  |
| 8 | MOL001999 | Scoparone | 74.75 | 0.09 | 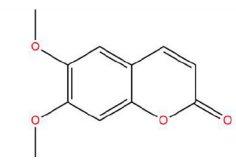 |
| 9 | MOL002347 | (R)-allantoin | 96.90 | 0.03 | 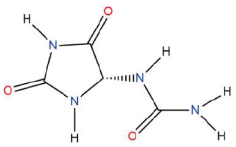 |
| 10 | MOL002959 | 3'-Methoxydaidzein | 48.57 | 0.24 | 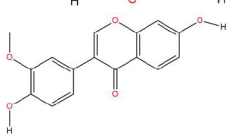 |
| 11 | MOL012297 | Puerarin | 24.03 | 0.69 | 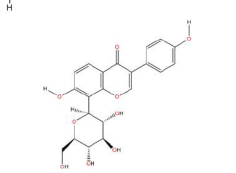 |
| 12 | MOL004631 | 7,8,4'-Trihydroxyisoflavone | 20.67 | 0.22 | 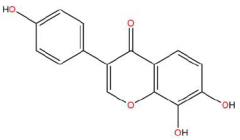 |
| 13 | MOL009720 | Daidzin | 14.32 | 0.73 | 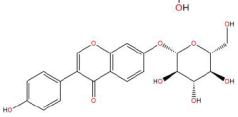 |

indicate that allantoin has strong drug activity. Scoparone is another compound with excellent pharmacological effects that has significant antihypertensive, anti-inflammatory, antioxidation, and anticoagulant effects (Huang et al., 1992; Cho et al., 2016; Xu et al., 2016; Jung et al., 2019). However, its DL is also well below 0.18. These examples demonstrate that although some compounds are not high for OB or DL, they do have high efficacy. Therefore, considering these factors, we decided to select all of the compounds related to RP in the TCMSP database as the candidate compounds. To sum up, a total of 18 compounds were selected as the candidate compounds of RP in this study. **Table 1** shows the thirteen active compounds from RP and their corresponding predicted OB, DL, and structure.

## Identification of the Related Targets and Genes of the Compounds in RP

After being collected from the TCMSP database and converted into the UniProt database, as well as deleting the redundant items, 13 active compounds in RP, and 183 known targets related to them were finally obtained. The details are described in Additional file: **Supplementary Table S1**.

## The Acquisition of Known Therapeutic Gene Targets for Hypertension

A total of 6,255 known therapeutic targets for hypertension were collected from the Gene Cards database. In addition, 11 known therapeutic targets for hypertension were obtained based on the OMIM database. After eliminating redundant targets, a total of 6,109 known therapeutic. Targets for hypertension were collected in this study. The details are described in Additional file: **Supplementary Table S2**.

## D-C-G-D Network Analysis

**Figure 2A** shows that 6,109 disease genes and 183 drug genes have 140 overlaps. This means that these 140 genes may be the key to the treatment of hypertension by RP. The 140 overlapping genes are detailed in Additional file: **Supplementary Table S3**.

To clarify the potential mechanism of RP acting on hypertension, we used Cytoscape software to build the D-C-G-D network, as shown in **Figure 2B**. The gray node represents RP. The red node represents hypertension. The 13 green nodes represent the active compounds in RP. The 140 purple nodes represent the overlapping genes between the disease and drug. The edges mean that nodes can interact with each other.

We conducted further network analysis by evaluating centralization and heterogeneity. The network centralization and heterogeneity are 0.885 and 2.442 and are different from each other, showing that some nodes are more concentrated in the network than others. This means that the compound-target space has a tendency for certain compounds and targets. Therefore, the network includes some compounds with multiple targets, such as genistein (degree=66), daidzein (degree=49), puerarin (degree=45), formononetin (degree=26), beta-sitosterol (degree=25), and scoparone (degree=14). Additionally, it means that RP can act on multiple targets through the same active compound. For example, puerarin can have an effect on 45 targets, such as VEGFA, PTGS2, AR, PPARG, and RELA, when treating hypertension. Studies have shown that puerarin can achieve anti-inflammatory effects by activating the NF-κB signaling pathway and antioxidant effects by inhibiting the Nrf2 pathway (Li et al., 2018; Liu et al., 2019; Wang et al., 2019). Detailed information about the active compounds and genes are described in Additional file: **Supplementary Table S4**.

## PPI Network Analysis

In this study, we constructed a PPI network of the 140 overlapping targets, which consisted of 140 nodes and 2,076 edges, as shown in **Figure 3A**. This means that the proteins have more interactions among themselves than would be expected for

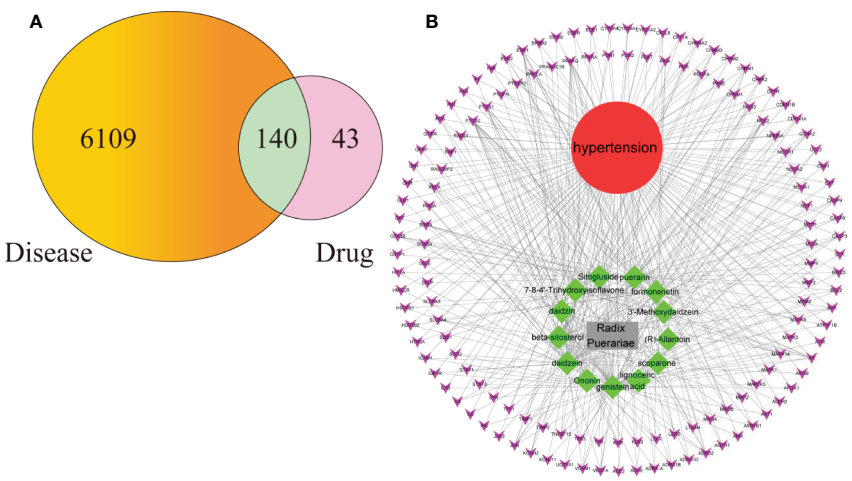


**FIGURE 2 | (A)** The 140 overlapping genes between the disease and drug. **(B)** The Drug-Compounds-Genes-Disease (D-C-G-D) network.

a random set of proteins of similar size drawn from the genome. Such an enrichment indicates that the proteins are at least partially biologically connected as a group. The light blue edges mean that the known interactions come from curated databases. The pink edges mean that the known interactions come from experimentally determined evidence. The green edges mean that the predicted interactions come from the gene neighborhood. The red edges mean that the predicted interactions come from the gene fusions. The dark blue edges mean that the predicted interactions come from gene co-occurrences. The yellow edges mean that the predicted interactions come from text mining. The black edges mean that the predicted interactions come from coexpression. The lavender edges mean that the others come from protein homology. The details of the PPI network are described in Additional file: **Supplementary Table S5**. We took the first 35 proteins in the PPI network for further analysis.

As seen in **Figure 3B**, proteins can be related to other proteins. This suggests that the therapeutic effect of RP on

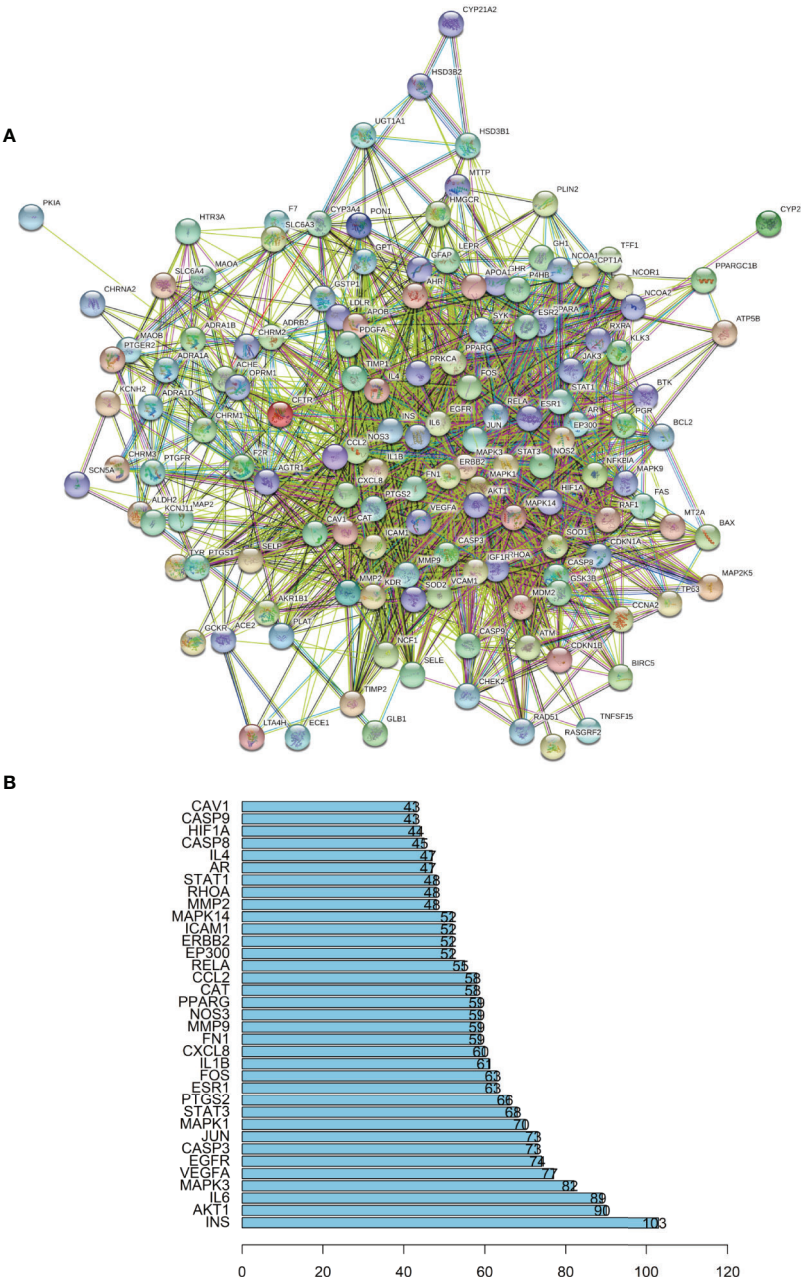


**FIGURE 3 | (A)** The protein-protein interaction (PPI) network. **(B)** The bar plot of the protein-protein interaction (PPI) network. The X-axis represents the number of neighboring proteins of the target protein. The Y-axis represents the target proteins.

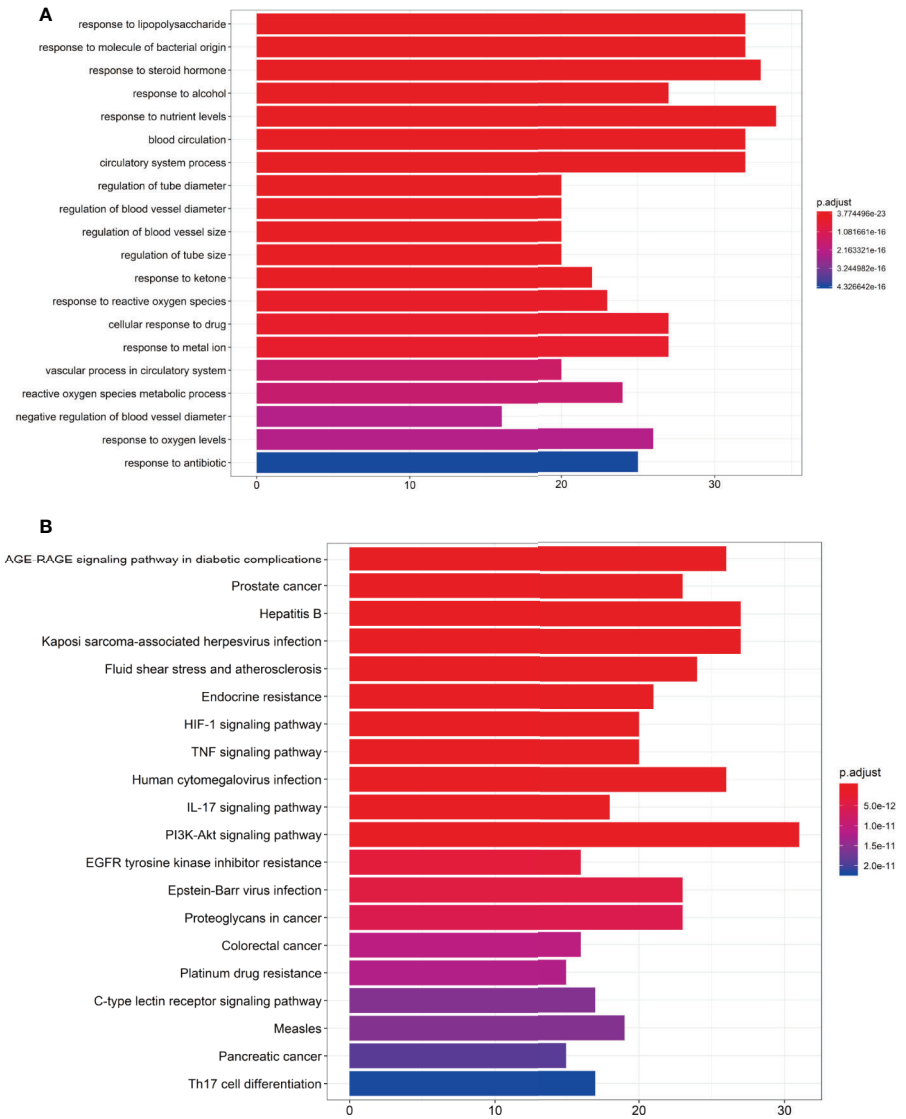


**FIGURE 4 | (A)** Gene Ontology (GO) analysis of the 140 overlapping gene symbols associated with hypertension. The X-axis represents the significant enrichment counts of these terms, while the Y-axis represents the categories of "biological process" in the GO of the target genes (p-value < 0.01). **(B)** The Kyoto Encyclopedia of Genes and Genomes (KEGG) pathway enrichment analysis. The X-axis represents the target counts in each pathway, and the Y-axis represents the main pathways (p-value < 0.01).

hypertension is likely to be achieved through multiple compounds, multiple targets, and multiple pathways.

## Gene Ontology Enrichment Analysis

To verify whether the 140 genes are related to hypertension, we conducted GO enrichment analysis to clarify the relevant biological processes, as shown in **Figure 4A**. The Y-axis represents the GO term. The X-axis indicates the number of genes enriched for the term. The redder the color, the smaller the value of p.adjust. This also means greater credibility and more importance. In contrast, the bluer the color, the greater the value of p.adjust. We used the first 20 terms from small to large according to the p-value for a brief demonstration. The details of the GO analysis are described in Additional file: **Supplementary Table S6**. The results indicated that numerous biological processes are involved in the treatment of hypertension, including response to lipopolysaccharide (GO:0032496), response to steroid hormone (GO:0048545), response to oxidative stress (GO:0006979), regulation of blood vessel diameter (GO:0097746), blood circulation (GO:0008015), regulation of blood vessel size (GO:0050880), negative regulation of blood vessel diameter (GO:0097756), and others.

## The KEGG Pathway Enrichment Analysis

The KEGG pathway enrichment analysis was performed by using the Bioconductor (R) software, as shown in **Figure 4B**.

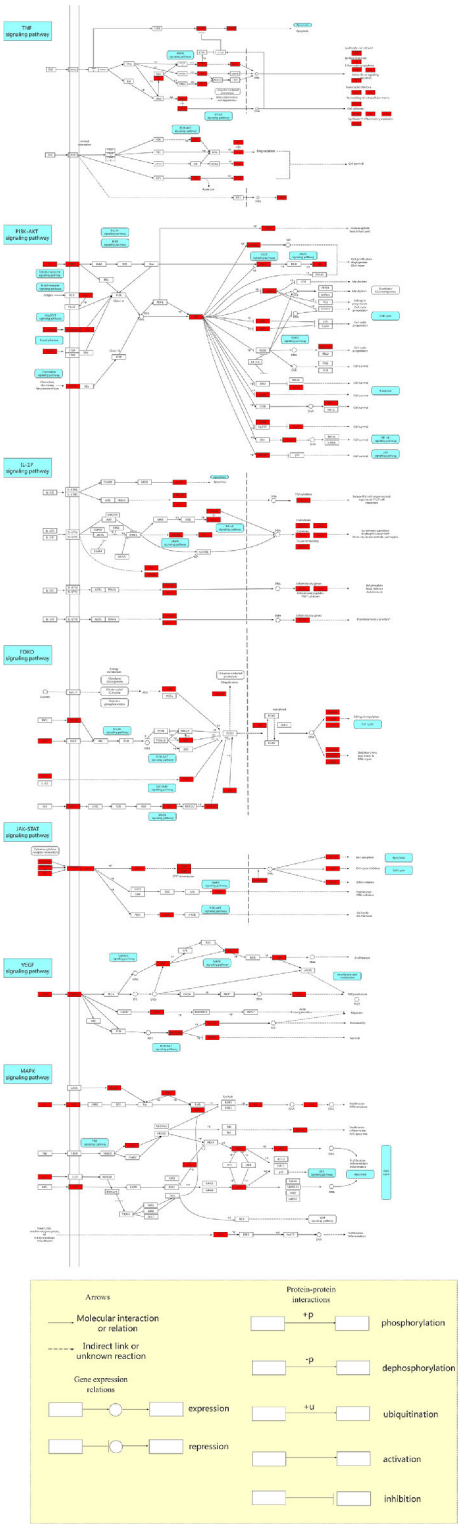


**FIGURE 5 |** The Kyoto Encyclopedia of Genes and Genomes (KEGG) pathway map of anti-hypertension for Radix Pueraria (RP). The red nodes within the predicted signaling pathway represent the targets relevant with the corresponding pathway. The yellow area below refers to the explanation of the notations used in the pathway map.

The Y-axis represents the pathway of the KEGG. The X-axis indicates the number of genes enriched in the pathway. The redder the color, the smaller the value of p.adjust, which also means more credibility and more importance. In contrast, the bluer the color, the greater the value of p.adjust. In this study, the 140 overlapping gene symbols were mapped to 157 pathways following KEGG pathway enrichment. We sorted the first 20 pathways from small to large according to the p-value for a brief demonstration. The details of the KEGG pathway enrichment analysis are described in Additional file: **Supplementary Table S7**.

According to the results, an integrated "RP pathway" has been constructed by the KEGG enrichment analysis, which can mainly be roughly divided into a proliferation module, apoptosis module, inflammation module, and others, as shown in **Figure 5**. In these pathways, the PI3K-Akt signaling pathway, TNF signaling pathway, IL-17 signaling pathway, FoxO signaling pathway, JAK-STAT signaling pathway, VEGF signaling pathway, MAPK signaling pathway, AMPK signaling pathway, NF-κB signaling pathway, calcium signaling pathway, mTOR signaling pathway, PPAR signaling pathway, cGMP-PKG signaling pathway, p53 signaling pathway, and Ras signaling pathway are considered the top priority. These signaling pathways can also interact with other pathways within the results.

In these modules, hypertension is thought to be associated with excessive endothelial cell proliferation (Hsueh and Anderson, 1992; Ueno et al., 2000; Landmesser et al., 2003). Studies have shown that hypertension can be treated by inhibiting the PI3K-Akt signaling pathway, increasing apoptosis and reducing cell proliferation (Intengan and Schiffrin, 2001; Wang et al., 2012; Sun et al., 2016). Activation of the PI3K-Akt signaling pathway and inhibition of apoptosis are involved in the pathogenesis of hypertension (Lin et al., 2013; Wu et al., 2013).

Chronic low-grade inflammation is one of the many putative mechanisms for hypertension, with elevated levels of inflammatory cytokines and activation of the immune system (Ruan and Gao, 2019). Some studies have suggested that the risk of hypertension is positively correlated with increased

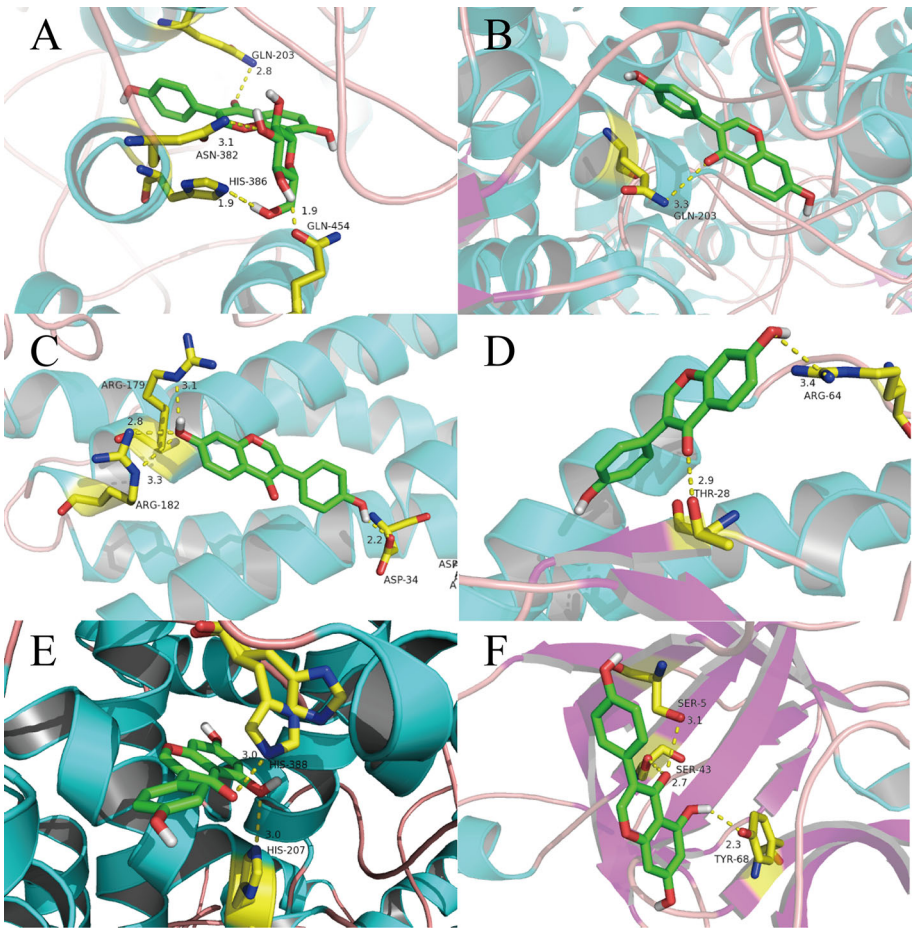


**FIGURE 6 |** Binding explorations of selected Compounds-Targets interactions. **(A):** puerarin with PTGS2; **(B)** daidzein with PTGS2; **(C)** daidzein with IL-6; **(D)** daidzein with IL-4; **(E)** genistein with PTGS2;**(F)** genistein with IL-1β. Molecules are represented by a ball-and-stick model, the hydrogen bonds are represented by a dotted line, and the distance is in angstroms. Atoms C, O, and N are green, red, and blue, respectively.

inflammation (Tomiyama et al., 2018; Jayedi et al., 2019). Moderate increases in blood pressure activate T cells, which in turn promote inflammation, which further increases blood pressure, leading to severe hypertension (Harrison et al., 2012). Studies have found that hypertension can be suppressed by reducing inflammation, and specific inflammatory pathways can improve blood pressure control (Mathieu et al., 2009; Chen et al., 2019).

Vascular endothelial growth factor receptor (VEGFR) can regulate the cardiovascular system (Olsson et al., 2006). The effects of VEGF-A on endothelial cells involves migration, proliferation, differentiation, and tube formation, leading to vascular germination and angiogenesis (Ferrara and Kerbel, 2005). There is evidence that the activation of the endothelin system is probably a reflection of the ECs activation status caused by the lack of VEGF, and it is a regulator of elevated blood pressure and, to a certain extent, may also be a regulator of renal injury (van den Meiracker and Danser, 2016). Inhibition of VEGF signaling leads to vascular dysfunction, kidney damage, and hypertension (Bhargava, 2009; Pandey et al., 2018).

## Computational Validation of Selected Ingredients-Targets Interactions

In general, the number and strength of a ligand bound to a receptor is determined largely by the inhibitory efficiency (Wang J. et al., 2017). Therefore, we explored the interactions and binding modes between the inflammatory factors IL-6, IL-4, IL-1β, and Prostaglandin G/H synthase 2 (PTGS2) with their active ingredients by molecular docking.

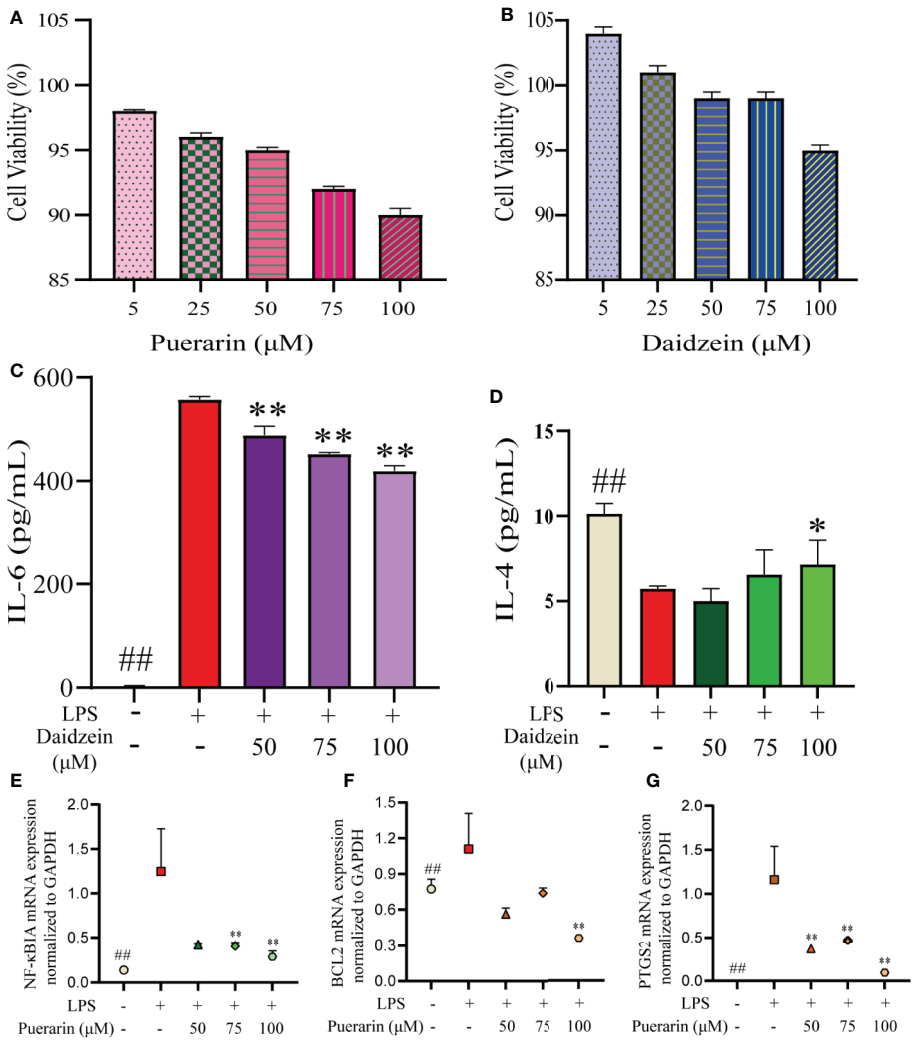


**FIGURE 7 |** Results of puerarin and daidzein on RAW 264.7 cells. RAW264.7 cells were incubated with LPS (1 μg/mL) for 24 h and then treated with puerarin or daidzein (50, 75, or 100 μM) for 24 h. The effects of puerarin **(A)** or daidzein **(B)** on the viability of RAW264.7 cells using the CCK-8 assay. Production of IL-6 **(C)** and IL-4 **(D)** was determined by ELISAs. mRNA expression of NF-κBIA **(E)** and BCL2 **(F)** and PTGS2 **(G)** was determined by qRT-PCR. ##$p < 0.01$ versus blank control group. *$p < 0.05$ LPS-treated group. **$p < 0.01$ LPS-treated group.

Puerarin has special pharmacologic effects and high content in RP. Hence, we first conducted molecular docking of puerarin with PTGS2. We can see clearly from **Figure 6A** that the O atom in the C-O double bond in puerarin interacts with the N atom on GLN-203 (2.8 Å) through H-bond. An O atom in a -OH group of puerarin interacts with the N atom on ASN-382 (3.1 Å). The H atoms in the two other -OH groups in different positions in puerarin interacts with the N and O atoms on HIS-386 (1.9 Å) and GLN454 (1.9 Å), respectively.

In **Figure 6B**, the molecular-docking result of daidzein with PTGS2 shows that the O atom in the C-O double bond in daidzein can interact with the N atom on GLN-203 (3.3 Å).

In **Figure 6C**, we can see that daidzein with IL-6 has four connection points. The O atom in a -OH group and ARG-182 (2.8 Å) and ARG-182 (3.3 Å) interacts with each other between each N atom. The H atom in this -OH group can interact with ARG-179 (3.1 Å) between N atom. The H atom in the other -OH group can interact with the O atom on ASP-34(2.2 Å).

As shown in **Figure 6D**, the O atom in the C-O double bond in daidzein is formed the O atom on THR-28 (2.9 Å) in IL-4. A hydrogen-bond between the -OH group of the benzene ring and ARG-64 (3.4 Å) are formed.

Due to that genistein has the highest degree, the molecular docking of genistein with PTGS2 was performed, with results displayed in **Figure 6E**. From this figure, clearly two weak H-bonds are observed forming between the O atom and a -OH group of genistein and HIS-388 (3.0 Å) and HIS-207 (3.0 Å), respectively.

In **Figure 6F**, the H-bonding interactions between genistein and IL-1β, including SER-43…O (2.7 Å), SER-5…O (3.1 Å), and TYR-68…H (2.3 Å), make genistein and IL-1β complex remain a stable conformation.

The results of molecular docking were also consistent with our cell-experiment results, which demonstrated that puerarin and daidzein had a significant anti-inflammatory effect.

Based on these data, we can consider that the interaction between these active compounds and targets is the basis of their biologic activity. It also means that RP has multiple compounds and multiple targets.

## Experimental Validation *In Vitro*

### CCK-8 Assay

First, we determined the effects of different doses of puerarin or daidzein on the viability of RAW264.7 cells using the CCK-8 assay (**Figures 7A, B**). Compared with the blank group, there was no significant decrease in the proliferation of RAW246.7 cells between puerarin or daidzein at the concentration of 5–100 μM. Therefore, three concentrations were selected (50, 75, 100 μmol/L) for subsequent experiments.

### Validation of Targets

To further evaluate the results obtained in systematic pharmacologic analyses, puerarin, or daidzein was selected from RP to examine potential anti-inflammatory effects using LPS (1 μg/mL)-stimulated RAW264.7 cells. We undertook ELISAs for IL-6 and IL-4 and qRT-PCR for NF-κBIA and BCL2 and PTGS2 to confirm the predicted anti-inflammatory effects of the compounds. The production of IL-6 was suppressed obviously with the increase of the concentration of daidzein, whereas IL-4 was generated more (**Figures 7C, D**). Simultaneously, a significant decrease in NF-κBIA, BCL2, and PTGS2 mRNA expressions were observed (**Figures 7E–G**).

# DISCUSSION

Hypertension is a clinical cardiovascular syndrome characterized by elevated systemic arterial pressure with or without multiple cardiovascular risk factors. It is also an important cause and risk factor for a variety of cardiovascular and cerebrovascular diseases, affecting the structure and function of the heart, brain, kidney, and other important organs, and eventually leading to organ failure (National Clinical Guideline Centre (UK), 2011; Moran et al., 2015). TCM has been used in clinical treatment in China for more than 2500 years (Robinson, 2011). Compared with western medicine, traditional Chinese medicine (TCM) has different antihypertensive targets (Zhao et al., 2010). Traditional Chinese medicine has accumulated much experience in the treatment of hypertension, obesity hypertension, refractory hypertension, and other aspects (Xu and Chen, 2008; Wang and Xiong, 2012; Xiong et al., 2013). However, its specific mechanism of pharmacological action has not been fully and comprehensively revealed (Wang et al., 2013a; Wang et al., 2013b; Xiong et al., 2014; Xiong, 2015). Therefore, it is imperative to explore the mechanism of RP in the treatment of hypertension by applying a systems pharmacology method combined with screening of active compounds, drug targets, and network and pathway analysis.

The results showed that there are 13 active compounds in RP influencing the 140 overlapping genes that play an important role in the process of treatment for hypertension. Puerarin is a well-known active compound in the treatment of hypertension (Zhou et al., 2014; Li et al., 2017). The therapeutic effect of puerarin on hypertension may be achieved by inhibiting the NF-κB pathway (Tan et al., 2017). Moreover, the key target of puerarin in reducing hypertension mechanism is believed to be NOS3, also called eNOS (Shi et al., 2019). The compound genistein from RP exhibited the highest number of interactions with various protein targets. Genistein can upregulate the expression of human endothelial nitric oxide synthase and lower blood pressure in spontaneously hypertensive rats and then treat hypertension (Xu et al., 2004; Cho et al., 2007; Si and Liu, 2008). It reduces hypertension through the PI3K/Akt/eNOS signaling pathway (Vera et al., 2007; Lin et al., 2012). In addition, daidzein has also been shown effective in treating hypertension (Furumoto et al., 2010).

On the other hand, the same target was found to be related to a variety of active compounds in RP, indicating that the active compounds in RP have a synergistic effect on the treatment of hypertension. PTGS2, namely, COX-2, is one of our predicted targets, which plays an important role in hypertension. It has been reported that selective cox-2 inhibition can treat hypertension through improving

vascular diastole and reducing inflammation and oxidative stress (Chenevard et al., 2003; Hermann et al., 2003; Solomon et al., 2004; Martelli et al., 2013). It was predicted that PTGS2 can be linked to 12 active compounds in RP, which reflects that TCM works through multiple active compounds acting on a single target. Meanwhile, puerarin was speculated to be associated with 48 targets, such as PTGS2, VEGFA, CASP3, JAK3, SATA3, et al, in agreement with the fact that a single active compound could act on multiple targets for TCM. The PPI network also showed complex interactions among the 140 overlapping genes. Through the analysis of its compounds and targets, the network reveals that RP may treat hypertension through multiple pathways and cellular processes. According to the GO enrichment analysis and the KEGG pathway enrichment analysis, we speculate that RP may exert a therapeutic effect by impacting on the proliferation module, apoptosis module, inflammation module, and others.

In total, 2,246 GO terms (2,062 BP, 82 CC, 150 MF) and 157 pathways were obtained by GO enrichment analysis and KEGG pathway enrichment analysis. We thought that the PI3K-Akt signaling pathway, TNF signaling pathway, IL-17 signaling pathway, FoxO signaling pathway, JAK-STAT signaling pathway, VEGF signaling pathway, MAPK signaling pathway, AMPK signaling pathway, NF-kappa B signaling pathway, calcium signaling pathway, mTOR signaling pathway, PPAR signaling pathway, cGMP-PKG signaling pathway, p53 signaling pathway, and Ras signaling pathway might be principle pathways involved in the process of the treatment. The JAK-STAT cascade (GO:0007259) is associated with hypertension, and hypertension can be reduced by negative regulation of this cascade (Wold et al., 2002).

Systems pharmacology is an acceptable strategy to predict the therapeutic mechanism and can provide us research direction effectively. Considering the possible spurious associations between one data base with another, it would be significant to verify. Therefore, our investigation applied *in vitro* cellular experiments and molecular docking to prove the validity of the prediction to some extent through verifying the inflammation pathway. Our results demonstrated that puerarin and daidzein from RP may have a therapeutic effect against hypertension, and the inhibition of inflammation would probably one of their approaches to produce anti-hypertension effect, especially through the IL-17 and NF-κB signaling pathway. *In vitro* studies and molecular-docking results also provided additional information for the screened compounds with potential anti-inflammatory effects, and validated the reliability of this screening strategy based on systems pharmacology. Meanwhile, there are a series of reported studies on the effects of puerarin on anti-hypertension through *in vivo* models, such as cats and SHR, and all suggests that puerarin exerts its anti-hypertensive effect, which is coincident with our research (Wong et al., 2011; Wu et al., 2014). Savoia, C. et al. concluded in their article that inflammation participates in the development and pathogenesis of hypertension (Savoia and Schiffrin, 2006). In order to illustrate the mechanism more clearly, our future research will focus on in-vivo study and validation of the other pathways.

## CONCLUSIONS

Our research systematically investigates RP from a whole action mechanism perspective in the treatment of hypertension and provides a basis for multi-compound synergies in follow-up research and a new approach to explore traditional Chinese medicine. RP can achieve the effect of anti-hypertension through multiple compounds, multiple targets, and multiple approaches. A total of 13 active compounds and 140 overlapping genes between RP and hypertension were screened by systems pharmacology combined with screening of active compounds and target predictions. The PPI network, GO enrichment analysis and KEGG pathway analysis suggested that the pharmacological mechanism of RP in the treatment of hypertension may be related to its involvement in the proliferation module, apoptosis module, inflammation module, et al. In general, the systems pharmacological method developed in this study provides an alternative strategy for a comprehensive understanding of the mechanism of RP in the treatment of hypertension.

## DATA AVAILABILITY STATEMENT

The data used to support the findings of this study are included within the article or within the **Supplementary Information File(s)**.

## AUTHOR CONTRIBUTIONS

SY and WW conceived and designed the studies. PLcompleted in vitro experiments. LY participated in this work. All authors participated in drafting of the manuscript and revising it before final submission.

## FUNDING

This work was supported by The National Key Research and Development Plan (2017YFC1702900).

## ACKNOWLEDGMENTS

This work was supported by The National Key Research and Development Plan (2017YFC1702900). The authors are thankful to Jiangxi University of Traditional Chinese Medicine for help in conducting this study.

## SUPPLEMENTARY MATERIAL

The Supplementary Material for this article can be found online at: https://www.frontiersin.org/articles/10.3389/fphar.2020.00345/full#supplementary-material

## REFERENCES


Alam, M. A., Al-Jenoobi, F. I., Al-Mohizea, A. M., and Ali, R. (2015). Understanding and managing oral bioavailability: physiological concepts and patents. *Recent Pat. Anticancer Drug Discovery* 10, 87–96. doi: 10.2174/1574892809666140917103834

Ashburner, M., Ball, C. A., Blake, J. A., Botstein, D., Butler, H., Cherry, J. M., et al. (2000). Gene ontology: tool for the unification of biology. *Nat. Genet.* 25, 25–29. doi: 10.1038/75556

Bhargava, P. (2009). VEGF kinase inhibitors: how do they cause hypertension? *Am. J. Physiol.-Regul. Integr. Comp. Physiol.* 297 (1), R1–R5. doi: 10.1152/ajpregu.90502.2008

Chen, G., Pan, S. Q., Shen, C., Pan, S. F., Zhang, X. M., He, Q. Y., et al. (2014). Puerarin inhibits angiotensin II-induced cardiac hypertrophy via the redox-sensitive ERK1/2, p38 and NF-kappaB pathways. *Acta Pharmacol. Sin.* 35, 463–475. doi: 10.1038/aps.2013.185

Chen, M. F., Tsai, J.-T., Chen, L.-J., Wu, T.-P., Yang, J.-J., Yin, L.-T., et al. (2014). Antihypertensive action of allantoin in animals. *BioMed. Res. Int*. 2014, 1–6. doi: 10.1155/2014/690135

Chen, J., Bundy, J. D., Hamm, L. L., Hsu, C. Y., Lash, J., Miller, E. R. III., et al. (2019). Inflammation and apparent treatment-resistant hypertension in patients with chronic kidney disease: the results from the CRIC study. *Hypertension* 73, 785–793. doi: 10.1161/HYPERTENSIONAHA.118.12358

Chenevard, R., Hürlimann, D., Béchir, M., Enseleit, F., Spieker, L., Hermann, M., et al. (2003). Selective COX-2 inhibition improves endothelial function in coronary artery disease. *Circulation* 107, 405–409. doi: 10.1161/01.CIR.0000051361.69808.3A

Cho, T. M., Peng, N., Clark, J. T., Novak, L., Roysommuti, S., Prasain, J., et al. (2007). Genistein attenuates the hypertensive effects of dietary NaCl in hypertensive male rats. *Endocrinology* 148 (11), 5396–5402. doi: 10.1210/en.2007-0245

Cho, D.-Y., Ko, H., Kim, J., Kim, B.-W., Yun, Y.-S., Park, J.-I., et al. (2016). Scoparone inhibits LPS-simulated inflammatory response by suppressing IRF3 and ERK in BV-2 microglial cells. *Molecules* 21, 1718. doi: 10.3390/molecules21121718

Ferrara, N., and Kerbel, R. S. (2005). Angiogenesis as a therapeutic target. *Nature* 438, 967–974. doi: 10.1038/nature04483

Furumoto, T., Fujii, S., and Tsutsui, H. (2010). Daidzein, soy phytoestrogen, selectively ameliorates obesity-related hypertension in mice and humans without affecting other metabolic derangements. *J. Hypertens.* 28, e377. doi: 10.1097/01.hjh.0000379367.11028.98

Go, H.-K., Rahman, M., Kim, G.-B., Na, C.-S., Song, C.-H., Kim, J.-S., et al. (2015). Antidiabetic effects of yam (*Dioscorea batatas*) and its active constituent, allantoin, in a rat model of streptozotocin-induced diabetes. *Nutrients* 7, 8532–8544. doi: 10.3390/nu7105411

Hamosh, A., Scott, A. F., Amberger, J. S., Bocchini, C. A., and McKusick, V. A. (2005). Online mendelian inheritance in man (OMIM), a knowledgebase of human genes and genetic disorders. *Nucleic Acids Res.* 33, D514–D517. doi: 10.1093/nar/gki033

Harrison, D. G., Marvar, P. J., and Titze, J. M. (2012). Vascular inflammatory cells in hypertension. *Front. Physiol.* 3, 128. doi: 10.3389/fphys.2012.00128

Hermann, M., Camici, G., Fratton, A., Hurlimann, D., Tanner, F. C., Hellermann, J. P., et al. (2003). Differential effects of selective cyclooxygenase-2 inhibitors on endothelial function in salt-induced hypertension. *Circulation* 108, 2308–2311. doi: 10.1161/01.CIR.0000101683.30157.0B

Hsia, C.-W., Ho, M.-Y., Shui, H.-A., Tsai, C.-B., and Tseng, M.-J. (2015). Analysis of dermal papilla cell interactome using STRING database to profile the *ex vivo* hair growth inhibition effect of a *Vinca* alkaloid drug, colchicine. *Int. J. Mol. Sci.* 16, 3579–3598. doi: 10.3390/ijms16023579

Hsueh, W. A., and Anderson, P. W. (1992). Hypertension, the endothelial cell, and the vascular complications of diabetes mellitus. *Hypertension* 20 (2), 253–263. doi: 10.1161/01.HYP.20.2.253

Huang, H.-C., Lee, C.-R., Weng, Y.-I., Lee, M.-C., and Lee, Y.-T. (1992). Vasodilator effect of scoparone (6,7-dimethoxycoumarin) from a Chinese herb. *Eur. J. Pharmacol.* 218, 123–128. doi: 10.1016/0014-2999(92)90155-W

Huang, J., Tang, H., Cao, S., He, Y., Feng, Y., Wang, K., et al. (2017). Molecular targets and associated potential pathways of danlu capsules in hyperplasia of mammary glands based on systems pharmacology. *Evid. Based Complement. Altern. Med.* 2017, 1–10. doi: 10.1155/2017/1930598

Hwang, Y. P., Kim, H. G., Hien, T. T., Jeong, M. H., Jeong, T. C., and Jeong, H. G. (2011). Puerarin activates endothelial nitric oxide synthase through estrogen receptor-dependent PI3-kinase and calcium-dependent AMP-activated protein kinase. *Toxicol. Appl. Pharmacol.* 257, 48–58. doi: 10.1016/j.taap.2011.08.017

Intengan, H. D., and Schiffrin, E. L. (2001). Vascular remodeling in hypertension: roles of apoptosis, inflammation, and fibrosis. *Hypertension* 38 (3), 581–587. doi: 10.1161/hy09t1.096249

Jayedi, A., Rahimi, K., Bautista, L. E., Nazarzadeh, M., Zargar, M. S., and Shab-Bidar, S. (2019). Inflammation markers and risk of developing hypertension: a meta-analysis of cohort studies. *Heart* 105, 686–692. doi: 10.1136/heartjnl-2018-314216

Jung, S. H., Lee, G. B., Ryu, Y., Cui, L., Lee, H. M., Kim, J., et al. (2019). Inhibitory effects of scoparone from chestnut inner shell on platelet-derived growth factor-BB-induced vascular smooth muscle cell migration and vascular neointima hyperplasia. *J. Sci. Food Agric*. 99 (9), 4397–4406. doi: 10.1002/jsfa.9674

Kim, S.-K. , Lee, S. , Lee, M.-K., and Lee, S. (2019). A systems pharmacology approach to investigate the mechanism of Oryeong-san formula for the treatment of hypertension. *J. Ethnopharm.* 244, 112–129. doi: 10.1016/j.jep.2019.112129

Landmesser, U., Dikalov, S., Price, S. R., McCann, L., Fukai, T., Holland, S. M., et al. (2003). Oxidation of tetrahydrobiopterin leads to uncoupling of endothelial cell nitric oxide synthase in hypertension. *J. Clin. Invest.* 111 (8), 1201–1209. doi: 10.1172/JCI200314172

Li, W., Zhao, W., Wu, Q., Lu, Y., Shi, J., and Chen, X. (2016). Puerarin improves diabetic aorta injury by inhibiting NADPH oxidase-derived oxidative stress in STZ-induced diabetic rats. *J. Diabetes Res.* 2016, 9. doi: 10.1155/2016/8541520

Li, X., Lin, Y., Zhou, H., Li, Y., Wang, A., Wang, H., et al. (2017). Puerarin protects against endothelial dysfunction and end-organ damage in Ang II-induced hypertension. *Clin. Exp. Hypertens.* 39, 58–64. doi: 10.1080/10641963.2016.1200603

Li, X., Yuan, T., Chen, D., Chen, Y., Sun, S., Wang, D., et al. (2018). Cardioprotective effects of puerarin-V on isoproterenol-induced myocardial infarction mice is associated with regulation of PPAR-ϒ/NF-κB pathway. *Molecules* 23, 3322. doi: 10.3390/molecules23123322

Lin, C. C., Lin, W.-N., Cheng, S.-E., Tung, W.-H., Wang, H.-H., and Yang, C.-M. (2012). Transactivation of EGFR/PI3K/Akt involved in ATP-induced inflammatory protein expression and cell motility. *J. Cell. Physiol.* 227 (4), 1628–1638. doi: 10.1002/jcp.22880

Lin, P.-P., Hsieh, Y.-M., Kuo, W.-W., Lin, Y.-M., Yeh, Y.-L., Lin, C.-C., et al. (2013). Probiotic-fermented purple sweet potato yogurt activates compensatory IGF-IR/PI3K/Akt survival pathways and attenuates cardiac apoptosis in the hearts of spontaneously hypertensive rats. *Int. J. Mol. Med.* 32 (6), 1319–1328. doi: 10.3892/ijmm.2013.1524

Liu, H., Wang, J., Zhou, W., Wang, Y., and Yang, L. (2013). Systems approaches and polypharmacology for drug discovery from herbal medicines: an example using licorice. *J. Ethnopharmacol.* 146, 773–793. doi: 10.1016/j.jep.2013.02.004

Liu, X., Liu, F., Ma, Y., Li, H., Ju, X., and Xu, J. (2019). Effect of puerarin, baicalin and berberine hydrochloride on the regulation of IPEC-J2 cells infected with enterotoxigenic *Escherichia coli*. *Evid. Based Complement. Altern. Med.* 2019, 15. doi: 10.1155/2019/7438593

Ma, C., Zhai, C., Xu, T., Lu, F., Zhang, S., Li, C., et al. (2019). A Systems Pharmacology-Based Study of the Molecular Mechanisms of San Cao Decoction for Treating Hypertension. *Evidence-Based Complement. Altern. Med.* 10010, 1–10. doi: 10.1155/2019/3171420

Martelli, A., Testai, L., Anzini, M., Cappelli, A., Di Capua, A., Biava, M., et al. (2013). The novel anti-inflammatory agent VA694, endowed with both NO-releasing and COX2-selective inhibiting properties, exhibits NO-mediated positive effects on blood pressure, coronary flow and endothelium in an experimental model of hypertension and endothelial dysfunction. *Pharmacol. Res.* 78, 1–9. doi: 10.1016/j.phrs.2013.09.008

Mathieu, P., Poirier, P., Pibarot, P., Lemieux, I., and Despres, J.-P. (2009). Visceral obesity: the link among inflammation, hypertension, and cardiovascular disease. *Hypertension* 53 (4), 577–584. doi: 10.1161/HYPERTENSIONAHA.108.110320

Mauri, A., Consonni, V., Pavan, M., and Todeschini, R. (2006). Dragon software: an easy approach to molecular descriptor calculations. *Match Commun. Math. Comput. Chem.* 56, 237–248.

Mocan, A., Carradori, S., Locatelli, M., Secci, D., Cesa, S., Mollica,A., et al. (2018). Bioactive isoflavones from Pueraria lobata root and starch: Different extraction techniques and carbonic anhydrase inhibition. *Food Chem. Toxicol.* 112, 441–447. doi: 10.1016/j.fct.2017.08.009

Moran, A. E., Odden, M. C., Thanataveerat, A., Tzong, K. Y., Rasmussen, P. W., Guzman, D., et al. (2015). Cost-effectiveness of hypertension therapy according to 2014 guidelines. *N. Engl. J. Med.* 372, 447–455. doi: 10.1056/NEJMsa1406751

National Clinical Guideline Centre (UK). (2011). Hypertension: the clinical management of primary hypertension in adults: update of clinical guidelines 18 and 34. *National Institute for Health and Clinical Excellence: Guidance* (UK: Royal College of Physicians).

Ogata, H., Goto, S., Sato, K., Fujibuchi, W., Bono, H., and Kanehisa, M. (1999). KEGG: Kyoto encyclopedia of genes and genomes. *Nucleic Acids Res.* 27, 29–34. doi: 10.1093/nar/27.1.29

Olsson, A. K., Dimberg, A., Kreuger, J., and Claesson-Welsh, L. (2006). VEGF receptor signalling? In control of vascular function. *Nat. Rev. Mol. Cell Biol.* 7, 359–371. doi: 10.1038/nrm1911

Pandey, A. K., Singhi, E. K., Arroyo, J. P., Ikizler, T. A., Gould, E. R., Brown, J., et al. (2018). Mechanisms of VEGF (vascular endothelial growth factor) inhibitor-associated hypertension and vascular disease. *Hypertension* 71, e1–e8. doi: 10.1161/HYPERTENSIONAHA.117.10271

Rebhan, M., Chalifa-Caspi, V., Prilusky, J., and Lancet, D. (1997). GeneCards: integrating information about genes, proteins and diseases. *Trends Genet.* 13, 163. doi: 10.1016/S0168-9525(97)01103-7

Robinson, N. (2011). Integrative medicine-traditional Chinese medicine, a model? *Chin. J. Integr. Med.* 17, 21–25. doi: 10.1007/s11655-011-0602-9

Ru, J., Li, P., Wang, J., Zhou, W., Li, B., Huang, C., et al. (2014). TCMSP: a database of systems pharmacology for drug discovery from herbal medicines. *J. Cheminform.* 6, 13. doi: 10.1186/1758-2946-6-13

Ruan, C. C., and Gao, P. J. (2019). Role of complement-related inflammation and vascular dysfunction in hypertension. *Hypertension* 73, 965–971. doi: 10.1161/HYPERTENSIONAHA.118.11210

Safran, M., Dalah, I., Alexander, J., Rosen, N., Iny Stein, T., Shmoish, M., et al. (2010). GeneCards version 3: the human gene integrator. *Database (Oxford)* 2010. baq020. doi: 10.1093/database/baq020

Savoia, C., and Schiffrin, E. L. (2006). Inflammation in hypertension. *Curr. Opin. Internal Med.* 5 (3), 245–251. doi: 10.1097/01.mnh.0000203189.57513.76

Shannon, P., Markiel, A., Ozier, O., Baliga, N. S., Wang, J. T., Ramage, D., et al. (2003). Cytoscape: a software environment for integrated models of biomolecular interaction networks. *Genome Res.* 13, 2498–2504. doi: 10.1101/gr.1239303

Shi, W., Yuan, R., Chen, X., Xin, Q. , Wang, Y., Shang, X., et al. (2019). Puerarin reduces blood pressure in spontaneously hypertensive rats by targeting eNOS. *Am. J. Chin. Med.* 47, 19–38. doi: 10.1142/S0192415X19500022

Si, H., and Liu, D. (2008). Genistein, a soy phytoestrogen, upregulates the expression of human endothelial nitric oxide synthase and lowers blood pressure in spontaneously hypertensive rats. *J. Nutr.* 138 (2), 297–304. doi: 10.1093/jn/138.2.297

Solomon, D. H., Schneeweiss, S., Levin, R., and Avorn, J. (2004). Relationship between COX-2 specific inhibitors and hypertension. *Hypertension* 44 (2), 140–145. doi: 10.1161/01.HYP.0000136134.31846.83

Song, W., Ni, S., Fu, Y., and Wang, Y. (2018). Uncovering the mechanism of maxing ganshi decoction on asthma from a systematic perspective: a network pharmacology study. *Sci. Rep.* 8, 17362. doi: 10.1038/s41598-018-35791-9

Su, G., Morris, J. H., Demchak, B., and Bader, G. D. (2014). Biological network exploration with cytoscape 3. *Curr. Protoc. Bioinform.* 47, 8.13.11–18.13.24. doi: 10.1002/0471250953.bi0813s47

Sun, H. J., Chen, D., Han, Y., Zhou, Y.-B., Wang, J.-J., Chen, Q., et al. (2016). Relaxin in paraventricular nucleus contributes to sympathetic overdrive and hypertension via PI3K-Akt pathway. *Neuropharmacology* 103, 247–256. doi: 10.1016/j.neuropharm.2015.12.023

Tan, C., Wang, A., Liu, C., Li, Y., Shi, Y., and Zhou, M.-S. (2017). Puerarin improves vascular insulin resistance and cardiovascular remodeling in salt-sensitive hypertension. *Am. J. Chin. Med.* 45, 1169–1184. doi: 10.1142/S0192415X17500641

Tao, W., Xu, X., Wang, X., Li, B., Wang, Y., Li, Y., et al. (2013). Network pharmacology-based prediction of the active ingredients and potential targets of Chinese herbal radix *Curcumae* formula for application to cardiovascular disease. *J. Ethnopharmacol.* 145, 1–10. doi: 10.1016/j.jep.2012.09.051

Tao, Z., Ge, Y., Zhou, N., Wang, Y., Cheng, W., and Yang, Z. (2016). Puerarin inhibits cardiac fibrosis via monocyte chemoattractant protein (MCP)-1 and the transforming growth factor-β1 (TGF-β1) pathway in myocardial infarction mice. *Am. J. Transl. Res.* 8, 4425–4433.

Tomiyama, H., Shiina, K., Vlachopoulos, C., Iwasaki, Y., Matsumoto, C., Kimura, K., et al. (2018). Involvement of arterial stiffness and inflammation in hyperuricemia-related development of hypertension. *Hypertension* 72, 739–745. doi: 10.1161/HYPERTENSIONAHA.118.11390

Ueno, H., Kanellakis, P., Agrotis, A., and Bobik, A. (2000). Blood flow regulates the development of vascular hypertrophy, smooth muscle cell proliferation, and endothelial cell nitric oxide synthase in hypertension. *Hypertension* 36 (1), 89–96. doi: 10.1161/01.HYP.36.1.89

van den Meiracker, A. H., and Danser, A. H. (2016). Mechanisms of hypertension and renal injury during vascular endothelial growth factor signaling inhibition. *Hypertension* 68, 17–23. doi: 10.1161/HYPERTENSIONAHA.116.07618

Vera, R., Sánchez, M., Galisteo, M., Villar, I. C., Jimenez, R., Zarzuelo, A., et al. (2007). Chronic administration of genistein improves endothelial dysfunction in spontaneously hypertensive rats: involvement of eNOS, caveolin and calmodulin expression and NADPH oxidase activity. *Clin. Sci.* 112 (3), 183–191. doi: 10.1042/CS20060185

Walters, W. P., and Murcko, M. A. (2002). Prediction of 'drug-likeness'. *Adv. Drug Deliv. Rev.* 54, 255–271. doi: 10.1016/S0169-409X(02)00003-0

Wang, J., and Xiong, X. (2012). Control strategy on hypertension in chinese medicine. *Evid. Based Complement. Altern. Med.* 2012, 284847. doi: 10.1155/2012/284847

Wang, M., Yang, H., Zheng, L.-Y., Zhang, Z., Tang, Y.-B., Wang, G.-L., et al. (2012). Downregulation of TMEM16A calcium-activated chloride channel contributes to cerebrovascular remodeling during hypertension by promoting basilar smooth muscle cell proliferation. *Circulation* 125 (5), 697–707. doi: 10.1161/CIRCULATIONAHA.111.041806

Wang, J., Feng, B., Yang, X., Liu, W., and Xiong, X. (2013a). Chinese herbal medicine for the treatment of prehypertension. *Evid. Based Complement. Altern. Med.* 2013, 493–521. doi: 10.1155/2013/493521

Wang, J., Feng, B., and Xiong, X. (2013b). Chinese herbal medicine for the treatment of obesity-related hypertension. *Evid. Based Complement. Altern. Med.* 2013, 757540. doi: 10.1155/2013/757540

Wang, C., Wang, W., Jin, X., Shen, J., Hu, W., and Jiang, T. (2016). Puerarin attenuates inflammation and oxidation in mice with collagen antibody-induced arthritis via TLR4/NF-kappaB signaling. *Mol. Med. Rep.* 14, 1365–1370. doi: 10.3892/mmr.2016.5357

Wang, S., Wang, H., and Lu, Y. (2017). Tianfoshen oral liquid: a CFDA approved clinical traditional Chinese medicine, normalizes major cellular pathways disordered during colorectal carcinogenesis. *Oncotarget* 8, 14549–14569. doi: 10.18632/oncotarget.14675

Wang, J., Li, Y., Yang, Y., Chen, X., Du, J., Zheng, Q., et al. (2017). A new strategy for deleting animal drugs from traditional chinese medicines based on modified yimusake formula. *Sci. Rep.* 7 (1), 1504–1526. doi: 10.1038/s41598-017-01613-7

Wang, L. Y., Fan, R. F., Yang, D. B., Zhang, D., and Wang, L. (2019). Puerarin reverses cadmium-induced lysosomal dysfunction in primary rat proximal tubular cells via inhibiting Nrf2 pathway. *Biochem. Pharmacol.* 162, 132–141. doi: 10.1016/j.bcp.2018.10.016

Wold, L. E., Relling, D. P., Duan, J., Norby, F. L., and Ren, J. (2002). Abrogated leptin-induced cardiac contractile response in ventricular myocytes under spontaneous hypertension: role of Jak/STAT pathway. *Hypertension* 39 (1), 69–74. doi: 10.1161/hy0102.100777

Wong, K. H., Li, G. Q., Li, K. M., Razmovski-Naumovski, V., and Chan, K. (2011). Kudzu root: Traditional uses and potential medicinal benefits in diabetes and cardiovascular diseases. *J. Ethnopharmacol.* 134, 584–607. doi: 10.1016/j.jep.2011.02.001

Wu, K. L. H., Wu, C.-A., Wu, C.-W., Chan, S. H. H., Chang, A. Y. W., and Chan, J. Y. H. (2013). Redox-sensitive oxidation and phosphorylation of PTEN contribute to enhanced activation of PI3K/Akt signaling in rostral ventrolateral medulla and neurogenic hypertension in spontaneously

hypertensive rats. *Antioxid. Redox Signal.* 18, 36–50. doi: 10.1089/ars.2011.4457

Wu, X. D., Wang, C., Zhang, Z. Y., Fu, Y., Liu, F. Y., and Liu, X. H. (2014). Puerarin attenuates cerebral damage by improving cerebral microcirculation in spontaneously hypertensive rats. *Evidence-Based Complement. Altern. Med.* 2014. doi: 10.1155/2014/408501

Wu, C. W., Lu, L., Liang, S. W., Chen, C., and Wang, S. M. (2016). Application of drug-target prediction technology in network pharmacology of traditional Chinese medicine. *Zhongguo Zhong Yao Za Zhi.* 41, 377–382. doi: 10.4268/cjcmm20160303

Xiong, X., Yang, X., Liu, Y., Zhang, Y., Wang, P., and Wang, J. (2013). Chinese herbal formulas for treating hypertension in traditional Chinese medicine: perspective of modern science. *Hypertens. Res.* 36, 570–579. doi: 10.1038/hr.2013.18

Xiong, X., Borrelli, F., de Sa Ferreira, A., Ashfaq, T., and Feng, B. (2014). Herbal medicines for cardiovascular diseases. *Evid. Based Complement. Altern. Med.* 2014, 809–741. doi: 10.1155/2014/809741

Xiong, X. (2015). Integrating traditional Chinese medicine into Western cardiovascular medicine: an evidence-based approach. *Nat. Rev. Cardiol.* 12, 374. doi: 10.1038/nrcardio.2014.177-c1

Xu, H., and Chen, K. (2008). Integrative medicine: the experience from China. *J. Altern. Complement. Med.* 14, 3–7. doi: 10.1089/acm.2006.6329

Xu, J. W., Ikeda, K., and Yamori, Y. (2004). Genistein inhibits expressions of NADPH oxidase p22phox and angiotensin II type 1 receptor in aortic endothelial cells from stroke-prone spontaneously hypertensive rats. *Hypertension Res.* 27 (9), 675–683. doi: 10.1291/hypres.27.675

Xu, X., Zhang, W., Huang, C., Li, Y., Yu, H., Wang, Y., et al. (2012). A novel chemometric method for the prediction of human oral bioavailability. *Int. J. Mol. Sci.* 13, 6964–6982. doi: 10.3390/ijms13066964

Xu, M., Cai, J., Wei, H., Zhou, M., Xu, P., Huang, H., et al. (2016). Scoparone protects against pancreatic fibrosis via TGF-β/Smad signaling in rats. *Cell. Physiol. Biochem.* 40, 277–286. doi: 10.1159/000452544

Yang, L., Liu, W., Hu, Z., Yang, M., Li, J., Fan, X., et al. (2019). A systems pharmacology approach for identifying the multiple mechanisms of action of the Wei Pi Xiao decoction for the treatment of gastric precancerous lesions. *Evid. Based Complement. Altern. Med.* 2019. 1–15. doi: 10.1155/2019/1562707

Yu, H., Chen, J., Xu, X., Li, Y., Zhao, H., Fang, Y., et al. (2012). A systematic prediction of multiple drug-target interactions from chemical, genomic, and pharmacological data. *PloS One* 7, e37608. doi: 10.1371/journal.pone.0037608

Yu, G., Wang, W., Wang, X., Xu, M., Zhang, L., Ding, L., et al. (2018). Network pharmacology-based strategy to investigate pharmacological mechanisms of zuojinwan for treatment of gastritis. *BMC Complement. Altern. Med.* 18, 292. doi: 10.1186/s12906-018-2356-9

Yuan, Y., Zong, J., Zhou, H., Bian, Z.-Y., Deng, W., Dai, J., et al. (2014). Puerarin attenuates pressure overload-induced cardiac hypertrophy. *J. Cardiol.* 63, 73–81. doi: 10.1016/j.jjcc.2013.06.008

Yuan, Y., Zhou, H., Wu, Q.-Q., Li, F.-F., Bian, Z.-Y., Deng, W., et al. (2016). Puerarin attenuates the inflammatory response and apoptosis in LPS-stimulated cardiomyocytes. *Exp. Ther. Med.* 11, 415–420. doi: 10.3892/etm.2015.2910

Zhang, W., Liu, C.-Q., Wang, P.-W., Sun, S.-Y., Su, W.-J., Zhang, H.-J., et al. (2010). Puerarin improves insulin resistance and modulates adipokine expression in rats fed a high-fat diet. *Eur. J. Pharmacol.* 649, 398–402. doi: 10.1016/j.ejphar.2010.09.054

Zhao, Y. H., Xu, Y. H., Guan, Y., and Xiang, P. (2010). Effects of yinian jiangya decoction containing serum on cytokines secretion of vascular endothelium of spontaneously hypertensive rats. *Chin. J. Integr. Med.* 16, 344–347. doi: 10.1007/s11655-010-0524-y

Zhou, Y. X., Zhang, H., and Peng, C. (2014). Puerarin: a review of pharmacological effects. *Phytother. Res.* 28, 961–975. doi: 10.1002/ptr.5083

**Conflict of Interest:** The authors declare that the research was conducted in the absence of any commercial or financial relationships that could be construed as a potential conflict of interest.

frontiers in Pharmacology

ORIGINAL RESEARCH
published: 25 March 2020
doi: 10.3389/fphar.2020.00297

# Traditional Chinese Medicine Formula *Kang Shuai Lao Pian* Improves Obesity, Gut Dysbiosis, and Fecal Metabolic Disorders in High-Fat Diet-Fed Mice

*Shuqing Gong[1], Tingting Ye[1], Meixia Wang[2,3], Mengying Wang[4], Yufei Li[1], Lina Ma[5], Yulian Yang[5], Yi Wang[1], Xiaoping Zhao[6], Li Liu[7], Min Yang[4]*, Huan Chen[2,3]* and Jing Qian[1]**

[1] Pharmaceutical Informatics Institute, College of Pharmaceutical Sciences, Zhejiang University, Hangzhou, China, [2] Key Laboratory of Microbial Technology and Bioinformatics of Zhejiang Province, Zhejiang Institute of Microbiology, Hangzhou, China, [3] NMPA Key Laboratory for Testing and Risk Warning of Pharmaceutical Microbiology, Zhejiang Institute of Microbiology, Hangzhou, China, [4] Chronic Disease Research Institute, Department of Nutrition and Food Hygiene, School of Public Health, Zhejiang University School of Medicine, Hangzhou, China, [5] School of Public Health, Zhejiang University School of Medicine, Hangzhou, China, [6] College of Preclinical Medicine, Zhejiang Chinese Medical University, Hangzhou, China, [7] Technical Center, Chiatai Qingchunbao Pharmaceutical Co. Ltd, Hangzhou, China

OPEN ACCESS

**Edited by:**
*Aiping Lu,*
*Hong Kong Baptist University, Hong Kong*

**Reviewed by:**
*Yanfang Zheng,*
*Fujian University of Traditional Chinese Medicine, China*
*Jianbo Wan,*
*University of Macau, China*

***Correspondence:**
*Min Yang*
*ymin36@zju.edu.cn*
*Huan Chen*
*chenhuan7809@gmail.com*
*Jing Qian*
*jingqian@zju.edu.cn*

**Specialty section:**
*This article was submitted to Ethnopharmacology, a section of the journal Frontiers in Pharmacology*

**Received:** *19 November 2019*
**Accepted:** *27 February 2020*
**Published:** *25 March 2020*

**Citation:**
*Gong S, Ye T, Wang M, Wang M, Li Y, Ma L, Yang Y, Wang Y, Zhao X, Liu L, Yang M, Chen H and Qian J (2020) Traditional Chinese Medicine Formula Kang Shuai Lao Pian Improves Obesity, Gut Dysbiosis, and Fecal Metabolic Disorders in High-Fat Diet-Fed Mice. Front. Pharmacol. 11:297. doi: 10.3389/fphar.2020.00297*

High-fat diet (HFD)-induced obesity is a risk factor for many metabolic disorders including cardiovascular diseases, diabetes, and fatty liver disease. Although there are accumulating evidences supporting the assumption that regulating gut microbiota as well as its metabolic status is able to mitigate obesity, the inner relationship between the obesity-related gut microbiota and the relevant metabolites are not well defined. In current study, we applied a traditional herbal formula *Kang Shuai Lao Pian* (KSLP) to HFD-fed mice and evaluated its effect against obesity. Emphases were addressed on identifying profiles of gut microbiota and fecal metabolites with the aid of 16S rRNA gene sequencing and non-target fecal metabolomics techniques. We showed that KSLP could improve HFD-induced obesity, glucose tolerance disorder, as well as gut dysbiosis. In the gut, KSLP corrected the increased abundance of Firmicutes and Proteobacteria, increased ratio of Firmicutes/Bacteroidetes, and decreased abundance of Bacteroidetes caused by HFD. KSLP also reversed HFD-induced significant changes in the abundance of certain genus including *Intestinimonas*, *Oscillibacter*, Christensenellaceae_R-7_group, Ruminococcaceae_UCG-010, and *Aliihoeflea*. Pearson correlation analysis indicated that except for Ruminococcaceae_UCG-010, other four genera had positive correlations with obesity. In addition, 22 key fecal metabolites responding to KSLP treatment were identified. Pearson correlation analysis showed that those metabolites are intimately related to KSLP effective genera of *Intestinimonas*, *Oscillibacter*, and Christensenellaceae_R-7_group. Our results indicate that KSLP is a promising traditional Chinese medicine (TCM) applicable for individuals with HFD habit. *Intestinimonas*, *Oscillibacter*, and Christensenellaceae_R-7_group might be responsible

for the regulatory effect of KSLP. Linking of obesity phenotypes with gut microbiota as well as fecal metabolites is therefore a powerful research strategy to reveal the mechanism of obesity and the targets of intervention.

**Keywords: Traditional Chinese medicine, high-fat diet, obesity, gut microbiota, fecal non-targeted metabolomics, correlation analysis**

## INTRODUCTION

Defined as a disease status related to various health problems and reduced life span (Hoyt et al., 2014), obesity has become a serious health issue in the past decades (James, 2008). It is estimated that more than 1 billion people are prone to be obese by the year 2030 worldwide (Kelly et al., 2008). Due to the accumulation of adipose tissue, obese individuals appear susceptible to metabolic disorders including insulin resistance, type 2 diabetes, fatty liver disease, and cardiovascular diseases (Kopelman, 2000). To date, there is still a lack of promising strategies for the prevention and treatment of obesity, partially due to the limited understanding of the mechanisms controlling the occurrence of obesity and the development of its related metabolic diseases.

Among the complex environmental and genetic factors, gut microbiota plays a critical role in regulating HFD-induced obesity and obesity-related metabolic diseases (Turnbaugh et al., 2006; Cani et al., 2009; Ridaura et al., 2013). It is recognized that diet has approximately 57% influence on the gut microbiota structure while genetic factors has approximately 12% (Tomasello et al., 2014). In line with clues that the occurrence of obese phenotype is associated with gut microbiosis characterized by richer abundance of Firmicutes and poorer Bacteroides in genetic obese ob/ob mice (Ley et al., 2005) and that transplantation of gut microbiota of human obese twins into mice fed with low-fat diet results in transmissible adiposity phenotypes (Ridaura et al., 2013), targeting the structure and function of gut microbiota could be a promising strategy for the prevention and treatment against obesity.

Gut microbiota affects nutrient acquisition, energy harvest, and metabolic pathways of the host (Devaraj et al., 2013; Le Chatelier et al., 2013). In the scenario of obesity, disorders of lipid, carbohydrate, bile acid, and amino acid metabolism are all likely related to compositional changes in gut microbiota (Caesar et al., 2010; Yokota et al., 2012; Devaraj et al., 2013; Neis et al., 2015). The investigation of fecal metabolomics, especially its association with the functional readout of gut microbiome, is of great value for the understanding of diet–microbiota–metabolism interactions (Cheng et al., 2018; Zierer et al., 2018).

Chinese herbal medicine has shown powerful capacity of improving both obesity and its metabolic diseases through the regulation of gut microbiota (Hasani-Ranjbar et al., 2009). Indeed, as gut microbiota composition is essential for the occurrence of obesity, varieties of bioactive substances from herb medicine were revealed to have positive impacts on gut microbiota and therefore could be used for the prevention or treatment of lipid metabolic disorders (Yu et al., 2018; Zhang et al., 2019b). For example, it is recently reported that the therapeutic effect of ganoderma lucidum against HFD-inducing obesity is actually working through the compositional regulation of gut microbiota (Chang et al., 2015; Chang et al., 2017). *Kang Shuai Lao Pian* (KSLP) is a famous traditional Chinese medicine (TCM) formulated from a court prescription of the Ming Dynasty. It comprises *Rehmannia glutinosa* (Gaertn.) DC., *Panax ginseng* C.A.Mey., *Asparagus cochinchinensis* (Lour.) Merr., *Ophiopogon japonicus* (Thunb.) Ker Gawl., *Lycium chinense* Mill., and *Poria cocos* (Schw.) Wolf. In China, it is a widely used health care product for delaying senescence. The application of KSLP could improve learning and memory but inhibit brain lipid peroxidation in D-galactose-induced aged rats (Tao, 2009). Although a direct link between HFD-induced obesity and KSLP has never been reported, there were clinical observations indicating people with long-term KSLP administration prone to have a lean appearance. Besides, we have revealed that while taking KSLP as food supplement for 6 weeks, mid-aged mice appeared to have relatively less white but more brown adipose tissue distribution (Gong et al., 2020). Therefore, it is worthwhile to investigate whether KSLP has any interventional effect on HFD-induced obesity. In the current study, we established an HFD-induced obesity mouse model and applied KSLP as an intervention. In addition to the assessments of body weight, adipose tissue distribution, and blood metabolites chemistry, 16S rRNA gene sequencing and fecal non-targeted metabolomics studies were apparently performed.

## MATERIALS AND METHODS

### KSLP Preparation

KSLP (Med-drug permit no. B20021021) was obtained from Chiatai Qingchunbao Pharmaceutical Co. Ltd. (Hangzhou, China). Composed of six herbs including *R. glutinosa* (Gaertn.) DC., *P. ginseng* C.A.Mey., *A. cochinchinensis* (Lour.) Merr., *O. japonicus* (Thunb.) Ker Gawl., *L. chinense* Mill., and *P. cocos* (Schw.) Wolf. with the mixed proportion of the respective compound being 409:167:26:26:26:77, the preparation of KSLP is followed as described in the patent (CN 1943707 B) (Zhou, 2012). The HPLC fingerprint results from three different batches (Batch 20171020, 20180302, and 20180716) were listed (**Supplementary Figure 1**). In the current study, KSLP (Batch 20171020) was dissolved in Milli-Q water and prepared as drug resuspension before use.

## Animals and Experimental Design

C57/BL6 mice (male, 6–8 weeks) were purchased from the Shanghai ReMed Biotechnology Co. Ltd. (Shanghai, China, www.remed-bio.com) and maintained under the following environment: 24–26°C, 40–60% humidity, 12-h light/dark cycle, food and water ad libitum. All of the animal experiments were performed at Zhejiang Province center for disease control and prevention. The Guide for the Care and Use of Laboratory Animals was followed (Mason and Matthews, 2012).

Mice were divided into four groups: normal diet (ND, $n = 5$), normal diet supplied with KSLP (ND_K, $n = 5$), high-fat diet (HFD, $n = 9$), and HFD supplied with KSLP (HFD_K, $n = 9$). The normal diet feed was supplied by Zhejiang experimental animal center and the implementation of the standard was GB14924.1-2001. The HFD feed was supplied by Research Diets (New Brunswick, NJ, USA) with the energy supply ratio being 60% fat, 20% protein, and 20% carbohydrate. Mice were supplied with either KSLP resuspension at 0.45 g/kg/day or the same amount of water by intragastric administration for 12 consecutive weeks, respectively.

The body weight of mice and food intake were measured every week. On the 9th week of the experimental period, oral glucose tolerance test (OGTT) was performed. At the end of the experiment, mice were fasted for 4 h before the eye blood was collected. Afterwards, samples of mice were collected for further studies. In detail, samples of visceral adipose tissue (VAT, including epididymal adipose, perirenal adipose, and mesentery adipose), subcutaneous adipose tissue (SAT), interscapular brown adipose tissue (BAT), and gastrocnemius muscles were extracted for weighting; intestine feces were collected and stored at −80°C till sent for 16S rRNA gene sequencing and non-targeted metabolomics analyses.

## Blood Biochemistry Test

Blood samples were kept still for 2 h before they were centrifuged at 3000 rpm for 15 min at 4°C. After centrifugation, the supernatants were collected for blood biochemistry test. Parameters including triglyceride (TG), total cholesterol (CHOL), low-density lipoprotein (LDL), high-density lipoprotein (HDL), and glucose were assayed on a Hitachi 7180 automatic biochemical analyzer (Kyoto, Japan).

## OGTT

For OGTT, mice were fasted for 4 h before they were intragastrically administered with glucose solution at a dosage of 2.5 g/kg. At baseline (0 min), 30, 60, and 120 min post glucose administration, tail blood was collected for the glucose level measuring (Super glucocard II GT-1640, ARKRAY Factory, Inc., Kyoto, Japan). A glucose curve was created and the area under the curve of glucose (AUC) was calculated according to the formula: AUC = (FPG/2 + 60 min PG + 120 min PG/2) × 1 h mmol·h/L (FPG: fasting plasma glucose).

## Gut Microbiota Sequencing and Data Analysis

Parts of fecal samples were sent to Zhejiang Tianke high-tech Co., Ltd (Hangzhou, China. http://www.tkgeneclub.com/tkgeneclub/index.html) for 16S rRNA gene sequencing. Total genomic DNA was extracted from 0.25 g of feces using the PowerSoil® DNA Isolation Kit (MO BIO, Cat. No. 12888, Carlsbad, CA, USA) according to the manufacturer's protocols. DNA concentration and purity were monitored on 1% agarose gels. According to the concentration, DNA was diluted to 1 ng/μl using sterile water. 16S rRNA genes were amplified used specific primer (16S V3–V4: 341F-806R) with the barcode. All PCR reactions were carried out with KAPA HiFi™ HotStart ReadyMix (2×). The PCR product was confirmed by using 1% agarose gel electrophoresis. The amplified products were purified with Beckman DNA Clean Beads and quantified by the Qubit 2.0 fluorometer (Invitrogen, Carlsbad, CA, USA). The library was diluted to 60 pM. The enriched library was loaded in Ion 530™ Chip and sequenced on an Ion S5™ platform (Thermo Fisher Scientific, Waltham, MA, USA) and about 500-bp single-end reads were generated. Raw sequencing data are available at the Sequence Read Archive (SRA) database of NCBI and connected to bioproject PRJNA565488.

Single-end reads were assigned to samples based on their unique barcode and truncated by cutting off the barcode and primer sequence. Quality filtering on the raw reads were performed under specific filtering conditions to obtain the high-quality clean reads according to the Cutadapt (https://cutadapt.readthedocs.io/en/stable/). The tags were compared with the reference database (Gold database, http://drive5.com/uchime/uchime_download.html) using UCHIME algorithm (UCHIME Algorithm, http://www.drive5.com/usearch/manual/uchime_algo.html) (Edgar et al., 2011) to detect chimera sequences and then the chimera sequences were removed (Haas et al., 2011). Then, the effective Tags were finally obtained. Operational Units (OTUs) were clustered with 97% similarity cutoff using Uparse (Uparse V8.1.1861, http://drive5.com/uparse/) (Edgar, 2013). Representative sequence for each OTU was screened for further annotation through the SILVA reference database (http://www.arb-silva.de/) (Quast et al., 2013) by uclust (http://drive5.com/usearch/manual/uclust_algo.html) (Edgar, 2010) at 90% threshold. Principal coordinates analysis (PCoA) was displayed by vegan package in R software (Version 3.2.2). The ACE index, Chao1 index, Shannon index, Simpson index, and rarefaction curve were calculated with QIIME (Version 1.9.1) and displayed with R software (Version 3.2.2). The ACE index, Chao1 index, Shannon index, and Simpson index used Wilcoxon rank-sum test for statistical significance comparison among groups. Significant differences in genus levels between two groups were calculated using R software for $t$ test to obtain $p$ values. Linear discriminant analysis (LDA) effect size (LEfSe) (http://huttenhower.sph.harvard.edu/galaxy) combined with the standard tests (Kruskal–Wallis rank-sum test and Wilcoxon rank-sum test) with linear discriminate analysis was used for statistical significance comparison.

## Gene Expression Analysis

The expression of Akkermansia was further analyzed using real-time qPCR as described elsewhere (Everard et al., 2013). The primers were ordered from Sangon Biotech (Shanghai, China) and 16S rDNA was amplified as an endogenous reference gene. The relative expression was calculated with the ΔΔCT method and expressed as the fold change in comparison to the control (ND group).

## Non-targeted Metabolomics Study

Parts of fecal samples were sent to Metabolon in cooperation with Calibra Diagnostics, Ltd. (Hangzhou, China, www.metabolon.com) for non-targeted metabolomics study. In brief, approximately 50 mg of feces was freeze-dried in a freeze drier (FreeZone 2.5L, LABCONCO, Kansas City, MO, USA) for 8 h. Afterwards, the samples were subjected to a MicroLab STAR® system (Hamilton, Switzerland) for automatic processing, which includes filtration, adding methanol to precipitate protein, and centrifugation before the supernatant of each sample was transferred to Evaporation System TurboVap® II for organic solvent removing and mobile phase reconstitution.

Ultrahigh Performance Liquid Chromatography–Tandem Mass Spectroscopy (UPLC-MS/MS): All methods utilized a Waters Acquity ultraperformance liquid chromatography and a Thermo Scientific Q-Exactive high-resolution/accurate mass spectrometer interfaced with a heated electrospray ionization (HESI-II) source and Orbitrap mass analyzer operated at 35,000 mass resolution. The concrete conditions of UPLC and MS as well as the method validation were described in detail in previous articles (Long et al., 2017).

Compounds were identified by automated comparison of the ion features in the experimental samples to a reference library of chemical standard entries that included retention time (RI), molecular weight (m/z), and chromatographic data (including MS/MS spectral data) on all molecules present in the library developed at Metabolon (Evans et al., 2009; Dehaven et al., 2010). Furthermore, biochemical identifications are based on three criteria: retention index within a narrow RI window of the proposed identification, accurate mass match to the library ± 10 ppm, and the MS/MS forward and reverse scores between the experimental data and authentic standards. The MS/MS scores are based on a comparison of the ions present in the experimental spectrum to the ions present in the library spectrum. While there may be similarities between these molecules based on one of these factors, the use of all three data points can be utilized to distinguish and differentiate biochemicals. More than 3300 commercially available purified standard compounds have been acquired and registered into LIMS for analysis on all platforms for determination of their analytical characteristics. Peaks were quantified using area under the curve. For studies spanning multiple days, a data normalization step was performed to correct variation resulting from instrument inter-day tuning differences. Essentially, each compound was corrected in run-day blocks by registering the medians to equal one (1.00) and normalizing each data point proportionately. ANOVA contrasts were used to identify biochemicals that differed significantly between experimental groups.

## Statistical Analysis

Data are presented as mean ± standard errors of the means (S.E.M.). Statistical differences were assessed over two groups by analysis of variance (ANOVA) using GraphPad Prism 7.0 software. In metabolomics research, statistical analyses are performed in ArrayStudio; Student's $t$ test was performed between two groups, while ANOVA was used among over two groups. A $p$ value less than 0.05 indicated statistical significance. Pearson correlation analysis was performed using SPSS and the corresponding heatmap was visualized using Excel and Adobe Illustrator.

# RESULTS

## KSLP Decreased Body Weight, White Adipose Tissue Ratio, and Improved Glucose Tolerance Disorder in HFD Mice

In the first panel of assessments, we compared the body weight, fat tissue distribution, and blood metabolic parameters among the groups of normal diet (ND), normal diet supplied with KLSP (ND_K), HFD, and HFD supplied with KSLP (HFD_K). As indicated in body weight curve (**Figure 1A**), ND group mice had slight body weight gain over the period of experiment, so did the ND_K group mice ($p > 0.05$, ND vs. ND_K). On the contrary, compared with ND mice, HFD group mice had a higher body weight gain speed. Starting from 3 weeks after HFD, the HFD mice had significant body weight gain as compared to ND mice ($p < 0.05$). The application of KSLP relieved the HFD-induced body weight gain. At the end of the experiment (12 weeks), the reduced body weight of HFD-K mice as compared to HFD were of statistical significance ($p < 0.05$). The inhibited body weight growing was not due to the inhibited appetite since the food intake between HFD and HFD_K groups had no significant difference (**Supplementary Figure 2**).

At the end of the experiment, samples of VAT (including epididymal adipose, perirenal adipose and mesentery adipose), SAT, and interscapular BAT were extracted and weighted for comparison. As indicated in **Figure 1B**, compared with ND mice, HFD mice had significant higher amounts of visceral adipose, subcutaneous adipose, as well as interscapular brown adipose ($p < 0.05$). KSLP reduced the net weight of these three types of fat tissues especially the visceral adipose (0.9858 ± 0.2058 vs. 1.559 ± 0.3042 g, $p < 0.05$). Notably, the reduced overall body weight of KSLP on HFD mice was not at the cost of muscle since KSLP treatment had no significant effect on the muscle weight of mice (**Supplementary Figure 3**).

Next, we detected lipid and glucose level (TG, CHOL, HDL, LDL, and glucose) for each mouse. As indicated in **Table 1**, except for the reduced level of TG ($p < 0.05$), KSLP had no effect on CHOL, HDL, LDL, and blood glucose on ND mice. As expected, HFD caused significant increased level of all the detected parameters of CHOL, HDL, LDL, and blood glucose ($p < 0.05$ or $p < 0.01$). While no regulatory effect of lipid metabolism as indicated by TG, CHOL, HDL, LDL, were

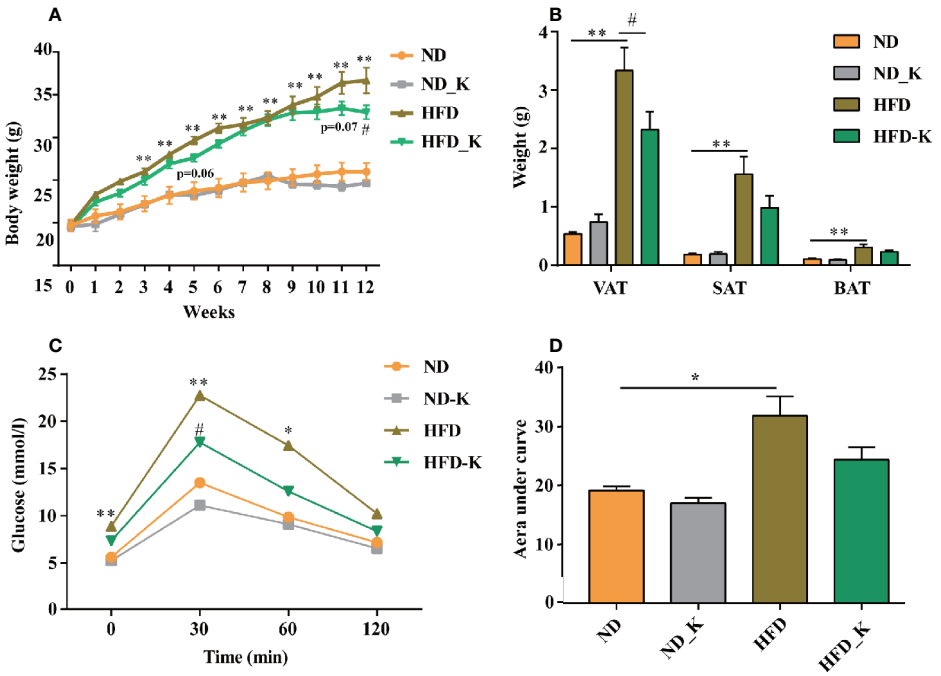


**FIGURE 1 |** KSLP reduced body weight and improved the glucose tolerance in HFD mice. **(A)** The changes of body weight during the experimental course. **(B)** The effects of HFD and KSLP on visceral adipose tissue (VAT), subcutaneous adipose tissue (SAT), and brown adipose tissue (BAT). **(C)** OGTT after 9 weeks of KSLP treatment. **(D)** AUC of each group was calculated during the oral glucose tolerance test. Compared with ND group, $^{*}p < 0.05$, $^{**}p < 0.01$. Compared with HFD group, $^{\#}p < 0.05$.

**TABLE 1 |** The serum lipid and glucose level in four groups.

| | ND | ND_K | HFD | HFD_K |
|---|---|---|---|---|
| TG (mmol/L) | 1.22 ± 0.08 | 0.88 ± 0.06** | 1.02 ± 0.04* | 0.94 ± 0.05 |
| CHOL (mmol/L) | 2.40 ± 0.10 | 2.41 ± 0.11 | 4.71 ± 0.24** | 4.12 ± 0.33 |
| HDL (mmol/L) | 1.70 ± 0.09 | 1.67 ± 0.08 | 2.83 ± 0.03** | 2.56 ± 0.21 |
| LDL (mmol/L) | 0.30 ± 0.03 | 0.32 ± 0.01 | 0.79 ± 0.14* | 0.65 ± 0.05 |
| Glucose (mmol/L) | 9.60 ± 0.39 | 7.19 ± 0.53 | 14.74 ± 1.74* | 10.03 ± 0.56# |

*Compared with ND group, $^{*}p < 0.05$, $^{**}p < 0.01$. Compared with HFD group, $^{\#}p < 0.05$.*

detected, KSLP significantly reduced the glucose level for HFD mice (14.74 ± 1.74 vs. 10.03 ± 0.56 mmol/L, $p < 0.05$).

The capacity for glucose metabolism was also evaluated by OGTT on the 9th week of the experiment. As indicated in **Figure 1C**, for each group of mice, the supplementation of glucose resulted in transient increase of blood glucose level at 30 min followed by the gradual decrease of that at 60 and 120 min. HFD mice presented higher levels of glucose at baseline (0 min) and at 30 and 60 min compared with ND mice ($p < 0.05$ or $p < 0.01$). Compared with HFD mice, HFD_K mice showed lower levels of glucose at each indicated time point, and at 30 min, the difference was statistically significant ($p < 0.05$). Similarly, while the AUC of glucose was calculated from the OGTT curve (**Figure 1D**), HFD mice had a significantly higher level of AUC compared to ND mice, and the AUC was marginally decreased in HFD_K group mice compared with HFD mice (**Figure 1D**). The OGTT results suggested that KSLP improved the glucose tolerance disorder in obesity mice.

## KSLP Modulated the Overall Structure of the Gut Microbiota in HFD Mice

To examine the effect of HFD and KSLP on the gut microbiota, we performed Life ION S5 sequencing targeting the V3–V4 regions of 16S rRNA gene. After selecting the effective reads, a total of 1,256,721 effective reads was generated, and each fecal sample produced an average of 44,883 ± 3769 effective reads. Rarefaction curve analysis reached stable level, indicating that the sequencing depth had covered rare new phylotypes and most of the diversity (**Figure 2A**).

The gut microbiota diversity and richness were evaluated by ACE, chao1, Shannon, and Simpson indexes (**Table 2**). While no obvious difference was noticed between the ND and ND_K group, significant reduced diversity and richness were found in the HFD group compared with the ND group ($p < 0.01$ for all the indexes). Compared with HFD, HFD_K group mice had increased index for all the four parameters, among which the changes in ACE was statistically significant (287.2 ± 3.3 vs. 305.7 ± 4.2, $p < 0.05$). Since obese individuals normally appear with decreased bacterial diversity in the gut (Turnbaugh et al., 2009), our result of KSLP brought up gut microbiota diversity in the HFD mice, indicating that those obese mice improved their body status.

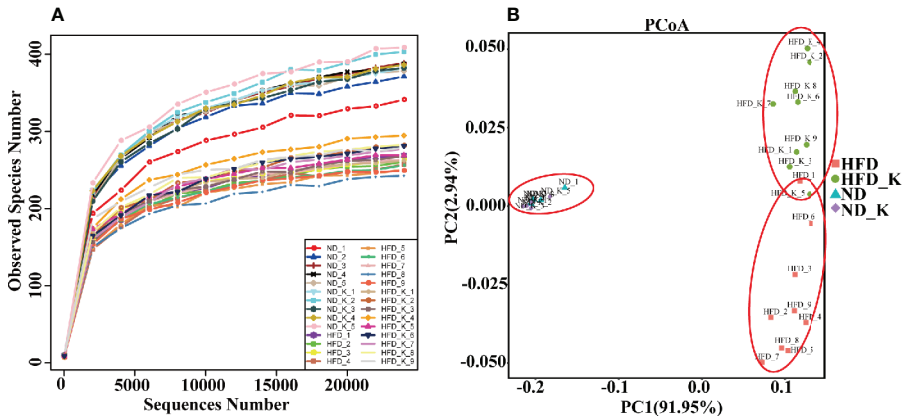


**FIGURE 2 |** KSLP reconstructed gut microbiota community in HFD mice. **(A)** Rarefaction curve analysis. The abscissa is the number of sequencing randomly extracted from a sample, and the ordinate is the number of OTUs that can be constructed based on the number of sequencing numbers. **(B)** Plots were generated using the principal coordinates analysis (PCoA).

**TABLE 2 |** The effects of HFD and KSLP on gut microbiota diversity.

| | ND | ND_K | HFD | HFD_K |
|---|---|---|---|---|
| ACE | 422.2 ± 7.7 | 443.6 ± 7.8 | 287.2 ± 3.3** | 305.7 ± 4.2# |
| Chao1 | 436.6 ± 11.7 | 450 ± 8.1 | 289.6 ± 3.6** | 306.4 ± 3.1 |
| Shannon | 6.45 ± 0.06 | 6.44 ± 0.05 | 5.64 ± 0.07** | 5.85 ± 0.10 |
| Simpson | 0.976 ± 0.002 | 0.972 ± 0.002 | 0.956 ± 0.003** | 0.962 ± 0.004 |

*Compared with ND group, **$p < 0.01$. Compared with HFD group, #$p < 0.05$.*

UniFrac-based PCoA was assessed to compare the overall microbiota structure for each group (**Figure 2B**). While ND and ND_K clusters merged into one, there appeared distinct clusters for ND/ND_K, HFD, and HFD_K groups. This result suggested that KSLP changed the overall gut microbiota composition in HFD mice but had no effect on ND mice.

## KSLP Regulated Gut Microbiota at Phylum and Family Levels in HFD Mice

The top 10 phyla in the relative abundance of gut microbiota were shown as histograms (**Figure 3A**), from which Firmicutes, Bacteroidetes, and Proteobacteria were listed as the top three dominant phyla in each group. Further comparison indicated that compared to the ND group, the HFD group had significantly increased relative abundance of Firmicutes and Proteobacteria but reduced relative abundance of Bacteroidetes. Notably, KSLP significantly reversed the phyla changes associated with HFD ($p < 0.05$ or $p < 0.01$, **Figure 3B**). In addition, we compared the ratio of Firmicutes/Bacteroidetes (F/B) as a featured sign of obesity among the four groups. As indicated in **Figure 3C**, HFD significantly increased the ratio of F/B, and its effect could be conversed by KSLP.

At the family level, in general, as indicated in **Figure 4A** and **Supplementary Table 1**, while ND and ND_K group mice presented very similar gut microbiota composition, HFD significantly affected the relative abundance of certain family and some of them could be reversed by KSLP. In detail, as Ruminococcaceae and Lachnospiraceae are dominant families in the phylum Firmicutes (Chi et al., 2018), HFD resulted in increased abundance of Ruminococcaceae but decreased abundance of Lachnospiraceae (**Figure 4B**). KSLP regulated the abundance of Ruminococcaceae in HFD mice to that similar to ND ones but did not affect that of Lachnospiraceae (**Figure 4B**). Besides, as Muribaculaceae, Prevotellaceae, Bacteroidaceae, and Rikenellaceae are members of the Bacteroidetes phylum, HFD diminished the relative abundance of Muribaculaceae and Prevotellaceae but did not affect that of Bacteroidaceae and Rikenellaceae (**Figure 4C**). Interestingly, KLSP had no impact on the relative abundance of the former two but increased the ones of the latter two (**Figure 4C**). In addition, HFD mice presented enriched Desulfovibrionaceae under Proteobacteria phylum as well as the Helicobacteraceae under Epsilonbacteraeota phylum, and KSLP decreased the abundance of both bacteria at a certain degree (**Figure 4D**).

## KSLP Regulated Gut Microbiota at the Genus Level in HFD Mice

At the genus level, the gut microbiota whose abundance significantly changed due to HFD (ND vs. HFD) and KSLP treatment (HFD vs. HFD_K) were evaluated. The list of the top ranked genera and the significantly changed ones are illustrated in **Figures 5A, B**. Overall, from the 50 top ranked genera in mean abundance between the ND and HFD group, 27 genera were significantly changed in response to HFD (**Figure 5A**). In detail, we observed significantly decreased abundance of the Prevotellaceae_UCG-001, *Muribaculum*, and Prevotellaceae_NK3B31_group of phylum Bacteroidetes in HFD compared with ND mice (**Figure 5A**). Notably, KSLP had no regulatory effect on those bacteria, but alternatively increased the abundance of other genera of bacteria in the category of phylum Bacteroidetes, i.e., Bacteroides, Alistipes, and Rikenellaceae_RC9_gut_group (**Figure 5B**). In addition, compared with the ND group, HFD mice had increased abundance of

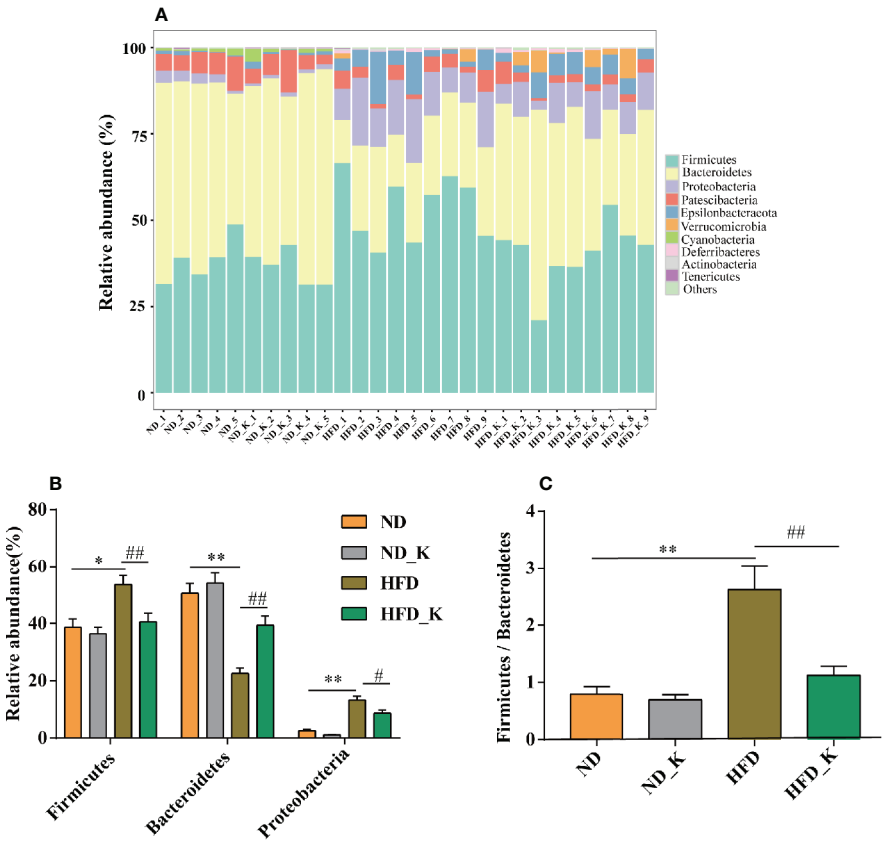


**FIGURE 3 |** KSLP affected the relative abundance of gut microbiota at the phylum level. **(A)** The relative abundance of the 10 top-ranked phyla were presented. **(B)** The relative abundance of Firmicutes, Bacteroidetes, and Proteobacteria. **(C)** The ratio of Firmicutes/Bacteroidetes. Compared with ND group, $^{*}p < 0.05$, $^{**}p < 0.01$. Compared with HFD group, $^{\#}p < 0.05$, $^{\#\#}p < 0.01$.

*Intestinimonas*, *Oscillibacter*, *Ruminiclostridium*, *Roseburia*, *Lactococcus*, Ruminococcaceae_UCG-010, *Anaerotruncus*, *Blautia*, and Christensenellaceae_R-7_group, all of which are of Firmicutes phylum, as well as increased abundance of *Bilophila* and *Aliihoeflea*, both of which are of Proteobacteria phylum (**Figure 5A**). Among them, five genera including *Intestinimonas*, *Oscillibacter*, Ruminococcaceae_UCG-010, Christensenellaceae_R-7_group, and *Aliihoeflea* were significantly reversed by the KSLP treatment in HFD mice (**Figure 5C**).

## Key Phylotypes Responding to the KSLP Treatment in HFD Mice

We also performed LEfSe analysis to identify the specific bacteria in the genus that were characteristic among the four groups. As shown in **Figure 6A**, discriminative features were identified with LDA score > 4.0. Referring to the ranked bacterial taxa, ND mice were enriched with g_Marivita, g_Lachnospiraceae_NK4A136_group, and g_Ruminococcaceae_UCG_014; ND_K mice with g_Alloprevotella; HFD mice with g_Intestinimonas, g_Helicobacter, g_Oscillibacter, and g_Ruminiclostridium; and HFD_K mice with g_Bacteroides, g_Alistipes, and g_Akkermansia. Of note, two of the four phylotypes of HFD, namely, *Intestinimonas* and *Oscillibacter*, were responsible for KSLP treatment (**Figure 5C**). We also noticed that Akkermansia was one of the characteristic genera for HFD_K group mice. The expression of Akkermansia was further analyzed using real-time qPCR analysis. The results demonstrated that compared with the HFD group, the expression level of Akkermansia in the HFD_K group was indeed increased (**Figure 6B**). Previous researches reported that the application of metformin resulted in slowing down body weight gain, improving glucose homeostasis, as well as enrichment of Akkermansia in diet-induced obese mice (Shin et al., 2014; Anhe et al., 2015). Besides, oral administration of Akkermansia (i.e., as a probiotic) could improve HFD induced metabolic disorders (Everard et al., 2013). Therefore, it can be considered that the beneficial effect of KSLP on HFD mice is related to enriched abundance of Akkermansia.

## KSLP Regulated Obesity-Related Gut Microbiota

As we have identified 27 genera that had significant abundance changes between ND and HFD groups, the correlation between these 27 genera and obesity-related parameters was calculated by Pearson correlation analysis. The result was summarized in **Supplementary Table 2** and presented as a heatmap (**Figure 7**). In general, there were nine genera intimately related to obesity phenotype, from which strong positive co-relationships

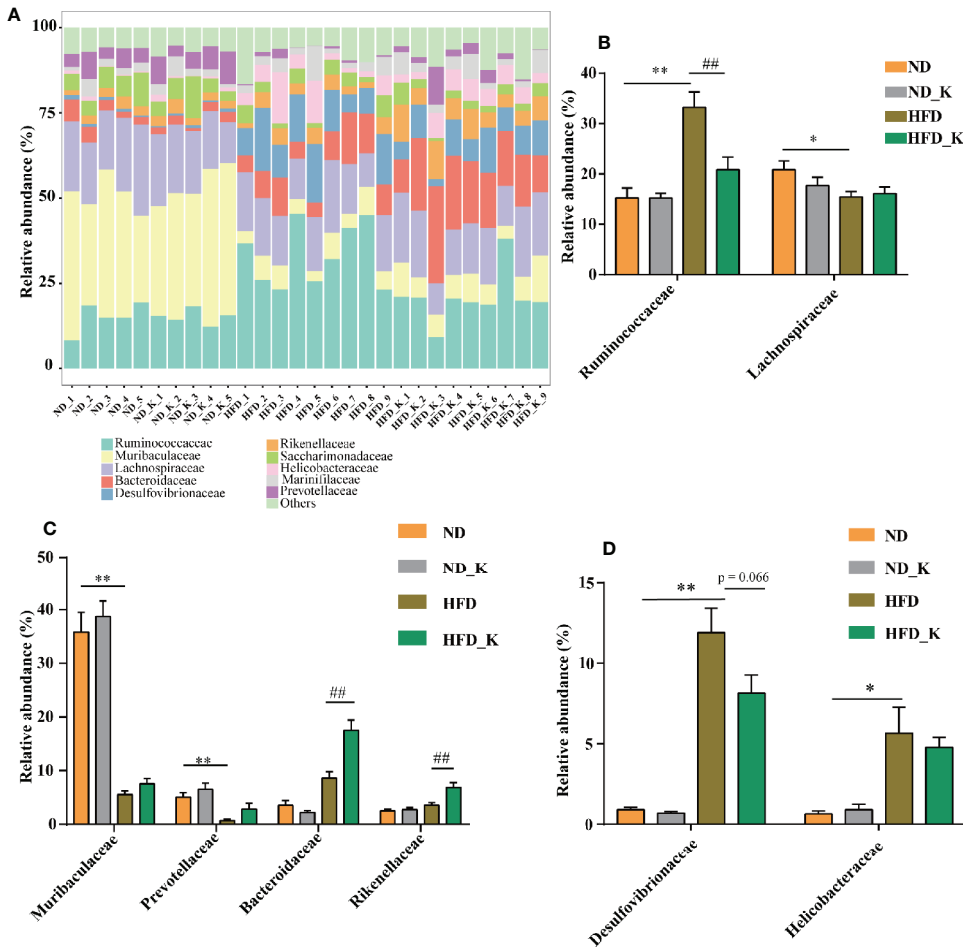


**FIGURE 4 |** KSLP affected the relative abundance of gut microbiota at the family level. **(A)** The relative abundance in the 10 top-ranked families was presented. **(B)** The relative abundance of Ruminococcaceae and Lachnospiraceae. **(C)** The changed abundance of families under Bacteroidetes phylum. **(D)** The relative abundance of Desulfovibrionaceae and Helicobacteraceae. Compared with ND group, $^{*}p < 0.05$, $^{**}p < 0.01$. Compared with HFD group, $^{\#\#}p < 0.01$.

were identified for *Intestinimonas*, *Oscillibacter*, *Lactococcus*, Christensenellaceae_R-7_group, and *Aliihoeflea*, while significant negative co-relationships were identified for Ruminococcaceae_UCG-014, Prevotellaceae_UCG-001, *Muribaculum*, and Family_XIII_AD3011_group (**Figure 7**). Of these nine genera, *Intestinimonas*, *Oscillibacter*, Christensenellaceae_R-7_group, and *Aliihoeflea* could be reversed by KSLP in HFD mice (**Figure 5C**). Therefore, *Intestinimonas*, *Oscillibacter*, Christensenellaceae_R-7_group, and *Aliihoeflea* might be targets of intervention for KSLP in HFD mice.

## KSLP Modulated Fecal Metabolomic Profiling in HFD Mice

We also conducted a global metabolomic profiling analysis using lyophilized fecal samples to check the metabolic situation of the gut in ND, ND_K, HFD, and HFD_K mice. In general, we have identified a total of 775 compounds of known identity (**Supplementary Table 3**). There were 439 metabolites changed in response to HFD, in which 188 were upregulated and 251 were downregulated (**Figure 8A**). Compared with the HFD group, 152 compounds changed, including 96 metabolites upregulated and 56 metabolites downregulated in the HFD_K group (**Figure 8A**). Two way-ANOVA analysis indicated that 514 metabolites could be affected by HFD and 120 metabolites could be affected by KSLP. Furthermore, 96 metabolites could be affected by both HFD and KSLP, in which the contents of 22 metabolites in response to HFD treatment could be reversed by KSLP (**Figure 8B** and **Supplementary Tables 4** and **5**).

## KSLP Regulated Obesity-Related Genera Along With Their Correlated Metabolites

Special attention was paid to reveal the novel inner relationship between the identified obesity-related gut microbiota and the reversed metabolites in response to KSLP in HFD mice. In this regard, we performed a correlation analysis by applying the four

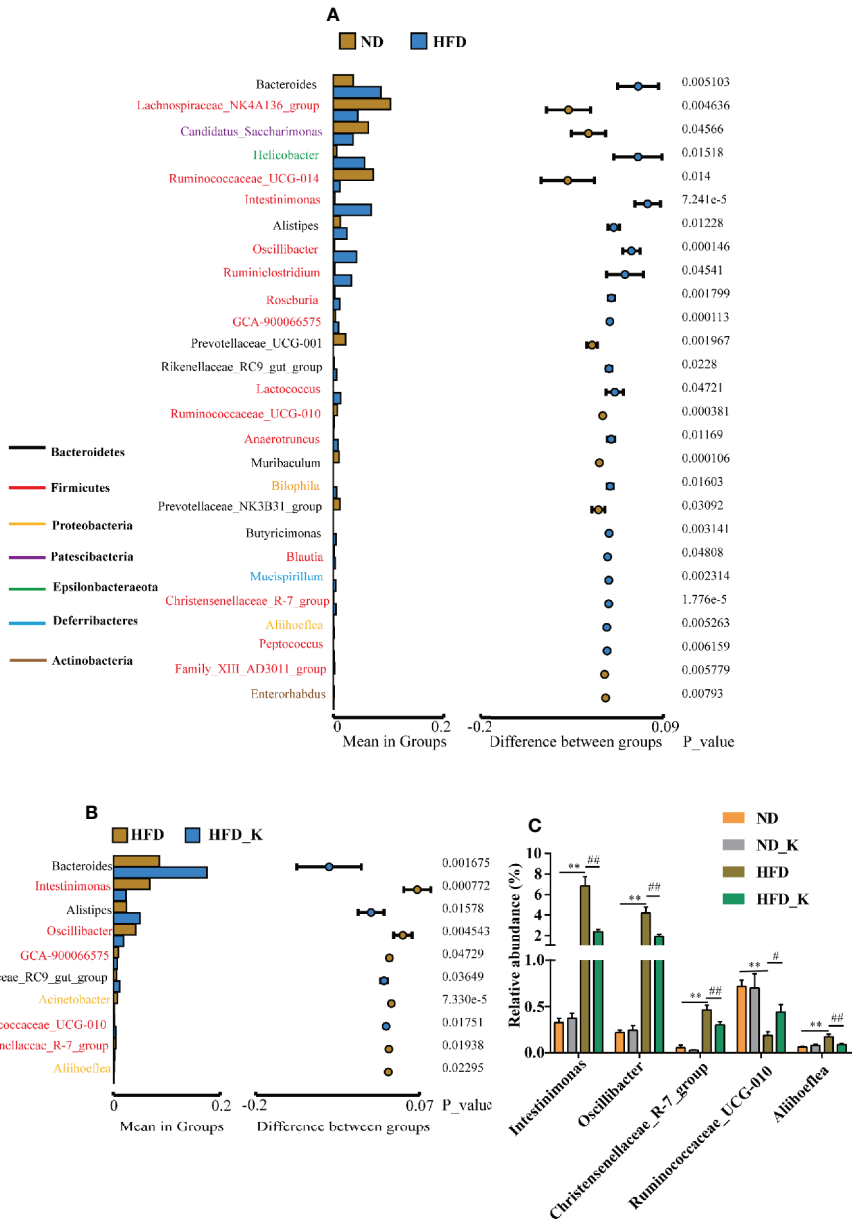


**FIGURE 5 |** KSLP affected the relative abundance of gut microbiota at the genus level. **(A)** Genera between ND and HFD groups with significant differences were presented. The list of genera with font color refers to their phyla. The histograms presented the mean relative abundance of genera whereas the circular colors represented the differences in confidence intervals. The *p* values for corresponding genus resulting from inter-group significance test were displayed. **(B)** Genera between HFD group and HFD_K group with significant differences were presented. **(C)** The genera responding to HFD and reversed by KSLP treatment. Compared with ND group, $^{**}p < 0.01$. Compared with HFD group, $^{\#\#}p < 0.01$, $^{\#}p < 0.05$.

identified KSLP-responsible-obesity-related genera of *Intestinimonas*, *Oscillibacter*, Christensenellaceae_R-7_group, and *Aliihoeflea*, as well as the 22 KSLP-responsible-HFD-related metabolites (**Supplementary Table 6**).

As indicated in the heatmap (**Figure 9**), *Intestinimonas*, *Oscillibacter*, and Christensenellaceae_R-7_group showed very similar metabolite relationship patterns, which positively correlated with histidylalanine, phenylalanylglycine, and gamma-CEHC, but negatively correlated with *N*-methylalanine, *N*,*N*,*N*-trimethyl-5-aminovalerate, (12 or 13)-methylmyristate (a15:0 or i15:0), 2-hydroxyarachidate*, 2-hydroxybehenate, 2-hydroxylignocerate*, 3-ketosphinganine, lanosterol, stigmastadienone, 2′-deoxyinosine, N6-methyladenosine, 2′-deoxyguanosine, 5,6-dihydrouridine, and hydroxymethylpyrimidine. As for *Aliihoeflea*, it presented weak correlation with the metabolites in the list except for the negative co-relationships with (12 or 13)-methylmyristate (a15:0 or i15:0) and 3-ketosphinganine.

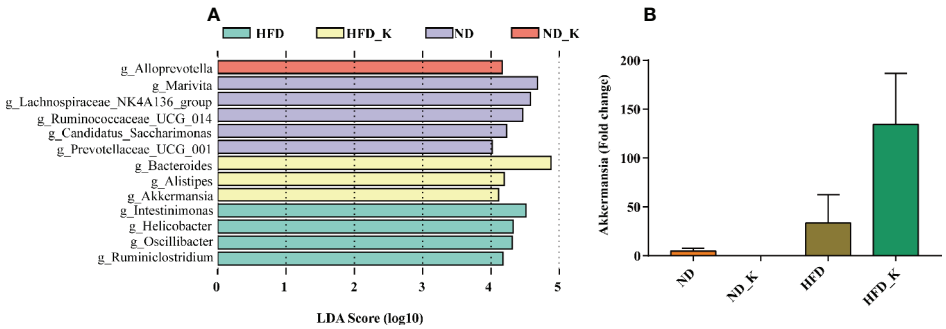


**FIGURE 6 |** Key phylotypes responding to the KSLP treatment in HFD mice. **(A)** Linear discriminant analysis (LDA) scores were computed for taxa with differential abundance in the fecal microbiota of ND (purple), ND_K (red), HFD (green), and HFD_K (yellow) mice. The LDA score indicated the effect size and ranking of each differentially abundant taxon (LDA > 4). **(B)** Real-time qPCR analysis. The relative expression of Akkermansia was expressed as the fold change in comparison to the ND group.

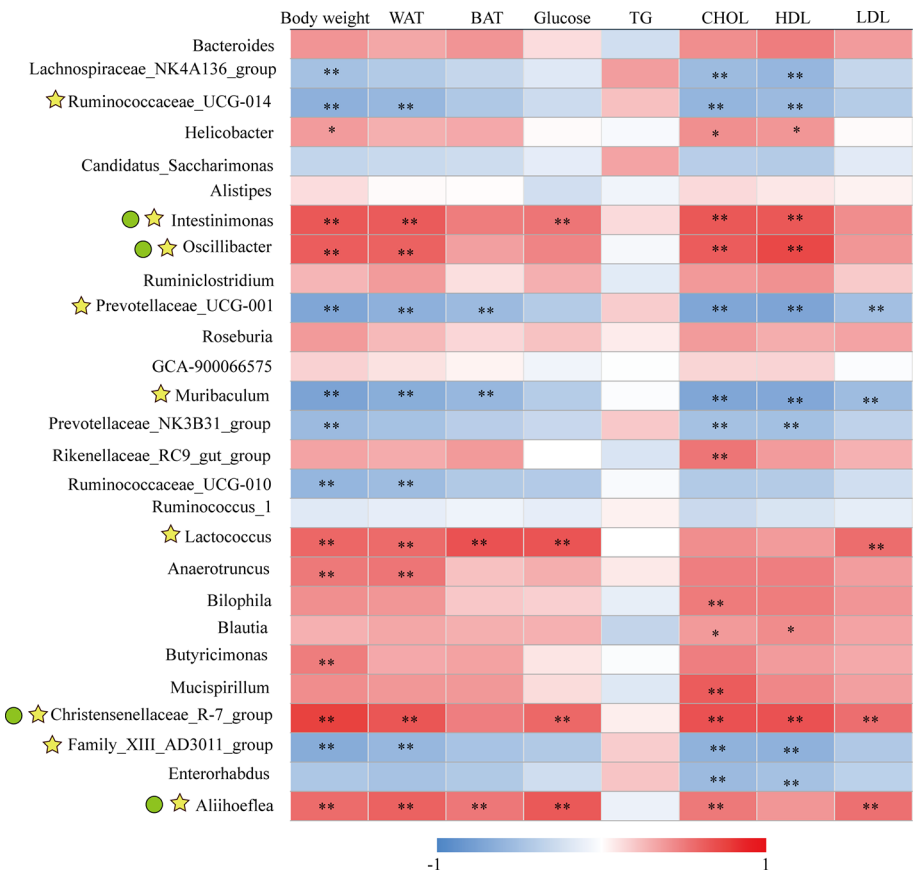


**FIGURE 7 |** The correlation between the changed genera responding to HFD and obesity-related index.*$|r| > 0.5$ and $p < 0.05$; **$|r| > 0.5$ and $p < 0.01$. Yellow asterisk: ≥4 obesity-related index were intimately correlated with certain genus; green cycle: (1) ≥4 obesity-related index were intimately correlated with certain genus; (2) reversed by KSLP treatment.

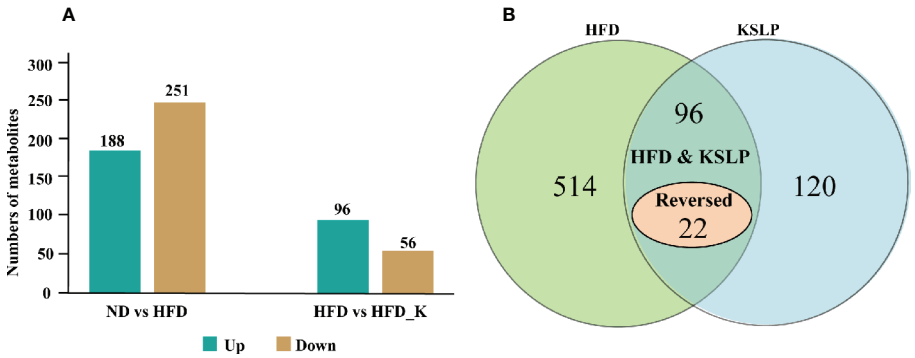


**FIGURE 8 |** Different metabolites among three groups. **(A)** Numbers of upregulated and downregulated metabolites. **(B)** The influencing factor of metabolites using two-way ANOVA.

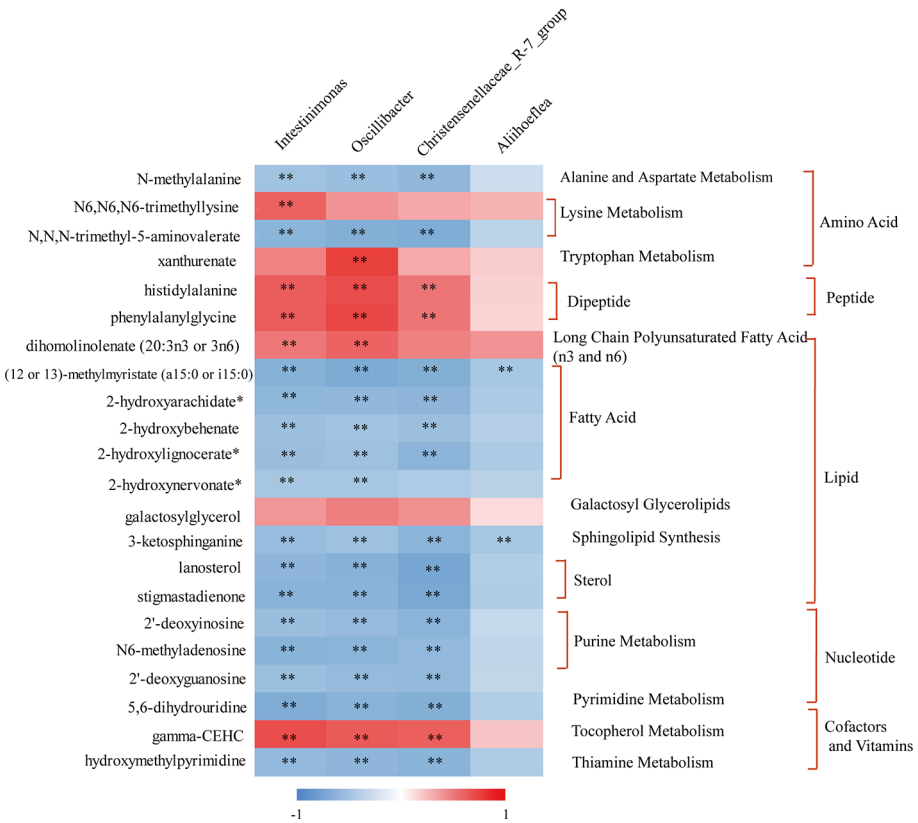


**FIGURE 9 |** The correlation between KSLP-responsible-obesity-related genera and reversed metabolites by KSLP. $^{**}|r| > 0.5$ and $p < 0.01$. The metabolites corresponding to the metabolic pathway were presented on the right.

## DISCUSSION

In this study, we observed significant differences in gut microbiota communities between the ND group and HFD group. At the phyla level, the gut of HFD-fed mice was characterized by increased abundance of Firmicutes and Proteobacteria, decreased abundance of Bacteroidales, as well as increased ratio of F/B, the profiling of which appeared similar to previously reported "obese gut" (Alard et al., 2016; Yu et al., 2018; Zhang et al., 2019b) and obesity-driven gut dysbiosis (Anhe et al., 2019; Jeong et al., 2019). In general, both Firmicutes and Bacteroidales are relevant with energy metabolism homeostasis (Ley et al., 2005). Take, for example, increased abundance of Firmicutes is believed to be beneficial for

obese individuals to harvest energy from food, subsequently absorb calories, and eventually gain body weight (Turnbaugh et al., 2006). Since KSLP alleviated the enrichment of Firmicutes, it is reasonable that KSLP could reduce the weight gain in HFD mice without interfering with their food intake.

At the family level, KSLP reversed the appearance of increased abundances of Ruminococcaceae and Desulfovibrionaceae in HFD mice. Ruminococcaceae, as a member of phylum Firmicutes, has been reported to be negatively correlated with hepatic encephalopathy (Bajaj et al., 2012), alcoholic cirrhosis (Bajaj et al., 2014), non-alcoholic fatty liver disease (Schnabl and Brenner, 2014), and intestinal leaking (Leclercq et al., 2014). In obesity-prone mice, the enriched Ruminococcaceae was revealed to be responsible for promoting fat synthesis (Duca et al., 2014). Our results showed that KSLP could reduce the abundance of Ruminococcaceae; therefore, it might be beneficial for reducing fat synthesis initiated by HFD. Desulfovibrionaceae, as a member of the Proteobacteria phylum, is known to be related to the production of endotoxin (Perez-Matute et al., 2015) and inflammation (Xiao et al., 2014). Our results of enriched Desulfovibrionaceae in HFD mice could be considered as a sign for the presence of gut inflammation, and KSLP might help in alleviating the occurrence of inflammation.

Other changes that happened in HFD mice at the family level were decreased abundance of Muribaculaceae and Prevotellaceae, which accounted for the decreased abundance of Bacteroidetes phylum. Interestingly, we noticed that although KSLP could effectively increase the overall abundance of Bacteroidetes phylum, it did not affect the abundance of Muribaculaceae and Prevotellaceae. Alternatively, it did increase two other family members of Bacteroidetes phylum: Bacteroidaceae and Rikenellaceae. Our result suggested that different to its effects on phyla Firmicutes and Proteobacteria, KSLP regulated the functional rather than compositional changes for family bacteria under the category of Bacteroidetes phylum.

At the genus level, Pearson correlations analysis between obesity-related parameters and the 27 changed genera responsible to HFD treatment verified nine obesity-associated genera, among which the abundance of *Intestinimonas*, *Oscillibacter*, Christensenellaceae_R-7_group, and *Aliihoeflea* could be reversed by KSLP. Notably, the roles of *Intestinimonas* and *Oscillibacter* in obesity have been reported. For instance, *Intestinimonas* is generally considered to be a beneficial genus with butyrate-producing capacity (Yang et al., 2019); nevertheless, the enrichment of which also presents in HFD rats (Lin et al., 2019). As for *Oscillibacter*, it is revealed to be positively correlated with the occurrence of obesity (Chang et al., 2015; Chang et al., 2017) probably through regulating fat synthesis (Duca et al., 2014). Until now, few studies revealed the roles of Christensenellaceae_R-7_group and *Aliihoeflea* in obesity. It seems that carnivorous individuals harbor abundance of Christensenellaceae_R-7_group, assigned to the Firmicutes phylum (Huang, 2018). Besides, destined as pathological Proteobacteria, the appearance of *Aliihoeflea* could be recognized as a sign reflecting gut disorder during the course of dextran sodium sulfate (DSS)-triggered colitis (Zhang et al., 2019a). In view of the above evidences, we believe that *Intestinimonas*, *Oscillibacter*, Christensenellaceae_R-7_group, and *Aliihoeflea* play crucial roles regarding the prevention effect of KSLP against HFD-induced obesity.

Gut microbiota affects host metabolism by ways of transformation, absorption, and metabolism of exogenous substances (Li et al., 2019). It is rational that the alternation of metabolites reflects the changes of gut microbiota profiles. In the current study, we performed Pearson correlation analysis to reveal the co-relation between the four identified obesity-related genera and the metabolites responding to KSLP. We found that there existed very similar metabolite relationship patterns of *Intestinimonas*, *Oscillibacter*, and Christensenellaceae_R-7_group. As summarized in **Figure 9**, those metabolites could be functionally categorized into amino acid, dipeptide, lipid metabolism, and others. Amino acids are believed to play critical roles in maintaining host gut homeostasis since their disorder happens in germ-free mice (Whitt and Demoss, 1975). The compositional changes of obesity-related gut microbiota may affect the production of certain amino acids as by-products of detrimental bacteria (Bested et al., 2013). Interestingly, it was recently revealed that xanthurenic acid and other products of tryptophan metabolism are related to the production and releasing of insulin (Oxenkrug, 2013). In our study, HFD mice had significantly increased level of xanthurenate in the gut. This, together with the fact that HFD mice appeared with poor glucose tolerance capacity, indicated that there might exist a correlation of HFD/gut microbiota/xanthurenate/glucose tolerance pipeline. Since the application of KSLP not only decreased the gut xanthurenate level, but also improved glucose tolerance capacity and reduced blood glucose level in HFD mice, a stimulated insulin production could be expected. Notably, there was no strong direct link between *Oscillibacter* itself and glucose (**Figure 7**); it is likely that a panel of microbiota, i.e., *Oscillibacter*, by working together with *Intestinimonas* or Christensenellaceae_R-7_group, functionally affects glucose metabolism. We also noticed that the content of fecal lanosterol was negatively related to the abundance of *Intestinimonas*, *Oscillibacter* and Christensenellaceae_R-7_group. Lanosterol is a precursor of cholesterol synthesis (Zhao et al., 2015), the reduced production of which in feces might be indicated for an increased cholesterol level in the serum. In HFD mice, supplementation with KSLP resulted in higher lanosterol than in feces of HFD mice alone; therefore, KSLP might impact sterol absorption in the intestine. Although not well defined, there are reports that highlight the regulatory roles of peptides and fatty acids in the scenario of obesity and its related metabolic disease (Zhao, 2011; Miyamoto et al., 2019). Taken together, our data suggest that KSLP may influence the abundance of *Intestinimonas*, *Oscillibacter*, and Christensenellaceae_R-7_group, which affects the fecal metabolites and whole-body physiology in HFD mice.

## CONCLUSIONS

In conclusion, our study provides sufficient evidences showing that KSLP is a promising TCM with prevention effects against HFD-induced obesity and is applicable for its consequent occurrence of metabolic diseases. The mode of action of KSLP is most likely *via*

modulating the gut microbiota. As a result, the obesity-related gut dysbiosis including the decreased diversity, increased F/B ratio, and enriched abundance of Proteobacteria could be corrected. *Intestinimonas*, *Oscillibacter*, and Christensenellaceae_R-7_group might be responsible for the regulatory effect of KSLP on obesity-related metabolic disorders, which involve amino acid, peptide, and lipid metabolism. In addition to the verification of the inner links among obesity, gut microbiota, and metabolic disorders, further investigations are required to verify the key targets of intervention as well as bioactive compounds in KSLP.

## DATA AVAILABILITY STATEMENT

The datasets generated for this study can be found in the PRJNA565488.

## AUTHOR CONTRIBUTIONS

JQ, HC, and MY conceived and designed the study. SG, MXW, TY, and MYW performed most of the experiments. SG, YL, LM, and YY analyzed and interpreted the data. LL provided the technical support. SG, JQ, and YW drafted the article. XZ contributed the constructional suggestions for revision. All authors made the final approval of the version to be submitted.

## FUNDING

This work was supported by grants from the National Key Scientific and Technological Project of China (2019ZX09201005) and the Science and Technology Department of Zhejiang Province of China (2018C02048).

## SUPPLEMENTARY MATERIAL

The Supplementary Material for this article can be found online at: https://www.frontiersin.org/articles/10.3389/fphar.2020.00297/full#supplementary-material

**SUPPLEMENTARY TABLE 1 |** The relative abundance of the top 10 families.

**SUPPLEMENTARY TABLE 2 |** Pearson correlation analysis between obesity-related parameters and genera.

**SUPPLEMENTARY TABLE 3 |** The effects of HFD and KSLP supplement on Mice feces metabolites.

**SUPPLEMENTARY TABLE 4 |** The metabolites in response to both the factors of HFD and KSLP.

**SUPPLEMENTARY TABLE 5 |** The metabolites in response to both the factors of HFD and KSLP, in which can be reversed by KSLP.

**SUPPLEMENTARY TABLE 6 |** The correlation coefficient between key genera and reversed metabolites.

## REFERENCES

Alard, J., Lehrter, V., Rhimi, M., Mangin, I., Peucelle, V., Abraham, A. L., et al. (2016). Beneficial metabolic effects of selected probiotics on diet-induced obesity and insulin resistance in mice are associated with improvement of dysbiotic gut microbiota. *Environ. Microbiol.* 18 (5), 1484–1497. doi: 10.1111/1462-2920.13181

Anhe, F. F., Roy, D., Pilon, G., Dudonne, S., Matamoros, S., Varin, T. V., et al. (2015). A polyphenol-rich cranberry extract protects from diet-induced obesity, insulin resistance and intestinal inflammation in association with increased Akkermansia spp. population in the gut microbiota of mice. *Gut* 64 (6), 872–883. doi: 10.1136/gutjnl-2014-307142

Anhe, F. F., Nachbar, R. T., Varin, T. V., Trottier, J., Dudonne, S., Le Barz, M., et al. (2019). Treatment with camu camu (Myrciaria dubia) prevents obesity by altering the gut microbiota and increasing energy expenditure in diet-induced obese mice. *Gut* 68, 453–464. doi: 10.1136/gutjnl-2017-315565

Bajaj, J. S., Hylemon, P. B., Ridlon, J. M., Heuman, D. M., Daita, K., White, M. B., et al. (2012). Colonic mucosal microbiome differs from stool microbiome in cirrhosis and hepatic encephalopathy and is linked to cognition and inflammation. *Am. J. Physiol. Gastrointest. Liver Physiol.* 303 (6), G675–G685. doi: 10.1152/ajpgi.00152.2012

Bajaj, J. S., Heuman, D. M., Hylemon, P. B., Sanyal, A. J., White, M. B., Monteith, P., et al. (2014). Altered profile of human gut microbiome is associated with cirrhosis and its complications. *J. Hepatol.* 60 (5), 940–947. doi: 10.1016/j.jhep.2013.12.019

Bested, A. C., Logan, A. C., and Selhub, E. M. (2013). Intestinal microbiota, probiotics and mental health: from Metchnikoff to modern advances: part III - convergence toward clinical trials. *Gut. Pathog* 5 (1), 4. doi: 10.1186/1757-4749-5-4

Caesar, R., Fak, F., and Backhed, F. (2010). Effects of gut microbiota on obesity and atherosclerosis via modulation of inflammation and lipid metabolism. *J. Intern Med.* 268 (4), 320–328. doi: 10.1111/j.1365-2796.2010.02270.x

Cani, P. D., Possemiers, S., Van de Wiele, T., Guiot, Y., Everard, A., Rottier, O., et al. (2009). Changes in gut microbiota control inflammation in obese mice through a mechanism involving GLP-2-driven improvement of gut permeability. *Gut* 58 (8), 1091–1103. doi: 10.1136/gut.2008.165886

Chang, C. J., Lin, C. S., Lu, C. C., Martel, J., Ko, Y. F., Ojcius, D. M., et al. (2015). Ganoderma lucidum reduces obesity in mice by modulating the composition of the gut microbiota. *Nat. Commun.* 6, 7489. doi: 10.1038/ncomms8489

Chang, C. J., Lin, C. S., Lu, C. C., Martel, J., Ko, Y. F., Ojcius, D. M., et al. (2017). Corrigendum: Ganoderma lucidum reduces obesity in mice by modulating the composition of the gut microbiota. *Nat. Commun.* 8, 16130. doi: 10.1038/ncomms16130

Cheng, W., Lu, J., Lin, W., Wei, X., Li, H., Zhao, X., et al. (2018). Effects of a galacto-oligosaccharide-rich diet on fecal microbiota and metabolite profiles in mice. *Food Funct.* 9 (3), 1612–1620. doi: 10.1039/c7fo01720k

Chi, L., Bian, X., Gao, B., Tu, P., Lai, Y., Ru, H., et al. (2018). Effects of the Artificial Sweetener Neotame on the Gut Microbiome and Fecal Metabolites in Mice. *Molecules* 23 (2), 367. doi: 10.3390/molecules23020367

Dehaven, C. D., Evans, A. M., Dai, H., and Lawton, K. A. (2010). Organization of GC/MS and LC/MS metabolomics data into chemical libraries. *J. Cheminform.* 2 (1), 9. doi: 10.1186/1758-2946-2-9

Devaraj, S., Hemarajata, P., and Versalovic, J. (2013). The human gut microbiome and body metabolism: implications for obesity and diabetes. *Clin. Chem.* 59 (4), 617–628. doi: 10.1373/clinchem.2012.187617

Duca, F. A., Sakar, Y., Lepage, P., Devime, F., Langelier, B., Dore, J., et al. (2014). Replication of obesity and associated signaling pathways through transfer of microbiota from obese-prone rats. *Diabetes* 63 (5), 1624–1636. doi: 10.2337/db13-1526

Edgar, R. C., Haas, B. J., Clemente, J. C., Quince, C., and Knight, R. (2011). UCHIME improves sensitivity and speed of chimera detection. *Bioinformatics* 27 (16), 2194–2200. doi: 10.1093/bioinformatics/btr381

Edgar, R. C. (2010). Search and clustering orders of magnitude faster than BLAST. *Bioinformatics* 26 (19), 2460–2461. doi: 10.1093/bioinformatics/btq461

Edgar, R. C. (2013). UPARSE: highly accurate OTU sequences from microbial amplicon reads. *Nat. Methods* 10 (10), 996–998. doi: 10.1038/nmeth.2604

Evans, A. M., DeHaven, C. D., Barrett, T., Mitchell, M., and Milgram, E. (2009). Integrated, nontargeted ultrahigh performance liquid chromatography/electrospray ionization tandem mass spectrometry platform for the identification and relative quantification of the small-molecule complement of biological systems. *Anal. Chem.* 81 (16), 6656–6667. doi: 10.1021/ac901536h

Everard, A., Belzer, C., Geurts, L., Ouwerkerk, J. P., Druart, C., Bindels, L. B., et al. (2013). Cross-talk between Akkermansia muciniphila and intestinal epithelium controls diet-induced obesity. *Proc. Natl. Acad. Sci. U. S. A* 110 (22), 9066–9071. doi: 10.1073/pnas.1219451110

Gong, S., Ye, T., Wang, M., Hong, Z., Liu, L., Chen, H., et al. (2020). Profiling the mid-adult cecal microbiota associated with host healthy by using herbal formula Kang Shuai Lao Pian treated mid-adult mice. *Chin. J. Nat. Med.* 18 (2), 90–102. doi: 10.3724/SP.J.1009.2019.000000

Haas, B. J., Gevers, D., Earl, A. M., Feldgarden, M., Ward, D. V., Giannoukos, G., et al. (2011). Chimeric 16S rRNA sequence formation and detection in Sanger and 454-pyrosequenced PCR amplicons. *Genome Res.* 21 (3), 494–504. doi: 10.1101/gr.112730.110

Hasani-Ranjbar, S., Nayebi, N., Larijani, B., and Abdollahi, M. (2009). A systematic review of the efficacy and safety of herbal medicines used in the treatment of obesity. *World J. Gastroenterol.* 15 (25), 3073–3085. doi: 10.3748/wjg.15.3073

Hoyt, C. L., Burnette, J. L., and Auster-Gussman, L. (2014). "Obesity is a disease": examining the self-regulatory impact of this public-health message. *Psychol. Sci.* 25 (4), 997–1002. doi: 10.1177/0956797613516981

Huang, D. (2018). *Relationship between gut microbiota structure and fecal fatty acids in different diets* (Haerbin, China: Master, Northeast Agricultural university).

James, W. P. (2008). The epidemiology of obesity: the size of the problem. *J. Intern Med.* 263 (4), 336–352. doi: 10.1111/j.1365-2796.2008.01922.x

Jeong, M. Y., Jang, H. M., and Kim, D. H. (2019). High-fat diet causes psychiatric disorders in mice by increasing Proteobacteria population. *Neurosci. Lett.* 698, 51–57. doi: 10.1016/j.neulet.2019.01.006

Kelly, T., Yang, W., Chen, C. S., Reynolds, K., and He, J. (2008). Global burden of obesity in 2005 and projections to 2030. *Int. J. Obes (Lond)* 32 (9), 1431–1437. doi: 10.1038/ijo.2008.102

Kopelman, P. G. (2000). Obesity as a medical problem. *Nature* 404 (6778), 635–643. doi: 10.1038/35007508

Le Chatelier, E., Nielsen, T., Qin, J., Prifti, E., Hildebrand, F., Falony, G., et al. (2013). Richness of human gut microbiome correlates with metabolic markers. *Nature* 500 (7464), 541–546. doi: 10.1038/nature12506

Leclercq, S., Matamoros, S., Cani, P. D., Neyrinck, A. M., Jamar, F., Starkel, P., et al. (2014). Intestinal permeability, gut-bacterial dysbiosis, and behavioral markers of alcohol-dependence severity. *Proc. Natl. Acad. Sci. U. S. A.* 111 (42), E4485–E4493. doi: 10.1073/pnas.1415174111

Ley, R. E., Backhed, F., Turnbaugh, P., Lozupone, C. A., Knight, R. D., and Gordon, J. I. (2005). Obesity alters gut microbial ecology. *Proc. Natl. Acad. Sci. U. S. A.* 102 (31), 11070–11075. doi: 10.1073/pnas.0504978102

Li, Q., Liu, F., Liu, J., Liao, S., and Zou, Y. (2019). Mulberry Leaf Polyphenols and Fiber Induce Synergistic Antiobesity and Display a Modulation Effect on Gut Microbiota and Metabolites. *Nutrients* 11 (5), 1017. doi: 10.3390/nu11051017

Lin, H., An, Y., Tang, H., and Wang, Y. (2019). Alterations of Bile Acids and Gut Microbiota in Obesity Induced by High Fat Diet in Rat Model. *J. Agric. Food Chem.* 67 (13), 3624–3632. doi: 10.1021/acs.jafc.9b00249

Long, T., Hicks, M., Yu, H. C., Biggs, W. H., Kirkness, E. F., Menni, C., et al. (2017). Whole-genome sequencing identifies common-to-rare variants associated with human blood metabolites. *Nat. Genet.* 49 (4), 568–578. doi: 10.1038/ng.3809

Mason, T. J., and Matthews, M. (2012). Aquatic environment, housing, and management in the eighth edition of the Guide for the Care and Use of Laboratory Animals: additional considerations and recommendations. *J. Am. Assoc. Lab. Anim. Sci.* 51 (3), 329–332. doi: 10.1186/1742-9994-9-9

Miyamoto, J., Igarashi, M., Watanabe, K., Karaki, S. I., Mukouyama, H., Kishino, S., et al. (2019). Gut microbiota confers host resistance to obesity by metabolizing dietary polyunsaturated fatty acids. *Nat. Commun.* 10 (1), 4007. doi: 10.1038/s41467-019-11978-0

Neis, E. P., Dejong, C. H., and Rensen, S. S. (2015). The role of microbial amino acid metabolism in host metabolism. *Nutrients* 7 (4), 2930–2946. doi: 10.3390/nu7042930

Oxenkrug, G. (2013). Insulin resistance and dysregulation of tryptophan-kynurenine and kynurenine-nicotinamide adenine dinucleotide metabolic pathways. *Mol. Neurobiol.* 48 (2), 294–301. doi: 10.1007/s12035-013-8497-4

Perez-Matute, P., Perez-Martinez, L., Aguilera-Lizarraga, J., Blanco, J. R., and Oteo, J. A. (2015). Maraviroc modifies gut microbiota composition in a mouse model of obesity: a plausible therapeutic option to prevent metabolic disorders in HIV-infected patients. *Rev. Esp. Quimioter.* 28 (4), 200–206.

Quast, C., Pruesse, E., Yilmaz, P., Gerken, J., Schweer, T., Yarza, P., et al. (2013). The SILVA ribosomal RNA gene database project: improved data processing and web-based tools. *Nucleic Acids Res.* 41 (Database issue), D590–D596. doi: 10.1093/nar/gks1219

Ridaura, V. K., Faith, J. J., Rey, F. E., Jiye, C., Duncan, A. E., Kau, A. L., et al. (2013). Gut microbiota from twins discordant for obesity modulate metabolism in mice. *Science* 341 (6150), 1079–U1049. doi: 10.1126/science.1241214

Schnabl, B., and Brenner, D. A. (2014). Interactions between the intestinal microbiome and liver diseases. *Gastroenterology* 146 (6), 1513–1524. doi: 10.1053/j.gastro.2014.01.020

Shin, N. R., Lee, J. C., Lee, H. Y., Kim, M. S., Whon, T. W., Lee, M. S., et al. (2014). An increase in the Akkermansia spp. population induced by metformin treatment improves glucose homeostasis in diet-induced obese mice. *Gut* 63 (5), 727–735. doi: 10.1136/gutjnl-2012-303839

Tao, T., P. (2009). Effects of KSLP on learning and memory and free radical metabolism in aging rats. *J. Zhejiang Univ. Tradit. Chin. Med.* 33 (6), 751–753. doi: 10.3969/j.issn.1005-5509.2009.06.007

Tomasello, G., Tralongo, P., Damiani, P., Sinagra, E., Di Trapani, B., Zeenny, M. N., et al. (2014). Dismicrobism in inflammatory bowel disease and colorectal cancer: changes in response of colocytes. *World J. Gastroenterol.* 20 (48), 18121–18130. doi: 10.3748/wjg.v20.i48.18121

Turnbaugh, P. J., Ley, R. E., Mahowald, M. A., Magrini, V., Mardis, E. R., and Gordon, J. I. (2006). An obesity-associated gut microbiome with increased capacity for energy harvest. *Nature* 444 (7122), 1027–1031. doi: 10.1038/nature05414

Turnbaugh, P. J., Hamady, M., Yatsunenko, T., Cantarel, B. L., Duncan, A., Ley, R. E., et al. (2009). A core gut microbiome in obese and lean twins. *Nature* 457 (7228), 480–484. doi: 10.1038/nature07540

Whitt, D. D., and Demoss, R. D. (1975). Effect of microflora on the free amino acid distribution in various regions of the mouse gastrointestinal tract. *Appl. Microbiol.* 30 (4), 609–615. doi: 10.1128/AEM.30.4.609-615.1975

Xiao, S., Fei, N., Pang, X., Shen, J., Wang, L., Zhang, B., et al. (2014). A gut microbiota-targeted dietary intervention for amelioration of chronic inflammation underlying metabolic syndrome. *FEMS Microbiol. Ecol.* 87 (2), 357–367. doi: 10.1111/1574-6941.12228

Yang, F., Li, J., Pang, G., Ren, F., and Fang, B. (2019). Effects of Diethyl Phosphate, a Non-Specific Metabolite of Organophosphorus Pesticides, on Serum Lipid, Hormones, Inflammation, and Gut Microbiota. *Molecules* 24 (10), 2003. doi: 10.3390/molecules24102003

Yokota, A., Fukiya, S., Islam, K. B., Ooka, T., Ogura, Y., Hayashi, T., et al. (2012). Is bile acid a determinant of the gut microbiota on a high-fat diet? *Gut. Microbes* 3 (5), 455–459. doi: 10.4161/gmic.21216

Yu, J., Guo, J., Tao, W., Liu, P., Shang, E., Zhu, Z., et al. (2018). Gancao-Gansui combination impacts gut microbiota diversity and related metabolic functions. *J. Ethnopharmacol.* 214, 71–82. doi: 10.1016/j.jep.2017.11.031

Zhang, F., Li, Y., Wang, X., Wang, S., and Bi, D. (2019a). The Impact of Lactobacillus plantarum on the Gut Microbiota of Mice with DSS-Induced Colitis. *BioMed. Res. Int.* 2019, 3921315. doi: 10.1155/2019/3921315

Zhang, Z., Xu, H., Zhao, H., Geng, Y., Ren, Y., Guo, L., et al. (2019b). Edgeworthia gardneri (Wall.) Meisn. water extract improves diabetes and modulates gut microbiota. *J. Ethnopharmacol.* 239, 111854. doi: 10.1016/j.jep.2019.111854

Zhao, L., Chen, X. J., Zhu, J., Xi, Y. B., Yang, X., Hu, L. D., et al. (2015). Lanosterol reverses protein aggregation in cataracts. *Nature* 523 (7562), 607–611. doi: 10.1038/nature14650

Zhao, M. (2011). Research status and trends of food-borne bioactive peptides structural characteristics and physiological activities. *Chin. J. Food Sci.* 11 (9), 69–81. doi: 10.3969/j.issn.1009-7848.2011.09.008

Zhou, X. (2012). *Traditional Chinese medicine mixture for anti-aging and preparation method* (Jinan: China patent application).

Zierer, J., Jackson, M. A., Kastenmüller, G., Mangino, M., Long, T., Telenti, A., et al. (2018). The fecal metabolome as a functional readout of the gut microbiome. *Nat. Genet.* 50 (6), 790–795. doi: 10.1038/s41588-018-0135-7

**Conflict of Interest:** Author LL was employed by company Chiatai Qingchunbao Pharmaceutical Co. Ltd.

The remaining authors declare that the research was conducted in the absence of any commercial or financial relationships that could be construed as a potential conflict of interest.

frontiers in Pharmacology

ORIGINAL RESEARCH
published: 03 April 2020
doi: 10.3389/fphar.2020.00423

# Buzhongyiqi Decoction Protects Against Loperamide-Induced Constipation by Regulating the Arachidonic Acid Pathway in Rats

*Wan-Jun Ju[1,2], Ze-kuo Zhao[1], Shao-Li Chen[1], Dan-dan Zhou[3], Wen-Ning Yang[4], Xiao-Ping Wen[1]* and Guang-Li Du[1]**

[1] Department of Formulaology, School of Basic Medical Sciences, Shanghai University of Traditional Chinese Medicine, Shanghai, China, [2] Department of Endocrinology, Shanghai Pudong New Area Hospital of Traditional Chinese Medicine, Shanghai, China, [3] R & D Department, GenChim Testing Co., Ltd, Shanghai, China, [4] School of Chinese Materia Medica, Beijing University of Chinese Medicine, Beijing, China

OPEN ACCESS

**Edited by:**
Aiping Lu,
Hong Kong Baptist University,
Hong Kong

**Reviewed by:**
Yong Wang,
Beijing University of Chinese Medicine, China
Wentzel Christoffel Gelderblom,
Cape Peninsula University of Technology, South Africa

***Correspondence:**
Xiao-Ping Wen
wxpglj@yahoo.com.cn
Guang-Li Du
duguangli2002@126.com

**Specialty section:**
This article was submitted to Ethnopharmacology, a section of the journal Frontiers in Pharmacology

**Received:** 04 September 2019
**Accepted:** 19 March 2020
**Published:** 03 April 2020

**Citation:**
Ju W-J, Zhao Z-k, Chen S-L, Zhou D-d, Yang W-N, Wen X-P and Du G-L (2020) Buzhongyiqi Decoction Protects Against Loperamide-Induced Constipation by Regulating the Arachidonic Acid Pathway in Rats. Front. Pharmacol. 11:423. doi: 10.3389/fphar.2020.00423

Constipation is a common gastrointestinal disorder without effective treatment approach. Buzhongyiqi decoction (BZYQD) is a classical formula that has been commonly used for gastrointestinal disorders for nearly 1,000 years. In this study, we aimed to investigate the protective effect of BZYQD against loperamide-induced constipation and its potential mechanism. Rats with loperamide-induced constipation were orally administered BZYQD. BZYQD treatment obviously increased the small intestinal transit rate and alleviated colon tissue pathological damage. Subsequently, serum metabolomics study was performed to identify the metabolites affected by BZYQD. Metabolomics identified that the levels of 17 serum metabolites, including prostaglandin $E_2$ ($PGE_2$), arachidonic acid (AA), and inositol, were significantly changed in BZYQD-treated group compared with those in the loperamide-induced group. Pathway analysis revealed that those metabolites were mainly associated with arachidonic acid metabolism, biosynthesis of unsaturated fatty acids, ascorbate and aldarate metabolism, inositol phosphate metabolism. Additionally, BZYQD treatment down-regulated the cyclooxygenase-2 expression and decrease production of the proinflammatory mediator $PGE_2$. Further study revealed that BZYQD administration decreased serum levels of the inflammatory factors IL-1β and TNF-α, inhibited phosphorylation of the nuclear transcription factor NF-κB, and down-regulated expression of the inflammatory factors IL-1β and IL-6 in the constipated rat colon. Moreover, BZYQD treatment also increased serum levels of inositol, motilin and gastrin, and promoted gastrointestinal motility. In conclusion, the present study suggested that BZYQD exerted a protective effect against loperamide-induced constipation, which may be associated with its role in regulation of multiple metabolic pathways.

**Keywords: constipation, Buzhongyiqi decoction, Metabolomics, Inflammation, rat**

## INTRODUCTION

Constipation is a clinically common gastrointestinal dysfunction with a prevalence of 5–20% worldwide (Suares and Ford, 2011). According to the Rome IV criteria, a typical symptom of chronic constipation is difficult, infrequent, or inadequate bowel movement (Mearin et al., 2016). Individuals with bowel movement every 3–4 days are at a higher risk of colon cancer, hemorrhoids, and other gastrointestinal diseases (Wu et al., 2010). Laxatives are widely prescribed as the main means to assist patients in passing stools (Li et al., 2019). However, these treatments have severe side effects. Therefore, development of more efficient and safe therapeutic/preventive agents and methods is still needed.

Traditional Chinese medicine (TCM) formulas have been widely used for the prevention and treatment of digestive diseases for thousands of years. Buzhongyiqi decoction (BZYQD) is a well-known TCM formula first described in Pi Wei Lun, a treatise on digestive system diseases written by the famous Chinese physician Li Gao (1180–1251 A.D. of the Chinese Yuan Dynasty) (He et al., 2017). BZYQD is comprised of eight herbs (**Table 1**) (Ji, 2006) and has been identified as an effective drug for improving the digestive system function, quality of life, and nutritional status in elderly patients with chronic obstructive pulmonary disease (Gou et al., 2016). Moreover, BZYQD is also a representative prescription that is increasingly applied to treat gastrointestinal dysfunction, such as constipation, in China (Wang et al., 1991; Sun Feng-Wei, 2016; Zhang, 2016; Dan, 2018). However, its mechanism of action has not yet been fully investigated.

Metabolomics represents a powerful discipline concerned with the comprehensive analysis of small molecules to discover biomarkers in biological systems (Schrimpe-Rutledge et al., 2016; Zhang et al., 2019). This method provides holistic insights into changes in the metabolic pathways during disease or drug treatment (Wu et al., 2017; Zheng et al., 2019). Therefore, metabolomics study is in perfect accordance with the holistic approach of TCM, and can provide clues to mechanism of action of TCM (Wu et al., 2017; Zheng et al., 2019). In the current study, the effect of BZYQD on loperamide-induced constipation in a rat model was investigated. Additionally, the underlying molecular mechanism of BZYQD in constipation was explored by serum metabolomics. Our results provide novel insights into the potential role of the herbal medicine BZYQD in treating gastrointestinal dysfunction diseases.

**TABLE 1** | Herbal constituents of BZYQD.

| Pharmaceutical name | Chinese name | Part used | Amount (g) |
|---|---|---|---|
| *Astragalus mongholicus* Bunge | Huangqi | Root | 18 |
| *Glycyrrhiza uralensis* Fisch. ex DC | Gancao | Root and rhizome | 9 |
| *Codonopsis pilosula* (Franch.) Nannf. | Dangshen | Root | 9 |
| *Angelica sinensis* (Oliv.) Diels | Danggui | Root | 3 |
| *Citrus* × aurantium L. | Chenpi | Pericarp | 6 |
| *Actaea heracleifolia* (Kom.) J. Compton | Shenma | Rhizome | 6 |
| *Bupleurum chinense* DC. | Chaihu | Root | 6 |
| *Atractylodes macrocephala* Koidz. | Baizhu | Rhizome | 9 |

## MATERIALS AND METHODS

### Chemical Compounds and Reagents

Chromatography-grade acetonitrile was purchased from Merck (Darmstadt, Germany). Water was purified using a Milli-Q water system (Millipore, Bedford, MA, USA). Chromatography-grade acetic acid, formic acid, and methanol were provided by Tedia Company (Fairfield, OH, USA). All the crude drugs including Radix Astragali (Huangqi in China, HQ), Radix Glycyrrhizae (Gancao in China, GC), Rhizoma Atractylodis Macrocephalae (Baizhu in China, BZ), Radix Codonopsis (Dangshen in China, DS), Radix Angelicae Sinensis (Danggui in China, DG), Pericarpium Citri Reticulatae (Chengpi in China, CP), Radix Bupleuri (Caihu in China, CH), and Rhizoma Cimicifugae (Shengma in China, SM) were purchased from Shanghai Kangqiao Chinese Medicine Tablet Co., Ltd (Shanghai, China) and authenticated by Gen Chim Testing Co., Ltd (Shanghai, China). Mosapride was purchased from Sigma-Aldrich (St. Louis, MO, USA).

### Preparation and Analysis of BZYQD

BZYQD was prepared according to our previously reported method. A mixture of HQ (18 g), DS (9 g), BZ (9 g), DG (3 g), GC (9 g), CP (6 g), SM (6 g), and CF (6 g) was added to 600 ml water and extracted at 100°C for 1 h. The extracted solution was filtered and spray-dried to obtain dry extract powder. The final ratio of BZYQD extract powder to raw herb was 37.80%. The total ion chromatogram of BZYQD extract that measured by LC-MS is shown as **Figure 1**.

### Animals and Experimental Design

Male 8-week-old Sprague–Dawley (SD) rats were provided by the Laboratory Animal Center of Shanghai University of Traditional Chinese Medicine. The animals were housed and acclimatized for one week prior to the experiment in a room at 20–22°C and 60–70% humidity under a 12 h-light and 12 h-dark cycle. All animal experiments were carried out in full compliance with the Guidance of Humane Care and Use of Laboratory and approved by the Committee on the Use of Live Animals for Teaching and Research in the Shanghai University of Traditional Chinese Medicine. Rats were randomly divided into four groups: control (normal control), loperamide, loperamide+BZYQD (1.73 g/kg of BZYQD extract powder), and loperamide +mosapride (positive group, 1.6 mg/kg), with 8 rats per group. Rats of the loperamide, loperamide+BZYQD, and loperamide +mosapride groups were treated with loperamide (4 mg/kg, b. w.), by subcutaneous injection twice per day at 09:00 and at 18:00 h for 1 week, and all the corresponding drugs was orally administered to the rats once daily from the third day. Rats in the control group and loperamide group orally received the normal saline. The scheme of the animal experiment is

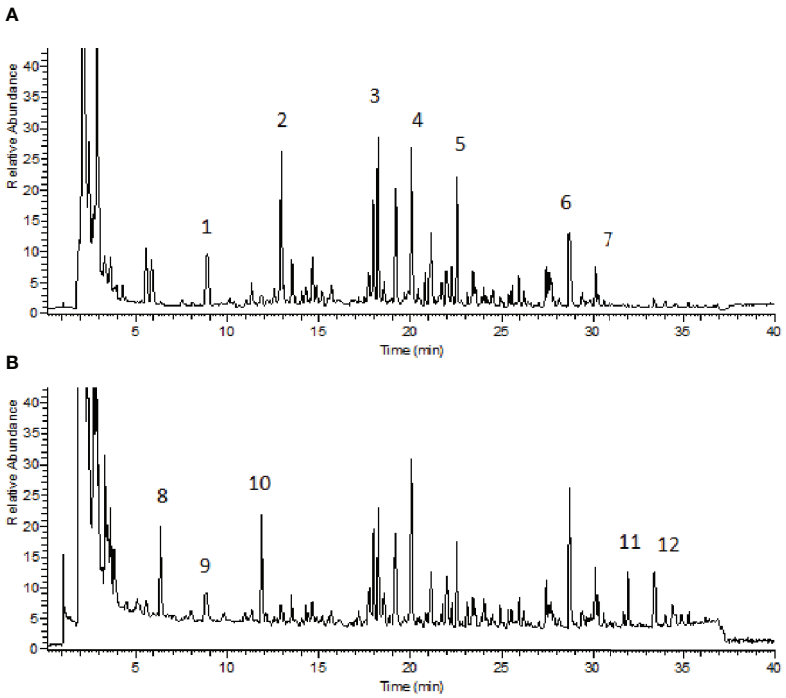


**FIGURE 1 |** Total ion chromatogram of BZYQD extract in negative-ion mode **(A)** and positive-ion mode **(B)**. 1: Piscidic acid; 2: Ferulic acid; 3: Liquiritin; 4: Hesperidin; 5: 2-feruloylpiscidic acid; 6: Glycyrrhizic Acid; 7: Saikosaponin D; 8: Synephrine; 9: Codonopyrrolidium B; 10: Tryptophan; 11: Nobiletin; 12: 3, 5, 6, 7, 8, 3', 4'-heptamethoxyflavone.

summarized in **Figure 2**. A 100% survival rate was recorded at the end point of the experiment.

## Measurement of Gastro-Intestinal Propulsion (GIP)

All the groups were exposed to fasting conditions and drank only water on the seventh day. GIP was measured through prepared Chinese ink. Thirty minutes later, all animals were fed with the prepared Chinese ink (10% charcoal in 5% gum Arabic) and were anesthetized. The small intestine was immediately dissected and put on a clean surface. The travelling distance of the charcoal meal from the pylorus was measured. The gastrointestinal propulsion was calculated based on the following formula: GIP = (Distance travelled by charcoal (cm)/total intestinal length (cm) ×100%. Then, the colon tissues were collected for further studies.

## Hematoxylin-Eosin Staining

Small intestine and colon tissues were fixed in 10% formaldehyde, dehydrated, embedded in paraffin, cut into 5-μm-thick sections, and stained with hematoxylin and eosin. Pathological changes were observed using the OlympusBX70 research microscope.

## Serum Metabolomics Study

### Sample Preparation

An aliquot of 100 μl acetonitrile containing the internal standards (IS, 10 μg/ml 2-chloro-L-phenylalanine in positive and negative modes) was added to 20 μl of serum samples. After vortex-mixing for 3 min, the mixture was centrifuged for 10 min at 16,000 rpm at 4°C, and 5 μl of the supernatant was injected for UPLC-MS/MS analysis. An equal aliquot from each serum sample was combined and mixed to prepare the quality control (QC) samples. The QC samples were processed by the same method as the other serum samples and analyzed randomly through the analytical batch to ensure the stability of the analytical process.

### Analysis Conditions

Sample analysis was performed using a UPLC-LTQ-Orbitrap system (Thermo Fisher Scientific, San Jose, CA, USA) and the samples were separated using a Waters ACQUITY UPLC BEH C18 column (2.1×100 mm, 1.7 μm) (Waters, Co., Milford, MA, USA). The mobile phases contained water with 0.1% formic acid (A) and acetonitrile with 0.1% formic acid (B). The elution steps were as follows: 10% B from 0.1–2 min, 10–40% B from 2.1–7 min, 40–80% B from 7.1–11 min, 80–90% B from 11.1–15 min, and 90% B for 0.5 min. At 15.5 min, B was adjusted to 10% and the column equilibrated for 4.5 min. The mass spectrometer parameters were as follows: ion spray voltage, 3.8 kV(+) and 3.2 kV(−); capillary and heater temperature, both 350°C; sheath and auxiliary gas flow rate, 45 and 15 psi, respectively; and S-Lens RF level, 60% (Li et al., 2017; Wu et al., 2017).

### Data Processing

Data preprocessing, identification of potential biomarkers, and pathway analysis were performed as reported previously (Huang

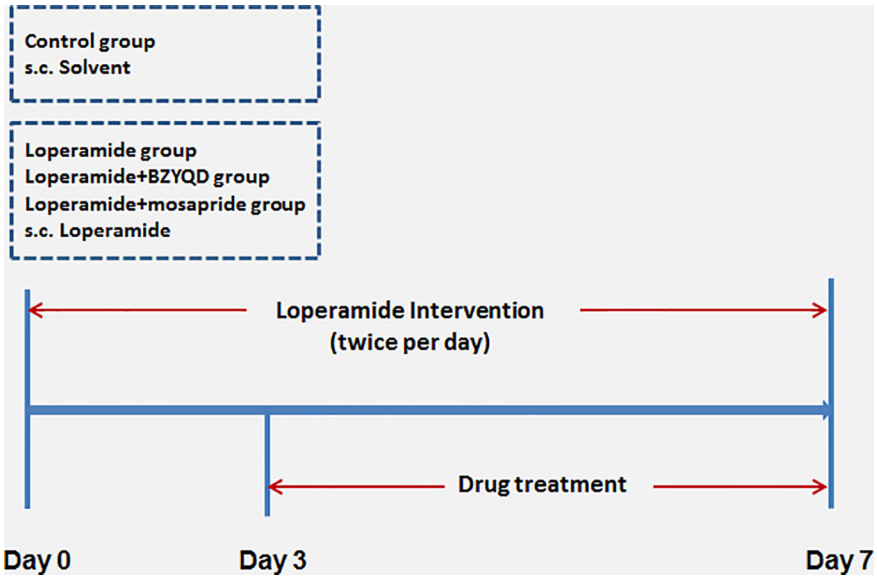


**FIGURE 2 |** Scheme of experiment. Buzhongyiqi decoction (BZYQD) treatment commenced on day 3, s.c: subcutaneous injection.

et al., 2013; Li et al., 2017). In brief, the raw data of UPLC-LTQ-Orbitrap were imported to SIEVE to perform peak extraction and matching. Retention time, m/z value, and corresponding intensities were recorded. These data were preprocessed as per the rules below: (1) the percentage of valid data in each group must be higher than 80%; (2) the relative standard deviation (RSD) in QC samples must be lower than 30%; (3) the intensities of each variable should be normalized by the intensity of the IS. After preprocessing, data were imported to SIMCA-P version 14.0 (Umetrics, Sweden) to perform principal components analysis (PCA) and orthogonal partial least squares discriminant analysis (OPLS-DA). The variable importance in projection (VIP) value was calculated in the OPLS-DA model and the Kruskal-Wallis test was conducted. Variables with VIP values more than 1 and P values less than 0.05 were considered potential biomarkers. These potential biomarkers were identified by searching databases such as HMDB (http://www.hmdb.ca/), KEGG (https://www.kegg.jp/), ChemSpider (http://www.chemspider.com/), and mzCloud (https://www.mzcloud.org/), and were finally validated by standard substances to confirm their identity.

## Immunohistochemistry Analysis

Dewaxed, hydrated colon tissue sections were pretreated with antigen retrieval fluid (pH 6.0), incubated with 3% $H_2O_2$ deionized water for 15 min to block endogenous peroxidase, and rinsed with PBS. IL-6 (1:400) and TNF-α (1:400) were added dropwise and samples incubated overnight at 4°C. The sections were immersed in PBS, and an IgG antibody and Fab fragment-HRP multimer were added dropwise. The mixture was incubated at 37°C for 30 min, and the samples were subsequently washed 5 times with PBS for 3 min each time. Samples were rinsed with distilled water, counter stained with hematoxylin, dehydrated with gradient alcohol, cleared with xylene, and sealed with resin. Positive immunostaining in five random visual fields of the slides was evaluated using an Olympus DP72 optical microscope at a magnification of ×200.

## Real-Time Polymerase Chain Reaction (PCR) Analysis

Total RNA was extracted from colon tissues using Trizol, and cDNA was subsequently synthesized using the Super Script cDNA synthesis kit. Real-time polymerase chain reaction (real-time PCR) was performed using the ABI-StepOnePlus sequence detection system (Applied Biosystems, CA, USA) using the Fast SYBR Green mix kit. The primers used are presented in **Table 2**. The relative target mRNA expression levels were calculated using the $2^{-\Delta\Delta Ct}$ method. The expression level of glyceraldehyde 3-phosphate dehydrogenase (*GAPDH*) mRNA was used as the endogenous reference control.

**TABLE 2 |** Primers of real-time PCR assay used in this study.

| GeneName | Specise | Primer sequence (5′-3′) |
|---|---|---|
| *Gapdh* | Rat | Forward primer AGGTCGGTGTGAACGGATTTTG |
| | | Reverse primer GGGGTCGTTGATGGCAACA |
| *NF-κB* | Rat | Forward primer GACGACACCTCTACACATAGCA |
| | | Reverse primer CCTCATCTTCTCCAGCCTTCTC |
| *IL-6* | Rat | Forward primer CCGGAGAGGAGACTTCACAG |
| | | Reverse primer CCATAGTGCAGGAGCGTACAGT |
| *IL-1β* | Rat | Forward primer TGACCCATGTGAGCTGAAAG |
| | | Reverse primer GGGATTTTGTCGTTGCTTGT |
| *TNF-α* | Rat | Forward primer TGATCCGAGATGTGGAACTG |
| | | Reverse primer CGAGCAGGAATGAGAAGAGG |
| *COX-2* | Rat | Forward primer TCTCCAACCTCTCCTACTAC |
| | | Reverse primer GCACGTAGTCTTCGATCACT |

## Western Blot Analysis

The colon samples were homogenized in a radioimmunoprecipitation assay buffer. The lysate proteins were separated using sodium dodecyl sulfate-polyacrylamide gel electrophoresis (SDS-PAGE) and were electro-blotted onto nitrocellulose membranes. The membranes were blocked for 1 h, and then incubated overnight with primary antibodies against p-NF-κB and NF-κB (Santa Cruz Biotechnologies, Inc., Santa Cruz, CA, USA) at 4°C. The membranes were subsequently washed with Tris-buffered saline/0.1% (v/v) Tween-20 and incubated for 1 h with secondary antibodies. After washing the membranes, the protein bands were detected using the FluorChem E image detection system (ProteinSimple, San Jose, CA, USA). β-actin was used as a loading control.

## Enzyme Linked Immunosorbent Assay (ELISA)

The protein levels of IL-1β and IL-6 in rat serum were measured using an ELISA kit (AMEKO Institute of Biotechnology, Shanghai, China) according to the manufacturer's instructions.

## Statistical Analysis

Data are expressed as the mean ± standard deviation (SD). The statistical differences among study groups were determined by one-way analysis of variance (ANOVA) followed by the least significant difference (LSD). For all comparisons, $P < 0.05$ was considered a statistically significant difference. Correlation coefficient (r) was determined using the Pearson's correlation.

# RESULTS

## Effect of BZYQD on Constipation in Loperamide Induced Rats

The body weight did not differ significantly between loperamide-induced group and normal control group (**Supplementary Figure 1**). The small intestinal transit rate and number of stools were significantly decreased in loperamide induced group than those in normal control group (**Figures 3A, B**). Treatment with BZYQD markedly increased the small intestinal transit rates and number of stools as compared to those in the loperamide group (**Figures 3A, B**). As compared with normal control group, the epithelial surface of the rat colon was damaged, mucosa was thinner, gland was reduced, goblet cells were reduced, and the inflammatory cells infiltrated in the lamina propria in the loperamide group; these histological

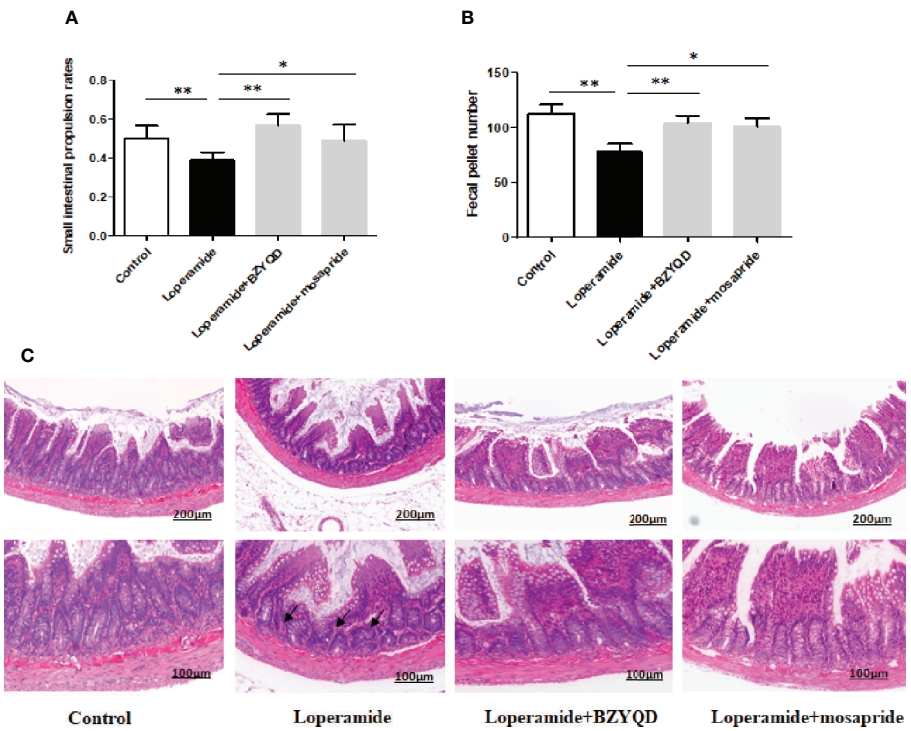


**FIGURE 3 |** Effect of BZYQD intervention on loperamide-induced constipation in rats. **(A)** Small intestinal transit rates of rats of Control group, Loperamide, Loperamide + BZYQD, and Loperamide + Mosapride groups. **(B)** Number of stools of rats of Control group, Loperamide, Loperamide + BZYQD, and Loperamide + Mosapride groups. **(C)** Hematoxylin and eosin (H&E)-staining for light microscopy analysis of colon sections in rats of the control group, Loperamide group, Loperamide + BZYQD group, Loperamide + Mosapride groups morphology. Arrow marks pointed to that epithelial surface of the rat colon was damaged, mucosa was thinner, gland was reduced, goblet cells were reduced, and the inflammatory cells infiltrated in the lamina propria in the loperamide group. n = 8; Original magnification ×100 or ×200; data are represented as mean ± SD. $^{\#}P < 0.05$ versus control group; $^{*}P < 0.05$versus loperamide group, $^{**}P < 0.01$ versus Loperamide group.

damages were significantly ameliorated by BZYQD treatment (**Figure 3C**).

## Effect of BZYQD on the Metabolism of Rats with Loperamide-Induced Constipation

As observed in the PCA plots, the QC samples were clustered closely under both positive and negative monitoring modes, which suggested a stable analysis method (**Figures 4A, B**). The OPLS-DA results indicated an appreciable separation of the data relating to these three groups (**Figures 4C, D**). After identification and screening, levels of 29 serum metabolites in the loperamide induced group were significantly different from those in the normal control group, and BZYQD treatment reversed levels of 17 of these metabolites (**Table 3**). Among these differential metabolites, four were identified using authenticated standards and others were deduced using accurate molecular weights and comparing tandem mass spectrometry fragments with data in metabolomics databases. The levels of metabolites in the three groups are presented as a heatmap (**Figure 4E**). To further explore the metabolic pathways that BZYQD influenced, these metabolites were imported into MetaboAnalyst (https://www.metaboanalyst.ca/) to conduct pathway analysis. The related metabolic pathways are listed in **Figure 5** and **Table 4**. The metabolic pathways influenced by BZYQD were arachidonic acid (AA) metabolism, biosynthesis of unsaturated fatty acids, ascorbate and aldarate metabolism, alactose metabolism, and inositol phosphate metabolism. According to the p value and –log (p) (Zhang et al., 2015; Wu et al., 2017), arachidonic acid metabolism is one of the main pathways that influenced by BZYQD.

## Effect of BZYQD on Inflammatory Response in Rats with Loperamide-Induced Constipation

As serum metabolomics revealed that the main pathway influenced by BZYQD was AA metabolism, we further investigated the effect of BZYQD on inflammation in loperamide-induced rat colon tissue. As shown in **Figures 6A, B**, level of serum metabolite $PGE_2$ was significantly increased in Loperamide group compared to that in the Control group, and it decreased by BZYQD treatment. Additionally, expression of cyclooxygenase 2 (COX-2), the key enzyme that produces $PGE_2$ from AA was also increased in Loperamide group and decreased in BZYQD group. Moreover, the serum levels of

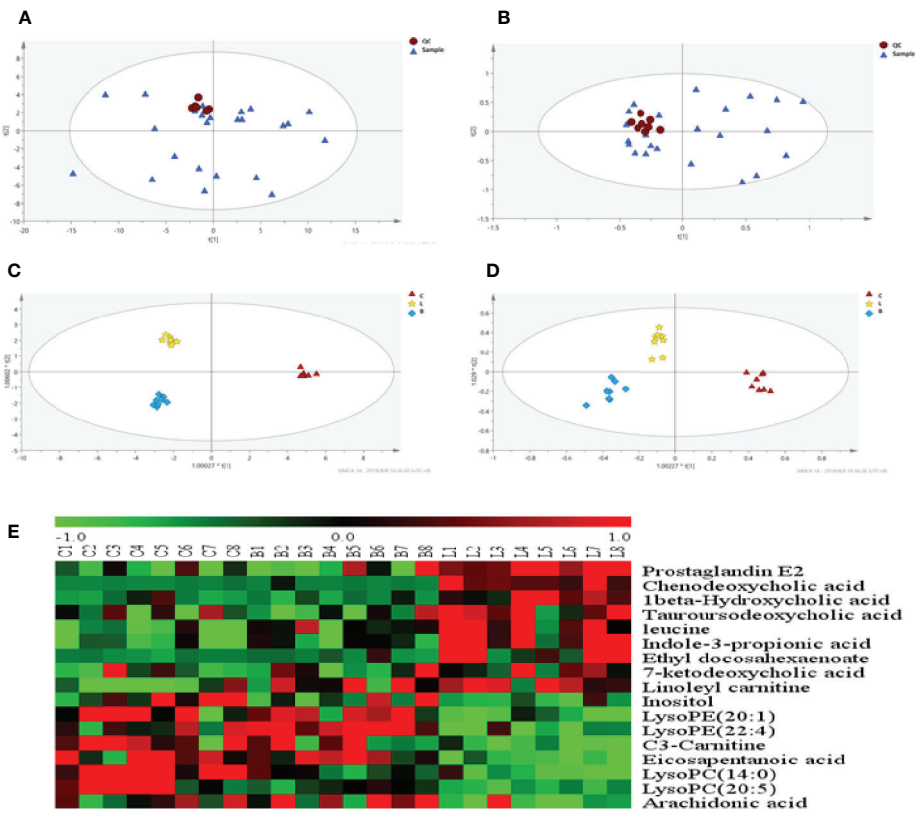


**FIGURE 4 |** Effect of BZYQD intervention on serum metabolic profiling in loperamide-treated rats. **(A, B)** PCA score plot in three groups, $R^2X = 0.513$, $Q^2 = 0.41$ in positive model. $R^2X = 0.567$, $Q^2 = 0.279$ in negative model. **(C, D)** OPLS-DA score plot in three groups, $R^2X = 0.788$, $R^2Y = 0.995$, $Q^2 = 0.515$ in positive model. $R^2X = 0.544$, $R^2Y = 0.918$, $Q^2 = 0.487$ in negative model. **(E)** Hierarchical clustering heat map of the differential metabolite levels in control (C), loperamide (L), and loperamide + BZYQD groups (B) (n = 8). The heat map indicated that the serum levels of nine metabolites (Green color) were decreased, and eight metabolites (Red color) were increased in loperamide + BZYQD group as compared with loperamide group.

**TABLE 3 |** Endogenous metabolites identified in the serum of rats included in this study.

| VIP | Time | Molecular ion | CompMW | Formula | Metabolites |
|---|---|---|---|---|---|
| 1.0830 | 8.22 | $[M-H]^-$ | 352.47 | $C_{20}H_{32}O_5$ | Prostaglandin E2 |
| 1.6241 | 8.16 | $[M-H]^-$ | 304.47 | $C_{20}H_{32}O_2$ | Arachidonic acid |
| 2.1715 | 6.29 | $[M-H]^-$ | 392.57 | $C_{24}H_{40}O_4$ | Chenodeoxycholic acid |
| 1.2442 | 6.37 | $[M-H]^-$ | 424.28 | $C_{24}H_{40}O_6$ | 1beta-Hydroxycholic acid |
| 1.8625 | 5.91 | $[M-H]^-$ | 499.70 | $C_{26}H_{45}NO_6S$ | Tauroursodeoxycholic acid |
| 1.2511 | 8.33 | $[M-H]^-$ | 180.16 | $C_6H_{12}O_6$ | Inositol |
| 1.4063 | 8.89 | $[M-H]^-$ | 549.37 | $C_{28}H_{56}NO_7P$ | LysoPC(20:1) |
| 1.1752 | 7.97 | $[M+H]^+$ | 571.17 | $C_{30}H_{52}NO_7P$ | LysoPC(22:4) |
| 1.9844 | 5.31 | $[M+H]^+$ | 131.17 | $C_6H_{13}NO_2$ | Leucine |
| 2.0029 | 5.31 | $[M+H]^+$ | 189.21 | $C_{11}H_{11}NO_2$ | IpA(Indole-3-propionic acid) |
| 1.5352 | 1.11 | $[M+H]^+$ | 161.20 | $C_7H_{15}NO_3$ | Carnitine |
| 1.2700 | 8.70 | $[M+H]^+$ | 302.22 | $C_{20}H_{30}O_2$ | Eicosapentanoic acid |
| 2.6147 | 6.39 | $[M+H]^+$ | 356.27 | $C_{24}H_{36}O_2$ | Ethyl docosahexaenoate |
| 1.5642 | 6.14 | $[M+H]^+$ | 406.27 | $C_{24}H_{38}O_5$ | 7-ketodeoxycholic acid |
| 1.7325 | 8.11 | $[M+H]^+$ | 423.33 | $C_{25}H_{45}NO_4$ | Linoelaidyl carnitine |
| 1.3189 | 7.58 | $[M+H]^+$ | 467.29 | $C_{22}H_{46}NO_7P$ | LysoPC(14:0) |
| 1.7046 | 7.63 | $[M+H]^+$ | 541.32 | $C_{28}H_{48}NO_7P$ | LysoPC(20:5) |

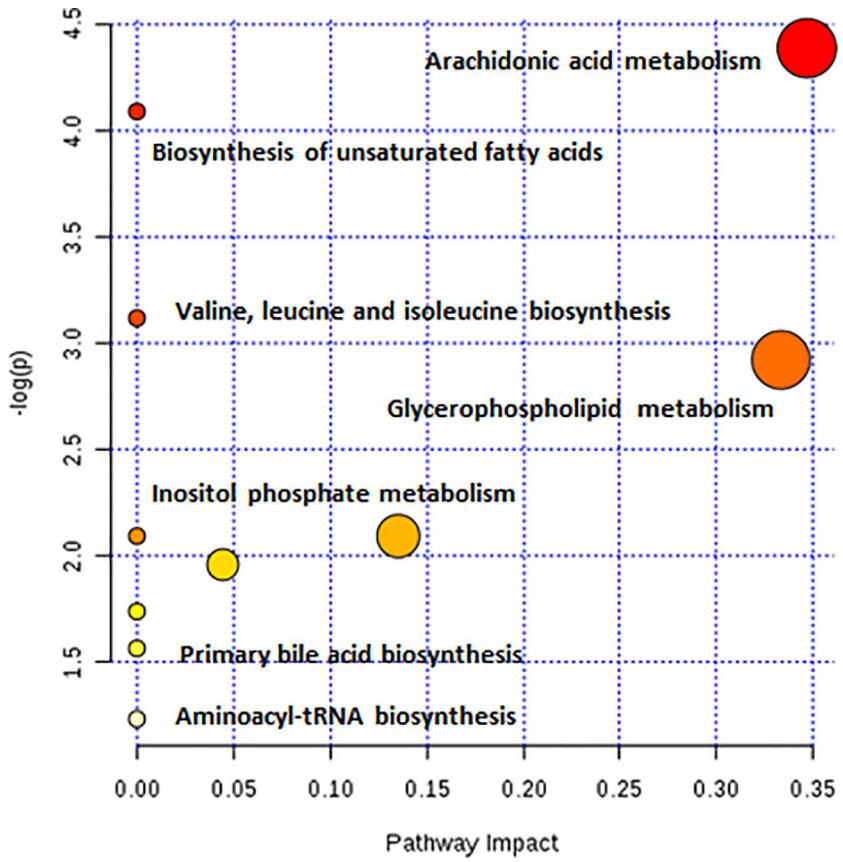


**FIGURE 5 |** Main pathway analysis associated with metabolites that were influenced by BZYQD.

inflammatory markers, such as IL-1β and TNF-α, were significantly increased in Loperamide group as compared with Control group. However, treatment with BZYQD decreased the serum levels of IL-1β and TNF-α (**Figures 6C, D**). Additionally, since differential metabolites, such as $PGE_2$, play an important role in the progression of inflammation, correlation between serum levels of $PGE_2$and those of IL-1β and TNF-α were tested using the Pearson's correlation. According to the correlation factor (r=0. 4669 or r=0. 4675) and *P*-value (p=0.0214 or p=0.0213), the results indicated serum levels of IL-1β and TNF-α had positive linear correlations

**TABLE 4 |** The metabolic pathways that influenced by BZYQD in loperamide-treated rats.

| Pathway Name | Total | Hits | p | -log (p) | Impact |
|---|---|---|---|---|---|
| Arachidonic acid metabolism | 36 | 2 | 0.012167 | 4.409 | 0.3468 |
| Biosynthesis of unsaturated fatty acids | 42 | 2 | 0.016393 | 4.1109 | 0.0000 |
| Ascorbate and aldarate metabolism | 9 | 1 | 0.043713 | 3.1301 | 0.0000 |
| Galactose metabolism | 26 | 1 | 0.12183 | 2.1052 | 0.0000 |
| Inositol phosphate metabolism | 28 | 1 | 0.13065 | 2.0353 | 0.1116 |
| Glycerophospholipid metabolism | 30 | 1 | 0.13939 | 1.9705 | 0.0444 |
| Primary bile acid biosynthesis | 46 | 1 | 0.20667 | 1.5767 | 0.0298 |

with $PGE_2$ levels (**Figures 6E, F**). The Pearson's correlation method was descripted as previously reported (Yan et al., 2017; Zheng et al., 2019). Additionally, the mRNA and protein expression of IL-1β and IL-6 in rat colon tissue was also investigated by real-time PCR and immunohistochemistry. As shown in **Figure 7**, the mRNA and protein expression of IL-1β and IL-6 was significantly increased in Loperamide group, and it decreased by BZYQD treatment (**Figure 7**). These results suggest that BZYQD treatment decreases loperamide-induced inflammation.

## Effect of BZYQD on NF-κB Signaling Pathway in Rats with Loperamide-Induced Constipation

$PGE_2$ is produced by AA through COX-2, which is regulated by NF-κB signaling pathway. Therefore, the mRNA and protein expression of p65 in rat colon tissue was further investigated by real-time PCR and western blotting. p65 mRNA expression and p65 and p-p65 protein levels were markedly increased in Loperamide group (**Figure 8**) than those in the control group. However, treatment with BZYQD significantly decreased p65 mRNA expression and p-p65 protein levels (**Figure 8**). This result indicated that BZYQD can regulate NF-κB signaling pathway.

## Effect of BZYQD on Serum levels of Gastrointestinal Hormone in Rats with Loperamide-Induced Constipation

The serum levels of gastrointestinal hormone of motilin and gastrin were detected by ELISA. The serum levels of motilin and gastrin were markedly decreased in Loperamide group (**Figure 9**) than those in the control group. However, treatment with BZYQD significantly increased serum levels of motilin and gastrin (**Figure 9**). This result indicated that BZYQD can promote gastrointestinal motility.

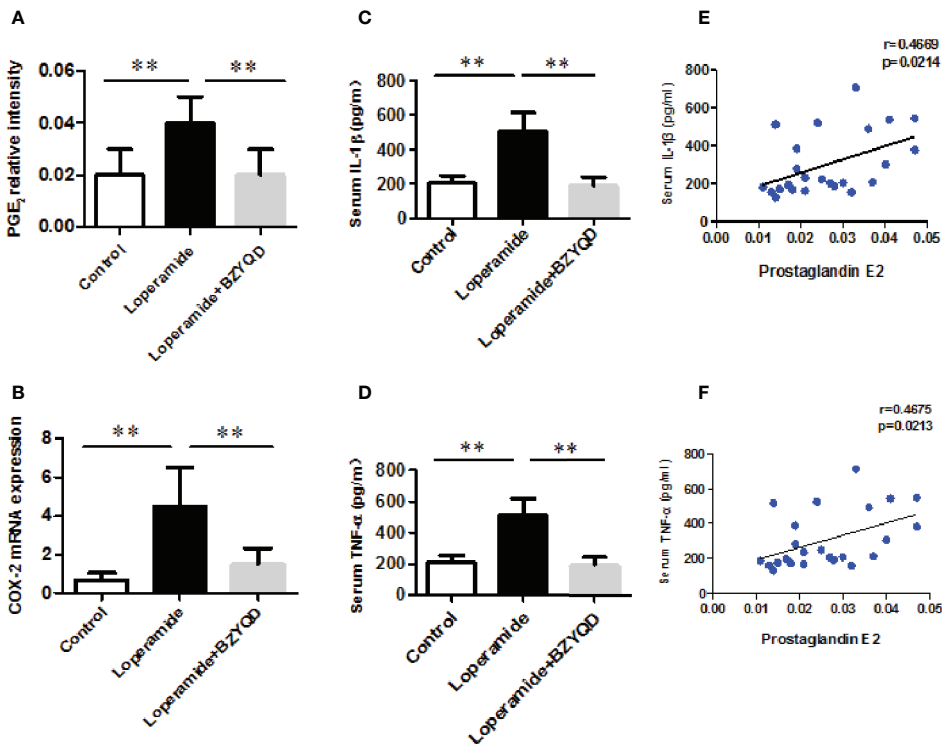


**FIGURE 6 |** Effect of BZYQD intervention on serum levels of inflammatory factors in loperamide-treated rats. **(A)** Serum levels of prostaglandin $E_2$ ($PGE_2$) in each group; **(B)** The mRNA expression of COX-2 in mice colon tissue; **(C)** Serum levels of IL-6 detected using ELISA in each group; **(D)** Serum levels of TNF-α detected using ELISA in each group; **(E)** The correlation between serum levels of IL-6 and serum metabolite $PGE_2$; **(F)** The correlation between serum levels of TNF-α and serum metabolite $PGE_2$; data are represented as mean ± SD (n = 8). $^{**}P < 0.01$ between two groups. Correlation factor (r) and *P*-value were determined using the Pearson's correlation analysis.

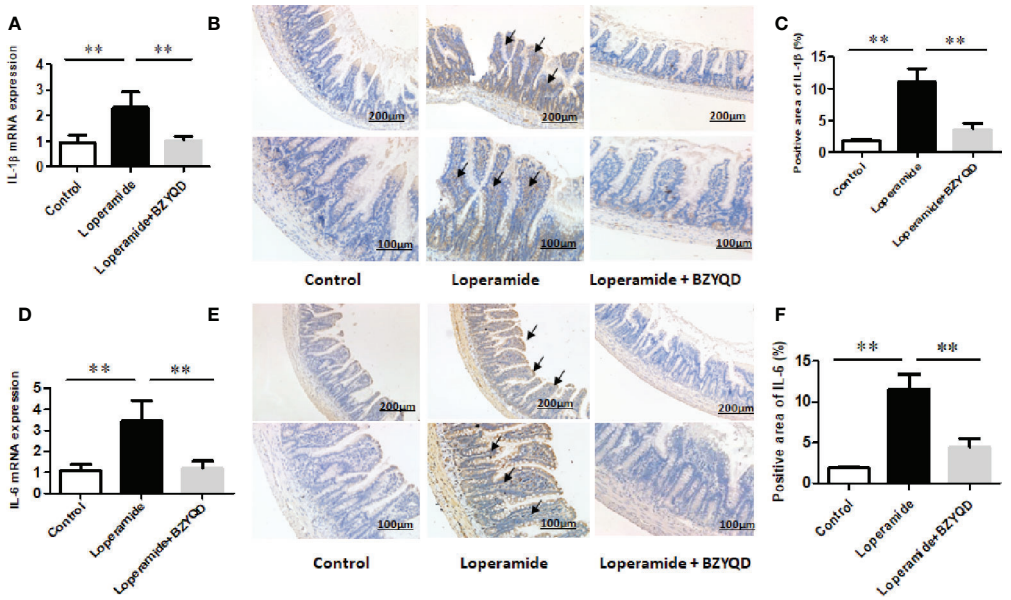


**FIGURE 7 |** Effect of BZYQD intervention on expression of colon inflammatory factors in loperamide-treated rats. BZYQD decreased the mRNA and protein expression of IL-1β and IL-6: **(A)** The mRNA expression of IL-1β of colon tissues that detected by real-time PCR; **(B)** Protein expression of IL-1β of colon tissues that detected using immunohistochemistry; **(C)** Quantification of protein expression of IL-1β of colon tissues. **(D)** The mRNA expression of IL-6 of colon tissues that detected by real-time PCR; **(E)** Protein expression of IL-6 of colon tissues that detected using immunohistochemistry; **(F)** Quantification of protein expression of 6 of colon tissues. Data are represented as mean ± SD. Arrow marks pointed to positive area expression. (n = 5). $^{**}P < 0.01$ between groups.

## DISCUSSION

BZYQD is a classic Chinese herbal formula used to treat gastrointestinal diseases (Gou et al., 2016), but its mechanism of action has not been fully studied. Loperamide is an anti-diarrheal drug commonly used in the clinic, and its mechanism of action mainly involves the inhibition of intestinal peristalsis and intestinal secretion (Zhang et al., 2018). Loperamide is widely used to establish animal constipation models to study the etiology and pathogenesis of constipation (Wu et al., 2010; Han et al., 2017; Zhang et al., 2018; Li et al., 2019). In this study, BZYQD treatment increased the intestinal propulsion rate and improved the colon tissue pathological damage induced by loperamide in a loperamide-induced rat constipation model. Mosapride is a commonly used drug to treat gastrointestinal dysfunction. Mosapride was reported to improve loperamide-induced constipation in rats (Li et al., 2019). In the current study, mosapride was used as a positive drug, and there was no significant difference between BZYQD and mosapride in improving constipation. Overall, our results indicate that BZYQD has protective effects against loperamide-induced constipation.

Metabolomics reveals molecular mechanism pathway by assessing differences in the production of metabolites or endogenous small molecules (Schrimpe-Rutledge et al., 2016). Metabolomics, thus, provides a holistic view of changes in metabolite levels due to drug interventions. TCM comprise a variety of crude herbs that exert a comprehensive therapeutic effect (Wu et al., 2017; Zheng et al., 2019). Metabolomics is very helpful in exploring the mechanisms of action of TCM (Wu et al., 2017; Zheng et al., 2019). In this study, metabolomics was used to analyze the influence of BZYQD on serum metabolites in a loperamide-induced constipation rat model. Our results showed that the levels of 29 metabolites were changed in the loperamide group compared with the control group, and 17 different metabolites were reversed by BZYQD. KEGG pathway analysis revealed that the major pathway that was influenced by BZYQD was the arachidonic acid metabolism, biosynthesis of unsaturated fatty acids, ascorbate and aldarate metabolism, inositol phosphate metabolism. Therefore, the regulation of those metabolic pathways may be key roles in BZYQD against loperamide-induced constipation.

Arachidonic acid metabolism plays an important role in the inflammatory network (Meirer et al., 2014). AA and prostaglandin $E_2$ ($PGE_2$) are both important metabolites involved in the AA metabolic pathway. AA is a type n-6 polyunsaturated fatty acid highly represented in the composition of phospholipids; moreover, it is the precursor of eicosanoids, such as $PGE_2$, thromboxanes, and leukotrienes, which are long-recognized mediators of inflammation (Akasaka and Ruan, 2016). There have been reports indicating that the increased release of $PGE_2$ can trigger an inflammatory response (Kawahara et al., 2015; Koeberle and Werz, 2015; Tsuge et al., 2019). In the present study, the serum metabolite $PGE_2$ was significantly increased in the loperamide-induced group and decreased upon BZYQD intervention. This result suggests that BZYQD administration may alleviate the inflammatory response induced by loperamide in constipation rats. Histopathological results showed that intervention with BZYQD reduced inflammatory cell infiltration and morphological damage in the colons of rats administered loperamide. Further study showed that BZYQD

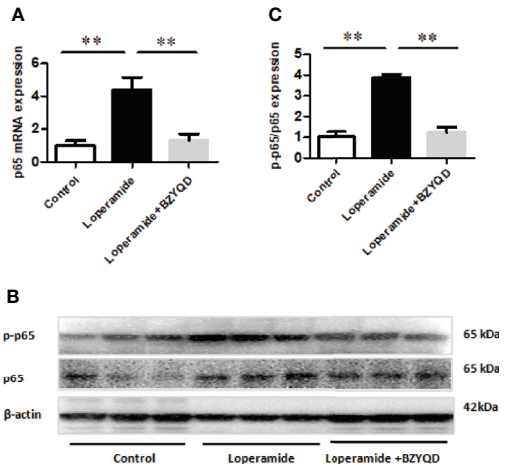


**FIGURE 8 |** Effect of BZYQD intervention on NF-κB signaling pathway in loperamide-treated rats. **(A)** The mRNA expression of p65 detected through real-time PCR. **(B)** The protein expression of p-p65 and p65 detected by western blot. **(C)** Ratio of protein expression of p-p65 and p65; data are represented as mean ± SD; n = 8 for real-time PCR and n = 3 for western blot. $^{**}P < 0.01$ between groups.

intervention reduced the levels of serum inflammatory factors IL-1β and TNF-α and colonic inflammatory factors IL-1β and IL-6 in constipation rats. Therefore, the above mentioned results also support the results of our metabolomics study. Previous studies have shown that the inflammatory response is closely related to gastrointestinal motility disorders (Ali et al., 2013). Infiltration of inflammatory cells into the digestive tract is a major histological change involved in gastrointestinal motility disorders (Ali et al., 2013). In addition, the release of inflammatory mediators also leads to changes in gastrointestinal motility (Ali et al., 2013). A recent study reported that loperamide-induced rats exhibit a significant colonic inflammatory response, and anti-inflammatory agents help to exert a laxative effect on constipation in these rats (Kim et al., 2019). Thus, consistent with our result, this study showed that inflammation may play an important role in the progression of constipation. Our results also suggested that BZYQD can alleviate the inflammatory response induced by loperamide and ameliorate constipation.

AA is catalyzed by COX-2 to produce the metabolite $PGE_2$ (Tsuge et al., 2019), while COX-2 expression is regulated by the NF-κB signaling pathway (Zha et al., 2014; Desai et al., 2018). In this study, we found that BZYQD can inhibit NF-κB phosphorylation in the colon of constipation rats, and down-regulate the expression of COX-2, thereby reducing the level of $PGE_2$. Therefore, our results suggest that the regulation of the arachidonic acid pathway by BZYQD may occur through the inhibition of the NF-κB signaling pathway. However, further exploration through future studies is needed. In addition, the release of inflammatory mediators is also known to induce acute inflammatory cell infiltration and promote NF-κB activity (Kawai and Akira, 2007; Gambhir et al., 2015; Merga et al., 2016). Here, we observed that BZYQD inhibited the activation of the NF-κB pathway, which may also contribute to its protective effect against loperamide-induced constipation.

There have been reported that inositol phosphate is associated with gastrointestinal hormone motilin and gastrin metabolism (Fang et al., 2010; Goze et al., 2010). In the current study, we have investigated the effect of BZYQD on the serum levels of

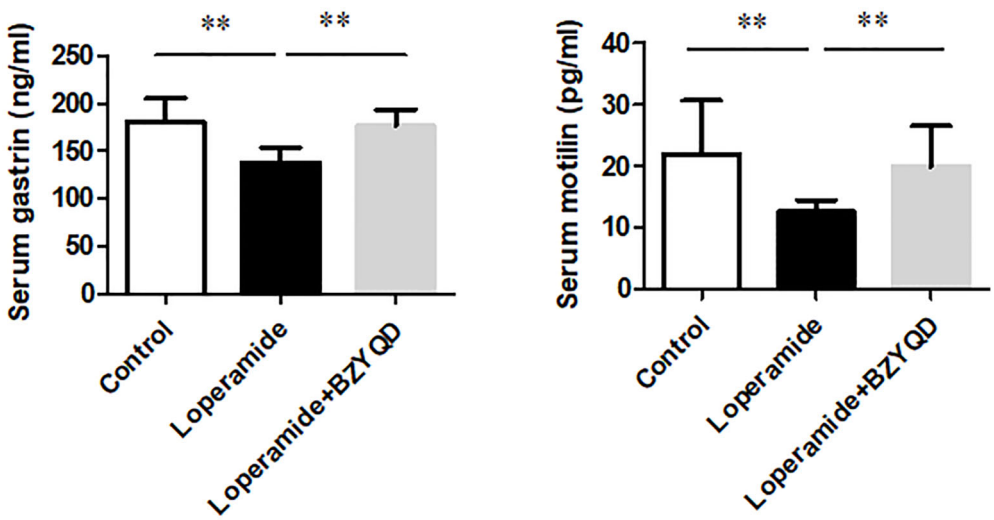


**FIGURE 9 |** Effect of BZYQD intervention on serum levels of motilin and gastrin in loperamide-treated rats. Data are represented as mean ± SD; n = 5. $^{**}P < 0.01$ between groups.

gastrointestinal hormone. Our results indicated that BZYQD increased the serum levels of gastrointestinal hormone motilin and gastrin. Therefore, those results suggested that treatment with BZYQD may promote the gastrointestinal motility of rats with loperamide-induced constipation.

In conclusion, the results of this study demonstrated that BZTQD intervention exerts a protective effect against loperamide-induced constipation, which may be associated with its role in regulation of multiple metabolic pathways.

## DATA AVAILABILITY STATEMENT

All datasets generated for this study are included in the article/ **Supplementary Material**.

## ETHICS STATEMENT

This study was carried out in accordance with the principles of China Regulations on the Administration of Laboratory Animals, the Decree No. 2 of National Science and Technology Commission of the People's Republic of China. The protocol was approved by the animal ethics committee of the Shanghai University of Traditional Chinese Medicine, China.

## AUTHOR CONTRIBUTIONS

W-JJ and Z-KZ performed the experiment. W-JJ completed this manuscript. G-LD designed the experiment. X-PW guided the experiment. S-LC, D-DZ, and W-NY assisted the experiments. X-PW and G-LD revised the article.

## FUNDING

The authors are grateful for the financial support from the National Natural Science Foundation of China (81573862).

## SUPPLEMENTARY MATERIAL

The Supplementary Material for this article can be found online at: https://www.frontiersin.org/articles/10.3389/fphar.2020.00423/full#supplementary-material

## REFERENCES

Akasaka, H., and Ruan, K. H. (2016). Identification of the two-phase mechanism of arachidonic acid regulating inflammatory prostaglandin E2 biosynthesis by targeting COX-2 and mPGES-1. *Arch. Biochem. Biophys.* 603, 29–37. doi: 10.1016/j.abb.2016.04.011

Ali, T., Choe, J., Awab, A., Wagener, T. L., and Orr, W. C. (2013). Sleep, immunity and inflammation in gastrointestinal disorders. *World J. Gastroenterol.* 19, 9231–9239. doi: 10.3748/wjg.v19.i48.9231

Dan, S.L.Y.J.X. (2018). Effects of Bushen Yiqi Decoction on Indexes of Hemotology and Intestinal Sensitivity in Patients with Constipation Predominant Irritable Bowel Syndrome. *World Chinses Med.* 13, 2196–2199. doi: 10.3969 /j.issn.1673-7202.2018.09.025

Desai, S. J., Prickril, B., and Rasooly, A. (2018). Mechanisms of Phytonutrient Modulation of Cyclooxygenase-2 (COX-2) and Inflammation Related to Cancer. *Nutr. Cancer* 70, 350–375. doi: 10.1080/01635581.2018.1446091

Fang, P., Dong, L., and Luo, J. Y. (2010). Effects of motilin on intracellular free calcium in cultured smooth muscle cells from the antrum of neonatal rats. *Acta Physiol. (Oxf.)* 199, 53–61. doi: 10.1111/j.1748-1716.2010.02079.x

Gambhir, S., Vyas, D., Hollis, M., Aekka, A., and Vyas, A. (2015). Nuclear factor kappa B role in inflammation associated gastrointestinal malignancies. *World J. Gastroenterol.* 21, 3174–3183. doi: 10.3748/wjg.v21.i11.3174

Gou, H., Gu, L. Y., Shang, B. Z., Xiong, Y., and Wang, C. (2016). Protective effect of Bu-Zhong-Yi-Qi decoction, the water extract of Chinese traditional herbal medicine, on 5-fluorouracil-induced intestinal mucositis in mice. *Hum. Exp. Toxicol.* 35, 1243–1251. doi: 10.1177/0960327115627686

Goze, C., Berge, G., M'kadmi, C., Floquet, N., Gagne, D., Galleyrand, J. C., et al. (2010). Involvement of tryptophan W276 and of two surrounding amino acid residues in the high constitutive activity of the ghrelin receptor GHS-R1a. *Eur. J. Pharmacol.* 643, 153–161. doi: 10.1016/j.ejphar.2010.06.018

Han, S. H., Park, K., Kim, E. Y., Ahn, S. H., Lee, H. S., and Suh, H. J. (2017). Cactus (Opuntia humifusa) water extract ameliorates loperamide-induced constipation in rats. *BMC Complement. Altern. Med.* 17, 49. doi: 10.1186/s12906-016-1552-8

He, M., Chen, W., Wang, M., Wu, Y., Zeng, J., Zhang, Z., et al. (2017). Simultaneous determination of multiple bioactive components of Bu-zhong-yi-qi-tang in rat tissues by LC-MS/MS: Application to a tissue distribution study. *J. Chromatogr. B. Anal. Technol. BioMed. Life Sci.* 1044, 177–184. doi: 10.1016/j.jchromb.2017.01.023

Huang, Y., Tian, Y., Li, G., Li, Y. Y., Yin, X. J., Peng, C., et al. (2013). Discovery of safety biomarkers for realgar in rat urine using UFLC-IT-TOF/MS and H-1 NMR based metabolomics. *Anal. Bioanal. Chem.* 405, 4811–4822. doi: 10.1007/s00216-013-6842-0

Ji, L. (2006). Fang Ji Xue. *Fang Ji Xue* 13, 2196–2199. doi: 10.18632/oncotarget.21385

Kawahara, K., Hohjoh, H., Inazumi, T., Tsuchiya, S., and Sugimoto, Y. (2015). Prostaglandin E2-induced inflammation: Relevance of prostaglandin E receptors. *Biochim. Biophys. Acta* 1851, 414–421. doi: 10.1016/j.bbalip.2014.07.008

Kawai, T., and Akira, S. (2007). Signaling to NF-kappaB by Toll-like receptors. *Trends Mol. Med.* 13, 460–469. doi: 10.1016/j.molmed.2007.09.002

Kim, J. E., Park, J. W., Kang, M. J., Choi, H. J., Bae, S. J., Choi, Y. S., et al. (2019). Anti-Inflammatory Response and Muscarinic Cholinergic Regulation during the Laxative Effect of Asparagus cochinchinensis in Loperamide-Induced Constipation of SD Rats 20. *Int. J. Mol. Sci*. doi: 10.3390/ijms20040946

Koeberle, A., and Werz, O. (2015). Perspective of microsomal prostaglandin E2 synthase-1 as drug target in inflammation-related disorders. *Biochem. Pharmacol.* 98, 1–15. doi: 10.1016/j.bcp.2015.06.022

Li, Y. F., Wu, J. S., Li, Y. Y., Dai, Y., Zheng, M., Zeng, J. K., et al. (2017). Chicken bile powder protects against alpha-naphthylisothiocyanate-induced cholestatic liver injury in mice. *Oncotarget* 8, 97137–97152.

Li, X., Liu, Y., Guan, W., Xia, Y., Zhou, Y., Yang, B., et al. (2019). Physicochemical properties and laxative effects of polysaccharides from Anemarrhena asphodeloides Bge. in loperamide-induced rats. *J. Ethnopharmacol.* 240, 111961. doi: 10.1016/j.jep.2019.111961

Mearin, F., Lacy, B. E., Chang, L., Chey, W. D., Lembo, A. J., Simren, M., et al. (2016). Bowel Disorders. *Gastroenterology.* 16, 222–225. doi: 10.1053/j.gastro.2016.02.031

Meirer, K., Steinhilber, D., and Proschak, E. (2014). Inhibitors of the arachidonic acid cascade: interfering with multiple pathways. *Basic Clin. Pharmacol. Toxicol.* 114, 83–91. doi: 10.1111/bcpt.12134

Merga, Y. J., O'hara, A., Burkitt, M. D., Duckworth, C. A., Probert, C. S., Campbell, B. J., et al. (2016). Importance of the alternative NF-kappaB activation pathway in inflammation-associated gastrointestinal carcinogenesis. *Am. J. Physiol. Gastrointest. Liver Physiol.* 310, G1081–G1090. doi: 10.1152/ajpgi.00026.2016

Schrimpe-Rutledge, A. C., Codreanu, S. G., Sherrod, S. D., and Mclean, J. A. (2016). Untargeted Metabolomics Strategies-Challenges and Emerging Directions. *J. Am. Soc. Mass Spectrom.* 27, 1897–1905. doi: 10.1007/s13361-016-1469-y

Suares, N. C., and Ford, A. C. (2011). Prevalence of, and risk factors for, chronic idiopathic constipation in the community: systematic review and meta-analysis. *Am. J. Gastroenterol.* 106, 1582–1591; quiz 1581, 1592. doi: 10.1038/ajg.2011.164

Sun Feng-Wei, Y. Q.-Y. (2016). Modified Buzhong Yiqi Decoction Treating 49 Cases of Senile Constipation of Spleen Deficiency Syndrome. *Liao Ning J. Tradit. Chin. Med.* 43, 554–556. doi: 1013192 / jissn1000-1719201603040

Tsuge, K., Inazumi, T., Shimamoto, A., and Sugimoto, Y. (2019). Molecular mechanisms underlying prostaglandin E2-exacerbated inflammation and immune diseases. *Int. Immunol.* doi: 10.1093/intimm/dxz021

Wang, N. J., Wang, J. H., Fu, D. Z., and Shao, T. Y. (1991). Study on pharmacological effects on Buzhongyiqi decocotion -the effects and mechanism of BZYQD on preventing or treating experimental gastric ulcer. *Pharmacol. Clinics Chin. Mater. Med.*, 1–5. doi: 10.13412/j.cnki.zyyl.1991.05.001

Wu, D., Wang, X., Zhou, J., Yuan, J., Cui, B., An, R., et al. (2010). Traditional Chinese formula, lubricating gut pill, improves loperamide-induced rat constipation involved in enhance of Cl- secretion across distal colonic epithelium. *J. Ethnopharmacol.* 130, 347–353. doi: 10.1016/j.jep.2010.05.018

Wu, J. S., Li, Y. F., Li, Y. Y., Dai, Y., Li, W. K., Zheng, M., et al. (2017). Huangqi Decoction Alleviates Alpha-Naphthylisothiocyanate Induced Intrahepatic Cholestasis by Reversing Disordered Bile Acid and Glutathione Homeostasis in Mice. *Front. Pharmacol.* 8, 938. doi: 10.3389/fphar.2017.00938

Yan, J., Xie, G., Liang, C., Hu, Y., Zhao, A., Huang, F., et al. (2017). Herbal medicine Yinchenhaotang protects against alpha-naphthylisothiocyanate-induced cholestasis in rats. *Scientific Report.* 7, 4211. doi: 10.1038/s41598-017-04536-5

Zha, L., Chen, J., Sun, S., Mao, L., Chu, X., Deng, H., et al. (2014). Soyasaponins can blunt inflammation by inhibiting the reactive oxygen species-mediated activation of PI3K/Akt/NF-kB pathway. *PloS One* 9, e107655. doi: 10.1371/journal.pone.0107655

Zhang, Z. H., Wei, F., Vaziri, N. D., Cheng, X. L., Bai, X., Lin, R. C., et al. (2015). Metabolomics insights into chronic kidney disease and modulatory effect of rhubarb against tubulointerstitial fibrosis. *Sci. Rep.* 5, 14472. doi: 10.1038/srep14472

Zhang, Y., Ge, T., Xiang, P., Mao, H., Tang, S., Li, A., et al. (2018). Therapeutic effect of protease-activated receptor 2 agonist SLIGRL-NH2 on loperamide-induced Sprague-Dawley rat constipation model and the related mechanism. *Drug Des. Devel Ther.* 12, 2403–2411. doi: 10.2147/DDDT.S160628

Zhang, X., Wang, Y., Li, X., Dai, Y., Wang, Q., Wang, G., et al. (2019). Treatment Mechanism of Gardeniae Fructus and Its Carbonized Product Against Ethanol-Induced Gastric Lesions in Rats. *Front. Pharmacol.* 10, 750. doi: 10.3389/fphar.2019.00750

Zhang, E. A. (2016). Clinical observation on functional constipation (qi deficiency type) with Buzhong Yiqi decoction. *J. Shanxi Coll. Tradit. Chin. Med.* 17, 42–43. doi: 10.13192/j.issn.1000-1719.2016.03.040

Zheng, M., Li, Y. Y., Wang, G. F., Jin, J. Y., Wang, Y. H., Wang, T. M., et al. (2019). Protective effect of cultured bear bile powder against dimethylnitrosamine-induced hepatic fibrosis in rats. *BioMed. Pharmacother.* 112, 108701. doi: 10.1016/j.biopha.2019.108701

**Conflict of Interest:** Author DZ was employed by company Gen Chim Testing Co., Ltd.

The remaining authors declare that the research was conducted in the absence of any commercial or financial relationships that could be construed as a potential conflict of interest.

frontiers in Pharmacology

ORIGINAL RESEARCH
published: 03 April 2020
doi: 10.3389/fphar.2020.00381

# Systems Pharmacology Approach to Investigate the Mechanism of Kai-Xin-San in Alzheimer's Disease

*Yunxia Luo[1,2†], Dongli Li[1†], Yanfang Liao[1†], Chuipu Cai[1], Qihui Wu[1], Hanzhong Ke[3,4], Xinning Liu[1], Huilin Li[2], Honghai Hong[5], Yumin Xu[6], Qi Wang[1,7*], Jiansong Fang[1,7*] and Shuhuan Fang[1,7*]*

[1] Science and Technology Innovation Center, Guangzhou University of Chinese Medicine, Guangzhou, China, [2] Department of Endocrinology, Fourth Clinical Medical College, Guangzhou University of Chinese Medicine, Shenzhen, China, [3] Department of Cancer Immunology and Virology, Dana-Farber Cancer Institute, Boston, MA, United States, [4] Department of Medicine, Harvard Medical School, Boston, MA, United States, [5] Department of Clinical Laboratory, The Third Affiliated Hospital of Guangzhou Medical University, Guangzhou, China, [6] Department of Encephalopathy First Affiliated Hospital of Henan University of Chinese Medicine, Zhengzhou, China, [7] Institute of Clinical Pharmacology, Guangzhou University of Chinese Medicine, Guangzhou, China

Alzheimer's disease (AD) is a complex neurodegenerative disease characterized by cognitive dysfunction. Kai-Xin-San (KXS) is a traditional Chinese medicine (TCM) formula that has been used to treat AD patients for over a thousand years in China. However, the therapeutic mechanisms of KXS for treating AD have not been fully explored. Herein, we used a comprehensive network pharmacology approach to investigate the mechanism of action of KXS in the treatment of AD. This approach consists of construction of multiple networks and Gene Ontology enrichment and pathway analyses. Furthermore, animal experiments were performed to validate the predicted molecular mechanisms obtained from the systems pharmacology-based analysis. As a result, 50 chemicals in KXS and 39 AD-associated proteins were identified as major active compounds and targets, respectively. The therapeutic mechanisms of KXS in treating AD were primarily related to the regulation of four pathology modules, including amyloid beta metabolism, tau protein hyperphosphorylation process, cholinergic dysfunction, and inflammation. In scopolamine-induced cognitive dysfunction mice, we validated the anti-inflammatory effects of KXS on AD by determining the levels of inflammation cytokines including interleukin (IL)-6, IL-1β, and tumor necrosis factor (TNF)-α. We also found cholinergic system dysfunction amelioration of KXS is correlated with upregulation of the cholinergic receptor CHRNB2. In conclusion, our work proposes a comprehensive systems pharmacology approach to explore the underlying therapeutic mechanism of KXS for the treatment of AD.

**Keywords: systems pharmacology, Kai-Xin-San, Alzheimer's disease, cholinergic system, neuroinflammation**

OPEN ACCESS

***Edited by:***
*Yonghua Wang,*
*Northwest A&F University, China*

***Reviewed by:***
*Jianxin Chen,*
*Beijing University of Chinese Medicine, China*
*Shiv Bahadur,*
*GLA University, India*

***Correspondence:**
*Qi Wang*
*wangqi@gzucm.edu.cn*
*Jiansong Fang*
*fangjs@gzucm.edu.cn*
*Shuhuan Fang*
*fangshuhuan@gzucm.edu.cn*

*†These authors have contributed equally to this work*

***Specialty section:***
*This article was submitted to Ethnopharmacology, a section of the journal Frontiers in Pharmacology*

***Received:*** *28 November 2019*
***Accepted:*** *12 March 2020*
***Published:*** *03 April 2020*

***Citation:***
*Luo Y, Li D, Liao Y, Cai C, Wu Q, Ke H, Liu X, Li H, Hong H, Xu Y, Wang Q, Fang J and Fang S (2020) Systems Pharmacology Approach to Investigate the Mechanism of Kai-Xin-San in Alzheimer's Disease. Front. Pharmacol. 11:381. doi: 10.3389/fphar.2020.00381*

## INTRODUCTION

Alzheimer's disease (AD), as the most common form of dementia, has become one of the leading causes of morbidity and mortality in the aged population. According to the World Alzheimer Report, up to 2019, there were over 50 million people living with dementia (Cao et al., 2018b; Gaugler and Al, 2019). Patients with AD suffer from a decline in learning and memory, cognitive deficits, and behavioral/personality changes, which lead to a heavy public health burden (Jia et al., 2018; Kumar and Tsao, 2019). As a complex multifactorial disease, AD is driven by extracellular deposition of beta amyloid (Aβ) and intracellular accumulation of tau protein. Current treatments can only provide limited symptomatic-relief benefits but fail to stop or reverse disease progression. Moreover, adverse effects, including diarrhea, nausea, and nightmares, further restrict the clinical treatment of AD (Masters et al., 2015). Therefore, there is an urgent need to discover novel therapeutic drugs with new mechanisms of action (MOAs) for treating AD.

Traditional Chinese medicine (TCM), which embraces centuries of knowledge and practical experience, has been used to treat many complex diseases in China for over 2,000 years (Cooper and Ma, 2017; Jiang et al., 2017). TCM has advantages for multi-targeting in intervention and treatment and has provided comprehensive prospects for understanding physiopathology and drug development for neurodegenerative diseases, including AD (Ho et al., 2010; Law et al., 2017). Kai-Xin-San (KXS) is a widely used TCM formula initially recorded in *Beiji Qianjin Yaofang* for treating dementia and depression in China since the Tang Dynasty. It is comprised of four herbs: *Panax ginseng C. A. Mey* (RENSHEN, RS), *Polygala tenuifolia Willd* (YUANZHI, YZ), *Acorus tatarinowii* (SHICHANGPU, SCP), and *Poria* (FULING, FL) (Cao et al., 2018a). Previous studies of KXS mainly focused on the mechanism of a single target-oriented pathway or neurotransmitter regulation, which cannot comprehensively illuminate the therapeutic effects and mechanism of action (MOA) of KXS for AD treatment (Lu et al., 2017; Wang et al., 2017; Cao et al., 2018a; Gao et al., 2018). Herein, there is a need to investigate the overall beneficial effects of KXS for treating AD using advanced approaches.

Systems pharmacology is a cutting-edge methodology that combines computational and experimental tools toward discovering novel therapeutic agents and understanding the therapeutic mechanisms of complex diseases. (Fang et al., 2017a; Fang et al., 2019). In recent years, systems pharmacology-based approaches have provided new insights into elucidating the mechanisms of TCM in the treatment of diseases such as cardiovascular diseases and AD (Zhou and Wang, 2014; Fang et al., 2017a; Cai et al., 2018). In this study, we employed a systems pharmacology approach to identify potential compounds, candidate targets, and therapeutic mechanisms of KXS against AD disease from a holistic prospect (**Figure 1**). Briefly, we first determined the comprehensive AD-associated genes and ingredients of KXS after integrating different data sources. We further predicted candidate targets based on a balanced substructure-drug-target network-based inference approach (bSDTNBI). Subsequently, the targets of KXS were mapped onto AD-relevant genes to determine their biological functions and corresponding AD pathways. Furthermore, we performed multiple level data analyses to reveal the MOA of KXS on AD treatment. Finally, we validated the proposed pharmacological mechanism of KXS in a scopolamine (SCOP)-induced AD mouse model.

## MATERIALS AND METHODS

### AD-Associated Gene Collection

Genes related to AD were collected from several public disease gene-related databases, including Malacard (https://www.malacards.org), DisGeNet database, GWAS catalog, HGMD

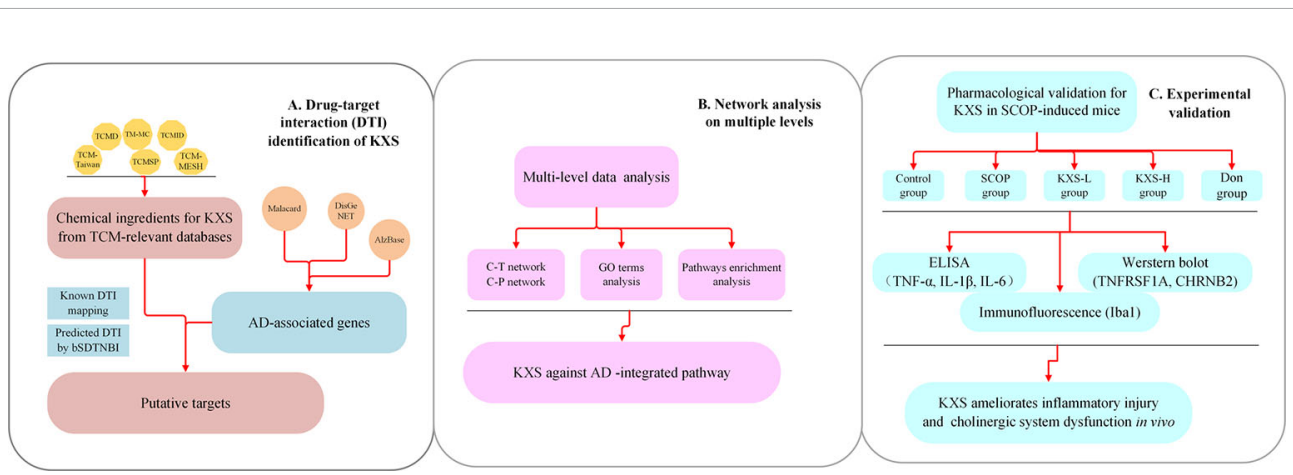


**FIGURE 1 |** Flowchart of the systems pharmacology approach for deciphering the therapeutic mechanisms of action of Kai-Xin-San (KXS) on Alzheimer's disease (AD). **(A)** Drug-target interaction (DTI) identification. **(B)** Network analysis of multiple data to investigate the therapeutic mechanisms of KXS on AD. **(C)** Experimental validation *in vivo* to explore the pharmacological mechanisms of KXS on AD.

(Pinero et al., 2017), AlzBase database (http://alz.big.ac.cn/alzBase/summary/Gene), and AlzPlatform. AlzPlatform is an AD-specific chemogenomics knowledgebase for target identification and drug discovery (Liu et al., 2014). Ultimately, a total of 447 AD-associated genes were obtained (**Supplementary Datasheet S1**).

## KXS Ingredient Collection

All ingredients in KXS (4 herbs) were collected from six TCM-related databases, including TCMID (Xue et al., 2013), TCM-Taiwan (Chen, 2011), TCMD (He et al., 2001), TCMSP (Ru et al., 2014), TM-MC (Kim et al., 2015), and TCM-MESH (Zhang et al., 2017). For each database, we extracted the chemical structures of each herb as an SDF file. Subsequently, six SDF files were merged to a single SDF, which contained all of the chemical structures from the six data sources. SMILES as well as InChIKey were generated by Open Babel (O'boyle et al., 2011) for each ingredient. After removing the duplicates, 1,118 ingredients in KXS were finally obtained.

## Target Identification for KXS

In this work, the known targets of KXS were extracted from our previous integrated database (Fang et al., 2017b), which contains 7,314 drug-target interactions (DTIs) connecting 751 targets and 2,388 natural products.

In a previous study, we developed predictive network models to identify new targets of natural products *via* the bSDTNBI approach (Fang et al., 2017b), which prioritized potential targets for known drugs and new chemical entities (NCEs) by resource-diffusion processes of the substructure drug-target network. During the course, two parameters including $\alpha$ and $\beta$ were imported to balance the initial resource allocation of different node types as well as the weighted values of different edge types. Moreover, parameter $\gamma$ was also utilized to balance the influence of hub nodes. The final parameters ($\alpha = \beta = 0.1$, $\gamma = -0.5$, and $k = 2$) of bSDTNBI were adopted from a previous study (Wu et al., 2016). Among the four network models developed using different types of fingerprints, bSDTNBI_KR performed best with the highest value of P (0.049), R (0.752), eP (27.02), eR (27.24), and AUC (0.959). Thus, bSDTNBI_KR was utilized to predict new targets of natural products in the global network.

## Network Construction

To comprehensively understand the complex interactions among herbs, compounds, targets, and pathways, herb-target and compound-target networks were constructed by Cytoscape (version 3.2.1) and Gephi (version 0.9.2). In the graphical network, the nodes represent compounds, targets, or herbs, while the edges denote links among them. The quantitative property "degree" was calculated as the number of edges linked to each node, indicating the importance of a given node in a network.

## Gene Ontology (GO) Enrichment Analysis

The biological significance of protein targets can be interpreted *via* GO enrichment analysis. In this work, we conducted a biological process (BP) interpretation by mapping AD-related genes (with a degree greater than 2) of KXS to the DAVID database (https://david.ncifcrf.gov/home.jsp) (Huang Da et al., 2009). DAVID is an integrated biological knowledgebase and analytic tool aimed at systematically extracting the biological meaning from large gene/protein lists.

## Pathway Construction and Analysis

To investigate the roles of protein targets in the pathophysiological network of AD and how KXS acts on AD by regulating certain pathways, an "AD-integrated pathway" was proposed based on our present understanding of AD pathology and target identification. In brief, the protein targets were first mapped to the Kyoto Encyclopedia of Genes and Genomes database (KEGG, http://www.genome.jp/kegg/) to obtain the potential pathways. Subsequently, pathways related to AD pathological processes were selected and incorporated into an "AD-integrated pathway" to analyze the therapeutic mechanisms of KXS for treating AD.

## Experimental Validation

### KXS Preparation

The four herbs in KXS (RS, FL, SCP, and YZ) were obtained from the First Affiliated Hospital of Guangzhou University of Chinese Medicine (Guangzhou, China) and were mixed at a ratio of 3:3:2:2 referenced the previous studies (Cao et al., 2012; Xu et al., 2019). The extraction process and quality control were implemented according to our previous study (Xu et al., 2019). Briefly, SCP was added to six parts of water as a solvent for 2 h, followed by heat reflux extraction for 8 h. Volatile oil and SCP dregs were saved. RS was extracted twice by 60% ethanol as solvent for each time with 1 hour. The extracts were combined and filtrated, and the RS dregs were saved. The dregs of SCP, RS, FL, and YZ were added to 10 parts of water and extracted twice, for 1 h each. All extracts were combined and evaporated on a rotary evaporator. Finally, volatile oil of SCP and original liquid after concentrated were mixed and refrigerated at −20°C for usage.

### AD Model and Drug Treatments

Kun-Ming mice (8 weeks old) weighing 30–35 g were obtained from Sibeifu Biotechnology (Beijing, China) and housed at 22 ± 2°C, with a relative humidity of 55% ± 5%, a 12 h light/dark cycle and *ad libitum* access to food and water. All animal procedures were performed in accordance with the principles and guidelines of the National Institutes of Health Guide for the Care and Use of Laboratory Animals and approved by the Guangzhou University of Chinese Medicine Animal Ethics Committee.

AD model was induced by intraperitoneally injected SCOP (3 mg/kg) for a consecutively week. In this week, Morris water maze and new objection recognition test were performed daily after 30 min of SCOP injection to evaluate animal model. In this study: mice were randomly allotted to five groups: Control group (n=10; 0.9% saline p.o.+ 0.9% saline, i.p.), SCOP group (n=10; 0.9% saline p.o.+ SCOP 3 mg/kg/d i.p.), low-dose KXS group (n=10; KXS 1.4 g/kg/d p.o.+ SCOP 3 mg/kg/d i.p.), high-dose KXS group (n=10; KXS 2.8 g/kg/d p.o.+ SCOP 3 mg/kg/d i.p.), and Don group (n=10; donepezil 3 mg/kg/d p.o.+ SCOP 3 mg/

kg/d i.p.). The mice were orally administered 0.9% saline, KXS, or donepezil mice for 14 continuous days. Memory impairment was induced by SCOP treatment (3 mg/kg body weight) for 7 days.

### Western Blot Analysis

The hippocampus and cortex were homogenized in SDS lysis buffer containing a protease inhibitor and phosphatase inhibitor mixture (Sigma-Aldrich). After sonication, lysates were centrifuged at 3,000×g and 4°C for 15 min. Supernatants were collected, and protein concentrations were determined by the Bradford assay (Bio-Rad). The same amounts of proteins were resolved on SDS-PAGE gels, transferred to PVDF membranes (Millipore), and probed with primary antibodies overnight at 4°C. Rabbit anti-TNFRSF1A (1:1,000, Abcam), anti-CHRNB2 (1:1,000, Abcam), and anti-β-actin (1:10,000, Abcam) were used as the primary antibodies. Immunoblots were visualized by the ECL western blot detection kit (Millipore) and quantified by densitometry and ImageJ software (National Institutes of Health) (Lee et al., 2017).

### Immunofluorescence

Mice were transcardially perfused with 0.9% saline. The mouse brains were fixed in 4% paraformaldehyde (PFA) for 72 h, followed by dehydration with different concentrations of ethanol and paraffin embedding. A paraffin microtome was used to cut 5-μm-thick coronal brain sections.

For immunofluorescence, sections were deparaffinized by ethanol and incubated with 3% $H_2O_2$. Antigen retrieval was performed by heating the sections in sodium citrate buffer (10 mM trisodium citrate, 0.5% Tween-20 in $H_2O$, pH 6.0) at 70°C for 30 min. Sections were then permeabilized and incubated with blocking solution containing the Iba-1 antibody (1:100, Abcam) overnight at 4°C. The sections were then stained with a fluorophore-conjugated secondary antibody (1:1,000, CST) for 1 h, followed by 4′6-diamino- 2-phenylindole (DAPI, Sigma) staining for another 1 h. Images were acquired by a fluorescence microscope Model DMi8 (Leica, Germany) and quantified using ImageJ software (National Institutes of Health) (Muhammad et al., 2019).

### ELISA Analysis

Mice cortical and hippocampal tissues were sequentially homogenized in ice-cold PBS, and the supernatants were centrifuged at 21,000×g for 20 min at 4°C. The levels of IL-1β, IL-6, and TNF-α were measured using an enzyme-linked immunosorbent assay (ELISA, Biological Technology, Jiangsu) (Karthivashan et al., 2018) according to the manufacturer's instructions.

### Statistical Analysis

All data were expressed as means ± SEM of at least three independent experiments. Statistical analyses were performed using SPSS (version 20.0, IBM, Armonk, NY). Statistical tests between multiple datasets were carried using a one-way analysis of variance (ANOVA) followed by Dunnett's *post hoc* test to determine statistical significance, as appropriate. A $P$ value < 0.05 was considered statistically significant.

## RESULTS AND DISCUSSION

### Collection of Chemical Ingredients in KXS

In the present study, a total of 1,118 compounds in KXS were collected from specific TCM-relevant databases after removing the duplicate structures. The numbers of ingredients for each herb in KXS were 628 (RS), 237 (YZ), 119 (FL), and 210 (SCP). Among the 1,118 chemical ingredients, there were 70 compounds that existed in more than one herb. For example, compound M449 (palmitic acid) could be found in all four herbs in the KXS formula. Candidate ingredients were defined if there were known targets or putative targets *via* bSTDNBI for a certain ingredient. Ultimately, 1,113 candidate compounds were obtained (**Supplementary Datasheet S1**).

### Identification of Putative Targets for the Ingredients in KXS

After merging the known DTIs and predicted DTIs by bSTDNBI, we identified 439 target proteins for 1,113 candidate compounds. We further identified 39 AD-associated targets for KXS by overlapping 439 potential targets into the curated human AD-associated 447 genes. Detailed information of the 39 AD-associated targets can be found in **Supplementary Datasheet S1**.

### Analysis of the Synergetic Actions of KXS Against AD

The TCM theory "Jun-Chen-Zuo-Shi" serves as the guide for physicians when formulating herbal prescriptions. Among the herbs in KXS, RS and FL serve as the "Jun" and "Chen" herbs to treat the major symptoms and signs of AD, while YZ and SCP act as the "Zuo" and "Shi" herbs for improving the therapeutic effects of the "Jun" and "Chen" herbs and guiding the herbs to the disease targets (Cao et al., 2018a). Herein, we investigated the distribution of AD-relevant targets among the four herbs (18 from RS, 9 from FL, 16 from SCP, 15 from YZ) *via* a Venn analysis (**Supplementary Figure S1**).

The four herbs covered all 39 AD-associated targets (**Figure S1**). Among the four herbs, RS covered the largest number (18) of AD targets for the "Jun" herb in KXS for treating AD, demonstrating the consistency of TCM theory. To exploit the synergistic MOAs of the KXS formula at the individual herb level, we constructed a herb-target network (**Figure 2**, H-T network). We found that the four herbs in KXS shared six common targets, suggesting that KXS could exert its magnifying effects by targeting these key targets. These targets include acetylcholinesterase (ACHE), beta-secretase 1 (BACE1), hydroxysteroid 17-beta dehydrogenase 10 (HSD17B10), mitogen-activated protein kinase 1 (MAPK1), peroxisome proliferator-activated receptor gamma (PPARG), and tumor necrosis factor (TNF). BACE plays a key role in neurotoxic Aβ generation (Moussa-Pacha et al., 2019). Tumor necrosis factor-α (TNF-α) has been confirmed to advance Aβ production through

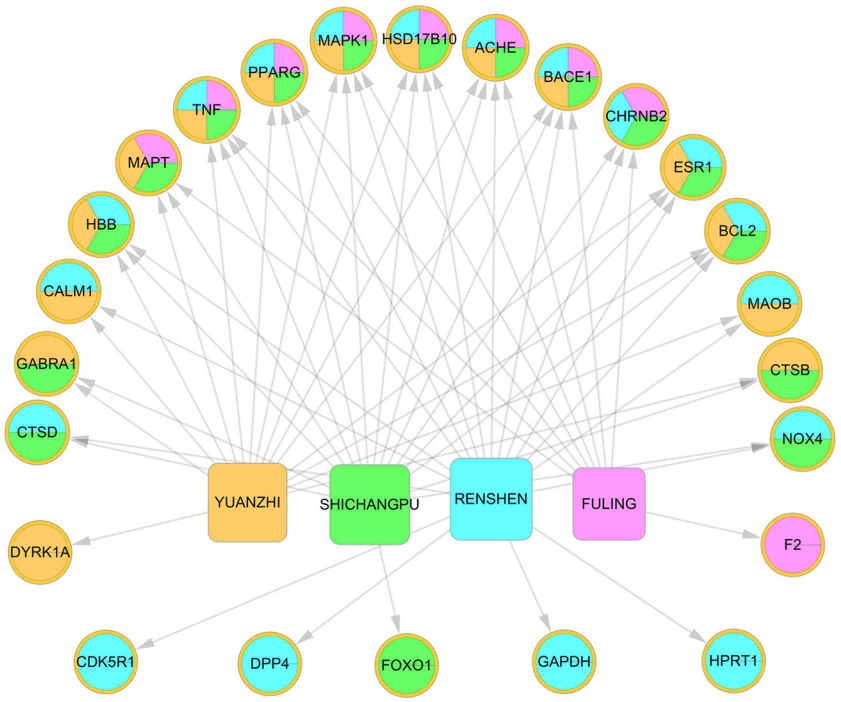


**FIGURE 2 |** Herb-target network of Kai-Xin-San (KXS). The ellipses represent the targets of KXS. The round rectangle indicates the herbs in KXS.

enhancing the expression of BACE1 and suppressing the clearance of Aβ (Yamamoto et al., 2007; Decourt et al., 2017). Moreover, ACHE regulates acetylcholine in the cholinergic system, which plays a role in the learning process in AD patients (Ferreira-Vieira et al., 2016). Therefore, it is likely that the four herbs in KXS are able to regulate several important AD-associated pathological processes to exert advanced or synergistic effects in AD intervention and treatment.

## Compound-Target (C-T) Network Analysis

To further decipher the therapeutic mechanism of KXS against AD, we constructed a AD-specific compound-target (C-T) network consisting of 1,936 C-T interactions (**Figure 3**). The C-T network comprises 40 known CTIs and 1,896 predicted CTIs connecting 1,021 compounds to 39 AD target proteins. Among the 1,021 ingredients, nine have a target degree (*N*) higher than five, including M909 (apigenin, *N*=9), M638 (4-aminobutyric acid, *N*=6), M326 (aspidinol, *N*=5), M429 (dodecanal, *N*=5), M621 (harmine, *N*=5), M8 (spinacen, *N*=5), and M903 (DL-catechin, *N*=5). For the 39 AD targets, five were targeted by more than 100 compounds (*D*): ACHE (*D*=454), MAPK1 (*D*=372), TNF (*D*=346), PPARG (*D*=261), and BACE1 (*D*=174). Previous studies have demonstrated that these targets are beneficial for AD patients. For example, inhibitors of ACHE (e.g., donepezil) can provide modest symptomatic relief for AD patients (Arvanitakis et al., 2019). Recently, both preclinical and clinical studies have indicated that PPARG agonists can improve learning and memory abilities in AD patients (Khan et al., 2019). BACE1 inhibitors have also been reported to repress the generation of neurotoxic amyloid protein (Dobrowolska Zakaria and Vassar, 2018; Moussa-Pacha et al., 2019). Overall, this AD-specific C-T network contributes to uncovering the MOA of chemicals in KXS against AD. The detailed information of the C-T network is provided in **Supplementary Datasheet S2**

## GO BP Enrichment Analysis

To illustrate the related signaling pathways involved in the treatment of AD with KXS, GO BP enrichment analysis was performed using ClueGO, a plug in of the Cytoscape software package. Only the top 20 significantly enriched (adjusted $P < 0.05$) signaling pathways were preserved for further analysis. Multiple signaling pathways were involved in the treatment of AD with KXS, including reactive oxygen species metabolic process, positive regulation of neuron death (apoptotic process), regulation of calcium ion transport into the cytosol, and nitric oxide biosynthetic process, etc. (**Figure 4**). These signaling pathways seem to play vital roles in AD-associated pathological processes. For instance, Aβ-induced neuron death is considered a central pathway in the pathogenesis of AD through oxidative stress, inflammation, apoptosis, or autophagy (Cao et al., 2018b; Kumar and Tsao, 2019).

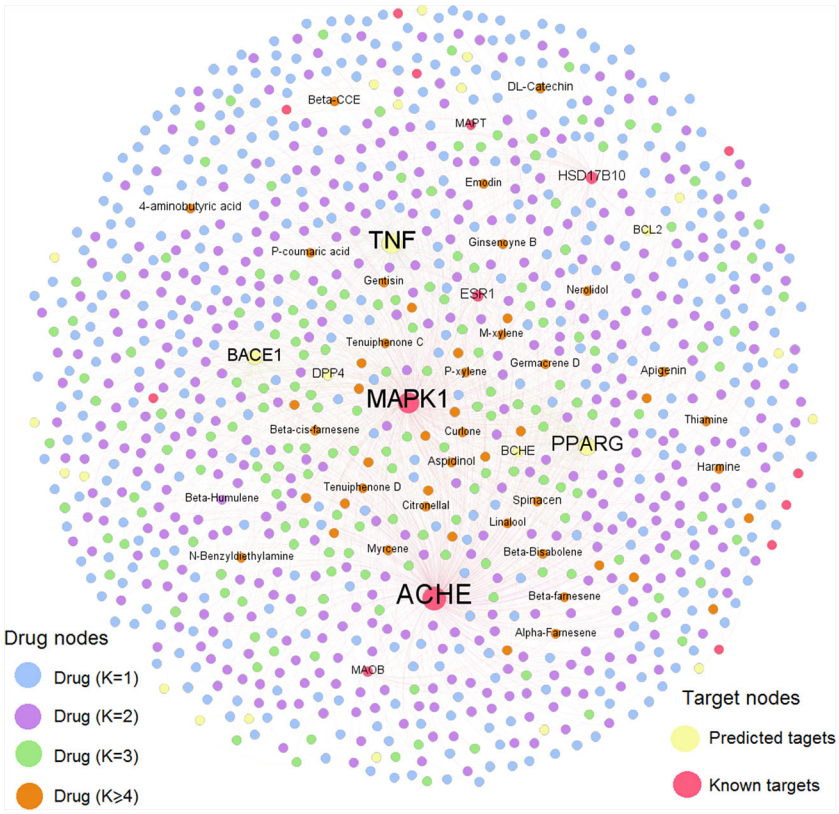


**FIGURE 3 |** Global compound-target network of the candidate ingredients of Kai-Xin-San (KXS).

## Integrated Pathway Analysis

In this analysis, pathways directly related to AD were incorporated into an "AD-integrated pathway" based on target identification for KXS and AD pathology, including the glucose homeostasis signaling pathway, ACHE-associated signaling pathway, Aβ-associated signaling pathway, tau hyperphosphorylated signaling pathway, and TNF-induced inflammation signaling pathway. As depicted in **Figure 5**, several pathophysiological modules were involved in this integrated pathway, such as glycolysis, cell death, survival, and synaptic plasticity. Here, four representative modules will be discussed to illustrate the underlying therapeutic mechanisms of KXS for AD treatment.

### Aβ-Associated Pathological Signaling Pathway Regulation Module

It is well known that abnormal Aβ aggregation and accumulation plays a critical role in the pathogenesis of AD. Amyloid precursor protein (APP) is cleaved by α-secretase, β-secretase, and γ-secretase *via* non-amyloidogenic and amyloidogenic pathways. In the non-amyloidogenic pathway, proteolysis of APP by α- and γ-secretases yields nonpathogenic fragments, including sAPPα and C-terminal fragments. However, the amyloidogenic pathway involves cleavage by β- and γ-secretases, leading to the production of sAPPβ, C-terminal fragments, and Aβs (Barage and Sonawane, 2015; Selkoe and Hardy, 2016). Accumulated Aβ can further directly or indirectly trigger other pathological processes, such as mitochondrial dysfunction and inflammation, inducing neuronal death in AD (Mao et al., 2012). Thus, targeting β- and γ-secretases is regarded as a primary therapeutic approach for reducing Aβ production in AD patients. As shown in **Figure 5**, KXS targets key proteins implicated in the Aβ-associated signaling pathway, including BACE1 (β-secretase 1), GAPDH (glycolytic glyceraldehyde-3-phosphate dehydrogenase), and SD17B10 (hydroxysteroid 17-beta dehydrogenase 10). GAPDH (glycolytic glyceraldehyde-3-phosphate dehydrogenase), an abundantly expressed oxidoreductase for glucose metabolism, has been reported to possess diverse non-glycolytic functions, including interaction with Aβ (El Kadmiri et al., 2014; Sen et al., 2018). Target prediction suggested that M693 (citric acid) could bind with GAPDH, which might alleviate Aβ accumulation by disturbing the cross-talk between Aβ and GAPDH (Gerszon and Rodacka, 2018). In addition, HSD17B10 (hydroxysteroid 17-beta dehydrogenase 10), a hydroxysteroid dehydrogenase localized in the mitochondria (He et al., 2018), was the potential target of the compounds in KXS, including M150, M388, and M500. This target has been recognized as a putative intracellular mediator of

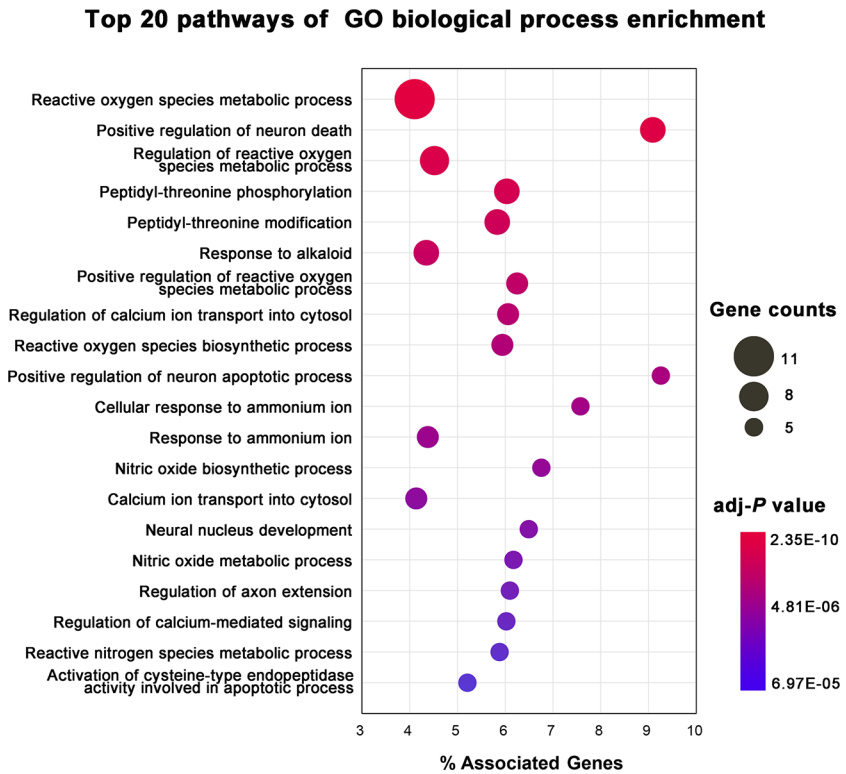


**FIGURE 4 |** Gene Ontology (GO) biological process enrichment analysis of targets of Kai-Xin-San (KXS) for the treatment of Alzheimer's disease (AD).

Aβ neurotoxicity *via* its dozen proteins that bind to Aβ (Reddy et al., 2012). Thus, KXS could disturb the combination of Aβ and HSD17B10 to alleviate mitochondria dysfunction as it activates β-secretase and γ-secretase and facilitates Aβ generation (Yang et al., 2014). Taken together, KXS might prevent and treat AD by regulating Aβ generation and aggregation.

## Neurofibrillary Tangles Regulation Module

NFTs (neurofibrillary tangles), aggregating by abnormal hyperphosphorylation of microtubule-associated protein tau (MAPT) in the brain, correlate well with the severity of cognitive deficits in AD patients (Simic et al., 2016; Jouanne et al., 2017). Tau protein can be hyperphosphorylated by various kinases including CDK5 (cyclin-dependent kinase 5) (Zhao et al., 2019) and GSK3B (glycogen synthase kinase 3beta) (Chu et al., 2017). Therefore, a reduction in tau protein levels (Wang and Mandelkow, 2015) as well as inhibition of tau protein hyperphosphorylation and aggregation are potential therapeutic avenues for AD treatment. As shown in **Figure 5**, KXS was predicted to target three crucial proteins (i.e., CDK5, GSK3B, and MAPT) involved in the regulation of NFTs. For example, the compounds M621, M622, and M909 were predicted to interact with CDK5 and GSK3B. Emerging evidence has revealed that inhibiting these kinases can prevent tau protein hyperphosphorylation and NFT formation (Congdon and Sigurdsson, 2018). Additionally, compounds such as M84, M257, and M686 were identified to bind to MAPT, suggesting that KXS might decrease tau protein levels to alleviate NFT formation and ameliorate Aβ-dependent neurotoxicity (Peters et al., 2019).

## Cholinergic System Dysfunction Regulation Module

The loss of cholinergic neurons in AD patients leads to learning and memory deficits (Ferreira-Vieira et al., 2016). Cholinesterase inhibitors can prevent the breakdown of acetylcholine and preserve its activity at cholinergic synapses (Hampel et al., 2018). **Figure 5** shows that the KXS formula regulates the cholinergic system signaling pathway by targeting ACHE (acetylcholinesterase) and CHRN2B (cholinergic receptor nicotinic beta 2 subunit). Four compounds, M21, M389, M597, and M944, interact with ACHE and CHRN2B, which might improve the level of acetylcholine and sustain its activity. Our previous study demonstrated that KXS could ameliorate cognitive function in SCOP-induced mice by regulating the cholinergic system through sustaining ACh levels, increasing ChAT activity, and decreasing AChE activity (Xu et al., 2019), which is in accordance with our systems pharmacology-based analysis.

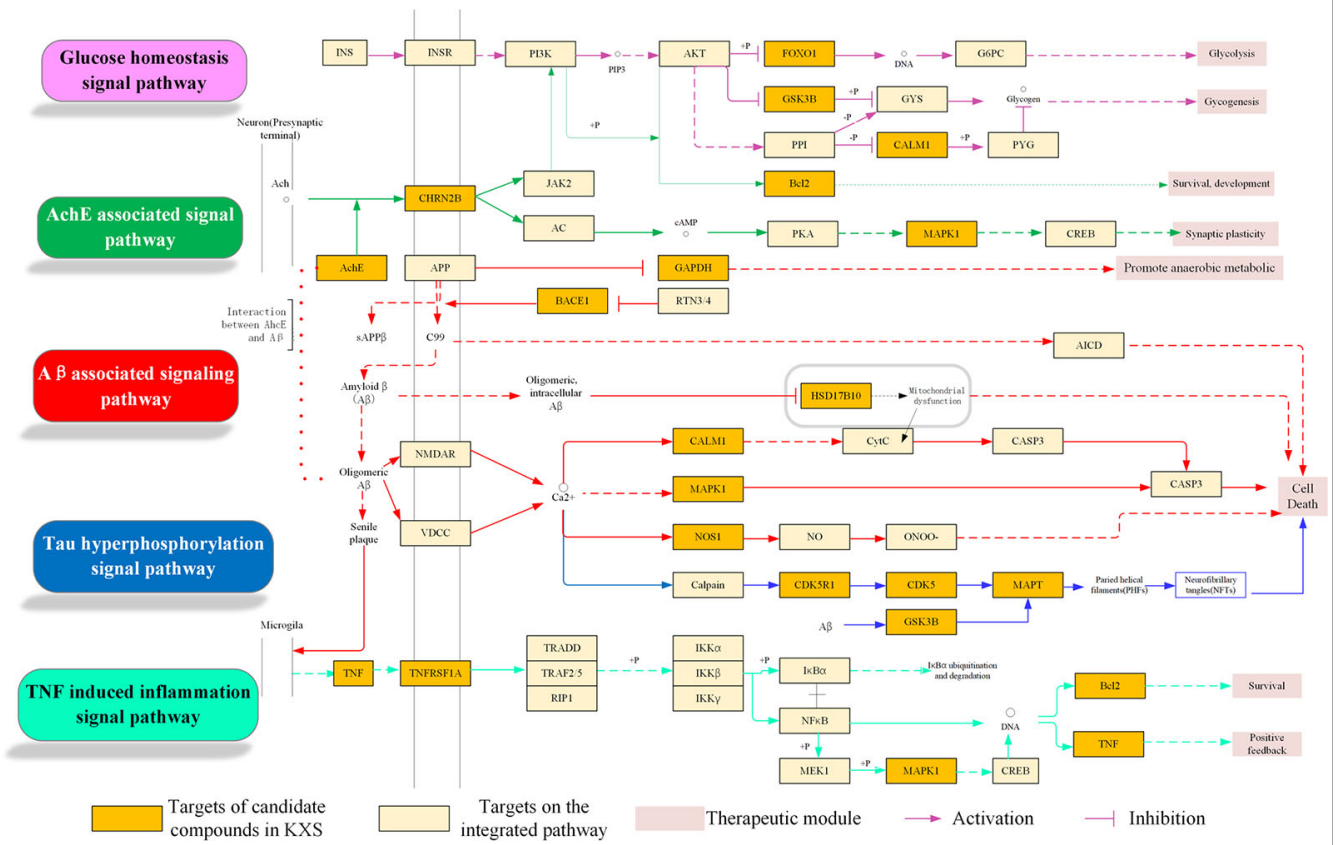


**FIGURE 5 |** Integrated Alzheimer's disease (AD)-pathway and Kai-Xin-San (KXS) action in the therapeutic modules.

### Neuroinflammation Regulation Module

Neuroinflammation refers to the inflammatory response in the central nervous system secondary to neuronal insult (Calsolaro and Edison, 2016). Activating microglia and astrocytes in AD leads to the production and release of inflammatory cytokines, including interleukin-6 (IL-6), interleukin-1β (IL-1β), and TNF-α (Heneka et al., 2015; Kinney et al., 2018; Ozben and Ozben, 2019). **Figure 5** suggests that KXS, a more specifically the compounds M230, M885, and M606, could modulate neuroinflammation in AD by regulating TNF-α and its receptor TNF-receptor superfamily 1A (TNFRSF1A). TNF-α can exacerbate Aβ burden by increasing γ-secretase activity and β-secretase production (Cheng et al., 2014; Chang et al., 2017) or bind to TNFRSF1A. This effect is partly mediated through MAPK1 signaling, which leads to the expression of molecules that participate in inflammation and amyloid genesis (Montgomery and Bowers, 2012; Decourt et al., 2017). Furthermore, IL-1β and IL-6 are able to enhance the amyloidogenic process of APP (Tachida et al., 2008) and the hyperphosphorylation of tau epitopes (Kitazawa et al., 2011). Suppression of either IL-1β or IL-6 can ameliorate neuroinflammation and neurodegeneration (Basu et al., 2004; Rothaug et al., 2016). In summary, KXS might prevent and treat AD by regulating neuroinflammation.

## Experimental Validation of KXS in SCOP-Induced Mice

### KXS Ameliorates Inflammatory Injury in SCOP-Induced Mice

The systems pharmacology analysis indicated that the therapeutic mechanism of KXS for AD involves several potential mechanisms, including the regulation of cholinergic system dysfunction and neuroinflammation.

Chronic neuroinflammation (sustained microglial activation and overproduction of pro-inflammatory cytokines) has been implicated in the pathophysiology of AD. To validate the mechanism of KXS on neuroinflammation *in vivo*, we measured proinflammatory cytokine levels in SCOP-induced mice treated with KXS. As shown in **Figure 6**, SCOP administration significantly increased the levels of TNF-α, IL-1β, and IL-6 compared to the non-treated control group ($P < 0.05$ or $P < 0.01$). However, KXS and Don significantly ($P < 0.05$) attenuated the upregulation of IL-1β, TNF-α, and IL-6 compared with the SCOP alone group both in the hippocampus and cortex.

TNFRSF1A is the main cell surface receptor for TNF. Next, we explored the expression of TNFRSF1A by western blotting. As shown in **Figure 7**, the protein expression of TNFRSF1A increased in the SCOP group in both the hippocampus and

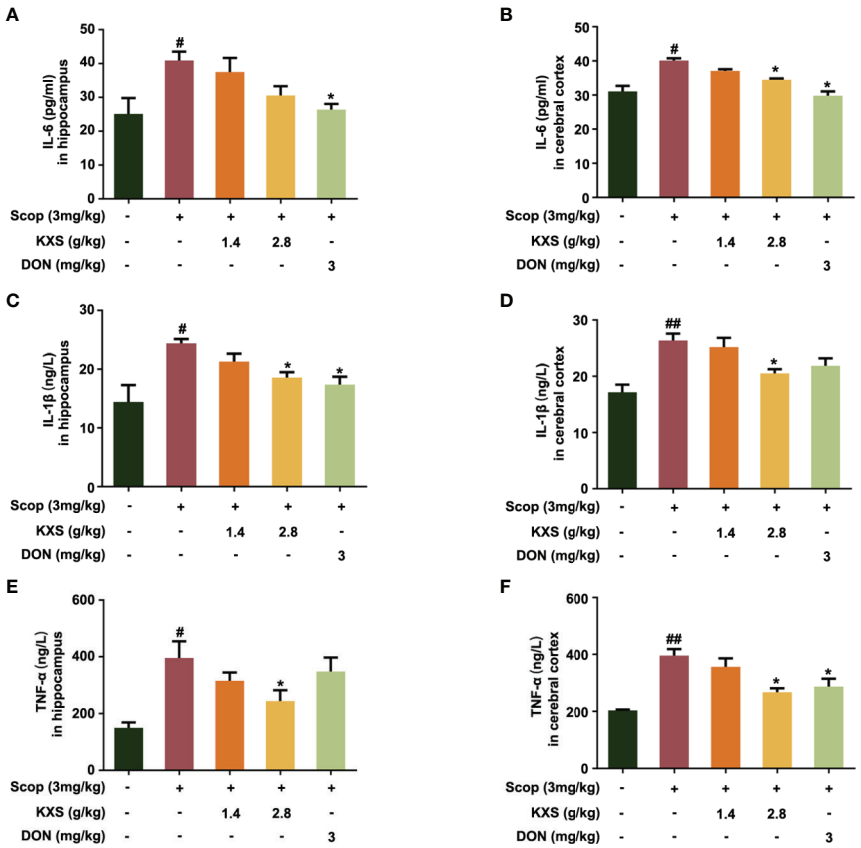


**FIGURE 6 |** Kai-Xin-San (KXS) attenuates inflammatory injury in scopolamine (SCOP)-induced mice. The levels of interleukin (IL)-6, IL-1β, and tumor necrosis factor (TNF)-α in the hippocampus **(A, C, E)** and cortex **(B, D, F)** were determined by ELISA. Data are expressed as means ± SEM. Difference was calculated using one-way ANOVA followed by Dunnett's *post hoc* test (n=5, $^{\#}P < 0.05$, $^{\#\#}P < 0.01$ the control group versus the SCOP group; $^{*}P < 0.05$ versus the SCOP group).

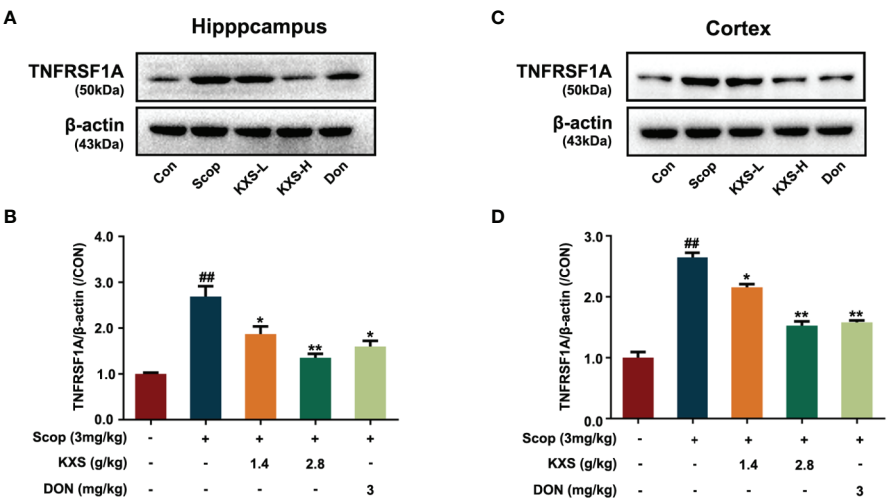


**FIGURE 7 |** Kai-Xin-San (KXS) decreases the protein expression of tumor necrosis factor receptor superfamily member 1A (TNFRSF1A) in scopolamine (SCOP)-induced mice. Western blot analysis showing the protein expression levels of TNFRSF1A in the hippocampus **(A)** and cortex **(C)**. Quantification of TNFRSF1A levels in panel **(A, B)** or **(C, D)** was normalized to that of actin. Data represent the means ± SEM (n=3, $^{\#\#}P < 0.01$ versus the control group; $^{*}P < 0.05$, $^{**}P < 0.01$ versus the SCOP group).

cortex ($P < 0.01$, vs. the control group). Both the low-dose and high-dose KXS groups and the DON wed group decreased TNFRSF1A expression ($P < 0.05$ or $P < 0.01$, vs. the SCOP group).

Microglia secrete a number of inflammatory cytokines including TNF-α, IL-1β, and IL-6 in response to inflammatory stimuli (Ozben and Ozben, 2019). To further probe the effect of KXS on neuroinflammation, we detected the expression of Iba-1, a microglia activation marker, in the hippocampus and cortex using immunofluorescence. As displayed in **Figure 8**, elevated microglia activation was observed in the SCOP group in the hippocampus (CA1) and cortex, whereas KXS and donepezil markedly attenuated microglia activation. These results demonstrate that KXS inhibits neuroinflammation in SCOP-induced mice

### KXS Attenuates Cholinergic System Dysfunction in SCOP-Induced Mice

In our previous study, we demonstrated that KXS could alleviate cholinergic system dysfunction in SCOP-induced mice by increasing ChAT activity and the Ach content, and decreasing AChE activity (Xu et al., 2019). However, the detailed mechanism remains unclear. In this study, a systems pharmacology-based analysis suggested that KXS could regulate the expression of the target protein CHRNB2 (a nicotinic acetylcholine receptor). CHRNB2 is lost in the brains of AD patients and knockout of the CHRNB2 gene impairs neuronal survival in aging (Cook et al., 2004). Therefore, we further investigated the effect of KXS on cholinergic dysfunction *via* CHRNB2 expression in SCOP-induced mice. As shown in **Figure 9**, SCOP significantly downregulated the expression of CHRNB2 compared to the control group in both the hippocampus and cortex ($P < 0.05$, $P < 0.01$, respectively). High-dose KXS and Donepezil remarkably increased the expression of CHRNB2 both in the hippocampus and cortex ($P < 0.05$, vs. the SCOP group). These data suggest that CHRNB2 may play an important role in the effects of KXS ameliorating cholinergic system dysfunction of SCOP-induced mice.

## CONCLUSION

To date, acetylcholinesterase inhibitors and NMDA receptor antagonists have been the primary choice for treating AD patients, showing marginal benefits for alleviating symptoms. The side effects are not ignorable and add to the ongoing AD burden. Therefore, it is urgent that novel and efficient curative remedies are discovered for AD patients. TCM efficacy in medical practice has been demonstrated for thousands of years. In contrast to western medicine, TCM formulas emphasize the regulation of interactions among all illness-associated elements within the abnormal body toward a

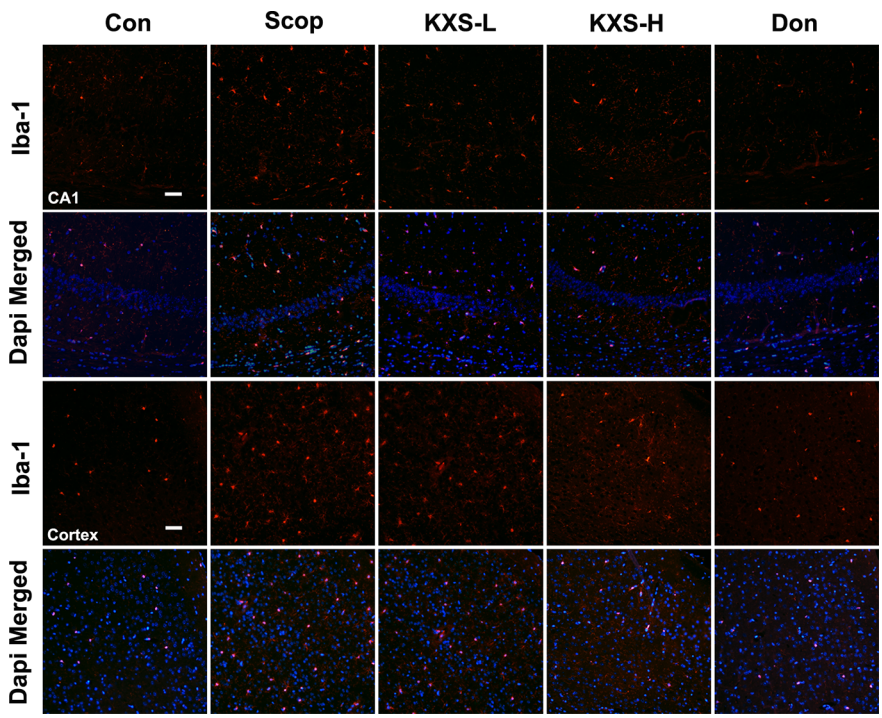


**FIGURE 8 |** Kai-Xin-San (KXS) attenuates microglia activation in scopolamine (SCOP)-induced mice. Immunofluorescence analysis in the hippocampus (CA1) and cortex. Microglia were stained with anti-Iba-1 (red) and the nuclei were stained with DAPI (blue). Scale bar: 50 μm. Con, control group; SCOP, scopolamine; KXS-L, low-dose Kai-Xin San (1.4 g/kg); KSX-H, high-dose Kai-Xin San (2.8 g/kg); Don, donepezil.

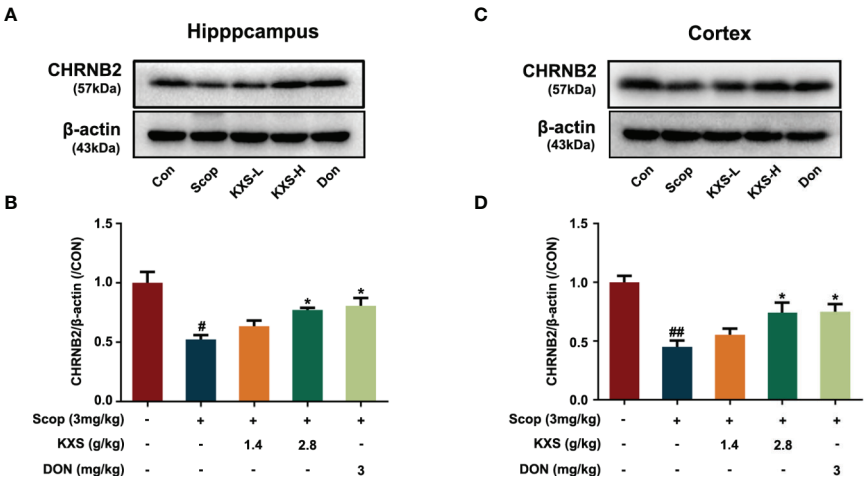


**FIGURE 9 |** Kai-Xin-San (KXS) increases the expression of nicotinic acetylcholine receptor beta 2 (CHRNB2) in scopolamine (SCOP)-induce mice. Western blot analysis of the protein expression of CHRNB2 in the hippocampus **(A)** and cortex **(C)**. Quantification of CHRNB2 level in panel **(A, B)** or **(C, D)** was normalized to that of actin. Data represent the means ± SEM (n=3, $^{\#}P < 0.05$, $^{\#\#}P < 0.01$ versus the control group; $^{*}P < 0.05$ versus the SCOP group).

balanced/normal condition. However, as TCM formulas contain hundreds of chemical components, the specific pharmacological mechanisms through which TCM prescriptions exert their effects against diseases are still difficult to illustrate.

KXS, a TCM formula that has been used for thousands of years in China to treat cognitive dysfunction, has been shown to improve learning and memory in animals studies. In this study, we developed an integrative systems pharmacology approach to illustrate the therapeutic mechanisms of KXS against AD. For the first time, we identified 39 AD-associated targets of KXS ingredients using known target mapping and *in silico* target prediction. Furthermore, we deciphered potential MOAs of KXS in AD treatment *via* a multiple data integration analysis, including an herb-target network analysis, compound-target network analysis, synergic action analysis, and integrated pathway analysis. Our systems pharmacology analysis was validated in *in vivo* experiments. The results showed that KXS could ameliorate cognitive dysfunction mainly through inhibiting the inflammation of microglia in SCOP-induced mice. More importantly, we found that the therapeutic effect of alleviating cholinergic system dysfunction involves the upregulation of the cholinergic receptor CHRNB2. Overall, these findings indicate that systems pharmacology could provide an alternative approach for exploring the complex MOAs of TCM and advance the comprehensive understanding of TCM.

## DATA AVAILABILITY STATEMENT

All datasets generated for this study are included in the article/**Supplementary Material**.

## ETHICS STATEMENT

The animal study was reviewed and approved by Guangzhou University of Chinese Medicine Animal Ethics Committee.

## AUTHOR CONTRIBUTIONS

SF and JF conceived and designed the experiments. YuL and DL conducted the experiments and wrote the manuscript. QWu, YaL, CC, HL, HH, YX and XL provided and analyzed some of the data. HK, QWa, JF, and SF reviewed and revised the manuscript.

## FUNDING

This work was supported by the National Natural Science Foundation of China (Nos. 81603318, 81673627, and 81904265), the Youth Scientific Research Training Project of GZUCM (No. 2019QNPY05), the Guangzhou Science Technology and Innovation Commission Technology Research Projects (No. 201805010005), and Key R & D and extension projects in Henan Province (No. 192102310166).

## SUPPLEMENTARY MATERIAL

The Supplementary Material for this article can be found online at: https://www.frontiersin.org/articles/10.3389/fphar.2020.00381/full#supplementary-material

**SUPPLEMENTARY DATASHEET S1 |** The detailed information of compounds of KXS and their corresponding targe.

**SUPPLEMENTARY DATASHEET S2 |** The detailed information of C-T network.

## REFERENCES


Arvanitakis, Z., Shah, R. C., and Bennett, D. A. (2019). Diagnosis and Management of Dementia: Review. *JAMA* 322, 1589–1599. doi: 10.1001/jama.2019.4782

Barage, S. H., and Sonawane, K. D. (2015). Amyloid cascade hypothesis: Pathogenesis and therapeutic strategies in Alzheimer's disease. *Neuropeptides* 52, 1–18. doi: 10.1016/j.npep.2015.06.008

Basu, A., Krady, J. K., and Levison, S. W. (2004). Interleukin-1: a master regulator of neuroinflammation. *J. Neurosci. Res.* 78, 151–156. doi: 10.1002/jnr.20266

Cai, H., Luo, Y., Yan, X., Ding, P., Huang, Y., Fang, S., et al. (2018). The Mechanisms of Bushen-Yizhi Formula as a Therapeutic Agent against Alzheimer's Disease. *Sci. Rep.* 8, 3104. doi: 10.1038/s41598-018-21468-w

Calsolaro, V., and Edison, P. (2016). Neuroinflammation in Alzheimer's disease: Current evidence and future directions. *Alzheimers Dement.* 12, 719–732. doi: 10.1016/j.jalz.2016.02.010

Cao, Y., Hu, Y., Liu, P., Zhao, H. X., Zhou, X. J., and Wei, Y. M. (2012). Effects of a Chinese traditional formula Kai Xin San (KXS) on chronic fatigue syndrome mice induced by forced wheel running. *J. Ethnopharmacol.* 139, 19–25. doi: 10.1016/j.jep.2011.08.030

Cao, C., Xiao, J., Liu, M., Ge, Z., Huang, R., Qi, M., et al. (2018a). Active components, derived from Kai-xin-san, a herbal formula, increase the expressions of neurotrophic factor NGF and BDNF on mouse astrocyte primary cultures via cAMP-dependent signaling pathway. *J. Ethnopharmacol.* 224, 554–562. doi: 10.1016/j.jep.2018.06.007

Cao, J., Hou, J., Ping, J., and Cai, D. (2018b). Advances in developing novel therapeutic strategies for Alzheimer's disease. *Mol. Neurodegener.* 13, 64. doi: 10.1186/s13024-018-0299-8

Chang, R., Yee, K.-L., and Sumbria, R. K. (2017). Tumor necrosis factor α Inhibition for Alzheimer's Disease. *J. Cent. Nerv. Syst. Dis.* 9, 1179573517709278. doi: 10.1177/1179573517709278

Chen, C. Y.-C. (2011). TCM Database@Taiwan: the world's largest traditional Chinese medicine database for drug screening in silico. *PloS One* 6, e15939. doi: 10.1371/journal.pone.0015939

Cheng, X., Shen, Y., and Li, R. (2014). Targeting TNF: a therapeutic strategy for Alzheimer's disease. *Drug Discovery Today* 19, 1822–1827. doi: 10.1016/j.drudis.2014.06.029

Chu, J., Lauretti, E., and Pratico, D. (2017). Caspase-3-dependent cleavage of Akt modulates tau phosphorylation via GSK3beta kinase: implications for Alzheimer's disease. *Mol. Psychiatry* 22, 1002–1008. doi: 10.1038/mp.2016.214

Congdon, E. E., and Sigurdsson, E. M. (2018). Tau-targeting therapies for Alzheimer disease. *Nat. Rev. Neurol.* 14, 399–415. doi: 10.1038/s41582-018-0013-z

Cook, L. J., Ho, L. W., Taylor, A. E., Brayne, C., Evans, J. G., Xuereb, J., et al. (2004). Candidate gene association studies of the alpha 4 (CHRNA4) and beta 2 (CHRNB2) neuronal nicotinic acetylcholine receptor subunit genes in Alzheimer's disease. *Neurosci. Lett.* 358, 142–146. doi: 10.1016/j.neulet.2004.01.016

Cooper, E. L., and Ma, M. J. (2017). Alzheimer Disease: Clues from traditional and complementary medicine. *J. Tradit. Complement Med.* 7, 380–385. doi: 10.1016/j.jtcme.2016.12.003

Decourt, B., Lahiri, D. K., and Sabbagh, M. N. (2017). Targeting Tumor Necrosis Factor Alpha for Alzheimer's Disease. *Curr. Alzheimer Res.* 14, 412–425. doi: 10.2174/1567205013666160930110551

Dobrowolska Zakaria, J. A., and Vassar, R. J. (2018). A promising, novel, and unique BACE1 inhibitor emerges in the quest to prevent Alzheimer's disease. *EMBO Mol. Med.* 10. e9717. doi: 10.15252/emmm.201809717

El Kadmiri, N., Slassi, I., El Moutawakil, B., Nadifi, S., Tadevosyan, A., Hachem, A., et al. (2014). Glyceraldehyde-3-phosphate dehydrogenase (GAPDH) and Alzheimer's disease. *Pathol. Biol.* (Paris) 62, 333–336. doi: 10.1016/j.patbio.2014.08.002

Fang, J., Wang, L., Wu, T., Yang, C., Gao, L., Cai, H., et al. (2017a). Network pharmacology-based study on the mechanism of action for herbal medicines in Alzheimer treatment. *J. Ethnopharmacol.* 196, 281–292. doi: 10.1016/j.jep.2016.11.034

Fang, J., Wu, Z., Cai, C., Wang, Q., Tang, Y., and Cheng, F. (2017b). Quantitative and Systems Pharmacology. 1. In Silico Prediction of Drug-Target Interactions of Natural Products Enables New Targeted Cancer Therapy. *J. Chem. Inf. Model* 57, 2657–2671. doi: 10.1021/acs.jcim.7b00216

Fang, J., Cai, C., Chai, Y., Zhou, J., Huang, Y., Gao, L., et al. (2019). Quantitative and systems pharmacology 4. Network-based analysis of drug pleiotropy on coronary artery disease. *Eur. J. Med. Chem.* 161, 192–204. doi: 10.1016/j.ejmech.2018.10.020

Ferreira-Vieira, T. H., Guimaraes, I. M., Silva, F. R., and Ribeiro, F. M. (2016). Alzheimer's disease: Targeting the Cholinergic System. *Curr. Neuropharmacol.* 14, 101–115. doi: 10.2174/1570159X13666150716165726

Gao, H. L., Zhang, A. H., Yu, J. B., Sun, H., Kong, L., Wang, X. Q., et al. (2018). High-throughput lipidomics characterize key lipid molecules as potential therapeutic targets of Kaixinsan protects against Alzheimer's disease in APP/PS1 transgenic mice. *J. Chromatogr. B. Analyt. Technol. BioMed. Life Sci.* 1092, 286–295. doi: 10.1016/j.jchromb.2018.06.032

Gaugler, J., and Al, E. (2019). 2019 Alzheimer's disease facts and figures. *Alzheimer's Dement.* 15, 321–387. doi: 10.1016/j.jalz.2019.01.010

Gerszon, J., and Rodacka, A. (2018). Oxidatively modified glyceraldehyde-3-phosphate dehydrogenase in neurodegenerative processes and the role of low molecular weight compounds in counteracting its aggregation and nuclear translocation. *Ageing Res. Rev.* 48, 21–31. doi: 10.1016/j.arr.2018.09.003

Hampel, H., Mesulam, M. M., Cuello, A. C., Farlow, M. R., Giacobini, E., Grossberg, G. T., et al. (2018). The cholinergic system in the pathophysiology and treatment of Alzheimer's disease. *Brain* 141, 1917–1933. doi: 10.1093/brain/awy132

He, M., Yan, X., Zhou, J., and Xie, G. (2001). Traditional Chinese Medicine Database and Application on the Web. *J. Chem. Inf. Comput. Sci.* 41, 273–277. doi: 10.1021/ci0003101

He, X. Y., Isaacs, C., and Yang, S. Y. (2018). Roles of Mitochondrial 17beta-Hydroxysteroid Dehydrogenase Type 10 in Alzheimer's Disease. *J. Alzheimers Dis.* 62, 665–673. doi: 10.3233/JAD-170974

Heneka, M. T., Carson, M. J., El Khoury, J., Landreth, G. E., Brosseron, F., Feinstein, D. L., et al. (2015). Neuroinflammation in Alzheimer's disease. *Lancet Neurol.* 14, 388–405. doi: 10.1016/S1474-4422(15)70016-5

Ho, Y. S., So, K. F., and Chang, R. C. (2010). Anti-aging herbal medicine–how and why can they be used in aging-associated neurodegenerative diseases? *Ageing Res. Rev.* 9, 354–362. doi: 10.1016/j.arr.2009.10.001

Huang Da, W., Sherman, B. T., and Lempicki, R. A. (2009). Systematic and integrative analysis of large gene lists using DAVID bioinformatics resources. *Nat. Protoc.* 4, 44–57. doi: 10.1038/nprot.2008.211

Jia, J., Wei, C., Chen, S., Li, F., Tang, Y., Qin, W., et al (2018). The cost of Alzheimer's disease in China and re-estimation of costs worldwide. *Alzheimers Dement.* 14, 483–491.

Jiang, Y., Gao, H., and Turdu, G. (2017). Traditional Chinese medicinal herbs as potential AChE inhibitors for anti-Alzheimer's disease: A review. *Bioorg. Chem.* 75, 50–61. doi: 10.1016/j.bioorg.2017.09.004

Jouanne, M., Rault, S., and Voisin-Chiret, A. S. (2017). Tau protein aggregation in Alzheimer's disease: An attractive target for the development of novel therapeutic agents. *Eur. J. Med. Chem.* 139, 153–167. doi: 10.1016/j.ejmech.2017.07.070

Karthivashan, G., Park, S. Y., Kweon, M. H., Kim, J., Haque, M. E., Cho, D. Y., et al. (2018). Ameliorative potential of desalted Salicornia europaea L. extract in multifaceted Alzheimer's-like scopolamine-induced amnesic mice model. *Sci. Rep.* 8, 7174. doi: 10.1038/s41598-018-25381-0

Khan, M. A., Alam, Q., Haque, A., Ashafaq, M., Khan, M. J., Ashraf, G. M., et al. (2019). Current Progress on Peroxisome Proliferator-activated Receptor Gamma Agonist as an Emerging Therapeutic Approach for the Treatment of Alzheimer's Disease: An Update. *Curr. Neuropharmacol.* 17, 232–246. doi: 10.2174/1570159X16666180828100002

Kim, S. K., Nam, S., Jang, H., Kim, A., and Lee, J. J. (2015). TM-MC: a database of medicinal materials and chemical compounds in Northeast Asian traditional medicine. *BMC Complement Altern. Med.* 15, 218. doi: 10.1186/s12906-015-0758-5

Kinney, J. W., Bemiller, S. M., Murtishaw, A. S., Leisgang, A. M., Salazar, A. M., and Lamb, B. T. (2018). Inflammation as a central mechanism in Alzheimer's disease. *Alzheimers Dement. (N Y)* 4, 575–590. doi: 10.1016/j.trci.2018.06.014

Kitazawa, M., Cheng, D., Tsukamoto, M. R., Koike, M. A., Wes, P. D., Vasilevko, V., et al. (2011). Blocking IL-1 signaling rescues cognition, attenuates tau

pathology, and restores neuronal beta-catenin pathway function in an Alzheimer's disease model. *J. Immunol.* 187, 6539–6549. doi: 10.4049/jimmunol.1100620

Kumar, A., and Tsao, J. W. (2019). "Alzheimer Disease," in *StatPearls* (Treasure Island (FL): StatPearls Publishing LLC).

Law, B. Y. K., Wu, A. G., Wang, M. J., and Zhu, Y. Z. (2017). Chinese Medicine: A Hope for Neurodegenerative Diseases? *J. Alzheimers Dis.* 60, S151–s160. doi: 10.3233/JAD-170374

Lee, S., Park, H. J., Jeon, S. J., Kim, E., Lee, H. E., Kim, H., et al. (2017). Cognitive Ameliorating Effect of Acanthopanax koreanum Against Scopolamine-Induced Memory Impairment in Mice. *Phytother. Res.* 31, 425–432. doi: 10.1002/ptr.5764

Liu, H., Wang, L., Lv, M., Pei, R., Li, P., Pei, Z., et al. (2014). AlzPlatform: an Alzheimer's disease domain-specific chemogenomics knowledgebase for polypharmacology and target identification research. *J. Chem. Inf. Model* 54, 1050–1060. doi: 10.1021/ci500004h

Lu, C., Shi, Z., Sun, X., Pan, R., Chen, S., Li, Y., et al. (2017). Kai Xin San aqueous extract improves Abeta1-40-induced cognitive deficits on adaptive behavior learning by enhancing memory-related molecules expression in the hippocampus. *J. Ethnopharmacol.* 201, 73–81. doi: 10.1016/j.jep.2016.10.002

Mao, P., Manczak, M., Calkins, M. J., Truong, Q., Reddy, T. P., Reddy, A. P., et al. (2012). Mitochondria-targeted catalase reduces abnormal APP processing, amyloid beta production and BACE1 in a mouse model of Alzheimer's disease: implications for neuroprotection and lifespan extension. *Hum. Mol. Genet.* 21, 2973–2990. doi: 10.1093/hmg/dds128

Masters, C. L., Bateman, R., Blennow, K., Rowe, C. C., Sperling, R. A., and Cummings, J. L. (2015). Alzheimer's disease. *Nat. Rev. Dis. Primers* 1, 15056. doi: 10.1038/nrdp.2015.56

Montgomery, S. L., and Bowers, W. J. (2012). Tumor necrosis factor-alpha and the roles it plays in homeostatic and degenerative processes within the central nervous system. *J. Neuroimmune Pharmacol.* 7, 42–59. doi: 10.1007/s11481-011-9287-2

Moussa-Pacha, N. M., Abdin, S. M., Omar, H. A., Alniss, H., and Al-Tel, T. H. (2019). BACE1 inhibitors: Current status and future directions in treating Alzheimer's disease. *Med. Res. Rev.* 40, 339–384. doi: 10.1002/med.21622

Muhammad, T., Ali, T., Ikram, M., Khan, A., Alam, S. I., and Kim, M. O. (2019). Melatonin Rescue Oxidative Stress-Mediated Neuroinflammation/Neurodegeneration and Memory Impairment in Scopolamine-Induced Amnesia Mice Model. *J. Neuroimmune Pharmacol.* 14, 278–294. doi: 10.1007/s11481-018-9824-3

O'boyle, N. M., Banck, M., James, C. A., Morley, C., Vandermeersch, T., and Hutchison, G. R. (2011). Open Babel: An open chemical toolbox. *J. Cheminf.* 3, 33. doi: 10.1186/1758-2946-3-33

Ozben, T., and Ozben, S. (2019). Neuro-inflammation and anti-inflammatory treatment options for Alzheimer's disease. *Clin. Biochem.* 72, 87–89. doi: 10.1016/j.clinbiochem.2019.04.001

Peters, F., Salihoglu, H., Pratsch, K., Herzog, E., Pigoni, M., Sgobio, C., et al. (2019). Tau deletion reduces plaque-associated BACE1 accumulation and decelerates plaque formation in a mouse model of Alzheimer's disease. *EMBO J.* 38, e102345. doi: 10.15252/embj.2019102345

Pinero, J., Bravo, A., Queralt-Rosinach, N., Gutierrez-Sacristan, A., Deu-Pons, J., Centeno, E., et al. (2017). DisGeNET: a comprehensive platform integrating information on human disease-associated genes and variants. *Nucleic Acids Res.* 45, D833–D839. doi: 10.1093/nar/ gkw943

Reddy, P. H., Tripathi, R., Troung, Q., Tirumala, K., Reddy, T. P., Anekonda, V., et al. (2012). Abnormal mitochondrial dynamics and synaptic degeneration as early events in Alzheimer's disease: implications to mitochondria-targeted antioxidant therapeutics. *Biochim. Biophys. Acta* 1822, 639–649. doi: 10.1016/j.bbadis.2011.10.011

Rothaug, M., Becker-Pauly, C., and Rose-John, S. (2016). The role of interleukin-6 signaling in nervous tissue. *Biochim. Biophys. Acta* 1863, 1218–1227. doi: 10.1016/j.bbamcr.2016.03.018

Ru, J., Li, P., Wang, J., Zhou, W., Li, B., Huang, C., et al. (2014). TCMSP: a database of systems pharmacology for drug discovery from herbal medicines. *J. Cheminf.* 6, 13. doi: 10.1186/1758-2946-6-13

Selkoe, D. J., and Hardy, J. (2016). The amyloid hypothesis of Alzheimer's disease at 25 years. *EMBO Mol. Med.* 8, 595–608. doi: 10.15252/emmm.201606210

Sen, T., Saha, P., and Sen, N. (2018). Nitrosylation of GAPDH augments pathological tau acetylation upon exposure to amyloid-beta. *Sci. Signal* 11, eaao6765. doi: 10.1126/scisignal.aao6765

Simic, G., Babic Leko, M., Wray, S., Harrington, C., Delalle, I., Jovanov-Milosevic, N., et al. (2016). Tau Protein Hyperphosphorylation and Aggregation in Alzheimer's Disease and Other Tauopathies, and Possible Neuroprotective Strategies. *Biomolecules* 6, 6. doi: 10.3390/biom6010006

Tachida, Y., Nakagawa, K., Saito, T., Saido, T. C., Honda, T., Saito, Y., et al. (2008). Interleukin-1 beta up-regulates TACE to enhance alpha-cleavage of APP in neurons: resulting decrease in Abeta production. *J. Neurochem.* 104, 1387–1393. doi: 10.1111/j.1471-4159.2007.05127.x

Wang, Y., and Mandelkow, E. (2015). Tau in physiology and pathology. *Nat. Rev. Neurosci.* 17, 22. doi: 10.1038/nrn.2015.1

Wang, N., Jia, Y. M., Zhang, B., Xue, D., Reeju, M., Li, Y., et al. (2017). Neuroprotective mechanism of Kai Xin San: upregulation of hippocampal insulin-degrading enzyme protein expression and acceleration of amyloid-beta degradation. *Neural Regener. Res.* 12, 654–659. doi: 10.4103/1673-5374.205107

Wu, Z., Lu, W., Wu, D., Luo, A., Bian, H., Li, J., et al. (2016). In silico prediction of chemical mechanism of action via an improved network-based inference method. *Br. J. Pharmacol.* 173, 3372–3385. doi: 10.1111/bph.13629

Xu, Y.-M., Wang, X.-C., Xu, T.-T., Li, H.-Y., Hei, S.-Y., Luo, N.-C., et al. (2019). Kai Xin San ameliorates scopolamine-induced cognitive dysfunction. *Neural Regener. Res.* 14, 794–804. doi: 10.4103/1673-5374.249227

Xue, R., Fang, Z., Zhang, M., Yi, Z., Wen, C., and Shi, T. (2013). TCMID: Traditional Chinese Medicine integrative database for herb molecular mechanism analysis. *Nucleic Acids Res.* 41, D1089–D1095. doi: 10.1093/nar/gks1100

Yamamoto, M., Kiyota, T., Horiba, M., Buescher, J. L., Walsh, S. M., Gendelman, H. E., et al. (2007). Interferon-gamma and tumor necrosis factor-alpha regulate amyloid-beta plaque deposition and beta-secretase expression in Swedish mutant APP transgenic mice. *Am. J. Pathol.* 170, 680–692. doi: 10.2353/ajpath.2007.060378

Yang, S. Y., He, X. Y., Isaacs, C., Dobkin, C., Miller, D., and Philipp, M. (2014). Roles of 17beta-hydroxysteroid dehydrogenase type 10 in neurodegenerative disorders. *J. Steroid Biochem. Mol. Biol.* 143, 460–472. doi: 10.1016/j.jsbmb.2014.07.001

Zhang, R. Z., Yu, S. J., Bai, H., and Ning, K. (2017). TCM-Mesh: The database and analytical system for network pharmacology analysis for TCM preparations. *Sci. Rep.* 7, 2821. doi: 10.1038/s41598-017-03039-7

Zhao, J., Li, X., Chen, X., Cai, Y., Wang, Y., Sun, W., et al. (2019). GRK5 influences the phosphorylation of tau via GSK3beta and contributes to Alzheimer's disease. *J. Cell Physiol.* 234, 10411–10420. doi: 10.1002/jcp.27709

Zhou, W., and Wang, Y. (2014). A network-based analysis of the types of coronary artery disease from traditional Chinese medicine perspective: potential for therapeutics and drug discovery. *J. Ethnopharmacol.* 151, 66–77. doi: 10.1016/j.jep.2013.11.007

**Conflict of Interest:** The authors declare that the research was conducted in the absence of any commercial or financial relationships that could be construed as a potential conflict of interest.

frontiers in Pharmacology

ORIGINAL RESEARCH
published: 28 April 2020
doi: 10.3389/fphar.2020.00526

# Kaempferol, a Major Flavonoid in Ginkgo Folium, Potentiates Angiogenic Functions in Cultured Endothelial Cells by Binding to Vascular Endothelial Growth Factor

*Wei-Hui Hu*[1,2,3†], *Huai-You Wang*[1,2†], *Yi-Teng Xia*[1,2], *Diana Kun Dai*[1,2], *Qing-Ping Xiong*[2,4], *Tina Ting-Xia Dong*[1,2], *Ran Duan*[1,2], *Gallant Kar-Lun Chan*[1,2], *Qi-Wei Qin*[3] *and Karl Wah-Keung Tsim*[1,2*]

[1] *Shenzhen Key Laboratory of Edible and Medicinal Bioresources, The Hong Kong University of Science and Technology, Nanshan, Shenzhen, China,* [2] *Division of Life Science and State Key Laboratory of Molecular Neuroscience, The Hong Kong University of Science and Technology, Hong Kong, Hong Kong,* [3] *Joint Laboratory of Guangdong Province and Hong Kong Region on Marine Bioresource Conservation and Exploitation, College of Marine Sciences, South China Agricultural University, Guangzhou, China,* [4] *Jiangsu Key Laboratory of Regional Resource Exploitation and Medicinal Research, Huaiyin Institute of Technology, Jiangsu, China*

Kaempferol is a major flavonoid in Ginkgo Folium and other edible plants, which is being proposed here to have roles in angiogenesis. Angiogenesis is important in both physiological and pathological development. Here, kaempferol was shown to bind with vascular endothelial growth factor (VEGF), probably in the heparin binding domain of VEGF: this binding potentiated the angiogenic functions of VEGF in various culture models. Kaempferol potentiated the VEGF-induced cell motility in human umbilical vein endothelial cells (HUVECs), as well as the sub-intestinal vessel sprouting in zebrafish embryos and formation of microvascular in rat aortic ring. In cultured HUVECs, application of kaempferol strongly potentiated the VEGF-induced phosphorylations of VEGFR2, endothelial nitric oxide synthase (eNOS) and extracellular signal-regulated kinase (Erk) in time-dependent and concentration-dependent manners, and in parallel the VEGF-mediated expressions of matrix metalloproteinases (MMPs), MMP-2 and MMP-9, were significantly enhanced. In addition, the potentiation effect of kaempferol was revealed in VEGF-induced migration of skin cell and monocyte. Taken together, our results suggested the pharmacological roles of kaempferol in potentiating VEGF-mediated functions should be considered.

**Keywords: kaempferol, *Ginkgo biloba*, VEGF, angiogenesis, herbal medicine**

OPEN ACCESS

***Edited by:***
*Aiping Lu,*
*Hong Kong Baptist University, Hong Kong*

***Reviewed by:***
*Hossein Hashempour, Azarbaijan Shahid Madani University, Iran*
*Xiujuan Li, Soochow University, China*

****Correspondence:***
*Karl Wah-Keung Tsim*
*botsim@ust.hk*

*†These authors have contributed equally to this work*

***Specialty section:***
*This article was submitted to Ethnopharmacology, a section of the journal Frontiers in Pharmacology*

***Received:*** *20 December 2019*
***Accepted:*** *03 April 2020*
***Published:*** *28 April 2020*

***Citation:***
*Hu W-H, Wang H-Y, Xia Y-T, Dai DK, Xiong Q-P, Dong TT-X, Duan R, Chan GK-L, Qin Q-W and Tsim KW-K (2020) Kaempferol, a Major Flavonoid in Ginkgo Folium, Potentiates Angiogenic Functions in Cultured Endothelial Cells by Binding to Vascular Endothelial Growth Factor. Front. Pharmacol. 11:526. doi: 10.3389/fphar.2020.00526*

## INTRODUCTION

It has been proved that angiogenesis is defined by the formation of new vessels from pre-existing blood vessels in the blood vascular system (Folkman and D'Amore, 1996), which is contributing a number of physiologic and pathologic processes, including wound healing, embryo development, malignancy, and chronic inflammation (Folkman, 1995; Carmeliet and Jain, 2000). The process of vessel formation is highly dynamic and complicated, which controls a large quantity of pro-angiogenic molecules and/or anti-angiogenic molecules (Rafii et al., 2002). Several steps are required during angiogenesis, including endothelial cell proliferation and migration, sequential degradation of basement membrane, and new vessel stabilization: the modulation of these steps potentiates, or suppresses, new blood vessel formation. A large number of growth factors and related receptors focusing on angiogenesis have been identified. Among these known angiogenic factors, vascular endothelial growth factor (VEGF) is a major regulator of angiogenesis acting as a major pro-angiogenic factor (Ferrara, 1996). VEGF has six members, i.e. from VEGF-A to VEGF-E and placenta growth factor. By binding to its receptors, i.e. from VEGF receptor 1 (VEGFR1) to VEGFR3, the VEGF members are responsible for the regulation of vascular functions. VEGF-A (corresponding to VEGF thereafter) and VEGFR2 are major players in angiogenesis.

Angiogenesis plays vital role in providing tissue regeneration, or sites of repair, with sufficient amounts of nutrient, oxygen and various growth factor: this process is also pre-requisite of removing waste products (Griffith and Naughton, 2002). Speeding up the angiogenic process should be an excellent way to repair tissue damages, e.g. caused by ischemia, and which therefore provides a strong support to development of therapeutic neovascularization (Timar et al., 2001; Emanueli and Madeddu, 2005). In having growth factor as therapeutic agent, the pharmacological activity of growth factor however fails to last very long *in vivo* due to its poor stability, especially those protein-type growth factors. Besides, the injection of high doses of protein-type angiogenic factors might induce side effects. Thus, the search on natural compounds having regulatory roles in angiogenesis could be a possible direction.

Traditional Chinese medicine (TCM) is an excellent source in finding new therapies for different diseases. Ginkgo Folium is a commonly used medicinal herb, which is known to contain a rich source of flavonoidic compounds. Kaempferol, named 3,4′,5,7-tetrahydoxyflavone, is highly enriched in Ginkgo Folium, and indeed this flavonoid is serving as one of the indicative chemicals in assessing quality of Ginkgo Folium, according to Chinese Pharmacopoeia (2015). Kaempferol has been demonstrated to have pharmacological activities, e.g. reducing mortality caused by coronary heart disease and decreasing myocardial infarction incidence (Hertog et al., 1993), inducing antioxidant activities by promoting expression of enzymes related with antioxidant effects (dismutase, heme oxygenase-1 and catalase) (Lin et al., 2003; Hong et al., 2009), inhibiting NF-κB activity for anti-inflammation effects (Wang et al., 2006), inducing osteoblastic differentiation (Guo et al., 2012), and weakening the damage of cigarette smoke in promoting immortalized lung epithelial cell growth (Puppala et al., 2007).

By using HerboChips as a drug screening platform, we have identified polydatin (Hu et al., 2019a) and resveratrol (Hu et al., 2019b) for its binding to VEGF; both of them are deriving from a TCM herb, Polygoni Cuspidati Rhizoma et Radix (Hu et al., 2018). The high affinity binding of polydatin and/or resveratrol to VEGF suppressed the angiogenic effects of VEGF, i.e. decreased the binding of VEGF to its receptors. In the screening of HerboChips, Ginkgo Folium was identified to be one of the positive hits in binding to VEGF. Further screening and fractionation of Ginkgo Folium, kaempferol was identified to bind VEGF; however, this binding, in contrast to polydatin and resveratrol, increased the angiogenic effects of VEGF both *in vitro* and *in vivo*. In this study, we revealed the pharmacological properties of kaempferol in affecting the signaling triggered by VEGF.

**Abbreviation:** MMP-2, matrix metalloproteinase-2; MMP-9, matrix metalloproteinase-P; Erk, extracellular signal-regulated kinase; eNOS, endothelial nitric oxide synthase; GAPDH, glyceraldehyde 3-phosphate dehydrogenase; VEGF, vascular endothelial growth factor; VEGFR1, VEGF receptor 1; VEGFR2, VEGF receptor 2; VEGFR3, VEGF receptor 3; HUVECs, human umbilical vein endothelial cells.

## MATERIALS AND METHODS

### Cell Lines and Chemicals

Human umbilical vein endothelial cells (HUVECs) were bought from Lonza (San Diego, CA): cell passages from three to six were used. Endothelial cells were cultured in EGM-2® BulletKit media according to the instructions (Lonza). RAW 264.7 cells were from American Type Culture Collection (ATCC, Manassas, VA) and human keratinocyte cell line (HaCaT) was obtained from Cell Lines Service (Heidelberg, Germany). RAW 264.7 cells were cultured in Dulbecco's modified Eagle's medium supplemented with 1% streptomycin, 1% penicillin, and 10% heat in-active fetal bovine serum (FBS), while HaCaT cells were cultured in Dulbecco's modified Eagle's medium added with 1% streptomycin, 1% penicillin, and 10% FBS. HUVECs, RAW264.7 cells, and HaCaT cells were maintained in a humidified atmosphere supplying 5% $CO_2$ and the temperature was set at 37°C. Human protein ($VEGF_{165}$) was recombinant and was obtained from R&D systems (Minneapolis, MN) and the following antibodies: matrix metalloproteinase (MMP)-2, MMP-9, phospho-p44/42 MAPK [extracellular signal-regulated kinase (Erk) 1/2] (Thr202/Tyr204), p44/42 MAPK (Erk1/2), phospho-endothelial nitric oxide synthase (eNOS) (Ser1177), and eNOS were from Cell Signalling Technology (Danvers, MA); glyceraldehyde 3-phosphate dehydrogenase (GAPDH) antibody and dexamethasone were purchased from Sigma-Aldrich (St. Louis, MO). Kaempferol was supplied by Testing Laboratory for Chinese Medicine of HKUST, and its purity was more than 98% analyzed by HPLC-DAD. For preparation of a stock solution of kaempferol, it was freshly dissolved in dimethyl sulfoxide (DMSO) with the concentration set at 100 mM.

## Immunoprecipitation Assay

Kaempferol solution (100 μl), at a concentration of 0.5 μM, was reacted with protein or biotinylated protein with or without heated at 95°C for 10 min. The reaction lasted for 1 h at 4°C. Then, the reacted solution was independently reacted with 100 μl of PureProteome Streptavidin Magnetic Beads. The binding reaction lasted for 24 h at 4°C. A magnetic stand was used to make the beads gathered at the magnet. Then, without touching the beads, the supernatant was gently gathered, and the VEGF complex and biotin-labeled VEGF complex were separately precipitated with acetonitrile (ACN) after washed with PBS solution for three times. The solution was injected into UPLC instrument equipped with an Agilent, Grace VisionHT C18 column (4.6 × 250 mm, 5 μm) to measure kaempferol's amount. The mobile phase was optimized as below: A, 0.1% formic acid in ACN; B, 0.2% diluted aqueous formic acid, and the optimized gradient elution was as followed: Solvent A was gradually increased from 8% to 18% by 12 min, from 18% to 24% by 24 min, from 24% to 25% by 5 min, from 25% to 40% by 15 min and finally increased from 40% to 75% by 96 min. The determined flow rate was 1 ml/min and the sample volume for injection was 10 μl. The sample temperature was maintained at room temperature. The column temperature was at 30°C. The wavelength of detector was at 360 nm.

The mass spectrometric detection was performed together with a Synapt™ quadrupole time-of-flight (Q-TOF) High-Definition Mass Spectrometer (Waters), equipped with an electrospray ionization source operated under positive ionization mode. The mobile phase consisted of 0.1% formic acid in ACN (A) and 0.2% diluted aqueous formic acid (B). The linear gradient of solvent was same as UPLC analysis, and there were two cycles of weak (90% ACN) and strong (20% ACN) solvent washing of the injecting system between different injections. The mass spectrometric parameters were determined as follows: capillary voltage, 2.5 kV; sample cone, 25 V; extraction cone, 4.0 V; source temperature, 120°C; and desolvation temperature at 350°C. Nitrogen was used in desolvation, and a cone gas was determined at a flow rate of 600 and 50 L/h, respectively. Argon acted as a collision gas. The sample was scanned and analyzed in full-scan mode with m/z set from 80 to 800 in 1-s scan interval. The sample was scanned and analyzed in full-scan mode with m/z set from 80 to 800 in 1-s scan interval in high-resolution mode.

## Molecular Docking

Protein (VEGF) structure was downloaded from Protein Data Bank (PDB), and kaempferol (PubChem: 5280863) was from NCBI-PubChem database. Before analysis, the structure of kaempferol was shifted into MOL2 mode with Chemoffice 2014 software (Cambridge Soft, Cambridge, MA), and the docking analysis was performed based on kaempferol-VEGF protein model. 40 × 40 × 40 Å grid points, as affinity (grid) maps, along with x, y, and z as well as 0.375 Å spacing, were optimized by application of AutoGrid program. The box center was optimized. The value of x was: 0.38 Å, y was −2.98 Å and z was 20.51 Å (Morris et al., 1998). The majority of binding modes were produced for possible bindings, and the energies could be roughly estimated (Grosdidier et al., 2011). The binding interactions were run using vina software; while values representing binding intensity were demonstrated under a PyMOL molecular graphic system.

## Cell Viability Assay

The 3-(4,5-dimethylthiazol-2-yl)-2,5-diphenyltetrazolium bromide (MTT) assay was firstly used to determine working concentration of kaempferol on cells. In short, HUVECs were seeded into each well of a sterile 96-well plate with density set at $5 \times 10^3$/well. After HUVECs treated with drugs for 48 h, MTT solution with concentration set at 5 mg/ml was freshly prepared, and 10 μl of MTT solution was used for each well. The viability of cells was determined (Hu et al., 2019a; Hu et al., 2019b). An assay to determine the release of LDH was performed by applying a cytotoxicity detection kit plus (LDH) (Roche Diagnostics, Indianapolis, IN) with referring to the instructions with the kit. To measure the LDH content of each group, the formula as followed was used: Cytotoxicity (%) = (experimental value − low control)/(high control − low control) × 100.

## Endothelial Cell Migration Assay

To determine the migration ability of cells *in vitro*, a wound-healing assay was performed (Hu et al., 2019a; Hu et al., 2019b). Briefly, $20 \times 10^4$ HUVECs in 1,000 μl of medium were plated onto each well of a sterile 12-well plate. After cells seeded for 24 h, with using a 200-μl pipette tip, a single wound was straightly made in the center of cell monolayer, and each well was rinsed with phosphate-buffered saline (PBS) which was pre-warmed to remove attached cells. Then, photos were captured under a phase-contrast microscope ($A_{t0}$). The treatment of drugs lasted for 8 h and after drug treatment, three scratched areas in each well were selected freely and taken pictures ($A_{t8}$). Finally, the wound area of endothelial cells before and after treatments of drugs was determined using Tscratch software (CSE lab, Switzerland). The recovery percentage of cells was quantized based on the formula as below: Recovery (%) = $A_{t0} - A_{t8}/A_{t0} \times 100\%$.

## Tube Formation Assay

Tube formation assay was performed according to previous descriptions (Ashton et al., 1999; Hu et al., 2019a). Briefly, 24-well-plate was firstly covered by matrigel, and which was firstly allowed to polymerize for 1 h at 37 °C. Upon matrigel was polymerized, cell cultures treated by VEGF (5 ng/ml) or kaempferol were placed onto each well pre-treated with matrigel. The density of cells was $20 \times 10^4$ cells/well. Medicine treatment was taken at 37°C and lasted for 8 h. After incubated with drugs, images of structures similar to tubes in each well were taken under a phase-contrast microscope. Pictures in control group and other groups treated by drugs were quantified according to the junction points. Branching points were counted manually.

## Zebrafish Angiogenesis Assay

Zebrafishes were fed in an environment supplied with flow water and regular aeration and the temperature was 28.5°C. The system was maintained at a cycle of 10 h: 14 h of dark/light. The

experimental conduction on zebrafish was performed strictly following the requirements and guidelines of Animal and Plant Care Facility, approval by Animal Ethics Committee of HKUST. Following previous experience, healthy embryos were picked (Hu et al., 2019a; Hu et al., 2019b). Dechlorinated embryos were kept in a 12-well plate. After dechlorinated, 8~10 embryos were placed in each well and freely divided into different groups. Embryos were treated with water containing VEGF or kaempferol or their combination. After incubated with drugs for 48 h, to check viability, eyes and morphological characteristics of embryos were observed. Next, paraformaldehyde (4%) was used to fix the embryos at 4°C, and fixation reaction lasted for 20 h. Then the embryos were washed by PBS with 0.1% Tween-20 solution (PBST), 50% methanol and methanol. Each time lasted for 5 min. After rinsed, samples were kept in methanol and stored at −20°C. Then, by using PBST solution, embryos underwent rinsed continuously for another four times, again, each time lasted for 5 min. To begin with alkaline phosphatase-based vascular staining assay, samples were immersed in buffer 9.5T and then kept in nitro-blue tetrazolium/5-bromo-4-chloro-3-indolyl-phosphate (NBT/BCIP) (Cell Signalling Technology). To remove the interference of NBT/BCIP, after staining, the embryos were washed with PBST until the solution was clear. Finally, pictures representing sub-intestinal vessels were captured by a digital camera (Olympus DP71) under a stereomicroscope (Nikon AZ100). The quantification of the areas and branches vessels in sub-intestinal parts was performed by using an ImageJ software.

## Aortic Ring Sprouting Assay

The kaempferol-potentiated VEGF-triggered micro-vessel outgrowth was assessed by performing aortic ring sprouting experiments with minor modifications (Nicosia and Ottinetti, 1990). Briefly, thoracic aortas were gently dissected from Sprague-Dawley rats (6-week-old), and the tissue was washed by PBS which was pre-warmed. With application of small scissors, the fibroadipose tissue around the aorta was cut off, and the aortas were gently cut into pieces of fragments with thick set at 1-mm under a microscope. Then, the fragments were placed into a 24-well plate precoated with matrigel (200 µl). To cover aortic fragments, another 100 µl of matrigel was added into each well. After matrigel polymerized and solidified for 1 h, 500 µl medium containing VEGF and different concentrations of kaempferol were used treat the fragments. Avastin, at a concentration of 200 µg/ml and serving as a control, was used to treat aortic fragments. After medicine treatment lasted for 8 days, pictures of aortic fragments were taken under a phase-contrast microscope. An ImageJ software was used to perform the quantification of sprouting area of microvessels.

## Western Blot Analysis

Western blotting test was performed to determine the expression levels of some key proteins, including MMP-2, MMP-9 as well as phosphorylated p44/42 MAPK (Erk1/2), eNOS (S1177)VEGFR1 (Y103), and VEGFR2 (Tyr1175). Prior to drug treatment, basal medium without serum was used to treat cells for 1 h. After treatment of drugs, aspiration of medium was performed and subsequently, cultures were lysed in freshly made low-salt lysis buffer (2% SDS, 200 mM 2-mercaptoethanol, 10% glycerol, 125 mM Tris–HCl, pH 6.8), and the samples were transferred into centrifuge tubes. The cell lysates in tubes were boiled at 95°C for three times, each for 5 min. The protein extracts were analyzed and separated by applying 7% or 8% acrylamide gel electrophoresis. Protein transferring reaction was taken at 4°C and nitrocellulose membranes was used here. Then, blocking reaction was taken for 60 min at room temperature by using 5% milk, which was prepared in a Tris-buffered saline containing 0.1% TBST. The membranes were immersed in primary antibody at 4°C. All primary antibodies used were diluted 1,000×, and the membranes were incubated with primary antibodies for 24 h. After incubated with primary antibody, membranes were washed and then subjected to react with horseradish peroxidase-conjugated secondary anti-rabbit antibody. Here, the secondary antibody was diluted at 1:2,000. After reacted with secondary antibody for 2 h, membranes were rinsed by TBST solution for four times, and each time lasted for 5 min. By dropping ECL (Invitrogen), the reactive bands in membrane were visualized. Pictures representing reactive bands were obtained by using Chemidoc Imaging System (Bio-Rad; Hercules, CA). The band intensities of control group and drug-treated groups, run on the same piece of gel and taken pictures under standardized ECL conditions, were analyzed and went on comparison by using the related software, which were performed based on a calibration plot from a parallel gel with one of the samples, diluted at a series of different ratios. To quantify Western blot in phosphorylation in each group, the band at 10 min for each group was compared with the band at 0 min after comparison with its corresponding total protein. Then, each group was compared with the control group.

## Fluorescence Intensity Analysis

HUVEC cells ($20 \times 10^4$) were plated into each well of a sterile 12-well plate. After cultured for 24 h, fresh medium supplemented with 5 ng/ml biotinylated VEGF, or together with kaempferol was used to treat cells. The group incubated with fresh medium only served as a background control. Drug treatment lasted for 24 h at 37°C, Then, to hybridize with the biotinylated VEGF, Streptavidin-Cy5™ was added into cultures, and the hybridization reaction lasted for 60 min at 37°C. After rinsed, cultures were under fixation in ethanol, and images were captured under a laser confocal fluorescent microscopy. The fluorescence intensity of each photo was quantified with application of relevant software.

## Skin Cell Migration Assay

A cell migration assay was used to determine wound recovery of skin cell *in vitro* by using HaCaT cells. Briefly, $50 \times 10^4$ HaCaT cells were seeded into each well of a sterile 6-well plate. After cells allowed to grow to a confluent monolayer, a scrape was performed in the middle of each well with application of a sterile P200 micropipette tip. At different time of drug treatment (0 and 16 h), pictures of wound area in each well were taken by using a phase-contrast microscope with randomly determined six points per well. The wound area was then analyzed with application of Image J software. The relative wound area was

obtained by calculation of dividing the change in the wound area of drug-treated group by that of the control group without drug treatment in each experiment.

## Monocyte Cell Migration Assay

A cell migration assay was performed to determine wound recovery of monocyte cell *in vitro* by using murine RAW 264.7 macrophages. Briefly, $60 \times 10^4$ macrophages were seeded into each well of a 12-well plate. After cells growing to a 90% confluence, a scrape was performed in the center of the monolayer in each well by using a sterile P200 micropipette tip. At different time of drug treatment (0 and 24 h), pictures of wound area in each well were taken by using a phase-contrast microscope with randomly determined six points per well. The number of cells located within the wound area was used to quantify cell migration and analyzed with application of Image J software. The relative cell number was obtained by calculation of dividing the change in the cell number of drug-treated group by that of the control group without drug treatment in each experiment.

## Statistical Analysis

Protein was determined by Bradford method (Hercules, CA). Statistical analysis was performed using one-way analysis of variance (ANOVA) followed by a Bonferroni multiple comparisons test using the SPSS 16.0 software. Data were shown as the mean ± standard error of the mean (SEM). The statistical significance was set at $p < 0.05$.

# RESULTS

## Kaempferol Binds VEGF

Kaempferol was identified to bind VEGF from our HerboChips screening. The chemical structure of kaempferol was shown (**Figure 1A**). Molecular docking was performed with PyMOL molecular graphic system and AutoDock tool. The proposed binding interaction between kaempferol and VEGF protein was shown (**Figure 1A**). The binding affinity between kaempferol and VEGF protein was estimated from −6.9 to −6.1. According to auto-docking result, the specific binding site of kaempferol to VEGF protein was shown to be located at heparin binding domain of the growth factor. This binding region is in contrast to that of polydatin or resveratrol (Hu et al., 2019a; Hu et al., 2019b). To confirm the binding of kaempferol to VEGF, an immuno-precipitation assay was applied here. The precipitated kaempferol in the sample having biotinylated VEGF was much higher than that deriving from without VEGF or with heated denatured VEGF (**Figure 1B**), suggesting the binding specificity. Moreover, the binding of kaempferol to VEGF was markedly displaced by heparin (**Figure 1C**). The precipitated kaempferol was further analyzed by LC-MS/MS analysis. The $[M+H]^+$ ion in positive mode at m/z 287.0557 was identified for kaempferol, and which produced smaller fragments of m/z 213.0540 and 157.0662 (**Figure 1D**). Therefore, the aforementioned results gave support to a direct binding interaction between VEGF protein and kaempferol.

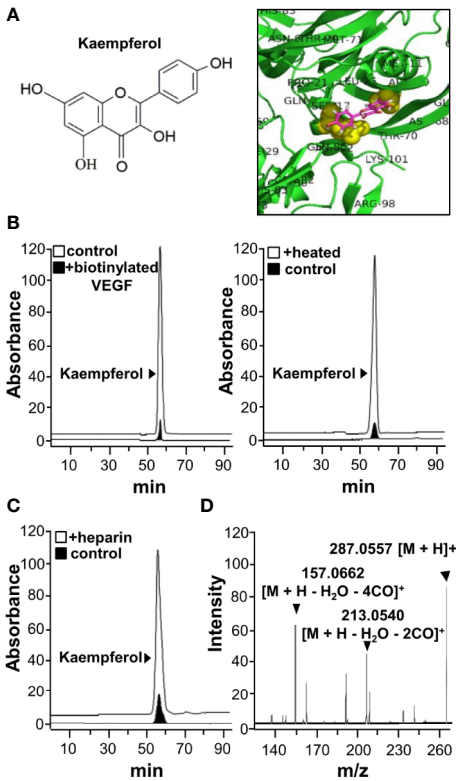


**FIGURE 1 |** Kaempferol binds with VEGF. **(A)** Structure of kaempferol (left) was shown, and protein structure of VEGF (i.e. VEGF-A) was downloaded from PDB for performing molecular auto-docking. Visualization of the binding interaction of kaempferol-VEGF was shown (right). VEGF: green; kaempferol: sticks, color of carbon: pink, oxygen: red, hydrogen: silver; the proposed binding site: yellow. **(B)** UPLC chromatogram was used to detect the amount of kaempferol in supernatant after biotinylated VEGF or VEGF (66.1 ng/ml) in an immunoprecipitation assay by streptavidin magnetic beads (left panel). The heated denature VEGF was tested for binding to kaempferol (right panel). **(C)** The binding of VEGF with kaempferol was interfered in the present of heparin (500 μg/ml; left panel). **(D)** Having an electrospray ionization (ESI) source with ionization set at the positive mode of a mass spectrometer, the mass-charge ratio of kaempferol was determined (right panel). The typical figure was demonstrated, $n = 3$. VEGF, vascular endothelial growth factor.

## Kaempferol Potentiates VEGF-Mediated Angiogenesis

Based on the binding between kaempferol and VEGF, we suspected that kaempferol might exert effects in VEGF-induced angiogenesis and cell proliferation. Having kaempferol up to 10 μM, the treatment on endothelial cells exerted no significant effects on cell viability (**Figure 2A**). The proliferation of endothelial cell was triggered by application of VEGF in a dose-dependent manner (**Supplementary Figure 1**), and which indicated that 5 ng/ml VEGF at the sub-maximum response could be used for the assay here. The cell proliferation, triggered by 5 ng/ml VEGF, was further potentiated, in a dose-dependent manner, in the presence of kaempferol (**Figure 2B**). Avastin, a monoclonal antibody against VEGF, served as a control to

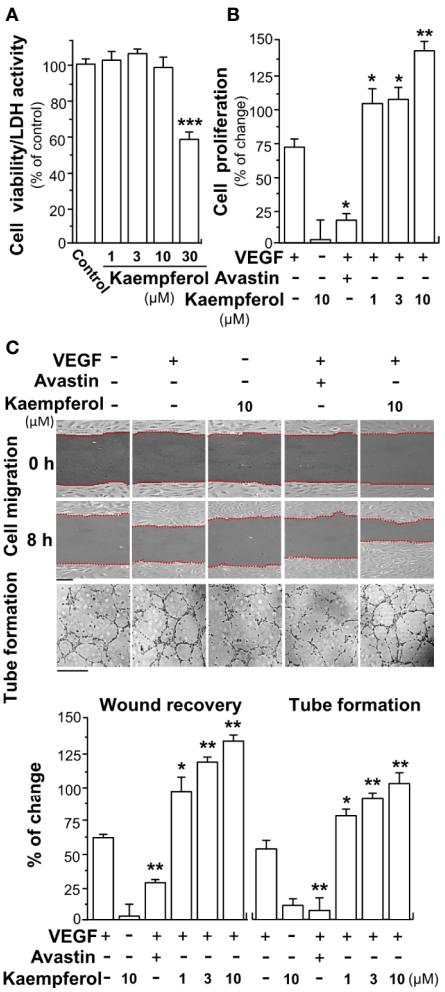


**FIGURE 2 |** Kaempferol promotes VEGF-mediated endothelial cell proliferation, cell migration, and tube formation. **(A)** Different concentrations of kaempferol were applied onto endothelial cells for 48 h, and MTT assay and LDH cytotoxicity assay were determined. **(B)** HUVECs were seeded onto a 96-well plate at 5,000 cells/well and treated with kaempferol for 48 h with or without VEGF. **(C)** In cell migration assay, HUVECs at 20 × $10^4$ cells/well were plated onto a 12-well plate. A wounded endothelial cell monolayer was created manually at the bottom of wells, and images representing recovery of wounds were taken at 0 and 8 h, separately, by a phase-contrast microscope. HUVECs were incubated with VEGF, with or without kaempferol or Avastin. In tube formation assay, endothelial cells were seeded onto a 12-well plate at 20 × $10^4$ per well. The well was pre-coated with matrigel. VEGF, together with or without kaempferol, was applied to treat cells for 8 h. To quantify the images of tube formation, three fields in one photo were randomly selected, and branching points were determined manually. In all experiments, VEGF was at a concentration of 5 ng/ml, and Avastin (a positive control) was set at 200 μg/ml. Data are demonstrated as mean ± SEM of the percentage of change as compared to control group, where $n = 4$; $p < 0.05$ *$p < 0.01$ **$p < 0.001$ (***) vs VEGF-treated group. Bar = 40 μm. MTT, 3-(4,5-dimethylthiazol-2-yl)-2,5-diphenyltetrazolium bromide; HUVEC, human umbilical vein endothelial cell.

suppress VEGF effect (Michael, 2014; Hu et al., 2019a; Hu et al., 2019b).

Endothelial cell migration and tube formation contribute to new blood vessel formation, and they are initiating the repairing of injured vessel. Here, the promoting effect of kaempferol on the migration of endothelial cells was determined by wound healing assay *in vitro*. The wound cultures were treated by VEGF, or together with kaempferol. As a control, the endothelial cell migration, induced by VEGF, was decreased in the present of Avastin (**Figure 2C**). Kaempferol alone exerted no effect on cell migration. The treatment of kaempferol and VEGF together in HUVECs significantly reduced the denuded area, i.e. increase wound recovery (**Figure 2C**). To further study the enhancing effects of kaempferol in angiogenesis, the tube formation was determined in VEGF-treated endothelial cells. After treated with VEGF, elongated and solid tube-like structures were formed. An interruption of capillary-like tubes was obviously revealed after Avastin treatment; however, the connections in capillary-like tubes were robustly increased after co-treatment of VEGF with kaempferol (**Figure 2C**). Kaempferol alone exerted no effect on tube formation. These pharmaceutical investigations contributed a lot to a conclusion that kaempferol could potentiate the VEGF-induced angiogenesis in cultured endothelial cells.

In zebrafish model, the neo-vascularization of sub-intestinal vessels was used to investigate the effect of kaempferol in VEGF-mediated angiogenesis *in vivo*. Zebrafish embryos were dechlorinated and subsequently incubated with VEGF, Avastin, or kaempferol. After treatment of VEGF, the blood microvessels in sub-intestinal part were elongated; besides, the area was broadened (**Figure 3**). There were few changes at sub-intestinal vessels in treatment of kaempferol alone. However, kaempferol applied together with VEGF could enhance the VEGF-mediated vessel formation of the embryos in a concentration-dependent manner (**Figure 3**). As expected, Avastin suppressed the VEGF-induced vessel formation.

The potentiating activities of kaempferol on VEGF-triggered angiogenic functions were also proved by performing an *ex vivo*

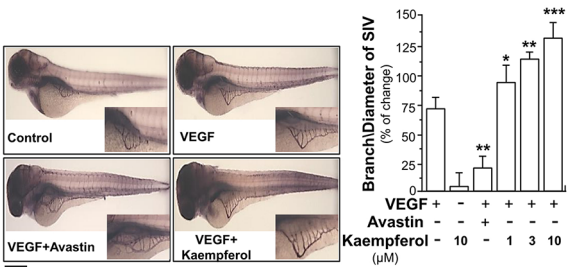


**FIGURE 3 |** Kaempferol potentiates angiogenesis *in vivo*. Healthy zebrafish embryos were picked out for each group and placed onto a 12-well plate with density set at 8–10 embryos/well. Embryos were fed with PU water containing 5 ng/ml VEGF with or without kaempferol or 200 μg/ml Avastin on 1st day of development. After drug treatment for 48 h, the fish embryos were stained. The blood vessels located in the sub-intestinal were captured for blood vessel formation. Images represented the basket of sub-intestinal vessels of the zebrafish embryos developed for 3 days. The branches and area of sub-intestinal vessels in control group and medicine-treated group were quantified with application of Image J software. Results are shown as the percentage of change as compared to control (no drug) in mean ± SEM, where $n = 3$; $p < 0.05$ *$p < 0.01$ **$p < 0.001$ (***) vs VEGF-treated group. Bar = 40 μm.

aortic ring sprouting assay. Rat aortic fragments were cultured on the matrigel and treated with drugs, including VEGF, Avastin or kaempferol. Section of aortic fragments was determined, and the angiogenic responses were monitored for eight days. The microvascular sprouting was visibly formed with the VEGF application; while fewer amounts of micro-vessels were formed in the group treated by Avastin (**Figure 4**). Kaempferol alone did not alter changes of aortic fragments. With co-applied VEGF, kaempferol prominently promoted the VEGF-induced neovascularization in aortic fragments in a concentration-dependent manner, i.e. promoting the outgrowth of microvascular outgrowth (**Figure 4**).

## Kaempferol Enhances VEGF-Induced Signaling

To demonstrate the role of kaempferol in potentiating VEGF-triggered angiogenic signaling mechanisms in endothelial cells, the expressions of phosphorylated VEGFR2, eNOS and Erk were determined here. After treated with VEGF, the expression levels of phosphorylated VEGFR2, an active form of VEGFR2, and total VEGFR2 were determined by Western blotting (**Figure 5A**). Comparing with the control group, VEGF treatment visibly enhanced the expressions of phosphorylated NOS in a time-dependent manner. The maximal activation was ~4-fold at 10 min (**Figure 5A**). Meanwhile, application of Avastin in endothelial cells markedly suppressed the VEGF-mediated phosphorylation of VEGFR2 in both time- and dose-dependent manners without altering the total expression of VEGFR2 protein. In cultured endothelial cells, kaempferol alone exerted no effect on VEGFR2 phosphorylation. The kaempferol-treated endothelial cells obviously potentiated the VEGF-triggered the expression of phosphorylated VEGFR2 in time- and dose-dependent manners:

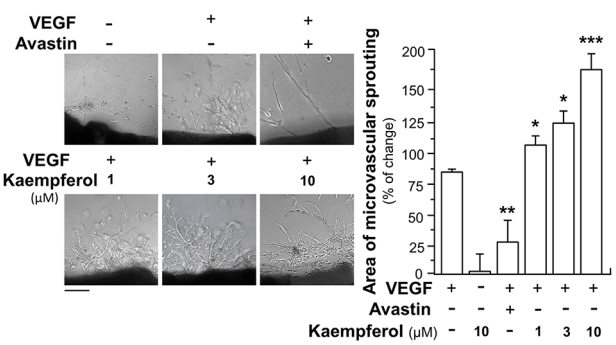


**FIGURE 4 |** Kaempferol potentiates angiogenesis *ex vivo* microvascular sprouting. Thoracic aortas were removed from 6-week-old Sprague-Dawley rats, and aortic ring fragments (cut into 1-mm thick) were cultured in matrigel and incubated with 5 ng/ml VEGF with or without kaempferol or 200 μg/ml Avastin. After drug treatment for 8 days, micovessels in each piece of fragment were captured for microvascular outgrowth. Images represented the microvascular outgrowth, and the area of microvascular sprouting in the control group and drug-treated group were quantified with application of Image J software. Results are shown as the percentage of change as compared to control (no drug) in mean ± SEM, where $n = 3$; $p < 0.05$ *$p < 0.01$ **$p < 0.001$ (***) vs VEGF-treated group. Bar = 40 μm.

the maximal increase could be achieved at ~6-fold (**Figure 5A**). Kaempferol binding to VEGF heparin binding domain was expected to increase the binding interaction of VEGF to its receptor VEGFR2, potentiating the receptor activation. To confirm this possibility, the binding activity of VEGF onto cell cultures was measured by using a fluorescence-labeled VEGF. Application of kaempferol increased the binding activity of VEGF to cells: this binding enhancement, triggered by kaempferol, was in a dose-dependent manner (**Figure 5B**).

In parallel, the applied VEGF increased the downstream mechanism signaling mediated by VEGFR2. The VEGF-induced expression levels of phosphorylated eNOS and Erk were potentiated by fivefold to ninefold in the co-treatment of kaempferol: the protein expression of total eNOS and Erk remained unchanged (**Figures 6A, B**). Avastin showed contrary effects in VEGF-mediated phosphorylations of eNOS and Erk, acting as a control (**Figures 6A, B**). Kaempferol alone did not alter the expressions of phosphorylated eNOS and Erk. These results suggested the kaempferol-bound VEGF might have stronger activation to its receptor.

We further investigated the signaling mechanism of kaempferol in angiogenic function by determining expressions of factors playing key roles in cell migration and invasion (Moses, 1997). Thus, the expressions of MMP-2 and MMP-9 were analyzed by performing Western blotting assay in endothelial cells treated by VEGF with or without kaempferol. Application of VEGF remarkedly increased the expression levels of MMP-2 and MMP-9 by ~5-fold and ~3-fold, respectively (**Figure 7**). At the same time, Avastin treatment attenuated the VEGF-mediated expressions. In cultured endothelial cells, kaempferol application alone showed no effect on expression levels of MMP-2 and MMP-9; while the co-treatment of kaempferol and VEGF induced expression levels of MMP-2 and MMP-9 proteins at ~9-fold and ~10-fold, respectively (**Figure 7**).

## Kaempferol Potentiates VEGF-Triggered Functions

Besides angiogenesis, we aimed to reveal the outcome of kapempferol binding to VEGF in affecting other biological activities of VEGF, at least in terms of activation of other forms of VEGF receptor. The moving ability of epidermal keratinocytes contributes to a high degree of wound re-epithelialization. Here, we investigated the VEGF-mediated wound healing process in cultured HaCaT cells. In a scratch wound-healing assay, the cells were incubated with VEGF, or kaempferol, and the cell migration across the wound space was analyzed after 16 h. Avastin exerted inhibitory effects on cell migration (**Figure 8**). In comparison with control group, the treatment of HaCaT cells with kaempferol and VEGF together significantly enhanced the cells migrating across the denuded space in a dose-dependent manner, which provided evidence to positive role of kaempferol in promoting VEGF-mediated migration of keratinocyte (**Figure 8**).

The VEGFR1 mRNA is being expressed in human peripheral blood monocytes, and VEGFR1 tyrosine kinase contributes greatly to VEGF-mediated cell migration of macrophages (Barleon et al., 1996). Here, the role of kaempferol in VEGF-

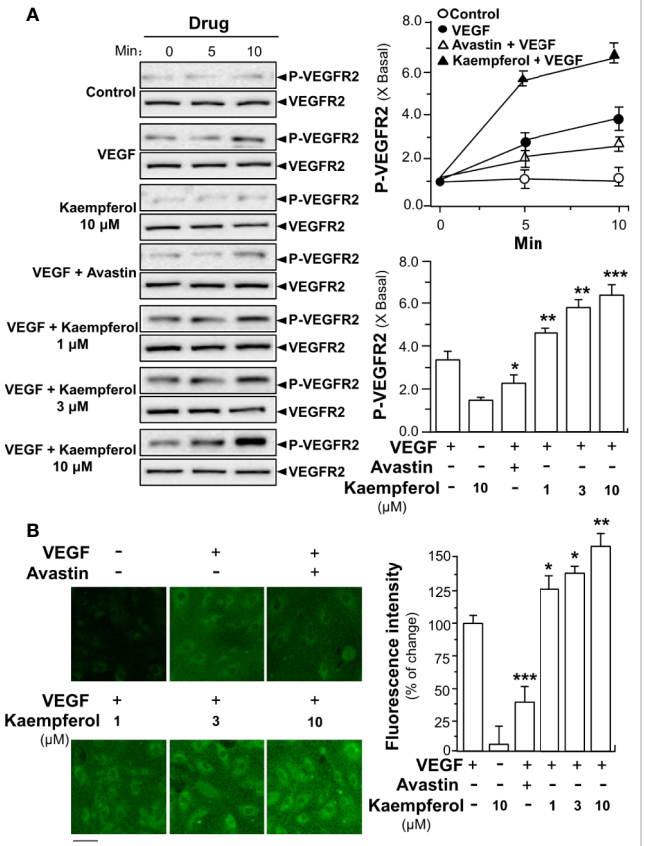


**FIGURE 5 |** Kaempferol enhances VEGF binding to VEGFR2 and its phosphorylation. **(A)** Endothelial cells were seeded onto each well of a 12-well plate with the density set at 20 × $10^4$ per well. VEGF (5 ng/ml), was used in presence or absence of kaempferol or Avastin (200 μg/ml). The cell lysates were collected at different time points. Western blotting (left panel) was used to probe phosphorylated and total expressions of VEGFR2. Quantitation was done at different time, as well as different drug treatments, at 10 min of activation (right panel). **(B)** Fluoresence-labeled VEGF (5 ng/ml) was applied onto HUVECs, with or without kaempferol, for 24 h. The fluorescence intensity in fluoresence-labeled VEGF minus background (no drug) was considered as 100%. Avastin (200 μg/ml) served as a control. Right panel is the quantitation values deriving from left panel of confocal micrograph. Data are indicated as X Basal setting as 1, or the percentage of change as compared to biotinylated VEGF group, mean ± SEM, where $n$ = 3–4; $p$ < 0.05 *$p$ < 0.01 **$p$ < 0.001 (***) vs VEGF-treated group. Bar = 40 μm.

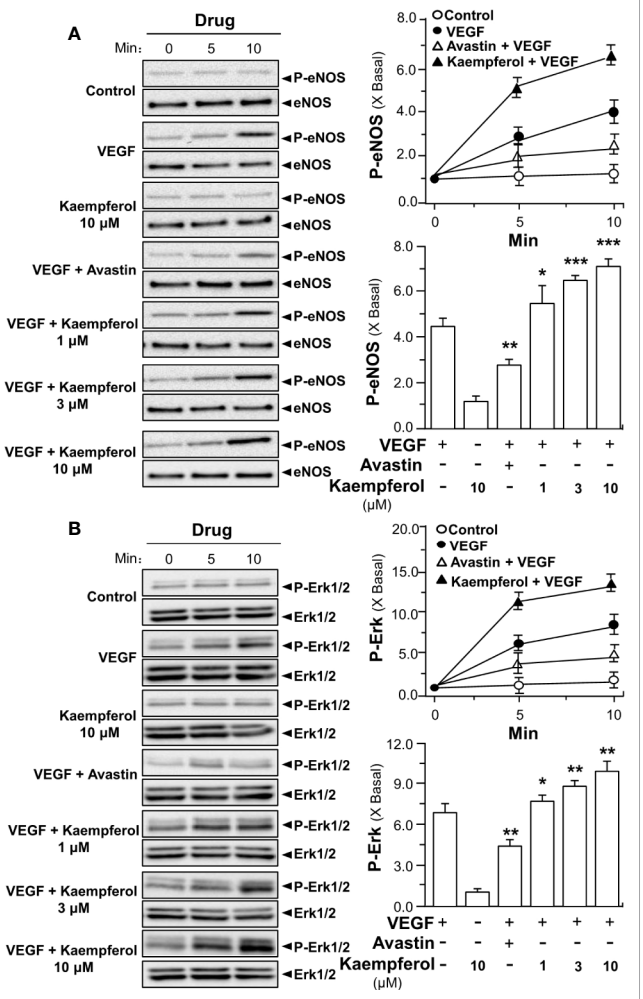


**FIGURE 6 |** Kaempferol potentiates VEGF-triggered phosphorylations of eNOS and Erk. 20 × $10^4$ HUVECs were seeded into each well of a 12-well plate. VEGF (5 ng/ml) was determined with or without kaempferol or Avastin (200 μg/ml). The lysates of endothelial cells were collected at different time intervals, as demonstrated. Phosphorylated and total proteins of eNOS **(A)** and Erk **(B)** were separately analyzed by Western blotting. Right panel is the quantitation values deriving from left panel. Quantitation was done at different time, as well as different drug treatments, at 10 min of activation. Results are expressed as the fold of change as compared to control (X Basal), where the control group (no drug) was set as 1, mean ± SEM, where $n$ = 3; $p$ < 0.05 *$p$ < 0.01 **$p$ < 0.001 (***) vs VEGF-treated group. eNOS, endothelial nitric oxide synthase; Erk, extracellular signal-regulated kinase.

induced wound healing process and phosphorylations of VEGFR1 in cultured macrophage cells was tested. In a cell migration assay, macrophages were incubated with VEGF, or kaempferol, and the cell migration across the wound space was analyzed after 24 h. Avastin demonstrated inhibitory effects on cell migration (**Figure 9A**). The treatment of macrophages with kaempferol and VEGF together obviously increased the cell migrating across the denuded space in a dose-dependent manner, supporting a positive role of kaempferol in migration of monocytes (**Figure 9A**). Besides, the effects of kaempferol on VEGF-mediated phosphorylations of VEGFR1 in macrophages were further tested by western blotting analysis. Application of VEGF markedly increased the phosphorylations of VEGFR1 by ~4-fold (**Figure 9B**). Meanwhile, kaempferol treatment alone demonstrated little effects on VEGFR1 phosphorylation; while the kaempferol-treated macrophages significantly up regulated the VEGF-induced VEGFR1 phosphorylation at ~6-fold, respectively (**Figure 9B**). Moreover, the treatments of SU5416 further blocked VEGF/kaempferol-induced phosphorylation, which almost restored back to the control level. Thus, it could be concluded that the signaling, induced by kaempferol, was similar to the selective VEGFR1 kinase inhibitor.

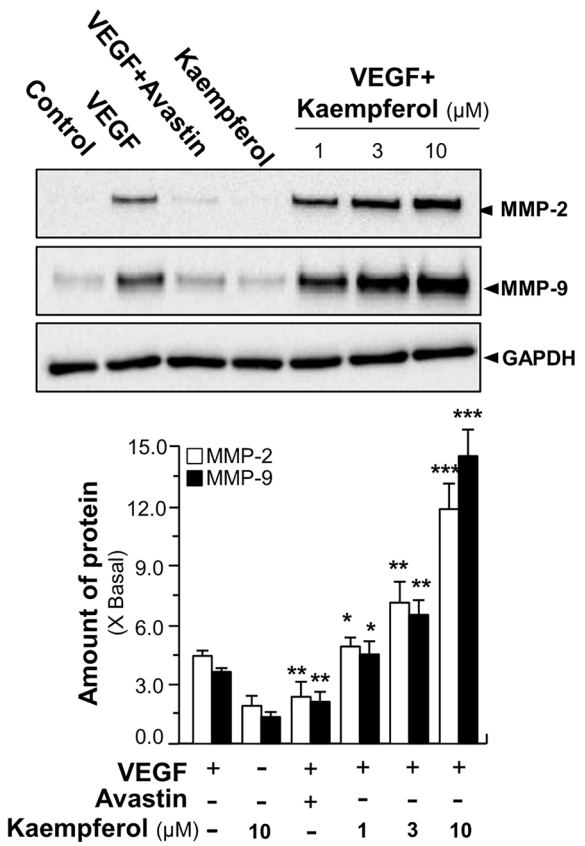


**FIGURE 7 |** Kaempferol enhances VEGF-triggered expressions of MMP-2 and MMP-9. HUVECs, at a density of 40 × $10^4$ per well, were seeded in a six-well plate. VEGF (5 ng/ml) was applied with or without Avastin or kaempferol at different concentrations. The cell lysates were collected after drug treatment. The protein expressions of MMP-2 and MMP-9 were determined by performing Western blotting (upper panel). GAPDH served as a loading control. Quantitation was done from the band intensity in Western blotting (lower panel). Results are expressed as the fold of change as compared to control (X Basal), where the control group (no drug) was set as 1, mean ± SEM, where $n = 3$; $p < 0.05$ *$p < 0.01$ **$p < 0.001$ (***) vs VEGF-treated group. MMP, matrix metalloproteinase; GAPDH, glyceraldehyde 3-phosphate dehydrogenase.

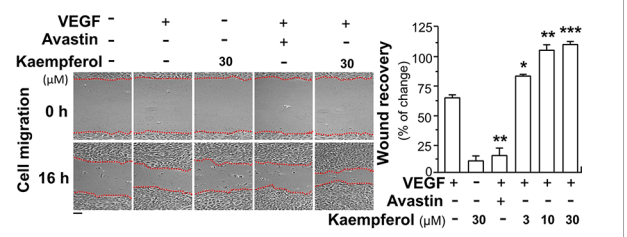


**FIGURE 8 |** Kaempferol enhances VEGF-triggered migration of HaCaT cells. Keratocytes (HaCaT cells) at 50 × $10^4$ cells/well were plated onto a six-well plate. A wounded skin cell monolayer was created manually at the bottom of wells, and pictures representing wound recovery were captured at 0 and 16 h, separately, by a phase-contrast microscope. HaCaT cells were incubated with VEGF, with or without kaempferol or Avastin. Data are demonstrated as mean ± SEM of the percentage of change as compared to control group, where $n = 3$; $p < 0.05$ *$p < 0.01$ **$p < 0.001$ (***) vs VEGF-treated group. Bar = 40 μm.

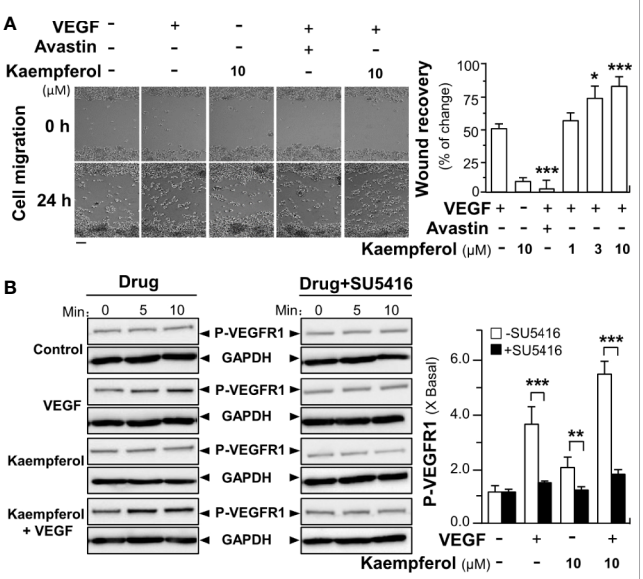


**FIGURE 9 |** Kaempferol promotes VEGF-induced migration of macrophages *via* VEGFR1 phosphorylation. **(A)** RAW264.7 cells at 60 × $10^4$ cells/well were seed onto a 12-well plate. A wounded monocyte cell monolayer was created manually at the center of wells, and images representing wound recovery were captured at 0 and 24 h, separately, under a phase-contrast microscope. Macrophages were incubated with VEGF, with or without kaempferol. The recovery of wound is measured by the cell occupant per unit area. Data are demonstrated as mean ± SEM of the percentage of change as compared to control group. Bar = 100 μm. **(B)** Macrophages were plated into a 12-well plate at 60 × $10^4$ cells per well. The cells were treated with VEGF (5 ng/ml) with or without kaempferol. An inhibitor for VEGFR1 (SU5416 at 50 μM) was used. Data are expressed as X Basal, where the control was set as 1. All data are in mean ± SEM, where $n = 3$; $p < 0.05$ 8$p < 0.01$ **$p <$ 0.001 (***) vs VEGF-treated group or indicated.

## DISCUSSION

TCM is a great source to find possible treatment of various diseases, and additionally there is a steady growth about the application of botanical dietary supplements. In our HerboChips drug screening, Ginkgo Folium was identified here by using VEGF as a target protein. Kaempferol, an abundant active flavonoid in Ginkgo Folium, was shown to bind VEGF, and subsequently which potentiated angiogenic effects of VEGF. The extract of Ginkgo Folium is one of the top 10 commonly used herbal products (Leung, 1982). Pharmacological activities of the leaves of *Ginkgo biloba* are proposed to have cardiac protection, stimulating blood flow, radical scavenging and enhancing activities of anti-platelet activating factors (Beek, 2000). Active constituents, e.g. bilobalide, ginkgolides and flavonoids, in Ginkgo Folium play functions in antioxidant (Chen et al., 1999), anti-ischemic (Chung and Harris, 1999) and anti-convulsant (Sasaki and Hatta, 1999). Kaempferol is not only found in Gingko Folium; this flavonoid is commonly found in many edible plants, e.g. apples, strawberries and beans.

Kaempferol has been reported to have anti-apoptosis (Choi and Ahn, 2008), anti-inflammation (Bobe et al., 2010), anti-oxidation (Tatsimo et al., 2012), and anti-carcinogenic effects (Gates et al., 2009). However, there are very few investigations targeting the potentiating effects of kaempferol in angiogenesis. Petpiroon et al. (2015) demonstrated that kaempferol could promote wound healing using a human keratinocyte model, which suggested the potentiating effect of kaempferol in angiogenesis. Angiogenesis contributes to pathologic processes in many diseases, including diabetes, ischemic heart disease, cancer, and chronic inflammation (Carmeliet, 2003). Here, we highlighted the pharmacological activities of kaempferol in VEGF-induced angiogenesis. Application of kaempferol in cultured HUVECs could significantly promote VEGF-mediated endothelial cell proliferation, cell migration and tube formation; and in *in vivo* the effects of kaempferol in angiogenesis were demonstrated in vessel formation of zebrafish embryos and micro-vessels outgrowth from aortic fragments. In addition, we illustrated the underlying mechanism signaling by which kaempferol positively controls the VEGF-triggered expressions of phosphorylated VEGFR2, eNOS, and Erk. Thus, the angiogenic effect of kaempferol is proposed to be initiated by its binding with VEGF, which therefore potentiates the activation of VEGF on its receptor. Besides, MMPs are known to play critical roles in initiation of angiogenesis, which contribute to re-organization of extracellular matrix, break down stroma and extracellular matrix proteins, and promote endothelial cells moving toward sources of growth factors (Herron et al., 1986; Liotta, 1986). The expressions of MMP-2 and MMP-9 were measured in VEGF-induced cultures, and which was potentiated by kaempferol.

In natural products, kaempferol has chemical analogs sharing a close structure similarity, e.g. quercetin and kaempferol-3-O-rutinoside. The difference between kaempferol and quercetin in pharmacological properties did exist in regulating pro-inflammatory genes (Crespo et al., 2008) and in interacting with immunoglobulin (Liu et al., 2008). Inspired by these studies, we have search possible interactions of VEGF with kaempferol analogs. According to the molecular docking analysis, quercetin and kaempferol-3-O-rutinoside could possibly bind to VEGF. In line to this notion, kaempferol-3-O-rutinoside has been shown to promote keratinocyte migration through FAK and Rac1 activation (Petpiroon et al., 2015).

Different growth factors, e.g. EGF, bFGF, VEGF, and PDGF, and their corresponding receptors are known to play key roles in angiogenic regulation. Among these growth factors, VEGF is considered as the most important one. VEGF reacts with two main VEGF receptors, namely VEGFR1 and VEGFR2, and VEGFR2 has been proved to be responsible for the majority of VEGF-mediated angiogenic activities. Once interacted with VEGFR2, VEGF takes the main responsibilities to activate downstream signaling, including eNOS and Erk, as to enhance angiogenic process. HerboChips screening is tailored to find compounds from natural source that bind to growth factors (Lee et al., 2016). In previous reports, polydatin and its closely related analogs, resveratrol, were shown to bind with VEGF, and this binding, similar to Avastin, inhibited angiogenic functions of VEGF (Hu et al., 2019a; Hu et al., 2019b). The inhibitory effects of polydatin/resveratrol in VEGF-treated cultures could be attributed to its occupation of possible binding sites between VEGF and VEGFR, which subsequently decreased the binding of VEGF to VEGFR. However, kaempferol is different to that of polydatin/resveratrol. The binding of kaempferol enhanced the VEGF-triggered phosphorylations of VEGFR2, eNOS, and Erk. The potentiating activity of kaempferol might be accounted by its direct binding with VEGF at the heparin binding domain, i.e. to increase the binding of VEGF to its receptor, which could be different from binding sites of polydatin/resveratrol to VEGF. Thus, kaempferol at low concentration could be used for treatment of ischemic heart disease related with angiogenesis, including coronary heart disease and myocardial infarction. Contrary, studies have proposed kaempferol could suppress angiogenesis through inhibiting VEGFR2 expression (Luo et al., 2012; Liang et al., 2015). However, the authors did not identify the interacting target of VEGF or VEGF receptor. Besides, a rather high concentration of kaempferol (i.e. 80 μM) was applied in their reports: this concentration of kaempferol showed cell death activity, as shown in our study, as well as in other (Liang et al., 2015).

The important roles of epidermal cell migration in wound healing have been reported (Gao et al., 2010; Walter et al., 2010). Indeed, the migration of keratinocyte toward the wound site is a step of great significance in restoring a barrier in cutaneous wounds (Santoro and Gaudino, 2005; Ranzato et al., 2008). Herein, we demonstrated, for the first time, that kaempferol has a positive effect on VEGF-mediated migration of human keratinocyte cells, which was consistent with our findings obtained based on endothelial cells. Because the migration of keratinocyte plays critical roles in the wound re-epithelialization, the information obtained from here should support development of kaempferol for clinical application as an active agent for wound healing and related applications.

VEGFR1 is being expressed in monocytes, and it is highly expressed during the differentiation of monocyte–macrophage lineage (Sawano et al., 2001). VEGFR1 promotes migration of macrophage through PI3K and PLCγ signaling pathways (Weddell et al., 2018). Here, we demonstrated that kaempferol could enhance VEGF-mediated migration of macrophage cells by enhancing VEGF-induced VEGFR1 phosphorylations. Because pro-inflammatory mediators are mainly produced by macrophages, and thus macrophage migration from circulation to injured tissues plays a vital role in wound healing. Polarization of macrophages is relating to the remodeling of homeostatic tissue, inflammation resolution and tissue repair (Mantovani et al., 2013). Thus, our investigations may shed light on the positive effects of kaempferol on macrophage migration, and tissue regeneration *via* modulation of macrophage through VEGFR1 signaling pathway.

## DATA AVAILABILITY STATEMENT

All datasets generated for this study are included in the article/ **Supplementary Material**.

## ETHICS STATEMENT

The animal study was reviewed and approved by Animal Ethics Committee of HKUST.

## AUTHOR CONTRIBUTIONS

W-HH wrote the paper and performed most of the experiments. KT revised the paper, conceived, and designed the research. H-YW took part in most of the experiments. Y-TX and KD helped to make gels for western blot assay and YT conducted HPLC. RD and Q-PX performed data analysis for the cell migration assay. GC helped to do cell culture. TD provided reagents and Q-WQ took part in screening of HerboChips analysis.

## FUNDING

This work is supported by Shenzhen Science and Technology Innovation Committee (ZDSYS201707281432317; JCYJ20170413173747440; JCYJ20180306174903174), China Post-doctoral Science Foundation (2019M653087), Zhongshan Municipal Bureau of Science and Technology (ZSST20SC03), Guangzhou Science and Technology Committee Research Grant (GZSTI16SC02; GZSTI17SC02), Hong Kong RGC Theme-based Research Scheme (T13-607/12R), Hong Kong Innovation Technology Fund (UIM/340, UIM/385, ITS/500/18FP; TCPD/17-9), TUYF19SC02, PD18SC01, and HMRF18SC06.

## ACKNOWLEDGMENTS

We would like to thank Prof. Zilong Wen and Shizheng Zhao from Division of Life Science of HKUST, for their assistance in zebrafish assay.

## SUPPLEMENTARY MATERIAL

The Supplementary Material for this article can be found online at: https://www.frontiersin.org/articles/10.3389/fphar.2020.00526/full#supplementary-material.

**SUPPLEMENTARY FIGURE 1 |** VEGF promotes endothelial cell proliferation in a concentration-dependent manner. HUVECs were seeded onto a 96-well plate at 5,000 cells/well and treated with or without VEGF at different concentrations. The cell viability was assayed by MTT after 48 h of treatment. Data are demonstrated as Mean ± SEM of the percentage of change as compared to control group (no VEGF), where $n = 5$.

## REFERENCES

Ashton, A. W., Yokota, R., John, G., Zhao, S., Suadicani, S. O., Spray, D. C., et al. (1999). Inhibition of endothelial cell migration, intercellular communication, and vascular tube formation by thromboxane *A. J. Biol. Chem.* 274, 35562–35570. doi: 10.1074/jbc.274.50.35562

Barleon, B., Sozzani, S., Zhou, D., Weich, H. A., Mantovani, A., and Marme, D. (1996). Migration of human monocytes in response to vascular endothelial growth factor (VEGF) is mediated via the VEGF receptor flt-1. *Blood* 87, 3336–3343. doi: 10.1182/blood.V87.8.3336.bloodjournal8783336

Beek, T. A. (2000). *Ginkgo biloba. 12th ed.* Vol. 1 (Amsterdam: Harwood Academic Publishers), 345–370.

Bobe, G., Albert, P. S., Sansbury, L. B., Lanza, E., Schatzkin, A., Colburn, N. H., et al. (2010). Interleukin-6 as a potential indicator for prevention of high risk adenoma recurrence by dietary flavonols in the polyp prevention trial. *Cancer Prev. Res. (Phila)* 3, 764–775. doi: 10.1158/1940-6207.CAPR-09-0161

Carmeliet, P., and Jain, R. K. (2000). Angiogenesis in cancer and other diseases. *Nature* 407, 249–257. doi: 10.1038/35025220

Carmeliet, P. (2003). Angiogenesis in health and disease. *Nat. Med.* 9, 653–660. doi: 10.1038/nm0603-653

Chen, C., Wei, T. T., Gao, Z., Zhao, B., Hou, J., Xu, H., et al. (1999). Different effects of the constituents of EGb761 on apoptosis in rat cerebellar granule cells induced by hydroxyl radicals. *Biochem. Mol. Biol. Int.* 47, 397–405. doi: 10.1080/15216549900201423

Choi, E. J., and Ahn, W. S. (2008). Kaempferol induced the apoptosis via cell cycle arrest in human breast cancer MDA-MB-453 cells. *Nutr. Res. Pract.* 2, 322–325. doi: 10.4162/nrp.2008.2.4.322

Chung, H. S., and Harris, A. (1999). *Ginkgo biloba* extract increases ocular blood flowvelocity. *J. Ocul. Pharmacol. Ther.* 15, 233–240. doi: 10.1089/jop.1999.15.233

Crespo, I., Mediavilla, M. V., Gutierrez, B., Campos, S. S., Tunon, M. J., and Gallego, J. J. (2008). A comparison of the effects of kaempferol and quercetin on cytokine-induced pro-inflammatory status of cultured human endothelial cells. *Br. J. Nutr.* 100, 968–976. doi: 10.1017/S0007114508966083

Emanueli, C., and Madeddu, P. (2005). Changing the logic of therapeutic angiogenesis for ischemic disease. *Trends Mol. Med.* 11, 207–216. doi: 10.1016/j.molmed.2005.03.007

Ferrara, N. (1996). Vascular endothelial growth factor. *Eur. J. Cancer* 32, 2413–2422. doi: 10.1016/s0959-8049(96)00387-5

Folkman, J., and D'Amore, P. A. (1996). Blood vessel formation: what is its molecular basis? *Cell* 87, 1153–1155. doi: 10.1016/s0092-8674(00)81810-3

Folkman, J. (1995). Angiogenesis in cancer, vascular, rheumatoid and other disease. *Nat. Med.* 1, 27–31. doi: 10.1038/nm0195-27

Gao, Z. X., Huang, D. Y., Li, H. X., Zhang, L. N., Lv, Y. H., and Cui, H. D. (2010). Scutellarin promotes in vitro angiogenesis in human umbilical vein endothelial cells. *Biochem. Biophys. Res. Commun.* 400, 151–156. doi: 10.1016/j.bbrc.2010.08.034

Gates, M. A., Vitonis, A. F., Tworoger, S. S., Rosner, B., Titus-Ernstoff, L., Hankinson, S. E., et al. (2009). Flavonoid intake and ovarian cancer risk in a population-based case-control study. *Int. J. Cancer* 124, 1918–1925. doi: 10.1002/ijc.24151

Griffith, L. G., and Naughton, G. (2002). Tissue engineering – current challenges and expanding opportunities. *Science* 295, 1009–1014. doi: 10.1126/science.1069210

Grosdidier, A., Zoete, V., and Michielin, O. (2011). Fast docking using the CHARMM force field with EADock DSS. *J. Comput. Chem.* 32, 2149–2159. doi: 10.1002/jcc.21797

Guo, J. Y., Choi, C. Y., Zheng, Y. Z., Chen, P., Dong, T. X., Wang, Z. T., et al. (2012). Kaempferol as a flavonoid induces osteoblastic differentiation via estrogen receptor signalling. *Chin. Med.* 7, 10–20. doi: 10.1186/1749-8546-7-10

Herron, G. S., Banda, M. J., Clark, E. J., Gavrilovic, J., and Werb, Z. (1986). Secretion of metalloproteinases by stimulated capillary endothelial cells. II. Expression of collagenase and stromelysin activities is regulated by endogenous inhibitors. *J. Biol. Chem.* 261, 2810–2813.

Hertog, M. G., Feskens, E. J., Hollman, P. C., Katan, M. B., and Kromhout, D. (1993). Dietary antioxidant flavonoids and risk of coronary heart disease: the Zutphen elderly study. *Lancet* 342, 1007–1011. doi: 10.1016/0140-6736(93)92876-u

Hong, J. T., Yen, J. H., Wang, L., Lo, Y. H., Chen, Z. T., and Wu, M. J. (2009). Regulation of heme oxygenase-1 expression and MAPK pathways in response to kaempferol and rhamnocitrin in PC12 cells. *Toxicol. Appl. Pharmacol.* 37, 59–68. doi: 10.1016/j.taap.2009.02.014

Hu, W. H., Chan, G. L., Lou, J. S., Wu, Q. Y., Wang, H. Y., Duan, R., et al. (2018). The extract of Polygoni Cuspidati Rhizoma et Radix suppresses the vascular endothelial growth factor-induced angiogenesis. *Phytomedicine* 42, 135–143. doi: 10.1016/j.phymed.2018.03.029

Hu, W. H., Wang, H. Y., Kong, X. P., Xiong, Q. P., Poon, K. M., Xu, L., et al. (2019a). Polydatin suppresses VEGF-induced angiogenesis through binding with VEGF and inhibiting its receptor signalling. *FASEB J.* 33, 532–544. doi: 10.1096/fj.201800750R

Hu, W. H., Duan, R., Xia, Y. T., Xiong, Q. P., Wang, H. Y., Chan, G. L., et al. (2019b). Binding of resveratrol to vascular endothelial growth factor (VEGF) suppresses angiogenesis by inhibiting the receptor signalling. *J. Agric. Food Chem.* 67, 1127–1137. doi: 10.1021/acs.jafc.8b05977

Lee, S. C., Zhang, M. L., Yan, L., Lam, Y. C., Dong, T. X., Lin, H. G., et al. (2016). Indication of nerve growth factor binding components from herbal extracts by HerboChip: a platform for drug screening on a chip. *Chin. Med.* 11, 34–44. doi: 10.1186/s13020-016-0107-8

Leung, A. Y. (1982). *Encyclopedia of common natural ingredients used in food, drugs and cosmetics* Vol. 1 (New York: Second John Wiley & Sons Publishers), 1–3.

Liang, F., Han, Y. X., Gao, H., Xin, S. C., Chen, S. D., Wang, N., et al. (2015). Kaempferol identified by zebrafish assay and fine fractionations strategy from *Dysosma versipellis* inhibits angiogenesis through VEGF and FGF pathways. *Sci. Rep.* 5, 14468. doi: 10.1038/srep14468

Lin, H. Y., Juan, S. H., Shen, S. C., Hsu, F. L., and Chen, Y. C. (2003). Inhibition of lipopolysaccharide-induced nitric oxide production by flavonoids in RAW264.7 macrophages involve heme oxygenase-1. *Biochem. Pharmacol.* 66, 1821–1832. doi: 10.1016/S0006-2952(03)00422-2

Liotta, L. A. (1986). Tumour invasion and metastases–role of the extracellular matrix: Rhoads Memorial Award lecture. *Cancer Res.* 46, 1–7.

Liu, Y. C., Yang, Z. Y., Du, J., Yao, X. J., Lei, R. X., Zheng, X. D., et al. (2008). Study on the interactions of kaempferol and quercetin with intravenous immunoglobulin by fluorescence quenching, fourier transformation infrared spectroscopy and circular dichroism spectroscopy. *Chem. Pharm. Bull.* 56, 443–451. doi: 10.1248/cpb.56.443

Luo, H., Rankin, G. O., Juliano, N., Jiang, B. H., and Chen, Y. C. (2012). Kaempferol inhibits VEGF expression and *in vitro* angiogenesis through a novel ERK-NFκB-cMyc-p21 pathway. *Food Chem.* 130, 321–328. doi: 10.1016/j.foodchem.2011.07.045

Mantovani, A., Biswas, S. K., Galdiero, M. R., Sica, A., and Locati, M. (2013). Macrophage plasticity and polarization in tissue repair and remodelling. *J. Pathol.* 229, 176–185. doi: 10.1002/path.4133

Michael, W. S. (2014). Pharmacokinetics, pharmacodynamics and pre-clinical characteristics of ophthalmic drugs that bind VEGF. *Expert. Rev. Clin. Pharmacol.* 7, 167–180. doi: 10.1586/17512433.2014.884458

Morris, G. M., Goodsell, D. S., and Halliday, R. S. (1998). Automated docking using a Lamarckian genetic algorithm and an empirical binding free energy function. *J. Comput. Chem.* 19, 1639–1662. doi: 10.1002/(SICI)1096-987X(19981115)

Moses, M. A. (1997). The regulation of neovascularization of matrix metalloproteinases and their inhibitors. *Stem Cells* 15, 180–189. doi: 10.1002/stem.150180

Nicosia, R. F., and Ottinetti, A. (1990). Modulation of microvascular growth and morphogenesis by reconstituted basement membrane gel in three dimensional cultures of rat aorta: A comparative study of angiogenesis in matrigel, collagen, fibrin, and plasma clot. *In Vitro Cell Dev. Biol.* 26, 119–128. doi: 10.1007/bf02624102

Petpiroon, N., Suktap, C., Pongsamart, S., Chanvorachote, P., and Sukrong, S. (2015). Kaempferol-3-*O*-rutinoside from *Afgekia mahidoliae* promotes keratinocyte migration through FAK and Rac1 activation. *J. Nat. Med.* 69, 340–348. doi: 10.1007/s11418-015-0899-3

Puppala, D., Gairola, C. G., and Swanson, H. I. (2007). Identification of kaempferol as an inhibitor of cigarette smoke-induced activation of the aryl hydrocarbon receptor and cell transformation. *Carcinogenesis* 28, 639–647. doi: 10.1093/carcin/bgl169

Rafii, S., Lyden, D., Benezra, R., Hattori, K., and Heissig, B. (2002). Vascular and haematopoietic stem cells: novel targets for anti-angiogenesis therapy? *Nat. Rev. Cancer* 2, 826–835. doi: 10.1038/nrc925

Ranzato, E., Patrone, M., Mazzucco, L., and Burlando, B. (2008). Platelet lysate stimulates wound repair of HaCaT keratinocytes. *Br. J. Dermatol.* 159, 537–545. doi: 10.1111/j.1365-2133.2008.08699.x

Santoro, M. M., and Gaudino, G. (2005). Cellular and molecular facets of keratinocyte reepithelization during wound healing. *Exp. Cell Res.* 304, 274–286. doi: 10.1016/j.yexcr.2004.10.033

Sasaki, K., and Hatta, S. (1999). Effects of bilobalide on gamma-aminobutyric acid levels and glutamic acid decarboxylase in mouse brain. *Eur. J. Pharmacol.* 367, 165–173. doi: 10.1016/s0014-2999(98)00968-6

Sawano, A., Iwai, S., Sakurai, Y., Ito, M., Shitara, K., and Nakahata, T. (2001). Flt-1, vascular endothelial growth factor receptor 1, is a novel cell surface marker for the lineage of monocyte-macrophages in humans. *Blood* 97, 785–791. doi: 10.1182/blood.v97.3.785

Tatsimo, S. J., Tamokou, J. D., Havyarimana, L., Csupor, D., Forgo, P., Hohmann, J., et al. (2012). Antimicrobial and antioxidant activity of kaempferol rhamnoside derivatives from *Bryophyllum pinnatum*. *BMC Res. Notes* 5, 158–164. doi: 10.1186/1756-0500-5-158

Timar, J., Dome, B., Fazekas, K., Janovics, A., and Paku, S. (2001). Angiogenesis-dependent diseases and angiogenesis therapy. *Pathol. Oncol. Res.* 7, 85–94. doi: 10.1007/BF03032573

Walter, M. N., Wright, K. T., Fuller, H. R., Macneil, S., and Johnson, W. E. (2010). Mesenchymal stem cell-conditioned medium accelerates skin wound healing: an *in vitro* study of fibroblast and keratinocyte scratch assays. *Exp. Cell Res.* 316, 1271–1281. doi: 10.1016/j.yexcr.2010.02.026

Wang, L., Tu, Y. C., Lian, T. W., Hung, J. T., Yen, J. H., and Wu, M. J. (2006). Distinctive antioxidant and anti-inflammatory effects of flavonols. *J. Agric. Food Chem.* 54, 9798–9804. doi: 10.1021/jf0620719

Weddell, J. C., Chen, S., and Imoukhuede, P. I. (2018). VEGFR1 promotes cell migration and proliferation through PLCγ and PI3K pathways. *Syst. Biol. Appl.* 4, 1–11. doi: 10.1038/s41540-017-0037-9

**Conflict of Interest:** The authors declare that the research was conducted in the absence of any commercial or financial relationships that could be construed as a potential conflict of interest.

frontiers in Pharmacology

ORIGINAL RESEARCH
published: 29 April 2020
doi: 10.3389/fphar.2020.00416

# Proteomics Unravels Emodin Causes Liver Oxidative Damage Elicited by Mitochondrial Dysfunction

*Yinhuan Zhang*[1], *Xiaowei Yang*[2], *Zhixin Jia*[1], *Jie Liu*[1], *Xiaoning Yan*[1], *Yihang Dai*[1] *and Hongbin Xiao*[1]*

[1] Research Center of Chinese Medicine Analysis and Transformation, Beijing University of Chinese Medicine, Beijing, China, [2] Institute of Chinese Materia Medica, China Academy of Chinese Medical Sciences, Beijing, China

Emodin is one of the main active compounds in many Chinese traditional herbs. Due to its potential toxic effect on the liver, the possible injury mechanism needs to be explored. In the present study, we investigated liver injury mechanisms of emodin on rats by the technology of proteomics. Firstly, 4530 proteins were identified from the liver of rats treated with emodin by label free proteomics. Inside, 892 differential proteins were selected, presenting a downward trend. Bioinformatics analysis showed that proteins interfered with by emodin were mainly involved in oxidation-reduction biological processes and mitochondrial metabolic pathways, such as mitochondrial fatty acid β-oxidation, citric acid cycle, and oxidative phosphorylation, which were further confirmed by western blot. The decrease in maximal respiration, ATP production, spare respiratory capacity, and coupling efficiency and increase in proton leakage were detected by seahorse XFe 24 analyzer, which confirmed the damage of mitochondrial function. The down-regulated expressions in antioxidant proteins were verified by western blot and a significant increase of ROS levels were detected in emodin group, which showed that emodin disrupted redox homeostasis in livers. Molecular docking revealed that the main targets of emodin might be acadvl and complex IV. Generally, emodin could induce oxidative stress in livers by directly targeting acadvl/complex IV and inhibiting fatty acid β-oxidation, citric acid cycle, and oxidative phosphorylation taken place in mitochondria.

**Keywords: Emodin, liver injury, proteomics, mitochondrial dysfunction, redox homeostasis**

OPEN ACCESS

***Edited by:***
*Wei Zhou,*
*The Affiliated Hospital of Shenzhen University, China*

***Reviewed by:***
*Jingwu Kang,*
*Shanghai Institute of Organic Chemistry (CAS), China*
*Songxiao Xu,*
*Artron BioResearch Inc., Canada*

***Correspondence:**
*Hongbin Xiao*
*hbxiao69@163.com*

***Specialty section:***
*This article was submitted to Ethnopharmacology, a section of the journal Frontiers in Pharmacology*

***Received:*** *05 December 2019*
***Accepted:*** *18 March 2020*
***Published:*** *29 April 2020*

***Citation:***
*Zhang Y, Yang X, Jia Z, Liu J, Yan X, Dai Y and Xiao H (2020) Proteomics Unravels Emodin Causes Liver Oxidative Damage Elicited by Mitochondrial Dysfunction. Front. Pharmacol. 11:416. doi: 10.3389/fphar.2020.00416*

## INTRODUCTION

Due to its wide and unpredictable effects, drug-induced liver injury (DILI) has become one of the main obstacles in drug safety development and clinical application. Hence, a better understanding of key signaling mechanisms driving initiation and progression of this untoward reaction may contribute to both early diagnosis and safe use of drugs. Critical events in the development of DILI are mitochondrial damage and oxidative stress (Lim et al., 2006; Berson et al., 2006). Mitochondria are important organelles; on one hand, they are the sources of power which are responsible for the production of the majority of adenosine triphosphate (ATP) through oxidative metabolism by tricarboxylic acid (TCA) cycle, fatty acid β-oxidation and oxidative phosphorylation (OXPHOS).

On the other hand, they are the main source of reactive oxygen species (ROS) in mammalian organs. Oxygen accepts a single electron derived from $FMN^{\cdot}$ of the FMNH2/FMN coenzyme of mitochondrial respiratory chain complex I (Turrens and Boveris, 1980) and double electron from $UQH^{\cdot}$ of the complex III (Boveris et al., 1976) to be reduced to form superoxide radicals and hydrogen peroxide, which constitute a constant source of the largest amount of ROS in the organism. Mitochondrial damage gives rise to the increase of ROS (Wang et al., 2013) such as the lack of any component of the TCA cycle or electron transport chain. Interestingly, to prevent oxidative damage, there is a set of scavenging systems including enzymatic and non-enzymatic antioxidants to protect cells from the attack by ROS (Valko et al., 2007). The imbalance between ROS and antioxidant defenses result in oxidative stress (Myatt and Cui, 2004; Burton and Jauniaux, 2011). Oxidative stress leads to the damage of important biomolecules and cells, which has a potential impact on the whole organism (Ďuračková, 2010). Moreover, oxidation stress can further damage the mitochondrial metabolic process (Duchen, 2004) and lead to liver injury.

Emodin (1, 3, 8-trihydroxy-6-methylanthraquinone) is a natural active compound isolated from *Rheum palmatum* (Wang et al., 2011), *Polygonum cuspidatum* (Wang et al., 2012), *Polygonum multifloyum* (Lee et al., 2011), *Aloe vera* (Naqvi et al., 2010), and *Cassia obtusifolia* (Yang et al., 2003) etc. As one of their mutual active ingredients, emodin is considered to be responsible for the toxic effect on livers (Yang et al., 2019). Previous studies have shown that emodin can elevate ROS levels accompanied by consumption of SOD and GSH (Ma et al., 2015; Jiang et al., 2017; Jiang et al., 2018) and lead to oxidative stress (Cui et al., 2014). Further studies have found that emodin can alter mitochondrial membrane potential (Cui et al., 2014), down-regulate GAPDH expression and MDH activities (Yang et al., 2018), and inhibit protein expressions and activities of mitochondrial respiratory chain (Lin et al., 2019), which implied that emodin has a potential damaging effect on liver mitochondrial function. Moreover, emodin can also induce DILI in the way of hepatocyte apoptosis *via* mitochondria-dependent pathways including up-regulating apoptosis protein expressions of cyt c, caspase 3, and caspase 9 (Yang et al., 2018). In addition, oxidative stress has been shown to destroy mitochondria metabolic processes (ie, Fatty acid oxidation, ATP production) (Galluzzi et al., 2012). In hepatocytes, the inhibition of mitochondrial function induces oxidative stress, which decreases fatty acid oxidation (Pettinelli et al., 2011; Bechmann et al., 2012). Our previous study had reported that emodin interfered with three fatty acid β-oxidation metabolites including N-undecanoyl glycine, L-palmitoyl carnitine, and eradi carnitine based on metabonomics (Liu et al., 2015a). Yet it is unclear how emodin induces oxidative stress by affecting mitochondrial metabolism function.

In recent years, mass spectrometry-based proteomics has been widely used to determine the modes of action and mechanisms involved in drug- or chemical-induced toxicity (Tan et al., 2012; Lee et al., 2013). A label-free approach generally quantifies based on peak intensity, and it has no sample limitation, so this approach has the ability to accurately quantitate more samples. Besides, there are few restrictions in terms of experimental conditions, so almost any type of sample can be used. Despite the popularity of proteomics, the information on emodin-induced hepatotoxicity is still limited which challenges toxicity monitoring and evaluation.

Therefore, in this study, we try to explore the effect of emodin on oxidative stress and mitochondrial function in rat livers using proteomic technology. This work is expected to sharpen understanding of the liver injury mechanism induced by emodin and provide reference for the further development and application of drugs containing emodin.

**Abbreviations:** DILI, drug-induced liver injury; ATP, adenosine triphosphate; TCA, tricarboxylic acid; OXPHOS, oxidative phosphorylation; ROS, reactive oxygen species; ALT, Serum alanine aminotransferase; AST, aspartate transaminase; HE, hematoxylin and eosin; SDS-PAGE, sodium dodecyl sulfate polyacrylamide gel electrophoresis; ECL, enhanced chemiluminescence; OCR, oxygen consumption rate; FCCP, carbonyl cyanide 4-(trifluoromethoxy) phenylhydrazone; Acads, Short-chain specific acyl-CoA dehydrogenase; Hadhb, Trifunctional enzyme subunit alpha; Ndufs5, NADH dehydrogenase (Ubiquinone) Fe-S protein 5; Sdhb, Succinate dehydrogenase [ubiquinone] iron-sulfur subunit; Uqcrh, ubiquinol-cytochrome c reductase hinge protein; Cox5a, Cytochrome c oxidase subunit 5A; Atp5g1, ATP synthase F(0) complex subunit C1G1; Cs, Citrate synthase; Idh3a, Isocitrate dehydrogenase [NAD] subunit alpha; Trx, thioredoxin; Prdx, Peroxiredoxins; Gpx, glutathione peroxidases; Glrx, Glutaredoxin.

# MATERIALS AND METHODS

## Drugs and Reagents

Emodin (1, 3, 8-trihydrow-6-meth-ylanthraquinone) was purchased from Chengdu Ruifen Si Biological Technology Co., Ltd. (Chengdu, China, purity≥98%). Electrophoresis agents [sodium lauryl sulfate (SDS), acrylamide, N, N'-Methylenebisacrylamide (Bis), Tris (hydroxymethyl) amino methane (Tris), Glycine (Gly), ammonium persulfate (Aps), N, N, N', N'-Tetramethylethylenediamine (TEMED), Bromophenol Blue (BPB), glycerol, urea, and mercaptoethanol] were obtained from Beijing Bio Dee Biotechnology Co.Ltd. (Beijing China). Hcl was purchased from Beijing Chemical Works (Beijing, China). A protease inhibitor cocktail was obtained from Roche (Mannheim, Germany). Coomassie Blue R250 was purchased from Sigma (USA).All other chemicals were of analytical grade reagent. Deionized water (R > 18.2 MΩ) used for all experiments was purified by using Millipore purification system (Billerica, MA, USA). Chloraldehyde hydrate (S24149) was purchased from Beijing Honghu United Chemical Products Co., Ltd. Skimmed milk powder (Q/NYLB 0039 S) was purchased from Yili Company. NaCl (PBZ0637-3) was purchased from Beijing Oubei Biotechnology Co., Ltd. Tween 20 and dithiothreitol were purchased from amresco, USA; iodoacetamide and ammonium bicarbonate were purchased from Beijing Inoke Technology Co., Ltd. Bradford Assay kits, ECL kits were purchased from Biyuntian Biotechnology Co., Ltd. Color prestained protein Marker was purchased from Abfans. PVDF membrane (Immobilon-P; Millipore Corp) was purchased from

Bedford, MA, USA. Seahorse XF cell mitochondrial stress test kit (oligomycin 2.5 mmol/L, carbonyl cyanide 4-(trifluoromethoxy) phenylhydrazone (FCCP) 2.5 mmol/L, Antimycin 2.5 mmol/L, Rotenone 2.5 mmol/L) were purchased from Agilent, USA. Anti-Ndufs3, Anti-Txn2, Anti-Prdx3, Anti-Gpx3, and Anti-Glrx5 were obtained from Bioss Co., Ltd. Anti-Atp5g1, Anti-Acads, Anti-Hadhb, Anti-Sdhb, Anti-Uqcrh, Anti-Cox5a, Anti-CS, and Anti-Idh3a were obtained from Abcam Co., Ltd (England).

## Animal Treatments

Male Sprague-Dawley rats (9 weeks old, 200-300 g) were purchased from Beijing Vital River Laboratory Animal Technology Co., Ltd. (Beijing, China). Rats were housed at a constant room temperature and humidity (21 ± 2°C; 45–55%) under a 12–h light/dark cycle. The rats had ad libitum access to food and water. All animal experiments were approved by the Committee on Animal Care and Use of Institute of Chinese Materia Medica, China Academy of Chinese Medical Sciences, and the protocol was approved by Animal Ethical and Welfare Committee of CACMS.

Twelve rats were randomly assigned to either a control group (6 rats) or an emodin group (6 rats). Rats in the emodin group were orally administrated with emodin (150 mg/kg daily, 10 times the clinical equivalent of rhubarb), and rats in the control group received the same volume of physiological saline. After four weeks administration, all rats were sacrificed. Blood was collected and centrifuged to get serum for pathological examination. After blood collection, livers of rats in each group were quickly removed by laparotomy and divided into several small pieces, some of which were fixed in 4% polyformaldehyde solution for histopathology, while the rest of the liver tissue samples were then immediately frozen by immersion in liquid nitrogen, and stored at -80°C for proteomic analysis.

## Extraction and Gel Separation of Rat Liver Proteins

Equal amounts of liver samples from all animals in each group were pooled and prepared. Three biological replicates were prepared for the control group and emodin group, which were used for proteomics study. The detailed steps of protein extraction are as follows: Rat livers were homogenized in the PBS buffer containing protease inhibitor cocktail with a high-throughput tissue homogenizer (Sceintz-48, Ningbo, China). Then, proteins of rat livers were extracted with 8 M urea and total protein concentration was detected with the Bradford Assay kit (P0006, Beyotime Institute of Biotechnology, China). After quantification, equal amounts of proteins (30 μg) were separated with 10 or 12% sodium dodecyl sulfate polyacrylamide gel electrophoresis (SDS-PAGE). The gels ran on the Bio-Rad electrophoresis system at 80 W/gel for 20 min and then ran at 120 W/gel until bromophenol blue reaches the bottom of the gel. The gels were stained using coomassie brilliant blue.

## Gel Tryptic Digestion

Protein bands of interest were excised from the preparative gels, and reduced with 25 mmol/L dithiotreitol, then alkylated in 55 mmol/L iodoacetamide and carried out overnight at 37°C with sequencing grade modified trypsin in 50 mmol/L ammonium bicarbonate. The peptides were extracted twice with 0.1% trifluoroacetic acid in 50% acetonitrile aqueous solution for 30 min. The extractions were centrifuged to reduce the volume. The digested peptides were dissolved into 0.1% formic acid. Equal amounts of proteins from rat livers were combined and analyzed by LC-MS/MS.

## Label-Free Quantitative Proteomics

The identification of trypsin-digested proteins was performed through a Thermo-Dionex Ultimate 3000 HPLC coupled to a Thermo LTQ-Orbitrap Velos Pro mass spectrometer. Peptides were separated on an analytical homemade fused silica capillary column (75 μm ID, 150 mm length; Upchurch, Oak Harbor, WA) which was packed with C-18 resin (300 A, 5 μm; Varian, Lexington, MA) at a flow rate 0.250 μL/min. Mobile phase A was 0.1% formic acid aqueous solution, and mobile phase B was 100% acetonitrile containing 0.1% formic acid. Data acquisition was performed using Xcalibur 2.0.7 software. Mass spectrometry acquisition was in positive ion mode. Detailed parameters are as follows: capillary voltage8 V, cone voltage 100 V, ion source voltage 2.4 kV, Data acquisition range m/z 400-1800, Scanning in centroid mode with 60000 resolution, Linear ion trap dynamic exclusion scanning mode is adopted in the detection of secondary mass spectrometry Orbitra, first level full scan with 10 strongest LTQ secondary scans, signals with the same m/z appeared within 20 s were dynamically eliminated using secondary scan. The secondary scan chose the CID mode, the collision gas is high-purity helium (99.99% He), collision standardized energy is controlled at 35%.

Proteins were identified by their peptide mass fingerprint data search against the Rattus norvegicus database with Proteome Discoverer (Version 1.4). The criteria of identification were set as the following: full tryptic specificity was required; two missed cleavages were allowed; carbamidomethylation was set as fixed modification; oxidation (M) were set as variable modifications; precursor ion mass tolerance was 10 ppm for all MS acquired in the Orbitrap mass analyzer; and fragment ion mass tolerance was 0.8 Da for all MS2 spectra acquired in the LTQ. High confidence score filter (FDR < 1%) was used to select the "hit" peptides. Finally, the proteins were identified and analyzed artificially to confirm the authenticity.

## Bioinformatics Analysis of Differentially Expressed Proteins

GO enrichment analysis with biological process and molecular function of potential targets were carried out for biological function annotation based on a DAVID bioinformatics database (https://david.ncifcrf.gov/gene2gene.jsp). KEGG Pathway database (http://www.genome.jp/kegg/pathway.html) was utilized to analyze the representative pathways of the differentially expressed proteins and a p-value ≤ 0.05 significant level was used. Protein interaction analysis was performed by string database (https://string-db.org/). The visualization of graphs was made by Cytoscape (version 3.6.0).

## Western Blot Analysis

Equal amounts of protein (30 μg) from each sample were separated on SDS-PAGE and electrophoretically transferred onto a PVDF membrane (Immobilon-P; Millipore Corp., Bedford, MA, USA) and blocked in 10% nonfat powdered milk in Tris-Buffered Saline Tween-20 (TBST: 10 mmol/L Tris-HCl; 150 mmol/L NaCl; 0.05% tween-20; pH 7.6) overnight at 4°C. The membranes were incubated in primary antibodies overnight at 4°C or at 37°C for 2 h. After washing three times in TBST, HRP-labeled Goat Anti-Mouse IgG antibody or HRP-labeled Goat Anti-Rabbit IgG antibody was added to membranes and incubated for 2 h at room temperature. The membranes were then washed three times in TBST for 15 min, followed by signal detection using an ECL detection kit from Millipore Corporation. β-actin was utilized as a housekeeping protein.

## Mitochondrial Stress Test Assay

Mitochondrial function was assessed using the Seahorse XFe 24 Analyzer (Agilent Technologies, Santa Clara, CA). 5, 000 L-02 cells per well were seeded on Cell-Tak coated Seahorse plates. L-02 cells were treated with 10.93 μmol/L of emodin for 24 h (Zhang et al., 2019) prior to assessing mitochondrial function. Cells were equilibrated in XF media before testing the mitochondrial oxygen consumption rate (OCR). The mitochondrial stress test was carried out *via* the manual steps described. Using the mitochondrial stress test inhibitors, oligomycin (0.5μmol/L), FCCP (0.5mol/L), and rotenone and antimycin A (10 μmol/L) were used to gain basal respiration, maximal respiration, ATP production, proton leak, spare respiratory capacity, and coupling efficiency.

## Measurement of Reactive Oxygen Species

Take 0.5 g liver tissue and homogenate on ice for 10 minutes with 0.09% normal saline using a high-throughput tissue homogenizer (Sceintz-48, Ningbo, China), and then centrifuge at 10000g for 10min at 4°C, collect the supernatant, then detect the level of ROS by Luminol chemiluminescence method.

## Molecular Docking

Three-dimensional structures of the target proteins were downloaded from Protein Data Bank database (https://www.rcsb.org/pdb/home/home.do). Firstly, emodin was imported into the Discovery Studio 3.5 software for hydrogenation optimization. Next, the three-dimensional structure of target proteins was introduced and optimized through dehydration, hydrogenation, and structural modification. Emodin was docked with target proteins respectively. The higher the total score, the more stable the binding between the ligand and the receptor. If the total score is ≥ 6, it can be inferred that there is a strong interaction between the component molecule and the corresponding protein target. Moreover, the closer the absolute value of crash is to 0, the more likely the target protein can be considered.

## Statistical Analysis

All experimental data obtained from rats were expressed as mean ± standard deviation (SD). The significance of the differences among different treatment groups was determined using Student's t-test by GraphPad Prism 6.0 software. The level $P < 0.05$ was considered to indicate a statistically significant difference.

# RESULTS

## Comparative Proteomic Analysis in Livers Between Emodin Group and Control Group

In order to elucidate the effects of emodin on liver function, we measured the activities of serum alanine aminotransfease (ALT) and aspartate transaminase (AST) in different groups before (Yang et al., 2018), results showed that in emodin group, increased ALT and AST levels were detected in rats and these changes were significant ($P < 0.05$). Histopathology observation showed that HE-stained hepatic sections in the control group were microscopically normal. After being treated with emoin (150 mg/kg daily) for four weeks, mild inflammation changes were found in the liver (Yang et al., 2018). Further, we explored the liver injury mechanism induced by emodin. To characterize the expressions of proteins in response to emodin exposure, the label-free quantitative proteomics technique was used. Firstly, equal amounts of the control group and emodin-treated group were initially separated by SDS-PAGE, then differentially expressed proteins were qualitatively and quantitatively tested by unlabeled methods. The experiment was repeated three times, and each sample identified approximately 4,530 proteins (≥1 peptide). According to $P < 0.05$ and $F > 1.2$ or $<0.67$, 892 differentially expressed proteins were screened and their expressions were all down-regulated under emodin administration. The 892 differentially expressed proteins data can be seen in **Table S1**. In order to analyze the biological significance of differential proteins, the David Bioinformatics Platform was used. The top 20 significantly enriched terms in Biological Process, Molecular Function, and Cellular Component categories were selected, according to $P < 0.05$, P-values were corrected using the Benjamini-Hochberg procedure, as shown in **Figure 1**. In the biological process category, proteins were mainly involved in the oxidation-reduction biological process, ATP metabolic process, or fatty acid β-oxidation. Based on cell composition, proteins were mainly attributed to extracellular exosome, mitochondria, and mitochondrial inner membrane. In the molecular function category, proteins were mainly involved in poly RNA binding, unfolded protein binding, and electron carrier activity (**Figure 1**). In addition, KEGG database was used to enrich differentially expressed proteins, according to BH-corrected P-values < 0.05, the top 20 pathways were screened. Results demonstrated that the differentially expressed proteins mainly participated in metabolic pathways, OXPHOS, and Biosynthesis of antibiotics (**Figure 2A**).

Redox reaction is the most basic motive force and the most common metabolic reaction mechanism of biological evolution and life activities. To explore the relationship between mitochondrial metabolism and redox disequilibrium under the influence of emodin, we mainly analyzed 101 proteins in oxidation-reduction biological process. The 101 proteins data

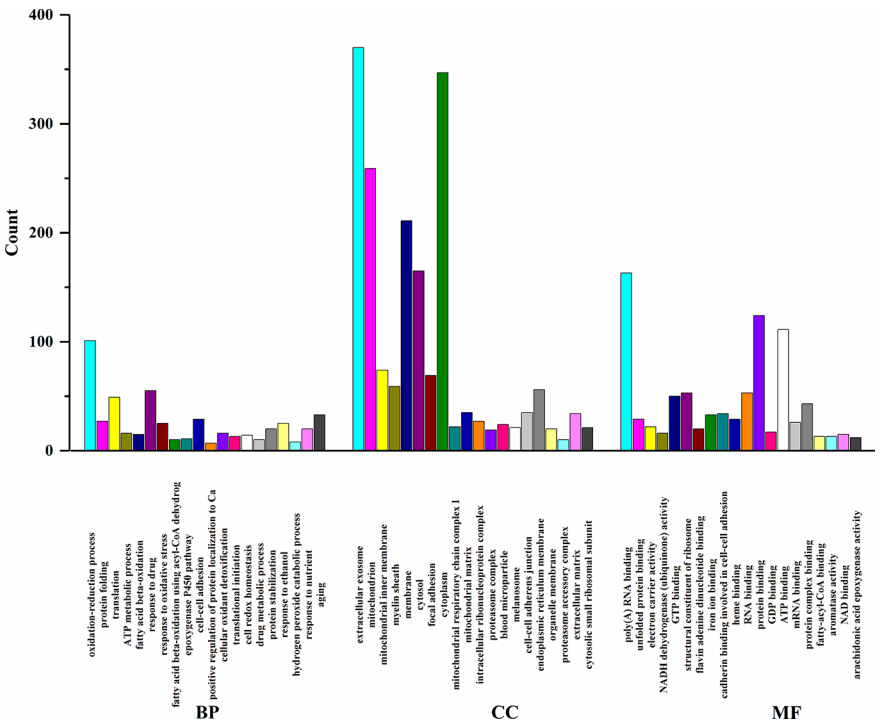


**FIGURE 1 |** GO enrichment analysis of differentially expressed proteins.

can be seen in **Table S2**. The proteins were submitted to string database for PPI network construction. High confidence of protein interaction data with a score of more than 0.7 were selected and hide disconnected nodes in the network. The results visualized by cytoscape (**Figure 2B**) showed that fatty acid degradation, TCA. and OXPHOS were involved. Taken together, by analyzing the proteomics data, it preliminarily speculated that emodin may mainly interfere with fatty acid β-oxidation, TCA, and OXPHOS to destroy redox homeostasis and cause hepatic injury.

## Emodin Led to Mitochondrial Dysfunction

Among the 892 differential proteins, we specifically found the key proteins involved in fatty acid β-oxidation (**Table S3**), mitochondrial respiratory chain (**Table S4**), and TCA cycle (**Table S5**) in proteomic data, whose protein expressions were down-regulated by emodin. Thus, we next tested if emodin can alter the metabolic activity of mitochondria. According to the functional identification and fold-change-ratio changes, Acads, Hadhb, Ndufs3, Ndufb7, Sdhb, Uqcrh, Cox5a, Atp5g1, Cs, and Idh3a were selected for western blot analysis. Results (**Figure 3A**) demonstrated that emodin inhibited protein expressions of Acads, Hadhb, Ndufs3, Ndufb7, Sdhb, Uqcrh, Cox5a, Atp5g1, Cs, and Idh3a in various degrees, which indicated that emodin might inhibit the function of fatty acid β-oxidation, TCA cycle, and OXPHOS taken place in mitochondria.

Next, a mitochondrial stress test was performed by sequential use of oligomycin, FCCP, rotenone, and antimycin A. The overall OCR profile was lower in the emodin group compared to the control group (**Figure 3B**). Between them, maximal respiration, ATP production, spare respiratory capacity, and coupling efficiency showed progressive decline with emodin treatment (**Figure 3C**). Only proton leak increased in the emodin group (**Figure 3C**) which can be increased by oxidative stress. However, basal respiration was not affected (**Figure 3C**). These results indicated that emodin disturbed the function of mitochondria by inhibiting the expressions of proteins related to fatty acid β oxidation, citric acid cycle, and mitochondrial respiratory chain.

## Emodin Destroyed Redox Equilibrium

Proteomic data showed that emodin mainly affected the redox biological process. Therefore, we investigated whether emodin can induce the generation of oxidative stress in livers. By detecting ROS with reference to protocol of ROS test kit (E004, Nanjing Jiancheng Bioengineering Research Institute), result showed that emodin led to a significant increase in ROS levels (**Figure 4A**).

Inhibition of the antioxidant defense system contributes to oxidative stress. By digging up the proteomic data, 11 antioxidant proteins were down-regulated (**Table S6**) in emodin group, including glutathione reductase, thioredoxin, glutathione peroxidase, and peroxide reductase protein. Based on western blot, proteins with high protein fold-change-ratio were chosen to be verified. The results (**Figure 4B**) showed that their protein expressions in the emodin group were significantly lower than

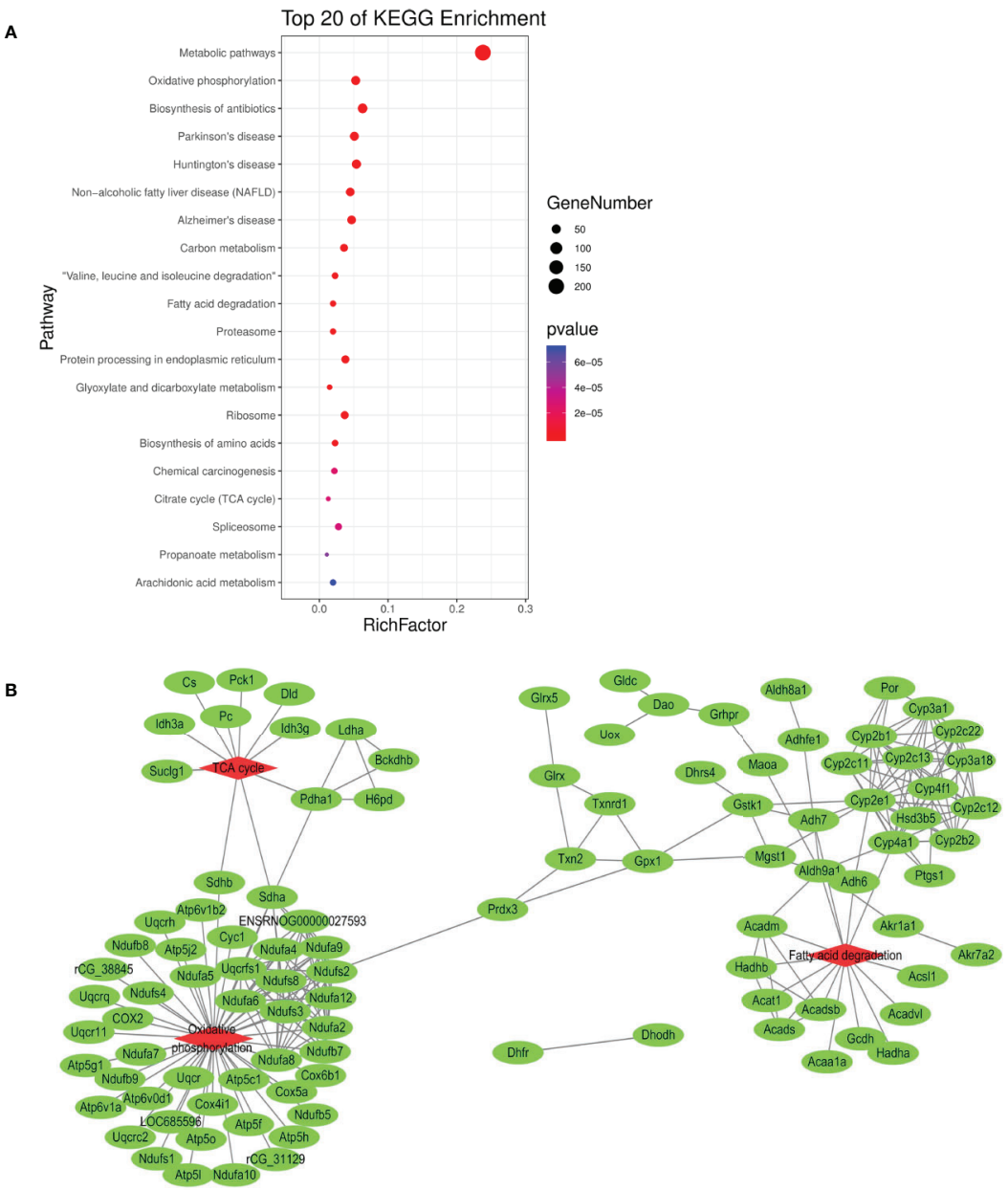


**FIGURE 2 | (A)** KEGG pathway analysis of differentially expressed proteins. **(B)** Interaction analysis of proteins involved in oxidation-reduction biological process. The green ellipse represents the proteins, and the red diamond represents the pathways.

those in the control group. Results showed that emodin inhibited antioxidant function in livers and induced oxidative stress.

## Exploration of Emodin Targets Through Molecular Docking

Molecular docking experiment was conducted to further explore the liver injury mechanism of emodin and to clarify the targets of emodin in affecting redox balance *via* mitochondrial metabolism. Firstly, fatty acid oxidation, TCA cycle, OXPHOS, and antioxidant related proteins in proteomic data were found in PDB database. Secondly, human proteins with ligands were selected. Proteins with emodin/ligand value close to 1 were selected to remove the negative results. Then, according to the total score, protein with high scores were selected. Generally, a total score greater than 6 was considered. The scores of Acadvl and complex IV were 7.6312 and 8.0158 respectively, hence, Acadvl and complex IV were selected (**Table S7**). The molecular docking results of emodin and ligands were shown in **Figure 5**. Emodin could form hydrogen bonds with His, Tyr, and Arg residues in Complex IV, and it also had hydrogen bonding forces

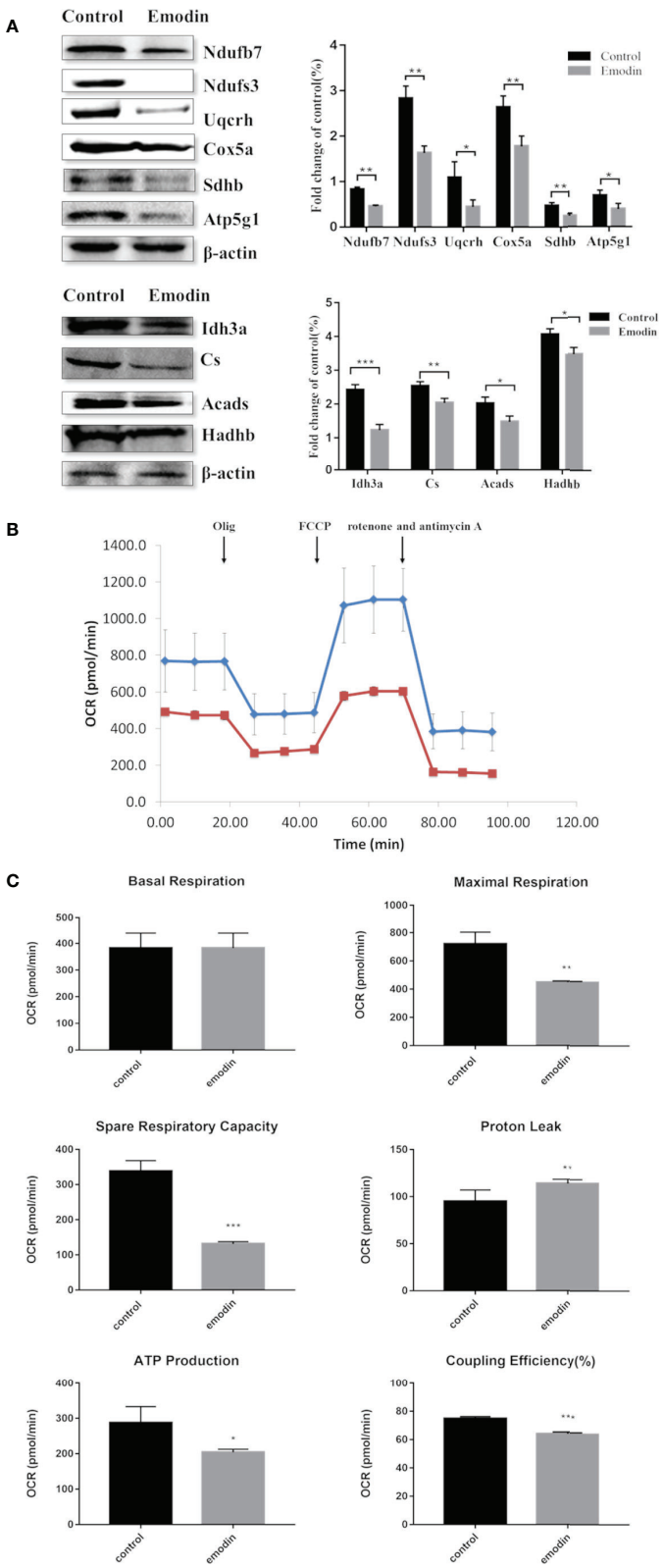


**FIGURE 3 | (A)** KEGG pathway analysis of differentially expressed proteins. **(B)** Interaction analysis of proteins involved in oxidation-reduction biological process. The green ellipse represents the proteins, and the red diamond represents the pathways.

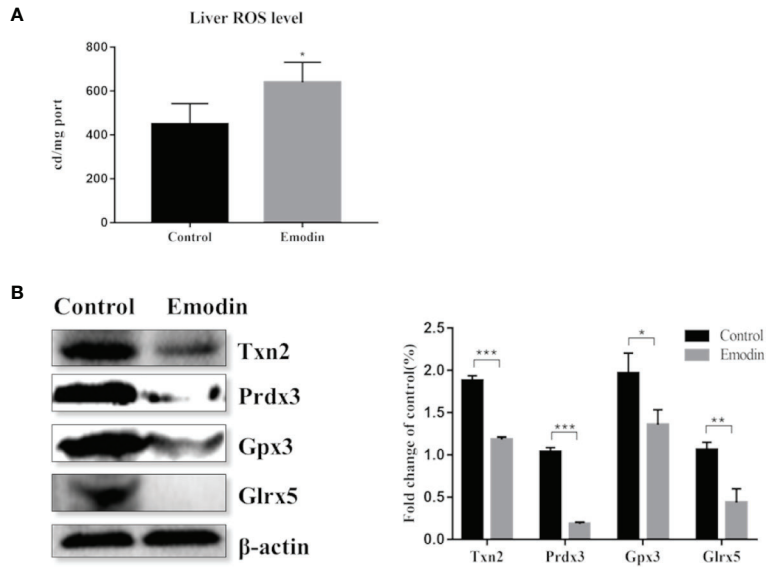


**FIGURE 4 | (A)** Change of the ROS level between the emodin group and the control group. **(B)** Western blot analysis of differentially expressed antioxidant proteins, including protein bands and relative abundance. Values are mean ± SD, n = 3. * for P value <0.05, ** for P value <0.01, *** for P value <0.001.

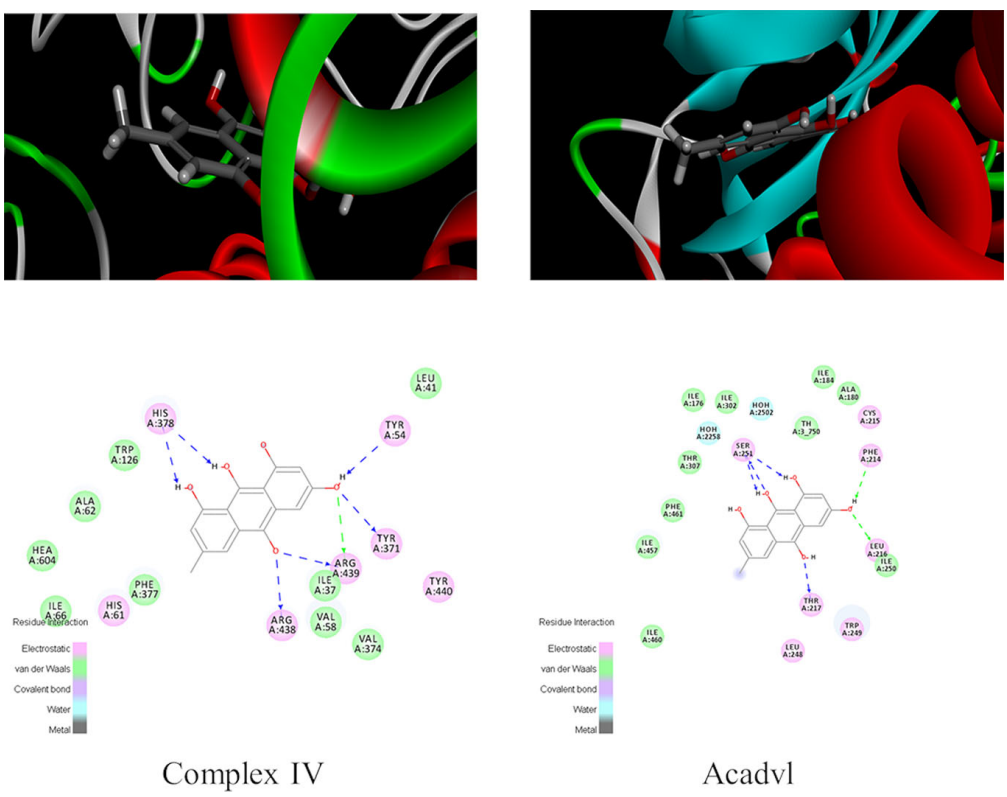


**FIGURE 5 |** Graphs of molecular docking results.

with Ser, Phe, Leu, and Thr of Acadvl. The results showed that there were interactions between emodin and residues of Acadvl and complex IV. Hence, Acadvl and complex IV may be the possible targets of emodin in liver injury signal pathway.

## DISCUSSION

Recent evidence suggested that oxidative stress and mitochondrial pathways cooperate to mediate the development of DILI induced by emodin. Here, we show that emodin can promote the occurrence of oxidative stress by impairment of fatty acid β-oxidation, TCA cycle, and OXPHOS as well as an imbalance in the expression of antioxidant enzymes. Hence, we prove a functional relationship between two major pathways driving the development of DILI and also provide additional insight into how emodin affected the mitochondrial metabolic process.

Serum ALT and AST are important enzyme indexes in liver disease screening. Analysis of serum samples from rats in the control and emodin groups indicated that emodin induced liver injury (Yang et al., 2018). Previous studies have also found that emodin induced liver injury *in vivo* and *in vitro* to some extent (Li et al., 2012; Zhang et al., 2010; Liu et al., 2015b; Ma et al., 2015; Jiang et al., 2017), similar to our observation.

Mitochondrial is an appealing target, as it plays an important role in the regulation of redox balance, which is crucial for cell life and death (Smith et al., 2012). Our proteomic analysis revealed emodin affected the redox balance by interfering with fatty acid β-oxidation, TCA cycle, and OXPHOS in mitochondria. Coenzyme A dehydrogenase and L-β-Hydroxyl acyl CoA dehydrogenase are involved in the fatty acid beta-oxidation pathway, which can catalyze dehydrogenation of fatty acyl CoA with FAD as auxiliary group and oxidize L-beta-hydroxyalkyl CoA at the same time, generating $FADH_2$ and NADH. CoA produced by fat degradation is further oxidized by TCA cycle, reducing NADH and $NAD^+$ to $FADH_2$ and NADH at the same time. Specifically, emodin bound to acadvl protein inhibited the normal expressions of downstream products. To adapt to this change, the body would appropriately down-regulate the protein expressions of key catalytic enzymes involved in downstream cascades, including L-β-Hydroxyl acyl CoA dehydrogenase, citrate synthase, isocitrate dehydrogenase, and succinate dehydrogenase, which were down-regulated in the proteomic data (**Table S3**, **S5**). Furthermore, it inhibited fatty acid β-oxidation, TCA cycle in downstream. The cascade feedback eventually caused the protein expression of CoA dehydrogenase to be down-regulated. Besides, the results of this cascade feedback indicated the decrease in NADH and FADH2 and the deformity of electron and energy production in mitochondria. In addition, our previous studies have found that emodin inhibited the transport of NADH and FADH2 to mitochondria (Yang et al., 2018). Moreover, the loss of hepatic fatty acid β-oxidation alters systemic lipid metabolism, which may be related to our previous studies that emodin can cause lipid accumulation in hepatocytes (Zhang et al., 2019). Electrons produced in the process of fatty acid beta-oxidation and TCA cycle are not only transferred to $O_2$ *via* complex I~IV but also drive proton transfer and ATP production.

Complex IV is a complex at the distal end of the mitochondrial respiratory chain, which can transfer a pair of hydrogen atoms removed from metabolism to oxygen to generate $H_2O$. Emodin passed through the outer membrane of mitochondria and acted on complex IV which was attached to the mitochondria inner membrane. On the one hand, it suppressed electron transfer of the respiratory chain, leading to a decrease in the production of intracellular ubiquinone, which in turn led to an increase in ROS (Kim et al., 2003). On the other hand, it inhibited the function of the mitochondrial respiratory chain, causing the down-regulation of protein expressions of the respiratory chain complex, which were reflected in the proteomics data (**Table S4**). It caused the decrease of mitochondrial maximal respiration and spare respiratory capacity and the increase of proton leakage (**Figure 3C**). ATP synthase is responsible for transferring protons out of the inner membrane to generate ATP. The down-regulation of ATP synthase restrained mitochondrial ATP production (**Figure 3C**). These findings suggested that emodin might interfere with fatty acid β-oxidation, TCA cycle, and OXPHOS by targeting to acadvl and complex IV.

Mitochondrial dysfunction may result in an excessive production of ROS, which was detected in the livers of the emodin group (**Figure 4A**). In order to maintain redox homeostasis, cells produce small molecule antioxidants as well as various antioxidant proteins (Walsh et al., 2009). $H_2O_2$ can be degraded by peroxiredoxins (Prdx) or by glutathione peroxidases (Gpx) which use thioredoxin (Trx) or GSH as electron donors (Finkel, 2003). Trx and glutaredoxin (Glrx) are important thiol-disulfide bond oxidoreductase which are responsible for the reduction of disulfide bonds in target proteins and are important components in the thioredoxin system and the glutamate reductase system. In the down-regulated proteins, 11 proteins related to redox regulatory were found (**Table S6**), which increased susceptibility to oxidative stress and contributed to the disruption of redox homeostasis and ultimately damaged biomolecules (Liu et al., 2009). Previous studies have found that emodin could induce oxidative stress by producing ROS and consuming antioxidants such as GSH and SOD (Ma et al., 2015; Jiang et al., 2017; Jiang et al., 2018). However, in this study, emodin could inhibit Prdx, Gpx, thioredoxin system and glutaredoxin system, which is a new discovery.

Mitochondria are crucial for cell function and viability, and play a central role in ROS generation (Cherukuri and Nelson, 2008; Chatterjee et al., 2008). Mitochondrial respiratory chain has been shown to be involved in ROS generation (Poyton et al., 2009). However, it remains to be determined how mitochondria metabolism initiates the generation of ROS under the influence of emodin. There are reports showing that emodin can induce suppression of respiratory chain complex function and cause mitochondrial dysfunction (Lin et al., 2019). Our results supported the fact that emodin, through targeting to acadvl and complex IV, impaired mitochondrial function by interfering with fatty acid β-oxidation, TCA cycle, and OXPHOS. The damage to mitochondrial function and imbalance of expressions of antioxidant enzymes could lead to further overproduction of

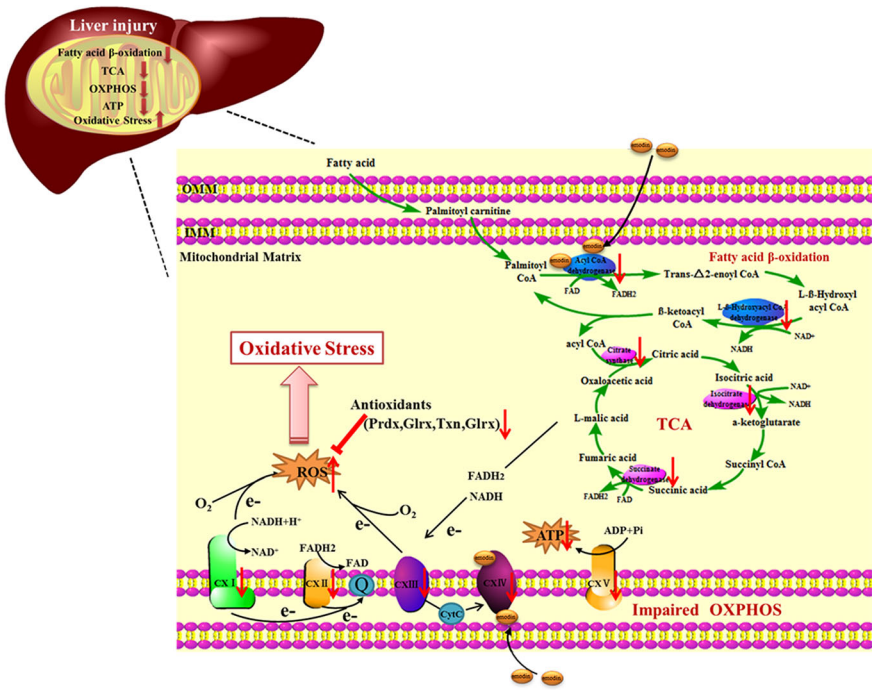


**FIGURE 6 |** The proposed mechanism of liver injury induced by emodin in SD rats.

ROS, which in turn leads to oxidative damage (**Figure 6**). Extensive research has shown that oxidative stress can lead to the development of chronic inflammation (Goldstein et al., 1992), which was revealed by histopathological evaluation.

## CONCLUSION

In this study, we aimed to explore the hepatotoxicity mechanisms of emodin on rats. Results showed that emodin (150 mg/kg daily) exposure for four weeks in SD rats could cause liver injury. Our experiments proved that oxidative stress injury caused by emodin may be the result of some deficiency in mitochondrial function, including fatty acid β-oxidation, TCA cycle, OXPHOS, and antioxidant defenses in rats *via* targeting to bind acadvl and complex IV.

## DATA AVAILABILITY STATEMENT

The original contributions presented in the study are included in the article/supplementary files, further inquiries can be directed to the corresponding author.

## ETHICS STATEMENT

All the animal experiments were approved by the Committee on Animal Care and Use of Institute of Chinese Materia Medica, China Academy of Chinese Medical Sciences (Beijing, China). This study was carried out in accordance with the principles of the Basel Declaration and recommendations of guidelines of the National Institutes of Health Conflict of Interest.

## AUTHOR CONTRIBUTIONS

YZ, XWY, and HX designed the experiments. YZ and XWY carried out the experiments. YZ and XWY analyzed the data. ZJ, JL, XNY, and YD contributed reagent/materials./analysis tools. YZ and HX wrote the manuscript.

## FUNDING

The project was financially supported by the National Science and Technology Major Project (2019ZX09201004-001) and the National Natural Science Foundation of China (NO. 81573839 and NO. 81774155). We thank The Center of Biomedical Analysis, Tsinghua University for the help.

## SUPPLEMENTARY MATERIAL

The Supplementary Material for this article can be foundonline at: https://www.frontiersin.org/articles/10.3389/fphar.2020.00416/full#supplementary-material

## REFERENCES


Bechmann, L. P., Hannivoort, R. A., Gerken, G., Hotamisligil, G. S., Traune, R. M., and Canbay, A. (2012). The interaction of hepatic lipid and glucose metabolism in liver diseases. *J. Hepatol.* 56, 952–964. doi: 10.1016/j.jhep.2011.08.025

Berson, A., Cazanave, S., Descatoire, V., Tinel, M., Grodet, A., Wolf, C., et al. (2006). The antiinflammatory drug, nimesulide (4-nitro-2-phenoxymethanesulfoanilide), uncouples mitochondria and induces mitochondrial permeability transition in human hepatoma cells: protection by albumin. *J. Pharmacol. Exp. Ther.* 318, 444–454. doi: 10.1124/jpet.106.104125

Boveris, A., Cadenas, E., and Stoppani, A. O. (1976). Role of ubiquinone in the mitochondrial generation of hydrogen peroxide. *Biochem. J.* 156 (2), 435–444. doi: 10.1042/bj1560435

Burton, G. J., and Jauniaux, E. (2011). Oxidative stress. *Best Pract. Res. Clin. Obstet. Gynaecol.* 25 (3), 287–299. doi: 10.1016/j.bpobgyn.2010.10.016

Chatterjee, S., Kundu, S., and Bhattacharyya, A. (2008). Mechanism of cadmium induced apoptosis in the immunocyte. *Toxicol. Lett.* 177, 83–89. doi: 10.1016/j.toxlet.2007.12.010

Cherukuri, D. P., and Nelson, M. A. (2008). Role of reactive oxygen species (ROS) and JNKs in selenite-induced apoptosis in HepG2 cells. *Cancer Biol. Ther.* 7, 697–698. doi: 10.4161/cbt.7.5.6088

Cui, Y. T., Liu, B., Xie, J., Xu, P., Habte-Tsion, H. M., and Zhang, Y. Y. (2014). The effect of emodin on cytotoxicity, apoptosis and antioxidant capacity in the hepatic cells of grass carp (Ctenopharyngodon idellus). *Fish Shellfish Immunol.* 38, 74–79. doi: 10.1016/j.fsi.2014.02.018

Duchen, M. R. (2004). Mitochondria in health and disease: perspectives on a new mitochondrial biology. *Mol. Aspects Med.* 25, 365–451. doi: 10.1016/j.mam.2004.03.001

Ďuračková, Z. (2010). Some current insights into oxidative stress. *Physiol. Res.* 59, 459–469.

Finkel, T. (2003). Oxidant signals and oxidative stress. *Curr. Opin. Cell Biol.* 15, 247–254. doi: 10.1016/s0955-0674(03)00002-4

Galluzzi, L., Kepp, O., Trojel-Hansen, C., and Kroemer, G. (2012). Mitochondrial control of cellular life, stress, and death. *Circ. Res.* 111, 1198–1207. doi: 10.1161/CIRCRESAHA.112.268946

Goldstein, A. R., White, R. H., Akuse, R., and Chantler, C. (1992). Long-term follow-up of childhood Henoch-Schonlein nephritis. *Lancet* 339, 280–282. doi: 10.1016/0140-6736(92)91341-5

Jiang, L. L., Zhao, D. S., Fan, Y. X., Yu, Q., Li, P., and Li, H. J. (2017). Detection of Emodin Derived Glutathione Adduct in Normal Rats Administered with Large Dosage of Polygoni Multiflori Radix. *Front. Pharmacol.* 8, 446. doi: 10.3389/fphar.2017.00446

Jiang, L. L., Jiang, Y., Zhao, D. S., Fan, Y. X., Yu, Q., Li, P., et al. (2018). CYP3A Activation and Glutathione Depletion Aggravate Emodin-Induced Liver Injury. *Chem. Res. Toxicol.* 31, 1052–1060. doi: 10.1021/acs.chemrestox.8b00117

Kim, J. S., He, L., and Lemasters, J. J. (2003). Mitochondrial permeability transition: a common pathway to necrosis and apoptosis. *Biochem. Biophys. Res. Commun.* 304, 463–470. doi: 10.1016/s0006-291x(03)00618-1

Lee, M. H., Kao, L., and Lin, C. C. (2011). Comparison of the antioxidant and transmembrane permeative activities of the different Polygonum cuspidatum extracts in phospholipid-based microemulsions. *J. Agric. Food Chem.* 59, 9135–9141. doi: 10.1021/jf201577f

Lee, Y. H., Goh, W. W., Ng, C. K., Raida, M., Wong, L., Lin, Q., et al. (2013). Integrative toxicoproteomics implicates impaired mitochondrial glutathione import as an off-target effect of troglitazone. *J. Proteome Res.* 12, 2933–2945. doi: 10.1021/pr400219s

Li, C. L., Ma, J., Zheng, L., Li, H. J., and Li, P. (2012). Determination of emodin in L-02 cells and cell culture media with liquid chromatography-mass spectrometry: application to a cellular toxicokinetic study. *J. Pharm. BioMed. Anal.* 71, 71–78. doi: 10.1016/j.jpba.2012.07.031

Lim, M. S., Lim, P. L., Gupta, R., and Boelsterli, U. A. (2006). Critical role of free cytosolic calcium, but not uncoupling, in mitochondrial permeability transition and cell death induced by diclofenac oxidative metabolites in immortalized human hepatocytes. *Toxicol. Appl. Pharmacol.* 217, 322–331. doi: 10.1016/j.taap.2006.09.012

Lin, L., Liu, Y., Fu, S., Qu, C., Li, H., and Ni, J. (2019). Inhibition of Mitochondrial Complex Function-The Hepatotoxicity Mechanism of Emodin Based on Quantitative Proteomic Analyses. *Cells* 8, pii: E263. doi: 10.3390/cells8030263

Liu, J., Yu, Z., Guo, S., Lee, S. R., Xing, C., Zhang, C., et al. (2009). Effects of neuroglobin overexpression on mitochondrial function and oxidative stress following hypoxia/reoxygenation in cultured neurons. *J. Neurosci. Res.* 87, 164–170. doi: 10.1002/jnr.21826

Liu, X. Y., Liu, Y. Q., Qu, Y., Cheng, M. C., and Xiao, H. B. (2015a). Metabolomic profiling of emodin-induced cytotoxicity in human liver cells and mechanistic study. *Toxicol. Res.* 4, 948–955. doi: 10.1039/c4tx00246f

Liu, X. Y., Liu, Y. Q., Cheng, M. C., and Xiao, H. B. (2015b). Metabolomic Responses of Human Hepatocytes to Emodin, Aristolochic Acid, and Triptolide: Chemicals Purified from Traditional Chinese Medicine. *J. Biochem. Mol. Toxicol.* 29, 533–543. doi: 10.1002/jbt.21724

Ma, J., Zheng, L., He, Y. S., and Li, H. J. (2015). Hepatotoxic assessment of Polygoni Multiflori radix extract and toxicokinetic study of stilbene glucoside and anthraquinones in rats. *J. Ethnopharmacol.* 162, 61–68. doi: 10.1016/j.jep.2014.12.045

Myatt, L., and Cui, X. (2004). Oxidative stress in the placenta. *Histochem. Cell Biol.* 122, 369–382. doi: 10.1007/s00418-004-0677-x

Naqvi, S., Ullah, M. F., and Hadi, S. M. (2010). DNA degradation by aqueous extract of Aloe vera in the presence of copper ions. *Indian J. Biochem. Biophys.* 47, 161–165. doi: 10.1089/ham.2010.1014

Pettinelli, P., Obregon, A. M., and Videla, L. A. (2011). Molecular mechanisms of steatosis in nonalcoholic fatty liver disease. *Nutr. Hosp.* 26, 441–450. doi: 10.1590/S0212-16112011000300003

Poyton, R. O., Ball, K. A., and Castello, P. R. (2009). Mitochondrial generation of free radicals and hypoxic signaling. *Trends Endocrinol. Metab.* 20, 332–340. doi: 10.1016/j.tem.2009.04.001

Smith, R. A., Hartley, R. C., Cocheme, H. M., and Murphy, M. P. (2012). Mitochondrial pharmacology. *Trends Pharmacol. Sci.* 33, 341–352. doi: 10.1016/j.tips.2012.03.010

Tan, F., Jin, Y., Liu, W., Quan, X., Chen, J., and Liang, Z. (2012). Global liver proteome analysis using iTRAQ labeling quantitative proteomic technology to reveal biomarkers in mice exposed to perfluorooctane sulfonate (PFOS). *Environ. Sci. Technol.* 46, 12170–12177. doi: 10.1021/es3027715

Turrens, J. F., and Boveris, A. (1980). Generation of superoxide anion by the NADH dehydrogenase of bovine heart mitochondria. *Biochem. J.* 191, 421–427. doi: 10.1042/bj1910421

Valko, M., Leibfritz, D., Moncol, J., Cronin, M. T., Mazur, M., and Telser, J. (2007). Free radicals and antioxidants in normal physiological functions and human disease. *Int. J. Biochem. Cell Biol.* 39, 44–84. doi: 10.1016/j.biocel.2006.07.001

Walsh, B., Pear, A., Suchy, S., Tartaglio, J., Visco, K., and Phelan, S. A. (2009). Overexpression of Prdx6 and resistance to peroxide-induced death in Hepa1-6 cells: Prdx suppression increases apoptosis. *Redox Rep.* 14, 275–284. doi: 10.1179/135100009X12525712409652

Wang, J. B., Zhao, H. P., Zhao, Y. L., Jin, C., Liu, D. J., Kong, W. J., et al. (2011). Hepatotoxicity or hepatoprotection? Pattern recognition for the paradoxical effect of the Chinese herb Rheum palmatum L. in treating rat liver injury. *PloS One* 6, e24498. doi: 10.1371/journal.pone.0024498

Wang, M., Zhao, R., Wang, W., Mao, X., and Yu, J. (2012). Lipid regulation effects of Polygoni Multiflori Radix, its processed products and its major substances on steatosis human liver cell line L02. *J. Ethnopharmacol.* 139, 287–293. doi: 10.1016/j.jep.2011.11.022

Wang, C. H., Wu, S. B., Wu, Y. T., and Wei, Y. H. (2013). Oxidative stress response elicited by mitochondrial dysfunction: Implication in the pathophysiology of aging. *Exp. Biol. Med. (Maywood)* . 238, 450–460. doi: 10.1177/1535370213493069

Yang, Y. C., Lim, M. Y., and Lee, H. S. (2003). Emodin isolated from Cassia obtusifolia (Leguminosae) seed shows larvicidal activity against three mosquito species. *J. Agric. Food Chem.* 51, 7629–7631. doi: 10.1021/jf034727t

Yang, X., Zhang, Y., Liu, Y., Chen, C., Xu, W., and Xiao, H. (2018). Emodin induces liver injury by inhibiting the key enzymes of FADH/NADPH transport in rat liver. *Toxicol. Res. (Camb.)* 7, 888–896. doi: 10.1039/c7tx00307b

Yang, J., Zhu, A., Xiao, S., Zhang, T., Wang, L., Wang, Q., et al. (2019). Anthraquinones in the aqueous extract of Cassiae semen cause liver injury in rats through lipidmetabolism disorder. *Phytomedicine* 64, 153059. doi: 10.1016/j.phymed.2019.153059

Zhang, R. C., Liu, B., Sun, Z. X., and Xu, D. Y. (2010). Effects of extract of Polygonum multiflorum on cell cycle arrest and apoptosis of human liver cell line L02. *Zhong Xi Yi Jie He Xue Bao* 8, 554–561. doi: 10.3736/jcim20100608

Zhang, Y. H., Yang, X. W., Dai, Y. H., and Xiao, H. B. (2019). Effects of emodin on lipid accumulation and inflammation in hepatocytes. *China J. Chin. Mater. Med.* 44, 2820–2826. doi: 10.19540/j.cnki.cjcmm.20190321.401

**Conflict of Interest:** The authors declare that the research was conducted in the absence of any commercial or financial relationships that could be construed as a potential conflict of interest.

frontiers in Pharmacology

ORIGINAL RESEARCH
published: 06 May 2020
doi: 10.3389/fphar.2020.00528

# Investigation of the Lipid-Lowering Mechanisms and Active Ingredients of Danhe Granule on Hyperlipidemia Based on Systems Pharmacology

*Kuikui Chen*[1], *Zhaochen Ma*[1], *Xiaoning Yan*[1], *Jie Liu*[1], *Wenjuan Xu*[2], *Yueting Li*[1], *Yihang Dai*[1], *Yinhuan Zhang*[1] *and Hongbin Xiao*[1]*

[1] Research Center of Chinese Medicine Analysis and Transformation & School of Chinese Materia Medica, Beijing University of Chinese Medicine, Beijing, China, [2] School of Life Sciences, Beijing University of Chinese Medicine, Beijing, China

OPEN ACCESS

**Edited by:**
*Wei Zhou,*
*The Affiliated Hospital of Shenzhen University, China*

**Reviewed by:**
*Na Lin,*
*Beijing Key Laboratory of Quality Evaluation of Traditional Chinese Medicine, China*
*Suhong Chen,*
*Zhejiang University of Technology, China*

***Correspondence:**
*Hongbin Xiao*
*hbxiao69@163.com*

**Specialty section:**
*This article was submitted to Ethnopharmacology, a section of the journal Frontiers in Pharmacology*

**Received:** *15 December 2019*
**Accepted:** *03 April 2020*
**Published:** *06 May 2020*

**Citation:**
*Chen K, Ma Z, Yan X, Liu J, Xu W, Li Y, Dai Y, Zhang Y and Xiao H (2020) Investigation of the Lipid-Lowering Mechanisms and Active Ingredients of Danhe Granule on Hyperlipidemia Based on Systems Pharmacology. Front. Pharmacol. 11:528. doi: 10.3389/fphar.2020.00528*

**Objective:** Investigate the active ingredients and underlying hypolipidemic mechanisms of Danhe granule (DHG).

**Methods:** The lipid-lowering effect of DHG was evaluated in hyperlipidemic hamsters induced by a high-fat diet. The ingredients absorbed into the blood after oral administration of DHG in hamsters were identified by ultra-high-performance liquid chromatography coupled with quadrupole time-of-flight mass spectrometry (UHPLC-Q-TOF/MS). A systems pharmacology approach incorporating target prediction and network construction, gene ontology (GO) enrichment and pathway analysis was performed to predict the active compounds and map the compounds-targets-disease network. Real-time polymerase chain reaction (RT-PCR) and Western blot were utilized to analyze the mRNA and protein expression levels of predicted targets.

**Results:** DHG remarkably lowered the levels of serum total cholesterol (TC), triglyceride (TG), low-density lipoprotein cholesterol (LDL-c), and arteriosclerosis index (AI), at the same time, elevated the levels of serum high-density lipoprotein cholesterol (HDL-c) and HDL-c/TC ratio in hyperlipidemic hamsters. Sixteen ingredients absorbed into blood after oral administration of DHG were identified as the possible components interacted with targets. Moreover, 65 potential targets were predicted after targets intersection and compounds–targets–disease network mapping. Then, compounds–targets–pathways network mapping revealed that six active compounds (emodin, naringenin, etc.) compounds could interact with 10 targets such as sterol regulatory element binding protein (SREBP) 1c, SREBP-2 and peroxisome proliferation-activated receptor (PPAR) α, regulate three lipid metabolism-related pathways including SREBP control of lipid synthesis pathway, PPAR signaling pathway and nuclear receptors in lipid metabolism and toxicity pathway, and further affect lipid metabolic processes including fatty acid biosynthesis, low-density lipoprotein receptor (LDLR)-mediated cholesterol uptake, bile acid biosynthesis, and cholesterol efflux. Experimental results indicated that DHG significantly increased SREBP-2, LDLR, PPARα, liver X receptor alpha (LXRα),

cholesterol 7α-hydroxylase (CYP7A1), and ATP binding cassette subfamily A member 1 (ABCA1) mRNA and protein expressions while decreased SREBP-1c and fatty acid synthase (FAS) mRNA, and protein expressions.

**Conclusion:** DHG possessed a good hypolipidemic effect that may be through affecting the mRNA and protein expressions of SREBP-1c, FAS, SREBP-2, LDLR, PPARα, LXRα, CYP7A1, and ABCA1, involving in fatty acid synthesis, LDLR-mediated cholesterol uptake, bile acid biosynthesis, and cholesterol efflux. This study further provided experimental evidence about its practical application for treating hyperlipidemia and its complications.

**Keywords: Danhe granule, hyperlipidemia, systems pharmacology, mechanism, active ingredients**

## INTRODUCTION

Cardiovascular diseases (CVDs) are the leading cause of death globally. Hyperlipidemia is one of the leading risk factors for the development and progression of CVDs, characterized by elevated serum total cholesterol (TC), serum triglycerides (TG), low-density lipoprotein cholesterol (LDL-c), and decreased serum high-density lipoprotein cholesterol (HDL-c) (Gupta et al., 2011). It is well known that reducing high lipid levels, especially for the circulating levels of TC and LDL-c, has a huge potential to lower the risks for CVDs (Ridker, 2014; Qu et al., 2018). Genetic background, environmental factors, and lifestyle preferences are the main factors that may contribute to the rising prevalence of hyperlipidemia (Mathur and Devi, 2016). In some cases, patients with hyperlipidemia also suffered from severe complications such as coronary artery disease, ischemic stroke, angina pectoris, and diabetes. The commonly used lipid-regulating drugs like statins, the inhibitors of the rate-limiting enzyme in cholesterol synthesis, are challenging to achieve a satisfactory therapeutic effect, but also accompanied by harmful side effects such as gastrointestinal tract issues and myopathy (Garnett, 1995; Tacherfiout et al., 2018). It was reported that the proportion of patients with myopathy caused by statins was about 10%, and an estimated 20% of the patients were statin-resistant or intolerant (Harper and Jacobson, 2007; Maningat and Breslow, 2011). Thus, it warrants to find alternative medicines for the treatment of hyperlipidemia.

In several Asian countries, such as China and Korea, herbs and traditional Chinese medicine (TCM) formulas were widely used to prevent and cure atherosclerosis and hyperlipidemia. Danhe granule (DHG) is a TCM formula which consists of *Salvia miltiorrhiza* Bunge (Danshen), *Reynoutria japonica* Houtt. (Huzhang), *Crataegus pinnatifida* Bunge (Shanzha), *Citrus* × *aurantium* L. (Chenpi), *Coix lacryma-jobi var. ma-yuen* (Rom.Caill.) Stapf (Yiyiren), and *Nelumbo nucifera* Gaertn. (Heye). It is originated from clinical prescriptions Danhe decoction that has been used in treating hyperlipidemia for many years. Modern pharmacology researches showed that some component herbs of DHG exhibited excellent hypolipidemic effects. For example, *Crataegus pinnatifida* Bge. could reduce blood lipid levels by inhibiting cholesterol biosynthesis and increasing lipid β oxidation (Ye et al., 2010; Niu et al., 2011). Meanwhile, researches also showed some bioactive monomer compounds such as naringin and salvianolic acid B possessed regulatory effects on lipid metabolism disorder (Yue et al., 2015; Liang et al., 2016). Although previous studies indicated that DHG had potential effects on hyperlipidemia (Ma et al., 2019), because of the complexity of components, the underlying lipid-lowering mechanisms, and effective components of DHG are not yet clear.

In TCM formula, the characteristics "multi-component, multi-target, and multi-pathway" present a tremendous challenge in understanding of the interactions between components and their mechanisms of action (Jiang et al., 2019). Fortunately, systems pharmacology, as a new discipline based on the basic theories of pharmacology and systems biology pharmacology, integrating pharmacology feature mapping, multiple targeting techniques, network pharmacology, and pathway analyses, has gradually become a powerful tool to investigate the therapeutic mechanisms of TCM (Su et al., 2019; Zhou et al., 2019). For example, Liu et al. found 33 compounds with potential anticancer effects from *Scutellaria barbata* D. Don and investigated their mechanisms in treating non-small cell lung cancer by systems pharmacology method (Liu et al., 2018). However, previous systems pharmacology studies usually consider drug-like compounds in herb databases. In contrast, whether the compounds can be absorbed into the blood is often neglected, which may lead to the results that the active ingredients and predicted targets deviate from the truth. The serum pharmacochemistry method

**Abbreviations:** DHG, Danhe granule; UHPLC-Q-TOF/MS, ultra-high performance liquid chromatography coupled with quadrupole time-of-flight mass spectrometry; GO enrichment, gene ontology enrichment; RT-PCR, real-time polymerase chain reaction; TC, total cholesterol; TG, triglyceride; LDL-c, low-density lipoprotein cholesterol; HDL-c, high-density lipoprotein cholesterol; NC, normal control group; HFD, high-fat diet group; Sim, simvastatin; DHG-L, DHG at low dosage; DHG-M, DHG at medium dosage; DHG-H, DHG at high dosage; SREBP, sterol regulatory element binding proteins; SREBP-1c, sterol regulatory element-binding protein-1c; FAS, fatty acid synthase; SREBP-2, sterol regulatory element binding protein 2; LDLR, low-density lipoprotein receptor; PPARα, peroxisome proliferation-activated receptor alpha; LXRα, liver X receptor alpha; CYP7A1, cholesterol 7α-hydroxylase; ABCA1, ATP binding cassette subfamily A member 1; CVD, cardiovascular disease; TCM, traditional Chinese medicine; TBA, total bile acid.

could help to discover the compounds absorbed into blood of the Chinese medicinal formula as the clues of active ingredients and is widely used to reveal the efficacy of TCMs (Yan et al., 2017). Therefore, the detected constituents absorbed into blood can provide the basis of chemical composition for further systems pharmacology investigation.

In this work, a systems pharmacology approach was employed to investigate the lipid-lowering mechanism and active components of DHG. The detailed flowchart is shown in **Figure 1**. First, the high-fat diet (HFD)-induced hyperlipidemic hamster model was used to evaluate the hypolipidemic effect of DHG. Then, a UPLC-Q-TOF/MS method was performed to identify the constituents absorbed into blood after DHG administration. On this basis, target prediction, network mapping, and pathway analysis were carried out to systematically explore the underlying reciprocity between active compounds, active targets and pathways. Finally, some crucial targets were experimentally validated. This work will serve to deepen the understanding of the effective substances and mechanisms of DHG in the treatment of hyperlipidemia and contribute to its development and application.

# MATERIALS AND METHODS

## Chemicals and Materials

Simvastatin (Hangzhou MSD Pharmaceutical Co., Ltd., China) was taken as a positive control. The HFD contained 10% lard, 10% egg yolk powder, 0.3% cholesterol, and 79.7% standard diet was provided by Beijing HFK Bioscience Co., Ltd., China. Reference standards (purity ≥ 98%) of gallic acid (M-017-161223), polydatin (M-017-161223), isoquercetin (Y-076-161216), hesperidin (110721-201818), salvianolic acid B (D-012-170417), emodin 8-*O*-$\beta$-D-glucoside (D-018-160928), hyperin (J-012-170317), nuciferine (111566-201706), quercetin (H-009-170426), nobiletin (C-015-170316), emodin (Must-16031601), and tanshinone II A (D-008-170508) were purchased from Chengdu Herbpurify Co., Ltd. (China). High-performance liquid chromatography (HPLC)-grade acetonitrile, methanol, and formic acid were supplied by Merck (Darmstadt, Germany). Ultrapure water was obtained using a Milli-Q water purification system from Millipore (Bedford, MA, USA). TC, TG, LDL-c, and HDL-c assay kits were purchased from Nanjing Jiancheng Bioengineering Institute (Nanjing, China). BCA protein assay kit was purchased from Beyotime (Shanghai, China). total bile acid (TBA) assay kit was provided by Crystal Chem (USA). Anti-SREBP-1c, anti-liver X receptor alpha (LXR$\alpha$), anti-cholesterol 7$\alpha$-hydroxylase (CYP7A1), and anti-ATP binding cassette subfamily A member 1 (ABCA1) were purchased from ImmunoWay Biotechnology Company (Newark, DE, USA). Anti-SREBP-2, anti-low-density lipoprotein receptor (LDLR), anti-fatty acid synthase (FAS), anti-peroxisome proliferation-activated receptor (PPAR)$\alpha$, and anti-GAPDH were obtained from Proteintech Group Inc. (Chicago, USA). Power sybr green pcr mix and Revert aid first strand cDNA synthesis kit were purchased from Thermo Fisher Scientific Inc. (St. Louis, MO, USA). The primer was provided by Sangon Biotech Co., Ltd. (Shanghai, China).

## DHG Preparation and HPLC Analysis

DHG (batch No. D1905007) was provided by the hospital preparation room, China–Japan Friendship Hospital (Beijing, China). Saliae Mil Tiorrhizae Radix et Rhizoma (Lot No.80270602) (the root and rhizome of *Salvia miltiorrhiza* Bunge a perennial herbal plant of the *Salvia* L. genus, the *Labiatae* family), Polygoni Cuspidati Rhizoma et Radix (Lot No.80510801) (the root and rhizome of *Reynoutria japonica* Houtt., genus *Reynoutria* Houtt., family *Polygonaceae*), Crataegi Fructus (Lot No.82230701) (the fruit of *Crataegus pinnatifida* Bunge the short arbor plants of the *Crataegus* L. genus, the *Rosaceae* family), Citri Reticulatae Pericarpium (Lot No. 81450601) (the peel of *Citrus* × *aurantium* L., genus *Citrus* L., family *Rutaceae*), Coicis Semen (Lot No. 70511101) (the mature kernel of *Coix lacryma-jobi var. ma-yuen* (Rom.Caill.) Stapf a perennial herbal plant of the *Coix* L. genus, the *Poaceae* family) and Nelumbinis Folium (Lot No. 83720701) (the leaf of *Nelumbo nucifera* Gaertn., genus *Nelumbo* Adans., family *Nelumbonaceae*) were obtained from Beijing San He Co., Ltd. (Beijing, China) and identified by Professor Xueyong Wang (School of Chinese Materia Medica, Beijing University of Chinese Medicine. Voucher specimens including Saliae Mil Tiorrhizae Radix et Rhizoma (No. CMAT-SM-201806), Polygoni Cuspidati Rhizoma et Radix (No. CMAT-PC-201809), Crataegi Fructus (No. CMAT-CP-201810), Citri Reticulatae Pericarpium (No. CMAT-CR-201811), Coicis Semen (No. CMAT-CL-201808), and Nelumbinis Folium. (No. CMAT-NN-201807) were deposited in School of Chinese Materia Medica, Beijing University of Chinese Medicine (Herbarium Code: BCMM). Besides, detailed drug materials information, including herbal material origin and the scan of the vouchers, was given in **Supplementary Table S1**. A mixture of Saliae Mil Tiorrhizae Radix et Rhizoma (1000g), Coicis Semen (3000g), Polygoni Cuspidati Rhizoma et Radix (1000g), Crataegi Fructus (1000g), Citri Reticulatae Pericarpium (1000g), and Nelumbinis Folium (1500g) at a weight ratio of 1:3:1:1:1:1.5 were extracted three times by refluxing with 12-fold of water (volume/weight) for 1 h each time. The liquid extract was filtered and concentrated to a density of 1.08 (60°C). 95% ethanol was added into the concentrated liquid to 60% ethanol concentration, and then it was precipitated at room temperature for 24 h. The supernatant was condensed and dried to yield 1060 g powder using the decompression drying method at 60°C.

The HPLC analysis of DHG was performed on Agilent 1260 Infinity HPLC system (Agilent Technologies, Waldbronn, Germany) with a ZORBAX Eclipse XDB-C18 column (4.6 × 250 mm, 5 μm) at a flow rate of 1.0 ml/min and a 30°C column temperature. The mobile phase was composed of solvent A (water-0.1% phosphoric acid) and solvent B (acetonitrile): 0–55 min, 5%–30% B; 55–60 min, 30%%95% B; 70–75 min, maintained at 95% B. The injection volume was 10 μl and the UV detection wavelength was set at 286 nm.

## Animals and Experimental Design

Healthy 4-week-old male Syrian golden hamsters weighing 90 ± 3 g were obtained from Beijing Vital River Laboratory Animal Technology Co., Ltd [SCXK(JING) 2016-0011]. All animals were housed in stainless steel wire-mesh cages individually in a room kept at 22 ± 2°C with 50%–60% relative humidity and a 12-h light/dark cycle and allowed free access to normal food and water. After acclimatization with the facility for a week, animals were randomly assigned to different dietary groups: the normal diet control group (NC) (n = 10) and the experimental group (n = 50). The experimental group was fed with a HFD, which was composed of 10% lard, 10% egg yolk powder, 0.3% cholesterol, and 79.7% standard diet. Animals had free access to both food and distilled water, which were provided fresh every day. After 2 weeks, dyslipidemia hamsters were determined according to the lipid levels including serum TC, TG, LDL-c, and HDL-c and divided into the HFD group (n = 10), three DHG-treated groups with a dose of 0.37 (1/3-fold clinical doses) g/kg/day (n = 10), 1.10 (clinical doses) g/kg/day (n = 10), and 3.3 (3-fold clinical doses) g/kg/day (n = 10), and 2.4 mg/kg/day of simvastatin (Sim) was used as positive control (n = 10). In subsequent an 8-week experiment, except for the NC group (n = 10), the remaining five groups were fed with the HFD. During the experiment, food intake was measured daily. Body weight was recorded every seven days. Feces of each hamster were collected third day prior to termination of the study for the analysis of cholesterol and bile acid.

This study was conducted in conformity with the policies and procedures of the Ethics Committee of Beijing University of Traditional Chinese Medicine (permit number: BUCM-4-2018091101-3048). At the end of the experiment, blood from each hamster was collected *via* puncturing the retro-orbital sinus with a capillary tube after overnight fasting. After collecting the blood, the adipose tissue, liver, heart, spleen, lung, kidney, and brain were removed, rinsed with a physiological saline solution, and weighed. The viscera index (%) = viscera weight (g)/body weight (g) ×100. Then the liver and adipose tissue were stored at −80°C.

## Biochemical Parameters

The serum sample was prepared by centrifugation of blood at 1000×g for 10 min at 4°C and stored at −80°C until analysis. Serum TC, TG, LDL-c, and HDL-c were measured by enzymatic colorimetric methods using commercial kits (Nanjing Jiancheng Bioengineering Institute, Nanjing, China). The total fat in feces was extracted with chloroform/methanol (2:1, v/v) according to the reported method (Folch et al., 1957). After lipid extraction, the TC concentration was assayed by commercial kits (Nanjing Jiancheng Bioengineering Institute, Nanjing, China). The TBA in feces was extracted by 75% ethanol at 50°C for 2 h (Ning et al., 2015), then the level of TBA was analyzed by commercial kits (Crystal Chem, USA). The atherogenic index (AI) was calculated by the equation AI = (TC −HDL-c)/HDL-c (Guo et al., 2011).

## Histological Analysis

For histological analysis of lipid accumulation in the liver, tissues were embedded in Tissue-TekOCT cryostat molds and frozen at −80°C. After the sections were obtained from the liver tissues above, the liver tissue sections were stained with 0.5% Oil Red O. The epididymal adipose tissues were fixed in 10% formalin, dehydrated, embedded in paraffin, and sectioned at 5 μm on to poly-L-lysine-coated slides. Then the sections were stained with hematoxylin and eosin, photographed with an upright fluorescence microscope (Nikon Instruments CO., Ltd, Japan).

## Serum Ingredients Analysis After DHG Taken Orally

### Sample Preparation

Six male Syrian golden hamsters (weighing from 95 to 110 g) were randomly divided into the experiment group (n = 4) and blank group (n = 2). The DHG was administrated by oral administration at a single dose of 3.30 (3-fold clinical doses) g/kg body weight to the experiment group. At the same time, an equivalent of distilled water was given to the blank group. For the collection of serum samples, the hamsters were anesthetized by intraperitoneal injection of 10% aqueous chloral hydrate after oral administration of the DHG. The blood samples were collected from the hepatic portal at 0.5, 1, 2, and 4 h, respectively. The collected samples were centrifuged at 4000 rpm for 15 min at 4°C and then mixed to obtain a pooled serum. The blank serum was collected in the same way. A volume of 2 ml serum samples was immediately treated with 6 ml acetonitrile to precipitate serum proteins. After centrifuged at 12,000 rpm for 15 min at 4°C, the supernatants were dried under a vacuum concentrator and dissolved in 200 μl methanol for LC-MS analysis.

### Analysis Method

The sample detection was performed by an Agilent 1290/6550 iFunnel Q-TOF MS system with both negative and positive ionization modes. Samples were separated by the Agilent Eclipse C18 RRHD (2.1 mm × 150 mm, 1.8 μm), the temperature was maintained at 40°C, and the injection volume was 2 μl. The mobile phase consisted of water–0.1% formic acid (A), and acetonitrile–0.1% formic acid (B) (5% B at 0–5 min, 5%–20% B at 5–15 min, 20%–35% B at 15–35 min, 35%–95% B at 35–45 min, 95%–100% B at 45–50 min) and the flow rate was 0.4 ml/min. The Dual AJS ESI source conditions were as follows: gas temperature, 200°C; gas flow, 14 L/min; nebulizer pressure, 45 psi; sheath gas temperature, 300°C; sheath gas flow, 12 L/min; capillary voltage, 3500 V (−)/4000 V (+); nozzle voltage, 1000 V; fragmentor voltage, 380 V; MS range, 100–1400 *m/z*. The sample collision energy was set at 10, 20, and 40 V. The mass spectral data were processed by Agilent Mass Hunter Qualitative Analysis B.07.00 software (version B.07.00, Agilent Technologies, USA).

## Network Construction

The network construction mainly includes the following three steps: (1) Disease target collection. DisGeNET is a discovery platform containing one of the largest collections of genes associated with human diseases, which was typically used for the discovery of information about disease-related targets (Zhu et al., 2018). After screening targets with relevance score ≥ 0.001 from DisGeNET database (http://www.disgenet.org/), the known therapeutic targets of treatment for hyperlipidemia were obtained. (2) DHG candidate

targets collection. Genecards is an integrative human genes database, which could be employed to search for target information related to compounds (Chen et al., 2019). The candidate targets of DHG (relevance score ≥1) were collected from Genecards Databases (http://www.genecards.org/) based on the 16 compounds identified in hamster serum. After retaining the common targets for disease and serum compounds of DHG, removing duplicate targets, and the compounds without targets, then the potential targets and active compounds were obtained for next network mapping. (3) The network construction. The active compounds–potential targets–disease network (C–T–D network) was established by mapping the potential targets with the active compounds and hyperlipidemia, made by Cytoscape (Version 3.6.0) (http://www.cytoscape.org/). The potential targets, which could be associated with other targets by the String database (https://string-db.org/), were used to conduct further gene ontology (GO) enrichment analysis and pathway analysis.

## GO Enrichment and Pathway Analysis

GO enrichment analysis with biological process and molecular function of potential targets were carried out for biological function annotation based on a Cytoscape (Version 3.6.0) plugin Clue GO (Version 2.5.5) with the criterion of $p$-value ≤ 0.01 and kappa score 0.7. In addition, the DAVID database (https://david.ncifcrf.gov/home.jsp, Version 6.8) was utilized to analyze the representative pathways of the potential targets, and a $p$-value ≤ 0.05 significant level was used. Meanwhile, the targets–pathways (T–P) network was conducted by Cytoscape (Version 3.6.0) to visualize the relationship of the potential targets and related pathways. Based on the pathway analysis, we focused on the three pathways associated with lipid metabolism. Then the compounds–targets–pathways (C–T–P) network was further mapped to investigate the relationship between compounds, targets, and pathways using Cytoscape (Version 3.6.0) similarly.

## RNA Extract, cDNA Synthesis, and Real-time PCR

Total RNA was prepared from livers using TRIzol reagent. cDNA was synthesized using Revertaid first strand cDNA synthesis kit. The quantitative real-time polymerase chain reaction (RT-PCR) reaction, containing target genes and SYBR Green PCR master mix, was performed on Bio-Rad CFX connect real-time system (Bio-Rad, USA). The sequences of the primers were listed in **Supplementary Table S2**. The PCR conditions were as follows: 95°C for 3 min, cycled at 95°C for 10 s, 55°C for 10 s, and 72°C for 30 s for 40 cycles, for melt curve from 55°C to 95°C with an interval at 0.5°C for 5 s. Each experiment was performed in triplicate. The relative levels of each gene expression were determined by the $2^{-\Delta\Delta Ct}$ method with GAPDH as an internal control to normalize all the mRNA levels.

## Western Blot Analysis

The liver tissue was homogenized in sodium chloride–Tris–EDTA buffer (250 mM sucrose, 10 mM Tris/HCl, 1 mM EDTA/Na, pH 8.0) with protease inhibitor. Total protein samples were separated by SDS-PAGE at 120 V for 1.5 h at room temperature and then electrotransferred onto PVDF membranes at 200 mA for 2.5 h at 4°C. To block non-specific binding site, the membranes were blocked with 5% non-fat dry milk in TBST for 2 h at room temperature, followed by incubated with primary antibodies overnight at 4°C including anti-rabbit SREBP-1c (1:1000, Immunoway), anti-rabbit SREBP-2 (1:1000, Proteintech), anti-rabbit LDLR (1:1000, Proteintech), anti-rabbit FAS (1:1000, Proteintech), anti-rabbit LXRα (1:1000, Immunoway), anti-rabbit CYP7A1 (1:1000, Immunoway), anti-rabbit PPARα (1:750, Proteintech), anti-rabbit ABCA1 (1:1000, Immunoway), and anti-rabbit GAPDH (1:1000, Proteintech). Afterward, the membranes were incubated with HRP-linked anti-IgG (1:2000, Proteintech) for 2 h at room temperature. Densitometric measurement of chemiluminescent bands was performed using Image Lab™ software on ChemiDoc XRS+ (Bio-Rad, USA).

## Statistical Analysis

Results were expressed as mean ± standard deviation (SD). Statistical analysis was performed with one-way analysis of variance (ANOVA) using the SPSS 19.0 program, and the differences in mean values among groups were assessed using Duncan's multiple range test. $p < 0.05$ was considered as statistically significant difference, and $p < 0.01$ was extremely significant difference.

# RESULTS

## HPLC Profile of DHG

Using the current HPLC method, the reproducibility analysis of the 11 batches of DHG samples was conducted (**Figure 2B**), and the results (similarities > 0.94) indicated that the preparation process of DHG was reasonable and feasible (**Supplementary Information** for details). Besides, to determine the main chemical composition of DHG, an HPLC analysis was performed and the chromatogram was shown in **Figure 2A**. Six compounds from the HPLC chromatographic peaks, including gallic acid, polydatin, isoquercetin, hesperidin, salvianolic acid B, and emodin-8-O-β-D-glucoside, were identified by comparing with standard references. The contents of these six compounds in the DHG sample (batch No. D1905007) were determined as 7.09, 4.37, 5.39, 9.62, 13.09, and 2.15 mg/g, respectively. The chromatograms of mixed standards and their structures were shown in **Supplementary Figure S1**.

## Protective Effects of DHG on Hyperlipidemia

### DHG Modulated Serum Lipid Levels

Firstly, we investigate the effect of DHG on serum lipid levels in hyperlipidemic hamsters. As shown in **Figures 3A–C**, the results show that the elevated serum levels of TC, TG, and LDL-c in dyslipidemia hamsters were significantly declined after treatment with DHG ($p < 0.01$). Notably, DHG-H therapy decreased the

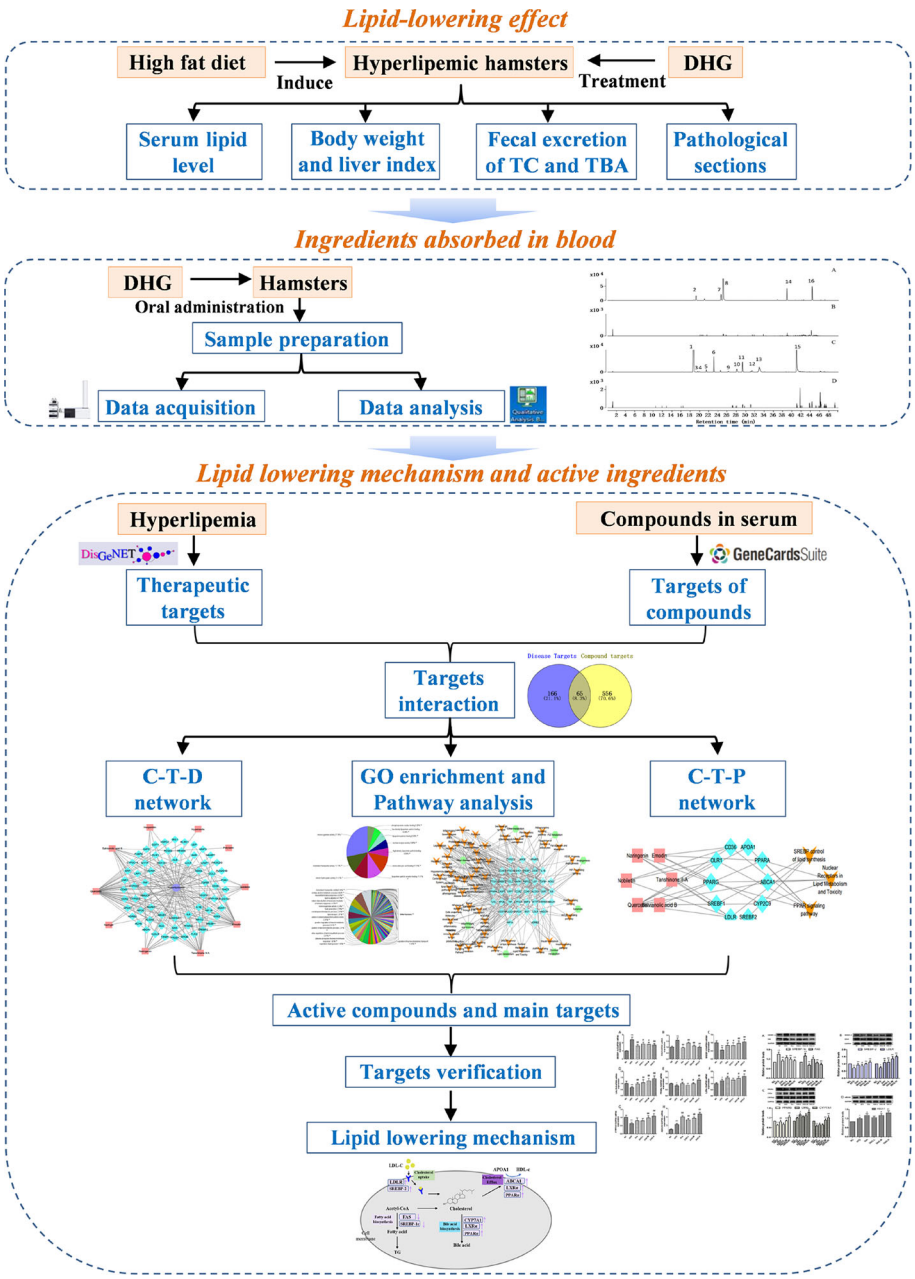


**FIGURE 1 |** The scheme of investigating the lipid-lowering mechanism and active ingredients of DHG based on systems pharmacology. DHG, Danhe granule.

serum TC, TG, and LDL-c level by 32.41%, 48.56%, and 28.23%, respectively, and enhanced the serum HDL-c level by 40.96% in hyperlipidemic hamsters (**Figure 3D**). From the data, DHG-H showed a similar effect as Sim in reducing serum TC, TG, and LDL-C levels, while a strong effect than Sim in improving serum HDL-c level. As seen in **Figures 3E, F**, HFD administration resulted in a significant increase in the AI ($p < 0.01$) and a decrease in serum HDL-c/TC ratio ($p < 0.01$) in hamster compared with the NC group. After 8 weeks of treatment, the serum HDL-c/TC ratio was significantly enhanced by DHG treatment compared to the HFD group ($p < 0.01$). Besides, the phenomenon was associated with a 34.01%, 37.77%, and 56.01% reduction in AI in DHG at low dosage (DHG-L), DHG at medium dosage (DHG-M), and DHG at high dosage (DHG-H) treatment group ($p < 0.01$). In addition, we also investigated the effect of DHG on the fecal excretion of TC and TBA in hamsters. As shown in **Table 1**, the fecal excretion of TC and TBA in hamsters was increased by HFD compared with the NC group ($p < 0.05$). DHG-H group exhibited a higher fecal TBA level compared with the HFD group ($p < 0.01$). Besides, the fecal

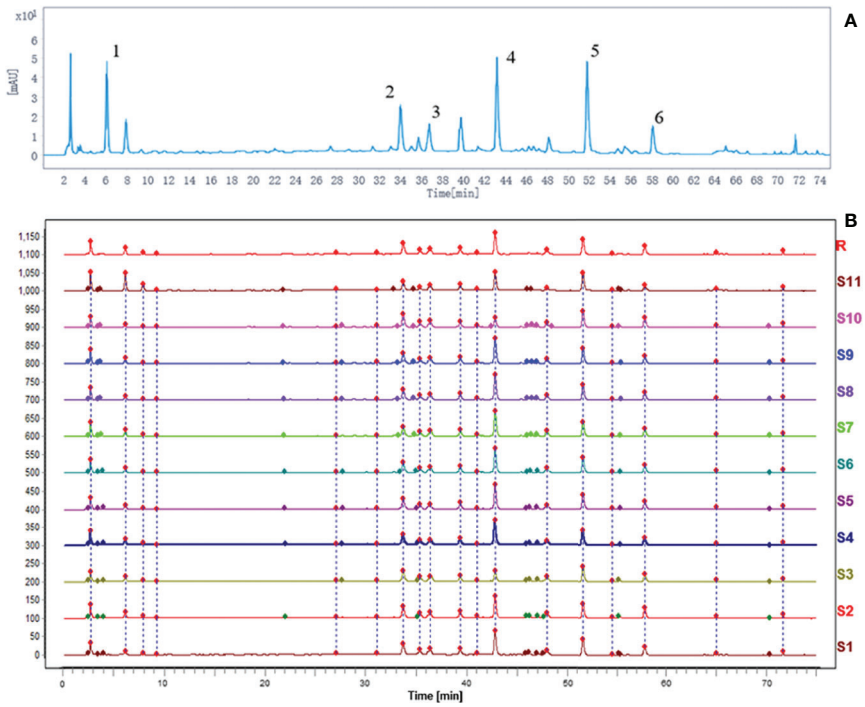


**FIGURE 2 |** HPLC fingerprint analysis of DHG. The HPLC chromatographic of DHG **(A)**. Comparability results of reproducibility of DHG samples **(B)**. The main components of DHG in the chromatograms are as follows: (1) gallic acid, (2) polydatin, (3) isoquercetin, (4) hesperidin, (5) salvianolic acid B, and (6) emodin-8-O-β-D-glucoside. HPLC, high-performance liquid chromatography.

TBA level was significantly enhanced by 21.67% and 32.51% with DHG-M and DHG-H treatment compared to the HFD group ($p < 0.05$), respectively. These data suggested that DHG has an excellent effect on improving blood lipid levels.

## DHG Reduced Body Weight Gain, Liver Index, and Fat Weight

Since hyperlipidemia often accompanied by body weight gain as well as fat increase and liver index change, we studied the effect of DHG on these aspects. The body weight of each group from the 10th week was recorded in **Figure 3G** and the weight gain of each group was shown in **Figure 3H**. The results indicated that the intake of the HFD diet induced a remarkable increase in the body weight and body weight gain of hamsters compared with the NC group ($p < 0.01$). Compared with the HFD group, DHG administration notably lowered the body weight in hyperlipidemic hamsters. Besides, DHG treatment significantly decreased body weight gain in hyperlipidemic hamsters by 16.60%, 28.01%, and 36.04%, respectively, at three dose levels. During the experimental period, there were no significant changes in daily food intake among different groups (**Figure 3I**), which indicated the changes in body weight in drug therapy groups were might mainly result from DHG treatment. As shown in **Table 2**, HFD led to a significant increase in the perirenal adipose tissue weight, epididymal adipose tissue weight and liver index compared with the NC group ($p < 0.01$). After treatment, DHG-M and DHG-H groups showed a significant decreasing trend in the liver index, the perirenal and epididymal adipose tissue weight in hyperlipidemic hamsters. Notably, DHG-H lowered perirenal adipose tissue weight, epididymal adipose tissue weight and liver index by 36.09%, 19.24%, and 15.19%, respectively. Besides, DHG and Sim treatments have little impact on other viscera indexes such as heart index, spleen index and lung index in hyperlipidemic hamsters (**Table 2**). These data indicated the beneficial effects of DHG on body weight, fat weight, and liver index in hyperlipidemic hamsters.

## Histopathological Changes in Liver and Adipose Tissues

To further evaluate the effects of DHG on the pathological changes of liver and adipose tissue, the Oil red O staining liver tissue and hematoxylin & eosin staining epididymal fat tissue were employed. As shown in **Figure 3J**, DHG substantially decreased the amount of fat accumulated in hyperlipidemic hamster liver. Moreover, histological analysis revealed that the Sim group and DHG-H group with fewer lipid droplets showed a more potent effect in inhibiting hepatic fat accumulation. In the hematoxylin and eosin staining of epididymal adipose tissue sections (**Figure 3K**), it's easy to see that the adipocyte size in the HFD group was larger than the NC group. Treatment with Sim and DHG-H suppressed enlargement of the adipocytes in epididymal adipose tissue in hyperlipidemic hamsters.

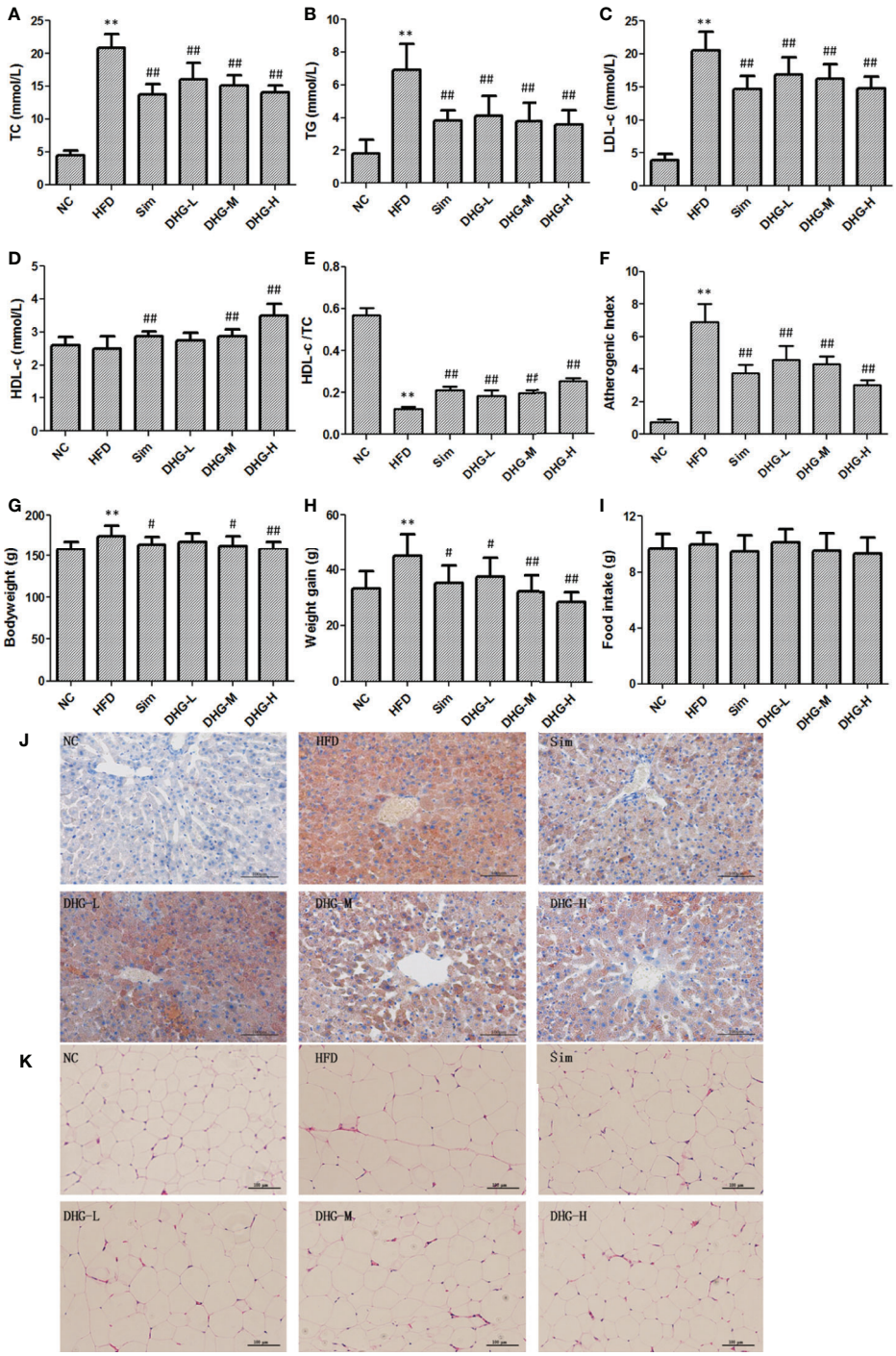


**FIGURE 3 |** Protective effect of DHG on hyperlipidemic hamsters induced by HFD. Values were mean ± SD, n =10. **(A)** Serum TC levels. **(B)** Serum TG levels. **(C)** Serum LDL-c levels. **(D)** Serum HDL-c levels. **(E)** HDL-c/TC ratio. **(F)** Atherosclerosis index. **(G)** Body weight in the 10th week. **(H)** Body weight gain of each group. **(I)** The food intake of each group. **(J)** Histological analysis of liver. Liver sections were stained with Oil Red O, Scale bar = 100 μm. **(K)** Histological analysis of epididymal adipose tissue. Epididymal adipose tissue sections were stained with hematoxylin and eosin, Scale bar = 100 μm. NC, normal control group; HFD, high-fat diet group; Sim, simvastatin (2.40 mg/kg/day); DHG-L, DHG at low dosage (0.37 g/kg/day); DHG-M, DHG at medium dosage (1.10 g/kg/day); DHG-H, DHG at high dosage (3.30 g/kg/day). TC, total cholesterol; TG triglyceride; LDL-c, low-density lipoprotein cholesterol; HDL-c, high-density lipoprotein cholesterol. $^{**}p < 0.01$ vs NC; $^{\#}p < 0.05$ vs HFD; $^{\#\#}p < 0.01$ vs HFD.

**TABLE 1 |** Effect of DHG on fecal excretion of TC and TBA levels in hamsters.

| Group | TC (μmol/g) | TBA (μmol/g) |
|---|---|---|
| NC | 3.05 ± 0.37 | 1.61 ± 0.28 |
| HFD | 5.45 ± 0.88** | 2.03 ± 0.43* |
| Sim | 6.18 ± 0.85 | 2.10 ± 0.35 |
| DHG-L | 6.34 ± 1.17 | 2.25 ± 0.54 |
| DHG-M | 6.65 ± 1.89 | 2.47 ± 0.42# |
| DHG-H | 7.48 ± 0.96## | 2.69 ± 0.21## |

*Values were mean ± SD, n = 10. TC, total cholesterol; TBA, total bile acids; NC, normal control group; HFD, high-fat diet group; Sim, simvastatin (2.40 mg/kg/day); DHG-L, DHG at low dosage (0.37 g/kg/day); DHG-M, DHG at medium dosage (1.10 g/kg/day); DHG-H, DHG at high dosage (3.3 g/kg/day). *p < 0.05, **p < 0.01 vs NC group; #p < 0.05, ##p < 0.01 vs HFD group.*

Databases (http://www.genecards.org/), 621 targets of compounds absorbed into the blood were predicted after filtering out the overlapping targets and targets with relevance score < 0.001. The target information of compounds is shown in **Supplementary Table S3**. Secondly, after consulting with the DisGeNET database (http://www.disgenet.org/), a total of 231 candidate targets of hyperlipemia with relevance score ≥1 were obtained (**Supplementary Table S4**). Finally, the 65 potential targets, which associated with both disease and serum ingredients, were screened out to generate a C–T–D network diagram to reflect the relationship between components, targets, and disease (**Supplementary Table S5**). As shown in **Figure 4A**,

**TABLE 2 |** Effect of DHG on perirenal and epididymal adipose tissue weight and relative viscera index of hyperlipidemic hamsters.

| Group | NC | HFD | Sim | DHG-L | DHG-M | DHG-H |
|---|---|---|---|---|---|---|
| Perirenal adipose tissue (g) | 2.29 ± 0.34 | 3.38 ± 0.50** | 2.35 ± 0.26## | 2.60 ± 0.37## | 2.35 ± 0.51## | 2.16 ± 0.37## |
| Epididymal adipose tissue (g) | 4.28 ± 0.31 | 5.25 ± 0.62** | 4.42 ± 0.53## | 4.67 ± 0.52# | 4.41 ± 0.85## | 4.24 ± 0.52## |
| Liver index (%) | 3.33 ± 0.31 | 5.53 ± 0.29** | 4.58 ± 0.51## | 5.35 ± 0.40 | 5.12 ± 0.38# | 4.69 ± 0.32## |
| Heart index (%) | 0.32 ± 0.02 | 0.32 ± 0.03 | 0.33 ± 0.02 | 0.32 ± 0.03 | 0.33 ± 0.03 | 0.33 ± 0.02 |
| Spleen index (%) | 0.07 ± 0.02 | 0.07 ± 0.01 | 0.08 ± 0.02 | 0.07 ± 0.01 | 0.07 ± 0.01 | 0.07 ± 0.02 |
| Lung index (%) | 0.39 ± 0.04 | 0.38 ± 0.02 | 0.41 ± 0.03 | 0.40 ± 0.02 | 0.40 ± 0.03 | 0.41 ± 0.03 |
| Kidney index (%) | 0.71 ± 0.05 | 0.68 ± 0.04 | 0.69 ± 0.07 | 0.67 ± 0.04 | 0.69 ± 0.05 | 0.68 ± 0.04 |
| Brain index (%) | 0.53 ± 0.03 | 0.51 ± 0.04 | 0.53 ± 0.03 | 0.52 ± 0.03 | 0.52 ± 0.05 | 0.54 ± 0.03 |

*Values were mean ± SD, n = 10. NC, normal control group; HFD, high-fat diet group; Sim, simvastatin (2.40 mg/kg/day); DHG-L, DHG at low dosage (0.37 g/kg/day); DHG-M, DHG at medium dosage (1.10 g/kg/day); DHG-H, DHG at high dosage (3.3 g/kg/day). **p < 0.01 vs NC; #p < 0.05 vs HFD; ##p < 0.01 vs HFD.*

## The Ingredients Absorbed Into Blood After Oral Administration of DHG

The ultra-high performance liquid chromatography coupled with quadrupole time-of-flight mass spectrometry (UHPLC-Q-TOF/MS) was employed to analyze the main ingredients absorbed into the blood after oral administration of DHG. According to the accurate mass measurements, reference standards, fragmentation behavior, and related literatures, a total of 16 prototype compounds in hamster serum from DHG were first identified, including polydatin, n-nornuciferine, hyperin, isoquercitrin, naringin, hesperidin, o-nornuciferine, nuciferine, quercetin, emodin 8-O-β-D-glucoside, naringenin, torachryson, nobiletin, emodin, and tanshinone II-A. The detailed information of the 16 compounds was summarized in **Table 3**. The detailed identification process can be seen in the **Supplementary Material**. The extracted ion chromatograms of the 16 compounds in dosed groups and blank groups in positive and negative ion modes were shown in **Supplementary Figure S2**, and the total ion chromatograms of DHG sample were shown in **Supplementary Figure S3**.

## Network Construction and Enrichment Analysis

### C–T–D Network

To intuitively reflect the relationship between compounds, targets and disease, Cytoscape 3.6.0 was employed to map out a C–T–D network diagram. Firstly, based on the Genecards

there were 10 components, 65 potential targets, and 1 disease contained in the C–T–D network. These 10 compounds were quercetin, emodin, polydatin, salvianolic acid B, tanshinone II-A, hesperidin, hyperoside, naringenin, naringin, and nobiletin. These compounds are mainly categorized as flavonoids, phenolic acids, anthraquinones, tanshinone, and stilbene glycosides. The 8 ones including quercetin, emodin, salvianolic acid B, tanshinone II-A, hesperidin, naringenin, naringin, and nobiletin of 10 compounds have high correlation degree (degree ≥ 3), which may play a significant role in the network. For instance, quercetin is a considerable compound of DHG with the highest number of target interaction (degree = 46). Previous studies have demonstrated that quercetin could reduce fat accumulation in the liver by regulating lipid metabolism genes (Jung et al., 2013). The LDLR (degree = 5) was targeted by four compounds from DHG, which played an important role in hepatic cholesterol metabolism (Li et al., 2018). Meanwhile, some active compounds were also linked to multiple targets, suggesting potential synergies between them. In summary, we first mapped the C–T–D network focusing on the ingredients absorbed into the blood to preliminary explain the effect of DHG on hyperlipidemia and screened 10 components and 65 potential targets.

### GO Enrichment Analysis

Firstly, the protein–protein interaction (PPI) network of the 65 common targets was built by String database (https://

**TABLE 3 |** The compounds identified in hamster serum after oral administration of DHG.

| No. | Rt (min) | Observed *m/z* | Error (ppm) | Formula | MS/MS fragments | Name |
|---|---|---|---|---|---|---|
| 1 | 18.75 | 389.1240 $[M-H]^-$ | 0.81 | $C_{20}H_{22}O_8$ | 227.0722, 185.0616, 143.0508 | Polydatin[a] |
| 2 | 19.26 | 282.1495 $[M+H]^+$ | −2.02 | $C_{18}H_{19}NO_2$ | 251.1093, 236.0849, 219.0828, 208.0897, 191.0875, 179.0867, 165.0709 | N-nornuciferine |
| 3 | 19.61 | 463.088 $[M-H]^-$ | 0.75 | $C_{21}H_{20}O_{12}$ | 300.0281, 271.0255, 255.0305, 243.0305, 178.9994, 151.0043 | Hyperin[a] |
| 4 | 20.01 | 463.0874 $[M-H]^-$ | 1.79 | $C_{21}H_{20}O_{12}$ | 300.0282, 271.0255, 255.0305, 243.0307, 227.0355, 151.0044 | Isoquercitrin |
| 5 | 21.46 | 579.1719 $[M-H]^-$ | 0.01 | $C_{27}H_{32}O_{14}$ | 271.0619, 227.0722, 175.0044, 151.0044, 119.0510, 107.0148, 93.0353 | Naringin |
| 6 | 23.1 | 609.1833 $[M-H]^-$ | −1.28 | $C_{28}H_{34}O_{15}$ | 325.0718, 301.0722, 286.0485, 257.0823, 242.0590, 164.0122, 151.0042, 125.0250 | Hesperidin[a] |
| 7 | 24.67 | 282.1493 $[M+H]^+$ | −1.45 | $C_{18}H_{19}NO_2$ | 265.1245, 250.1006, 235.0772, 219.0815, 207.0816, 191.0862, 179.0859 | O-nornuciferine |
| 8 | 25.13 | 296.1642 $[M+H]^+$ | 1.23 | $C_{19}H_{21}NO_2$ | 265.1246, 250.1008, 235.0773, 219.0819, 207.0821, 191.0869, 179.0866 | Nuciferine[a] |
| 9 | 26.25 | 717.1463 $[M-H]^-$ | −0.59 | $C_{36}H_{30}O_{16}$ | 519.0933, 339.0510, 321.0406, 295.0613, 185.0248, 109.0299 | Salvianolic acid B[a] |
| 10 | 28.06 | 301.0358 $[M-H]^-$ | −1.2 | $C_{15}H_{10}O_7$ | 273.0394, 245.0440, 178.9979, 151.0028, 121.0284, 107.0145 | Quercetin[a] |
| 11 | 29.29 | 431.0992 $[M-H]^-$ | −1.57 | $C_{21}H_{20}O_{10}$ | 269.0458, 240.0436, 225.0564, 210.0320, 197.0604, 181.0666 | Emodin 8-O-β-D-glucoside[a] |
| 12 | 31.12 | 271.0616 $[M-H]^-$ | −1.69 | $C_{15}H_{12}O_5$ | 151.0042, 119.0508, 107.0144 | Naringenin |
| 13 | 32.92 | 245.0824 $[M-H]^-$ | −1.95 | $C_{14}H_{14}O_4$ | 230.0594, 215.0362, 187.0396, 159.0458 | Torachryson |
| 14 | 38.98 | 403.1395 $[M+H]^+$ | −1.73 | $C_{21}H_{22}O_8$ | 388.1115, 373.0918, 359.1090, 327.0858, 211.0253, 165.0555 | Nobiletin[a] |
| 15 | 40.97 | 269.0461 $[M-H]^-$ | −1.88 | $C_{15}H_{10}O_5$ | 241.0514, 225.0565, 197.0615 | Emodin[a] |
| 16 | 44.21 | 295.1327 $[M+H]^+$ | −0.08 | $C_{19}H_{18}O_3$ | 277.1235, 266.0922, 262.0991, 252.0794, 249.1276, 235.0755, 206.1095, 191.0855, 179.0870 | Tanshinone II A[a] |

[a]*Compared with authentic compounds.*

string-db.org/) based on the STRING score values (with the highest confidence 0.9), and the targets with no connection with any others were neglected in our following study. Then, to further investigate the 48 remained potential targets, GO enrichment analysis, including molecular function and biological processes, was performed by ClueGO (version 2.5.5). For molecular functions analysis (**Supplementary Figure S4A**), the 10 significant GO terms associated with hyperlipidemia were enriched, such as cholesterol transporter activity, steroid hydroxylase activity, lipoprotein particle receptor binding, high-density lipoprotein particle binding, lipoprotein particle receptor binding, and low-density lipoprotein particle binding, etc. Moreover, as shown in **Supplementary Figure S4B**, the GO enrichment results revealed that these potential targets were involved in many biological processes, including cholesterol transporter activity, secondary alcohol metabolic process, lipid localization, lipid storage, regulation of plasma lipoprotein particle levels, positive regulation of steroid metabolic process, etc. The results indicated that these targets were associated with the pathogenesis of hyperlipidemia and related diseases. At the same time, many molecular functions and biological processes, such as cholesterol transporter activity, lipoprotein particle receptor binding and lipid localization, were closely related to lipid metabolism, which suggested that lipid metabolism may play an essential role in the pathogenesis or treatment mechanism of hyperlipidemia, and we will focus on it.

## C–T–P Network

To further elucidate the underlying curative mechanisms of DHG for the treatment of hyperlipidemia, the 48 remained potential targets with the STRING score values (with the highest confidence 0.9) were mapped onto the DAVID database (https://david.ncifcrf.gov/home.jsp, Version 6.8) to enrich their relevant pathways. As a result, a total of 52 pathways were obtained based on the criterion of $p < 0.05$, which were divided into eight groups such as inflammatory and immune, apoptosis, lipid metabolism, angiogenesis, etc. The detail information of the pathways was presented in **Supplementary Table S6**. Moreover, to visually reflect the relationship between targets and pathways, a T–P network containing 41 targets and 52 pathways classified into 8 groups were mapped, and the results suggested that these targets may affect many pathways to regulate the pathologic processes of hyperlipidemia (**Supplementary Figure S5**). Since lipid metabolism disorder is the core part of hyperlipidemia, we focused on the three pathways closely associated with lipid metabolism, including PPAR signaling pathway, SREBP control of lipid synthesis pathway, and nuclear receptors in lipid metabolism and toxicity pathway (**Table 4**). To further investigate the relationship between components, targets, and the three pathways, a C–T–P network diagram was mapped. As shown in **Figure 4B**, the network diagram displays that six active compounds connected with 10 targets affecting three pathways. These six active compounds are quercetin, emodin, salvianolic acid B, tanshinone II-A, naringenin, and nobiletin (**Figure 5**). The SREBP control of lipid synthesis pathway involves in lipid biosynthesis and LDLR-modulated cholesterol uptake. The PPAR signaling pathway and nuclear receptors in lipid metabolism and toxicity pathway play an important role in the conversion of cholesterol to bile acid and cholesterol efflux. In the three pathways, the targets SREBPs and PPARα are transcription regulators involved in

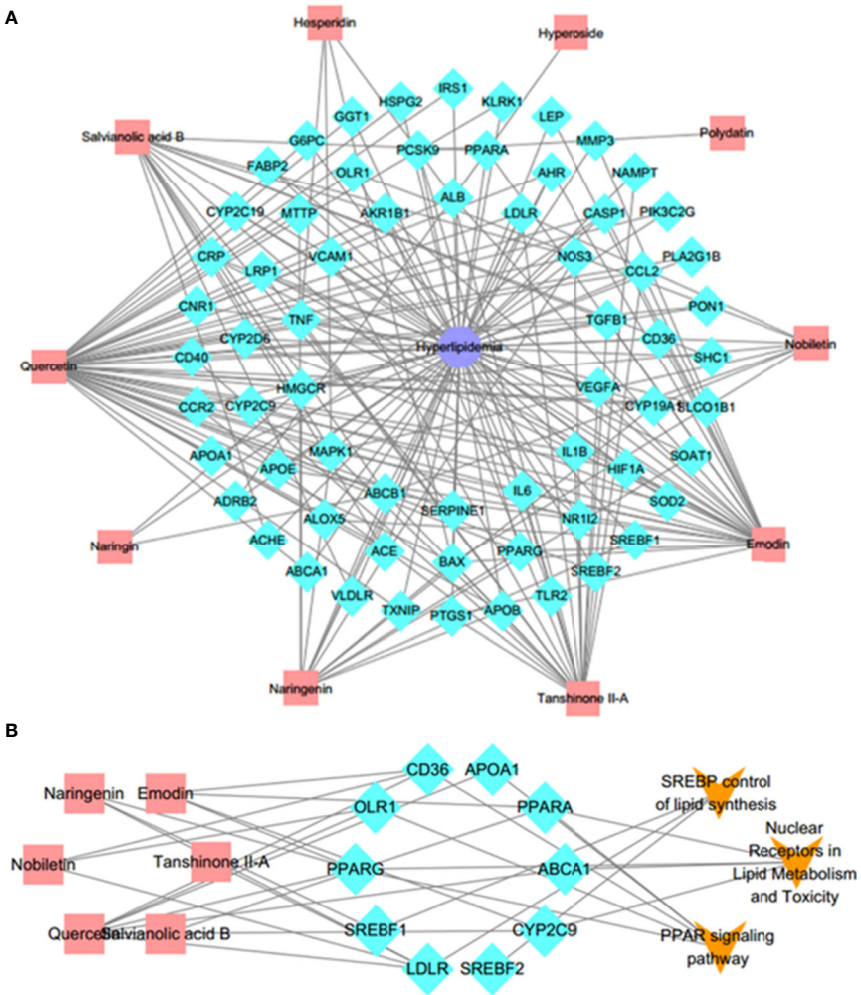


**FIGURE 4 |** C–T–D network and C–T–P network. **(A)** Active C–T–D network of 10 compounds and 65 common potential targets in treatment of hyperlipemia. The aquamarine rhombus nodes represent the targets, red rectangle nodes delineate the compounds, and indigo octagon nodes delineate the disease. **(B)** C–T–P network. The C–T–P network was constructed by linking compounds, targets, and their related pathways. The nodes represent compounds (red rectangle), targets (aquamarine rhombus), and pathways (orange v-shaped). C–T–D, compounds–potential targets–disease; C–T–P, compounds–targets–pathways.

**TABLE 4 |** The detail information of three pathways mainly involved in lipid metabolism.

| No. | Pathway | Targets | Count | Relevant targets | *p*-Value | Benjamini | Category | References |
|---|---|---|---|---|---|---|---|---|
| 1 | PPAR signaling pathway | PPARα, APOA1, CD36, OLR1, PPARG | 5 | RXR, LXRα, CYP7A1, PPARβ, PPARγ, APOAV | 6.35E-04 | 0.005524 | Lipid metabolism | (Hansjörg et al., 1993; Wu and Xu, 2016) |
| 2 | SREBP control of lipid synthesis | SREBF1, LDLR, SREBF2 | 3 | SCAP, SRE1, HMGCS | 0.008613 | 0.306643 | Lipid metabolism | (Eberle et al., 2004; Giudetti et al., 2013) |
| 3 | Nuclear receptors in lipid metabolism and toxicity | PPARα, CYP2C9, PPARG, ABCA1 | 4 | LXRα, CYP7A1, CYP27B1, ABCG1, ABCG5 | 0.024963 | 0.414386 | Lipid metabolism | (Beaven and Tontonoz, 2006) |

hyperlipidemia-related lipid metabolism processes. SREBP-1c (SREBF-1) and its target gene FAS could regulate the biosynthesis of fatty acids, further influencing the biosynthesis of TGs (Dentin et al., 2005). SREBP-2 (SREBF-2) and its related gene LDLR involved in cholesterol uptake (Kartawijaya et al., 2016). The target PPARα and its related genes LXRα, CYP7A1, and ABCA1 played a regulatory role in the process in the transformation of cholesterol into bile acids and cholesterol efflux (Wang et al., 2001; Basso et al., 2003; Cao et al., 2012; Ramakrishna et al., 2017). Taken together, these results indicated that the lipid-lowering mechanism of DHG may be that the 6 active components (quercetin,

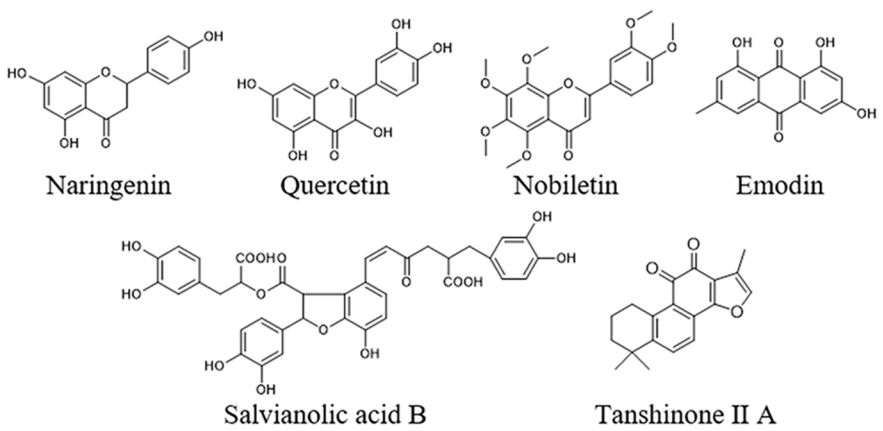


**FIGURE 5 |** Chemical structures of the six active compounds in DHG including naringenin, nobiletin quercetin, emodin, salvianolic acid B, and tanshinone II A.

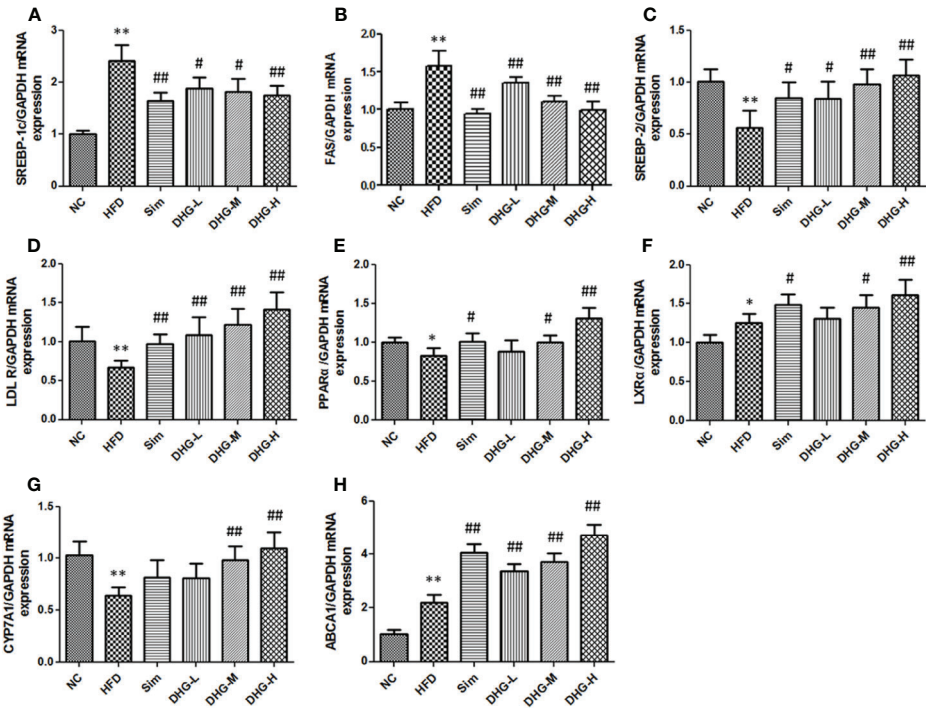


**FIGURE 6 |** Effect of DHG on mRNA expression of genes in hamster liver by RT-PCR. Values are mean ± SD, n = 5. **(A)** SREBP-1c mRNA. **(B)** FAS mRNA. **(C)** SREBP-2 mRNA. **(D)** LDLR mRNA. **(E)** PPARα mRNA. **(F)** LXRα mRNA. **(G)** CYP7A1 mRNA. **(H)** ABCA1 mRNA. RT-PCR, real-time polymerase chain reaction; SREBP-1c, sterol regulatory element-binding protein-1c; FAS, fatty acid synthase; SREBP-2, sterol regulatory element binding protein 2; LDLR, low density lipoprotein receptor; PPARα, peroxisome proliferation-activated receptor alpha; LXRα, liver X receptor alpha; CYP7A1, cholesterol 7α-hydroxylase; ABCA1, ATP binding cassette subfamily A member 1. $^{*}p < 0.05$ vs NC; $^{**}p < 0.01$ vs NC; $^{\#}p < 0.05$ vs HFD; $^{\#\#}p < 0.01$ vs HFD.

emodin, salvianolic acid B, etc.) acted on some important targets such as SREBP-1c, SPEBP-2 and PPARα, which could affect three pathways, including PPAR signaling pathway, SREBP control of lipid synthesis pathway and nuclear receptors in lipid metabolism and toxicity pathway, and further involve in and influence lipid metabolic processes. Besides, some crucial targets, including SREBP-1c, FAS, SREBP-2, LDLR, PPARα, ABCA1, LXRα, and CYP7A1 in the pathways, were selected to investigate the hypolipidemic mechanism of DHG further.

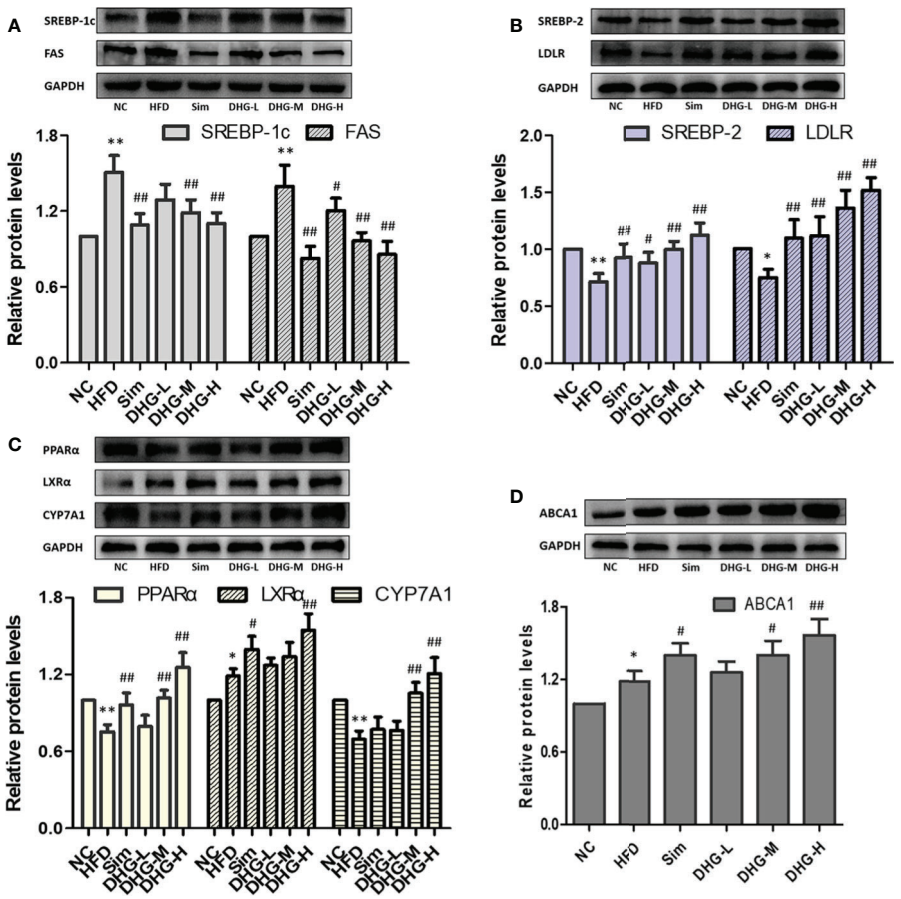


**FIGURE 7 |** Effect of DHG on protein expression of targets in hamster liver by Western blot. Values are mean ± SD, n = 3. **(A)** SREBP-1c, FAS. **(B)** SREBP-2, LDLR. **(C)** PPARα, LXRα, CYP7A1. **(D)** ABCA1. $^{*}p < 0.05$, $^{**}p < 0.01$ vs NC group; $^{\#}p < 0.05$, $^{\#\#}p < 0.01$ vs HFD group. The expression levels were normalized by GAPDH.

## Effect of DHG on the Expression of mRNA and Protein of Key Targets

To elucidate the molecular mechanism of DHG in treating hyperlipidemia, the mRNA and protein expressions of the targets predicted above were measured by RT-PCR and Western blot. The targets SREBP-1c and FAS play an important role in the biosynthesis of fatty acids (Horton, 2002). As shown in **Figures 6A, B**, and **7A**, compared with the NC group, the mRNA and protein expressions of SREBP-1c and FAS in HFD group were significantly increased ($p < 0.01$). Interesting, DHG-M and DHG-H obviously inhibited the mRNA and protein expressions of SREBP-1c and FAS in hyperlipidemic hamster liver ($p < 0.05$). A remarkably lower hepatic mRNA and protein expressions of SREBP-2 and LDLR were observed in HFD group than those in NC group ($p < 0.05$) (**Figures 6C, D**, **7B**). While treated with DHG, the mRNA and protein expression levels of SREBP-2 and LDLR were significantly increased in three DHG groups vs. HFD group ($p < 0.01$). The targets PPARα, LXRα and CYP7A1 could regulate the metabolism of cholesterol transformed into bile acids. As seen in **Figures 6E–G** and **7C**, HFD induced a down-regulation of PPARα and CYP7A1 mRNA and protein expressions ($p < 0.05$), while an up-regulation of LXRα mRNA and protein expressions ($p < 0.05$). After DHG-H treatment for 8 weeks, the mRNA and protein expressions of the PPARα, LXRα, and CYP7A1 were enhanced ($p < 0.01$). ABCA1 plays a major in cholesterol efflux by transporting intracellular cholesterol to the extracellular fluid (Wang and Tall, 2003). As shown in **Figures 6H** and **7D**, the mRNA and protein expression levels of ABCA1 were significantly up-regulated by DHG-M and DHG-H, compared with HFD group ($p < 0.05$).

# DISCUSSION

In China, the TCM formula is a conventional, safe and effective means for treating hyperlipidemia. In our study, DHG, derived from clinical prescriptions Danhe decoction, showed a strong hypolipidemic effect. The results showed that DHG significantly decreased the levels of serum TC, TG, LDL-

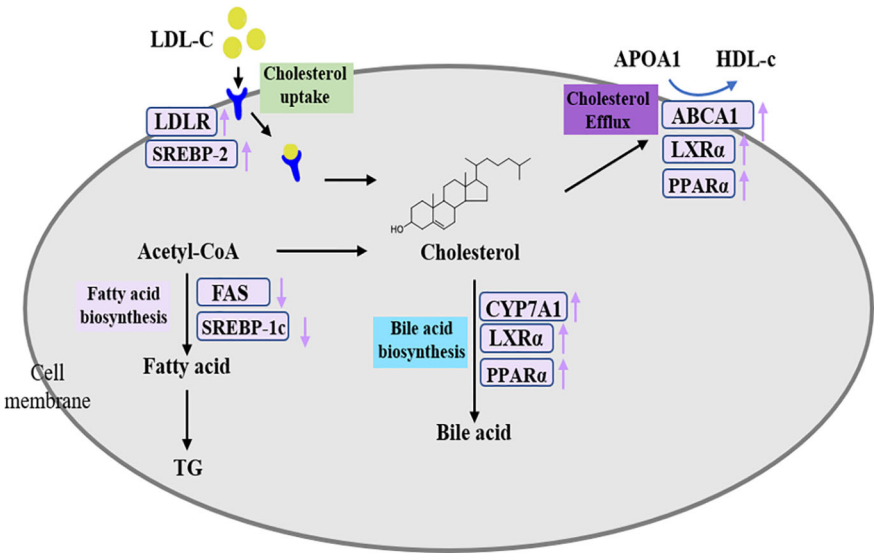


**FIGURE 8 |** The proposed mechanism of DHG in treatment of hyperlipidemia.

c, and AI, enhanced the level of serum HDL-c and HDL-c/TC ratio in hyperlipidemic hamsters. Long-term hyperlipidemia may induce atherosclerosis and further cause CVDs such as coronary artery disease. The HDL-c/TC ratio could predict the risk of coronary artery disease and the atherosclerosis index (AI) was also usually taken as the indicator of the risk of atherosclerosis (Yang et al., 2008; Sathiya et al., 2014). It is noteworthy that DHG-H was more effective than Sim in elevating levels of serum HDL-c and HDL-c/TC ratio, lowering the AI value, which suggested DHG has the potential application in inhibiting coronary artery disease and atherosclerosis. Besides, DHG treatment not only inhibited the fat accumulation in the liver, but also inversed the increase of body weight gain, liver index, and related adipose tissue weight in hyperlipidemic hamsters, which further confirmed that the DHG had a beneficial lipid-lowering effect.

Systems pharmacology has gradually become an effective method to study the active components and mechanisms of action of TCM (Zhou et al., 2019; Zhang et al., 2019). Different from most of the previous studies that usually consider ingredients from herbal databases, we take the compounds that are detected in the hamster blood as the compound source to carry out systems pharmacology research. In the present study, the 16 prototype compounds, such as polydatin, nuciferine and hyperin were identified from the hamster serum, which are the first report of the chemical constituents of DHG *in vivo*. Moreover, focusing on these ingredients absorbed into the blood, further systems pharmacology results indicated that 6 active compounds, including quercetin, emodin, salvianolic acid B, tanshinone II-A, naringenin, and nobiletin, may modulate some key targets (SREBP-1c, SPEBP-2, PPARα, and so on), involved in 3 closely lipid metabolism-related pathways. These six active compounds may be the potential material basis for the lipid-lowering effect of DHG. Previous studies have shown that quercetin, naringenin, and nobiletin, as flavonoids, are known for their protection against CVDs though lowering hepatic lipid accumulation, inhibiting hepatic fatty acid synthesis and increasing fatty acid oxidation (Jung et al., 2013; Hil et al., 2014; Mulvihill et al., 2016; Zhang et al., 2018). Emodin, as anthraquinones, could regulate lipid metabolism *via* the inhibition of lipid accumulation and lipogenesis (Tzeng et al., 2012; Cao et al., 2016). Salvianolic acid B and tanshinone II-A could attenuate atherosclerotic lesions by reducing vascular oxidative stress or regulating lipid metabolism (Xu et al., 2011; Zhang et al., 2011; Yue et al., 2015). Moreover, for PPAR signaling pathway and nuclear receptors in lipid metabolism and toxicity pathway, PPARα plays a role in scavenging circulating or cellular lipids by forming heterodimers with retinoid X receptor and regulating the expressions of genes involved in lipid metabolism such as biosynthesis of bile acids, cholesterol efflux, and so on (Ogata et al., 2009; Filip-Ciubotaru et al., 2011; Ramakrishna et al., 2017). In SREBP control of lipid synthesis pathway, SREBPs could bind to the LDL receptor promoter to enhance the expression of LDLR on cell surface to promote the internalization of plasma LDL (Ochiai et al., 2015).

The SREBPs are important transcription factors that regulate lipid homeostasis by regulating the expressions of related genes in cholesterol homeostasis, fatty acid synthesis, and TG

metabolism. SREBP-1c preferentially activates genes of fatty acid and TG metabolism, whereas SREBP-2 preferentially activates genes of cholesterol metabolism (Horton, 2002). Fatty acids, as raw materials for the synthesis of TGs, are closely related to the synthesis of TGs. FAS directly catalyzed the biosynthesis of fatty acids and modulated by SREBP-1c. The systems pharmacology results showed that the target SREBP-1c could be regulated by naringenin. Meanwhile, researchers have found that naringenin could inhibit hepatic fatty acids synthesis by decreasing SREBP-1c and other related genes mRNA levels in rats (Hashimoto and Ide, 2015). Moreover, our results indicated that DHG suppressed the SREBP-1c and FAS mRNA and protein expressions in hyperlipidemic hamsters, which could contribute to explain the effects of DHG on lowering serum TG level and inhibiting hepatic lipid accumulation. In humans, LDL receptor-mediated uptake and HDL-mediated reverse transports are important transport methods responsible for nearly 60-70% total plasma cholesterol (Zhang et al., 2013; Ridker, 2014). In general, LDL-c is removed from the circulation mainly by liver uptake *via* LDLR that internalizes bound LDL particles through endocytosis. The increase of LDLR expression will enhance the uptake and removal of LDL-c. LDLR is a known target gene of SREBP-2 (Kartawijaya et al., 2016). By C-T-P network mapping, we discovered that the target SREBP-2 could be modulated by quercetin and LDLR is connected to naringenin, nobiletin, quercetin and tanshinone II-A. Research has revealed quercetin could induce SREBP-2 and LDLR expression in hepG2 cells (Moon et al., 2012). In addition, naringenin, nobiletin, and tanshinone II-A were also reported to up-regulate the LDLR expression to affect lipid metabolism (Morin et al., 2008; Chen et al., 2016; Bawazeer et al., 2017). In the present study, our results suggested that DHG treatment increased the SREBP-2 and LDLR mRNA and protein expressions, which may be the main reason for the reduction of serum LDL-c effect by DHG. PPARα is a transcription factor that belongs to the nuclear receptor superfamily and plays important roles in metabolic regulation and affects the different links of lipid metabolism, including fatty acid uptake, fatty acid oxidation, cholesterol elimination and transport, etc. (Chinetti et al., 2001; Ogata et al., 2009). From the C-T-P network, PPARα is targeted by emodin and salvianolic acid B. Previous investigators have demonstrated that the two active compounds could regulate the expression of the target PPARα (Liu et al., 2010; Huang et al., 2016). CYP7A1, the rate-limiting enzyme in the classical bile acid biosynthetic pathway, catalyzing about 2/5 synthesized cholesterol transformed into bile acids, has a critical function in keeping homeostasis of cholesterol (Li et al., 2011; Cao et al., 2012). It is reported that PPARα and LXRα mediate feed-forward induction of CYP7A1, contributing to the clearance of excess cholesterol by increasing the formation of bile acids (Beaven and Tontonoz, 2006; Singh et al., 2013; Ramakrishna et al., 2017). In this study, DHG-H treatment significantly increased the mRNA and protein expressions of PPARα, LXRα, and CYP7A1, and enhanced the fecal TC and TBA levels in hyperlipidemic hamsters. These results suggested that the lipid-lowering effects of DHG may be related to the biosynthesis of bile acids. ABCA1, a trans-membranous protein, plays a key role in the regulation of cholesterol efflux (Li et al., 2018). The chief functions of ABCA1 are transporting intracellular cholesterol to the extracellular fluid and reducing the level of intracellular cholesterol by uniting it with HDL, which is regulated in a PPARα-LXRα-ABCA1 dependent manner (Hossain et al., 2008; Liu et al., 2015; Vijayakumar and Nachiappan, 2017). Based on the C-T-P network, the target ABCA1 is connected with quercetin. Quercetin demonstrated a protective effect against atherosclerosis partly through increasing the expression of ABCA1 (Jia et al., 2019). Our results showed that DHG up-regulated the mRNA and protein expressions of PPARα, LXRα, and ABCA1, which could help to explain the HDL-c-elevating effect of DHG. In summary, as shown in **Figure 8**, DHG may exert a hypolipidemic effect by affecting some targets such as some targets, such as SREBP-1c, SREBP-2 and PPARα, and further involving in lipid metabolic processes including fatty acid biosynthesis, LDLR-mediated cholesterol uptake, bile acid biosynthesis and cholesterol efflux.

Regardless, this study still has some limitations. First, we did not carry out experimental research on the targets of monomer active ingredients. Moreover, other species should also be considered in future experimental study.

## CONCLUSION

In this study, DHG exhibited excellent hypolipidemic effects in HFD-induced hyperlipidemic hamsters by multiple aspects, including improving blood lipid, reducing liver fat accumulation, and lowering body weight gain and liver index, etc. Then, systems pharmacology investigations focusing on the 16 main compounds absorbed into blood after oral administration of DHG showed that 6 active compounds, namely, quercetin, emodin, salvianolic acid B, tanshinone II-A, naringenin, and nobiletin, may affect some key targets such as SREBP-1c, SREBP-2 and PPARα, which were involved in three closely lipid metabolism-related pathways including PPAR signaling pathway, SREBP control of lipid synthesis pathway, and nuclear receptors in lipid metabolism and toxicity pathway. Further studies indicated that the hypolipidemic mechanisms of DHG were associated with the up-regulation of SREBP-2, LDLR, PPARα, LXRα, CYP7A1, and ABCA1 mRNA and protein expression levels, the down-regulation of SREBP-1c and FAS mRNA and protein expression levels. This work demonstrated that DHG has a good hypolipidemic effect, and provided an efficient way to understand the active ingredients and underlying mechanisms of DHG.

## DATA AVAILABILITY STATEMENT

All datasets generated for this study are included in the article/ **Supplementary Material**.

## ETHICS STATEMENT

The animal study was reviewed and approved by the Ethics Committee of Beijing University of Traditional Chinese Medicine (Beijing, China). This study was carried out in accordance with the principles of the Basel Declaration and recommendations of guidelines of the National Institutes of Health Conflict of Interest.

## AUTHOR CONTRIBUTIONS

KC, HX, JL, and WX conceived and designed the experiments. KC and ZM performed the experiments. ZM and XY analyzed the data. YL, YD, and YZ contributed reagents/materials/analysis tools. KC and XY wrote and edited the paper.

## FUNDING

This work was financially supported by the National Science and Technology Major Project (2019ZX09201004-001), the National Natural Science Foundation of China (No. 81573839 and No. 81774155), and the Fundamental Research Funds for the Central Universities (No. 2018-JYB-XS058).

## SUPPLEMENTARY MATERIAL

The Supplementary Material for this article can be found online at: https://www.frontiersin.org/articles/10.3389/fphar.2020.00528/full#supplementary-material

## REFERENCES

Basso, F., Freeman, L., Knapper, C. L., Remaley, A., Stonik, J., Neufeld, E. B., et al. (2003). Role of the hepatic abca1 transporter in modulating intrahepatic cholesterol and plasma hdl cholesterol concentrations. *J. Lipid Res.* 44, 296–302. doi: 10.1194/jlr.M200414-JLR200

Bawazeer, N. A., Choudary, H., Zamzami, M. A., Abdulaal, W. H., Zeyadi, M., ALbukhari, A., et al. (2017). Possible regulation of LDL-receptor by naringenin in HepG2 hepatoma cell line. *Afr. J. Tradit. Complem.* 14, 278–287. doi: 10.21010/ajtcam.v14i1.30

Beaven, S. W., and Tontonoz, P. (2006). Nuclear receptors in lipid metabolism: targeting the heart of dyslipidemia. *Annu. Rev. Med.* 57, 313–329. doi: 10.1146/annurev.med.57.121304.131428

Cao, Y., Bei, W., Hu, Y., Cao, L., Huang, L., Wang, L., et al. (2012). Hypocholesterolemia of Rhizoma Coptidis alkaloids is related to the bile acid by up-regulated CYP7A1 in hyperlipidemic rats. *Phytomedicine* 19, 686–692. doi: 10.1016/j.phymed.2012.03.011

Cao, Y., Chang, S., Dong, J., Zhu, S., Zheng, X., Li, J., et al. (2016). Emodin ameliorates high-fat-diet induced insulin resistance in rats by reducing lipid accumulation in skeletal muscle. *Eur. J. Pharmacol.* 780, 194–201. doi: 10.1016/j.ejphar.2016.03.049

Chen, H. C., Chen, P. Y., Wu, M. J., Tai, M. H., and Yen, J. H. (2016). Tanshinone II-A modulates low density lipoprotein uptake via down-regulation of PCSK9 gene expression in HepG2 Cells. *PloS One* 11, e0162414. doi: 10.1371/journal.pone.0162414

Chen, Y., Dong, J., Liu, J., Xu, W., Wei, Z., Li, Y., et al. (2019). Network pharmacology-based Investigation of protective mechanism of *Aster tataricus* on lipopolysaccharide-induced acute lung injury. *Int. J. Mol. Sci.* 20, 543. doi: 10.3390/ijms20030543

Chinetti, G., Lestavel, S., Bocher, V., Remaley, A. T., Neve, B., Torra, I. P., et al. (2001). PPAR-alpha and PPAR-gamma activators induce cholesterol removal from human macrophage foam cells through stimulation of the ABCA1 pathway. *Nat. Med.* 7, 53–58. doi: 10.1038/83348

Dentin, R., Girard, J., and Postic, C. (2005). Carbohydrate responsive element binding protein (ChREBP) and sterol regulatory element binding protein-1c (SREBP-1c): two key regulators of glucose metabolism and lipid synthesis in liver. *Biochimie* 87, 81–86. doi: 10.1016/j.biochi.2004.11.008

Eberle, D., Hegarty, B., Bossard, P., Ferré, P., and Foufelle, F. (2004). SREBP transcription factors: master regulators of lipid homeostasis. *Biochimie* 86, 839–848. doi: 10.1016/j.biochi.2004.09.018

Filip-Ciubotaru, F., Foia, L., Manciuc, C., and Grigore, C. (2011). PPARs: structure, mechanisms of action and control. note i. *Rev. Med. Chir. Soc. Med. Nat. Iasi.* 115, 477–484.

Folch, J., Lee, M., and Stanley, G. H. S. (1957). A simple method for isolation and purification of total lipids from animal tissue. *J. Biol. Chem.* 226, 497–509. doi: 10.1007/BF02927425

Garnett, W. R. (1995). Interactions with hydroxymethylglutaryl-coenzyme A reductase inhibitors. *Am. J. Health-Syst. Ph.* 52, 1639–1645. doi: 10.1093/ajhp/52.15.1639

Giudetti, A. M., Damiano, F., Gnoni, G. V., and Siculella, L. (2013). Low level of hydrogen peroxide induces lipid synthesis in brl-3a cells through a cap-independent srebp-1α activation. *Int. J. Biochem. Cell B.* 45, 1419–1426. doi: 10.1016/j.biocel.2013.04.004

Guo, J., Bei, W. J., Hu, Y. M., Tang, C. P., He, W., Liu, X. B., et al. (2011). A new TCM formula FTZ lowers serum cholesterol by regulating HMG-CoA reductase and CYP7A1 in hyperlipidemic rats. *J. Ethnopharmacol.* 135, 299–307. doi: 10.1016/j.jep.2011.03.012

Gupta, A., Sehgal, V., and Mehan, S. (2011). Hyperlipidemia: an updated review. *Inter. J. Biopharm. Toxicol. Res.* 1, 81–89.

Hansjörg, K., Mahfoudi, A., Dreyer, C., Hihi, A. K., and Wahli, W. (1993). Peroxisome proliferator-activated receptors and lipid metabolism. *Ann. N.Y. Acad. Sci.* 684, 157–173. doi: 10.1111/j.1749-6632.1993.tb32279.x

Harper, C. R., and Jacobson, T. A. (2007). The broad spectrum of statin myopathy: from myalgia to rhabdomyolysis. *Curr. Opin. Lipidol.* 18, 401–408. doi: 10.1097/mol.0b013e32825a6773

Hashimoto, T., and Ide, T. (2015). Activity and mRNA levels of enzymes involved in hepatic fatty acid synthesis in rats fed naringenin. *J. Agr. Food Chem.* 63, 9536–9542. doi: 10.1021/acs.jafc.5b03734

Hil, H. V. D., Schothorst, E. M. V., Stelt, I., Swarts, H. J. M., Vennma, D., Sailer, M., et al. (2014). Quercetin decreases high-fat diet induced body weight gain and accumulation of hepatic and circulating lipids in mice. *Genes Nutrition.* 9, 418. doi: 10.1007/s12263-014-0418-2

Horton, J. D. (2002). Sterol regulatory element-binding proteins: transcriptional activators of lipid synthesis. *Biochem. Soc. Trans.* 30, 1091–1095. doi: 10.1042/bst0301091

Hossain, M. A., Tsujita, M., Gonzalez, F. J., and Yokoyama, S. (2008). Effects of Fibrate drugs on expression of ABCA1 and HDL biogenesis in hepatocytes. *J. Cardiovasc. Pharm.* 51, 258–266. doi: 10.1097/fjc.0b013e3181624b22

Huang, M. Q., Zhou, C. J., Zhang, Y. P., Zhang, X. Q., Xu, W., Lin, J., et al. (2016). Salvianolic acid B ameliorates hyperglycemia and dyslipidemia in db/db mice through the AMPK pathway. *Cell Physiol. Biochem.* 40, 933–943. doi: 10.1159/000453151

Jia, Q., Cao, H., Shen, D., Li, S., Yan, L., Chen, C., et al. (2019). Quercetin protects against atherosclerosis by regulating the expression of PCSK9, CD36, PPARγ, LXRα and ABCA1. *Int. J. Mol. Med.* 44, 893–902. doi: 10.3892/ijmm.2019.4263

Jiang, Y. Y., Liu, N., Zhu, S. R., Hu, X. M., Chang, D. N., and Liu, J. X. (2019). Elucidation of the mechanisms and molecular targets of Yiqi shexue formula

for treatment of primary immune thrombocytopenia based on network pharmacology. *Front. Pharmacol.* 10, 1136. doi: 10.3389/fphar.2019.01136

Jung, C. H., Cho, I., Ahn, J., Jeon, T. I., and Ha, T. Y. (2013). Quercetin reduces high-fat diet-induced fat accumulation in the liver by regulating lipid metabolism genes. *Phytother. Res.* 27, 139–143. doi: 10.1002/ptr.4687

Kartawijaya, M., Han, H. W., Kim, Y., and Lee, S. M. (2016). Genistein upregulates LDLR levels via jnk-mediated activation of srebp-2. *Food Nutr. Res.* 60, 31120. doi: 10.3402/fnr.v60.31120

Li, T., Matozel, M., Boehme, S., Kong, B., Nilsson, L. M., Guo, G., et al. (2011). Overexpression of cholesterol 7α-hydroxylase promotes hepatic bile acid synthesis and secretion and maintains cholesterol homeostasis. *Hepatology* 53, 996–1006. doi: 10.1002/hep.24107

Li, X., Guo, J., Liang, N., Jiang, X., Song, Y., Ou, S., et al. (2018). 6-gingerol regulates hepatic cholesterol metabolism by up-regulation of LDLR and cholesterol efflux-related genes in hepg2 cells. *Front. Pharmacol.* 9, 159. doi: 10.3389/fphar.2018.00159

Liang, J., Wang, C., Peng, J., Li, W., Jin, Y., Liu, Q., et al. (2016). Naringin regulates cholesterol homeostasis and inhibits inflammation via modulating NF-κB and ERK signaling pathways in vitro. *Die Pharmazie-An. Int. J. Pharm. Sci.* 71, 101–108. doi: 10.1691/ph.2016.5629

Liu, T., Xu, Q. L., Zhao, Y., Li, X. J., Liu, C. Q., and Yang, S. Y. (2010). Effects of emodin on the lipid level and the expression of hepatic lipid metabolism in non-alcoholic fatty liver rats. *Chin. Tradit. Herbal Drugs* 41, 1516–1518.

Liu, R., Li, J., Cheng, Y., Huo, T., Xue, J., Liu, Y., et al. (2015). Effects of ellagic acid-rich extract of pomegranates peel on regulation of cholesterol metabolism and its molecular mechanism in hamsters. *Food Funct.* 6, 780–787. doi: 10.1039/C6FO00347H

Liu, J., Jiang, M., Li, Z., Zhang, X., Li, X., Hao, Y., et al. (2018). A novel systems pharmacology method to investigate molecular mechanisms of Scutellaria barbata D. Don for non-small cell lung cancer. *Front. Pharmacol.* 9, 1473. doi: 10.3389/fphar.2018.01473

Ma, Z. C., Chen, K. K., Li, Y. T., Su, R. B., L, Q., Yang, J., et al. (2019). Determinationof 25 characteristic components in Danhe Granules by LC-MS and consistency analysis of preparations. *Chin. Tradit. Herbal Drugs* 50, 5970–5979. doi: 10.7501/j.issn.0253-2670.2019.24.009

Maningat, P., and Breslow, J. L. (2011). Needed: pragmatic clinical trials for statin-intolerant patients. *New Engl. J. Med.* 365, 2250–2251. doi: 10.1056/NEJMp1112023

Mathur, M., and Devi, V. K. (2016). Potential of novel drug delivery strategies for the treatment of hyperlipidemia. *J. Drug Targeting* 24, 1–40. doi: 10.3109/1061186x.2016.1172586

Moon, J., Lee, S. M., Do, H. J., Cho, Y., Chung, J. H., and Shin, M. J. (2012). Quercetin up-regulates LDL receptor expression in HepG2 cells. *Phytother. Res.* 26, 1688–1694. doi: 10.1002/ptr.4646

Morin, B., Nichols, L. A., Zalasky, K. M., Davis, J. W., Manthey, J. A., and Holland, L. J. (2008). The citrus flavonoids hesperetin and nobiletin differentially regulate low density lipoprotein receptor gene transcription in HepG2 liver cells. *J. Nitr.* 138, 1274–1281. doi: 10.1093/jn/138.7.1274

Mulvihill, E. E., Burke, A. C., and Huff, M. W. (2016). Citrus flavonoids as regulators of lipoprotein metabolism and atherosclerosis. *Annu. Rev. Nutr.* 36, 13.1–13.25. doi: 10.1146/annurev-nutr-071715-050718

Ning, N., He, K., Wang, Y., Zou, Z., Wu, H., Li, X., et al. (2015). Hypolipidemic effect and mechanism of palmatine from coptis chinensis in hamsters fed high-fat diet. *Phytother. Res.* 29, 668–673. doi: 10.1002/ptr.5295

Niu, C., Chen, C., Chen, L., Cheng, K., Yeh, C., and Cheng, J. (2011). Decrease of blood lipids induced by Shan-Zha (fruit of crataegus pinnatifida) is mainly related to an increase of PPARα in liver of mice fed high-fat diet. *Horm. Metab. Res.* 43, 625–630. doi: 10.1055/s-0031-1283147

Ochiai, A., Miyata, S., Shimizu, M., Inoue, J., and Sato, R. (2015). Piperine induces hepatic low-density lipoprotein receptor expression through proteolytic activation of sterol regulatory element-binding proteins. *PloS One* 10, e0139799. doi: 10.1371/journal.pone.0139799

Ogata, M., Tsujita, M., Hossain, M. A., Akita, N., Gonzalez, F. J., Staels, B., et al. (2009). On the mechanism for PPAR agonists to enhance ABCA1 gene expression. *Atherosclerosis* 205, 413–419. doi: 10.1016/j.atherosclerosis.2009.01.008

Qu, L., Li, D., Gao, X., Li, Y., Wu, J., and Zou, W. (2018). Di'ao Xinxuekang capsule, a Chinese medicinal product, decreases serum lipids levels in high-fat diet-fed apoe$^{-/-}$mice by downregulating PCSK9. *Front. Pharmacol.* 9, 1170. doi: 10.3389/fphar.2018.01170

Ramakrishna, R., Kumar, D., Bhateria, M., Gaikwad, A. N., and Bhatta, R. S. (2017). 16-dehydropregnenolone lowers serum cholesterol by up-regulation of cyp7a1 in hyperlipidemic male hamsters. *J. Steroid Biochem.* 168, 110–117. doi: 10.1016/j.jsbmb.2017.02.013

Ridker, P. M. (2014). LDL cholesterol: controversies and future therapeutic directions. *Lancet* 384, 607–617. doi: 10.1016/S0140-6736(14)61009-6

Sathiya, R., Velu, V. K., Niranjan, G., Srinivasan, A. R., Amirtha, G. B., Ramesh, R., et al. (2014). A comparative study of serum uric acid levels and lipid ratios in coronary artery disease patients. *Int. J. BioMed. Sci.* 10, 124–128.

Singh, V., Jain, M., Misra, A., Khanna, V., Rana, M., Prakash, P., et al. (2013). Curcuma oil ameliorates hyperlipidaemia and associated deleterious effects in golden syrian hamsters. *Brit. J. Nutr.* 110, 437–446. doi: 10.1017/S0007114512005363

Su, X., Li, Y., Jiang, M., Zhu, J., Zheng, C., Chen, X., et al. (2019). Systems pharmacology uncover the mechanism of anti-non-small cell lung cancer for *Hedyotis diffusa* Willd. *BioMed. Pharmacother.* 109, 969–984. doi: 10.1016/j.biopha.2018.10.162

Tacherfiout, M., Petrov, P. D., Mattonai, M., Ribechini, E., Ribot, J., Bonet, M. L., et al. (2018). Antihyperlipidemic effect of a rhamnus alaternus leaf extract in triton-induced hyperlipidemic rats and human hepg2 cells. *BioMed. Pharmacother.* 101, 501–509. doi: 10.1016/j.biopha.2018.02.106

Tzeng, T., Lu, H., Liou, S., Chang, C., and Liu, I. (2012). Emodin protects against high-fat diet-induced obesity via regulation of AMP-activated protein kinase pathways in white adipose tissue. *Planta Med.* 78, 943–950. doi: 10.1055/s-0031-1298626

Vijayakumar, R., and Nachiappan, V. (2017). Cassia auriculata, flower extract attenuates hyperlipidemia in male Wistar rats by regulating the hepatic cholesterol metabolism. *BioMed. Pharmacother.* 95, 394–401. doi: 10.1016/j.biopha.2017.08.075

Wang, N., and Tall, A. R. (2003). Regulation and mechanisms of ATP-binding cassette transporter A1-mediated cellular cholesterol efflux. *Arterioscl. Throm Vas.* 23, 1178–1184. doi: 10.1161/01.ATV.0000075912.83860.26

Wang, N., Silver, D. L., Thiele, C., and Tall, A. R. (2001). ATP-binding Cassette Transporter A1 (ABCA1) functions as a cholesterol efflux regulatory protein. *J. Biol. Chem.* 276, 23742–23747. doi: 10.1074/jbc.M102348200

Wu, X., and Xu, J. (2016). New role of hispidulin in lipid metabolism: PPARα activator. *Lipids* 51, 1249–1257. doi: 10.1007/s11745-016-4200-7

Xu, S., Little, P. J., Lan, T., Huang, Y., Le, K., Wu, X., et al. (2011). Tanshinone II-A attenuates and stabilizes atherosclerotic plaques in apolipoprotein-e knockout mice fed a high cholesterol diet. *Arch. Biochem. Biophys.* 515, 72–79. doi: 10.1016/j.abb.2011.08.006

Yan, G., Wang, X., Zhang, A., Hui, S., Ying, Z., and Hui, S. (2017). "Serum pharmacochemistry of TCM for determining the active ingredients of Shuanghuanglian formulae," in *Serum Pharmacochemistry of Traditional Chinese Medicine*. Eds. X. Wang, A. Zhang and H. Sun (New York: Elsevier), 155–169. doi: 10.1016/B978-0-12-811147-5.00011-X

Yang, R. L., Shi, Y. H., Hao, G., Li, W., and Le, G. W. (2008). Increasing oxidative stress with progressive hyperlipidemia in human: relation between malondialdehyde and atherogenic index. *J. Clin. Biochem. Nutr.* 43, 154–158. doi: 10.3164/jcbn.2008044

Ye, X. L., Huang, W. W., Chen, Z., Li, X. G., Li, P., Lan, P., et al. (2010). Synergetic effect and structure-activity relationship of 3-hydroxy-3-methylglutaryl coenzyme a reductase inhibitor from crataegus pinnatifida bge. *J. Agr. Food Chem.* 58, 3132–3138. doi: 10.1021/jf903337f

Yue, J., Li, B., Jing, Q., and Guan, Q. (2015). Salvianolic acid B accelerated ABCA1-dependent cholesterol efflux by targeting PPAR-γ and LXRα. *Biochem. Bioph. Res. Co* 462, 233–238. doi: 10.1016/j.bbrc.2015.04.122

Zhang, F., Guo, M. J., Gu, L. Y., and Fan, Y. C. (2011). Effects of salvianolic acid b on stability of atherosclerotic plaque in apolipoprotein e gene knock-out mice treated with stz and high fat diet. *Chin. J. Arterioscl.* 19, 885–890. doi: 10.1038/cmi.2011.4

Zhang, L., Yuan, F., Liu, P., Fei, L., Huang, Y., Xu, L., et al. (2013). Association between pcsk 9 and ldlr gene polymorphisms with coronary heart disease: case-control study and meta-analysis. *Clin. Biochem.* 46, 727–732. doi: 10.1016/j.clinbiochem.2013.01.013

Zhang, J., Zhao, L., Cheng, Q., Ji, B., Yang, M., Sanidad, K. Z., et al. (2018). Structurally different flavonoid subclasses attenuate high-fat and high-fructose diet induced metabolic syndrome in rats. *J. Agr. Food Chem.* 66, 12412–12420. doi: 10.1021/acs.jafc.8b03574

Zhang, J. Y., Hong, C. L., Chen, H. S., Zhou, X. J., Zhang, Y. J., Efferth, T., et al. (2019). Target identification of active constituents of Shen Qi Wan to treat kidney yang deficiency using computational target fishing and network pharmacology. *Front. Pharmacol.* 10, 650. doi: 10.3389/fphar.2019.00650

Zhou, W., Chen, Z. Y., Wang, Y. H., Li, X. M., Lu, A. P., Sun, X. Z., et al. (2019). Systems pharmacology-based method to assess the mechanism of action of weight-loss herbal intervention therapy for obesity. *Front. Pharmacol.* 10, 1165. doi: 10.3389/fphar.2019.01165

Zhu, B., Zhang, W., Lu, Y., Hu, S., Gao, R., Sun, Z., et al. (2018). Network pharmacology-based identification of protective mechanism of Panax Notoginseng Saponins on aspirin induced gastrointestinal injury. *BioMed. Pharmacother.* 105, 159–166. doi: 10.1016/j.biopha.2018.04.054

**Conflict of Interest:** The authors declare that the research was conducted in the absence of any commercial or financial relationships that could be construed as a potential conflict of interest.

frontiers in Pharmacology

ORIGINAL RESEARCH
published: 14 May 2020
doi: 10.3389/fphar.2020.00694

# Resveratrol: Multi-Targets Mechanism on Neurodegenerative Diseases Based on Network Pharmacology

*Wenjun Wang[1,2†], Shengzheng Wang[3†], Tianlong Liu[1,4†], Yang Ma[2†], Shaojie Huang[1], Lu Lei[1], Aidong Wen[1*] and Yi Ding[1*]*

*[1] Department of Pharmacy, Xijing Hospital, Fourth Military Medical University, Xi'an, China, [2] Department of Pharmacy, Shaanxi University of Chinese Medicine, Xi'an, China, [3] Department of Medicinal Chemistry, School of Pharmacy, Fourth Military Medical University, Xi'an, China, [4] Department of Pharmacy, 940 Hospital of PLA Joint Logistics Support Forces, Lanzhou, China*

Resveratrol is a natural polyphenol in lots of foods and traditional Chinese medicines, which has shown promising treatment for neurodegenerative diseases (NDs). However, the molecular mechanisms of its action have not been systematically studied yet. In order to elucidate the network pharmacological prospective effects of resveratrol on NDs, we assessed of pharmacokinetics (PK) properties of resveratrol, studied target prediction and network analysis, and discussed interacting pathways using a network pharmacology method. Main PK properties of resveratrol were acquired. A total of 13,612 genes related to NDs, and 138 overlapping genes were determined through matching the 175 potential targets of resveratrol with disease-associated genes. Gene Ontology (GO) function analysis and Kyoto Encyclopedia of Genes and Genomes (KEGG) pathway enrichment were performed to obtain more in-depth understanding of resveratrol on NDs. Accordingly, nodes with high degrees were obtained according using a PPI network, and AKT1, TP53, IL6, CASP3, VEGFA, TNF, MYC, MAPK3, MAPK8, and ALB were identified as hub target genes, which showed better affinity with resveratrol in silico studies. In addition, our experimental results demonstrated that resveratrol markedly enhanced the decreased levels of Bcl-2 and significantly reduced the increased expression of Bax and Caspase-3 in hippocampal neurons induced by glutamate exposure. Western blot results confirmed that resveratrol inhibited glutamate-induced apoptosis of hippocampal neurons partly by regulating the PI3K/AKT/mTOR pathway. In conclusion, we found that resveratrol could target multiple pathways forming a systematic network with pharmacological effects.

**Keywords: resveratrol, neurodegenerative diseases (NDs), network pharmacology, multitargets, apoptosis**

OPEN ACCESS

***Edited by:***
*Wei Zhou,*
*The Affiliated Hospital of Shenzhen University, China*

***Reviewed by:***
*Jianhua Chen,*
*Shanghai Jiao Tong University, China*
*Jianping Chen,*
*Guangzhou University of Chinese Medicine, China*

****Correspondence:***
*Aidong Wen*
*adwen-2004@hotmail.com*
*Yi Ding*
*dingyi.007@163.com*

*[†]These authors have contributed equally to this work*

***Specialty section:***
*This article was submitted to Ethnopharmacology, a section of the journal Frontiers in Pharmacology*

***Received:*** *28 November 2019*
***Accepted:*** *27 April 2020*
***Published:*** *14 May 2020*

***Citation:***
*Wang W, Wang S, Liu T, Ma Y, Huang S, Lei L, Wen A and Ding Y (2020) Resveratrol: Multi-Targets Mechanism on Neurodegenerative Diseases Based on Network Pharmacology. Front. Pharmacol. 11:694. doi: 10.3389/fphar.2020.00694*

## INTRODUCTION

Neurodegenerative diseases (NDs) are multifactorial debilitating disorders that are characterized by progressive dysfunction and neuronal injury, which preferentially affect the normal functioning of the brain including learning and memory (Jakaria et al., 2019). Examples of NDs are Alzheimer's diseases (AD), Parkinson's disease (PD), Huntington's diseases (HD), amyotrophic lateral sclerosis (ALS), and spinocerebellar ataxia (SCA) (Rahman et al., 2019). Notwithstanding, although the different clinical and neuropathological characteristics of each ND (Raza et al., 2018), there are several common pathological mechanisms of NDs, which are characterized by multiple targets. Most importantly, NDs are typically characterized by loss of neurons (Velmurugan et al., 2018). Some studies suggested that the pathogenesis of these kinds of diseases is the result of multiple pathological mechanisms or processes, such as glutamate excitotoxicity, oxidative stress, and abnormal apoptosis (Huang et al., 2018). Some symptomatic treatments are offered, but particular therapies have not been found owing to conventional philosophy of "one gene, one drug, one disease" (Esteves, 2017). Accordingly, the multitargeted natural products with substantial pharmacological activities are most likely to have potential advantages. Resveratrol is a natural polyphenol with a stilbene scaffold (**Figure 1**) in numerous foods including grapes, mulberries, and blueberries, which has shown many beneficial properties including antioxidant, antiinflammation, neuroprotective, and even antiaging activities. And resveratrol has revealed appealing outcomes as treatment for several NDs in preclinical studies (Penalver et al., 2018). But the mechanism by which resveratrol displays its protective function is not extremely well comprehended yet (Sanchez-Melgar et al., 2019).

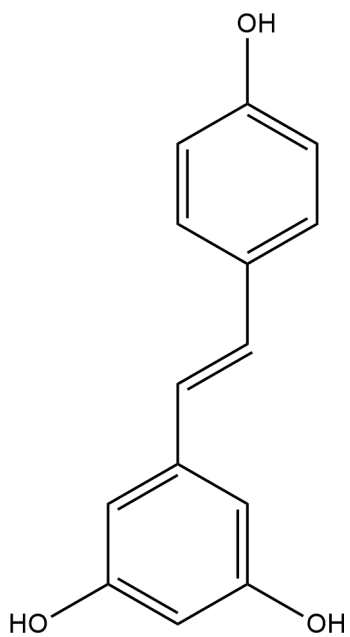


**FIGURE 1 |** Chemical structure of resveratrol (PubChem CID: 445154).

Network pharmacology as an emerging discipline located on the general concepts of systems biology (Zhou et al., 2019), which was utilized to systematically evaluate pharmacological effects of multiingredient medicine (Zhang R. et al., 2019). In addition, it similarly has been provided lately for revealing the molecular mechanisms of various complicated chronic diseases, such as NDs and cardiocerebral vascular diseases (Wang W. et al., 2019). Therefore, network analysis based on lots of existing databases enables us to produce a preliminary understanding of the mechanisms by which multitarget drugs treat complex diseases.

In present study, we illuminated the pharmacological actions of resveratrol on NDs systematically utilizing network pharmacology methods. Resveratrol was hypothesized to have therapeutic effects on NDs through multiple-targets mechanism. First, pharmacokinetic (PK) parameters of resveratrol were acquired from Traditional Chinese Medicine Systems Pharmacology Database (TCMSP) server. Potential candidate targets of resveratrol and therapeutic target genes of NDs were gathered respectively. Then, the potential candidate target genes were predicted *via* network pharmacology databases. In addition, multitarget of resveratrol network was constructed to supply a methodical overview. Furthermore, pivotal target genes, Gene Ontology (GO) function analysis and KEGG pathway enrichment were evaluated by STRING database and DAVID database. Finally, key targets and signaling pathways were identified by western blot. Network pharmacology analysis workflow was shown in **Figure 2**.

## MATERIAL AND METHODS

### Assessment of PK Parameters

PK parameters of resveratrol were acquired from TCMSP database version 2.3 (http://tcmspw.com/tcmsp.php) (Ru et al., 2014), which is a phytochemical database for TCMs or related ingredients. Meanwhile, the information of absorption, distribution, metabolism, and excretion (ADME) properties of a drug with potential biological activities also can be acquired, such as oral bioavailability (OB), drug likeness (DL), Caco-2 permeability (Caco-2), blood-brain barrier (BBB). In this study, with the chemical name "resveratrol" as the keyword, and PK properties of resveratrol were searched in the search box.

### Construction and Identification of Target Genes

All of genes associated to resveratrol were gathered from the databases: TCMSP database version 2.3 (http://tcmspw.com/tcmsp.php), TCM Database@Taiwan (http://tcm.cmu.edu.tw/) (Chen, 2011), the Comparative Toxicogenomics Database (CTD, http://ctdbase.org/) (Davis et al., 2019), and the Encyclopedia of Traditional Chinese Medicine (ETCM, www.nrc.ac.cn:9090/ETCM/) (Xu et al., 2019). Subsequently, the official names of gene were drawn from UniProt database (http://www.uniprot.org/) (Uniprot, 2019) by restricting the types to "Homo sapiens." Then, different genes' ID terms were converted into UniProt IDs. And a resveratrol-targets relationship dataset was constructed.

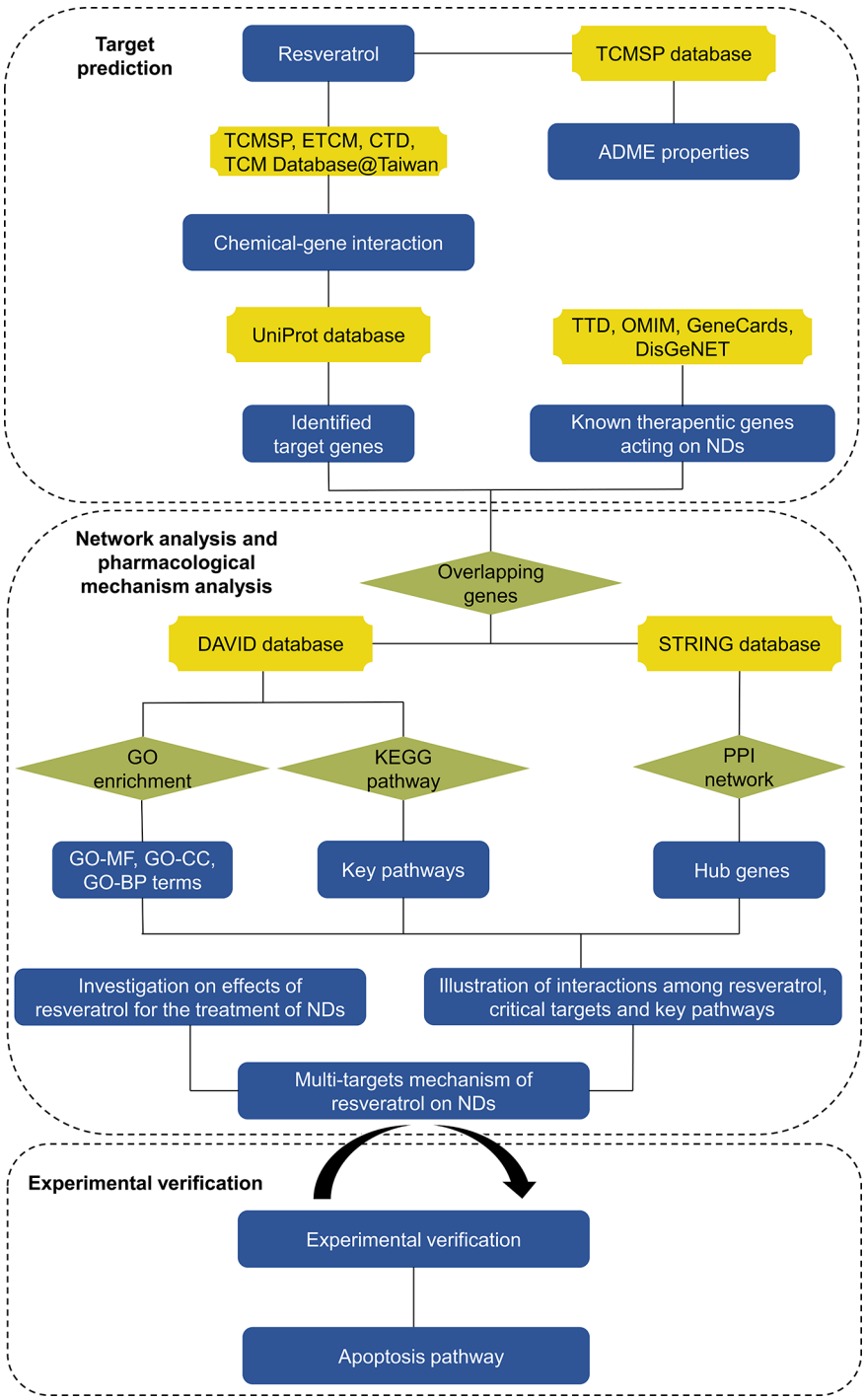


**FIGURE 2 |** The flowchart of pharmacology analysis.

## Gene Dataset Acquisition of NDs

With "NDs," "ADs," "PD," "HDs," "ALS," and "SCA" as the keywords, then therapeutic target genes of NDs were acquired from the Therapeutic Target Database (TTD, https://db.idrblab.org/ttd/) (Wang et al., 2020), the Online Mendelian Inheritance in Man (OMIM, http://www.omim.org/) (Amberger et al., 2015), GeneCards (https://www.genecards.org/) (Fishilevich et al., 2016) and a database of gene-disease associations (DisGeNET, http://www.disgenet.org/) (Pinero et al., 2017), and just "Homo sapiens" proteins linked to NDs were selected.

## GO Function Enrichment and KEGG Pathway Analysis

A pharmacology network is comprised of nodes and edges. The entities that make up the nodes of the networks are resveratrol NDs and related target genes. The Cytoscape version 3.7.2 was used to constructed networks, which is a java based open source software (Demchak et al., 2014). Functional pathways of resveratrol related to NDs were analyzed using GO enrichment and KEGG pathways analysis based upon the database for Annotation, Visualization and Integrated Discovery (DAVID) version 6.8 (https://david.ncifcrf.gov/) (Ke et al., 2019). $P < 0.05$ suggested the enrichment degree had statistically significant and the pathway results might be essential functional mechanisms of resveratrol in the treatment of NDs.

## Construction of Target Protein-Protein Interaction (PPI) Data

The potential interprotein interactions were obtained from STRING database version 11.0 (https://string-db.org/), which is a database of known and predicted protein-protein interactions (Ge et al., 2018). The software produces scores information for each pair of protein. The higher the score, the more confident the target protein's interactions were. Thus, the potential targets of resveratrol on NDs were imported into STRING tool to acquire potential interprotein interactions. We selected a high confidence score > 0.7 with the species restricted to "Homo sapiens" (Szklarczyk et al., 2019). Then, target genes with high degree, betweenness, and closeness were selected as the hub genes of NDs.

## *In Silico* Docking Study of Resveratrol With Key Targets

A study of in silico docking of resveratrol with key targets was conducted by Autodock Vina (Trott and Olson, 2010). For this purpose, resveratrol was prepared and optimized using the PubChem database (https://www.ncbi.nlm.nih.gov/), then converted to the PDB file format. Receptor structures were downloaded from the RCSB Web site (http://www.rcsb.org/pdb) in PDB format. Before docking, the original crystal ligands and water molecules were removed from the protein-ligand complexes. Hydrogen atoms and charge were added, and default settings were selected for other parameters. The theoretical binding affinities of resveratrol to proteins are predicted based on docking score.

## Cell Culture and Treatments

The study was reviewed and approved by Ethics Committee of Animal Experimentation of the Fourth Military Medical University (Xi'an China). Primary hippocampal neurons were prepared from embryonic d15 mouse embryos. Embryonic brain tissue was mechanically triturated and centrifuged. Neurons were cultured in the atmosphere of 5%/95% CO2/air at 37°C using the Dulbecco's modified Eagle's medium (DMEM) which contains 10% fetal bovine serum, 100 U/ml of penicillin, and 100 μg/ml streptomycin. The coincubation model incorporating samples and glutamate (25 mM) was used to evaluate the protective effects of resveratrol (50 mg/ml) on glutamate-induced apoptotic cells. The equivalent volume of PBS and resveratrol were used in the control groups, respectively. To investigate the involvement of PI3K/AKT/mTOR in the effects of resveratrol, phosphatidylinositol-3-kinase (PI3K) inhibitors, LY294002 (10 μM) was added to glutamate-stimulated hippocampal neurons. All operations were repeated over three times.

## Western Blot Analysis

Primary hippocampal neurons were lysed at indicated time points with 40-μl RIPA ice-cold lysis buffer (Rockford, IL, USA) supplemented with protease inhibitor (Vazyme Biotech, Nanjing, China) for 30 min and centrifuged at 9,000 g for 10 min at 4°C. The protein concentrations were analyzed by the BCA (Rockford, IL, USA). Equal amounts of proteins were separated and transferred to a PVDF membrane (Millipore, USA). The membranes were blocked with 3% BSA in TBS/T and stained with primary antibodies (1:1,000) and antibodies for β-actin (1:10,000) overnight at 4°C. Membranes were then probed with peroxidase conjugated secondary antibody at a 1:10,000 dilution. The antigen-antibody complexes were detected with an ECL reagent (Rockford, IL, USA). Primary antibodies used for western blotting were mouse antibodies. Secondary antibodies used were peroxidase conjugated goat antimouse antibodies.

## Statistical Analysis

The data of the experiment was expressed as means ± SEM and analyzed using one-way ANOVA. $P < 0.05$ was a significant difference and $P < 0.01$ is a very significant difference.

# RESULTS

## PK Parameters

The information of resveratrol on 12 main characteristics like Caco-2 and BBB for drug screening and evaluation (**Table 1**). Significantly, OB is the primary feature of oral medications because it plays a critical part in assessing the effectiveness of

**TABLE 1** | Pharmacological and molecular properties of resveratrol.

| Molecular Formula | MW | AlogP | Hdon | Hacc | OB (%) | Caco-2 | BBB | DL | FASA- | TPSA | RBN | HL |
|---|---|---|---|---|---|---|---|---|---|---|---|---|
| $C_{14}H_{12}O_3$ | 228.26 | 3.01 | 3 | 3 | 19.07 | 0.80 | –0.01 | 0.11 | 0.49 | 60.69 | 2 | – |

*MW, molecular weight; AlogP value represents the partition coefficient between octanol and water; Hdon and Hacc are measures of the hydrogen-bonding ability of a molecule expressed in terms of number of possible hydrogen-bond donors and acceptors, respectively; OB, oral bioavailability; Caco-2, Caco-2 permeability; BBB, blood-brain barrier; DL, drug-likeness; FASA-, fractional water accessible surface area of all atoms with negative partial charge; TPSA is a physico chemical property describing the polarity of molecules; RBN is the number of bonds which allow free rotation around themselves; HL, drug half-life.*

drug distribution for systemic circulation. In spite of the low bioavailability of resveratrol (its OB was calculated to be 19.07%), there are lots of evidence that resveratrol has the therapeutic potential on neurodegeneration (Yang et al., 2017). Furthermore, resveratrol has a relatively small molecular weight and moderate blood-brain barrier permeability with a BBB value of −0.01.

## Potential Target Genes and Network Analysis

A total of 182 candidate target genes were identified (**Supplementary Table 1**). Afterwards, seven were duplicated and therefore removed, 175 unique target genes for resveratrol remained (**Figure 3A**). Based on gene databases, we determined 13,612 genes concerned NDs (**Supplementary Table 2**). Then, 138 overlapping genes were identified through matching the potential targets of resveratrol with disease-associated genes (**Figure 3B**). Despite the different clinical and neuropathological characteristics of each ND, which are characterized by multiple targets, the underlying causes at the molecular level are almost similar (Suresh et al., 2020). Therefore, resveratrol reveled multitarget effects, which can regulate the variety of changes associated with NDs, unlike specific target drugs.

## GO Term Enrichment and Pathway Analysis

To elucidate the function and pharmacological mechanism of resveratrol, we conducted GO enrichment and KEGG pathway analysis of the 138 determined targets. GO analysis (**Supplementary Table 3**) is determined by the biological process (BP), cell component (CC), and molecular function (MF) terms. An introduction of the GO enrichment was discovered with the leading five enriched entries in the BP, CC, and MF terms (**Figure 4A**, $P < 0.05$). Especially, the enriched BP ontologies were dominated by positive regulation of transcription from RNA polymerase II promoter, DNA-templated transcription, and negative regulation of apoptotic process, etc. The enriched MF ontologies were dominated by ATP binding, DNA binding, and so on. The nucleus accounted for the largest proportion in CC analysis (42 target genes). Then, a total of 119 significant pathways were acquired ($P < 0.05$). Among them, 20 significant pathways were showed in **Figure 4B**. As shown, FoxO, PI3K-Akt, p53 and apoptosis signaling pathways may be the interaction pathways to apply their combined results versus NDs.

## PPI Network of Target Genes

The 138 target genes were submitted to STRING tool to acquire PPI relationships. We selected high-confidence target protein based on interaction with a score of > 0.7 to ensure the dependability of the study, and got the network of PPI relationships (**Figure 5A**). The targets with high degree, betweenness, and closeness were chosen as the hub genes for NDs (**Figure 5B**). And the predicted mode of action of 10 hub genes was shown in **Figure 5C**. The hub genes were including RAC-alpha serine/threonine-protein kinase (AKT1), cellular tumor antigen p53 (TP53), interleukin 6 (IL6), caspase-3

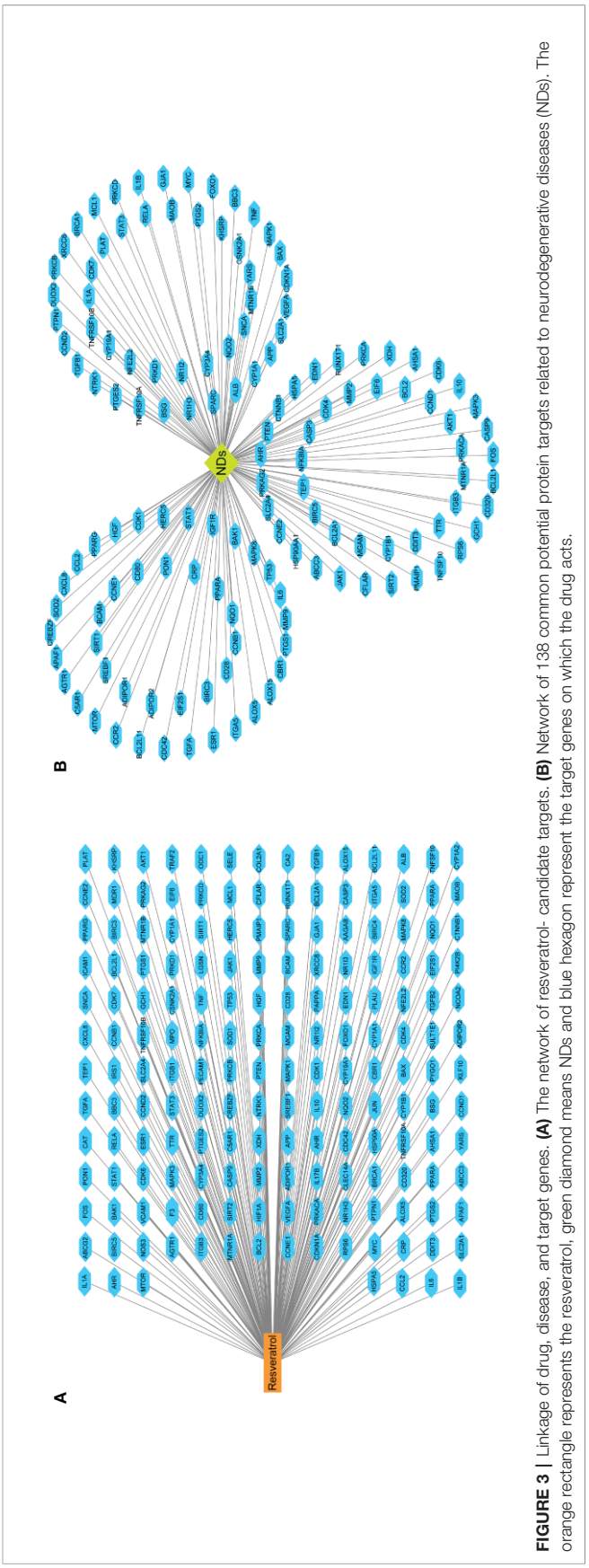


**FIGURE 3** | Linkage of drug, disease, and target genes. **(A)** The network of resveratrol- candidate targets. **(B)** Network of 138 common potential protein targets related to neurodegenerative diseases (NDs). The orange rectangle represents the resveratrol, green diamond means NDs and blue hexagon represent the target genes on which the drug acts.

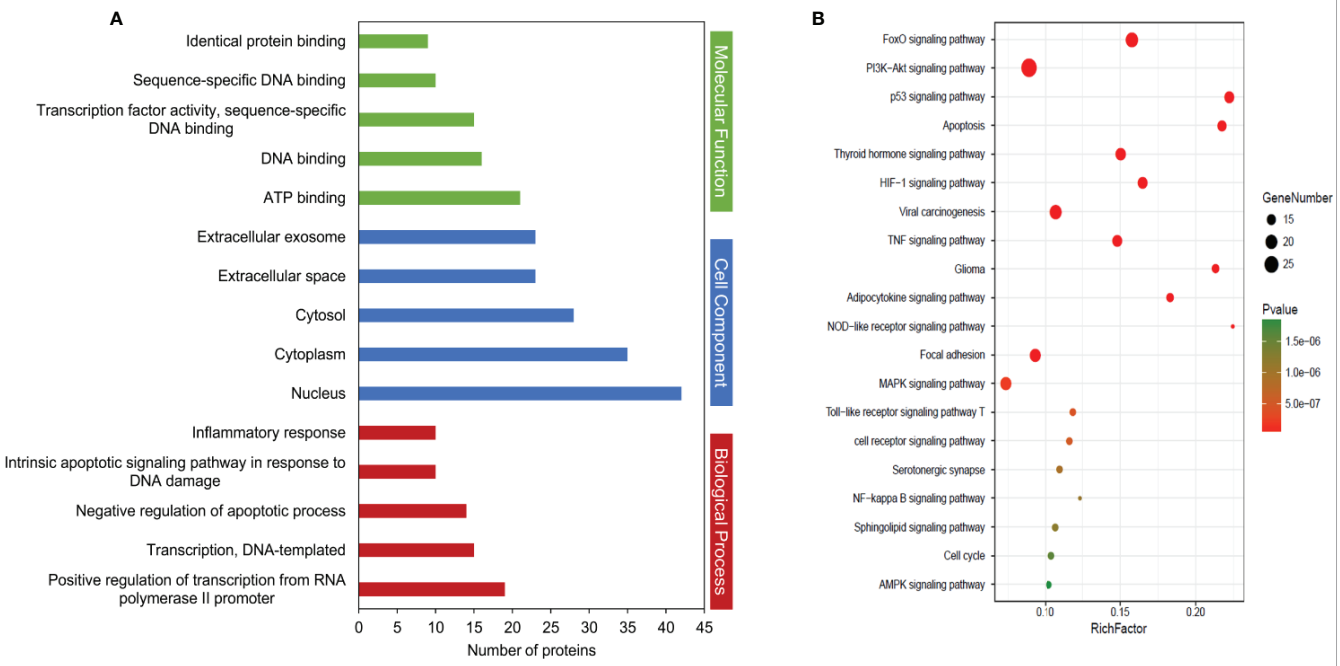


**FIGURE 4 |** Kyoto Encyclopedia of Genes and Genomes (KEGG) pathways and Gene Ontology (GO) analyses by database for Annotation, Visualization and Integrated Discovery (DAVID) database. **(A)** GO enrichment analysis of target proteins. The number of GO entries in the functional categories of cell composition (CC), molecular function (MF), and biological process (BP) ($P < 0.05$). **(B)** KEGG pathways of target genes ($P < 0.05$).

(CASP3), vascular endothelial growth factor A (VEGFA), tumor necrosis factor (TNF), myc proto-oncogene protein (MYC), mitogen-activated protein kinase 3 (MAPK3), mitogen-activated protein kinase 8 (MAPK8), and serum albumin (ALB). Among the above 10 hub proteins, such as AKT1, TP53, CASP3, and TNF, are involved in external or internal apoptotic pathways. Therefore, Resveratrol may play a protective role in NDs by regulating the apoptotic pathways involved in AKT1, TP53, CASP3, and TNF proteins (**Figure 6**).

## Molecular Docking Analysis

In silico studies were conducted to study the binding affinity of resveratrol with key target receptors. The results revealed that docking scores of resveratrol with AKT1, TP53, IL6, CASP3, VEGFA, TNF, MYC, MAPK3, MAPK8, and ALB ranged from −4.8 to −8.9. Particularly, resveratrol had the highest docking score with AKT1 (docking score: −8.9), which indicated that resveratrol was well located inside the binding site with AKT1. Other hub proteins also showed better affinity with resveratrol, as shown in **Figure 7** and **Table 2**.

## Experimental Validation

The protective effects of resveratrol on glutamate−induced injury in the culture model *in vitro* were determined. In fact, FoxO, PI3K-Akt, and p53 signaling pathways are also involved in regulating apoptosis (Akhter et al., 2014). Thus, based on the hub targets and KEGG pathway enrichment, we chose the apoptosis-related protein Bax, Bcl-2, and Caspase-3 for validation the mechanisms underlying the neuroprotective effects of resveratrol. Resveratrol markedly reinforced the decreased levels of Bcl-2 in glutamate treated hippocampal neurons ($P < 0.01$). Meanwhile, resveratrol significantly reduced the increased expression of Bax and Caspase-3 induced by glutamate exposure ($P < 0.01$, **Figure 8**).

The results of molecular docking showed that resveratrol was well located inside the binding site with AKT and PI3K (docking score: −7.5, **Figure 9A**), the upstream protein of AKT. It is well known that PI3K/AKT/mTOR signaling pathway is an important pathway mediating cell survival and differentiation, proliferation, apoptosis, and metastasis (Hou et al., 2018). Then we further confirmed whether resveratrol inhibited glutamate-induced apoptosis of hippocampal neurons by regulating the PI3K/AKT/mTOR pathway. The results revealed that resveratrol significantly reinforced the decreased the levels of p-PI3K, p-AKT, and p-mTOR after glutamate exposure ($P <0.05$, $P <0.01$). Additionally, LY294002 (PI3K inhibitor) significantly attenuated the effects of resveratrol ($P <0.05$, $P <0.01$), which can be observed from the protein expression of p-PI3K, p-AKT, p-mTOR and Bcl-2, Bax, and Caspase-3 (**Figure 9**). These results suggested that resveratrol plays a neuroprotective role partly by activating the PI3K/AKT/mTOR pathway to inhibit the apoptosis of neurons.

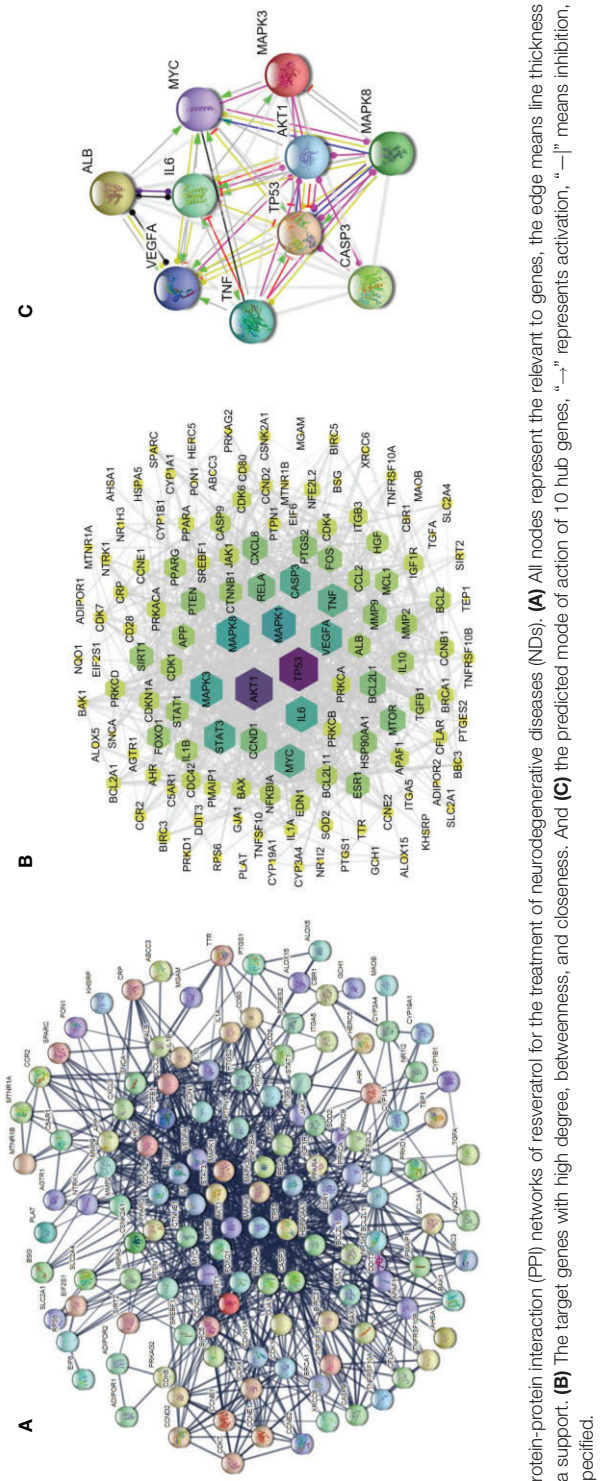


**FIGURE 5 |** Protein-protein interaction (PPI) networks of resveratrol for the treatment of neurodegenerative diseases (NDs). **(A)** All nodes represent the relevant to genes, the edge means line thickness indicates the strength of data support. **(B)** The target genes with high degree, betweenness, and closeness. And **(C)** the predicted mode of action of 10 hub genes, "→" represents activation, "—|" means inhibition, and "—•" represents unspecified.

## DISCUSSION AND CONCLUSION

NDs are common ailments in the elderly, and they are rapidly rising in prevalence as members of society age (Bianchi et al., 2019). And NDs vary in pathophysiology, such as memory and cognitive impairments, and the ability to move, speak, and breathe is affected. There is an urgent need to search for more effective therapeutic strategies to curb the progress of NDs. Moreover, it is important to gain insight into the causes and mechanisms of each disease (Gitler et al., 2017). Current advances in network pharmacology have provided brand-new chances to elucidate the treatment of certain complex diseases with certain drugs (Zhang et al., 2016). In this study, 12 very important PK properties of resveratrol were acquired from the TCMSP database. A total of 13,612 genes relevant to NDs, and 138 overlapping genes were identified through matching the potential targets of resveratrol with disease-associated genes. To acquire a more in-depth understanding of resveratrol on NDs, we performed GO function analysis and KEGG pathway enrichment. Accordingly, genes with degree, betweenness and closeness of differential expression were gotten according utilizing a PPI network, and AKT1, TP53, IL6, CASP3, VEGFA, TNF, MYC, MAPK3, MAPK8, and ALB were identified as hub nodes. These hub targets showed better affinity with resveratrol in silico studies. In addition, our experimental results demonstrated that suggested that resveratrol plays a neuroprotective role partly by activating the PI3K/AKT/mTOR pathway to inhibit the apoptosis of neurons.

Toxicity and PK are the most important characteristics should be given priority in drug research (Zhang Y.F. et al., 2019). Resveratrol is a natural nonflavonoid polyphenol, but its intense metabolism and particularly low OB seem to limit its application in human therapeutics. However, resveratrol nanoformulations are being looked upon as a resolution to these PK issues (Summerlin et al., 2015). Additionally, Lipinski's rule of five can determine some main drug properties: the compounds with molecular weight from 180 to 500 Dalton are viewed as more druggable, AlogP value is less than 5, numbers of possible hydrogen-bond donors and acceptors are less than 5 and 10, respectively (Chagas et al., 2018). And resveratrol could be up to these standards, suggesting it could be considered a lead compound that can be structurally optimized. Thus, resveratrol is a prospect for drug development.

A growing number of studies have suggested that resveratrol is a multitarget treatment for NDs. In this study, AKT1, TP53, IL6, CASP3, VEGFA, TNF, MYC, MAPK3, MAPK8, and ALB were identified as hub genes in the PPI analysis. Similarly, several previous studies have addressed gene expression changes. The majority of these studies compared the transcriptional levels of genes in cells or animals. AKT1 exerts major influences on the regulation of cell proliferation, cell survival, and protein synthesis (Ahmad et al., 2014; Palmieri et al., 2017). In fact, resveratrol has been shown to be protective in cellular and animal models of neurodegeneration by enhancing AKT1 activity (Zhang et al., 2014; Wang et al., 2018). TP53 is a crucial protein in NDs (Goiran et al., 2018). Several studies consistently suggested that TP53-dependent apoptotic cells are

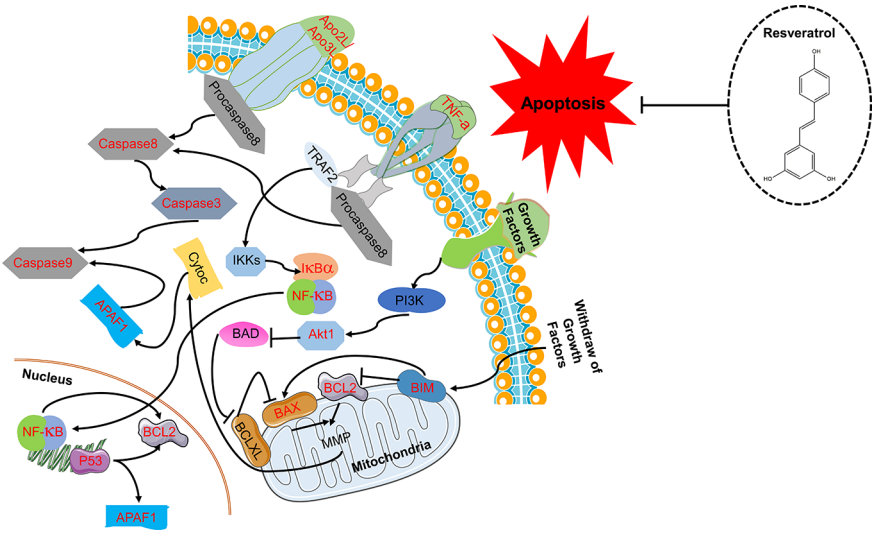


**FIGURE 6 |** Resveratrol plays a protective role in neurodegenerative diseases (NDs) by regulating the apoptotic pathways involved in AKT1, TP53, CASP3, and TNF proteins.

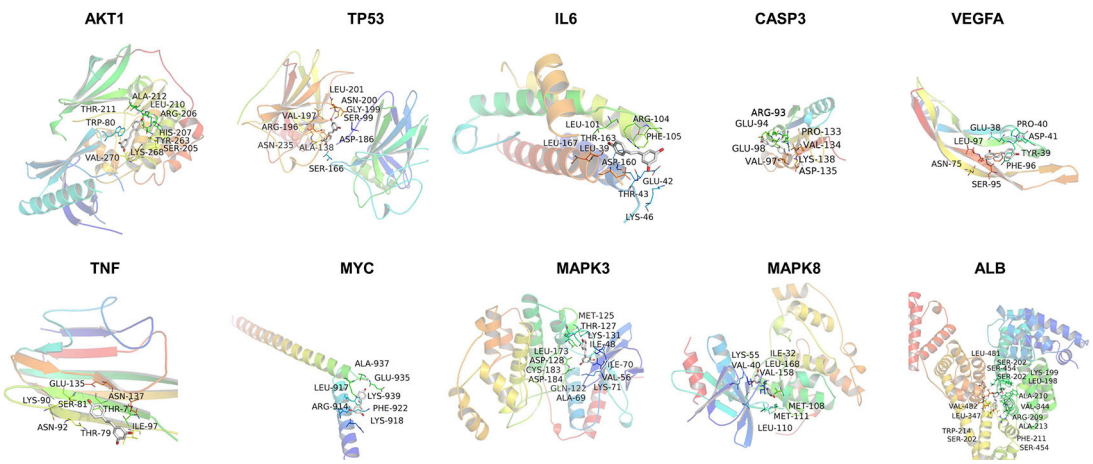


**FIGURE 7 |** Structural interactions of resveratrol key target receptors in silico studies.

**TABLE 2 |** The docking scores and binding sites of resveratrol with key proteins.

| Target (PDB ID) | Drug | Binding sites with the amino acid | Docking score |
|---|---|---|---|
| AKT1 (4EKL) | Resveratrol | ALA212, THR211, TRP80, VAL270, LYS268, SER205, TYR263 HIS207, ARG206, LEU210 | −8.9 |
| TP53 (6SHZ) | | VAL197, LEU201, ASN235, ALA138, SER166, ASP186, SER99, GLY199, ASN200, ARG196 | −6.4 |
| IL6 (4ZS7) | | LEU101, ARG104, THR163, PHE105, LEU167, ASP160, GLU42, LEU39, THR43, LYS46 | −7.1 |
| CASP3 (6BFK) | | LYS138, PRO133, ASP135, VAL134, GLU94, ARG93, GLU98, VAL97 | −5.9 |
| VEGFA (4KZN) | | GLU38, PRO40, LEU97, ASN75, SER95, PHE96, TYR39, ASP41 | −5.2 |
| TNF (6OOY) | | GLU135, ASN137, LYS90, SER81, THR77, ASN92, THR79, ILE97 | −4.8 |
| MYC (6G6J) | | ALA937, GLU935, LEU917, LYS939, ARG914, PHE922,LYS918 | −5.9 |
| MAPK3 (2ZOQ) | | MET125, THR127, LYS131, ILE48, GLN122, ASP184, CYS183, ASP128, LEU173 ILE70, VAL56, LYS71, ALA69 | −7.4 |
| MAPK8 (4YR8) | | LYS55, ILE32, VAL40, LEU168, VAL158, MET108, MET111, LEU110 | −6.8 |
| ALB (6QIO) | | LEU481, SER202, SER454, LYS199, LEU18, ALA210, VAL344, ARG209, ALA213, PHE211, SER454, VAL482, LEU347, TRP214 | −8.9 |

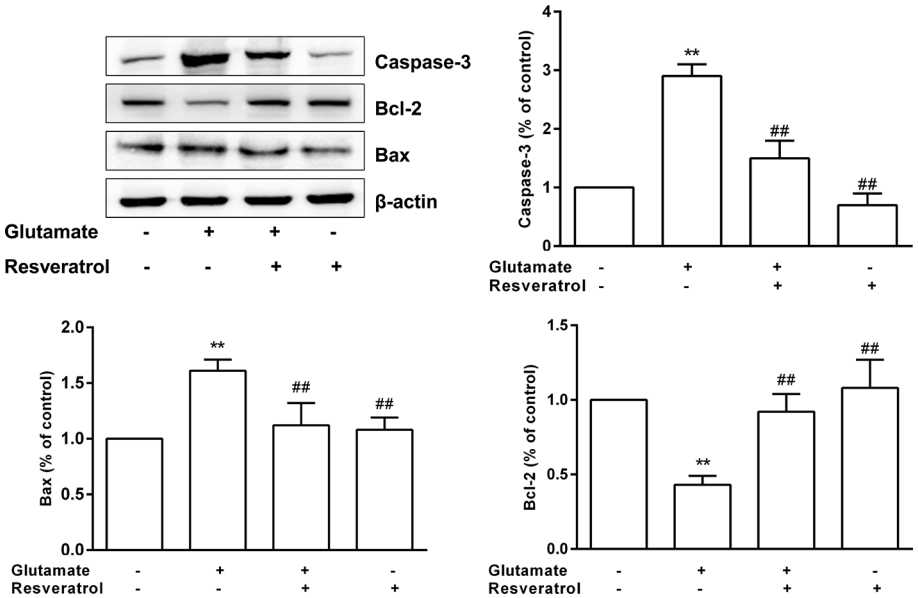


**FIGURE 8 |** Effects of resveratrol on the expression of Caspase-3, Bcl-2, and Bax induced by glutamate exposure in hippocampal neurons. $^{**}P < 0.01$ compared with control; $^{\#\#}P < 0.01$ compared with glutamate alone.

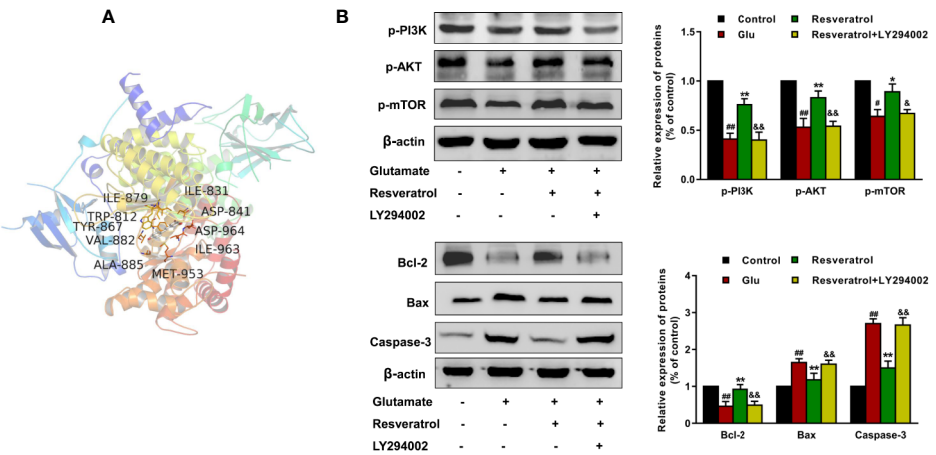


**FIGURE 9 |** Resveratrol inhibited glutamate-induced apoptosis of hippocampal neurons by regulating the PI3K/AKT/mTOR pathway. **(A)** Structural interactions of resveratrol with PI3K (PDB ID: 6AUD) in silico studies. **(B)** Effects of resveratrol on protein expression of p-PI3K, p-AKT, p-mTOR, Bcl-2, Bax, and Caspase-3 after glutamate-induced apoptosis of hippocampal neurons. $^{\#\#}P < 0.01$ compared with control; $^{*}P < 0.05$ and $^{**}P < 0.01$ compared with glutamate alone; $^{\&}P < 0.05$ and $^{\&\&}P < 0.01$ compared with resveratrol treated.

detectable in specific locations in PD and AD (Checler et al., 2018). Neuroinflammation is intensively demonstrated to be related with various NDs (Qi et al., 2019). Especially, the findings of the meta-analysis demonstrated higher peripheral concentrations of IL-6 and TNF in patients with PD (Qin et al., 2016). CASP3 plays a crucial function in intrinsic and extrinsic pathways of programed cell death and in cell proliferation. Previous study reported that the administration of resveratrol could increase proinflammatory cytokine levels and inhibit apoptosis in the hippocampus (Shen et al., 2019). VEGFA is a proangiogenic factor, which also involves in neuroprotection, neurogenesis, synaptic plasticity, and modulation of inflammation and astrocyte proliferation (Harris et al., 2018; Wei et al., 2018). Recently, human induced pluripotent stem cells, which are produced from somatic cells by overexpressing four reprogramming factors (including MYC), were applying in the cellular therapy of NDs (Berry et al., 2018). ALB is the most plentiful protein in blood plasma and cerebrospinal fluid, where

it contributes substantially to regulate the osmotic pressure and metabolic processes (Ts et al., 2017). Studies have demonstrated that resveratrol stabilizes the protein structure and regulates the development of fibrils along the preliminary stage of the ALB aggregation pathway (Stirpe et al., 2016). Simultaneously, MAPK is a crucial target for chronic inflammatory diseases such as AD (Criscuolo et al., 2017). It was reported that resveratrol reduced the upregulated protein expression of AMPK to prevent alcohol –induced neurodegeneration (Gu et al., 2018).

GO and KEGG pathway analyses were performed to better understand the interactions of the target genes. In results, GO analysis revealed that target genes were majorly related to the BPs of positive regulation of transcription from RNA polymerase II promoter, DNA-templated transcription, and negative regulation of apoptotic process, etc. The enriched MF ontologies were dominated by ATP binding, DNA binding, and so on. The nucleus accounted for the largest proportion in CC analysis. Furthermore, KEGG pathway analysis indicated that FoxO signaling pathway, PI3K-Akt signaling pathway and apoptosis, etc. may be the interaction pathways to apply their combined results versus NDs. These results followed the previous reports that above pathways participate in crucial functions in the progression of NDs (Huang et al., 2019; Qi et al., 2019; Rai et al., 2019).

NDs are typically characterized by loss of neurons. Studies have confirmed that apoptosis is an important molecular biological mechanism that is closely related to NDs (Ghavami et al., 2014). Wang N. et al. (2019) reported that resveratrol improves cognitive function of rats and reduces oxidative stress-induced neuronal damage in the frontal cortex and hippocampus by inhibiting neuronal apoptosis. In present study, among the 10 hub proteins from PPI network, such as AKT1, TP53, CASP3, and TNF, are involved in external or internal apoptotic pathways (**Figure 6**). And FoxO, PI3K-Akt, and p53 signaling pathways are also involved in regulating apoptosis. Apoptosis is a process of programmed cell death, which is vital for normal neural development (Ghavami et al., 2014). Under pathologic conditions, apoptosis also coresponsible for the loss of neurons associated with NDs (Maino et al., 2017). The proteins of Bcl-2 family, caspases and Apaf1 are main molecular components of the apoptosis program (Burek et al., 2006). Particularly, Bax gene is the first known proapoptotic member (Li et al., 2017). It has been reported that Bax promotes the release of cytochrome C by transferring it to the mitochondrial membrane, accordingly promoting downstream cell apoptosis (Kosten et al., 2008). Bcl-2 is a key member of the antiapoptotic Bcl-2 family (Garner et al., 2017). Overexpressed Bcl-2 has been demonstrated to protect nerve cells from damage by neurotoxins (Laulier and Lopez, 2012). Caspase-3 is a type of proapoptotic enzyme that plays the role of the apoptotic executor (Zhang Y. et al., 2019). Our results demonstrated that resveratrol markedly enhanced the decreased levels of Bcl-2 and significantly reduced the increased expression of Bax and Caspase-3 in hippocampal neurons induced by glutamate exposure. Then, Western blot results further confirmed that resveratrol inhibited glutamate-induced apoptosis of hippocampal neurons partly by regulating the PI3K/AKT/mTOR pathway. This further suggested that resveratrol plays a protective role against NDs through the apoptosis pathway.

In summary, resveratrol is an active and promising compound that is expected to be developed as a safe and effective multitarget drug against NDs. Our network pharmacological analysis of resveratrol predicted that the therapeutic effects of resveratrol related to NDs through mechanisms regulated by active compounds and apoptosis associated signaling pathways, such as PI3K/AKT/mTOR pathway. Further verification experiments study is necessary to explore and the key mechanisms resveratrol.

## DATA AVAILABILITY STATEMENT

All datasets generated for this study are included in the article/ **Supplementary Material**.

## ETHICS STATEMENT

The study was reviewed and approved by Ethics Committee of Animal Experimentation of the Fourth Military Medical University (Xi'an China).

## AUTHOR CONTRIBUTIONS

YD, WW, and AW conceived and proposed the idea. WW, SW, YM, and TL designed the research, analyzed the data and wrote the paper. SH, LL, and YD revised the manuscript. All authors read the final manuscript.

## FUNDING

This work was supported by the National Natural Science Foundation of China (No. 81603385) and the Booster Plan of Xijing Hospital (XJZT18D06).

## SUPPLEMENTARY MATERIAL

The Supplementary Material for this article can be found online at: https://www.frontiersin.org/articles/10.3389/fphar.2020.00694/full#supplementary-material

**SUPPLEMENTARY TABLE 1 |** The identified 175 potential targets of resveratrol.

**SUPPLEMENTARY TABLE 2 |** The identified 13612 genes relevant to NDs.

**SUPPLEMENTARY TABLE 3 |** The enriched GO terms and KEGG pathways based upon DAVID database.

## REFERENCES


Ahmad, F., Nidadavolu, P., Durgadoss, L., and Ravindranath, V. (2014). Critical cysteines in Akt1 regulate its activity and proteasomal degradation: implications for neurodegenerative diseases. *Free Radic. Biol. Med.* 74, 118–128. doi: 10.1016/j.freeradbiomed.2014.06.004

Akhter, R., Sanphui, P., and Biswas, S. C. (2014). The essential role of p53-up-regulated modulator of apoptosis (Puma) and its regulation by FoxO3a transcription factor in beta-amyloid-induced neuron death. *J. Biol. Chem.* 289, 10812–10822. doi: 10.1074/jbc.M113.519355

Amberger, J. S., Bocchini, C. A., Schiettecatte, F., Scott, A. F., and Hamosh, A. (2015). OMIM.org: Online Mendelian Inheritance in Man (OMIM(R)), an online catalog of human genes and genetic disorders. *Nucleic Acids Res.* 43, D789–D798. doi: 10.1093/nar/gku1205

Berry, B. J., Smith, A. S. T., Young, J. E., and Mack, D. L. (2018). Advances and Current Challenges Associated with the Use of Human Induced Pluripotent Stem Cells in Modeling Neurodegenerative Disease. *Cells Tissues Organs* 205, 331–349. doi: 10.1159/000493018

Bianchi, V. E., Herrera, P. F., and Laura, R. (2019). Effect of nutrition on neurodegenerative diseases. A systematic review. *Nutr. Neurosci.* 4, 1–25. doi: 10.1080/1028415X.2019.1681088

Burek, M., Maddika, S., Burek, C. J., Daniel, P. T., Schulze-Osthoff, K., and Los, M. (2006). Apoptin-induced cell death is modulated by Bcl-2 family members and is Apaf-1 dependent. *Oncogene* 25, 2213–2222. doi: 10.1038/sj.onc.1209258

Chagas, C. M., Moss, S., and Alisaraie, L. (2018). Drug metabolites and their effects on the development of adverse reactions: Revisiting Lipinski's Rule of Five. *Int. J. Pharmaceutics* 549, 133–149. doi: 10.1016/j.ijpharm.2018.07.046

Checler, F., Goiran, T., and Alves Da Costa, C. (2018). Nuclear TP53: An unraveled function as transcriptional repressor of PINK1. *Autophagy* 14, 1099–1101. doi: 10.1080/15548627.2018.1450022

Chen, C. Y. (2011). TCM Database@Taiwan: the world's largest traditional Chinese medicine database for drug screening in silico. *PloS One* 6, e15939. doi: 10.1371/journal.pone.0015939

Criscuolo, C., Fabiani, C., Cerri, E., and Domenici, L. (2017). Synaptic Dysfunction in Alzheimer's Disease and Glaucoma: From Common Degenerative Mechanisms Toward Neuroprotection. *Front. Cell Neurosci.* 11, 53. doi: 10.3389/fncel.2017.00053

Davis, A. P., Grondin, C. J., Johnson, R. J., Sciaky, D., Mcmorran, R., Wiegers, J., et al. (2019). The Comparative Toxicogenomics Database: update 2019. *Nucleic Acids Res.* 47, D948–D954. doi: 10.1093/nar/gky868

Demchak, B., Hull, T., Reich, M., Liefeld, T., Smoot, M., Ideker, T., et al. (2014). Cytoscape: the network visualization tool for GenomeSpace workflows. *F1000Res* 3, 151. doi: 10.12688/f1000research.4492.2

Esteves, A. R. (2017). Editorial: New Avenues and Therapeutic Strategies for the Treatment of Neurodegenerative Diseases. *Curr. Pharm. Des.* 23, 667–668. doi: 10.2174/1381612823999170201153809

Fishilevich, S., Zimmerman, S., Kohn, A., Iny Stein, T., Olender, T., Kolker, E., et al. (2016). Genic insights from integrated human proteomics in GeneCards. *Database (Oxford)* 2016, baw030. doi: 10.1093/database/baw030

Garner, T. P., Lopez, A., Reyna, D. E., Spitz, A. Z., and Gavathiotis, E. (2017). Progress in targeting the BCL-2 family of proteins. *Curr. Opin. Chem. Biol.* 39, 133–142. doi: 10.1016/j.cbpa.2017.06.014

Ge, Q., Chen, L., Tang, M., Zhang, S., Liu, L., Gao, L., et al. (2018). Analysis of mulberry leaf components in the treatment of diabetes using network pharmacology. *Eur. J. Pharmacol.* 833, 50–62. doi: 10.1016/j.ejphar.2018.05.021

Ghavami, S., Shojaei, S., Yeganeh, B., Ande, S. R., Jangamreddy, J. R., Mehrpour, M., et al. (2014). Autophagy and apoptosis dysfunction in neurodegenerative disorders. *Prog. Neurobiol.* 112, 24–49. doi: 10.1016/j.pneurobio.2013.10.004

Gitler, A. D., Dhillon, P., and Shorter, J. (2017). Neurodegenerative disease: models, mechanisms, and a new hope. *Dis. Model Mech.* 10, 499–502. doi: 10.1242/dmm.030205

Goiran, T., Duplan, E., Rouland, L., El Manaa, W., Lauritzen, I., Dunys, J., et al. (2018). Nuclear p53-mediated repression of autophagy involves PINK1 transcriptional down-regulation. *Cell Death Differ.* 25, 873–884. doi: 10.1038/s41418-017-0016-0

Gu, X., Cai, Z., Cai, M., Liu, K., Liu, D., Zhang, Q., et al. (2018). AMPK/SIRT1/p38 MAPK signaling pathway regulates alcoholinduced neurodegeneration by resveratrol. *Mol. Med. Rep.* 17, 5402–5408. doi: 10.3892/mmr.2018.8482

Harris, R., Miners, J. S., Allen, S., and Love, S. (2018). VEGFR1 and VEGFR2 in Alzheimer's Disease. *J. Alzheimers Dis.* 61, 741–752. doi: 10.3233/JAD-170745

Hou, X., Xiao, H., Zhang, Y., Zeng, X., Huang, M., Chen, X., et al. (2018). Transient receptor potential channel 6 knockdown prevents apoptosis of renal tubular epithelial cells upon oxidative stress via autophagy activation. *Cell Death Dis.* 9 1015. doi: 10.1038/s41419-018-1052-5

Huang, L., Wang, S., Ma, F., Zhang, Y., Peng, Y., Xing, C., et al. (2018). From stroke to neurodegenerative diseases: The multi-target neuroprotective effects of 3-n-butylphthalide and its derivatives. *Pharmacol. Res.* 135, 201–211. doi: 10.1016/j.phrs.2018.08.007

Huang, Y., Zhu, X., Chen, K., Lang, H., Zhang, Y., Hou, P., et al. (2019). Resveratrol prevents sarcopenic obesity by reversing mitochondrial dysfunction and oxidative stress via the PKA/LKB1/AMPK pathway. *Aging (Albany NY)* 11, 2217–2240. doi: 10.18632/aging.101910

Jakaria, M., Kim, J., Karthivashan, G., Park, S. Y., Ganesan, P., and Choi, D. K. (2019). Emerging signals modulating potential of ginseng and its active compounds focusing on neurodegenerative diseases. *J. Ginseng Res.* 43, 163–171. doi: 10.1016/j.jgr.2018.01.001

Ke, Z. B., Cai, H., Wu, Y. P., Lin, Y. Z., Li, X. D., Huang, J. B., et al. (2019). Identification of key genes and pathways in benign prostatic hyperplasia. *J. Cell Physiol.* 234, 19942–19950. doi: 10.1002/jcp.28592

Kosten, T. A., Galloway, M. P., Duman, R. S., Russell, D. S., and D'sa, C. (2008). Repeated unpredictable stress and antidepressants differentially regulate expression of the bcl-2 family of apoptotic genes in rat cortical, hippocampal, and limbic brain structures. *Neuropsychopharmacology* 33, 1545–1558. doi: 10.1038/sj.npp.1301527

Laulier, C., and Lopez, B. S. (2012). The secret life of Bcl-2: apoptosis-independent inhibition of DNA repair by Bcl-2 family members. *Mutat. Res.* 751, 247–257. doi: 10.1016/j.mrrev.2012.05.002

Li, M., Qi, Y., Wei, J., Lu, L., Zhao, X., and Zhou, L. (2017). N6-Isopentenyladenosine promoted HeLa cell apoptosis through inhibitions of AKT and transforming growth factor beta-activated kinase 1 activation. *Tumour Biol.* 39, 1010428317695966. doi: 10.1177/1010428317695966

Maino, B., Paparone, S., Severini, C., Ciotti, M. T., D'agata, V., Calissano, P., et al. (2017). Drug target identification at the crossroad of neuronal apoptosis and survival. *Expert Opin. Drug Discovery* 12, 249–259. doi: 10.1080/17460441.2017.1280023

Palmieri, M., Pal, R., Nelvagal, H. R., Lotfi, P., Stinnett, G. R., Seymour, M. L., et al. (2017). mTORC1-independent TFEB activation via Akt inhibition promotes cellular clearance in neurodegenerative storage diseases. *Nat. Commun.* 8, 14338. doi: 10.1038/ncomms14338

Penalver, P., Belmonte-Reche, E., Adan, N., Caro, M., Mateos-Martin, M. L., Delgado, M., et al. (2018). Alkylated resveratrol prodrugs and metabolites as potential therapeutics for neurodegenerative diseases. *Eur. J. Med. Chem.* 146, 123–138. doi: 10.1016/j.ejmech.2018.01.037

Pinero, J., Bravo, A., Queralt-Rosinach, N., Gutierrez-Sacristan, A., Deu-Pons, J., Centeno, E., et al. (2017). DisGeNET: a comprehensive platform integrating information on human disease-associated genes and variants. *Nucleic Acids Res.* 45, D833–D839. doi: 10.1093/nar/gkw943

Qi, G., Mi, Y., Fan, R., Li, R., Liu, Z., and Liu, X. (2019). Nobiletin Protects against Systemic Inflammation-Stimulated Memory Impairment via MAPK and NF-kappaB Signaling Pathways. *J. Agric. Food Chem.* 67, 5122–5134. doi: 10.1021/acs.jafc.9b00133

Qin, X. Y., Zhang, S. P., Cao, C., Loh, Y. P., and Cheng, Y. (2016). Aberrations in Peripheral Inflammatory Cytokine Levels in Parkinson Disease: A Systematic Review and Meta-analysis. *JAMA Neurol.* 73, 1316–1324. doi: 10.1001/jamaneurol.2016.2742

Rahman, S., Datta, M., Kim, J., and Jan, A. T. (2019). CRISPR/Cas: An intriguing genomic editing tool with prospects in treating neurodegenerative diseases. *Semin. Cell Dev. Biol.* 96, 22–31. doi: 10.1016/j.semcdb.2019.05.014

Rai, S. N., Dilnashin, H., Birla, H., Singh, S. S., Zahra, W., Rathore, A. S., et al. (2019). The Role of PI3K/Akt and ERK in Neurodegenerative Disorders. *Neurotox. Res.* 35, 775–795. doi: 10.1007/s12640-019-0003-y

Raza, S. S., Wagner, A. P., Hussain, Y. S., and Khan, M. A. (2018). Mechanisms underlying dental-derived stem cell-mediated neurorestoration in

neurodegenerative disorders. *Stem Cell Res. Ther.* 9, 245. doi: 10.1186/s13287-018-1005-z

Ru, J., Li, P., Wang, J., Zhou, W., Li, B., Huang, C., et al. (2014). TCMSP: a database of systems pharmacology for drug discovery from herbal medicines. *J. Cheminform.* 6, 13. doi: 10.1186/1758-2946-6-13

Sanchez-Melgar, A., Albasanz, J. L., Palomera-Avalos, V., Pallas, M., and Martin, M. (2019). Resveratrol Modulates and Reverses the Age-Related Effect on Adenosine-Mediated Signalling in SAMP8 Mice. *Mol. Neurobiol.* 56, 2881–2895. doi: 10.1007/s12035-018-1281-8

Shen, J., Qu, C., Xu, L., Sun, H., and Zhang, J. (2019). Resveratrol exerts a protective effect in chronic unpredictable mild stress-induced depressive-like behavior: involvement of the AKT/GSK3beta signaling pathway in hippocampus. *Psychopharmacol. (Berl)* 236, 591–602. doi: 10.1007/s00213-018-5087-1

Stirpe, A., Pantusa, M., Rizzuti, B., De Santo, M. P., Sportelli, L., Bartucci, R., et al. (2016). Resveratrol induces thermal stabilization of human serum albumin and modulates the early aggregation stage. *Int. J. Biol. Macromol.* 92, 1049–1056. doi: 10.1016/j.ijbiomac.2016.08.014

Summerlin, N., Soo, E., Thakur, S., Qu, Z., Jambhrunkar, S., and Popat, A. (2015). Resveratrol nanoformulations: challenges and opportunities. *Int. J. Pharm.* 479, 282–290. doi: 10.1016/j.ijpharm.2015.01.003

Suresh, S. N., Chakravorty, A., Giridharan, M., Garimella, L., and Manjithaya, R. (2020). Pharmacological tools to modulate autophagy in neurodegenerative diseases. *J. Mol. Biol.* 432, 2822–2842. doi: 10.1016/j.jmb.2020.02.023

Szklarczyk, D., Gable, A. L., Lyon, D., Junge, A., Wyder, S., Huerta-Cepas, J., et al. (2019). STRING v11: protein-protein association networks with increased coverage, supporting functional discovery in genome-wide experimental datasets. *Nucleic Acids Res.* 47, D607–D613. doi: 10.1093/nar/gky1131

Trott, O., and Olson, A. J. (2010). AutoDock Vina: improving the speed and accuracy of docking with a new scoring function, efficient optimization, and multithreading. *J. Comput. Chem.* 31, 455–461. doi: 10.1002/jcc.21334

Ts, C., Hj, L., Jy, H., Mh, L., and Hi, K. (2017). Molecular Insights into Human Serum Albumin as a Receptor of Amyloid-β in the Extracellular Region. *J. Am. Chem. Soc.* 139, 15437–15445. doi: 10.1021/jacs.7b08584

Uniprot, C. (2019). UniProt: a worldwide hub of protein knowledge. *Nucleic Acids Res.* 47, D506–D515. doi: 10.1093/nar/gky1049

Velmurugan, B. K., Rathinasamy, B., Lohanathan, B. P., Thiyagarajan, V., and Weng, C. F. (2018). Neuroprotective Role of Phytochemicals. *Molecules* 23, 2485. doi: 10.3390/molecules23102485

Wang, H., Dong, X., Liu, Z., Zhu, S., Liu, H., Fan, W., et al. (2018). Resveratrol Suppresses Rotenone-induced Neurotoxicity Through Activation of SIRT1/Akt1 Signaling Pathway. *Anat. Rec. (Hoboken)* 301, 1115–1125. doi: 10.1002/ar.23781

Wang, N., He, J., Pan, C., Wang, J., Ma, M., Shi, X., et al. (2019). Resveratrol Activates Autophagy via the AKT/mTOR Signaling Pathway to Improve Cognitive Dysfunction in Rats With Chronic Cerebral Hypoperfusion. *Front. Neurosci.* 13, 859. doi: 10.3389/fnins.2019.00859

Wang, W., Liu, T., Yang, L., Ma, Y., Dou, F., Shi, L., et al. (2019). Study on the multi-targets mechanism of triphala on cardio-cerebral vascular diseases based on network pharmacology. *BioMed. Pharmacother.* 116, 108994. doi: 10.1016/j.biopha.2019.108994

Wang, Y., Zhang, S., Li, F., Zhou, Y., Zhang, Y., Wang, Z., et al. (2020). Therapeutic target database 2020: enriched resource for facilitating research and early development of targeted therapeutics. *Nucleic Acids Res.* 48, D1031–D1041. doi: 10.1093/nar/gkz981

Wei, H., Zhu, X., and Li, Y. (2018). Application value of serum biomarkers for choosing memantine therapy for moderate AD. *J. Neurol.* 265, 1844–1849. doi: 10.1007/s00415-018-8926-4

Xu, H. Y., Zhang, Y. Q., Liu, Z. M., Chen, T., Lv, C. Y., Tang, S. H., et al. (2019). ETCM: an encyclopaedia of traditional Chinese medicine. *Nucleic Acids Res.* 47, D976–D982. doi: 10.1093/nar/gky987

Yang, X., Xu, S., Qian, Y., and Xiao, Q. (2017). Resveratrol regulates microglia M1/M2 polarization via PGC-1alpha in conditions of neuroinflammatory injury. *Brain Behav. Immun.* 64, 162–172. doi: 10.1016/j.bbi.2017.03.003

Zhang, J., Feng, X., Wu, J., Xu, H., Li, G., Zhu, D., et al. (2014). Neuroprotective effects of resveratrol on damages of mouse cortical neurons induced by beta-amyloid through activation of SIRT1/Akt1 pathway. *Biofactors* 40, 258–267. doi: 10.1002/biof.1149

Zhang, W., Bai, Y., Wang, Y., and Xiao, W. (2016). Polypharmacology in Drug Discovery: A Review from Systems Pharmacology Perspective. *Curr. Pharm. Des.* 22, 3171–3181. doi: 10.2174/1381612822666160224142812

Zhang, R., Zhu, X., Bai, H., and Ning, K. (2019). Network Pharmacology Databases for Traditional Chinese Medicine: Review and Assessment. *Front. Pharmacol.* 10, 123. doi: 10.3389/fphar.2019.00123

Zhang, Y., Li, Y., Wang, Y., Wang, G., Mao, L., Zhang, D., et al. (2019). Effects of resveratrol on learning and memory in rats with vascular dementia. *Mol. Med. Rep.* 20, 4587–4593. doi: 10.3892/mmr.2019.10723

Zhang, Y. F., Huang, Y., Ni, Y. H., and Xu, Z. M. (2019). Systematic elucidation of the mechanism of geraniol via network pharmacology. *Drug Des. Devel. Ther.* 13, 1069–1075. doi: 10.2147/DDDT.S189088

Zhou, W., Chen, Z., Wang, Y., Li, X., Lu, A., Sun, X., et al. (2019). Systems Pharmacology-Based Method to Assess the Mechanism of Action of Weight-Loss Herbal Intervention Therapy for Obesity. *Front. Pharmacol.* 10, 1165. doi: 10.3389/fphar.2019.01165

**Conflict of Interest:** The authors declare that the research was conducted in the absence of any commercial or financial relationships that could be construed as a potential conflict of interest.

frontiers in Pharmacology

ORIGINAL RESEARCH
published: 21 May 2020
doi: 10.3389/fphar.2020.00633

# A Novel Approach Based on Metabolomics Coupled With Intestinal Flora Analysis and Network Pharmacology to Explain the Mechanisms of Action of Bekhogainsam Decoction in the Improvement of Symptoms of Streptozotocin-Induced Diabetic Nephropathy in Mice

*Xianglong Meng*[1,2], *Junnan Ma*[1], *An Na Kang*[1], *Seok Yong Kang*[1,3], *Hyo Won Jung*[1,3]* *and Yong-Ki Park*[1,3]*

[1] Department of Herbology, College of Korean Medicine, Dongguk University, Gyeongju, South Korea, [2] Experimental Teaching Center, College of Chinese Materia Medica and Food Engineering, Shanxi University of Chinese Medicine, Jinzhong, China, [3] Korean Medicine R&D Center, Dongguk University, Gyeongju, South Korea

OPEN ACCESS

**Edited by:**
*Wei Zhou,*
*The Affiliated Hospital of Shenzhen University, China*

**Reviewed by:**
*Sol Cristians,*
*National Autonomous University of Mexico, Mexico*
*Hong Zheng,*
*Wenzhou Medical University, China*

***Correspondence:**
*Hyo Won Jung*
*tenzing2@hanmail.net*
*Yong-Ki Park*
*yongki@dongguk.ac.kr*

**Specialty section:**
*This article was submitted to Ethnopharmacology, a section of the journal Frontiers in Pharmacology*

**Received:** *28 October 2019*
**Accepted:** *21 April 2020*
**Published:** *21 May 2020*

**Citation:**
*Meng X, Ma J, Kang AN, Kang SY, Jung HW and Park Y-K (2020) A Novel Approach Based on Metabolomics Coupled With Intestinal Flora Analysis and Network Pharmacology to Explain the Mechanisms of Action of Bekhogainsam Decoction in the Improvement of Symptoms of Streptozotocin-Induced Diabetic Nephropathy in Mice. Front. Pharmacol. 11:633. doi: 10.3389/fphar.2020.00633*

Bekhogainsam decoction (BHID), a representative prescription for the treatment of diabetes mellitus (DM) and diabetic complications in both traditional Korean and Chinese medicine, was examined for its ability to ameliorate diabetic nephropathy (DN), and its mechanism of action was evaluated by metabolomics, gut microbiota, and network pharmacology. In this study, male specific pathogen-free C57BL/6 mice were intraperitoneally injected with streptozotocin (STZ, 100 mg/kg) once per day for 3 days consecutively, and were then orally administered BHID at 100 and 500 mg/kg, and metformin at 250 mg/kg once per day for 4 weeks. Our results showed that the administration of BHID to mice with STZ-induced DN prevented physiological and serological changes, structural damage, and kidney dysfunction. Based on a metabolomics test with serum, the profoundly altered metabolites in the BHID treatment group were identified. Thirty-six BHID-related proteins and four signaling pathways, including valine, leucine, and isoleucine biosynthesis, nicotinate and nicotinamide metabolism, tryptophan metabolism, and alanine, aspartate, and glutamate metabolism pathways, were explored. Principal coordinates analysis (PCoA) of the gut microbiota revealed that BHID treatment significantly affected the flora composition. In addition, the network pharmacology analysis revealed that BHID acted through phosphatidylinositol-3-kinase/protein kinase B (PI3K/Akt) and MAPK-related protein targets. Our findings on the anti-DN effects of BHID and its mechanism of

action, from the perspective of systems biology, have provided scientific evidence to support the clinical treatment of patients with diabetes, and implied that BHID has the potential to prevent the progression of DN.

**Keywords: Bekhogainsam decoction, diabetic nephropathy, metabolomics, gut microbiota, network pharmacology**

## INTRODUCTION

Diabetic nephropathy (DN), which is recognized as one of the most serious complications of type 2 diabetes mellitus (T2DM), is associated with proteinuria, hypertension, edema, and renal dysfunction and failure (Alicic et al., 2017). DN more commonly occurs in patients who have had T2DM for more than 10 years. However, its pathophysiology has not been fully elucidated because of the complexity of DN pathogenesis.

In traditional Korean medicine (TKM) and traditional Chinese medicine (TCM) theories, "wasting-thirst" (termed Sogal syndrome in TKM and Xiaoke syndrome in TCM) probably equate to the term "T2DM" in Western medicine (Xu et al., 2016). This syndrome refers to a Yin-deficient condition that causes heat in the body to increase, resulting in symptoms such as polydipsia, polyphagia, and polyuria as the disease progresses. The most serious condition of wasting-thirst syndrome is DN, which involves kidney problems and excessive urination.

Bekhogainsam decoction (BHID), created by Chang Chung-Ching in the Treatise on Febrile Disease (Shang Han Lun) is composed of Gypsum fibrosum (a mineral containing $CaSO_4 \bullet 2 H_2O$), Anemarrhenae rhizome (the rhizome of *Anemarrhena asphodeloides* Bge.), Ginseng radix et rhizome (the root and rhizome of *Panax ginseng* C. A. Mey.), and Glycyrrhizae radix et rhizome (the root and rhizome of *Glycyrrhiza uralensis* Fisch. ex DC.) and Polished round-grained rice (the endosperm of *Oryza sativa* L. seeds) and is known to impact the lung and stomach through a unique effect of clearing heat and promoting fluid movement (Tong et al., 2012). The monarch, minister, assistant, and messenger medicines in TKM or TCM prescriptions reflect the overall concept of traditional medicine (TM). The effective action of TCM prescription is mediated through the whole function of the compatibility of medicines. In this prescription, Gypsum fibrosum is the monarch medicine, which is pungent and cold and relieves the heat of Qi. As a minister medicine, Anemarrhenae rhizoma is bitter, cold, smooth, and good at purging fire and nourishing Yin. The combination of the two components can exert a very strong effect on reducing heat, nourishing Yin, and moistening dryness. Ginseng radix et rhizoma is an assistant medicine that can nourish Qi and Yin. Glycyrrhizae radix et rhizoma and polished round-grained rice can be used as messenger medicines to replenish Qi, and to relieve fire without hurting the spleen and stomach. Given the compatibility of these medicines, BHID has strong clearing effects on heat, relieves fidgetiness, and nourishes Qi generative fluid. BHID is also a commonly used prescription to treat patients with T2DM in traditional clinics. Despite the fact that BHID is a representative prescription for diabetes, little is known about its effects on diabetic complications, especially DN, or the underlying mechanisms of action.

Metabolomics is the qualitative and quantitative analysis of metabolites with a molecular mass below 1,000 in the *in vivo* study using high-throughput instruments (Beger et al., 2016). It can be used to identify specific molecular markers in certain physiological and pathological conditions, and can be used to study the pathogenesis of metabolic diseases and the mechanism of action of therapeutic drugs (Barnes et al., 2016). With regard to the pathogenesis of T2DM treated with TM theories based on metabolomics (Cui et al., 2018; Lin et al., 2019), some studies have been reported that act as good examples for the present study.

Intestinal flora is the most stable of the colonizing microorganisms in the human body. With the continuous development of DNA sequencing, metabolomics, proteomics, and computer technology, research on microbial flora has expanded, and the mystery of microbial flora has gradually been uncovered (Zhang B. et al., 2019). Recent studies have found that intestinal flora can significantly regulate the secretion of insulin, glucagon, and other hormones, and play an important role in the development of insulin resistance (Hanning and Diaz-Sanchez, 2015; Horie et al., 2017; Barko et al., 2018).

Network pharmacology is a new subject based on the theory of systems biology (Yuan et al., 2017). Specific signal nodes are selected for multi-target drug molecular design through network analysis of biological systems. Network pharmacology emphasizes the regulation of multiple pathways of signal pathways to improve the therapeutic effect of drugs and reduce the toxic and side effects, conferring improvements in the success rate of clinical trials of new drugs and reduce the drug development costs. Owing to the complexity of traditional medicine prescriptions, the pharmacological mechanisms of the anti-DM or anti-DN actions are difficult to clarify. In accordance with the modern pharmacodynamic mechanism of TM, the current "one target and one drug" mode can be transferred to a new "network target and multicomponent" mode based on network pharmacology (Zhang et al., 2019). Network pharmacology is also one of the new methods and focus points of TM modern research, and provides an abundance of information about single herbs or the prescriptions of potential bioactive components and the active mechanisms at the molecular and systematic level.

Therefore, in the present study, we investigated the effects of BHID in mice with streptozotocin (STZ)-induced DN, along with the underlying mechanism; in particular, we focused on renal dysfunction through the assessment of metabolomics, gut microbiota, and network pharmacology based on the perspective of systems biology, to reveal the modern scientific interpretation of BHID in the treatment of DM and DN.

# MATERIAL AND METHODS

## Preparation of the BHID Extract and Quality Control

The characteristics of constituent drugs in BHID, based on traditional prescription theory, were presented in **Table 1**. All constituent drugs in BHID in **Table 1** were purchased from Medicinal Materials Company (Kwangmyungdang Medicinal Herbs, Ulsan, Korea). These species were authenticated by Prof. Xiangping Pei (Shanxi College of Traditional Chinese Medicine) before use. Voucher specimens (no. SXTCM-Meng-2019001 for Gypsum fibrosum; no. SXTCM-Meng-2019002 for Anemarrhenae rhizoma; SXTCM-Meng-2019003 for Ginseng radix et rhizoma; SXTCM-Meng-2019004 for Glycyrrhizae radix et rhizoma; SXTCM-Meng-2019005 for polished round-grained rice) were deposited in the Herbarium of Shanxi College of Traditional Chinese Medicine (SXTCM), Taiyuan, China. All drugs were mixed (total 190.52 g in **Table 1**), ground, and extracted with 1.9052 L of boiling water for 3 h. The extract was then filtered through Whatman No. 1 filter paper (GE Healthcare UK Limited, UK), concentrated under a vacuum rotary evaporator, and lyophilized in a freeze-dryer (II Shin BioBase Co., Yangju, Korea). The BHID extract (yield = 33.99%) was stored at 4°C until use; it was then dissolved in distilled water for use.

In view of the different chemical structures that yield different pharmacodynamic effects, we performed quality control analysis of the BHID extract by using high-performance liquid chromatography (HPLC) under three different chromatographic conditions. The mobile phase for mangiferin and neo-mangiferin consisted of acetonitrile (A) and deionized water with 0.1% phosphoric acid (B). The gradient elution program was as follows: 3% A, 0–10 min; 15% A, 10–25 min. The detection wavelength was set at 258 nm. The mobile phase for liquiritin and ammonium glycyrrhetate consisted of acetonitrile (A) and deionized water with 0.1% phosphoric acid (B). The gradient elution program was as follows: 19% A, 0–8 min; 19%–50% A from 8–35 min; 50%–100% A from 35–36 min; then 100%–19% A from 36–40 min. The detection wavelength was set at 237 nm. The mobile phase for ginsenoside-Rg1 consisted of acetonitrile (A) and deionized water with 0.1% phosphoric acid (B), and the isocratic elution program was as follows: 25% A at 0–25 min. The detection wavelength was set at 218 nm. All HPLC analyses were performed with a U3000 series system (Thermo Fisher Scientific, Waltham, MA, USA) and samples were separated on a Tnature C18 column (250 × 4.6 mm, 5 μm, Waters, Milford, MA, USA). The HPLC pattern of components in BHID water extract has been reported elsewhere (Ding et al., 2007; Ablat et al., 2015; Song et al., 2015). The flow rate was 1.0 ml/min, the injection volume was 10 μl, and the column temperature was maintained at 30°C. Liquiritin, ammonium glycyrrhetate, mangiferin, neo-mangiferin, and ginsenoside-Rg1 standards (production batch numbers 18060604, 18083102, 18051002, 18041112, and 18071601, respectively) were purchased from Chengdu Pufei De Biotech Co., Ltd. (Chengdu, Sichuan, China). The mass fractions of all standard reagents were ≥ 98%.

## Animals and Preparation of Diabetic Animal Model

Five-week-old male specific pathogen-free (SPF) C57BL/6 mice (body weight 18–19 g) were purchased from Orient Bio Inc. (Seongnam, Korea). The mice were permitted a 1-week acclimation period to the SPF laboratory conditions (IVC systems, LAB & BIO, Changwon, Korea) before the experiments were started. The mice were kept under a 12 h/12 h light/dark cycle, at 23°C±2°C, with 50%±10% humidity, and were administered sterile filtered water, and used corn cobs as bedding. All animals were handled in accordance with the animal welfare guidelines issued by the Korean National Institute of Health and the Korean Academy of Medical Sciences for the care and use of laboratory animals and approved by the Institutional Animal Care and Use Committee of Dongguk University (IACUC-2017-012).

After adaptive breeding, all mice were randomly divided into five groups ($n$=7 per group): the normal group; the STZ-induced diabetic control group; the low-dose BHID treatment group, the high-dose BHID treatment group, and the metformin-treated group. With the exception of the mice in the normal group, DN was induced in all mice by STZ intraperitoneal injections at 100 mg/kg of body weight (b.w.) (Sigma-Aldrich, St. Louis, MO, USA) once per day for 3 days consecutively (Glastras et al., 2016). Animals with

**TABLE 1** | Composition of Bekhogainsam decoction (BHID) and the characteristics of each constituent drugs.

| Drug name/ English name | Scientific name (Family) | Medicinal part | Weight (g) in BHID | Channel tropism | Medicinal efficacies | Role in the prescription |
|---|---|---|---|---|---|---|
| Gypsum fibrosum | – | Gypsum (mineral) | 75 | lung, stomach | Clear heat, purge fire, relieve agitation, stop thirst, heal wounds, and promote tissue regeneration | Monarch |
| Anemarrhenae rhizoma | *Anemarrhena asphodeloides* Bge. | Rhizome | 30 | lung, stomach, kidney | Clear heat and purge fire, generate fluids, and moisten dryness | Minister |
| Ginseng radix et rhizoma. | *Panax ginseng* C. A. Mey. | Root, Rhizome | 15 | lung, spleen, heart | Replenish the primordial qi, tonify spleen and lung, promote fluid production, and induce tranquilization | Assistant |
| Glycyrrhizae radix et rhizoma | *Glycyrrhiza uralensis* Fisch. ex DC. | Root, Rhizome | 10.52 | heart, lung, spleen, stomach | Tonify spleen and replenish qi, dispel phlegm and arrest cough, relieve spasm and pain, clear heart and relieve toxicity, harmonize all medicines | Messenger |
| Polished round-grained rice | *Oryza sativa* L | Endosperm of seeds | 60 | spleen, stomach, lung | Invigorate qi and strengthen the spleen, relieve polydipsia | Messenger |

blood glucose concentrations of >300 mg/dl were used for the study. Mice in the low- and high-dose BHID treatment groups were administered 100 and 500 mg/kg b.w. BHID (peroral injection, p.o.), and mice in the metformin-administered group were treated with 250 mg/kg metformin (p.o.). The mice in the normal and STZ-induced diabetic control groups were treated with an equal volume of saline at the same time. All drugs were administered orally once per day for 4 weeks. All mice were administered a sterile standard diet (3.1 kcal, 14% protein, Harlan Teklad, Madison, WI, USA) for the entire experimental period. After a 4-week administration period, all mice were fasted for 12 h and then sacrificed. Samples of the blood, feces, and kidneys were harvested for further analysis on a clean bench. Subsequently, the intestinal feces were collected under sterile conditions, and then placed into sterile tubes and stored in liquid nitrogen.

## Measurement of Physiological Characteristics

Changes in physiological parameters, such as body weight, water, food intake, and fasting blood glucose (FBG) levels, were measured once per week for 4 weeks. In addition, blood samples were collected by cutting the tip of the tails, and 24 h urine volumes were collected in the metabolic cages from all mice at the end of the experimental period.

## Measurement of Serological and Urine Markers

A commercial ELISA kit (Crystal Chem, Springfield, IL, USA) was used to measure the insulin concentration in the serum in accordance with the manufacturer's protocol. The levels of aspartate aminotransferase (AST), alanine aminotransferase (ALT), glucose, total cholesterol (TC), triglyceride (TG), HDL-cholesterol (HDL-C), urea nitrogen (UN), creatinine (Cr), and microalbumin/urine creatine (MA/UCREA) were measured in the serum or urine samples by using an automatic biochemistry analyzer (Fuji Dri-chem 700i, Fujifilm, Tokyo, Japan).

## Histopathological Observation

The kidney tissues were fixed in 4% paraformaldehyde in 0.1 M PBS, embedded in paraffin, and cut into 5-mm sections. To observe structural damage to renal tissue, sections were stained with hematoxylin and eosin (H&E), periodic acid-Schiff (PAS), and Masson's trichrome (M-T). The sections were visualized using light microscopy, and digital images were captured and analyzed.

## Metabolomic Profiling

Serum samples were thawed at 4°C on ice. Then, 100 μl of sample was taken and placed in an EP tube, extracted with 400 μl of extraction solvent (methanol: acetonitrile = 1:1 [v/v], containing an internal standard, L-2 chlorophenylalanine at 2 μg/ml), vortexed for 30 s, treated with ultrasound for 5 min (during incubation in ice water), and incubated for 1 h at -20°C to precipitate proteins. The solutions were then centrifuged at 12,000 rpm for 15 min at 4°C. The supernatant was transferred into fresh EP tubes, and the extracts were dried in a vacuum concentrator without heating, and reconstituted in 200 μl of the extraction solvent (acetonitrile: water = 1:1 [v/v]). The reconstituted solution was vortexed for 30 s and sonicated for 10 min (in a 4°C water bath), centrifuged for 15 min at 12,000 rpm at 4°C. The supernatant was transferred into a fresh 2 ml LC-MS glass vial, 10 μl aliquots from each sample were collected and pooled as QC samples, and the supernatant was collected for UHPLC-QTOF-MS analysis.

LC-MS/MS analyses were performed using a UHPLC system (Thermo Fisher Scientific, Waltham, MA, USA) with a Thermo C18 column (1.9 μm; 2.1 × 50 mm). The mobile phase consisted of acetonitrile (A) and deionized water with 0.1% methanoic acid (B), and the following elution gradient was used: 0–1 min, 5%–5% A; 1–5 min, 5%–15% A; 5–7 min, 15%–15% A; 7–14 min, 15%–100% A; 14–19 min, 100%–100% A; 19–20 min, 100%–5% A; 20–22 min, 5%–5% A. The mobile phase was delivered at 0.3 ml $min^{-1}$, and the injection volume was 3 μl.

The Triple TOF mass spectrometer was used for its ability to acquire MS/MS spectra on a full MS dd-ms2 during the LC-MS experiment. In this mode, the electrospray capillary voltage was 3.2 kV in positive and negative ionization mode, the atomized gas velocity was 35 $L{\cdot}min^{-1}$, the auxiliary air velocity was 5 $L{\cdot}min^{-1}$, the ion source temperature was 320°C, and the auxiliary heater temperature was 350°C. The NCE values of energy collision were 25, 35, and 45, respectively.

The LC/Q/TOF-MS metabolomic profiling data were imported into Compound Discoverer 3.0 to perform the metabolic feature extraction by the adoption of a molecular feature extraction algorithm (Thermo Fisher, Inc., Santa Clara, CA, USA). The parameters were set as follows: mass range, 100–1,500; mass deviation, $5{\times}10^{-6}$; retention time deviation, 0.05 min; SNR threshold, 3. SIMCA-P (Version 14.1, Umetrics AB, Umea, Sweden) was used for multivariate statistical analysis of the integral values obtained from LC-MS findings. The mean centered data were used for principle component analysis (PCA). The modeling of sample classes was performed using orthogonal projection to latent structure-discriminant analysis (OPLS-DA) algorithm at a unit variance-scaled modality. After the OPLS-DA test, only the integral, with variable importance in the projection (VIP) values of >1.5 and a p-value of <0.05 from Student's *t*-test, was considered to be the potential differential metabolite. The disturbed metabolites and metabolic pathways were identified by open database sources, including the Human Metabolome Database[1], KEGG[2], and MetaboAnalyst[3]. Heat maps were constructed using Pyplot[4](Version 2.0.2).

## Gut Microbiota Analysis

Mouse fecal samples were randomly selected from each group and thawed at 4°C on ice. The total microbial DNA was extracted by using a commercial DNA kit (OmegaBio-tek, Norcross, GA, USA) in accordance with the manufacturer's protocol. The primers were obtained according to the conservative region design, and the end of the primers was amended with a sequencing connector to amplify the bacterial V3–V4 region of

[1] http://www.hmdb.ca/
[2] http://www.genome.jp/kegg/
[3] http://www.metaboanalyst.ca/faces/home.xhtml
[4] http://matplotlib.org/index.html

the 16S rRNA gene. Polymerase chain reaction (PCR) amplification was conducted, and the PCR products were extracted from 1% agarose gel, and purified using the AxyPrep DNA Gel Extraction Kit (Axygen Biosciences, Union City, CA, USA) in accordance with the manufacturer's instructions and quantified using a Quantus™ fluorometer (Promega, Madison, WI, USA). The purified amplicons were sequenced using an Illumina HiSeq 2500 (Illumina, San Diego, CA, USA) in accordance with the manufacturer's guidelines. Alpha diversity analysis, operational taxonomic units (OTUs) clustering analysis, and beta diversity analysis were conducted successively.

## Network Pharmacology Profiling

Chemical ingredients and the targets of BHID were obtained from the Traditional Chinese Medicine Systems Pharmacology database[5] (TCMSP), a Bioinformatics Analysis Tool for Molecular mechANism of Traditional Chinese Medicine[6] (BATMAN-TCM), and the relevant literature.

In consideration of the complexity of the changes in pharmacodynamic chemical components in the formula, the compounds were screened for both the pharmacokinetic and pharmacodynamic properties (oral bioavailability (OB) >30% and drug-likeness (DL) >0.18). The related targets of DN were collected from Genecards[7] and the Online Mendelian Inheritance in Man (OMIM) database[8], respectively. Venn diagram analysis was used for a comprehensive analysis of BHID, directly related genes, and targets of DN. A comprehensive, integrated analysis of BHID, directly related genes, and DN targets was performed using a Venn analysis. The overlap was presumed to be the group of potential targets, and these were used in the network pharmacology analysis. An interaction network was established among active ingredients, putative targets, and the DN-associated targets of BHID. The interaction network was visualized using Cytoscape 3.7.1 software[9]. STRING 11.0[10] was chosen to establish the protein-protein interaction network (PPI network). The Database for Annotation, Visualization, and Integrated Discovery[11] was used to perform Gene Ontology (GO) function enrichment analysis, and the Kyoto Encyclopedia of Genes and Genomes (KEGG)[2] Pathway Database was used for pathway enrichment analysis of BHID.

## Quantitative PCR Assay

Total RNA was isolated by using NucleoZOL reagent (MACHEREY-NAGEL GmbH & Co.KG., Duren, Germany) in accordance with the manufacturer's instructions. RNA concentration was measured using a spectrophotometer (NanoDrop Technologies, Inc., Wilmington, DE, USA). cDNA was generated with 1 μg of total RNA using a Reverse Transcription System kit (Promega, Fitchburg, WI, USA). PCR was performed using a SYBR Green kit (Agilent Technologies, West Cedar Creek, TX, USA) and primers specific to the target genes, namely: PKC-α: 5′-CCCATTCCAGAAGGAGATGA-3′ (forward, accession no. NM_011101.3) and 5′-TTCCTG TCAGCAAGCATCAC-3′ (reverse, accession no. NM_011101.3); α-SMA: 5′-ACTGCCGAGCGTGAGATTGT-3′ (forward, accession no. XM_006526606.2) and 5′-TGATGCT GTTATAGGTGGTTTCG-3′ (reverse, accession no. XM_0065 26606.2); TGF-β1: 5′-CGAAGCGGACTACTATGCTAAAGAG-3′ (forward, accession no. NM_011577.2) and 5′-TGGTTTTCTCATAGATGGCGTTG-3′ (reverse, accession no. NM_011577.2); GAPDH: 5′-CAGCCTCGTCCCGTAGACA-3′ (forward, accession no. XM_017321385.1) and 5′-CGCTCCTGGAAGATGGTGAT-3′ (reverse, accession no. XM_017321385.1). Gene expression was evaluated by the ΔΔCT method with GAPDH as a housekeeping gene.

## Western Blotting Analysis

Kidney tissues were isolated by using T-PER tissue protein extraction reagent (Thermo Fisher Scientific, Waltham, MA, USA). The protein content was measured using a Bradford assay, separated using SDS-PAGE and transferred to a nitrocellulose membrane. The membranes were incubated in 5% skimmed milk, dissolved in Tris-buffered saline with 1% Tween-20 (TBST), pH 7.5, for 30 min at RT for blocking, and then incubated with anti-PKCα, I-κB, NF-κB (p 65), α-SMA, TGF-β1, COX-2 (Santa Cruz Biotechnology, Santa Cruz, Dallas, TX, USA), iNOS (BD Biosciences, San Jose, CA, USA), total-AKT (Ser473), phospho-AKT (Ser473), total-IRS (Ser 307), phospho-IRS (Ser 307), PI3K (p85) (Cell Signaling Technology, Danvers, MA, USA), and β-actin (Sigma-Aldrich, Inc., St. Louis, MO, USA) antibodies at 1:1,000 overnight at 4°C and incubated with HRP-conjugated mouse or rabbit secondary antibodies for 3 h at RT. Blots were scanned and analysed with ChemiDoc™ MP imaging system.

## Statistical Analysis

Data analyses were conducted using GraphPad Instat software (ver. 5.0; GraphPad Software, La Jolla, CA, USA). The data were expressed as the mean ± standard deviation (SD) of seven mice in each group. The significance of treatment effects was determined by one-way analysis of variance (ANOVA) followed by Tukey's post-hoc analysis. The p-value of 0.05 was considered to indicate statistical significance.

# RESULTS

## HPLC Profiles of BHID

As shown in **Figure 1**, the HPLC profiles of BHID contained peaks reflecting the main compounds: mangiferin and neo-mangiferin in Anemarrhenae rhizome; liquiritin and ammonium glycyrrhetate in Glycyrrhizae radix et rhizome; and ginsenoside-Rg1 in Ginseng radix et rhizoma. The equations of the calibration curves for these reference compounds were Y=131.48X–0.0552 (r=0.9992) for liquiritin, Y=43.268X+0.3934

[5] http://lsp.nwu.edu.cn/tcmsp.php/
[6] http://bionet.ncpsb.org/batman-tcm/
[7] http://www.genecards.org/
[8] http://www.omim.org/
[9] https://cytoscape.org/
[10] https://string-db.org/cgi/input.pl/
[11] https://david.ncifcrf.gov/

(r=0.9991) for ammonium glycyrrhetate, Y=643.55X+0.0189 (r=0.9998) for mangiferin, Y=351.79X+2.4417 (r=0.9991) for neo-mangiferin, and Y=4.4811X+0.0258 (r=0.9999) for ginsenoside-Rg1; the content determination of the five compounds in BHID are shown in **Table 2**.

## Effects of BHID on Physiological and Serological Changes in Diabetic Nephropathy Mice

Over 4 weeks, the administration of BHID at low (100 mg/kg) and high (500 mg/kg) doses significantly reduced the increase in food intake ($p$<0.0001 and $p$<0.001, respectively) and water ($p$<0.0001, respectively) intake compared with the DN control group (**Table 3**). Moreover, the administration of BHID significantly increased body weight in weeks 3 ($p$<0.01 for low-dose treatment and $p$<0.05 for high-dose treatment, respectively) and 4 ($p$<0.05 for low-dose) compared with the DN control group (**Table 3**). In addition, low doses of BHID significantly increased the ratio of the kidney to the body weight compared with the DN control group ($p$<0.05) after administration for 4 weeks (**Figure 2A**). The administration of high doses of BHID and metformin also resulted in the same trend, but without significant differences.

As shown in **Table 3**, an increase in FBG levels in the DN control group ($p$<0.0001 throughout the experimental period) was significantly reduced by BHID administration ($p$<0.0001 for low-dose treatment and $p$<0.001 for high-dose treatment in week 3) and metformin ($p$<0.0001 in week 4). As shown in **Figure 2B**, BHID also reduced the elevated levels of serum glucose at both low ($p$<0.001) and high ($p$<0.01) doses. Moreover, the BHID treatment groups showed a greater glucose lowering effect than 250 mg/kg metformin. As shown in **Figure 2C**, BHID administration induced significant increases in serum insulin levels at low ($p$<0.01) and high ($p$<0.001) doses compared with the control group (**Figure 2C**). Metformin also significantly decreased insulin levels ($p$<0.001). The levels of triglyceride (TG, **Figure 2D**) and total cholesterol (TC, **Figure 2E**) were not significantly changed by the administration of BHID, whereas the levels of HDL-cholesterol (HDL-C, **Figure 2F**) were significantly higher in the low-dose BHID treatment group. In addition, the serum levels of AST (**Figure 2G**) and ALT (**Figure 2H**) were increased significantly ($p$<0.05 for AST and $p$<0.01 for ALT) in the control group compared with the normal group, and these increases were reduced significantly by BHID administration in both the low-dose ($p$<0.05 for AST and $p$<0.05 for ALT) and high-dose ($p$<0.05 for AST and $p$<0.05 for ALT) treatment group compared with the control group. Metformin induced a significant reduction in ALT levels ($p$<0.05).

## Effects of BHID on Kidney Dysfunction in Mice With DN

As shown in **Figure 3A**, a significant increase in MA/UCREA was observed in the DN control group compared with the normal group. The administration of BHID ($p$<0.001 for high dose) or metformin ($p$<0.0001) for 4 weeks significantly decreased MA/UCREA levels relative to the control group. In addition, the BHID-treated groups showed significant decreases in urea nitrogen (**Figure 3B**) and creatinine (**Figure 3C**) levels with low-dose ($p$<0.0001) and high-dose ($p$<0.0001 for urea nitrogen and $p$<0.001 for creatinine, respectively) treatment, respectively. Metformin also led to significant decreases in urea nitrogen ($p$<0.0001) and creatinine ($p$<0.0001). BHID and metformin also significantly reduced the increasing levels ($p$<0.01 for low-dose BHID and $p$<0.001 for metformin treatment) of urea nitrogen (**Figure 3D**) and creatinine ($p$<0.01 for low-dose BHID treatment, **Figure 3E**) in the sera of mice with DN. Finally, a significant decrease in 24 h urine volume ($p$<0.05) was observed in the group administered low-dose BHID (**Figure 3F**).

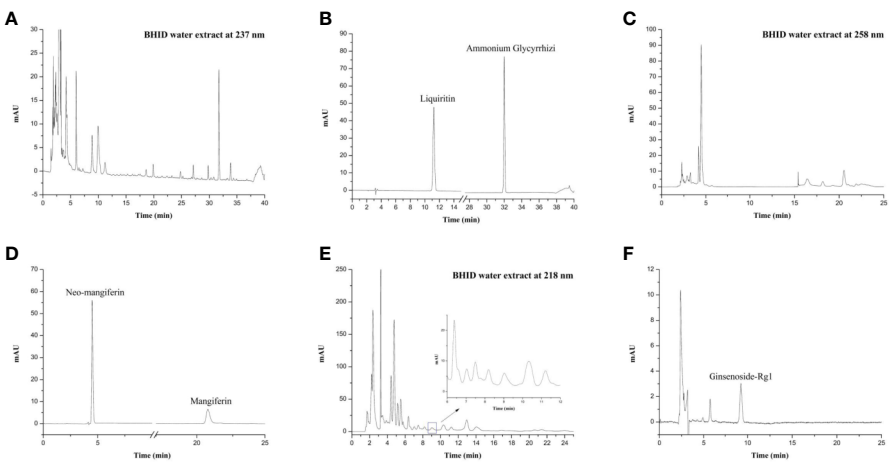


**FIGURE 1 |** High-performance liquid chromatography (HPLC) profiles of Bekhogainsam decoction (BHID). HPLC patterns of the BHID extract at 237 nm **(A)**, 258 nm **(B)**, and 218 nm **(E)**, and the standard compounds, liquiritin, ammonium glycyrrhetate, mangiferin, neo-mangiferin, and ginsenoside-Rg1 at 237 nm **(B)**, 258 nm **(D)**, and 218 nm **(F)**.

**TABLE 2 |** Quantification of Bekhogainsam decoction (BHID) by high-performance liquid chromatography (HPLC) analysis.

| Component name | Ratio (mg/g) |
|---|---|
| Liquiritin | $0.123±6.54×10^{-4}$ |
| Ammonium glycyrrhetate | $1.14±7.88×10^{-3}$ |
| Mangiferin | $0.186±4.07×10^{-3}$ |
| Neo-mangiferin | $1.103±1.09×10^{-2}$ |
| Ginsenoside-Rg1 | $0.110±2.16×10^{-2}$ |

## Effects of BHID on Histopathologic Changes in the Kidney Tissue of Mice With DN

The effects of BHID on histopathological changes in the kidney of mice with DN are shown in **Figure 4**. The kidney tissues were stained with H&E, PAS, and M-T. Hematoxylin and eosin staining revealed well-opened glomerular capillary loops in the normal group. In the DN control group, morphological changes,

**TABLE 3 |** Food intake, water intake, body weight, and fasting blood glucose (FBG) parameters of mice with streptozotocin (STZ)–induced diabetic nephropathy (DN) treated with Bekhogainsam decoction (BHID).

| | Weeks | Normal | Control | BHID-100 | BHID-500 | Met-250 |
|---|---|---|---|---|---|---|
| Food intake (g) | 1 | 18.43±0.73 | $74.43±2.87^{a****}$ | 71.14±0.64 | 71.14±0.83 | 72.29±1.39 |
| | 2 | 30.57±1.59 | $68.29±1.28^{a****}$ | $47.40±7.23^{b****}$ | $49.25±11.50^{b****}$ | $44.86±12.02^{b****}$ |
| | 3 | 26.29±1.39 | $74.14±3.94^{a****}$ | $54.00±3.35^{b****}$ | $57.00±12.53^{b***}$ | $60.86±2.29^{b***}$ |
| | 4 | 18.71±2.37 | $63.50±2.69^{a****}$ | $43.00±1.41^{b****}$ | $43.50±13.16^{b****}$ | $49.83±2.73^{b**}$ |
| Water intake (ml) | 1 | 29.43±0.90 | $289.29±11.16^{a****}$ | $238.29±4.37^{b**}$ | $172.83±45.88^{b****}$ | $194.29±5.60^{b****}$ |
| | 2 | 29.71±2.76 | $288.57±11.25^{a****}$ | $162.00±35.44^{b****}$ | $150.00±46.90^{b****}$ | $200.00±15.12^{b****}$ |
| | 3 | 31.86±2.80 | $261.43±22.95^{a****}$ | $157.00±24.00^{b****}$ | $180.00±50.87^{b****}$ | $215.00±21.88^{b**}$ |
| | 4 | 31.14±2.53 | $261.67±36.70^{a****}$ | $170.00±10.80^{b****}$ | $141.25±50.05^{b****}$ | 236.67±4.71 |
| Bodyweight (g) | 1 | 17.86±1.36 | $17.86±1.96^{a****}$ | 17.43±1.99 | 16.40±2.58 | 17.14±1.46 |
| | 2 | 25.29±1.75 | $18.86±1.81^{a****}$ | 18.60±3.20 | 19.00±1.22 | 18.14±1.73 |
| | 3 | 24.86±1.36 | $14.80±1.17^{a****}$ | $19.00±3.16^{b*}$ | $19.75±1.92^{b**}$ | $19.00±1.77^{b*}$ |
| | 4 | 24.57±0.73 | $15.75±1.09^{a****}$ | $20.33±2.36^{b*}$ | 20.00±1.63 | 19.20±1.94 |
| FBG (mg/dl) | 1 | 151.29±6.30 | $490.29±12.43^{a****}$ | 476.29±46.96 | 470.17±17.53 | 493.00±10.05 |
| | 2 | 160.71±7.59 | $507.43±18.39^{a****}$ | 444.00±81.39 | 449.00±26.42 | 508.33±25.85 |
| | 3 | 141.57±17.88 | $420.86±83.13^{a****}$ | $189.50±90.50^{b****}$ | $242.33±68.39^{b***}$ | 478.43±49.47 |
| | 4 | 152.25±21.60 | $574.67±36.39^{a****}$ | 472.00±21.31 | 478.00±128.08 | $407.20±88.82^{b****}$ |

*Normal, normal group; Control, STZ-induced DN control group; BHID-100, BHID 100 mg/kg treatment group; BHID-500, BHID 500 mg/kg treatment group; and Met-250, Metformin 250 mg/kg treatment group. Data are expressed as the mean ± S.D. (n=7 per group); *P < 0.05, **P < 0.01, and ***P < 0.001, ****P < 0.0001 vs. normal (a) or control (b) groups.*

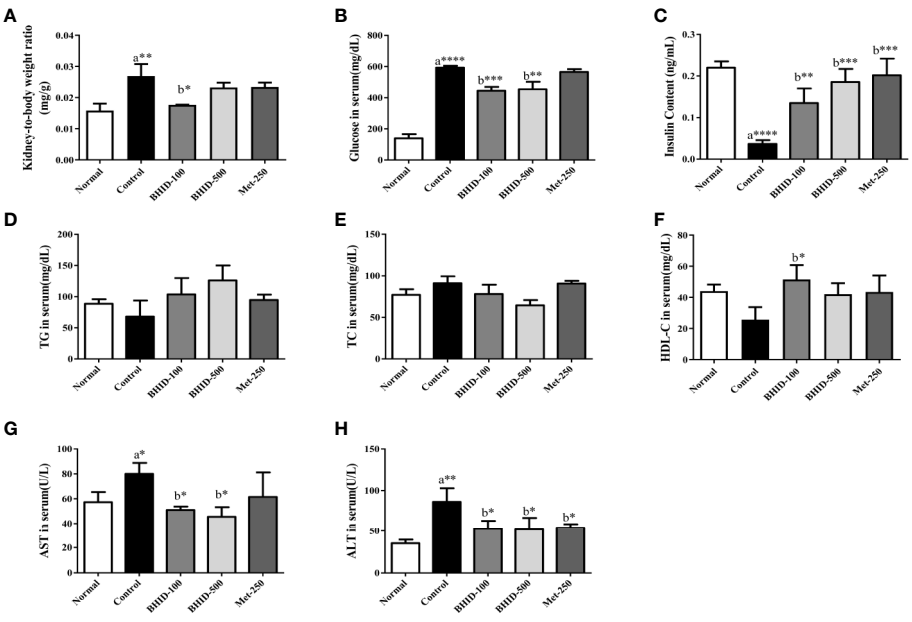


**FIGURE 2 |** Effects of Bekhogainsam decoction (BHID) on physiological and serological changes in mice with diabetic nephropathy (DN). Kidney to body weight ratio **(A)** and serum levels of glucose **(B)**, insulin **(C)**, triglyceride (TG) **(D)**, total cholesterol (TC) **(E)**, HDL-cholesterol (HDL-C) **(F)**, aspartate aminotransferase (AST) **(G)**, and alanine aminotransferase (ALT) **(H)**. Normal, normal group; Control, streptozotocin (STZ)–induced DN control group; BHID-100, BHID 100 mg/kg treatment group; BHID-500, BHID 500 mg/kg treatment group; and Met-250, Metformin 250 mg/kg treatment group. Data are expressed as the mean ± standard deviation (SD) (*n*=7 per group); *P < 0.05, **P < 0.01, and ***P < 0.001 , ****P < 0.0001 vs. normal (a) or control (b) groups.

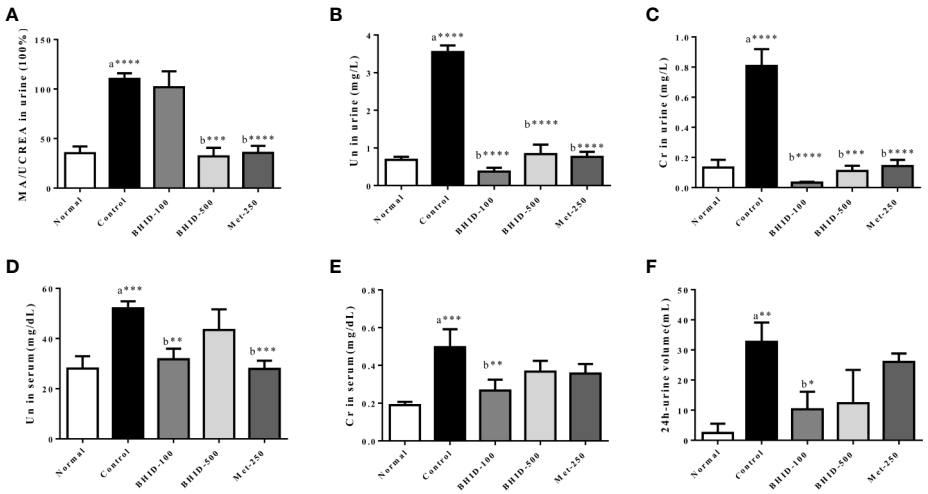


**FIGURE 3 |** Effects of Bekhogainsam decoction (BHID) on kidney dysfunction in mice with diabetic nephropathy (DN). The urine levels of microalbumin/urine creatine (MA/UCREA) **(A)**, urea nitrogen (UN) **(B)**, createnine (Cr) **(C)**, and UN **(D)**, serum levels of Cr **(E)**, and urine volumes for 24 h at week 4 **(F)**. Normal, normal group; Control, streptozotocin (STZ)–induced DN control group; BHID-100, BHID 100 mg/kg treatment group; BHID-500, BHID 500 mg/kg treatment group; and Met-250, Metformin 250 mg/kg treatment group. The data are expressed as the mean ± standard deviation (*n*=7 per group). *P < 0.05, **P < 0.01, and ***P < 0.001, ****P < 0.0001 vs. normal (a) or control (b) group.

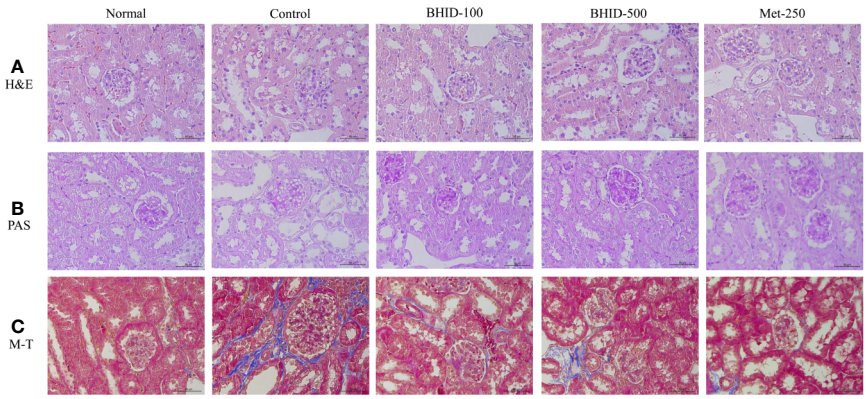


**FIGURE 4 |** Effects of Bekhogainsam decoction (BHID) on histological changes in kidney tissues in mice with diabetic nephropathy (DN). Tissue staining with hematoxylin and eosin (H&E) **(A)**, periodic acid-Schiff (PAS) **(B)**, and Masson's trichrome (M-T) **(C)**. Normal, normal group; Control, streptozotocin (STZ)–induced DN control group; BHID-100, BHID 100 mg/kg treatment group; BHID-500, BHID 500 mg/kg treatment group; and Met-250, Metformin 250 mg/kg treatment group. All tissues were observed using a light microscope; representative images are shown (×400).

including mesangial hyperplasia, irregular distortions, and glomerular basement membrane thickening, were observed. However, histological changes in glomerular and tubular structures were, to some extent, prevented in both the BHID-treatment groups and the metformin treatment group. PAS clearly revealed increased thickness of the glomerular basement membrane (GBM), hypertrophy, and mesangial matrix expansion in the control group. M-T staining also revealed an increased intensity of fibrosis in response to accumulation of extracellular matrix proteins in the control group. However, all destructive changes in mice with DN were ameliorated markedly by administration of both the low and high doses of BHID and metformin.

## Effects of BHID on the Expression of Fibrosis Regulators in Renal Tissues of Diabetic Nephropathy Mice

To investigate the effects of BHID on renal fibrosis in DN, we measured the mRNA and protein expression of renal fibrosis regulators (PKCα, TGF-β1, and α-SMA) by qPCR and western blotting (**Figure 5A**), respectively. The expression of PKC-α (**Figures 5B, E**) and TGF-β1 (**Figures 5C, F**) in kidney tissues

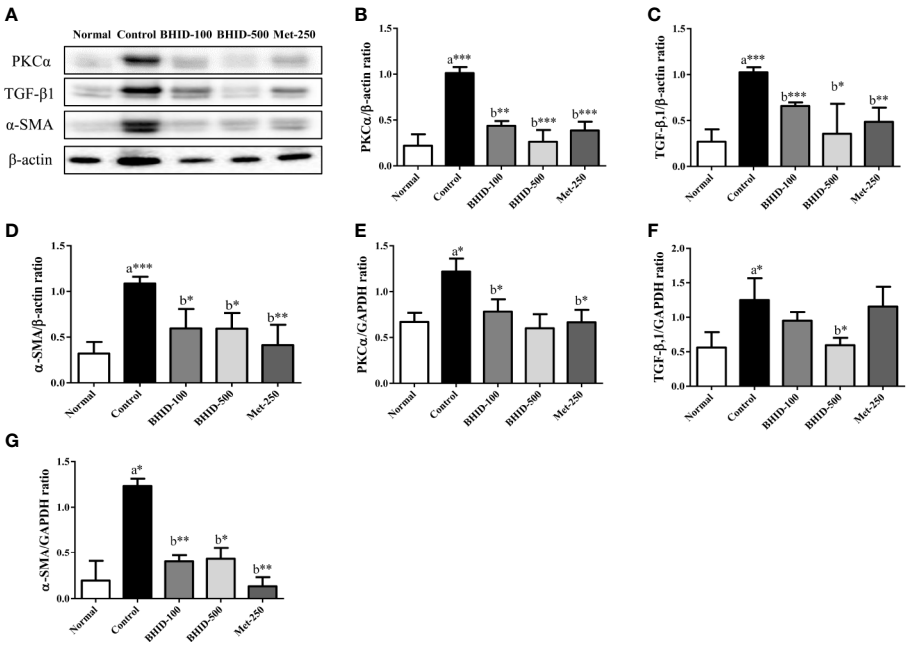


**FIGURE 5 |** Effects of Bekhogainsam decoction (BHID) on the expression of PKCα, TGF-β1, and α-SMA in the kidney tissue of mice with diabetic nephropathy (DN). Expression of PKCα, TGF-β1, and α-SMA was determined by western blotting **(A–D)** and qPCR **(E–G)**, respectively. Relative expression of PKCα **(B**, **E)**, TGF-β1 **(C**, **F)**, and α-SMA **(D**, **G)** were calculated using β-actin or GAPDH for normalization. Normal, normal group; Control, streptozotocin (STZ)–induced DN control group; BHID-100, BHID 100 mg/kg treatment group; BHID-500, BHID 500 mg/kg treatment group; and Met-250, Metformin 250 mg/kg treatment group. The data are expressed as the mean ± standard deviation ($n$=7). *P<0.05, **P<0.01, and ***P<0.001 vs. normal (a) or control (b) group.

was significantly increased in the DN control group compared with the normal group ($p$<0.001 for protein, $p$<0.05 for mRNA for both regulators). The expression of PKCα in kidney tissues of mice with DN was attenuated by the administration of low-dose ($p$<0.01 for protein and $p$ <0.05 for mRNA) and high-dose ($p$<0.001 for protein) BHID as well as by metformin ($p$<0.001 for mRNA and $p$<0.05 for protein). We also found that the expression of TGF-β1 was increased significantly ($p$<0.001 for protein and $p$<0.05 for mRNA) in the control group relative to the normal group (**Figures 5C, F**). BHID administration significantly inhibited TGF-β1 protein ($p$<0.001 for low dose and $p$<0.05 for high dose) and mRNA ($p$<0.05 for high dose) expression compared with the control group. Metformin also significantly decreased TGF-β1 protein expression ($p$<0.01).

A significant increase in α-SMA protein ($p$<0.001, **Figure 5D**) and mRNA ($p$<0.05, **Figure 5G**) expression was observed in the control group relative to the normal group. The administration of BHID significantly decreased the expression of α-SMA protein ($p$<0.05 for low and high dose) and mRNA ($p$<0.01 for low dose and $p$<0.05 for high dose) compared with the control group. Metformin administration also significantly inhibited α-SMA expression ($p$<0.01 for mRNA and protein).

## Differential Metabolite Analysis of Serum

In the present study, high-dose (500 mg/kg) BHID improved the symptoms of mice with STZ-induced DN. Therefore, the high-dose BHID was selected as the optimal effective dose for metabolic analysis and used in the subsequent screening for metabolic differences. The metabolite profiles of all serum samples were analyzed to determine the relative levels of the metabolites based on UHPLC-Q/TOF-MS analyses, and the base peak intensity chromatograms of a representative serum sample in each group are shown in **Supplementary Figure 1**. In the positive ion mode, more components were detected, and the multivariate statistical analysis was dependent on this mode.

First, PCA was conducted on serum samples. Clear differences in the serum metabolome were observed among all four groups (**Figure 6A**), especially between the control and other groups. The BHID and metformin group samples more closely resembled the normal group than the control group.

OPLS-DA and S-plot were then performed and compared to identify and characterize metabolites (**Figures 6B–D**). The significant differences in serum samples were observed between the control and BHID groups ($R^2Y$=0.822, $Q^2$=-0.146). There were 36 specific metabolic biomarkers that distinguished between the BHID and control group, including: xanthine, hypoxanthine, mesalazine, kanamycin, acetyl-β-methylcholine, uracil, taurocholic acid, elaidolinolenic acid, choline, adenosine, PPG acrylate n10, 2,3-dihydroxypropyl stearate, kinoprene, 2-(14,15-epoxyeicosatrienoyl) glycerol, tridemorph, lactate, quinbolone, memantine, sorbitan monolaurate, sparfloxacin, 3b-hydroxy-5-cholenoic acid, O-glutaroyl-L-carnitine, (+/-)-muscone, tretinoin, ricinoleic acid, niacinamide,

leucoline, decanoyl-coenzyme A, tryptophan, isoleucine, glutamine, valine, acetate, SCHEMBL1824118, and isoleucine. The heat map for these metabolites in the BHID and control groups is shown in **Figure 6E**. These data points were clustered into four distinct groups in the plot map, with a clear separation of the normal, control, BHID, and metformin samples.

The biomarkers that were altered in the BHID group were identified to be involved in four main pathways based on metabolic pathway analysis with MetaboAnalyst 4.0. The impact values of (a) valine, leucine, and isoleucine biosynthesis; (b) nicotinate and nicotinamide metabolism; (c) tryptophan metabolism; (d) alanine, aspartate, and glutamate

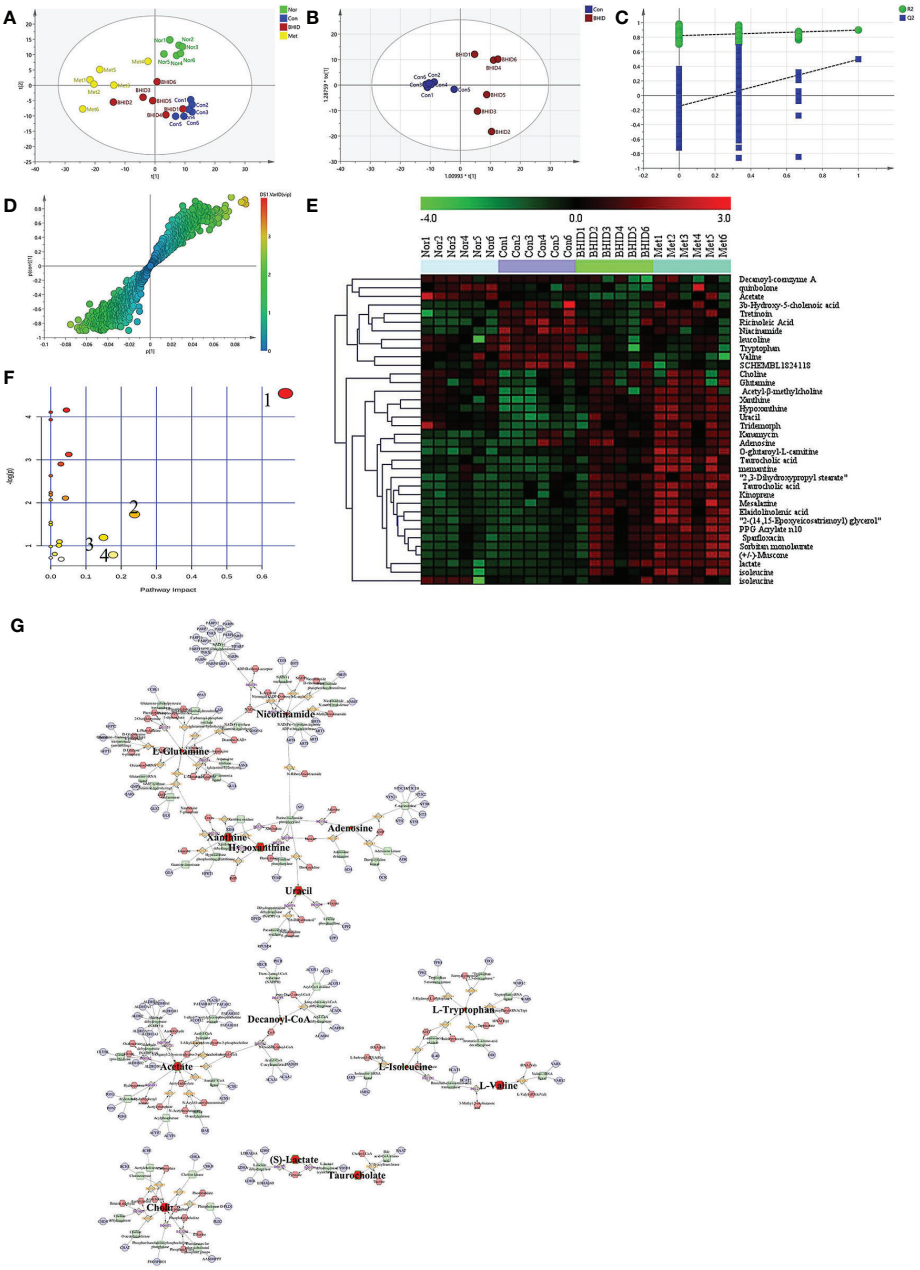


**FIGURE 6 |** Differential metabolite analysis of serum. The principle component analysis (PCA) analysis in different groups **(A)** and orthogonal projection to latent structure-discriminant analysis (OPLS-DA) analysis between control and Bekhogainsam decoction (BHID)–treatment group **(B)**. The permutation test of the OPLS-DA mode between the control and BHID groups **(C)** and the S-plot analysis **(D)**. The heat map of potential metabolites **(E)** and the summary of pathway analysis of differential metabolites **(F)**: valine, leucine, and isoleucine biosynthesis (1); nicotinate and nicotinamide metabolism (2); tryptophan metabolism (3); and alanine, aspartate, and glutamate metabolism (4). Metabolite-reaction–enzyme-gene graph **(G)**. The hub metabolites are presented in bold font. Nor, normal group; Con, streptozotocin (STZ)–induced DN control group; BHID, BHID 500 mg/kg group; and Met, metformin 250 mg/kg group.

metabolism were 0.67, 0.24, 0.18, and 0.15, respectively, and those metabolic pathway were the key metabolites in each pathway (**Figure 6F**).

The key metabolites from the metabolic pathway analysis were loaded into MetScape, and a metabolite–reaction–enzyme–gene graph was established to obtain an overview of all BHID metabolites on DN (**Figure 6G**). Adenosine, hypoxanthine, L-glutamine, uracil, xanthine, nicotinamide, acetate, decanoyl-Co, L-isoleucine, L-tryptophan, L-valine, (S)-lactate, taurocholate, and choline were selected as the hub metabolites of the correlation network in BHID on DN, based on their degree of influence.

## Gut Microbiota Analysis

The Shannon curves (**Figure 7A**) and Rank curves (**Figure 7B**) of each group were relatively gentle and concentrated, indicating that the amount of sequencing data was sufficient to reflect the majority of microbial information in the samples. The Shannon value provides an indication of the diversity of the intestinal flora in the samples (**Figure 7A**). The abscissa represents the number of sequences and the ordinate represents the Shannon index value. The higher the community diversity, the greater the Shannon value. The richness of intestinal flora and evenness were shown by the Rank abundance curves (**Figure 7B**). The length of the abscissa reflects the richness of the intestinal flora. The wider the curve, the richer the composition. The uniformity of the composition of the flora was reflected by the shape of the curve: a flatter curve indicates a more uniform composition.

OTUs at the 97% similarity level were obtained by cluster tags, and taxonomy notes were made on OTUs based on the taxonomy databases of Silva (for bacteria) and UNITE (for fungi). After the intersection was prepared using a OTUs-Venn diagram, we found that there were 400 shared OTUs for four groups (**Figure 7C**); the information on phylum, class, order, family, genus, and species level for each sample is shown in **Figures 7D–H**. The phylogenetic tree of OTUs at the genus taxonomic level is shown in **Figure 7I**.

To compare the similarity of different samples in species diversity, the principal coordinates analysis (PCoA) (**Figure 8A**) and Unweighted Pair-group Method with Arithmetic Mean (UPGMA) histogram of the cluster tree (**Figures 8B–E**) were obtained by beta diversity analysis. Owing to weighted UniFrac PCoA analysis, the points of the BHID group were widely distributed between the normal and DN control groups, and the metformin groups did not show a significant callback effect. Thus, it is suggested that BHID may be more effective in restoring the structure of gut microbiota towards that observed in the control group compared with metformin.

In our research, Metastats was used to investigate the biomarkers with a statistically significant difference (LDA score>4). There were significant differences between the normal and DN control groups with regard to the flora structures, specifically for: Patescibacteria and Deferribacteres at the phylum level; Saccharimonadia, Actinobacteria, and Deferribacteres at the class level; Saccharimonadales, Corynebacteriales, Deferribacterales, and Enterobacteriales at the order level; Saccharimonadaceae, Atopobiaceae, Rikenellaceae, Corynebacteriaceae Deferribacteraceae, Enterobacteriaceae, and Aerococcaceae at the family level; and Candidatus_Saccharimonas, Peptococcus, f_Erysipelotrichaceae, Anaerovorax, Butyricicoccus, Alistipes, Facklamia, A2, f_Ruminococcaceae, Coriobacteriaceae_UCG-002, Corynebacterium_1, Mucispirillum, Enterobacter, UBA1819, Kerstersia, Acetatifactor, Desulfovibrio, Turicibacter, ASF356, Brevundimonas at the genus level.

After BHID administration, the following significant differences were identified between the control and the BHID treatment groups for the flora structure: Actinobacteria at the phylum level; Coriobacteriia, Oxyphotobacteria, and Erysipelotrichia at the class level; Coriobacteriales, Chloroplast, and Erysipelotrichales at the order level; Atopobiaceae, uncultured_bacterium, Erysipelotrichaceae, Clostridiales_vadinBB60_group at the family level, Peptococcus, Roseburia, Coriobacteriaceae_UCG-002, f_Clostridiales_vadinBB60_group, Kerstersia, and Acetatifactor at the genus level. The above significant differences were further verified by ANOVA (**Supplementary Figure 2**). Correlation analysis was performed and the results are presented as a network diagram (**Supplementary Figure 4**).

## Network Pharmacology Analysis and Verification

To explore the potential ingredients and molecular targets of BHID that have an effect on DN, we conducted a network pharmacological analysis. We identified 153 potentially active compounds and 472 gene targets corresponding to those potentially active compounds in BHID. We also searched for 2,298-related DN target genes. A Venn intersection target diagram was built, and 193 common targets were identified (**Supplementary Figure 4**).

For a comprehensive identification of the mechanism of BHID on DN, we constructed a network between BHID active components, the corresponding targets, and DN-related genes (**Figure 9A**). In combination with high-frequency node analysis in the PPI network (**Figure 9B**), we were surprised to see AKT1 (protein kinase B1), IL6 (interleukin 6), MAPK3 (mitogen-activated protein kinase 3), and TP53 (tumor protein P53) at the center of the network (**Figure 9C**).

GO (**Figure 9E**) and KEGG (**Figure 9D**) analyses were conducted for pathway enrichment to identify the relevant pathways and functions based on putative targets. Functional analysis revealed that the MAPK signaling pathway and the PI3K/Akt signaling pathway significantly enriched the DN-related pathways. Moreover, functional analysis data revealed that these putative targets not only modulated cell proliferation, apoptosis, growth, and inflammatory response, but also tuned the phosphatase binding and protein serine/threonine kinase (PI3K/Akt) signaling pathways.

These data provided a theoretical basis for the possibility that the antagonistic activity of BHID against DN may be related to the activity of PI3K/Akt- and MAPK-related targets. These predicted results were verified by western blotting (**Figure 10**).

Significant inhibition of Akt ($p<0.05$, **Figure 10B**) and IRS-1 (**Figure 10D**) phosphorylation and PI3K ($p<0.01$, **Figure 10C**) expression was observed in the DN control group compared with the normal group. The administration of BHID at low and high doses increased PI3K expression, but the effect was not

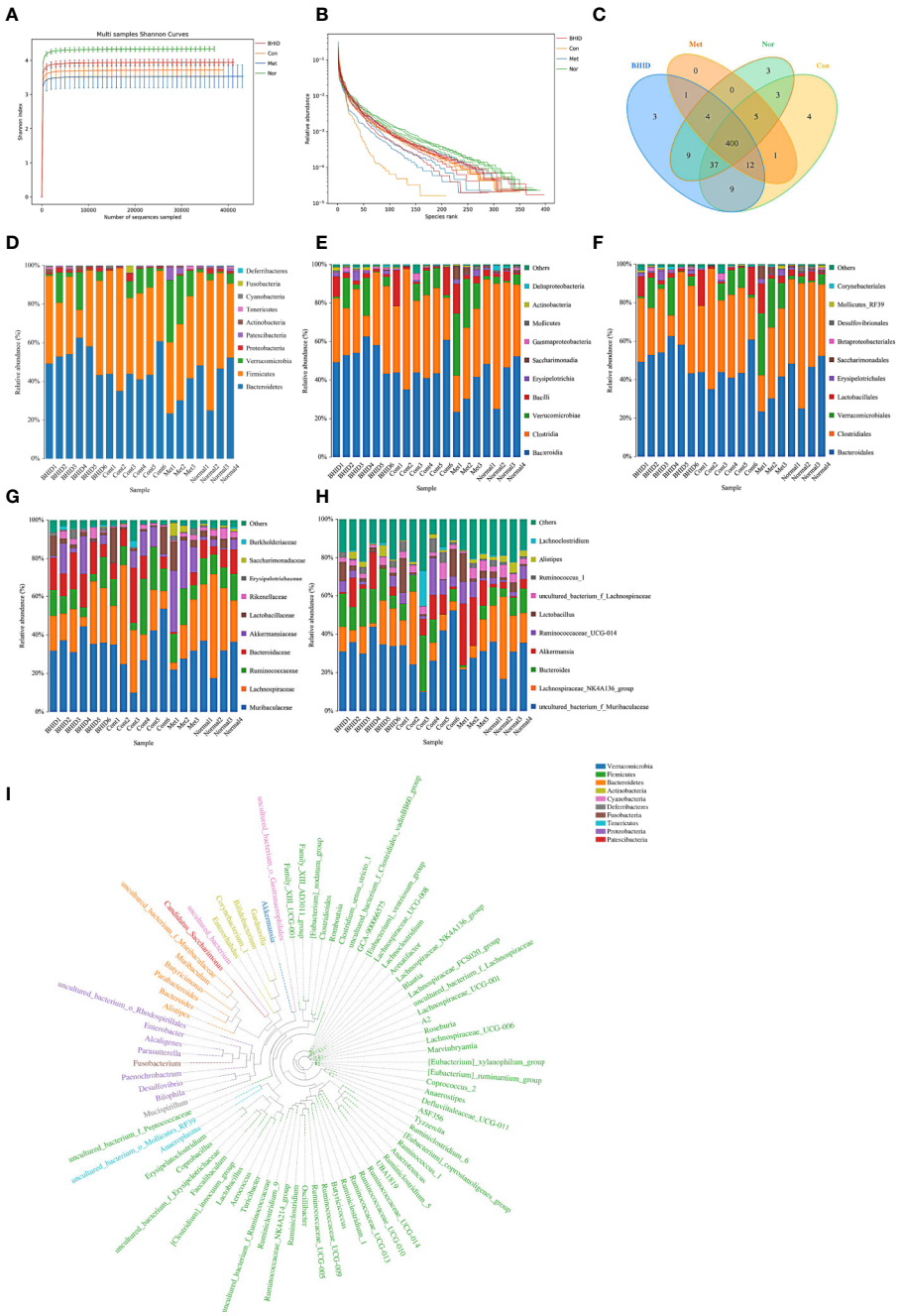


**FIGURE 7 |** Overall structural modulation of gut microbiota. Shannon curves for all groups **(A)** and rank curves **(B)**. Shared and special operational taxonomic unit (OTUs) for the normal, control, Bekhogainsam decoction (BHID), and metformin groups **(C)**. The information of phylum, class, order, family, and genus level for each sample **(D–H)**. The phylogenetic tree of OTUs at the genus taxonomic level **(I)**. Nor, normal group; Con, streptozotocin (STZ)–induced diabetic nephropathy (DN) control group; BHID, BHID 500 mg/kg group; and Met, metformin 250 mg/kg group.

significant. Moreover, BHID administration significantly increased Akt phosphorylation at low doses ($p<0.05$) and IRS-1 phosphorylation at high doses ($p<0.05$) compared with the control group. Metformin had little effect on the Akt/PI3K and IRS-1 pathways.

For the expression of the inflammatory mediators involved in the MAPK pathway (**Figure 11A**), significant increases in iNOS ($p<0.01$, **Figure 11C**) and COX-2 ($p<0.001$, **Figure 11B**) occurred in the DN control group compared with the normal group. However, BHID administration significantly decreased

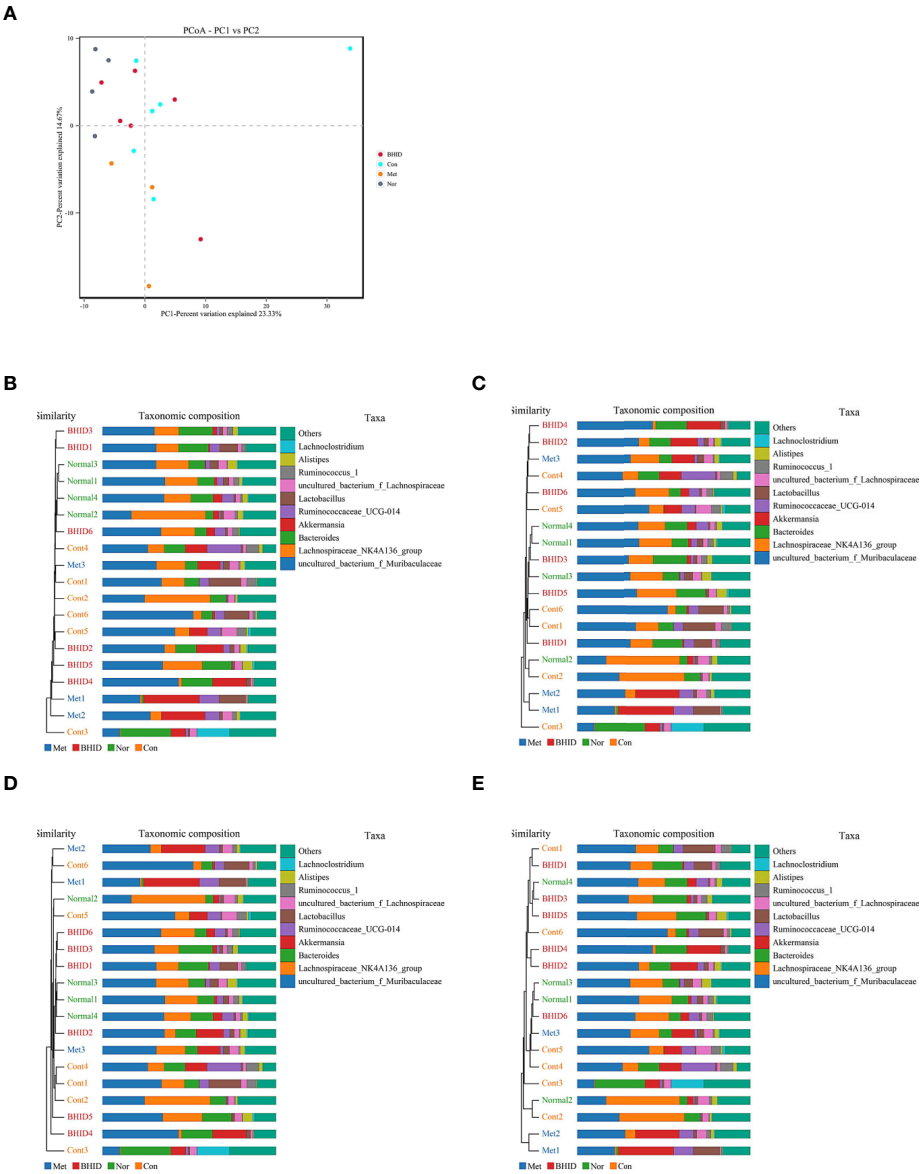


**FIGURE 8 |** Multivariate analysis for gut microbiota. Weighted UniFrac principal coordinates analysis (PCoA) analysis of gut microbiota based on the operational taxonomic unit (OTU) data **(A)** and Unweighted Pair-group Method with Arithmetic Mean (UPGMA) histogram of cluster tree **(B–E)**, respectively. Nor, normal group; Con, streptozotocin (STZ)–induced diabetic nephropathy (DN) control group; BHID, BHID 500 mg/kg group; and Met, metformin 250 mg/kg group.

the expression of iNOS ($p<0.05$ for low dose and $p<0.01$ for high dose), and COX-2 ($p<0.05$ for low dose and $p<0.001$ for high dose) relative to the control group. Metformin also significantly inhibited their expression ($p<0.05$ for iNOS and COX-2 for $p<0.001$) in the kidney tissue.

Significant increases in the expression of I-κBα and decreases in the expression of NF-κB were observed in response to BHID at low ($p<0.05$ for I-κBα and $p<0.05$ for NF-κB; **Figures 11D, E**) and high ($p<0.001$ for I-κBα and $p<0.05$ for NF-κB; **Figures 11D, E**) doses compared with the DN control group. Metformin also significantly increased I-κBα expression ($p<0.01$) and decreased NF-κB expression ($p<0.01$) in the kidney tissue.

## DISCUSSION

DN is a diabetic complication known as wasting-thirst disease, Sogal, or Xiaoke syndrome in traditional medicine. BHID is a representative prescription for the control of diabetic symptoms, such as excessive consumption of fluid owing to intense heat in

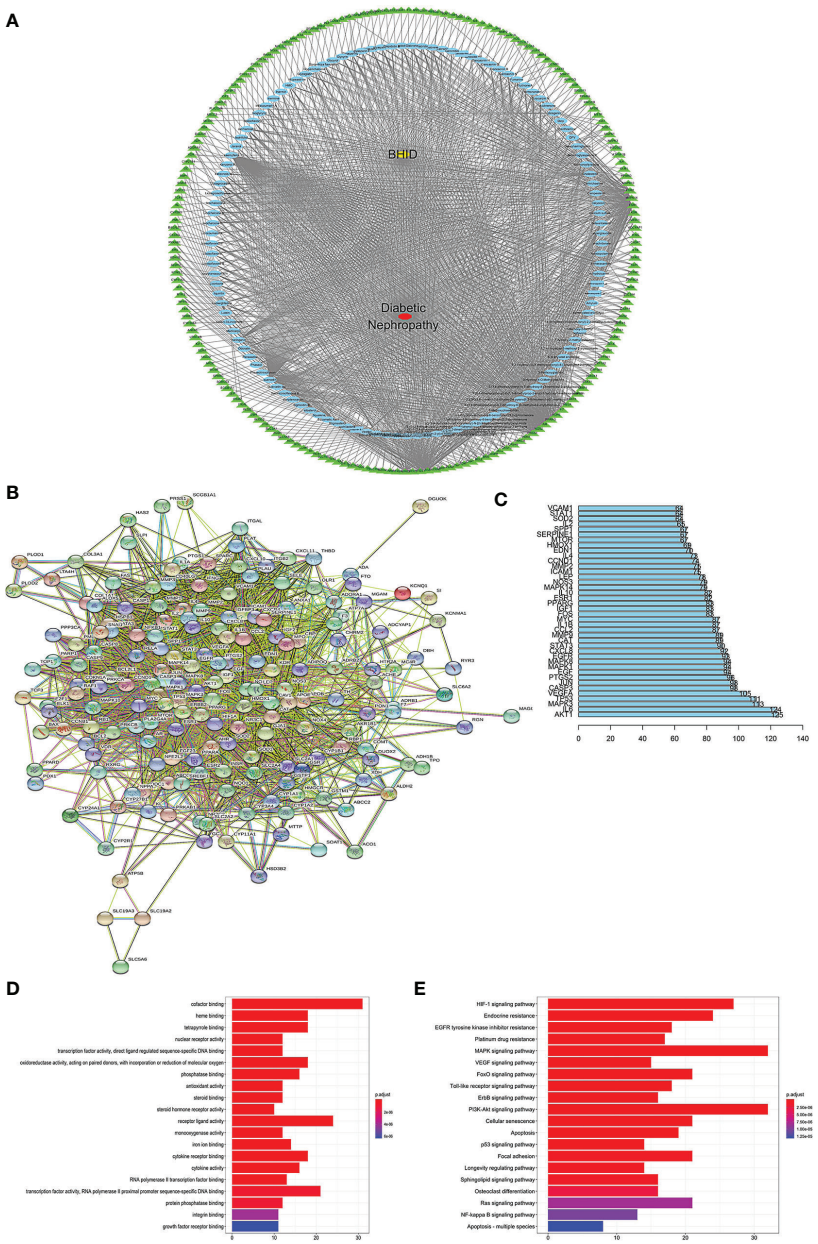


**FIGURE 9 |** Network construction, pathway, and functional enrichment analysis of the effect of Bekhogainsam decoction (BHID) on diabetic nephropathy (DN). Potential active ingredient-target-disease network **(A)**: Different color symbols as mentioned here: disease (red), BHID (yellow), targets (green), and compounds (blue). Protein-protein interaction (PPI) network **(B)** Node information as mentioned here: query proteins and first shell of interactors (colored nodes), second shell of interactors (white nodes), proteins of unknown 3D structure (empty nodes), some 3D structure is known or predicted (filled nodes), curated databases (), experimentally determined (), gene neighborhood (), gene fusions (), gene co-occurrence (), text mining (), co-expression (), and protein homology (). **(C)** Frequency analysis of protein targets. **(D)** Kyoto Encyclopedia of Genes and Genomes (KEGG) pathway enrichment analysis The gradual change in color represented the change in probability. **(E)** Gene Ontology (GO) function analysis. The gradual change in color represents the change in probability.

the spleen and stomach, and for the restoration of yin-deficient conditions. One of the constituents of BHID, Gypsum fibrosum is one mineral with hydro calcium fibriform crystallized polymeric and traditionally used to clear heat of lung and stomach at qi system in China and Korea. It has various characteristics, such as heart clearing, wound healing, purging of fire, and promotion of tissue regeneration (Li et al., 2006; Zhang B. et al., 2019). The Anemarrhenae rhizome clears heat and purges fire from the lung and kidney by generating fluids, moistens dryness, and has been reported to exert antithrombotic,

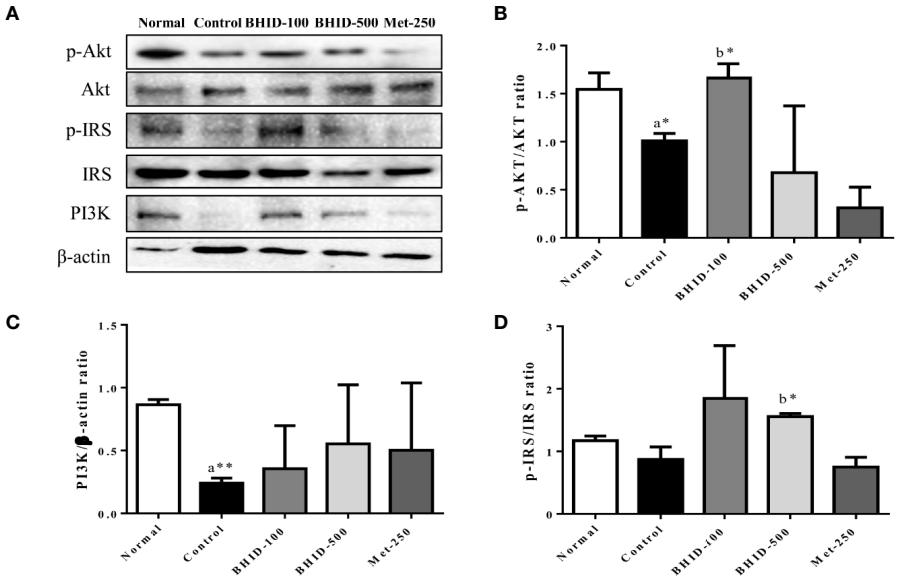


**FIGURE 10 |** Effects of Bekhogainsam decoction (BHID) on the PI3K/AKT and IRS-1 signaling pathways in the kidney tissue of mice with diabetic nephropathy (DN). Phosphorylation of Akt-Ser473, IRS-Ser307, and PI3K p85 was assessed by western blotting **(A)**. Relative expression of Akt-Ser 473 **(B)**, IRS-Ser307 **(C)**, and PI3K p85 **(D)** was calculated with the total and phosphorylated-forms or β-actin for normalization. Normal, normal group; Control, streptozotocin (STZ)–induced DN control group; BHID-100, BHID 100 mg/kg treatment group; BHID-500, BHID 500 mg/kg treatment group; and Met-250, Metformin 250 mg/kg treatment group. The data are expressed as the mean ± standard deviation (*n*=7). *p<0.05 and **p<0.01 vs. normal (a) or control (b) group.

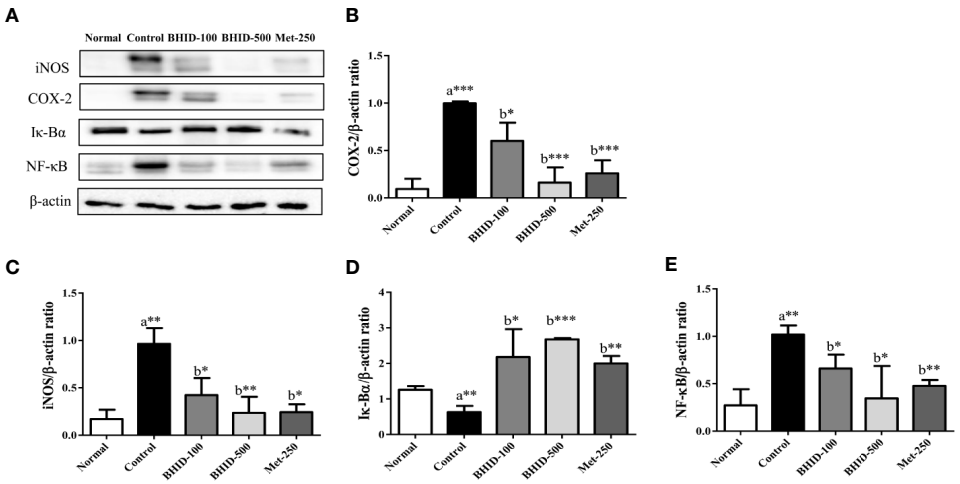


**FIGURE 11 |** Effects of Bekhogainsam decoction (BHID) on the expression of iNOS, COX-2, I-κB, and NF-κB in the kidney tissue of mice with diabetic nephropathy (DN) **(A)**. The expression of iNOS **(C)**, COX-2 **(B)**, I-κBα **(D)**, and NF-κB p65 **(E)** was assessed by western blotting. The relative expression was calculated with β-actin for normalization. Normal, normal group; Control, streptozotocin (STZ)–induced DN control group; BHID-100, BHID 100 mg/kg treatment group; BHID-500, BHID 500 mg/kg treatment group; and Met-250, Metformin 250 mg/kg treatment group. The data are expressed as the mean ± standard deviation (*n*=7). *P<0.05, **P<0.01, and ***P<0.001, vs. normal (a) or control (b) group.

antidiabetic, anticolitic, and antiallergic effects in modern pharmacology (Lu et al., 2011; Jang et al., 2013; Li et al., 2013; Makino et al., 2014). Glycyrrhizae radix et rhizoma is the most frequently used crude drug in traditional medicine for the treatment of a variety of diseases (Nose et al., 2017; Wang et al., 2018). Specifically, it contains glycyrrhizin, which is a bioactive compound known to exert antidiabetic activities through the amelioration of insulin resistance, hyperglycemia,

dyslipidemia, and oxidative stress (Li et al., 2006; Sen et al., 2011; Sil et al., 2013; Rani et al., 2017). Polished round-grained rice is a rice-grain sprout commonly used to invigorate spleen function, promote digestion, and improve the appetite, and is applied as a source of energy in So-gal syndrome with polydipsia. Ginseng radix et rhizoma is known as the "King of Herbs" because of its varied effects, including improving fitness, preventing fatigue, prolonging life, regulating blood sugar levels, soothing the nerves, and enhancing immunity. Ginseng radix et rhizoma has been shown to exert various pharmacological activities toward specific diseases, such as dementia, diabetes, respiratory infections, and cancer, *via* its constituent compounds, ginsenosides Rb1, Rg1, and Rg3 (Mancuso & Santangelo, 2017; Mohanan et al, 2018). From HPLC analysis, mangiferin and neomangiferin in Anemarrhenae rhizoma, liquiritin, and ammonium glycyrrhetate in Glycyrrhizae radix et rhizoma, and ginsenoside-Rg1 in Ginseng radix et rhizoma in BHID were identified as main compounds in BHID. This result will assist in the control the quality of BHID and will support further studies, such as pharmacodynamics experiments.

Experimental studies have tended to focus on the clinical treatment of BHID in DM. The antidiabetic effects of BHID and its components have been known and used for thousands of years to effectively treat DM, and it has been studied in many *in vivo* experiments (Chang et al., 2006). However, little is known about its individual effects on diabetic complications, especially DN, and the mechanisms responsible for these effects. Therefore, we performed a detailed evaluation of the effects of BHID on STZ-induced DN in mice and identified the molecular mechanisms responsible for its effects on DN. STZ is a naturally occurring antineoplastic alkylating agent that is particularly toxic to insulin-producing beta cells in the pancreas and thus induces experimental DM and DN. We induced DN in mice by 3 days' consecutive STZ injection; conferring systematic and serious histopathological damage in the kidney as well as typical diabetic symptoms, such as hyperglycemia, polydipsia, and polyuria with weight loss. The administration of low and high doses of BHID significantly decreased the increases in food and water intake, urine volume, and blood glucose and triglyceride levels, and significantly increased insulin secretion. These findings indicate that BHID can improve the diabetic symptoms of hyperglycemia, polydipsia, and urorrhagia in DN.

The liver is an important target organ for the regulation of metabolic functions, including insulin sensitivity and gluconeogenesis. The clinical diagnosis of damage to the structural integrity of the liver is usually tested by monitoring the activity of serum AST and ALT. Traditional medicine theory considers the liver and kidney to be homologous; specifically, although their structure and function are different, the origin of the liver and kidney is the same, and their physiological and pathological characteristics are therefore closely related. In the present study, the administration of BHID protected the liver against STZ-induced diabetic toxicity, resulting in decreased AST and ALT levels in DN mice.

The pathogenesis of DN is not fully established; however, it is generally believed to be related to genetics, hyperglycemia, hemodynamic changes, and the production of various cytokines (Piccoli et al., 2015). The glucose transporter (Glut) family is the most important membrane protein for the control of glucose uptake and use, and is distributed widely in the brain, kidney, skeletal muscle, myocardium, and adipose tissues (Colberg et al., 2010). Diabetes with hyperglycemia and insulin deficiency is associated with the loss of GLUT4 expression and translocation, which increases diacylglycerol synthesis (DAG) and activates the PKC pathway (Melloni et al., 1987). The PKC family consists of at least 10 serine/threonine protein kinases that play a central role in various cellular activities, such as the control of growth, differentiation, and apoptosis (Nishizuka, 1986). Therefore, activation of the DAG/PKC signaling pathway can trigger the polyol pathway, oxidative stress, and glycosylated terminal products involved in the occurrence of diabetic complications. This pathway also regulates the permeability of glomerular endothelial cells and, simultaneously, the synthesis and transformation of extracellular matrix in kidney tissue (Sajan and Farese, 2012; Yang and Zhang, 2015). PKC participates in the injury of glomerular podocytes by activation of the TGF-β1 signaling pathway (Xiao et al., 2018). TGF-β1, one of the most critical fibrogenic factors, increases the synthesis of extracellular matrix (ECM) in the mesangial area of the kidney and accelerates thickening of the glomerular basement membrane, thereby inducing glomerular sclerosis and renal failure. Therefore, the PKC/TGF-β1 signaling pathway plays an important role in glomerular sclerosis (Chang et al., 2016) and renal interstitial fibrosis (Wang et al., 2017). Alpha-SMA, a characteristic marker of myofibroblasts, is increased in the kidney tissue during the transformation of renal tubular epithelial cells into mesenchymal cells (Niu et al., 2014). In this study, we found that expression of PKCα, TGF-β1, and α-SMA was increased in the kidney tissue of DN mice, and this increase in expression was markedly suppressed by the administration of BHID. These results indicated that BHID inhibited renal fibrosis in DN through the downregulation of PKCα/TGF-β1/α-SMA expression. We also observed the protective effects of BHID against morphological destruction and fibrosis by using H&E, PAS, and Masson's trichrome staining.

The theory of "Yin-Yang Balance" and the practice of "BianZheng" in TKM and TCM have many common themes with the holism and systemic theory of systems biology. The concept of systems biology medicine has supported the advancement of TM research for medicine. The study of metabolomics, intestinal flora, and network pharmacology will help to achieve the internationalization and modernization of TM. In our study, BHID altered DN in mice through the inhibition of renal injury, as evidenced by metabolomics coupled with intestinal flora and network pharmacology analyses.

After the anti-DN potential was tested, the mechanism of BHID action was examined by a metabolomics analysis of the serum. The results showed that 36 specific metabolic biomarkers and four main metabolic pathways were affected by BHID treatment. These metabolites and metabolic pathways were

closely related to various nutrients, such as carbohydrates, proteins, fat, vitamins, and trace elements (Sarkozy et al., 2014). Moreover, valine, leucine, and isoleucine biosynthesis, which is the most important metabolic pathway for insulin sensitivity (Kaiser et al., 2018), had the highest impact value. Alanine, aspartate, and glutamate metabolism pathways are the signature pathologic metabolic pathways involved the metabolic disorders of DM (Engskog et al., 2017). Moreover, analysis of the gut microbiota verified that these amino acid metabolic disorders may be considered to provide feedback on intestinal flora. Thus, we can confirm the potential and efficiency of BHID in DM or DN through serum metabolomics analysis.

Moreover, BHID can alter microbial composition. The pathogenesis of DM and DN is correlated with inflammation in the intestinal flora. In our study, significant differences were found for Patescibacteria and Deferribacteres at the phylum level between the DN control group and BHID treatment group. More seriously, the worst and serious for the homogeneity and abundance imbalance can be observed in the control group. In combination with the biochemical and pathological indices, we showed that there was an inherent inevitability between the imbalance of intestinal flora and the occurrence of DM or DN. After BHID oral administration, there was a significant difference in Actinobacteria at the phylum level between the control and the BHID treatment group. Actinobacteria is the most important flora that causes intestinal inflammation and ulcers, and stimulates multiple inflammatory reactions (Burge et al., 2019). Our results showed that the administration of BHID can suppress inflammatory reactions by altering the composition of the intestinal flora. More importantly, Coriobacteriia is an important flora for glucose metabolism and the conversion and absorption of medicinal ingredients that can improve the symptoms of DN or STZ-induced DN in mice (Kikuchi et al., 2019). Moreover, the oral administration of BHID can improve the growth of probiotics, such as Clostridiales and Peptococcus, to maintain the homeostasis of the intestinal flora. Recent research has shown that the effects of Ginseng radix et rhizoma and Anemarrhenae rhizoma on obesity, cancer, and DM are mediated through the regulation of the composition of the intestinal flora (Xiao et al., 2016; Dong et al., 2019). In our study, significant differences were observed in the structure of the intestinal flora at the phylum, class, order, family, genus, and species levels between the normal and control, and control and BHID-treatment groups, and a high frequency of interconnected flora was also summarized. To the best of our knowledge, the present study is the first to demonstrate the effect of BHID or its components on the modulation of gut microbiota.

To further understand the molecular mechanism of the effects of BHID on DN, a network between BHID active components, the corresponding targets, and DN-related genes was established based on network pharmacology analysis. We concluded that BHID antagonism against DN may be related to the activity of PI3K/Akt- and MAPK-related targets. This hypothesis was further verified by western blotting. Beta-cell apoptosis in the pancreas, insulin resistance, and hyperglycemia induce the excessive production of inflammatory mediators, iNOS, and COX-2, through activation of the NF-κB signaling pathway in DN (Lu et al., 2014). Moreover, the phosphorylation of serine residues in the insulin receptor (IRS-1) results in diminished enzymatic activity in the PI3K/Akt pathway in DN. Previous studies have reported that the NF-κB pathway was activated in various tissues, including kidney tissues of DN (Wang et al., 2015; Gao et al., 2018). The PI3K/Akt pathway is one of the TGF-β1 downstream signaling pathways that can resist podocyte apoptosis by controlling purine adenosine, protein overload, hemodynamic disorder, and other conditions, and can give rise to proteinuria in DN (Saleem, 2015). In this study, we found that BHID administration in mice with STZ-induced DN effectively inhibited the expression of iNOS and COX-2 in the kidney tissue of mice with through the suppression of the I-κB/NF-κB signaling pathway, as well as activation of the PI3K/Akt signaling pathway.

Moreover, metformin is the most common classical drug used in the clinical treatment of T2DM; it can increase glucose utilization in the body by peripheral cells, prevent liver and kidney glycogenogenesis, reduce the synthesis and output of glucose by the liver and kidney, and inhibit glucose uptake by cells in the intestinal wall (Hostalek et al., 2015). It suppresses glucose synthesis from multiple links, promotes glucose conversion and absorption, and reduces blood glucose levels in patients with diabetes (van Stee et al., 2018). However, long-term use causes nausea, vomiting, diarrhea, fatigue, and other adverse reactions (Hostalek et al., 2015). In our results, BHID effectively decreased the kidney-to-body ratio, urine volume, serum levels of glucose, AST, and ALT, and increased insulin- and HDL-cholesterol compared with metformin. With regard to kidney damage, BHID reduced fibrosis, inflammation, and insulin resistance through the inhibition of TGF-β1 and COX-2 expression, and the activation of Akt and IRS-1 compared with metformin. These results indicated that BHID is a good candidate for traditional medicine prescription and as an alternative to metformin for the treatment of DN in clinics.

To the best of our knowledge, our study is the first to report the anti-DN effects of BHID in a mouse model, as shown by metabolomics coupled with analysis of the intestinal flora and network pharmacology, in which the holistic view of systems biology runs through the whole study. However, the content of the five main chemical substances in the BHID was measured, and the possible changes in the chemical compositions of each drug during the decocting process and metabolic labeling *in vivo*. In our study, we aimed to establish the internal relevance between metabolomics, intestinal flora, and network pharmacology with limited evidence; therefore, further explanation and evidence should be identified and explored to strengthen this relevance, and the core metabolites should be determine.

## CONCLUSION

The administration of 100 and 500 mg/kg BHID in mice with STZ-induced DN for 4 weeks improved diabetic conditions, such as physiological and serological imbalances and damage to the liver and kidney. In the analysis of metabolomics coupled with gut microbiota and network pharmacology, BHID was shown to alter the metabolites and gut floral structures, and the protective effect of BHID against the DN-induced damage to the kidney is underlying the activation of the PI3K/MAPK pathway. Our findings suggested that there is scientific evidence for the beneficial effects of BHID in the clinical treatment of patients with diabetes and for the prevention of DN progression.

## DATA AVAILABILITY STATEMENT

The raw data supporting the conclusions of this article will be made available by the authors, without undue reservation, to any qualified researcher.

## ETHICS STATEMENT

All animals were handled according to the animal welfare guidelines issued by the Korean National Institute of Health and the Korean Academy of Medical Sciences for the care and use of laboratory animals and approved by the Institutional Animal Care and Use Committee of Dongguk University (IACUC-2017-012).

## AUTHOR CONTRIBUTIONS

Y-KP and HJ designed the study. XM, JM, SK, AK, and HJ performed the experiment and conducted a statistical analysis. XM and HJ wrote the manuscript. All authors revised the manuscript and approved the final version of the manuscript.

## FUNDING

This research was supported by the Basic Science Research Program through the National Research Foundation of Korea (NRF) funded by the Ministry of Education (Grant No. 2016R1D1A2B01012117 & 2016R1D1A1B04935601).

## SUPPLEMENTARY MATERIAL

The Supplementary Material for this article can be found online at: https://www.frontiersin.org/articles/10.3389/fphar.2020.00633/full#supplementary-material

## REFERENCES

Ablat, N., Niyazi, G., and Abudujiapaer, A. (2015). Simultaneous determination of glycyrrhizic acid and liquiritin in Zukamu capsules by HPLC. *Chin. J. Inform. Trad. Chin. Med.* 22 (15), 83–85. doi: 10.3969/j.issn.1005-5304.2015.12.021

Alicic, R. Z., Rooney, M. T., and Tuttle, K. R. (2017). Diabetic kidney disease: Challenges, progress, and possibilities. *Clin. J. Am. Soc Nephrol.* 12, 2032–2045. doi: 10.2215/CJN.11491116

Barko, P. C., McMichael, M. A., Swanson, K. S., and Williams, D. A. (2018). The gastrointestinal microbiome: Review. *J. Vet. Intern. Med.* 32, 9–25. doi: 10.1111/jvim.14875

Barnes, S., Benton, H. P., Casazza, K., Cooper, S. J., Cui, X., Du, X., et al. (2016). Training in metabolomics research. I. Designing the experiment, collecting and extracting samples and generating metabolomics data. *J. Mass Spectrom.* 51, 461–475. doi: 10.1002/jms.3782

Beger, R. D., Dunn, W., Schmidt, M. A., Gross, S. S., Kirwan, J. A., Cascante, M., et al. (2016). Metabolomics enables precision medicine: "A White Paper, Community Perspective". *Metabolomics* 12, 149. doi: 10.1007/s11306-016-1094-6

Burge, K., Gunasekaran, A., Eckert, J., and Chaaban, H. (2019). Curcumin and intestinal inflammatory diseases: Molecular mechanisms of protection. *Int. J. Mol. Sci.* 20 (8). doi: 10.3390/ijms20081912

Chang, M. S., Oh, M. S., Kim, D. R., Jung, K. J., Park, S., Choi, S. B., et al. (2006). Effects of okchun-san, a herbal formulation, on blood glucose levels and body weight in a model of Type 2 diabetes. *J. Ethnopharmacol.* 103, 491–495. doi: 10.1016/j.jep.2005.08.039

Chang, A. S., Hathaway, C. K., Smithies, O., and Kakoki, M. (2016). Transforming growth factor-beta1 and diabetic nephropathy. *Am. J. Physiol. Renal. Physiol.* 310, F689–F696. doi: 10.1152/ajprenal.00502.2015

Colberg, S. R., Sigal, R. J., Fernhall, B., Regensteiner, J. G., Blissmer, B. J., Rubin, R. R., et al. (2010). Exercise and type 2 diabetes: the American College of Sports Medicine and the American Diabetes Association: joint position statement executive summary. *Diabetes Care* 33, 2692–2696. doi: 10.2337/dc10-1548

Cui, X., Qian, D. W., Jiang, S., Shang, E. X., Zhu, Z. H., and Duan, J. A. (2018). Scutellariae Radix and Coptidis Rhizoma improve glucose and lipid metabolism in T2DM rats via regulation of the metabolic profiling and MAPK/PI3K/Akt signaling pathway. *Int. J. Mol. Sci.* 19 (11). doi: 10.3390/ijms19113634

Ding, X., AN, N., Yao, D., and Zhao, Y. (2007). Change of ginsenoside Rg1 and ginsenoside Re in different compatibilities of Renshen Baihu decoction. *Chin. Tradit. Herbal Drugs* 05, 702–704. doi: 10.3321/j.issn:0253-2670.2007.05.023

Dong, L., Li, Y., Xu, J., Yang, J., Wei, G., Shen, L., et al. (2019). Biofertilizers regulate the soil microbial community and enhance *Panax ginseng* yields. *Chin. Med.* 14, 20. doi: 10.1186/s13020-019-0241-1

Engskog, M. K., Ersson, L., Haglof, J., Arvidsson, T., Pettersson, C., and Brittebo, E. (2017). beta-N-Methylamino-L-alanine (BMAA) perturbs alanine, aspartate and glutamate metabolism pathways in human neuroblastoma cells as determined by metabolic profiling. *Amino Acids* 49, 905–919. doi: 10.1007/s00726-017-2391-8

Gao, X., Liu, H., An, Z., and He, Q. (2018). QiDiTangShen granules reduced diabetic kidney injury by regulating the phosphorylation balance of the tyrosine and serine residues of insulin receptor substrate 1. *Evid. Based Complement. Alternat. Med.* 2018, 2503849. doi: 10.1155/2018/2503849

Glastras, S. J., Chen, H., Teh, R., McGrath, R. T., Chen, J., Pollock, C. A., et al. (2016). Mouse models of diabetes, obesity and related kidney disease. *PloS One* 11 (8), e0162131. doi: 10.1371/journal.pone.0162131

Hanning, I., and Diaz-Sanchez, S. (2015). The functionality of the gastrointestinal microbiome in non-human animals. *Microbiome* 3, 51. doi: 10.1186/s40168-015-0113-6

Horie, M., Miura, T., Hirakata, S., Hosoyama, A., Sugino, S., Umeno, A., et al. (2017). Comparative analysis of the intestinal flora in type 2 diabetes and nondiabetic mice. *Exp. Anim.* 66, 405–416. doi: 10.1538/expanim.17-0021

Hostalek, U., Gwilt, M., and Hildemann, S. (2015). Therapeutic use of metformin in prediabetes and diabetes prevention. *Drugs* 75 (10), 1071–1094. doi: 10.1007/s40265-015-0416-8

Jang, S. E., Jeong, J. J., Hyam, S. R., Han, M. J., and Kim, D. H. (2013). Anticolitic effect of the rhizome mixture of Anemarrhena asphodeloides and Coptidis chinensis (AC-mix) in mice. *Biomol. Ther. (Seoul)* .21 (v5), 398–404. doi: 10.4062/biomolther.2013.048

Kaiser, J. C., King, A. N., Grigg, J. C., Sheldon, J. R., Edgell, D. R., Murphy, M. E. P., et al. (2018). Repression of branched-chain amino acid synthesis in *Staphylococcus aureus* is mediated by isoleucine via CodY, and by a leucine-rich attenuator peptide. *PloS Genet.* 14, e1007159. doi: 10.1371/journal.pgen.1007159

Kikuchi, K., Saigusa, D., Kanemitsu, Y., Matsumoto, Y., Thanai, P., Suzuki, N., et al. (2019). Gut microbiome-derived phenyl sulfate contributes to albuminuria in diabetic kidney disease. *Nat. Commun.* 10, 1835. doi: 10.1038/s41467-019-09735-4

Li, X., Liu, Y. F., Xiang, X. R., Zhou, Y. B., and Zhang, Z. L. (2006). [Comparative study of the effects of Gypsum Fibrosum and Gypsum Fibrosum Preparatum in promoting granulation]. *Zhong Xi Yi Jie He Xue Bao* 4, 624–627. doi: 10.3736/jcim20060617

Li, X., Cui, X., Wang, J., Yang, J., Sun, X., Li, X., et al. (2013). Rhizome of Anemarrhena asphodeloides counteracts diabetic ophthalmopathy progression in streptozotocin-induced diabetic rats. *Phytother. Res.* 27, 1243–1250. doi: 10.1002/ptr.4866

Li, G., Che, N. C., Geng, J. G., Zhao, H., Wang, Z. Q., Guo, X. X., et al. (2014). Discussion of changes of TGF-β1, Smad-4, α-SMA and PDGF in DN rat liver before and after treatment in traditional Chinese Medicine based on the "liver and kidney share the same origin". *Chin. J. Basic Med. Tradit. Chin. Med.* 20, 459–461.

Lin, H. T., Cheng, M. L., Lo, C. J., Lin, G., Lin, S. F., Yeh, J. T., et al. (2019). (1)H Nuclear magnetic resonance (NMR)-based cerebrospinal fluid and plasma metabolomic analysis in type 2 diabetic patients and risk prediction for diabetic microangiopathy. *J. Clin. Med.* 8 (6). doi: 10.3390/jcm8060874

Lu, W. Q., Qiu, Y., Li, T. J., Tao, X., Sun, L. N., and Chen, W. S. (2011). Antiplatelet and antithrombotic activities of timosaponin B-II, an extract of Anemarrhena asphodeloides. *Clin. Exp. Pharmacol. Physiol.* 38, 430–434. doi: 10.1111/j.1440-1681.2011.05530.x

Lu, H. J., Tzeng, T. F., Liou, S. S., Da Lin, S., Wu, M. C., and Liu, I. M. (2014). Polysaccharides from Liriopes Radix ameliorate streptozotocin-induced type I diabetic nephropathy via regulating NF-kappaB and p38 MAPK signaling pathways. *BMC Complement. Altern. Med.* 14, 156. doi: 10.1186/1472-6882-14-156

Makino, T., Shiraki, Y., and Mizukami, H. (2014). Interaction of gypsum and the rhizome of Anemarrhena asphodeloides plays an important role in anti-allergic effects of byakkokakeishito in mice. *J. Nat. Med.* 68, 505–512. doi: 10.1007/s11418-014-0827-y

Mancuso, C., and Santangelo, R. (2017). *Panax ginseng* and *Panax quinquefolius*: From pharmacology to toxicology. *Food Chem. Toxicol.* 107, 362–372. doi: 10.1016/j.fct.2017.07.019

Melloni, E., Pontremoli, S., Michetti, M., Sacco, O., Cakiroglu, A. G., Jackson, J. F., et al. (1987). Protein kinase C activity and hexamethylenebisacetamide-induced erythroleukemia cell differentiation. *Proc. Natl. Acad. Sci. U. S. A.* 84, 5282–5286. doi: 10.1073/pnas.84.15.5282

Mohanan, P., Subramaniyam, S., Mathiyalagan, R., and Yang, D. C. (2018). Molecular signaling of ginsenosides Rb1, Rg1, and Rg3 and their mode of actions. *J. Ginseng Res.* 42, 123–132. doi: 10.1016/j.jgr.2017.01.008

Nishizuka, Y. (1986). Studies and perspectives of protein kinase C. *Science* 233 (4761), 305–312. doi: 10.1126/science.3014651

Niu, H., Nie, L., Liu, M., Chi, Y., Zhang, T., and Li, Y. (2014). Benazepril affects integrin-linked kinase and smooth muscle alpha-actin expression in diabetic rat glomerulus and cultured mesangial cells. *BMC Nephrol.* 15, 135. doi: 10.1186/1471-2369-15-135

Nose, M., Tada, M., Kojima, R., Nagata, K., Hisaka, S., Masada, S., et al. (2017). Comparison of glycyrrhizin content in 25 major kinds of Kampo extracts containing Glycyrrhizae Radix used clinically in Japan. *J. Nat. Med.* 71, 711–722. doi: 10.1007/s11418-017-1101-x

Piccoli, G. B., Grassi, G., Cabiddu, G., Nazha, M., Roggero, S., Capizzi, I., et al. (2015). Diabetic kidney disease: A syndrome rather than a single disease. *Rev. Diabet. Stud.* 12, 87–109. doi: 10.1900/RDS.2015.12.87

Rani, R., Dahiya, S., Dhingra, D., Dilbaghi, N., Kim, K. H., and Kumar, S. (2017). Evaluation of anti-diabetic activity of glycyrrhizin-loaded nanoparticles in nicotinamide-streptozotocin-induced diabetic rats. *Eur. J. Pharm. Sci.* 106, 220–230. doi: 10.1016/j.ejps.2017.05.068

Sajan, M. P., and Farese, R. V. (2012). Insulin signalling in hepatocytes of humans with type 2 diabetes: excessive production and activity of protein kinase C-iota (PKC-iota) and dependent processes and reversal by PKC-iota inhibitors. *Diabetologia* 55, 1446–1457. doi: 10.1007/s00125-012-2477-5

Saleem, M. A. (2015). One hundred ways to kill a podocyte. *Nephrol. Dial. Transplant.* 30, 1266–1271. doi: 10.1093/ndt/gfu363

Sarkozy, M., Fekete, V., Szucs, G., Torok, S., Szucs, C., Barkanyi, J., et al. (2014). Anti-diabetic effect of a preparation of vitamins, minerals and trace elements in diabetic rats: a gender difference. *BMC Endocr. Disord.* 14, 72. doi: 10.1186/1472-6823-14-72

Sen, S., Roy, M., and Chakraborti, A. S. (2011). Ameliorative effects of glycyrrhizin on streptozotocin-induced diabetes in rats. *J. Pharm. Pharmacol.* 63, 287–296. doi: 10.1111/j.2042-7158.2010.01217.x

Sil, R., Ray, D., and Chakraborti, A. S. (2013). Glycyrrhizin ameliorates insulin resistance, hyperglycemia, dyslipidemia and oxidative stress in fructose-induced metabolic syndrome-X in rat model. *Indian J. Exp. Biol.* 51, 129–138.

Song, Z., Wu, Y., and Gao, H. (2015). Determination of neomangiferin, mangiferin, and isomangiferin in Anemarrhenae Rhizoma before and after stir-frying with salt-water by HPLC. *Drug Clinic.* 30, 145–148. doi: 10.7501/j.issn.1674-5515.2015.02.007

Tong, X. L., Dong, L., Chen, L., and Zhen, Z. (2012). Treatment of diabetes using traditional Chinese medicine: past, present and future. *Am. J. Chin. Med.* 40, 877–886. doi: 10.1142/S0192415X12500656

van Stee, M. F., de Graaf, A. A., and Groen, A. K. (2018). Actions of metformin and statins on lipid and glucose metabolism and possible benefit of combination therapy. *Cardiovasc. Diabetol.* 17, 94. doi: 10.1186/s12933-018-0738-4

Wang, W. W., Zhang, F. L., Chen, J. H., Chen, X. H., Fu, F. Y., Tang, M. R., et al. (2015). Telmisartan reduces atrial arrhythmia susceptibility through the regulation of RAS-ERK and PI3K-Akt-eNOS pathways in spontaneously hypertensive rats. *Can. J. Physiol. Pharmacol.* 93, 657–665. doi: 10.1139/cjpp-2014-0416

Wang, Z., Han, Z., Tao, J., Wang, J., Liu, X., Zhou, W., et al. (2017). Role of endothelial-to-mesenchymal transition induced by TGF-beta1 in transplant kidney interstitial fibrosis. *J. Cell Mol. Med.* 21, 2359–2369. doi: 10.1111/jcmm.13157

Wang, R., Li, Y., Huai, X. D., Zheng, Q. X., Wang, W., Li, H. J., et al. (2018). Design and preparation of derivatives of oleanolic and glycyrrhetinic acids with cytotoxic properties. *Drug Des. Dev. Ther.* 12, 1321–1336. doi: 10.2147/DDDT.S166051

Xiao, C., Yang, L., Zhang, L., Liu, C., and Han, M. (2016). Effects of cultivation ages and modes on microbial diversity in the rhizosphere soil of *Panax ginseng*. *J. Ginseng Res.* 40, 28–37. doi: 10.1016/j.jgr.2015.04.004

Xiao, Y. H., He, X. Y., Han, Q., Yang, F., and Zhou, S. X. (2018). Atorvastatin prevents glomerular extracellular matrix formation by interfering with the PKC signaling pathway. *Mol. Med. Rep.* 17, 6441–6448. doi: 10.3892/mmr.2018.8724

Xu, L., Ren, H., Gao, G., Zhou, L., Malik, M. A., and Li, P. (2016). The progress and challenges in metabolic research in China. *IUBMB Life*. 68, 847–853. doi: 10.1002/iub.1563

Yang, J., and Zhang, J. (2015). Influence of protein kinase C (PKC) on the prognosis of diabetic nephropathy patients. *Int. J. Clin. Exp. Pathol.* 8, 14925–14931.

Yuan, H., Ma, Q., Cui, H., Liu, G., Zhao, X., Li, W., et al. (2017). How can synergism of traditional medicines benefit from network pharmacology? *Molecules* 22 (7). doi: 10.3390/molecules22071135

Zhang, B., Yue, R., Chen, Y., Yang, M., Huang, X., Shui, J., et al. (2019). Gut microbiota, a potential new target for Chinese herbal medicines in treating diabetes mellitus. *Evid. Based Complement. Alternat. Med.* 2019, 2634898. doi: 10.1155/2019/2634898

Zhang, R., Zhu, X., Bai, H., and Ning, K. (2019). Network pharmacology databases for traditional Chinese medicine: review and assessment. *Front. Pharmacol.* 10, 123. doi: 10.3389/fphar.2019.00123

**Conflict of Interest:** The authors declare that the research was conducted in the absence of any commercial or financial relationships that could be construed as a potential conflict of interest.

frontiers in Pharmacology

ORIGINAL RESEARCH
published: 19 June 2020
doi: 10.3389/fphar.2020.00933

# Multi-Component Comparative Pharmacokinetics in Rats After Oral Administration of *Fructus aurantii* Extract, Naringin, Neohesperidin, and Naringin-Neohesperidin

*Jinbin Yuan[1]*, Feiting Wei[1], Xizhen Luo[1], Min Zhang[1,2], Rifa Qiao[1], Minyong Zhong[1], Haifang Chen[1] and Wuliang Yang[1]**

*[1] Key Laboratory of Modern Preparation of TCM, Ministry of Education, Jiangxi University of Traditional Chinese Medicine, Nanchang, China, [2] Nanchang Key Laboratory of Quality Control and Safety Evaluation of Traditional Chinese Medicine, Nanchang Institute for Food and Drug Control, Nanchang, China*

OPEN ACCESS

**Edited by:**
*Aiping Lu,*
*Hong Kong Baptist University, Hong Kong*

**Reviewed by:**
*Anurag Khatkar,*
*Maharshi Dayanand University, India*
*Fan Yang,*
*Henan University of Science and Technology, China*

***Correspondence:**
*Jinbin Yuan*
*kings2008@163.com*
*Wuliang Yang*
*yangwuliang@163.com*

**Specialty section:**
*This article was submitted to Ethnopharmacology, a section of the journal Frontiers in Pharmacology*

**Received:** *10 December 2019*
**Accepted:** *08 June 2020*
**Published:** *19 June 2020*

**Citation:**
*Yuan J, Wei F, Luo X, Zhang M, Qiao R, Zhong M, Chen H and Yang W (2020) Multi-Component Comparative Pharmacokinetics in Rats After Oral Administration of Fructus aurantii Extract, Naringin, Neohesperidin, and Naringin-Neohesperidin. Front. Pharmacol. 11:933. doi: 10.3389/fphar.2020.00933*

Citrus × aurantium L., Chinese name: *Fructus Aurantii* (FA) has been largely used as Qi-invigorating herb in China for centuries. The main components (meranzin hydrate, naringin, neohesperidin, meranzin, nobiletin) have good physiological activity with relatively high abundance in FA. Few multi-component comparative pharmacokinetics are simultaneously accessible for the flavone glycosides, polymethoxy flavones, and coumarins in FA. In this work, a reliable and rapid ultra-high performance liquid chromatography-tandem mass spectrometry (UPLC-MS/MS) method was established and validated to determine the five ingredients in the SD rat plasma, and further applied to the pharmacokinetic studies after oral administration of monomer, drugs in compatibility, and FA extract. After hydrolysis with $\beta$-glucuronidase and sulfatase, the concentration of naringin and neohesperidin in rat plasma were expressed respectively by the total concentration of naringenin and hesperitin which was determined by UPLC-MS/MS. Double-peak phenomenon was observed for naringin and neohesperidin, which may be due to the enterohepatic circulation or multiple site absorption of the two flavone glycosides. Meranzin hydrate and meranzin (coumarins) were absorbed rapidly ($T_{max,}$ about 1.0 h) but eliminated slowly ($t_{1/2z}$ exceeds 6.5 h). Nobiletin, a typical polymethoxy flavone, was also rapidly absorbed according to $T_{max}$ and $AUC_{(0\text{-}t)}$. DAS 3.1 software suggests the pharmacokinetic profiles of the five components in rats be depicted as a two-compartment pharmacokinetic model. There were significant differences in pharmacokinetic parameters for naringenin and hesperetin between the compatibility, FA extract group *vs* monomer group: ① remarkable increases in the values of $AUC_{(0-\infty)}$, $AUC_{(0-t)}$ and $C_{max}$; ② obvious decrease of $CL_{Z/F}$; and ③ longer $t_{max}$ and $t_{1/2z}$. The results suggest that compatibility can promote mutual absorption and affect the elimination behaviors.

**Keywords: Citrus × aurantium L., *Fructus aurantii*, naringin, neohesperidin, pharmacokinetics, ultra-high performance liquid chromatography-tandem mass spectrometry**

## INTRODUCTION

*Fructus aurantii* (FA), also called Zhiqiao in Chinese, refers to the dried unripe fruit of *Citrus* × *aurantium* L. or its cultivar (Rutaceae). FA is a very important Qi-invigorating herb in China for thousands of years, and it vigorously modulates the motion of Qi and fortifies the spleen and stomach (Committee of National Pharmacopoeia of RP China, 2015). Modern pharmacological researches have established that FA possesses astoundingly biomedical properties, such as prokinetic effect (Qiu et al., 2011; Zhou et al., 2018), antidepression activity (Wu et al., 2015), anti-inflammation function (Parhiz et al., 2015), anticarcinogenic activity (Park et al., 2014), antihepatotoxicity (Renugadevi and Prabu, 2010), antihypersensitivity (Kobayashi et al., 2015), and hypoglycemic and hypolipidemic effects (Jia et al., 2015). It is well known that the primary chemical compositions in FA are flavonoids, alkaloids, volatile oils, and coumarins (Li et al., 2016). In which the main bioactive compounds are considered to be naringin, neohesperidin, meranzin hydrate (MH), meranzin, Naringenin, hesperetin nobiletin, tangeretin, and auraptene (Qiu et al., 2011; Yuan et al., 2012; Li et al., 2016; Wang et al., 2018; Zhang et al., 2018; Chen et al., 2019).

The therapeutic effects of a drug and its components are closely related to their pharmacokinetic characteristics. The pharmacokinetics of naringin and/or neohesperidin have been extensively studied in rats (Felgines et al., 2000; Fang et al., 2006; Li et al., 2010; Lee et al., 2017; Zeng et al., 2019), dogs (Mata-Bilbao et al., 2007), rabbits (Hsiu et al., 2002), and human beings (Ishii et al., 1996; Ishii et al., 1997; Bai et al., 2020). Multi-component pharmacokinetics can also be accessible for several flavones in FA (Tong et al., 2012; Wang et al., 2018; Zhang et al., 2018). Very recently, the comparative pharmacokinetics of naringin and neohesperidin between different model rats (Xu et al., 2019) and different herbs (Li et al., 2019) have been reported. As a whole, the above pharmacokinetic evaluation mainly focused on pure monomers (mainly flavones) (Ishii et al., 1996; Ishii et al., 1997; Felgines et al., 2000; Hsiu et al., 2002; Fang et al., 2006; Mata-Bilbao et al., 2007; Li et al., 2010; Lee et al., 2017), the extract of a single herb (Tong et al., 2012; Wang et al., 2018; Zhang et al., 2018), or the study of the pharmacokinetic interaction between two or more herbs (Li et al., 2019; Xu et al., 2019). Few pharmacokinetic data can be accessible for the other compounds, such as MH, meranzin, and nobiletin.

Our previous study indicated that the components (MH, meranzin, and nobiletin) have good physiological activity with relatively high abundance in FA besides naringin and neohesperidin. We also found that the drug quality is closely related to the content proportion of naringin *vs* neohesperidin in FA, which can partly elucidate the geo-authentic origin of the medicinal plant (Chen et al., 2019). So, it is interesting to investigate the pharmacokinetic differences of naringin and neohesperidin between the different forms (monomer, compatibility, and extract).

Some literatures indicated that naringin and neohesperidin transiently exist in the plasma, and the glucuronides/sulfates of their aglycones (naringenin and hesperetin) were the main circulating metabolites (Felgines et al., 2000; Fang et al., 2006; Xu et al., 2019). Free naringenin and hesperetin can be easily obtained from the naringenin-glucronaide and hesperetin-glucronaide in plasma by hydrolysis with $\beta$-glucuronidase and sulfatase. In addition, naringenin and hesperetin are relatively low content in FA. So, the concentration of the absorbed naringin and neohesperidin can be detected in the corresponding aglycone form (naringenin and hesperetin).

Hence, a rapid and sensitive ultra-high performance liquid chromatography-tandem mass spectrometry (UPLC-MS/MS) method was developed and validated for the simultaneous determination of the main components (naringin, neohesperidin, MH, meranzin, and nobiletin) in rat plasma, and used for the pharmacokinetic study of the compounds in different forms: monomer, compatibility, and extract.

## MATERIALS AND METHODS

### Crude Drugs

*Fructus aurantii*, the dry immature fruit of *Citrus* × *aurantium* L., were provided by Jiangxi Zhihui Chinese Medicinal Materianls Co. Ltd. The coordinates of plant picking is 115.226067 East longitude and 28.030638 North latitude (Wucheng Town, Zhangshu, Jiangxi, China). The crude drugs were identified as *Citrus junos* Sieb. ex Tanaka by Professor Wuliang Yang from Jiangxi University of Traditional Chinese Medicine (JXUTCM), China. Voucher specimens are preserved in the Herbarium of Pharmacognosy in JXUTCM.

### Chemicals and Reagents

Standards including neohesperidin, naringin, meranzin hydrate, naringenin, hesperetin, meranzin, and nobiletin were purchased from Chengdu Desite Biotech Co., Ltd. (Chengdu, China), and their purities were not lower than 98% according to HPLC analysis. Quercetin (Internal standard, IS) (HPLC ≥ 98%) was purchased from Chengdu Mansite Pharmaceticcal Co., Ltd. (Chengdu, China). $\beta$-glucuronidase and sulfate esterase were purchased from Shanghai Yuanye Bio-Technology Co., Ltd. (Shanghai, China), Formic acid was purchased from Shanghai Aladdin Bio-Chem Technology Co. Ltd. (Shanghai, China). Chromatographic reagent Methanol (Merck, Germany) and acetonitrile (Tedia, USA) were used throughout. Deionized Water was purified by Milli-Q purification system (Millipore, MA, USA). All other chemical regents were of analytical grade.

### Apparatus and UPLC–MS/MS Conditions

The UPLC-MS/MS system consisting of Shimadzu Ultra-High Performance Liquid Chromatograph LC-30A and Triple Quadrupole Mass Spectrometer (LCMS-8050, SHIMADZU, Japan).

### Liquid Chromatography

The chromatographic separation was achieved on an Agilent $C_{18}$ column (2.1x100mm, 1.8μm, Agilent, United States) with temperature at 40°C; The mobile phase was composed of water (containing 0.1% formic acid) (solvent A) and Acetonitrile (solvent B). The gradient elution procedures (0.01–5 min, 30 to 50% B, 5–7min, 50% B, 7–7.5min, 50–30% B, 7.5–10.5min, 30% B); The flow rate was 0.3 ml/min and injection volume was 1.0 μl (Yuan et al., 2017).

### Mass Spectrometry

The mass spectrometer was operated in negative mode for quercetin (IS), naringenin, and hesperetin, and positive mode for meranzin hydrate, meranzin, nobiletin. Quantification was obtained using multiple reaction monitoring (MRM) mode in the following positive/negative MS/MS scan segments. Segment I: 1.5–2.3min in positive mode, meranzin hydrate; Segment II: 2.2–4.5min in negative mode quercetin (IS), naringenin, and hesperetin; Segment III: 4.4–7.5min in positive mode for meranzin and nobiletin. The optimal MS parameters were as follows: Interface ESI, Nebulizing Gas Flow of 3.0 L/min; Heating Gas Flow of 10 L/min; Interface Temperature of 300°C; DL Temperature of 250°C; Heat Block Temperature of 400°C; Drying Gas Flow of 10 L/min; Nebulizing Gas of 3.0 L/min, Drying Gas F1 of 10.0 L/min, Conversion Dy: 10 kV, Detector Volt: 1.92 kV. MS/MS operating conditions were optimized by infusion of the standard solution (200 ng/ml) of each analyte and I.S. into the ESI source *via* a syringe pump. The optimal MRM parameters for these compounds are shown in **Table 1**.

## Animals

Male Sprague-Dawley (SD) rats [Certificate No. SCXK(Xiang) 2016-0002] weighing 200 ± 20 g were purchased from Hunan Silaike Laboratory Animal Ltd (Changsha, China). The animals were kept in a controlled breeding room with the following conditions: a temperature of 22 ± 2°C, a relative humidity of (65 ± 5)%, and a 12 h light- dark cycle (Yuan et al., 2017). The Experimental Animal Ethic Committee of JXUTCM approved all animal protocols. The animal experiments were carried out according to the European Community guidelines for the use of experimental animals.

## Sample Preparation

### Preparation of FA Extract

The dried drug was extracted twice by refluxing with boiling Methanol (1:10, w/v) for 2 h, then the two filtrates were merged and evaporated to dryness under vacuum (Tong et al., 2012). The extract (14.56 g) was weighed and the extract yield was 29.14%. The obtained extract was stored at 4 °C until use. To count the dosage, the contents of the main compounds in the FA extract were quantitatively measured by HPLC (Zhang et al., 2018; Chen et al., 2019), and the contents of naringin, neohesperidin, meranzin hydrate, meranzin and nobiletin in the extract were 171.6, 167.5, 1.98, 0.94, and 1.70 mg/g raw herb, respectively (see supplementary material: **Figure S1**).

### Preparation of Calibration Standards and Quality Control (QC) Samples

The stock solutions of the mixed standards were prepared in methanol with the concentrations of meranzin hydrate (194 μg/ml), naringenin (491 μg/ml), hesperetin (494 μg/ml), meranzin (209 μg/ml), nobiletin (528 μg/ml), and quercetin (IS) (303 μg/ml). All solutions were stored at 4 °C. The concentrations of each analyte in standard mixture solutions were as follows: 19.4 μg/ml for meranzin hydrate, 14.73 μg/ml for naringenin, 12.35 μg/ml for hesperetin, 4.18 μg/ml for meranzin, and 2.112 μg/ml for nobiletin. Then, the standard mixture solution was diluted to a series of concentration (1/2, 1/5, 1/10, 1/20, 1/50, 1/100, 1/250, 1/500, 1/1,000, and 1/2,000) as calibration curves. QC samples were prepared at three concentration levels containing meranzin hydrate (19.4, 388, and 19,400 ng/ml), naringenin (14.73, 294.6, and 14,730 ng/ml), hesperetin (12.35, 247, and 12,350 ng/ml), meranzin (4.18, 83.6, and 4,180 ng/ml), and nobiletin (2.112, 42.2, and 2,112 ng/ml). These samples were stored at −80°C until analysis.

### Biological Sample Preparation

The 20 μl of $\beta$-glucuronidase and 15 μl of sulfatase were added into 50 μl of plasma sample. After vortexed for 30 s, the mixture was incubated at 37°C for 2 h in a water bath, then placed in ice water for 5 min to terminate the reaction (Xu et al., 2019). IS solution (20 μl, 5 μg/ml) and acetonitrile (1.0 ml) were added into the mixture and vortexed for 2 min. The mixture was centrifuged at 4,000 rpm at 4°C for 10 min, and the supernatant (850 μl) was transferred into a new eppendorf tube and evaporated to dryness. The residue was redissolved in 100 μl of 50% methanol, and vortexed for 3 min, then centrifuged at 14,000 rpm at 4°C for 10 min, finally the supernatant was used for UPLC-MS/MS analysis.

## Method Validation

This method was validated according to the current US FDA Bioanalytical Method Validation Guidance (Guidance for Industry: Bioanalytical Method Validation, 2001). The

**TABLE 1** | MRM detection parameters for the five components and IS.

| Components | Precursor ion | $Q_1$ (V) | Collision energy (eV) | $Q_3$ (V) | Product ion |
|---|---|---|---|---|---|
| Meranzin hydrate | 279.10 | -13.00 | -33.00 | -25.0 | 131.10 |
| Naringenin | 271.10 | 13.00 | 18.00 | 14.00 | 151.05 |
| Hesperetin | 301.05 | 15.00 | 24.00 | 15.00 | 164.05 |
| Meranzin | 261.10 | -12.00 | -29.00 | -26.0 | 131.10 |
| Nobiletin | 403.15 | -18.00 | -28.00 | -27.00 | 373.10 |
| Quercetin (IS) | 301.10 | 14.00 | 22.00 | 13.00 | 151.00 |

following parameters were determined: selectivity, linearity, LLOQ, LOD, precision, accuracy, extraction recovery, matrix effect, and stability.

### Linearity Parameters

To assess the linearity ranges, a series of the mixed standard solutions (six concentration levels) were prepared in triplicate. Each calibration curve (y = ax + b) was established by plotting the peak area ratio of analyte to IS (y) against the concentrations (x) of the calibration solution with a least square linear regression. The limit of detection (LOD) and limit of quantification (LOQ) were determined when the peak height was three times and ten times the background noise, respectively (Yuan et al., 2017).

### Specificity and Selectivity

Blank plasma samples or the samples spiked with the IS were detected for endogenous or IS interference (Zhang et al., 2018). Specificity and selectivity were investigated by comparing the chromatograms of five individual batches of blank plasma samples, the samples spiked with the 5 analytes and IS, and plasma samples at 0.75 h after oral administration of FA extracts.

### Accuracy and Precision

The intra- and inter-day precisions and accuracies were calculated by an analysis of variance based on the replicate analysis of QC samples, and the work was accompanied by a standard calibration curve on each analytical run (Yuan et al., 2017). Five samples were measured for each concentration level on the optimal conditions five times within the same day for intra-day variance, and the three different days for inter-day variance. The analytic precision was denoted as the RSD (relative standard deviation), and the accuracy was considered the RE (relative error) of the measured average deviated from the nominal value. The precision and accuracy values (RSD%) were required to be within ±20% for LLOQ (lower limit of quantification) and within ±15% for other concentrations.

### Extraction Recovery and Matrix Effect

The extraction recoveries of the compounds were assessed by comparing the mean peak areas from five plasma samples in the pre-extraction spiked with the analytes and the post-extraction at three QC levels. The matrix effects were evaluated by comparing the peak areas obtained from the spiked plasma matrix with the pure standard solutions at the same concentrations. There was no matrix effect if the ratio was between 85–115%.

### Stability

The QC samples were assayed under several different conditions to evaluate the stability of the compounds in rat plasma. For the short-term stability, fresh plasma samples were kept at room temperature for 24 h before the sample preparation. After keeping the samples at room temperature for 24 h, post-preparation stability was tested. Freeze-thaw cycles (-20 °C/room temperature) stability were not treated at -20°C for freezing-room temperature melting three times (repeated freezing and thawing three times). In each freeze-thaw cycle, the samples were frozen and stored at -20 °C for 24 h, and subsequently thawed at room. To evaluate the long-term stability of QC plasma samples, following storage at -20 °C for one month. The stability data were acceptable when the bias was within ±15% of the actual value (Yuan et al., 2017).

## Pharmacokinetics

Rats were randomly divided into the following four groups (6 rats in each group): naringin (NA), neohesperidin (NHE), naringin-neohesperidin (NA-NHE), and FA extract group. The oral administration doses were selected according to the literatures (Tong et al., 2012; Yang et al., 2012; Committee of National Pharmacopoeia of RP China, 2015; Wang et al., 2018; Zhang et al., 2018; Chen et al., 2019), the contents of the five components in FA, and the preliminary experiments. The specific doses were as follows: FA extract (10.8 g/kg of the original medicinal material), 10 ml/kg; naringin and neohesperidin, 1.85 g/kg and 1.81 g/kg, respectively. The drug was suspended in 0.5% CMC-Na.

Blood samples (about 0.5 ml) were collected from the ocular vein using dried heparinized tubes from each six rats at 0, 0.083, 0.167, 0.25, 0.5, 0.75, 1, 1.5, 2.0, 4.0, 6.0, 8.0, 10.0, 12.0, 14.0, 24.0, and 30.0 h after dosing. The rats were intragastric administrated with 1.5 ml of water at the time points of 0.25, 0.5, 2, 4, and 6 h, respectively. The rats had free access to water during the experiment. The blood samples were then immediately centrifuged at 4,000 rpm for 10 min. The plasma was frozen and stored at −80°C until analysis.

The plasma concentration of the studied compounds was determined according to the daily calibration curve. The pharmacokinetic parameters, including $C_{max}$ (the peak drug plasma concentration), $T_{max}$ (the time to $C_{max}$), $AUC_{(0\text{-}t)}$ (the area under the plasma concentration-time curve from 0 to the last time point), $AUC_{(0-\infty)}$ (the area under the plasma concentration-time curve from 0 to time infinity), $MRT_{(0-t)}$ (average residence time from 0 to the last time point), and $t_{1/2z}$ (the elimination half-life) were fitted with the proprietary DAS 3.1 pharmacokinetic program (Chinese Pharmacological Society).

## Statistical Analysis

All statistical analyses were performed using the SPSS 21.0 software package from SPSS, Inc. (Chicago, IL, USA). **P* values < 0.05, or ***P* values < 0.01 was considered statistically significant difference.

# RESULTS

## UPLC-MS/MS Conditions

According to the direct full-scan ESI mass spectra, the ion intensities of naringenin, hesperetin, and quercetin (IS) was higher in negative mode, and the other three compounds (meranzin hydrate, meranzin, and nobiletin) got greater sensitivity in positive mode. So, the switch scan method (ESI +/-) was used for the corresponding compounds, and the

product ion mass spectra of the six compounds are shown in **Figure 1**.

Based on previous work, chromatographic conditions such as the constituents and the gradient profiles of the mobile phase were further improved to adapt the separation and detection of six components in rat plasma. In addition, the optimum mobile phase was water (containing 0.1% formic acid) and acetonitrile.

Various sample preparation methods including protein precipitation with methanol and acetonitrile were investigated to obtain an efficient cleanup of the biological samples. In this work, acetonitrile was chosen as the protein precipitation agent with simplicity and efficiency.

## Specificity

Typical chromatograms of blank, spiked plasma and plasma samples are shown in **Figure 2**. No interference was found between endogenous compounds or xenobiotics. The developed method results in six single sharp peaks at the retention time of meranzin hydrate, quercetin (IS), naringenin, hesperetin, meranzin, and nobiletin were 2.03, 2.46, 3.29, 3.63, 5.09, and 5.84 min, respectively.

## Linearity Parameters

The linearity parameters of the five components in rat plasma using weighed ($1/x^2$) least-squares linear regression analysis are summarized in **Table 2**. Within the investigated linear range, good linearity data was obtained with correlation coefficients >0.9941. The results indicate the proposed UPLC-MS/MS method has a wide linear range and high sensitivity.

## Precision and Accuracy

The precision and accuracy results are shown in **Table 3**, intra-day precision was less than 7.9%, intra-day accuracy was between -8.66 to 9.68%, and inter-day precision was less than 10% for the five compounds. Inter-day accuracies were in the range of -9.34–9.94% expressed by relative errors (RE%). The relative standard deviation and relative error values did not exceed ± 15% (**Table 3**), this indicate the accuracy and precision are acceptable.

## Extraction Recovery and Matrix Effect

The extraction recovery and matrix effect were summarized in **Table 4**. The recoveries were between 82.33 to 89.92%, and the matrix effects of the five compounds were in the range of 94.36–101.65%. These data indicate that the UPLC-MS/MS method provides suitable, reproducible, and reliable data and can be used as an analytical tool in rat plasma.

## Stability

The stability data under different experimental conditions are summarized in **Table 5**. The results showed all RSD% were less than 8.8% and RE% were in the range from -13.50 to 14.81%, which suggested that rat plasma samples containing 5 analytes were stable under routine laboratory conditions and no additional procedures were necessary to stabilize the sample for pharmacokinetic studies.

## Pharmacokinetics

The proposed UPLC-MS/MS method was applied to a multi-component pharmacokinetic study of meranzin hydrate, naringenin, hesperetin, meranzin, and nobiletin in SD rats after oral administration of the extract, NA, NHE, and NA-NHE. The plasma concentration-time profiles of the five

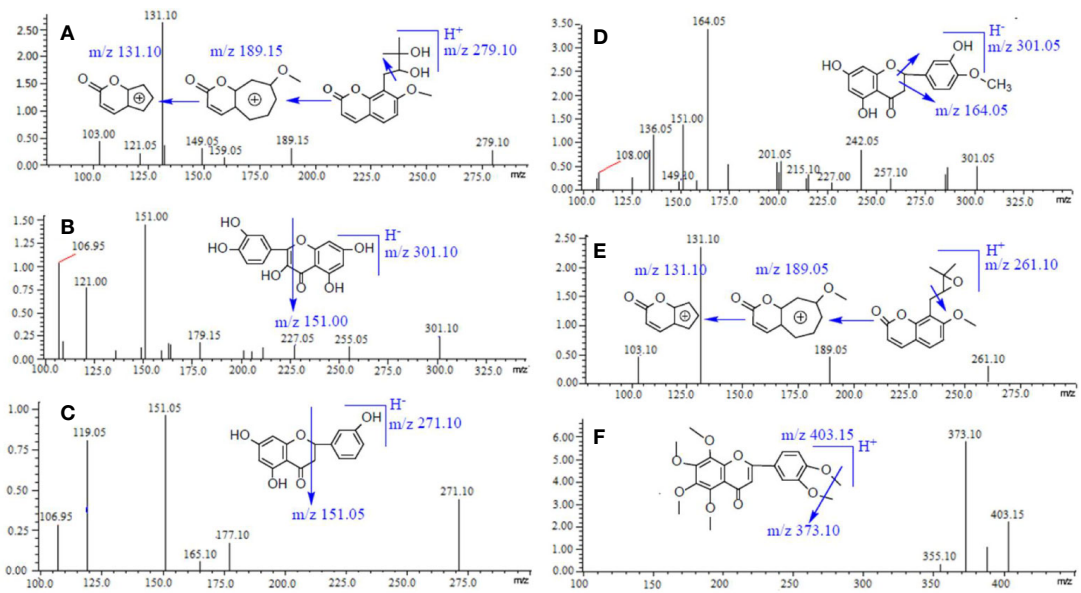


**FIGURE 1 |** Chemical structures and product ion mass spectra of Meranzin hydrate **(A)**, Quercetin (IS) **(B)**, Naringenin **(C)**, Hesperidin **(D)**, Meranzin **(E)**, and Nobiletin **(F)**.

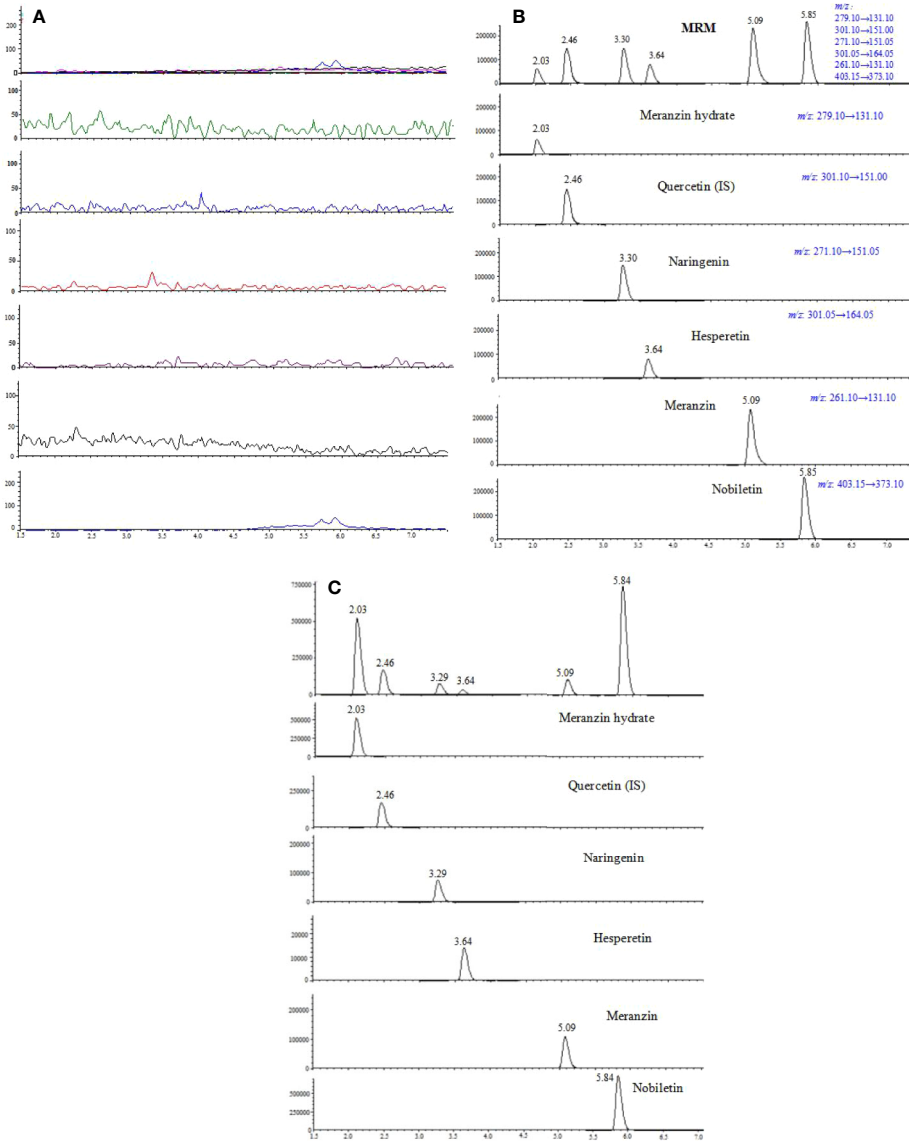


**FIGURE 2 |** Representative multiple reaction monitoring (MRM) chromatograms of meranzin hydrate, naringenin, hesperetin, meranzin, nobiletin, and quercetin (IS) in rat plasma: **(A)** blank plasma, **(B)** blank plasma spiked with the 5 analytes and quercetin (IS), and **(C)** plasma sample collected at 0.75 h after oral administration of FA extract (10.8 g/kg) to rats.

**TABLE 2 |** Linear parameters of the compounds in rat plasma.

| Components | Calibration curves | Correlation coefficients | Range (ng/mL) | LLOQ (ng/mL) | LOD (ng/mL) |
|---|---|---|---|---|---|
| Meranzin hydrate | $y = 0.001x + 0.0653$ | $r^2 = 0.9941$ | 1.94 ~ 3880 | 1.94 | 0.59 |
| Naringenin | $y = 0.0021x + 0.0383$ | $r^2 = 0.9981$ | 1.473 ~ 2946 | 1.473 | 0.45 |
| Hesperetin | $y = 0.0017x - 0.0031$ | $r^2 = 0.9994$ | 1.235 ~ 2470 | 1.235 | 0.37 |
| Meranzin | $y = 0.0207x - 0.0033$ | $r^2 = 0.9998$ | 0.418 ~ 836 | 0.418 | 0.13 |
| Nobiletin | $y = 0.0778x - 0.1077$ | $r^2 = 0.9961$ | 0.2112 ~ 422.4 | 0.2112 | 0.06 |

components were shown in **Figure 3**, and the corresponding pharmacokinetic parameters were shown in **Tables 6** and **7**. The physiological disposition conformed to a two-compartment model of the 5 analytes in rats fitted by the DAS 3.1 software. The results suggested that there were significant differences in pharmacokinetic parameters of naringenin and hesperetin between different drug forms, including $AUC_{(0-t)}$, $AUC_{(0-\infty)}$, $C_{max}$, $t_{max}$, $t_{1/2z}$, and $CL_{Z/F}$. The main differences including

**TABLE 3 |** Intra-day and inter-day precisions and accuracies of the analytes from QC samples prepared in rat plasma (n=6).

| Components | Spiked concentration (ng/mL) | Intra-day | | | Inter-day | | |
|---|---|---|---|---|---|---|---|
| | | Concentration measured (ng/mL) | Precision (RSD,%) | Accuracy (RE,%) | Concentration measured (ng/mL) | Precision (RSD,%) | Accuracy (RE,%) |
| Meranzin hydrate | 3.88 | 3.94 ± 0.10 | 2.6 | 1.52 | 3.98 ± 0.24 | 6.0 | 2.65 |
| | 77.6 | 73.57 ± 5.77 | 7.8 | 5.19 | 71.38 ± 4.24 | 6.0 | -8.01 |
| | 3880 | 3557.39 ± 20.27 | 0.6 | 8.31 | 3517.64 ± 56.07 | 1.6 | -9.34 |
| Naringenin | 2.946 | 2.92 ± 0.16 | 5.6 | -0.98 | 2.97 ± 0.21 | 7.2 | 0.69 |
| | 58.92 | 64.03 ± 3.83 | 6.0 | 8.68 | 63.79 ± 4.18 | 6.6 | 8.27 |
| | 2946 | 2981.99 ± 39.27 | 1.3 | 1.22 | 2969.13 ± 58.10 | 2.0 | 0.78 |
| Hesperetin | 2.47 | 2.62 ± 0.06 | 2.3 | 6.02 | 2.56 ± 0.15 | 5.8 | 3.50 |
| | 49.4 | 51.38 ± 3.35 | 6.5 | 4.01 | 50.37 ± 3.96 | 7.9 | 1.96 |
| | 2470 | 2320.26 ± 10.40 | 0.5 | -6.06 | 2296.49 ± 31.09 | 1.4 | 7.02 |
| Meranzin | 0.836 | 0.78 ± 0.06 | 7.2 | -6.18 | 0.76 ± 0.05 | 6.5 | -9.27 |
| | 16.72 | 15.27 ± 0.72 | 4.7 | -8.66 | 15.25 ± 1.00 | 6.6 | -8.80 |
| | 836 | 829.63 ± 7.05 | 0.9 | -0.76 | 823.28 ± 11.34 | 1.4 | -1.52 |
| Nobiletin | 0.4424 | 0.41 ± 0.03 | 7.9 | -4.01 | 0.42 ± 0.05 | 10 | 0.29 |
| | 8.44 | 9.26 ± 0.29 | 3.2 | 9.68 | 9.28 ± 0.44 | 4.8 | 9.94 |
| | 422.4 | 410.48 ± 26.76 | 6.5 | -2.82 | 376.29 ± 32.40 | 8.6 | -10.92 |

**TABLE 4 |** Extraction recovery and matrix effects of the analytes in rat plasma (n = 6).

| Components | Concentration (ng/mL) | Extraction recovery (%) | | Matrix effect (%) | |
|---|---|---|---|---|---|
| | | Mean ± SD | RSD(%) | Mean ± SD | RSD(%) |
| Meranzin hydrate | 7.76 | 83.44 ± 5.37 | 6.4 | 100.28 ± 6.14 | 6.1 |
| | 77.6 | 87.89 ± 6.33 | 7.2 | 100.94 ± 4.85 | 4.8 |
| | 776 | 88.13 ± 3.40 | 3.5 | 97.88 ± 4.45 | 4.5 |
| Naringenin | 5.892 | 82.33 ± 1.58 | 1.9 | 94.36 ± 4.85 | 5.1 |
| | 58.92 | 86.12 ± 4.02 | 4.7 | 98.34 ± 6.36 | 6.5 |
| | 589.2 | 89.33 ± 1.88 | 2.1 | 100.31 ± 4.86 | 4.8 |
| Hesperetin | 4.94 | 87.79 ± 4.51 | 5.1 | 95.95 ± 7.08 | 7.4 |
| | 49.4 | 89.15 ± 6.10 | 6.8 | 99.51 ± 4.62 | 4.6 |
| | 494 | 88.93 ± 3.17 | 3.6 | 98.64 ± 1.65 | 1.7 |
| Meranzin | 1.672 | 82.97 ± 5.88 | 7.1 | 101.08 ± 4.97 | 4.9 |
| | 16.72 | 88.50 ± 4.46 | 5.0 | 96.90 ± 5.39 | 5.6 |
| | 167.2 | 88.04 ± 3.40 | 3.9 | 98.84 ± 7.72 | 7.8 |
| Nobiletin | 0.8448 | 83.63 ± 0.06 | 7.7 | 101.65 ± 6.80 | 6.7 |
| | 8.44 | 89.92 ± 1.78 | 2.0 | 100.17 ± 6.86 | 6.9 |
| | 84.48 | 89.85 ± 2.20 | 2.4 | 99.16 ± 6.83 | 6.9 |

**TABLE 5 |** Stability of the 5 analytes in rat plasma (n = 6).

| Components | Concentration (ng/mL) | Short-term Stability | | Free–thaw Stability | | Long-term Stability | |
|---|---|---|---|---|---|---|---|
| | | RSD (%) | RE (%) | RSD (%) | RE (%) | RSD (%) | RE (%) |
| Meranzin hydrate | 3.88 | 7.2 | 4.71 | 4.6 | 5.77 | 5.9 | 7.62 |
| | 77.6 | 1.9 | 1.55 | 3.8 | 0.71 | 2.2 | 3.19 |
| | 3880 | 0.5 | 7.43 | 1.5 | 7.63 | 2.6 | 6.85 |
| Naringenin | 2.946 | 2.8 | -3.02 | 0.3 | -4.36 | 7.6 | -0.84 |
| | 58.92 | 1.2 | 14.81 | 2.8 | 8.14 | 1.2 | 12.09 |
| | 2946 | 3.9 | -13.49 | 3.5 | -10.94 | 4.2 | -9.76 |
| Hesperetin | 2.47 | 7.6 | 4.10 | 10 | 7.78 | 4.7 | 5.03 |
| | 49.4 | 5.6 | -9.20 | 5.0 | -10.70 | 4.3 | -8.58 |
| | 2470 | 8.7 | -13.50 | 8.0 | -12.68 | 5.3 | -7.81 |
| Meranzin | 0.836 | 2.7 | -6.25 | 1.6 | -9.71 | 4.9 | -10.98 |
| | 16.72 | 13 | -8.40 | 1.6 | 11.07 | 8.8 | -13.52 |
| | 836 | 2.1 | -2.81 | 2.6 | -6.01 | 5.9 | -7.37 |
| Nobiletin | 0.4224 | 1.1 | 7.01 | 8.2 | 2.21 | 4.9 | 5.83 |
| | 8.44 | 4.3 | 7.89 | 2.5 | 10.46 | 3.9 | 6.71 |
| | 422.4 | 0.3 | 0.80 | 0.3 | -1.72 | 1.7 | -3.36 |

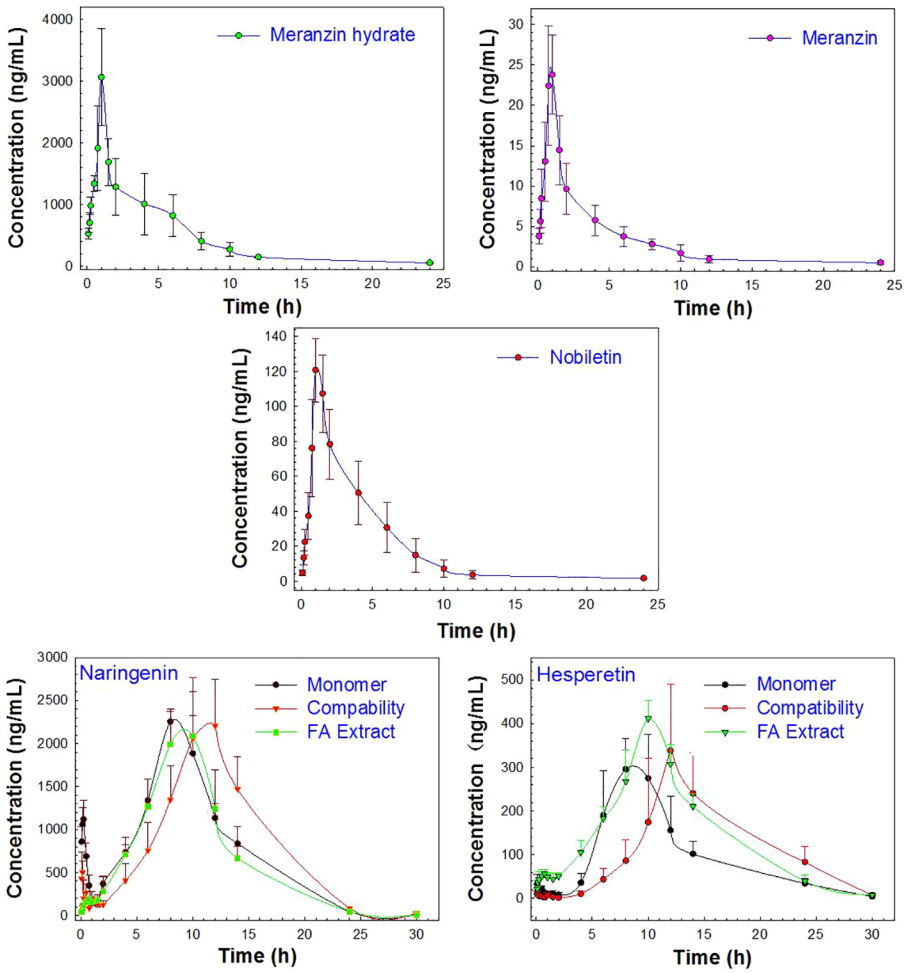


**FIGURE 3 |** The profiles of the mean plasma concentration over time after oral administration of the monomer (NA or NHE), the compatibility (NA-NHE), and FA extract (FA) form (mean ± SD, n = 6).

remarkable increases in the values of $AUC_{(0-\infty)}$, $AUC_{(0-t)}$ and $C_{max}$, obvious decrease of $CL_{Z/F}$, and longer $t_{max}$ and $t_{1/2z}$. The comparisons of $C_{max}$ and $AUC_{(0-t)}$ of different groups were shown in **Figure 4**.

## DISCUSSION

UPLC-MS/MS is a powerful analytical tool for the trace compounds in biosamples with high selectivity and sensitivity (Yuan et al., 2017). Various influencing factors were investigated carefully including separation and detection conditions in this work, and the optimal analytical parameters were obtained for the studied analytes. In addition, the mass spectrometer can be switched freely between ESI (Electro-spray Ionization) +/- detection modes in a single injection, and it ensures that each analyte can get the best response. Therefore, the developed method achieved higher sensitivity than the literatures did with lower LODs (see **Table 2**).

A study (Wang et al., 2018) has reported that flavone glycosides (naringin, hesperidin, and neohesperidin) could not been detected in the rat plasma even after orally administering 30 g/kg FA decoction, which might be associated with the hydrolysis caused by microbial bacterial from the gastrointestinal tract (Hsiu et al., 2002). Naringin can be quickly absorbed, and metabolized into its aglycone and naringenin glucuronide. Hesperidin was also quickly transferred to hesperetin due to the similar structure (Hu et al., 2015; Wang et al., 2018). In general, naringin and hesperidin are hydrolyzed in the gastrointestinal tract by the enzymes of intestinal bacteria followed by absorption and conjugation of their aglycones, and the main present forms are naringenin and hesperitin glucuronide/sulfatase conjugations and a small amount of the free aglycones in plasma (Xu et al., 2019). Therefore, the concentration of naringin and neohesperidin in mouse plasma were expressed respectively by the total (free + conjugated) concentration of naringenin and hesperitin which was determined by UPLC-MS/MS after hydrolysis with $\beta$-glucuronidase and sulfatase in this work.

**TABLE 6 |** Pharmacokinetic parameters of the 5 compounds in male SD rats after oral administration of FA extract (mean ± SD, n = 6).

| Parameter | Components | | | | |
|---|---|---|---|---|---|
| | **Meranzin hydrate** | **Naringenin** | **Hesperetin** | **Meranzin** | **Nobiletin** |
| $C_{max}$ (μg/L) | 3356.68 ± 91.03 | 2448.08 ± 225.62 | 424.89 ± 11.13 | 27.74 ± 2.85 | 130.28 ± 4.78 |
| $T_{max}$ (h) | 0.96 ± 0.10 | 9.33 ± 1.03 | 9.67 ± 0.82 | 0.92 ± 0.13 | 1.17 ± 0.26 |
| $t_{1/2z}$ (h) | 6.50 ± 1.20 | 2.56 ± 0.17 | 3.40 ± 0.46 | 6.52 ± 0.63 | 2.10 ± 0.37 |
| $AUC_{(0-t)}$ (μg/L*h) | 11091.22 ± 2824.56 | 19617.11 ± 2623.90 | 4295.33 ± 314.81 | 76.90 ± 14.69 | 472.64 ± 118.70 |
| $AUC_{(0-\infty)}$ (μg/L*h) | 11620.50 ± 2763.67 | 19651.18 ± 2634.06 | 4337.25 ± 325.91 | 80.41 ± 15.49 | 480.11 ± 116.51 |
| $MRT_{(0-t)}$ (h) | 5.17 ± 0.34 | 9.71 ± 0.56 | 11.42 ± 0.37 | 4.82 ± 0.76 | 4.23 ± 0.50 |
| $MRT_{(0-\infty)}$ (h) | 6.57 ± 0.95 | 9.75 ± 0.56 | 11.65 ± 0.42 | 6.39 ± 2.22 | 4.80 ± 0.99 |
| $V_{z/F}$ (L/kg) | 9.36 ± 3.56 | 2.06 ± 0.29 | 12.24 ± 1.67 | 476.8 ± 70.2 | 150.97 ± 46.98 |
| CLz/F (L/h/kg) | 0.97 ± 0.23 | 0.56 ± 0.08 | 2.50 ± 0.18 | 138.66 ± 27.24 | 23.60 ± 5.67 |

**TABLE 7 |** Pharmacokinetic parameters of naringin (NA) and neohesperidin (NHE) after oral administration of monomer, the compatibility of NA-NHE, and FA extract form (mean ± SD, n = 6).

| Parameter | Groups of NA | | | Groups of NHE | | |
|---|---|---|---|---|---|---|
| | **NA** | **NA-NHE** | **FA** | **NHE** | **NA-NHE** | **FA** |
| $C_{max}$ (μg/L) | 2317.25 ± 130.51 | 2573.79 ± 158.38* | 2448.08 ± 225.62 | 358.85 ± 14.09 | 419.73 ± 9.88** | 424.89 ± 11.13** |
| $T_{max}$ (h) | 8.67 ± 1.03 | 11.33 ± 1.03 | 9.33 ± 1.03 | 9.00 ± 1.10 | 12.00 ± 1.27 | 9.67 ± 0.82 |
| $t_{1/2z}$ (h) | 2.70 ± 0.23 | 2.80 ± 0.35 | 2.56 ± 0.17 | 4.35 ± 0.81 | 3.13 ± 0.29 | 3.40 ± 0.46 |
| $AUC_{(0-t)}$ (μg/L*h) | 21336.35 ± 2347.74 | 23670.00 ± 3087.55 | 19617.11 ± 2623.90 | 2848.13 ± 395.44 | 3448.04 ± 552.57 | 4295.33 ± 314.81** |
| $AUC_{(0-\infty)}$ (ug/L*h) | 21386.91 ± 2368.44 | 23776.17 ± 3078.88 | 19651.18 ± 2634.06 | 2903.91 ± 396.58 | 3488.92 ± 571.92 | 4337.25 ± 325.91 |
| $MRT_{(0-t)}$ (h) | 9.59 ± 0.29 | 11.48 ± 0.51 | 9.71 ± 0.56 | 11.29 ± 0.93 | 14.60 ± 1.30 | 11.42 ± 0.37 |
| $MRT_{(0-\infty)}$ (h) | 9.65 ± 0.30 | 11.58 ± 0.52 | 9.75 ± 0.56 | 11.88 ± 1.04 | 14.81 ± 1.40 | 11.65 ± 0.42 |
| $V_{z/F}$ (L/kg) | 0.34 ± 0.04 | 0.32 ± 0.06 | 2.06 ± 0.29 | 3.96 ± 1.66 | 2.38 ± 0.31 | 12.24 ± 1.67 |
| CLz/F (L/h/kg) | 0.09 ± 0.01 | 0.08 ± 0.01 | 0.56 ± 0.08 | 0.63 ± 0.09 | 0.53 ± 0.10 | 2.50 ± 0.18 |

**P < 0.05, **P < 0. 01 for NA-NHE group & FA extract group vs monomer group.*

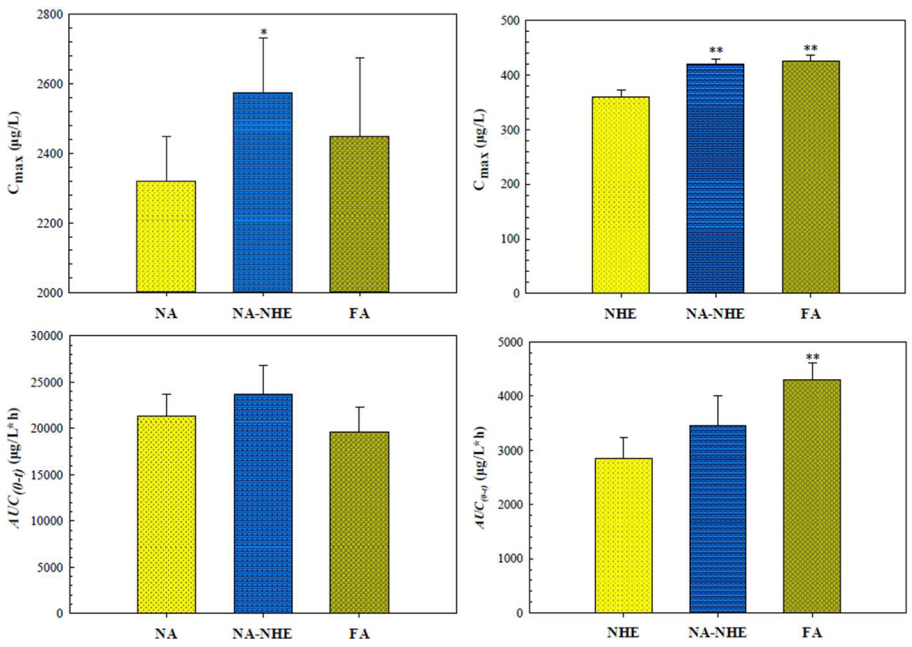


**FIGURE 4 |** Comparison of $C_{max}$ and $AUC_{(0-t)}$ of naringin (NA) and neohesperidin (NHE) after oral administration of monomer (NA or NHE), the compatibility (NA-NHE), and FA extract (FA) form. (mean ± SD, n = 6). **P* < 0.05, ***P* < 0. 01 for NA-NHE group & FA extract group *vs* monomer group.

As shown in **Figure 3**, the change trend in concentration-time profiles of naringenin and hesperetin are basically consistent with previous reports (Xu et al., 2010; Tong et al., 2012; Xu et al., 2019): both had double peaks. The double-peak phenomenon may be due to the enterohepatic circulation and drug reabsorption of naringin and neohesperidin in rats, which was also reported for other flavonoid glycosides from the extract of TCM (Ma et al., 2006; Lu et al., 2007; Zhang et al., 2012; Okada et al., 2017). In addition, these components can be detected in rat plasma within 5 min after dosing with a short $T_{max}$ (less than 1 h), and which indicates that they be absorbed easily and rapidly after oral administration. The values of $C_{max}$ and AUC of naringenin and hesperitin are relatively big, which indicates their bioavailability is not as low as reported in the literatures (Ma et al., 2006). The metabolic behaviors of the flavonoid glycosides might also be explained by the enterohepatic circulation or multiple site absorption (Wang et al., 2016). Meanwhile, the double-peak phenomenon and the so-called low bioavailability might also suggest that the reabsorption of the metabolites secreted in bile for FA should be more obvious.

Meranzin hydrate and meranzin, as the typical coumarins, were absorbed rapidly ($T_{max}$, about 1 h) but eliminated slowly ($t_{1/2z}$ exceeds 6.5 h). Nobiletin, a polymethoxy flavone, was also rapidly absorbed with $T_{max}$ value of 1.17 ± 0.26 h and $AUC_{(0\text{-}t)}$ value of 472.64 ± 118.70, which was consistent with the previous report (Onoue et al., 2013; Shen et al., 2019). The average $t_{1/2z}$ of nobiletin was 2.10 ± 0.37 h in rats, suggested that nobiletin should be rapidly distributed and eliminated (Shen et al., 2019), which was partly different from the previous report, probably owing to the interactions among components in FA extract (Qiao et al., 2012; Zhang et al., 2018).

Statistical moment analysis (corresponding to non-compartmental model) and compartmental model analysis can be simultaneously performed in a run of batch analysis by DAS 3.1. In the current *in vivo* data analysis, the non-compartmental model has become the mainstream processing method and has been recommended by the drug review authorities in various countries (Yuan et al., 2017; Xu et al., 2019). In particular, the statistical moment analysis is more reliable for the drugs with double-peak phenomena. In this work, naringenin and hesperetin are found to have exactly these pharmacokinetic properties. So, the statistical moment parameters are shown in **Tables 6** and **7**. In the compartmental model analysis, various models and different statistical weights were compared in this work, and two-compartment parameters were found to be the optimal fitting values with the minimum AIC (Akaike's Information Criterion) and the best R (correlation coefficient) values (Yuan et al., 2017; Yang et al., 2019). The compartmental model parameters are shown in **Tables S1** and **S2**.

As mentioned above, the pharmacokinetic characteristics of naringenin and hespeietin are closely related with enterohepatic circulation or multiple site absorption/reabsorption, which indicates their pharmacokinetics may be affected by the forms in which they exist. Therefore, we design the following four groups to investigate the effects: pure monomer (naringenin and hesperitin), compatibility (NA-NHE), and FA extract group. The results demonstrated that there were significant differences in pharmacokinetic parameters between different drug forms, including $AUC_{(0-t)}$, $AUC_{(0-\infty)}$, $C_{max}$, $t_{max}$, $t_{1/2z}$, and $CL_{Z/F}$. The main differences were observed between the compatibility group and the other two groups: ① remarkable increases in the values of $AUC_{(0-\infty)}$, $AUC_{(0-t)}$ and $C_{max}$; ② obvious decrease of $CL_{Z/F}$; and ③ longer $t_{max}$ and $t_{1/2z}$. The comparisons of $C_{max}$ and $AUC_{(0-t)}$ between different groups were shown in **Figure 4**. The results suggest that compatibility can promote mutual absorption and affect the metabolic behaviors. Drug-drug interactions often occur, and the detailed effect of compatibility on the pharmacokinetics needs further study.

## CONCLUSION

The proposed UPLC-MS/MS method was suitable for the accurate determination of meranzin hydrate, naringenin, hesperetin, meranzin, and nobiletin in rat plasma with high selectivity and sensitivity. The analytical method has been successfully used for the pharmacokinetic studies following oral administration of monomer, drugs in compatibility, and FA extract. The five components in FA can rapidly be absorbed. Drug compatibility can promote mutual absorption and affect the metabolic behaviors.

## DATA AVAILABILITY STATEMENT

All datasets generated for this study are included in the article/ **Supplementary Material**.

## ETHICS STATEMENT

The animal study was reviewed and approved by The Experimental Animal Ethic Committee of Jiangxi University of Traditional Chinese Medicine.

## AUTHOR CONTRIBUTIONS

JY, FW, and WY conceived and designed the experiments. FW, XL, RQ, MZha, MZho, and HC performed the experiments. FW, JY, and WY analyzed the data. JY and FW wrote the paper. All authors contributed to the article and approved the submitted version.

## FUNDING

This work was financially supported by the National Natural Science Foundation of China (No. 81860698 and 81760680) and the Double First-class Discipline of Jiangxi Province (No. JXSYLXK-ZHYAO064).

## ACKNOWLEDGMENTS

Junwei He (Research Center for the Resourcing of Traditional Chinese Medicine and Minority Medicine, Jiangxi University of Traditional Chinese Medicine) kindly provided some standards, such as quercetin.

## SUPPLEMENTARY MATERIAL

The Supplementary Material for this article can be found online at: https://www.frontiersin.org/articles/10.3389/fphar.2020.00933/full#supplementary-material

## REFERENCES

Bai, Y., Peng, W., Yang, C. P., Zou, W., Liu, M. H., Wu, H., et al. (2020). Pharmacokinetics and metabolism of naringin and active metabolite naringenin in rats, dogs, humans, and the differences between species. *Front. Pharmacol.* 11, 364. doi: 10.3389/fphar.2020.00364

Chen, H., Gao, M., Luo, X. Q., Chen, H. F., Yuan, J. B., and Yang, W. L. (2019). Principal component analysis and discriminant analysis of 12 effective chemical constituents in *Aurantii Fructus* from different areas. *Chin. Tradit. Herb. Drugs* 50 (14), 3433–3437. doi: 10.7501/j.issn.0253-2670.2019.14.025

Committee of National Pharmacopoeia of RP China (2015). *National pharmacopoeia of RP China: 247. 2015 edition* (Beijing: China Medical Science and Technology Press).

Fang, T. Z., Wang, Y. G., Ma, Y., Su, W. W., Bai, Y., and Zhao, P. Y. (2006). A rapid LC/MS/MS quantitation assay for naringin and its two metabolites in rats plasma. *J. Pharm. Biomed. Anal.* 40 (2), 454–459. doi: 10.1016/j.jpba.2005.07.031

Felgines, C., Texier, O., Morand, C., Manach, C., Scalbert, A., Régerat, F., et al. (2000). Bioavailability of the flavanone naringenin and its glycosides in rats. *Am. J. Physiol-Gastr. L.* 279 (6), G1148–G1154. doi: 10.1152/ajpgi.2000.279.6.G1148

Hsiu, S. L., Huang, T. Y., Hou, Y. C., Chin, D. H., and Chao, P. D. L. (2002). Comparison of metabolic pharmacokinetics of naringin and naringenin in rabbits. *Life Sci.* 70 (13), 1481–1489. doi: 10.1016/S0024-3205(01)01491-6

Hu, D. D., Han, Q. B., Zhong, L. L. D., Li, Y. H., Lin, C. Y., Ho, H. M., et al. (2015). Simultaneous determination of ten compounds in rat plasma by UPLC-MS/MS: application in the pharmacokinetic study of Ma-Zi-Ren-Wan. *J. Chromatogr. B.* 1000, 136–146. doi: 10.1016/j.jchromb.2015.07.03

Ishii, K., Furuta, T., and Kasuya, Y. (1996). Determination of naringin and naringenin in human plasma by high-performance liquid chromatography. *J. Chromatogr. B.* 683 (2), 225–229. doi: 10.1016/0378-4347(96)00114-4

Ishii, K., Furuta, T., and Kasuya, Y. (1997). Determination of naringin and naringenin in human urine by high-performance liquid chromatography utilizing solid-phase extraction. *J. Chromatogr. B.* 704 (1-2), 299–305. doi: 10.1016/S0378-4347(97)00474-X

Jia, S., Hu, Y., Zhang, W. N., Zhao, X. Y., Chen, Y. H., Sun, C. D., et al. (2015). Hypoglycemic and hypolipidemic effects of neohesperidin derived from *Citrus aurantium* L. @ in diabetic KK-A$^{y}$ mice. *Food Funct.* 6 (3), 878–886. doi: 10.1039/C4FO0093b

Kobayashi, S., Kato, T., Azuma, T., Kikuzaki, H., and Abe, K. (2015). Anti-allergenic activity of polymethoxyflavones from Kaempferia parviflora. *J. Funct. Foods.* 13 (13), 100–107. doi: 10.1016/j.jff.2014.12.029

Lee, J. T., Pao, L. H., Hsieh, C. D., Huang, P. W., and Hu, O. Y. P. (2017). Development and validation of an LC-MS/MS method for simultaneous quantification of hesperidin and hesperetin in rat plasma for pharmacokinetic studies. *Anal. Methods-UK.* 9 (22), 3329–3337. doi: 10.1039/c7ay00051k

Li, X. H., Xiong, Z. L., Lu, S., Zhang, Y., and Li, F. M. (2010). Pharmacokinetics of naringin and its metabolite naringenin in rats after oral administration of Rhizoma Drynariae extract assayed by UPLC-MS/MS. *Chin. J. Nat. Med.* 8 (1), 40–46. doi: 10.1016/S1875-5364(10)60005-2

Li, P., Zeng, S. L., Duan, L., Ma, X. D., Dou, L. L., Wang, L. J., et al. (2016). Comparison of *Aurantii Fructus Immaturus* and *Aurantii Fructus* based on multiple chromatographic analysis and chemometrics methods. *J. Chromatogr. A.* 1469, 96–107. doi: 10.1016/j.chroma.2016.09.061

Li, P., Zeng, S. L., Wang, Z. Y., Yin, Q., Bi, Z. M., and Liu, E. H. (2019). Simultaneous Quantification of Five Flavanone Glycosides in Rat Plasma by Ultra-Performance Liquid Chromatography-Tandem Mass Spectrometry: Application to a Comparative Pharmacokinetic Study of *Aurantii Fructus Immaturus* and *Aurantii Fructus* Extracts. *J. AOAC Int.* 102 (3), 781–787. doi: 10.5740/jaoacint.18-0285

Lu, T., Song, J., Huang, F., Deng, Y. X., Xie, L., Wang, G. J., et al. (2007). Comparative pharmacokinetics of baicalin after oral administration of pure baicalin, Radix scutellariae extract and Huang-Lian-Jie-Du-Tang to rats. *J. Ethnopharmacol.* 110 (3), 412–418. doi: 10.1016/j.jep.2006.09.036

Ma, Y., Li, P. B., Chen, D. W., Fang, T. Z., Li, H. T., and Su, W. W. (2006). LC/MS/MS quantitation assay for pharmacokinetics of naringenin and double peaks phenomenon in rats plasma. *Int. J. Pharm.* 307 (2), 292–299. doi: 10.1016/j.ijpharm.2005.10.018

Mata-Bilbao, M. D. L., Andrés-Lacueva, C., Roura, E., Jáuregui, O., Escribano, E., Torre, C., et al. (2007). Absorption and pharmacokinetics of grapefruit flavanones in beagles. *Brit. J. Nutr.* 98 (1), 86–92. doi: 10.1017/S0007114507707262

Okada, N., Murakami, A., Urushizaki, S., Matsuda, M., Kawazoe, K., and Ishizawa, K. (2017). Extracts of immature orange (*Aurantii Fructus Immaturus*) and citrus unshiu peel (*Citri Unshiu Pericarpium*) induce P-glycoprotein and cytochrome P450 3A4 expression via upregulation of pregnane X receptor. *Front. Pharmacol.* 8, 84. doi: 10.3389/fphar.2017.00084

Onoue, S., Nakamura, T., Uchida, A., Ogawa, K., Yuminoki, K., Hashimoto, N., et al. (2013). Physicochemical and biopharmaceutical characterization of amorphous solid dispersion of nobiletin, a citrus polymethoxylated flavone, with improved hepatoprotective effects. *Eur. J. Pharm. Sci.* 49 (4), 453–460. doi: 10.1016/j.ejps.2013.05.014

Parhiz, H., Roohbakhsh, A., Soltani, F., Rezaee, R., and Iranshahi, M. (2015). Antioxidant and anti-inflammatory properties of the citrus flavonoids hesperidin and hesperetin: an updated review of their molecular mechanisms and experimental models. *Phytother. Res.* 29 (3), 323–331. doi: 10.1002/ptr.5256

Park, K. I., Park, H. S., Kim, M. K., Hong, G. E., Nagappan, A., Lee, H. J., et al. (2014). Flavonoids identified from Korean Citrus aurantium L. inhibit Non-Small Cell Lung Cancer growth in vivo and in vitro. *J. Funct. Foods.* 7, 287–297. doi: 10.1016/j.jff.2014.01.032

Qiao, X., Ye, M., Xiang, C., Wang, Q., Liu, C. F., Miao, W. J., et al. (2012). Analytical strategy to reveal the in vivo process of multi-component herbal medicine: a pharmacokinetic study of licorice using liquid chromatography coupled with triple quadrupole mass spectrometry. *J. Chromatogr. A.* 1258, 84–93. doi: 10.1016/j.chroma.2012.08.041

Qiu, X. J., Huang, X., Chen, Z. Q., Ren, P., Huang, W., Qin, F., et al. (2011). Pharmacokinetic study of the prokinetic compounds meranzin hydrate and ferulic acid following oral administration of Chaihu-Shugan-San to patients with functional dyspepsia. *J. Ethnopharmacol.* 137 (1), 205–213. doi: 10.1016/j.jep.2011.05.009

Renugadevi, J., and Prabu, S. M. (2010). Cadmium-induced hepatotoxicity in rats and the protective effect of naringenin. *Exp. Toxicol. Pathol.* 62 (2), 171–181. doi: 10.1016/j.etp.2009.03.010

Shen, X. F., Li, L., Ma, Q. H., Chen, H., Wang, J. P., Lv, L., et al. (2019). Pharmacokinetic study of eight bioactive components following oral administration of Zhiqiao Gancao decoction and its clinical efficacy observation. *Biomed. Chromatogr.* 34 (2), e4706. doi: 10.1002/bmc.4706

Tong, L., Zhou, D. D., Gao, J., Zhu, Y. H., Sun, H., and Bi, K. S. (2012). Simultaneous determination of naringin, hesperidin, neohesperidin, naringenin and hesperetin of Fractus aurantii extract in rat plasma by liquid chromatography tandem mass spectrometry. *J. Pharm. Biomed. Anal.* 58, 58–64. doi: 10.1016/j.jpba.2011.05.001

Wang, J. J., Shi, Q. S., Wu, C. Y., and Feng, F. (2016). Dynamic metabolic profile of Zhi-Zi-Da-Huang decoction in rat urine based on hybrid liquid chromatography–mass spectrometry coupled with solid phase extraction. *J. Chromatogr. B.* 1036, 100–113. doi: 10.1016/j.jchromb.2016.10.003

Wang, W. B., Zhao, L. L., Huang, H. Y., Yao, J. M., Zhou, L., Wang, D. S., et al. (2018). Development of an Ultra-High Performance Liquid Chromatography Method for Simultaneous Determination of Six Active Compounds in *Fructus aurantii* and Rat Plasma and Its Application to a Comparative Pharmacokinetic Study in Rats Administered with Different Doses. *J. Anal. Methods Chem.* 2018, 7579136. doi: 10.1155/2018/7579136

Wu, M., Zhang, H. W., Zhou, C., Jia, H. M., Ma, Z., and Zou, Z. M. (2015). Identification of the chemical constituents in aqueous extract of Zhi-Qiao and evaluation of its antidepressant effect. *Molecules.* 20 (4), 6925–6940. doi: 10.3390/molecules.20046925

Xu, F. G., Liu, Y., Dong, H. J., Song, R., and Zhang, Z. J. (2010). Pharmacokinetic comparison in rats of six bioactive compounds between Da-Cheng-Qi decoction and its parent herbal medicines. *Nat. Prod. Commun.* 5 (5), 795–800. doi: 10.1177//1934578X1000500523

Xu, Z. R., Jiang, C. H., Fan, S. Y., Yan, R. J., Xie, N., and Wu, C. Z. (2019). Comparative pharmacokinetics of naringin and neohesperidin after oral administration of flavonoid glycosides from Aurantii Fructus Immaturus in normal and gastrointestinal motility disorders mice. *Chin. Herb. Med.* 11 (3), 314–320. doi: 10.1016/j.chmed.2019.03.011

Yang, C. P., Liu, M. H., Zou, W., Guan, X.-L., Lai, L., and Su, W. W. (2012). Toxicokinetics of naringin and its metabolite naringenin after 180-day repeated oral administration in beagle dogs assayed by a rapid resolution liquid chromatography/tandem mass spectrometric method. *J. Asian. Nat. Prod. Res.* 14 (1), 68–75. doi: 10.1080/10286020.2011.632369

Yang, F., Yang, F., Wang, G. Y., Kong, T., and Liu, B. B. (2019). Pharmacokinetics of florfenicol and its metabolite florfenicol amine in crucian carp (Carassius auratus) at three tempetatures after single oral administration. *Aquaculture.* 503, 446–451. doi: 10.1016/j.aquaculture.2019.01.037

Yuan, J. B., Li, M., Chen, H. F., Yang, W. L., Luo, X. Q., Liu, Y. Y., et al. (2012). An HPLC method for the determination of auraptene in dog plasma: application to pharmacokinetic study. *Lat. Am. J. Pharm.* 31 (2), 251–256. doi: 10.1358/dof.2012.37.3.1745227

Yuan, J. B., Ren, G., Liang, J., Wang, C. Z., Yan, Z. H., Huang, Q., et al. (2017). Comparative studies on the multi-component pharmacokinetics of Aristolochiae Fructus and honey-fried Aristolochiae Fructus extracts after oral administration in rats. *BMC Complem. Altern. Med.* 17 (1), 1–11. doi: 10.1186/s12906-017-1626-2

Zeng, X., Su, W. W., Zheng, Y. Y., He, Y. D., He, Y., Rao, H. Y., et al. (2019). Pharmacokinetics, tissue distribution, metabolism, and excretion of naringin in aged rats. *Front. Pharmacol.* 10, 34. doi: 10.3389/fphar.2019.00034

Zhang, J. Z., Gao, W. Y., Hu, X., Liu, Z., and Liu, C. X. (2012). The influence of compatibility of traditional Chinese medicine on the pharmacokinetic of main components in *Fructus aurantii*. *J. Ethnopharmacol.* 144 (2), 277–283. doi: 10.1016/j.jep.2012.09.009

Zhang, X. H., Han, L. R., Liu, J., Xu, Q. Y., Guo, Y. X., Zheng, W., et al. (2018). Pharmacokinetic study of 7 compounds following oral administration of *Fructus aurantii* to depressive rats. *Front. Pharmacol.* 9, 131. doi: 10.3389/fphar.2018.00131

Zhou, L., Cui, M., Zhao, L. L., Wang, D. S., Tang, T., Wang, W. B., et al. (2018). Potential Metabolic Drug–Drug Interaction of *Citrus aurantium* L. (*Rutaceae*) Evaluating by Its Effect on 3 CYP450. *Front. Pharmacol.* 9, 895. doi: 10.3389/fphar.2018.00895

**Conflict of Interest:** The authors declare that the research was conducted in the absence of any commercial or financial relationships that could be construed as a potential conflict of interest.

frontiers in Pharmacology

ORIGINAL RESEARCH
published: 02 October 2020
doi: 10.3389/fphar.2020.512877

# A Novel Network Pharmacology Strategy to Decode Mechanism of Lang Chuang Wan in Treating Systemic Lupus Erythematosus

*Yao Gao[1,2†], Ke-xin Wang[1,2†], Peng Wang[1†], Xiao Li[1], Jing-jing Chen[2,3], Bo-ya Zhou[4], Jun-sheng Tian[1], Dao-gang Guan[5,6*], Xue-mei Qin[1*] and Ai-ping Lu[2*]*

[1] Modern Research Center for Traditional Chinese Medicine, Shanxi University, Taiyuan, China, [2] Institute of Integrated Bioinformedicine and Translational Science, Hong Kong Baptist University, Hong Kong, Hong Kong, [3] Zhijiang College, Zhejiang University of Technology, Shaoxing, China, [4] Department of Ultrasound, Eighth Affiliated Hospital of Sun Yat-sen University, Shenzhen, China, [5] Department of Biochemistry and Molecular Biology, School of Basic Medical Sciences, Southern Medical University, Guangzhou, China, [6] Guangdong Provincial Key Laboratory of Single Cell Technology and Application, Southern Medical University, Guangzhou, China

OPEN ACCESS

**Edited by:**
Thomas Efferth,
Johannes Gutenberg University Mainz, Germany

**Reviewed by:**
Gang Bai,
Nankai University, China
Jianping Chen,
Guangzhou University of Chinese Medicine, China
Rufeng Wang,
Beijing University of Chinese Medicine, China

***Correspondence:**
Dao-gang Guan
guandg0929@hotmail.com
Xue-mei Qin
qinxm@sxu.edu.cn
Ai-ping Lu
aipinglu@hkbu.edu.hk

[†]These authors have contributed equally to this work

**Specialty section:**
This article was submitted to Ethnopharmacology, a section of the journal Frontiers in Pharmacology

**Received:** 18 November 2019
**Accepted:** 11 September 2020
**Published:** 02 October 2020

**Citation:**
Gao Y, Wang K-x, Wang P, Li X, Chen J-j, Zhou B-y, Tian J-s, Guan D-g, Qin X-m and Lu A-p (2020) A Novel Network Pharmacology Strategy to Decode Mechanism of Lang Chuang Wan in Treating Systemic Lupus Erythematosus. Front. Pharmacol. 11:512877. doi: 10.3389/fphar.2020.512877

Complex disease is a cascade process which is associated with functional abnormalities in multiple proteins and protein-protein interaction (PPI) networks. One drug one target has not been able to perfectly intervene complex diseases. Increasing evidences show that Chinese herb formula usually treats complex diseases in the form of multi-components and multi-targets. The key step to elucidate the underlying mechanism of formula in traditional Chinese medicine (TCM) is to optimize and capture the important components in the formula. At present, there are several formula optimization models based on network pharmacology has been proposed. Most of these models focus on the 2D/3D similarity of chemical structure of drug components and ignore the functional optimization space based on relationship between pathogenetic genes and drug targets. How to select the key group of effective components (KGEC) from the formula of TCM based on the optimal space which link pathogenic genes and drug targets is a bottleneck problem in network pharmacology. To address this issue, we designed a novel network pharmacological model, which takes Lang Chuang Wan (LCW) treatment of systemic lupus erythematosus (SLE) as the case. We used the weighted gene regulatory network and active components targets network to construct disease-targets-components network, after filtering through the network attribute degree, the optimization space and effective proteins were obtained. And then the KGEC was selected by using contribution index (CI) model based on knapsack algorithm. The results show that the enriched pathways of effective proteins we selected can cover 96% of the pathogenetic genes enriched pathways. After reverse analysis of effective proteins and optimization with CI index model, KGEC with 82 components were obtained, and 105 enriched pathways of KGEC targets were consistent with enriched pathways of pathogenic genes (80.15%). Finally, the key components in KGEC of LCW were evaluated by *in vitro* experiments. These results indicate that the proposed model with good accuracy in screening the

KGEC in the formula of TCM, which provides reference for the optimization and mechanism analysis of the formula in TCM.

**Keywords: Lang Chuang Wan, systemic lupus erythematosus, network pharmacology, optimization space, effective proteins, contribution index**

## INTRODUCTION

The key group of effective components (KGEC) in a formula of traditional Chinese medicine (TCM) refer to the pharmacologically active components that are closely related to the positive response to the therapy of the diseases. How to determine the KGEC that play leading roles in the treatment of specific disease is a difficult problem due to the high complexity of the chemical composition and the incompletely understanding the complex multi-targets mechanism of TCM. Selecting the KGEC in the formula of TCM is an important direction in the reduction of non-active components and analysis of the treatment mechanism of formula. At present, there are several formula optimization models based on network pharmacology have been proposed. Most of these models focus on the 2D/3D similarity of chemical structure of drug or components, and ignore the optimized functional space, which couldrepresent effective relationships between drug targets and pathogenetic genes (Wang et al., 2018; Xie et al., 2018; Duan et al., 2019). Increasing evidences confirm that the monomer component of TCM exerts important pharmacological effects through the protein-protein interactions (PPI) (Chen and Cui, 2017; Gan et al., 2018; Guo et al., 2019). Thus, it is desirable to design a module to detect the KGEC and infer the potential mechanisms of formula on complex disease based on chemical properties analysis, targets prediction, and construction of functional optimization space.

Systemic Lupus Erythematosus (SLE) is an autoimmune disease involving multiple systems and organs, with complicated clinical manifestations and persistent. Most of them are found in young women, and the incidence ratio of male to female is 1: 5 ~ 10 (Veeranki and Choubey, 2010; Dorner and Furie, 2019). Previous researches indicate that the SLE may be related to heredity, immune disorder, endocrine abnormality and environmental factors. Currently, western medicine mainly adopts non-steroidal anti-inflammatory drugs, antimalarial drugs, glucocorticoids, immunosuppressive agents, plasma treatment, and systemic lymph node irradiation therapy for the treatment of SLE (Loram et al., 2015; Wallace, 2015). However, so far these drugs and methods can only temporarily control the disease. At the same time, some toxic and side effects of western medicine are becoming increasingly apparent. Intervention therapy of TCM can not only effectively relieve clinical symptoms, but also reduce the toxic and side effects of western medicine (Huang et al., 2016; Ma et al., 2016). Increasing evidences proved that TCM play important roles in both acute and remission phases of SLE.

In recent years, TCM has been widely used in the treatment of SLE and has achieved remarkable results. With the continuous improvement of its therapeutic effect, it has gradually attracted the attention of medical experts and scholars at home and abroad (Ma et al., 2016). At present, the TCM formula, Lang Chuang Wan (LCW) is widely used in the treatment of SLE with TCM. LCW generally comprised of 16 herbs: *Lonicera japonica* Thunb. (Jinyinhua, 53.6 g), *Forsythia suspensa* (Thunb.) Vahl (Lianqiao, 53.6 g), *Taraxacum mongolicum* Hand. (Pugongying, 53.6 g), *Coptis chinensis* Franch. (Huanglian, 13.4 g), *Rehjnannia glutinosa* Libosch. (Dihuang, 53.6 g), *Rheum officinale* Baill. (Dahuang, 20.1 g), *Glycyrrhiza uralensis* Fisch. (Gancao, 13.4 g), *Scolopendra subspinipes mutilans* L. Koch (Wugong, 2.42 g), *Paeonia ladiflora* Pall. (Chishao, 26.8 g), *Angelica sinensis* (Oliv.) Diels (Danggui, 13.4 g), *Salvia miltiorrhiza* Bge. (Danshen, 13.4 g), *Scrophularia ningpoensis* Hemsl. (Xuanshen, 53.6 g), *Prunus persica* (L.) Batsch (Taoren, 26.8 g), *Carthamus tinctorius* L. (Honghua, 20.1 g), *Cryptotympana pustulata* Fabricius (Chantui, 53.6 g), and *Fritillaria thunbergii* Miq. (Zhebeimu, 26.8 g). In this Chinese formula, Flos Lonicerae, Fructus Forsythiae and Herba Taraxaci have the function of clearing heat-toxin, eliminating carbuncles, and resolving masses, Coptidis Rhizoma has the function of clearing heart fire, the Rehmanniae Radix mainly focus on cooling blood, nourishing yin and promoting fluid production, Radix et Rhizoma Rhei play roles in clearing heat cooling blood promoting blood circulation; Glycyrrhrizae Radix used for clearing heat-toxin harmonizing various drugs; Radix Paeoniae Rubra, Saviae Miltiorrhizae Radix and Carthami Flos usually used for clearing heat cooling blood; Scolopendra used for removing toxic substance resolving masses, detumescence, and relieving pain; Radix Angelicae Sinensis used for nourishing and activating blood; Radix Scrophulariae used for clearing heat-toxin nourishing yin for lowering fire; Semen Persicae used for promoting blood circulation removing blood stasis; Periostracum Cicadae used for clearing heat; Bulbus Fritillariae Thunbergii used for clearing heat dissipating phlegm and resolving masses. The whole recipe has the functions of clearing away heat and toxic materials, cooling blood and promoting blood circulation. In pharmacologic studies, LCW may has the effect of inhibiting humoral immune function and enhancing cellular immune function. Additionally, LCW also obvious inhibitory effect on acute and chronic inflammation and allergy in rats, and can promote fibrinolytic activity. These studies confirmed that the LCW could be beneficial in the treatment of patients with SLE at comprehensive level. Nevertheless, not any document expounds the key components and underlying therapeutic mechanism of LCW for clinically benefit to SLE (Wang, 1989; Wang et al., 1991).

**Abbreviations:** CI, Contribution index; DL, Drug-likeness; GO, Gene Ontology; KGEC, Key group of effective components; KEGG, Kyoto Encyclopedia of Genes and Genomes; LCW, Lang Chuang Wan; OB, Oral bioavailability; PPI, Protein-protein interactions; SLE, Systemic lupus erythematosus; TCM, Traditional Chinese medicine.

Currently, a novel network pharmacology module was designed to detect the KGEC and elucidate the therapeutic mechanisms of LCW in the treatment of SLE. During this process, the weighted gene regulatory network of SLE disease was constructed and used for constructing of optimization space. All LCW components were collected from databases and literature. The potential active components were selected from all components based on published ADME-related models; the targets of these active components were predicted by three published prediction tools. The active components and their targets were used for building the components-targets (C-T) network. The weighted gene regulatory network and C-T networks were used to construct optimization space to determine the effective proteins. The effective proteins selected from optimization space were used to screen the effective components. The contribution index (CI) module was employed to optimize effective components and get the KGEC, which would be used to illustrate the molecular mechanism of LCW in the therapy of SLE. Finally, the key components in KGEC of LCW were evaluated by *in vitro* experiments.

# METHODS

## Construct Weighted Gene Regulatory Network of SLE

In order to construct comprehensive weight gene network of SLE, the PPI data were derived from public databases BioGRID, STRING, Dip, HPRD, Intact, Mint and Reactome (Guan et al., 2014). Genes from DisGeNET (Pinero et al., 2017) were reported to be related to SLE were extracted and mapped to the PPI network to construct the weighted gene regulatory network of SLE. Cytoscape (Version 3.5.1) was utilized to visualize the network.

## LCW Content Determination

### Reagents and Chemicals

High performance liquid chromatography (HPLC)-grade acetonitrile and HPLC grade formic acid were obtained from Thermo-Fisher (USA). Reference standards provided by the National Institute on Drug Abuse of China:Hydroxysafflor-Yellow-A (batch number: 111637-200502), amygdalin (batch number: 110820-200403), paeoniflorin (batch number: 0905-9805), caffeic acid (batch number: 110728-200506), phillyrin (batch number: 120908-200914), liquiritin (batch number:111610-200503), peimisine (batch number: 0750-9303), harpagoside (batch number: 712-9403), rhein (batch number: 0902-200207), Z-Ligustilide (batch number: 927-9908), berberine (batch number: 0713-200107), tanshinone II a (batch number: 0766-200011), catalpol (batch number: 0808-9602). The purities of all standards were no less than 98% and suitable for liquid chromatography-tandem mass spectrometry (LC-MS/MS) analysis. LCW was purchased from Changchun Overseas Pharmaceutical Co. Ltd.

### Preparation of Samples and Standard Solution

LCW (batch number: 20190601) was grinded into powder. Each sample of LCW powder (0.5 g) was weighed precisely and ultrasonically extracted in 50 ml hydrochloric-acid methanol (1:100) for 30 min. Supplement the weight lost with hydrochloric acid-methanol (1:100) solution and then filtered through 0.22 μm nylon membrane filters. The filtrate was analyzed directly by UPLC-ESI-MS/MS. At the same time, a stock solution containing 13 reference standards was prepared in methanol. All solutions were stored at 4°C prior to analysis.

### Instrument and UPLC-ESI-MS/MS Conditions

Chemical profiling of LCW and reference standards were detected by an Agilent ultra-performance liquid chromatography system (UHPLC) (Agilent, USA) coupled to a Q-trap 3200 (AB SCIEX, USA). Chromatography separation was carried out on a Waters ACQUITYUPLC HSS T3 column (2.1 mm × 100 mm, 1.8 μm) maintained at 40°C. The mobile phase consisted of 0.1% formic acid in water (A) and 0.1% formic acid in acetonitrile (B), and run under the following program: 0 ~ 1 min, 15% B; 1 ~ 4 min, 15 ~ 45% B; 4 ~ 10 min, 45 ~ 60% B, 10 ~ 15 min, 60 ~ 90% B; 15 ~ 18 min, 90 ~ 95% B. The sample injection volume was 5 μl and the flow rate was set at 0.2 ml/min. The mass spectrometer was fitted with an electrospray ionization source and the mass detection was operated in both positive and negative ion modes with the following setting: ion source temperature, 500°C; Sheath gas velocity, 50 psi; Auxiliary gas flow rate, 12 L/min; scan range, m/z 150–900.

## Collect and Select Chemical Components of LCW

All components of LCW were collected from four published natural product data sources: TCMSP database (Ru et al., 2014), Traditional Chinese Medicine integrated database (Xue et al., 2013), Traditional Chinese Medicine database@Taiwan (Chen, 2011), and YaTCM (Li et al., 2018). For all components, the initial structure formats (e.g., mol2 and SDF) were transformed into unified SDF format using Open Babel toolkit (version 2.4.1). Subsequently, the properties of components were retrieved from TCMSP, including molecular weight (MW), oral bioavailability (OB), Caco-2 permeability (Caco-2), and DL (drug-likeness).

Three ADME-related models, including OB, Caco-2, and DL, were employed to screen the bioactive molecules. OB (%F) represents the percentage of an orally administered dose of unchanged drug that reaches the systemic circulation, which reveals the convergence of the ADME process (Xu et al., 2012). High oral bioavailability is often a key indicator to determine the drug-like property of bioactive molecules as therapeutic agents. The components with suitable OB≥30% were chosen as candidate components for further research. Human intestinal cell line Caco-2 is used as an efficient *in vitro* model to study the passive diffusion of drugs across the intestinal epithelium, the ingredients' transport rates (nm/s) in Caco-2 monolayers represent the intestinal epithelial permeability in TCMSP. Components with Caco-2>-0.4 were chosen as the candidate components, because the components with a Caco-2 value less than -0.4 were not permeable. Drug-likeness is a qualitative concept used in drug design for an estimate on how "drug-like" a prospective compound is, which helps to optimize pharmacokinetic and pharmaceutical properties, such as

solubility and chemical stability. The "drug-like" level of the components is 0.18, which is used as a selection criterion for the "drug-like" components in the traditional Chinese herbs (Tao et al., 2013). After ADME screening, some components that did not meet the three screening criteria were also selected because of their high content and high biological activity. These will be used in conjunction with ADME screening as a follow-up study.

## Predict Targets of Active Components

To obtain the targets of active components in LCW, the commonly used prediction tools, i.e., Similarity Ensemble Approach (SEA) (Tao et al., 2013), HitPick (Liu X. et al., 2013), and Swiss Target Prediction (Gfeller et al., 2014), were employed to identify the targets. All chemical structures were prepared and converted into canonical SMILES using Open Babel toolkit (version 2.4.1).

## Define the Optimization Space and Evaluate the Effective Proteins

Construction of the optimization space is able to maximize the search for targets of small molecules that are highly relevant to pathogenetic genes. Firstly, we used the weighted gene regulatory network and active components targets network to construct the disease-targets-components network. Degree is an important topological property in the network that can be used to evaluate the importance of nodes in the network. The nodes with higher degree than the average degree of all nodes in the disease-targets-components network were identified as hub nodes. Following this rule, the passed nodes and their edges in the disease-targets-components network were kept and defined as optimization space. The whole process can be described as follows:

We defined $\mathrm{Net}_{ppi} = \{N, E\}$, $N$ means nodes that represent proteins, $E$ means edges that represent protein–protein interactions derived from public databases BioGRID, STRING, Dip, HPRD, Intact, Mint, and Reactome. $T_{tar} = \{P_{1tar}, P_{2tar}\ldots\ \ldots P_{ntar}\}$ means the predicted targets of active components. $D_{dis} = \{G_{1dis}, G_{2dis}\ldots\ \ldots G_{ndis}\}$ means the pathogenic genes of SLE. The optimization space can be calculated by the following steps.

$$L_{tar} = \{P_{1tar}, P_{2tar} \ldots\ldots P_{ntar}\}$$

$$L_{dis} = \{P_{1dis}, P_{2dis} \ldots\ldots P_{ndis}\}$$

$$Net_{tarppi} = \{N_{tar}, E_{tar}\} = Net_{ppi} \cap L_{tar}\ ,\ Net_{tar} \in N;\ E_{tar} \in E$$

$$Net_{disppi} = \{N_{dis}, E_{dis}\} = Net_{ppi} \cap L_{dis}\ ,\ Net_{dis} \in N;\ E_{dis} \in E$$

$$Net_{tar-dispi} = Net_{ppi} \cap Net_{disppi} \cap Net_{tarppi}$$

$$D_{avg} = \left(\sum_{i=1}^{k} d_i\right)/k$$

$$OptS = \cup_{i=1}^{k}\ d_{\left(Net_{tar-dispi}\right)i} > D_{avg}$$

Where $Net_{tar^{ppi}}$ is the network of predicted targets, the $Net_{dis^{ppi}}$ is the network of pathogenic genes.$Net_{tar-dis^{ppi}}$ represents the disease-targets-components network. $D_{avg}$ is the average degree of all nodes in the disease-targets-components network. $k$ means the number of nodes in the disease-targets-components network. OptS represent the optimization space. The nodes in the optimization space were identified as effective proteins.

## Develop a CI Model to Select KGEC

To optimize effective components and get the KGEC, which would be used to illustrate the molecular mechanism of LCW in the therapy of SLE. Active components which are associated with effective proteins were extracted as $\lambda = \{\lambda_1, \lambda_2, \lambda_3\ldots\ \ldots\ \lambda_m\}$, The target number of each active compounds be defined as $\omega = \{\omega_1, \omega_2, \omega_3\ldots\ \ldots\omega_m\}$, then coverage of the target number for each active compounds defined as $v = \{v_1, v_2, v_3\ldots\ \ldots\ v_m\}$, the dynamic-0-1 knapsack algorithm can be described as:

Input: $v$ and $\omega$, the number of active components m and the number of effective $v$ proteins W.

Output: The optimal KGEC.

*for* $\omega \leftarrow 0$ *to* $W$ *do*
  $c[0, \omega] \leftarrow 0$
*end for*
*for* $i \leftarrow 0$ *to* $m$ *do*
  $c[i, 0\ ] \leftarrow 0$
  *for* $\omega \leftarrow 1$ *to* $W$ *do*
    *if* $\omega_i \ll \omega$ *then*
      *if* $v_i + c[i-1,\ \omega - \omega_i] > c[i-1, \omega]$ *then*
        $c[i, \omega] \leftarrow v_i + c[i-1,\ \omega - \omega_i]$
      *else*
        $c[i, \omega] \leftarrow c[i-1, \omega]$
      *end if*
      *else*
      $c[i, \omega] \leftarrow c[i-1, \omega]$
      *end if*
    *end for*
*end for*
*return* $CI = c[k, W]$

## Gene Ontology and Pathway Analysis

To analyze the main function of the targets, the clusterProfiler package of R software was used to perform Gene Ontology (GO) analysis. $p$-values were set at 0.05 as the cut-off criterion. The clusterProfiler package of R software (Yu et al., 2012) was employed to classify the biological terms and to analyze the gene cluster enrichment automatically. The latest pathway data were obtained from the Kyoto Encyclopedia of Genes and Genomes (KEGG) database (Draghici et al., 2007) for KEGG pathway enrichment analyses. $p$-values were set at 0.05 as the

cut-off criterion. The ggplot2 package was used to create graphs in R statistical programming language (version 3.4.2). The results of analysis were annotated by Pathview (Luo et al., 2017) in the R Bioconductor package (https://www.bioconductor.org/).

## Experimental Validation

### Chemicals and Reagents

Liquiritin and ferulic acid (≧98% purity by HPLC, PUYI BIOLOGY; Jangsu, China). Resiquimod (≧99.6%, Topscience Co., Ltd. China). Fetal bovine serum (FBS) (Sangon Biotech (Shanghai) Co., Ltd., China). RPMI-1640 (Sangon Biotech (Shanghai) Co., Ltd., China). β-actin, Phospho-ERK1/2, Phospho-AKT, and Phospho-PI3K (CST, USA).

### Cell Culture and Drug Treatment

RAW 264.7 cells (Cell Bank of Chinese Academy of Sciences, China) were cultured in DMEM-H with 10% FBS at 37°C, in an atmosphere containing 5% $CO_2$, humidified 95%. RAW 264.7 cells were seeded on 96-well plates with $1\times10^4$ per/well, 100 mm dishes with $1\times10^6$ per/dishes, and cultured for 24 h. After incubation, the RAW 264.7 cells were co-incubated with different concentrations of liquiritin, ferulic acid, and resiquimod for 24 h. The concentration of resiquimod was selected at 0.1 μg/ml.

### Cell Viability Assay

RAW 264.7 cells were seeded in 96-well plates. After drug treatment, the culture medium was removed, 100 μl 0.5 mg/ml MTT (Sangon Biotech (Shanghai) Co., Ltd., China) solution was added. After 4 h, the culture medium was removed and 100 μl DMSO (Sangon Biotech (Shanghai) Co., Ltd., China) was added. The absorbance at 570 nm was measured with a microplate reader (BioTek Epoch, USA). Cell viability is expressed as a percentage of the control.

### Measurement of IL-6 Levels

The cells were cultured in 6-well plates. After relevant treatment, the cells were collected and centrifuged to obtain a cell pellet and supernatant. The cell pellet and supernatant were stored at −80°C until required for analysis. The level of IL-6 was determined by commercial assay kits (Nanjing Jiancheng, China).

### Western Blot Analyses

RAW 264.7 cells were seeded in 100 mm dishes. At the end of the treatments, the cells were harvested and washed twice with cold PBS. The cells were lysed with RIPA lysis buffer (Beyotime, China) containing 1% phenylmethylsulfonylfluoride (PMSF, Beyotime, China). The whole-cell lysates were centrifuged at 12,000 rpm/min for 15 min at 4°C, and the supernatants were collected. Protein concentrations were determined by bicinchoninic acid assay. Equal amounts of protein (50 μg) were separated by electrophoresis on 12% sodium dodecyl sulphate polyacrylamide gels and transferred onto PVDF membranes. These membranes were incubated with 5% (w/v) non-fat milk powder in Tris-buffered saline containing 0.1% (v/v) Tween-20 (TBST) for 2 h to block nonspecific binding sites. The membranes were then incubated overnight at 4°C with the primary antibodies. After washing with TBST, the membranes were incubated for 2 h at room temperature with the fluorescent secondary antibodies. After rewashing with TBST, the membranes were scanning by a fluorescent scanner (Odclyssey CLX, Gene company limi ed, USA).

# RESULTS

In this report, a novel network pharmacology module was designed to detect the KGEC and elucidate the therapeutic mechanisms of LCW in the treatment of SLE (**Figure 1**). Firstly, all LCW components were collected from databases and literature. Next, the potential active components were selected from all LCW components based on published ADME-related models. The targets of these active components were predicted by three online prediction tools. Then the weighted gene regulatory network and active components targets network were used to construct optimization space for determining the effective proteins. The effective proteins were used to select the KGEC based on CI module and then the KGEC was used to infer the underlying molecular mechanism of LCW in treating SLE. Finally, the key components in KGEC of LCW were evaluated by *in vitro* experiments.

## Construct Weighted Gene Regulatory Network of SLE

Construction and analysis of weighted gene regulatory network is the basis and key step to understand the pathogenesis and provide intervention strategies of SLE. In order to construct a comprehensive weighted gene network of SLE, the PPI data sets from public databases BioGRID, STRING, Dip, HPRD, Intact, Mint and Reactome were used to construct the PPI network. 1201 genes from DisGeNET which confirmed associated with SLE were extracted and mapped to the PPI network to construct the weighted gene regulatory network of SLE. The weighted gene regulatory network contains 950 nodes and 6,984 edges (**Figure 2**). The number of literature reports of one node represent the weight of the node (**Table S1**). Eight out of top 30 genes with the highest weight in the gene regulatory network enriched in the common SLE pathways (hsa05322), including TNF (Geng et al., 2014), HLA-DRB1 (Shimane et al., 2013), IFNG (Leng et al., 2016), CD40LG (Wu et al., 2016), IL10 (Liu P. et al., 2013), FCGR3A (Kyogoku et al., 2013), FCGR2A (Bentham et al., 2015) and TRIM21 (Kyriakidis et al., 2014). These genes are also enriched in cytokine-cytokine receptor interaction, T cell receptor signaling pathway and Th17 cell differentiation, which are closely related to SLE (**Figure 3**). These results indicate that the weight gene regulatory network and weight genes can reflect the pathogenesis of SLE, which also provides a reliable reference for the next step to construct the optimization space.

## Chemical Components Analysis

Thirteen components in the chromatograms of the LCW sample were identified and assigned by comparing the retention time with those of the reference compounds (**Figure 4**). The 13

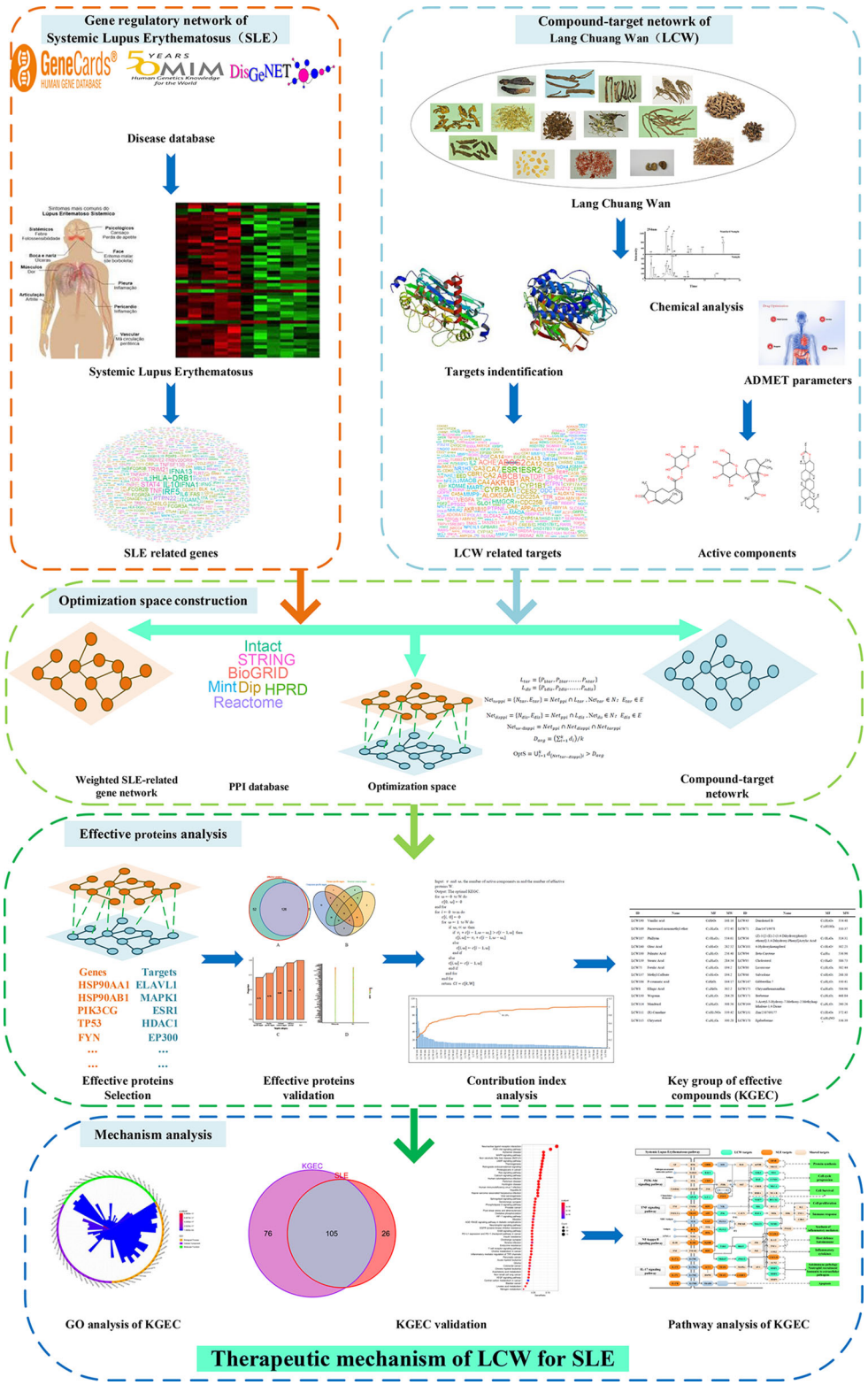


**FIGURE 1** | The flowchart of our proposed network pharmacology approach. Experimental methods include gene regulatory network of SLE, compound-target netowrk of LCW, optimization space construction, effective proteins analysis and mechanism analysis. SLE represents systemic lupus erythematosus, LCW represents Lang Chuang Wan, KGEC represents key group of effective components.

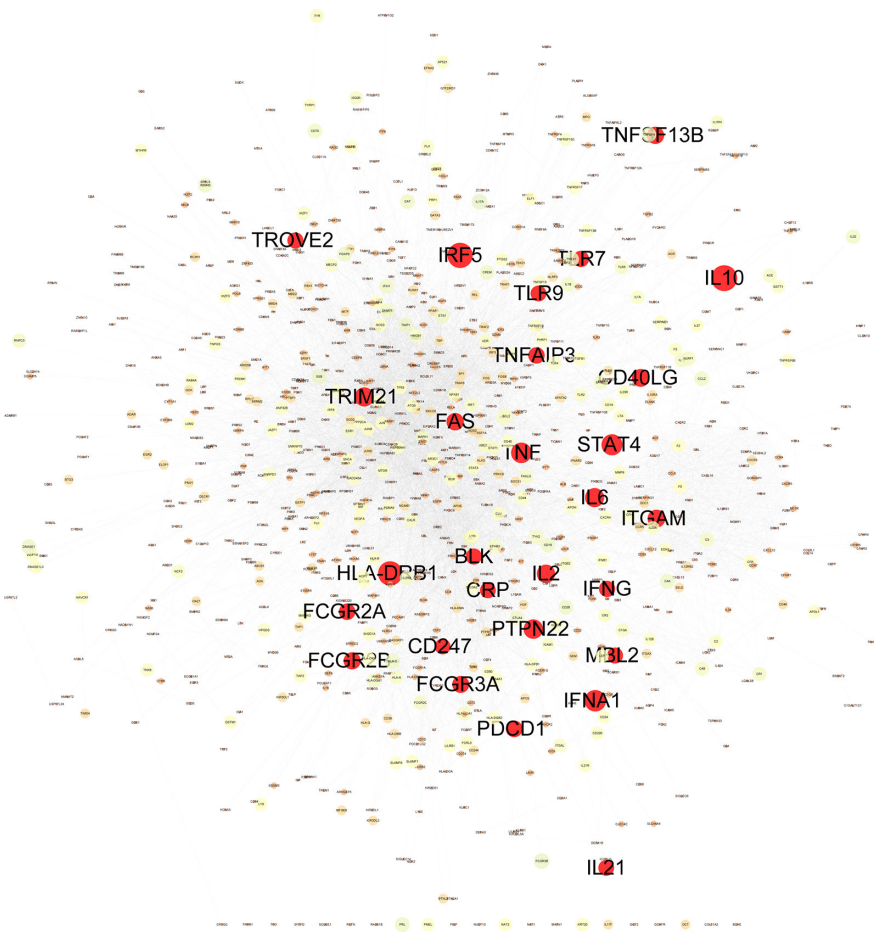


**FIGURE 2** | Weighted gene regulatory network of SLE. The weighted gene regulatory network contains 950 nodes and 6,984 edges. The number of literature reports of one node represent the weight of the node. The red nodes list the top 30 of SLE pathogenetic genes in the weighted gene regulatory network.

components are hydroxysafflor-Yellow-A, amygdalin, paeoniflorin, caffeic acid, phillyrin, liquiritin, peimisine, harpagoside, rhein, Z-Ligustilide, berberine, tanshinone II a, and catalpol (**Table 1**). The pharmacopoeia defines that the content of berberine should not be less than 0.4 mg/g, and we get the content of berberine as 0.57 mg/g by chemical analysis. These results confirmed that the content of berberine in LCW meets the requirements of pharmacopoeia. Chemical Components analysis provides a reference for the screening of active components in LCW for further analysis.

## Select Potential Active Components

By a systematic search of components from public databases of 16 herbs, a total of 1693 components were retrieved in LCW in **Table 2**. The detail information of these components was provided in **Table S2**. TCM formula usually contains multiple components, only a few components have satisfactory pharmacodynamic and pharmacokinetic properties. In this study, three ADME-related models, OB, Caco-2, and DL were employed to screen the active components. The components with OB values higher than 30%, Caco-2 values higher than -0.4 and DL values higher than 0.18 were retained for further investigation. After ADME screening, some components that did not meet the three screening criteria were selected because of their high content and high biological activity, which has been reported in the literature and our UPLC-ESI-MS/MS analysis. Finally, 193 active components were filtered out of the 1,693 components of LCW. The detail information was shown in **Table S3**.

## Shared Components of Herbs in LCW

As can be seen from **Table S2**, there exist more than 20 active components shared by two or more herbs in LCW. For example, beta-sitosterol (LCW5), a common component of 10 herbs such as CS, DH, DG, HH, JYH, LQ, TR, XS, ZBM, and PGY, shows an inhibitory effect on the expression of proinflammatory cytokine interleukin IL-6 and TNF-α, which display the properties of anti-inflammatory and immune-modulating in the treatment of SLE (Fraile et al., 2012). Caffeic acid (LCW23) shared by, DS, JYH, PGY, and LQ was well-known for its pharmacological properties

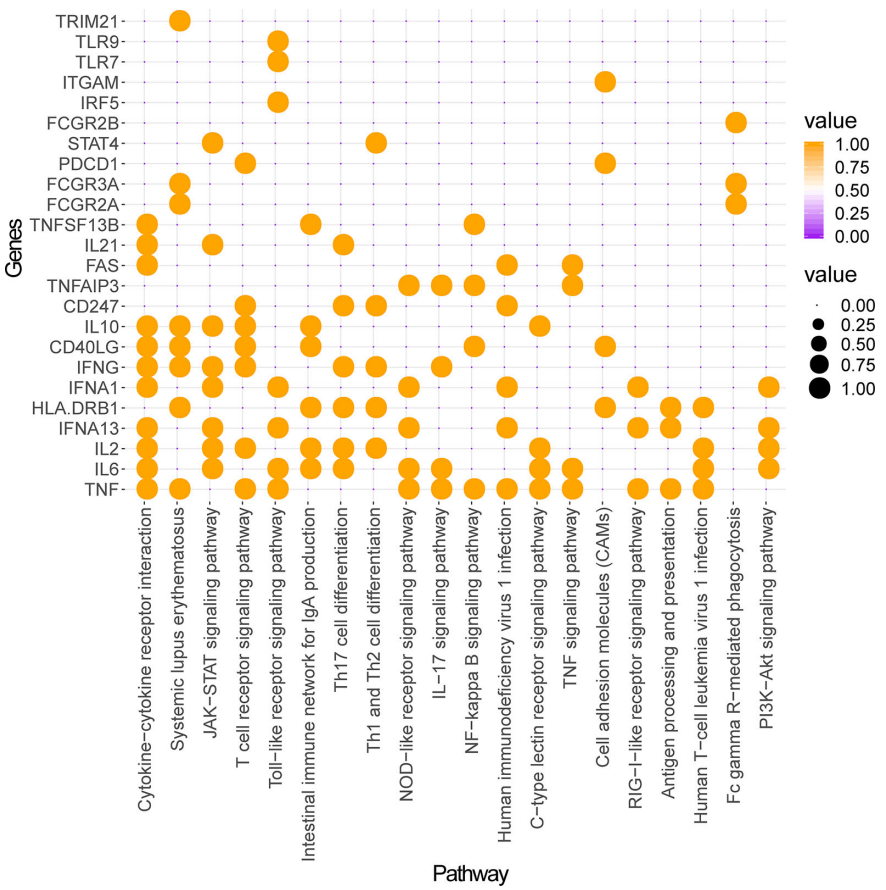


**FIGURE 3** | Pathway enrichment analysis of top 30 weighted genes of SLE. The ordinate represents genes and the abscissa represents enriched pathways. Orange nodes represent genes enriched in a given pathway and no nodes represent genes not enriched in this pathway.

such as antiviral, anti-inflammatory, anti-carcinogenic, and immunomodulatory activities (Espindola et al., 2019). It has also been revealed that the administration of caffeic acid not only protect rats from cisplatin-induced oxidative stress and gastrointestinal toxicity but also reverse the activities of enzymes superoxide dismutase, catalase, glutathione reductase, and glutathione peroxidase near to their normal level, which are related to the SLE and that may be used to infer underlying mechanism of LCW on SLE (Iraz et al., 2006). Kaempferol (LCW77), a shared component of GC, HH, JYH, and LQ, was a common type of dietary flavonoid with anti-oxidative and anti-inflammatory properties. Studies also indicated that kaempferol decreased lipopolysaccharide (LPS)-induced TNF-α and IL-1 expression by increasing the number of activated macrophages, which has been reported associating with SLE (Lee et al., 2018). Additionally, quercetin (LCW97) in HH, JYH, LQ, and HL was one type of flavonoid compound with anti-cancer, anti-inflammatory and immune-regulating activities. The treatment of pristane-induced SLE model mice with liposomal quercetin found that quercetin achieves SLE therapeutic effect is by reducing the level of autoantibody expression (Dos Santos et al., 2018).

## Specific Components of Herbs in LCW

Except the shared components, most of the herbs possess their specific ingredients. For example, luteolin (LCW25), the specific component of JYH, protects against vascular inflammation in mice and TNF-α induced monocyte adhesion to endothelial cells *via* suppressing IKBα/NF-kappa B signaling pathway, which has been reported associating with SLE. Phillyrin (LCW187), one of the most effective constituents in LQ, has good antibacterial and anti-inflammatory activity, which can regulate MyD88/IκBα/NF-kappa B signaling pathway by controlling the expression of IκBα, IL-1β, IL-6 and TNF-α, which would be a benefit to SLE (Yang et al., 2017). As the major component of HL, epiberberine (LCW178) has broad biological activities, including antihyperlipidemic and antihyperglycemic effects as well as anti-inflammatory and antioxidant effects, and inhibits urease activity (Li et al., 2015) which suggested the MAPK signaling pathway could be used as the therapy target. Berberine (LCW172) was the quality marker of LCW in Chinese Pharmacopeia (China, 2015), and has anti-inflammatory effects, suppresses the expression of proinflammatory cytokines likely due to its capacity of AMPK activation, which could be used to illustrate the molecular mechanism of LCW in the

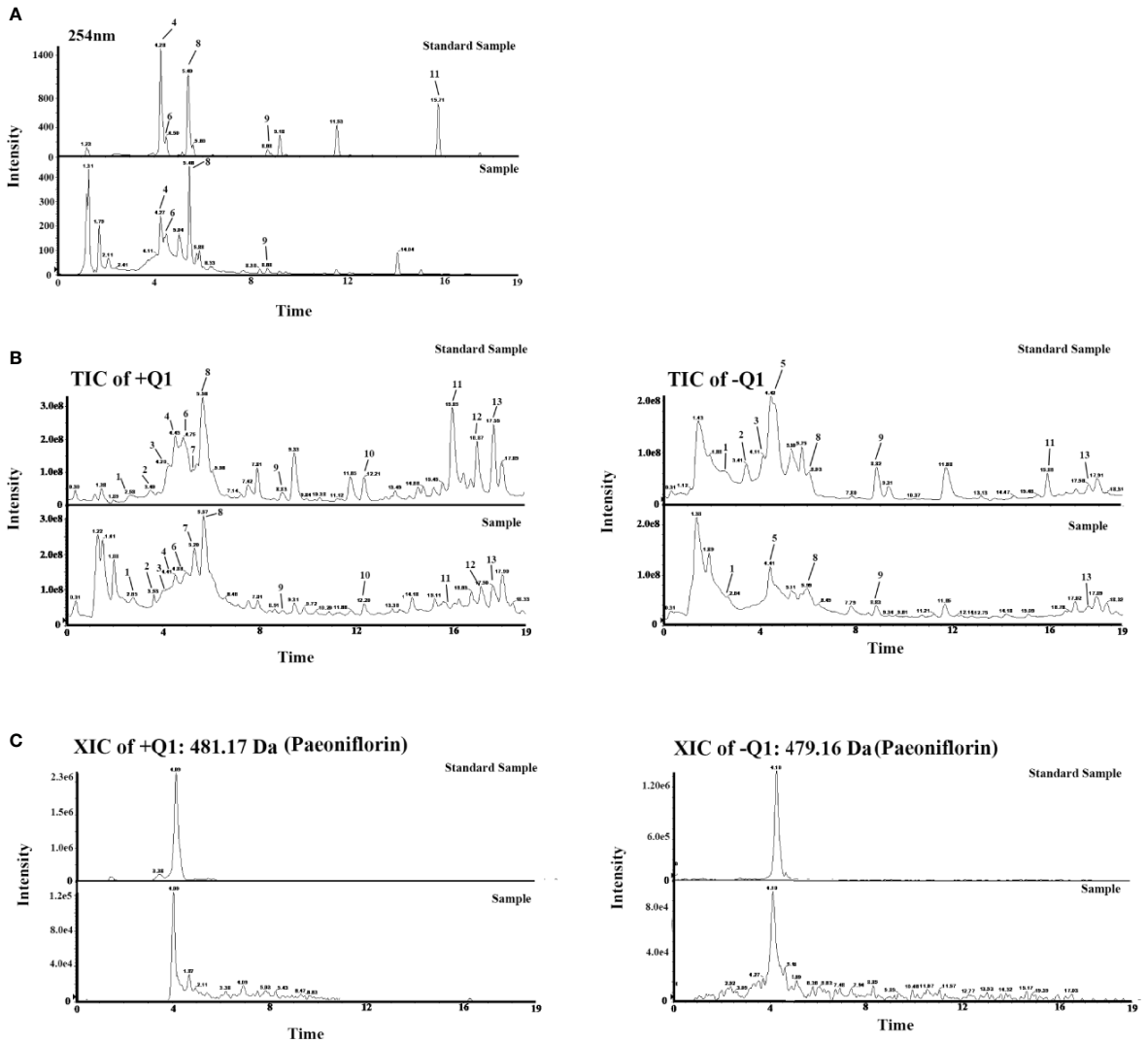


**FIGURE 4** | **(A)** Chromatograms of LCW and standard samples. **(B)** Total ion Current (TIC) chromatograms of LCW and standards samples. **(C)** Extracted ion current (XIC) chromatograms of paeoniflorin in LCW and standard samples. 1) Hydroxysafflor-Yellow-A, 2) Amygdalin, 3) Paeoniflorin, 4) Caffeic Acid, 5) Phillyrin, 6) Liquiritin, 7) Peimisine, 8) Harpagoside, 9) Rhein, 10) Z-Ligustilide, 11) Berberine, 12) Tanshinone II a, and 13) Catalpol.

**TABLE 1** | Information of chemical components in LCW.

| No | TR | Name | Formula | Molecular Weight | m/z | ion | Area (Standard) | Area (LCW) | Content (mg) |
|---|---|---|---|---|---|---|---|---|---|
| 1 | 2.56 | Hydroxysafflor-Yellow-A | $C_{27}H_{32}O_{16}$ | 612.17 | 613.18 | M+H | 1.06E+07 | 7.19E+05 | 0.34 |
| 2 | 3.41 | Amygdalin | $C_{20}H_{27}NO_{11}$ | 457.16 | 458.17 | M+H | 1.36E+06 | 8.70E+04 | 0.32 |
| 3 | 4.1 | Paeoniflorin | $C_{23}H_{28}O_{11}$ | 480.16 | 481.17 | M+H | 2.79E+07 | 3.15E+05 | 0.06 |
| 4 | 4.42 | Caffeic Acid | $C_9H_8O_4$ | 180.04 | 181.05 | M+H | 3.75E+06 | 1.14E+06 | 1.52 |
| 5 | 4.48 | Phillyrin | $C_{29}H_{36}O_{15}$ | 624.20 | 623.19 | M-H | 9.24E+07 | 3.57E+06 | 0.19 |
| 6 | 4.7 | Liquiritin | $C_{21}H_{22}O_9$ | 418.13 | 419.14 | M+H | 2.40E+06 | 4.30E+05 | 0.89 |
| 7 | 5.1 | Peimisine | $C_{27}H_{45}NO_3$ | 431.34 | 430.33 | M-H | 6.98E+05 | 5.28E+04 | 0.38 |
| 8 | 6.08 | Harpagoside | $C_{24}H_{30}O_{11}$ | 494.18 | 493.17 | M-H | 2.31E+07 | 2.11E+06 | 0.46 |
| 9 | 8.81 | Rhein | $C_{15}H_8O_6$ | 284.03 | 285.04 | M+H | 1.07E+07 | 3.30E+06 | 1.54 |
| 10 | 12.19 | Z-Ligustilide | $C_{12}H_{14}O_2$ | 190.10 | 191.11 | M-H | 5.77E+06 | 2.24E+06 | 1.94 |
| 11 | 15.89 | Berberine | $C_{17}H_{17}N$ | 235.14 | 236.15 | M-H | 5.10E+06 | 5.84E+05 | 0.57 |
| 12 | 16.87 | Tanshinone II a | $C_{19}H_{18}O_3$ | 294.13 | 295.14 | M+H | 1.61E+08 | 3.94E+06 | 0.12 |
| 13 | 17.57 | Catalpol | $C_{15}H_{22}O_{10}$ | 362.12 | 363.13 | M+H | 7.06E+06 | 3.35E+05 | 0.24 |

**TABLE 2** | The number of LCW components collected in the published databases.

| Herbs | components | Herbs | components |
|---|---|---|---|
| *Lonicera japonica* Thunb. (JYH) | 239 | *Paeonia ladiflora* Pall. (CS) | 75 |
| *Forsythia suspensa* (Thunb.) Vahl (LQ) | 153 | *Angelica sinensis* (Oliv.) Diels (DG) | 126 |
| *Taraxacum mongolicum* Hand. (PGY) | 77 | *Salvia miltiorrhiza* Bge. (DS) | 203 |
| *Coptis chinensis* Franch. (HL) | 33 | *Scrophularia ningpoensis* Hemsl. (XS) | 47 |
| *Rehjnannia glutinosa* Libosch. (DH) | 76 | *Prunus persica* (L.) Batsch (TR) | 66 |
| *Rheum officinale* Baill. (DH) | 92 | *Carthamus tinctorius* L. (HH) | 190 |
| *Glycyrrhiza uralensis* Fisch. (GC) | 280 | *Cryptotympana pustulata* Fabricius (CT) | 8 |
| *Scolopendra subspinipes mutilans* L. Koch (WG) | 8 | *Fritillaria thunbergii* Miq. (ZBM) | 17 |
| Total | | 1693 | |

therapy of SLE (Liu et al., 2019). Thus, these components could be considered as curative elements in treating SLE.

## C-T Network Construction of Active Components

To explore the therapeutic mechanism of LCW in the treatment of SLE, 193 active components and 1,220 targets (**Table S4**) were used to construct the component-target network (**Figure 5**). This network contain 6,399 component-target associations. The average number of targets of per component is 33.16. It shows that the multi-targets characteristics of LCW for treating of SLE. Among these components, vanillic acid (LCW190, degree = 510) has the highest number of targets, followed by ferulic acid (LCW75, degree = 480), kaempferol (LCW77, degree = 300), palmitic acid (LCW100, degree = 252), luteolin (LCW25, degree = 220), protocatechuic acid (LCW29, degree = 182), beta-sitosterol (LCW5, degree = 170), stigmasterol (LCW2, degree = 170), and caffeic acid (LCW23, degree = 148). Most of these components were reported associated with the inflammation and immune-related pathways of SLE. Such as vanillic acid, a well-known flavonoid, significantly decreased the increased serum levels of TNFα and IL-6 on concanavalin a-induced liver injury in mice (Itoh et al., 2010). Moreover, it could down-regulate LPS-induced COX-2 and nitric oxide production in mouse peritoneal macrophages *in vitro* (Kim et al., 2011). Ferulic acid reduced the translocation of NF-E2-related factor 2

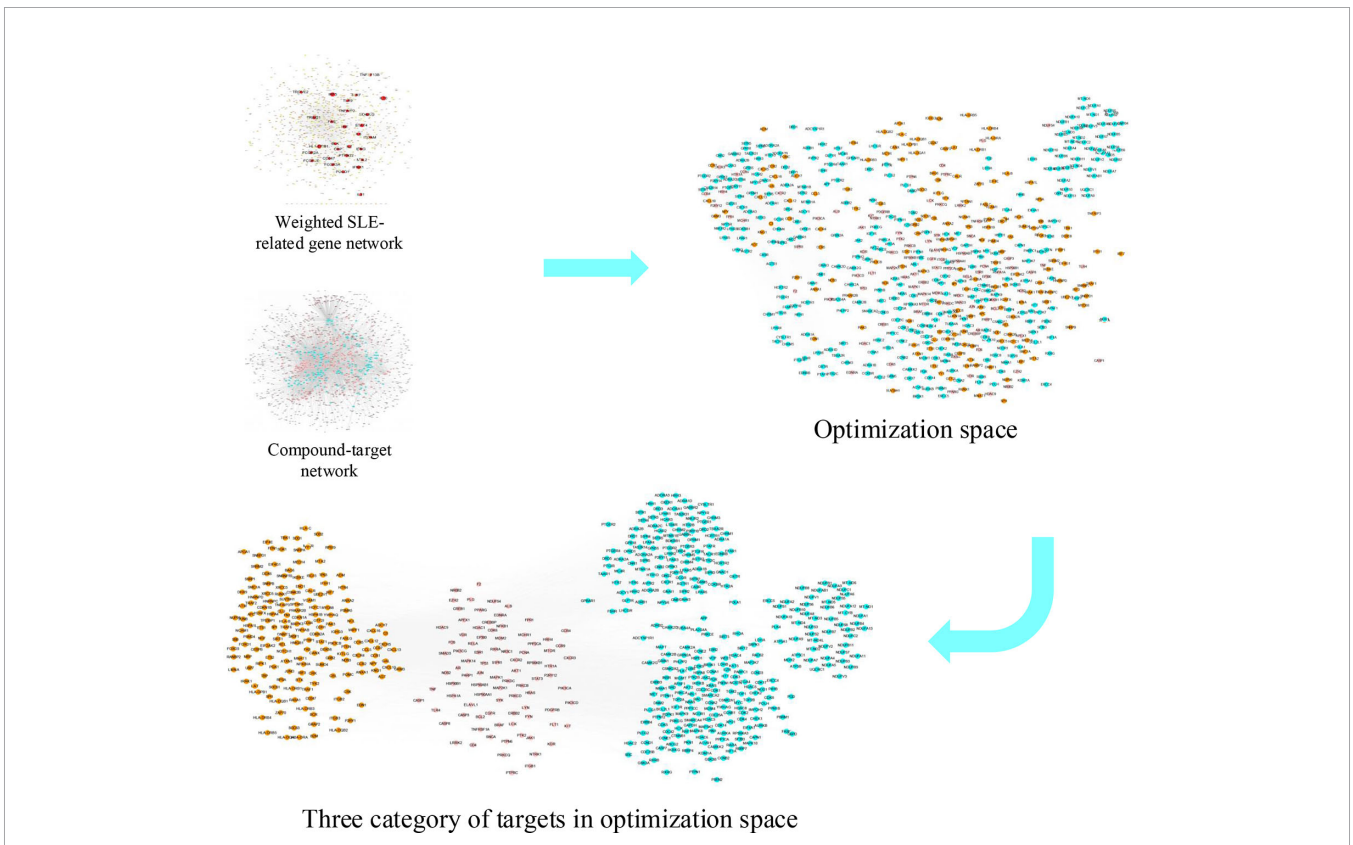


**FIGURE 5** | Optimization space construction. Optimization space includes three category targets, pink nodes represent essential common targets, orange nodes represent disease-specific targets, cyan nodes represent component-specific targets.

(NRF2) and nuclear transcription factor-κB (NF-kappa B) into the nuclei through a reduction of the expression of phosphorylated IKK and consequently inhibited IL-6 and NF-kappa B promoter activity. These data suggested that ferulic acid play anti-inflammatory roles by regulating IKK/NF-kappa B signaling pathway (Lampiasi and Montana, 2016). Protocatechuic acid inhibits Toll-like receptor-4 dependent activation of NF-kappa B by suppressing activation of the Akt, mTOR, JNK, and p38-MAPK (Nam and Lee, 2018). The function of remaining components in the treatment of SLE has been described in *Shared Components of Herbs in LCW* and *Specific Components of Herbs in LCW* sections. These results demonstrated that the crucial roles of these components in the treatment of SLE and further confirmed that these components work in a multi-target manner to treat SLE.

In the component-target network, the mean degree of targets for different components is 5.25. The top 20 targets with larger weight are ESR1, IL2, IL1B, TLR9, and ACE, etc. Interestingly, majority of these targets are related to immunity and inflammation, which are confirmed associated with the pathogenesis of SLE and that maybe indicate potential therapeutic mechanisms of LCW on SLE. For example, ESR1 polymorphism and its interaction with smoking and drinking contribute to susceptibility of SLE (Zhou et al., 2017); In addition, IL2 stimulates T cell proliferation and activation and regulates the adaptive immune response by stimulating both T-regulatory cells and activation-induced cell death in antigen-activated T cells. Some research reports indicated that IL2 region seems to play a role in the response to rituximab in SLE patients (Marquez et al., 2013); Moreover, TLR9 plays important role in immunopathology of SLE, because increased apoptosis and/or clearance deficiencies in SLE are considered to result in increased amounts of circulating plasma DNA, which may act as TLR agonists and subsequently provide B cell activation signals (Celhar et al., 2012). It is worth mention that 287-bp Alu insertion/deletion (I/D) of ACE gene was association with SLE and renal injury (Xu et al., 2007). Some other SNPs, such as A5466C, T3892C, A240T, C1237T, G2215A, A2350G, and C3409T, of ACE gene may affect the risk of certain autoimmune diseases including IgA nephropathy and lupus nephropathy (Li et al., 2010). Overall, these results suggested that LCW act synergistically to treat SLE by regulating inflammation, and immunity and further confirmed that targets of LCW were regulated by multi-components in the treatment of SLE.

## Effective Proteins Selection and Validation From Optimization Space

Here, we used the weighted gene regulatory network and active components targets network to construct disease-targets-components network. This network contains 1,829 nodes and 24,841 edges. Degree is an important topological property in the network that can be used to evaluate the importance of nodes in the network. For each node $i$ in disease-targets-components network, if the degree of a node is more than the average degree of all nodes in a network, such node is believed to play a critical role in the network structure, and can be treated as a hub node (Liu et al., 2016). Following this rule, the passed nodes and their edges in the disease-targets-components network were kept and defined as optimization space. The optimization space contains 565 nodes and 15,550 edges, each node represents one effective protein, and thus we identified 565 effective proteins from the optimization space. There are three categories of effective proteins in optimization space. The first category is the direct interactions between the component targets and pathogenic genes. We defined this category as the essential common targets. The second category is the interactions of disease-specific targets. The third category is the interactions of component-specific targets (**Figure 5** and **Table S5**).

To test whether the effective proteins we selected from optimization space could cover the pathogenic genes of SLE at functional level. We performed functional pathway analysis using effective proteins and SLE pathogenic genes, respectively. Among them, the effective proteins enriched in 178 pathways ($p < 0.05$), and the pathogenic genes enriched in 131 pathways ($p < 0.05$). The effective proteins enriched pathways were found to cover 96% of the pathogenic genes enriched pathways (**Figure 6A**). Additionally, in order to test whether the effective proteins in optimization space can be replaced by essential common targets, disease-specific targets or component-specific targets for further optimization. We performed pathway analysis on essential common targets, disease-specific targets, and component-specific targets, respectively. Results show that the coverage proportion of enriched pathways of three categories compare with the enriched pathways of pathogenic genes is 89%, 78%, 71%, respectively (**Figures 6B, C**), which are far less than that of the effective proteins. These results confirmed the accuracy and reliability of our approach to construct optimization space and further demonstrated that the effective proteins selected in the optimization space play a key role in the pathogenesis of SLW.

According to the results of KEGG analysis, these effective proteins were frequently involved in PI3K-Akt signaling pathway (hsa04151), Th17 cell differentiation (hsa04659), T cell receptor signaling pathway (hsa04660), TNF signaling pathway (hsa04668), MAPK signaling pathway (hsa04010), Toll-like receptor signaling pathway (hsa04620), NF-kappa B signaling pathway (hsa04064), IL-17 signaling pathway (hsa04657), and B cell receptor signaling pathway (hsa04662) (**Figure 6D**). PI3K/Akt/mTOR signaling pathway plays an important role in cellular proliferation and growth signaling. Increased activity of Akt can reduce expression of its substrate p27kip1 in SLE (Besliu et al., 2009). This defect seems to be involved in SLE lymphocytes passage by G1/S cell cycle checkpoint. Therefore, SLE lymphocytes accumulate in S and G2/M cell cycle phases towards apoptosis or proliferation. Previous research found that abnormal activation of the PI3K/AKT signaling pathway by upregulation of CDKs and downregulation of p27Kip1 and p21WAF1/CIP1 increased the proliferation of T lymphocytes might participate in the pathogenesis of SLE in SLE patients (Tang et al., 2009). The KEGG analysis and literature reported suggested that majority of them are related to immunity and inflammation, which are confirmed associated with the pathogenesis of SLE and that may be a potential therapeutic mechanism of LCW on SLE.

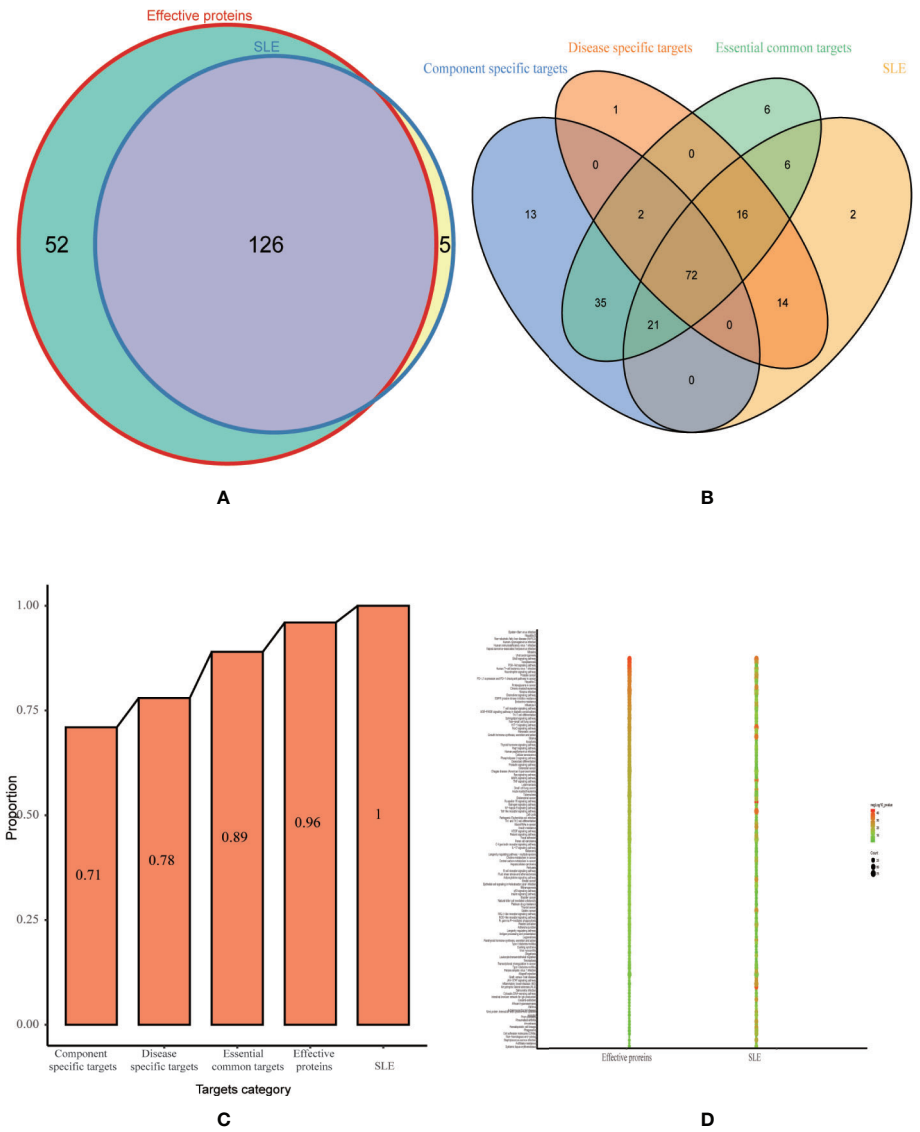


**FIGURE 6** | Validation of optimization space. **(A)** Venn diagram for pathway enrichment analysis of effective proteins and SLE related genes. **(B)** Venn diagram for pathway enrichment analysis of essential component-specific targets, disease-specific targets, essential common targets and SLE related genes. **(C)** The proportion histogram of enriched pathways of three categories (component-specific targets, disease-specific targets, essential common targets) and effective proteins compare with the enrichment pathways of pathogenic genes. **(D)** Bubble diagram for common pathway enrichment analysis of effective proteins and SLE related genes.

## KGEC Selection and Validation

The CI module was established to capture the KGEC, which would be used to illustrate the molecular mechanism of LCW in the therapy of SLE. According to the contribution accumulation results, the top 11 components including vanillic acid (LCW190), pinoresinol monomethyl ether (LCW169), phillyrin (LCW187), oleic acid (LCW160), palmitic acid (LCW100), stearic acid (LCW139), ferulic acid (LCW75), methyl caffeate (LCW137), p-coumaric acid (LCW186), ellagic acid (LCW8), and wogonin (LCW130) contribute to 51.89% target coverage of effective proteins. For further analysis, 82 components which can contribute to 90.18% targets coverage of effective proteins were selected as KGEC (**Figure 7** and **Table 3**). Among these components in KGEC, some of them belongs to different single herbs in LCW have the function of clearing away heat and toxic materials: JYH (18), LQ (19), PGY (14), HL (5), and WG (2). And some of them in different herbs have the function of cooling blood and promoting blood circulation: DH (3), CS (9), DG (4), DS (25), XS (6), TR (5), HH (21), CT (2), and ZBM (1). Higher targets coverage of effective proteins proved that the KGEC may play the leading role and generate combination effects in the treatment of SLE.

In order to investigate the function of LCW in the treatment of SLE, we performed pathway analysis using KGEC targets and

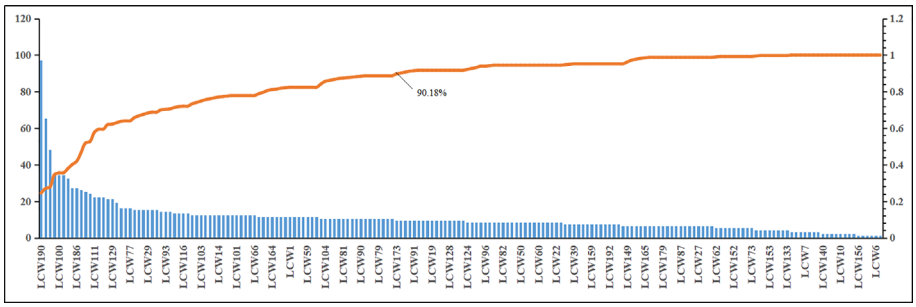


**FIGURE 7** | The CI and CI accumulation for KGEC selection in LCW. The bar diagram and trend line diagram are used to visualize the targets coverage of effective proteins of the LCW components and the contribution accumulation results, respectively.

**TABLE 3** | The information of selected KGEC in LCW.

| ID | Name | MF | MW | ID | Name | MF | MW |
|---|---|---|---|---|---|---|---|
| LCW190 | Vanillic acid | $C_8H_8O_4$ | 168.16 | LCW43 | Danshenol B | $C_{22}H_{26}O_4$ | 354.48 |
| LCW169 | Pinoresinol monomethyl ether | $C_{21}H_{24}O_6$ | 372.45 | LCW71 | Zinc14719978 | $C_{19}H18O_4$ | 310.37 |
| LCW187 | Phillyrin | $C_{27}H_{34}O_{11}$ | 534.61 | LCW36 | (Z)-3-[2-(E)-2-(3,4-Dihydroxyphenyl) ethenyl]-3,4-Dihydroxy-Phenyl]Acrylic Acid | $C_{17}H_{14}O_6$ | 314.31 |
| LCW160 | Oleic acid | $C_{18}H_{34}O_2$ | 282.52 | LCW101 | 6-Hydroxykaempferol | $C_{15}H_{10}O_7$ | 302.25 |
| LCW100 | Palmitic acid | $C_{16}H_{32}O_2$ | 256.48 | LCW94 | Beta-carotene | $C_{40}H_{56}$ | 536.96 |
| LCW139 | Stearic acid | $C_{18}H_{36}O_2$ | 284.54 | LCW95 | Cholesterol | $C_{27}H_{46}O$ | 386.73 |
| LCW75 | Ferulic acid | $C_{10}H_{10}O_4$ | 194.2 | LCW80 | Licoricone | $C_{22}H_{22}O_6$ | 382.44 |
| LCW137 | Methyl caffeate | $C_{10}H_{10}O_4$ | 194.2 | LCW66 | Salviolone | $C_{18}H_{20}O_2$ | 268.38 |
| LCW186 | P-coumaric acid | $C_9H_8O_3$ | 164.17 | LCW147 | Gibberellin 7 | $C_{19}H_{22}O_5$ | 330.41 |
| LCW8 | Ellagic acid | $C_{14}H_6O_8$ | 302.2 | LCW175 | Chrysanthemaxanthin | $C_{40}H_{56}O_3$ | 584.96 |
| LCW130 | Wogonin | $C_{16}H_{12}O_5$ | 284.28 | LCW171 | Beta-amyrin acetate | $C_{32}H_{52}O_2$ | 468.84 |
| LCW114 | Mandenol | $C_{20}H_{36}O_2$ | 308.56 | LCW164 | 3-Acetyl-5-Hydroxy-7-Methoxy-2-Methylnaphthalene-1,4-Dione | $C_{14}H_{12}O_5$ | 260.26 |
| LCW111 | (R)-Canadine | $C_{20}H_{21}NO_4$ | 339.42 | LCW131 | Zinc238769177 | $C_{21}H_{24}O_6$ | 372.45 |
| LCW115 | Chryseriol | $C_{16}H_{12}O_6$ | 300.28 | LCW178 | Epiberberine | $C_{20}H_{18}NO_4^+$ | 336.39 |
| LCW138 | Myristic acid | $C_{14}H_{28}O_2$ | 228.42 | LCW70 | Zinc13341234 | $C_{18}H_{16}O_8$ | 360.34 |
| LCW161 | Sitogluside | $C_{35}H_{60}O_6$ | 576.95 | LCW1 | Baicalin | $C_{21}H_{18}O_{11}$ | 446.39 |
| LCW129 | Rutin | $C_{27}H_{30}O_{16}$ | 610.57 | LCW24 | Clionasterol | $C_{29}H_{50}O$ | 414.79 |
| LCW174 | Cholesteryl ferulate | $C_{37}H_{54}O_4$ | 562.91 | LCW41 | Cryptotanshinone | $C_{19}H_{20}O_3$ | 296.39 |
| LCW143 | Stachyose | $C_{24}H_{42}O_{21}$ | 666.66 | LCW45 | Deoxyneocryptotanshinone | $C_{19}H_{22}O_3$ | 298.41 |
| LCW118 | Ethyl Linolenate | $C_{20}H_{34}O_2$ | 306.54 | LCW59 | Nortanshinone | $C_{17}H_{12}O_4$ | 280.29 |
| LCW77 | Kaempferol | $C_{15}H_{10}O_6$ | 286.25 | LCW106 | Pyrethrin II | $C_{22}H_{28}O_5$ | 372.5 |
| LCW170 | 3beta-Acetyl-20,25-epoxydammarane-24alpha-ol | $C_{32}H_{54}O_4$ | 502.86 | LCW97 | Quercetin | $C_{15}H_{10}O_7$ | 302.25 |
| LCW38 | 2-(4-Hydroxy-3-Methoxyphenyl)-5-(3-Hydroxypropyl)-7-Methoxy-3-Benzofurancarboxaldehyde | $C_{20}H_{20}O_6$ | 356.4 | LCW180 | GA121-isolactone | $C_{23}H_{32}O_5Si$ | 330.41 |
| LCW185 | Isoscopoletin | $C_{10}H_8O_4$ | 192.18 | LCW104 | Amygdalin | $C_{20}H_{27}NO_{11}$ | 457.48 |
| LCW29 | Protocatechuic Acid | $C_7H_6O_4$ | 154.13 | LCW134 | Esculetin | $C_9H_6O_4$ | 178.15 |
| LCW127 | (-)-Phillygenin | $C_{21}H_{24}O_6$ | 372.45 | LCW68 | Tournefolic acid A | $C_{17}H_{12}O_6$ | 312.29 |
| LCW126 | Isolariciresinol | $C_{20}H_{24}O_6$ | 360.44 | LCW110 | Magnograndiolide | $C_{15}H_{22}O_4$ | 266.37 |
| LCW31 | Tanshinone II a | $C_{19}H_{18}O_3$ | 294.37 | LCW81 | Methoxy-7-Hydroxycoumarin | $C_{16}H_{12}O_6$ | 300.28 |
| LCW93 | Shinpterocarpin | $C_{20}H_{18}O_4$ | 322.38 | LCW84 | Glabridin | $C_{20}H_{20}O_4$ | 324.4 |
| LCW108 | Quercetagetin | $C_{15}H_{10}O_8$ | 318.25 | LCW135 | Ethyl Caffeate | $C_{11}H_{12}O_4$ | 208.23 |
| LCW113 | Palmatine | $C_{21}H_{22}NO_4^+$ | 352.44 | LCW55 | Miltionone II | $C_{19}H_{20}O_4$ | 312.39 |
| LCW54 | Miltionone I | $C_{19}H_{20}O_4$ | 312.39 | LCW90 | Liquiritin | $C_{21}H_{22}O_9$ | 418.43 |
| LCW116 | Corymbosin | $C_{19}H_{18}O_7$ | 358.37 | LCW3 | 3-Epi-Beta-Sitosterol | $C_{29}H_{50}O$ | 414.79 |
| LCW25 | Luteolin | $C_{15}H_{10}O_6$ | 286.25 | LCW123 | Arctiin | $C_{27}H_{34}O_{11}$ | 534.61 |
| LCW9 | Paeoniflorigenone | $C_{17}H_{18}O_6$ | 318.35 | LCW181 | GA122-isolactone | $C_{23}H_{32}O_5Si$ | 416.6 |
| LCW11 | Paeonol | $C_9H_{10}O_3$ | 166.19 | LCW79 | Licochalcone B | $C_{16}H_{14}O_5$ | 286.3 |
| LCW103 | 7,8-dimethyl-1H-pyrazino[2,3-g]quinazoline-2,4-dione | $C_{12}H_{10}N_4O_2$ | 242.26 | LCW188 | Protocatechualdehyde | $C_7H_6O_3$ | 138.13 |
| LCW122 | Bicuculline | $C_{20}H_{17}NO_6$ | 367.38 | LCW26 | Sugiol | $C_{20}H_{28}O_2$ | 300.48 |
| LCW32 | 3-Hydroxymethylenetanshinquinone | $C_{18}H_{14}O_4$ | 294.32 | LCW34 | Tanshinone II b | $C_{19}H_{18}O_4$ | 310.37 |
| LCW51 | Isotanshinone IIa | $C_{19}H_{18}O_3$ | 294.37 | LCW173 | Carthamone | $C_{21}H_{20}O_{11}$ | 448.41 |
| LCW14 | Zinc15211904 | $C_{17}H_{18}O_6$ | 318.35 | LCW98 | Lignan | $C_{25}H_{30}O_8$ | 458.55 |

SLE pathogenic genes, respectively. Among them, the KGEC targets enriched in 181 pathways ($p < 0.05$), and the pathogenic genes enriched in 131 pathways ($p < 0.05$). The KGEC targets enriched pathways were found to cover 80.15% of the pathogenic genes enriched pathways (**Figure 8**). These major targets of KEGG were frequently involved in PI3K-Akt signaling pathway (hsa04151), HIF-1 signaling pathway (hsa04066), MAPK signaling pathway (hsa04010), T cell receptor signaling pathway (hsa04660), IL-17 signaling pathway (hsa04657), B cell receptor signaling pathway (hsa04662), TNF signaling pathway (hsa04668), Toll-like receptor signaling pathway (hsa04620), NF-kappa B signaling pathway (hsa04064), JAK-STAT signaling pathway (hsa04630) and Th1 and Th2 cell differentiation (hsa04658), etc. For example, the PI3K-Akt signaling pathway (hsa04151) was essential to cellular proliferation and growth. In addition, it was correlated with autoimmune diseases due to its activation in lymphocytes, which are developed features of systemic autoimmunity (Ge et al., 2017). NF-kappa B was an essential modulator in the pathogenesis of SLE in the context of the increasing immune

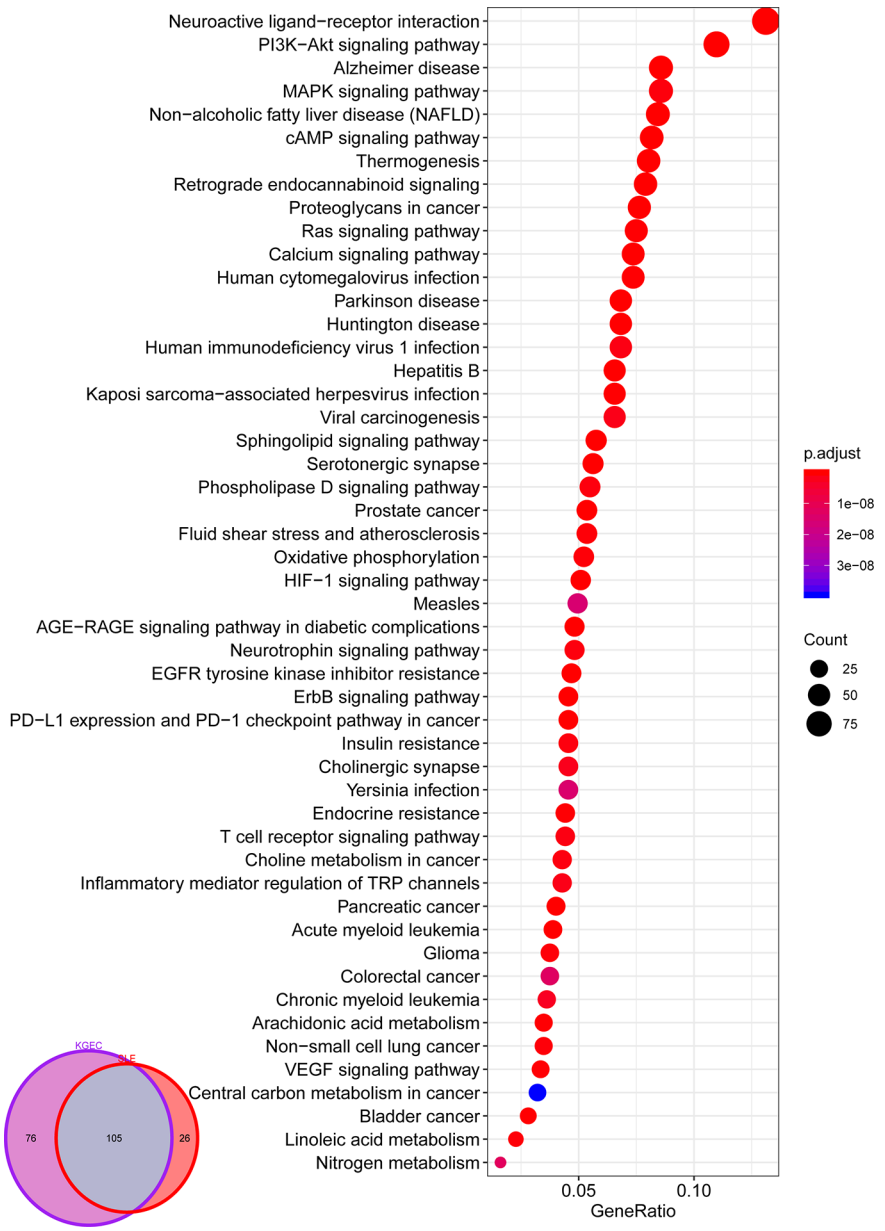


**FIGURE 8** | Pathway enrichment analysis of KGEC Targets. Veen diagram for pathway enrichment analysis of KGEC targets and SLE related genes; The size of the circle represents the number of genes enriched in the pathways, and the color change of the circle represents the significant degree of the enriched genes in the pathways.

deficiencies (Wong et al., 1999). The TLR family in the NF-kappa B pathway was responsible for sensing microbial pathogens and occupied an important position in innate immune responses. So TLR signals in B cells amplified anti-dsDNA autoantibody and enhanced one SLE characteristic, autoantibody production (Papadimitraki et al., 2006). This result suggested that the strategy of combining the optimization space with the CI model to optimize the herbal formula is reliable and the predicted KGEC may play therapy role by mediating multiple inflammation-related pathways.

## GO Enrichment Analysis of KGEC Targets

GO enrichment analysis based on clusterProfiler package of R software was performed to identify the biological functional of the primary targets with $p$-values <0.05. In order to further dissect the combination effects of LCW, all the targets interacting with KGEC of LCW were enriched by GO enrichment analysis (**Figure 9**).

GO analysis showed that the targets of KGEC were enriched in biological processes related to inflammation and immunity. For example, the pathways of inflammation are regulation of inflammatory response (GO:0050727, LYN, PTGS2, PPARG, PTPRC, etc.), leukocyte activation involved in inflammatory response (GO:0002269, PTPRC, LRRK2, TNF, JUN, TLR2, etc.), production of molecular mediator involved in inflammatory response (GO:0002532, TNF, KDM6B, CXCR2, ELANE, CNR1, etc.), and inflammatory response to antigenic stimulus (GO:0002437, LYN, TLR4, F2, SERPINE1, NOS2, etc.). Important genes involved in inflammation in these pathways include TNF, NOS2, TLR2, etc. these genes are involved in inflammation of SLE (Oates et al., 2003; Marques et al., 2016; Zhao et al., 2017). The pathways of immunity are regulation of innate immune response (GO:0045088, PTPN22, LYN, PPARG, JAK1, EP300, etc.), immune response-regulating cell surface receptor signaling pathway (GO:0002768, PTPN22, BLK, LYN, PTPRC, EP300, etc.), regulation of production of molecular mediator of immune response (GO:0002700, PTPRC, IL1B, IL2, TLR9, TNF, etc.), B cell activation involved in immune response (GO:0002312, PTPRC, IL2, TLR4, LGALS1, ABL1, etc.) and T cell differentiation involved in immune response (GO:0002292, IL2, MTOR, STAT3, RORA, RORC, etc.). Important genes involved in inflammation in these pathways include PTPN22, TLR4, MTOR. These genes are involved in inflammation of SLE (Lai et al., 2015; Wong-Baeza et al., 2015; Morris et al., 2016). SLE is an autoimmune disease characterized by the presence of circulating immune complexes and inflammation in multiple organs and tissues. GO analysis confirmed that LCW treat SLE through regulation of inflammation and immune therapy.

Interestingly, LCW regulates the GO cellular component of SLE, including mitochondrial respiratory chain complex I (GO: 0005747, SNCA, NDUFS4, NDUFA4, NDUFA1, NDUFA10, etc.), mitochondrial respiratory chain (GO:0005746, SNCA, NDUFS4, NDUFA4, NDUFA1, NDUFA10, etc.), and

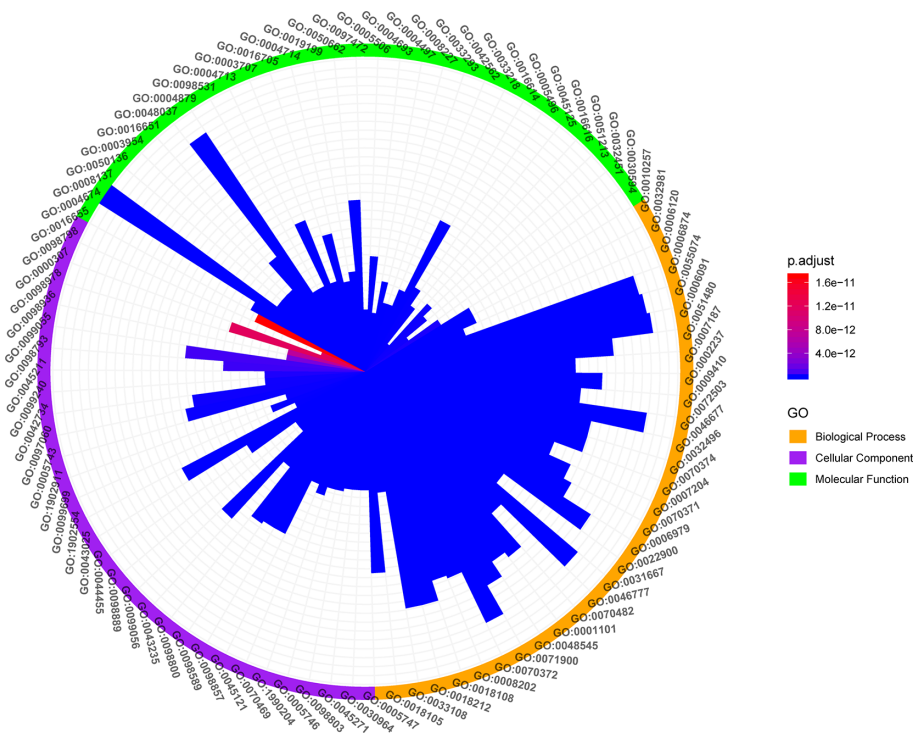


**FIGURE 9** | GO enrichment analysis of KGEC Targets. The Orange, purple and bright green color on the circle represent biological processes, cellular component and molecular function, respectively. The color change of the bar represents the significant degree of the enriched genes in the GO items.

oxidoreductase complex (GO:1990204, SNCA, NDUFS4, P4HB, NOX1, NOX4, etc.). Accumulating evidence indicates that mitochondrial dysfunction plays important roles in the pathogenesis of SLE, including mitochondrial DNA damage, mitochondrial dynamics change, abnormal mitochondrial biogenesis and energy metabolism, oxidative stress, inflammatory reactions (Lee et al., 2016). Given the accumulating evidence for mitochondrial release during inflammatory pathogenesis, these observations point to a role for mitochondria both in the stimulation of the innate immune system and as a potential source of autoantigens. Our results indicated that LCW may play a role in the treatment of SLE by modulating targets on the mitochondria.

Moreover, LCW regulates the GO molecular function of SLE including protein serine/threonine kinase activity (GO: 0004674, LRRK2, MAPK1, MTOR, EGFR, PRKCB, etc.), transcription factor activity (GO:0098531, PPARG, RXRA, ESR1, STAT3, VDR, etc.), and protein tyrosine kinase activity (GO:0004713, BLK, LYN, JAK1, EPHB2, HSP90AA1, etc.). Increasing evidence confirmed enzymes play different roles in regulating inflammation and immunity (Cunninghame Graham et al., 2007; Suarez-Fueyo et al., 2011). Our results indicate that LCW may affect different types of enzyme functions in the treatment of SLE.

## KEGG Enrichment Analysis of KGEC Targets

SLE is a chronic autoimmune disease involving multiple organs and systems characterized by the production of multiple autoantibodies. Previous studies confirmed that SLE-associated pathways could be decomposed into several functional modules such as immune response, synthesis of inflammatory mediators, autoimmune pathology, neutrophil recruitment, immunity to extracellular pathogens, cell cycle progression, protein synthesis, apoptosis, and so forth. Increasing evidence indicate that PI3K-Akt signaling pathway (hsa04151), TNF signaling pathway (hsa04668), NF-kappa B signaling pathway (hsa04064) and IL-17 signaling pathway (hsa04657) response to these functional modules. Such as, PI3K-Akt signaling pathway (hsa04151) has been reported involved in the inhibition of apoptosis, cell proliferation and expression of inflammatory cytokines. TNF signaling pathway (hsa04668) can induce a wide range of intracellular signal pathways including apoptosis and cell survival as well as inflammation and immunity. NF-kappa B signaling pathway (hsa04064) is the generic name of a family of transcription factors that function as dimers and regulate genes involved in immunity, inflammation and cell survival. While IL-17 signaling pathway (hsa04657) work as a subset of cytokines consisting of IL-17A-F, plays crucial roles in both acute and chronic inflammatory responses. For exploring the mechanism of LCW in the treatment of SLE at the system level, we constructed a comprehensive signaling pathway use four important molecular pathways (**Figure 10**).

These four pathways play important roles in the treatment of SLE. In order to define the position of LCW targets on the pathways, we consider the first three columns as upstream and the rest as a downstream position of the pathway. Among them, PI3K-Akt signaling pathway (hsa04151) is one of the top pathways in the treatment of SLE with KGEC in LCW. KGEC regulates 10 targets located upstream of PI3K-Akt signaling

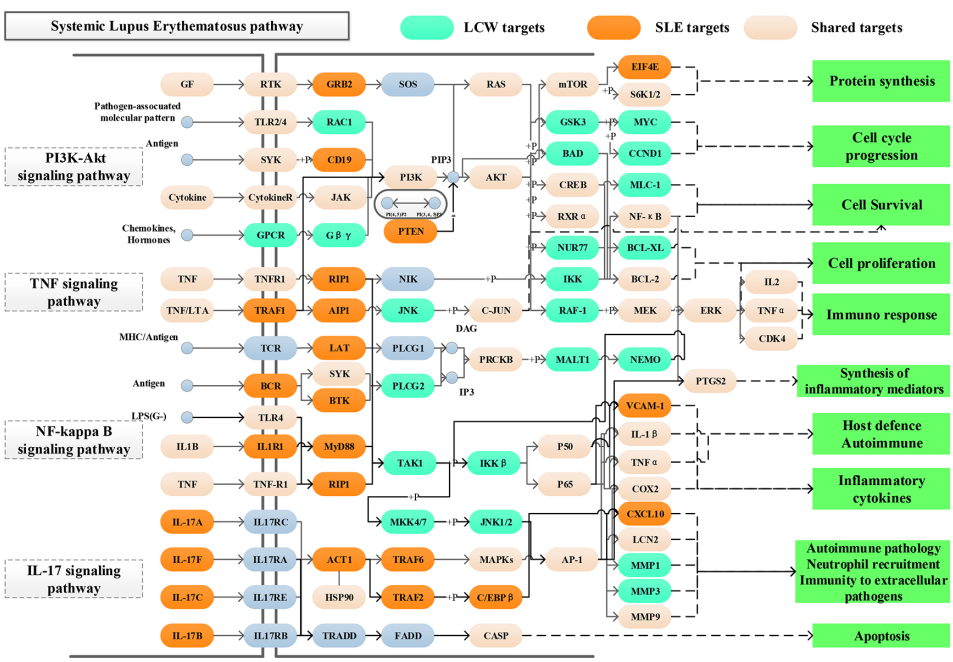


**FIGURE 10** | Distribution of targets of KGEC on the comprehensive signaling pathway. Different colors represent different types of targets. Light green represents the targets of LCW, orange represents the pathogenetic genes of SLE, and pink represents shared targets, respectively.

pathway (hsa04151), such as RTK, TLR2/4 and JAK, and 24 targets located downstream pathways, such as PI3K, AKT, and mTOR. The downstream targets account for more than 70%. KGEC may activate downstream of the PI3K and AKT proteins through the upstream TLR2/4, resulting in downstream GSK3, RXRα, and CREB cascade amplification, which are closely related to SLE immune response, cell proliferation and protein synthesis (Bentham et al., 2015). Most of the targets of KGEC regulating TNF signaling pathway (hsa04668) are located downstream of the pathway, such as JNK, C-JUN and RAF-1. In addition, it can also be seen (**Figure 10**) that KGEC can also affect the activation of PI3K and AKT proteins downstream of TNF to play a role in the treatment of SLE. Therefore, KGEC in LCW plays a key role in the treatment of SLE by regulating the TNF-PI3K-AKT key cascade to synergistically affect the process of immunity and inflammation.

NF-kappa B signaling pathway (hsa04064) and IL-17 signaling pathway (hsa04657) are also important pathways in the treatment of SLE by LCW. The targets regulated by KGEC are more downstream of the pathway. For example, 19 targets such as TAK1, IL-1 β, and COX2 of KGEC are located downstream of NF-kappa B signaling pathway (hsa04064). KGEC in LCW can affect upstream BCR, and then activate downstream AP-1, to further affect a series of inflammatory and immune-related proteins such as IL-1 β, TNF α, and COX2 related to SLE. The 12 targets of KGEC, such as MAPKs, AP-1 and LCN2, in the IL-17 signaling pathway (hsa04657) are located downstream of the pathway. KGEC in LCW can activate downstream AP-1, through upstream MAPKs, and affect a series of inflammatory and immune-related proteins such as LCN2, MMP1, and MMP3 related to SLE (Marques et al., 2016). Therefore, KGEC in LCW can also play a role in the treatment of SLE by regulating the NTF-MAPKs-AP-1 key cascade to synergistically affect the process of immunity and inflammation.

## Experimental Validation *In Vitro*

The effect of liquiritin and ferulic acid in KGEC was assessed in RAW 264.7 cells. As shown in **Figure S1**, 10–100 μM of liquiritin and ferulic acid revealed no obvious effects. To evaluate the anti-inflammatory effect of liquiritin and ferulic acid, the level of IL-6 was detected. Exposure of RAW 264.7 cells to resiquimod significantly elevated the level of IL-6 ($p < 0.01$). In contrast, pretreatment with liquiritin and ferulic acid significantly attenuated the phenomenon induced by resiquimod (**Figures 11A, B**). According to the anti-inflammatory effect of liquiritin and ferulic acid, 50 μM liquiritin and ferulic acid were used in subsequent research. Therefore, liquiritin and ferulic acid concentration of 50 μM were used to evaluate the effect on resiquimod-induced RAW 264.7 cells. Exposure of RAW 264.7 cells to resiquimod significantly elevated the protein expression of IL- p-ERK1/2, p-AKT, and p-PI3K. In contrast, treatment with liquiritin and ferulic acid significantly attenuated the phenomenon induced by resiquimod (**Figures 11C–F**). Our results demonstrated that liquiritin and ferulic acid inhibited the phenomenon production in resiquimod induced RAW264.7 cells.

## DISCUSSION

The main purpose of formula optimization is to reduce the non-pharmacological factors and improve the curative effect of the

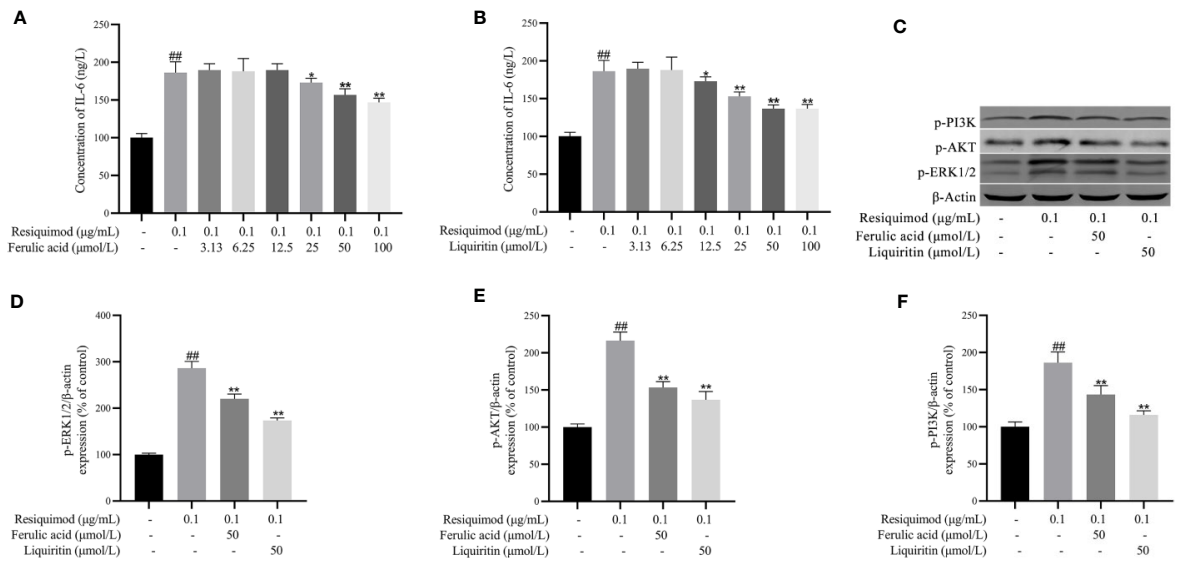


**FIGURE 11** | Effects of ferulic acid **(A)** and liquiritin **(B)** on resiquimod-induced RAW 264.7 cells IL-6 cytokines expression and the protein expression of p-ERK1/2, p-AKT, and p-PI3K of resiquimod induced RAW264.7 cells **(C–F)**. $^{\#\#}p < 0.01$, compared with control group. $^{*}p < 0.05$, $^{**}p < 0.01$, compared with the resiquimod group.

formula. Although different medicinal herbs are composed as the formula according to the theory of TCM, whether the herbs or the components in the formula are necessary, especially for a specific indication is still need analysis and verification. Through optimization of formula, the medicine herbs or ingredient with effect can be screened, so that the formula is more simplified and the drug effect is more clarified.

In order to better optimize the classical formula with clinical curative effect, effective proteins, common targets, disease-specific targets, component-specific targets and KGEC targets were defined as changed target-data sets. Mathematical methods and network pharmacology were employed to investigate the coverage percentage of changed target-data sets related functional analysis on that of the disease pathogenesis genes. The changed target-data sets response to different targets of various herbs and different chemical components in each formula. To find the relatively optimal KGEC, the strategy of optimization space definition and reverse searching for components was applied and evaluated based on changed target-data sets, which provide a methodological reference for the research and development of new drugs based on TCM.

At present, how to optimize and obtain the KGEC and analyze their mechanism of action is the basis for quantification of TCM. The research of TCM emphasizes the holistic view, integrity and synergy. Network pharmacology has the characteristics of systematization and integrity, which is consistent with the philosophy of TCM research. Network pharmacology emphasizes multi-targets regulation of signal pathways to improve the therapeutic effect of drugs and reduce toxic and side effects. At present, network pharmacology is widely used in the treatment of complex diseases in TCM. For example, to determine the molecular mechanism of TCM formula in the treatment of complex diseases, such as "treating different diseases with the same treatment, treating the same diseases with different treatment", but there are few research reports based on network pharmacology to study the optimization of formula in TCM. Thus, we propose an integrative strategy to optimize LCW based on network pharmacology, obtain the key components of LCW in the treatment of SLE, and analyze the potential mechanism of these components.

In the process of analyzing the therapeutic mechanism, network pharmacology has formed its own analytical rules, in the first step, select active components through ADME/T screening based on the chemical properties of components in TCM. Then predict targets and analyze potential mechanisms. This flowchart really solves the molecular mechanism of some formulas of TCM in treating complex diseases. Such as: Hua Yu Qiang Shen Tong Bi formula treats rheumatoid arthritis (Wang et al., 2019), Shen Qi Wan treats kidney yang deficiency syndrome (Zhang et al., 2019), and Huo Xiang Zheng Qi formula treats functional dyspepsia (Zhao et al., 2018). However, there still exists some problems, such as false positive and noise in the predicted targets of components. Here we propose a strategy to optimize active components and decode molecular mechanism of LCW in the treatment of SLE. In this strategy, we build an optimization space and extract effective proteins based on the associations of component targets and pathogenetic genes to reduce the false positive and noise.

The result shows that the enriched functional pathways of effective protein can cover 96% of the enriched functional pathways of pathogenetic genes. It proves that our strategy of constructing target-based optimization space to select effective proteins is appropriate and reliable. Based on the effective proteins provided by optimization space, we calculated the accumulation contribution degree by using the CI model, and the accumulation contribution degree of 82 active components reach more than 90% was finally optimized as KGEC. KEGG and Go analysis confirmed that the targets of our optimized KGEC are closely related to the pathogenesis of SLE in pathways and functional annotation. This proves once again the reliability of our optimization space and CI model.

Currently, our network pharmacology model provides a powerful tool for exploring the compatibility and mechanism of TCM formula. Cellular experiments were applied to prove the reliability of the network pharmacology model through verifying the protective effects of components in KGEC of LCW on the inflammation of mice RAW264.7 cells induced by resiquimod. In addition, in order to better evaluate the reliability of our proposed network pharmacology model, *in vivo* study will be conducted to verify the efficacy and mechanism of active components in the treatment of SLE in our future research.

## DATA AVAILABILITY STATEMENT

The raw data supporting the conclusions of this manuscript will be made available by the authors, without undue reservation, to any qualified researcher.

## AUTHOR CONTRIBUTIONS

A-pL, X-mQ, and D-gG provided the concept and designed the study. YG, K-xW, PW, XL, J-jC, B-yZ, and J-sT conducted the analyses and wrote the manuscript. YG, K-xW, PW, XL, J-jC, B-yZ, and J-sT participated in data analysis. A-pL, X-mQ, and D-gG contributed to revising and proof-reading the manuscript. All authors contributed to the article and approved the submitted version.

## FUNDING

This study is financially supported by the Startup fund from Southern Medical University [grant No. G619280010], the Natural Science Foundation Council of China [grant No. 31501080], Hong Kong Baptist University Strategic Development Fund [grant No. SDF13-1209-P01, SDF15-0324-P02(b) and SDF19-0402-P02], Hong Kong Baptist University Interdisciplinary Research Matching Scheme [grant No. RC/IRCs/17-18/04], the General Research Fund of Hong Kong

Research Grants Council [grant No. 12101018, 12100719, 12102518] and the National S&T Major Project for "Major New Drugs Innovation and Development" [2017ZX09301047].

## SUPPLEMENTARY MATERIAL

The Supplementary Material for this article can be found online at: https://www.frontiersin.org/articles/10.3389/fphar.2020.512877/full#supplementary-material.

**SUPPLEMENTARY TABLE 1 |** The information of SLE genes.

**SUPPLEMENTARY TABLE 2 |** The information of LCW components.

**SUPPLEMENTARY TABLE 3 |** The information of LCW active components.

**SUPPLEMENTARY TABLE 4 |** The relationship between components and targets.

**SUPPLEMENTARY TABLE 5 |** The information of effective proteins.

**SUPPLEMENTARY FIGURE 1 |** Effects of ferulic acid **(A)** and liquiritin **(B)** on cell viabilities.

## REFERENCES


Bentham, J., Morris, D. L., Graham, D. S. C., Pinder, C. L., Tombleson, P., Behrens, T. W., et al. (2015). Genetic association analyses implicate aberrant regulation of innate and adaptive immunity genes in the pathogenesis of systemic lupus erythematosus. *Nat. Genet.* 47 (12), 1457–1464. doi: 10.1038/ng.3434

Besliu, A. N., Pistol, G., Marica, C. M., Banica, L. M., Chitonu, C., Ionescu, R., et al. (2009). PI3K/Akt signaling in peripheral T lymphocytes from systemic lupus erythematosus patients. *Roum Arch. Microbiol Immunol.* 68 (2), 69–79.

Celhar, T., Magalhaes, R., and Fairhurst, A. M. (2012). TLR7 and TLR9 in SLE: when sensing self goes wrong. *Immunol. Res.* 53 (1–3), 58–77. doi: 10.1007/s12026-012-8270-1

Chen, S. J., and Cui, M. C. (2017). Systematic Understanding of the Mechanism of Salvianolic Acid A via Computational Target Fishing. *Molecules* 22 (4), 1–10. doi: 10.3390/molecules22040644

Chen, C. Y. (2011). TCM Database@Taiwan: the world's largest traditional Chinese medicine database for drug screening in silico. *PloS One* 6 (1), e15939. doi: 10.1371/journal.pone.0015939

Cunninghame Graham, D. S., Akil, M., and Vyse, T. J. (2007). Association of polymorphisms across the tyrosine kinase gene, TYK2 in UK SLE families. *Rheumatol. (Oxford)* 46 (6), 927–930. doi: 10.1093/rheumatology/kel449

Dorner, T., and Furie, R. (2019). Novel paradigms in systemic lupus erythematosus. *Lancet* 393 (10188), 2344–2358. doi: 10.1016/s0140-6736(19)30546-x

Dos Santos, M., Poletti, P. T., Favero, G., Stacchiotti, A., Bonomini, F., Montanari, C. C., et al. (2018). Protective effects of quercetin treatment in a pristane-induced mouse model of lupus nephritis. *Autoimmunity* 51 (2), 69–80. doi: 10.1080/08916934.2018.1442828

Draghici, S., Khatri, P., Tarca, A. L., Amin, K., Done, A., Voichita, C., et al. (2007). A systems biology approach for pathway level analysis. *Genome Res.* 17 (10), 1537–1545. doi: 10.1101/gr.6202607

Duan, H., Zhai, K. F., Khan, G. J., Zhou, J., Cao, T. Y., Wu, Y. Q., et al. (2019). Revealing the Synergistic Mechanism of Multiple Components in Compound Fengshiding Capsule for Rheumatoid Arthritis Therapeutics by Network Pharmacology. *Curr. Mol. Med.* 19 (4), 303–314. doi: 10.2174/1566524019666190405094125

Espindola, K. M. M., Ferreira, R. G., Narvaez, L. E. M., Silva Rosario, A. C. R., da Silva, A. H. M., Silva, A. G. B., et al. (2019). Chemical and Pharmacological Aspects of Caffeic Acid and Its Activity in Hepatocarcinoma. *Front. Oncol.* 9, 541. doi: 10.3389/fonc.2019.00541

Fraile, L., Crisci, E., Cordoba, L., Navarro, M. A., Osada, J., and Montoya, M. (2012). Immunomodulatory properties of beta-sitosterol in pig immune responses. *Int. Immunopharmacol.* 13 (3), 316–321. doi: 10.1016/j.intimp.2012.04.017

Gan, Y., Zheng, S., Zhao, J., Zhang, C., Gao, T., Liao, W., et al. (2018). Protein network module-based identification of key pharmacological pathways of Curcuma phaeocaulis Val. acting on hepatitis. *J. Ethnopharmacol* 221, 10–19. doi: 10.1016/j.jep.2018.03.004

Ge, F., Wang, F., Yan, X., Li, Z., and Wang, X. (2017). Association of BAFF with PI3K/Akt/mTOR signaling in lupus nephritis. *Mol. Med. Rep.* 16 (5), 5793–5798. doi: 10.3892/mmr.2017.7367

Geng, L., Li, X., Feng, X., Zhang, J., Wang, D., Chen, J., et al. (2014). Association of TNF-alpha with impaired migration capacity of mesenchymal stem cells in patients with systemic lupus erythematosus. *J. Immunol. Res.* 2014:169082. doi: 10.1155/2014/169082

Gfeller, D., Grosdidier, A., Wirth, M., Daina, A., Michielin, O., and Zoete, V. (2014). SwissTargetPrediction: a web server for target prediction of bioactive small molecules. *Nucleic Acids Res.* 42 (Web Server issue), W32–W38. doi: 10.1093/nar/gku293

Guan, D., Shao, J., Zhao, Z., Wang, P., Qin, J., Deng, Y., et al. (2014). PTHGRN: unraveling post-translational hierarchical gene regulatory networks using PPI, ChIP-seq and gene expression data. *Nucleic Acids Res.* 42 (Web Server issue), W130–W136. doi: 10.1093/nar/gku471

Guo, P., Cai, C., Wu, X., Fan, X., Huang, W., Zhou, J., et al. (2019). An Insight Into the Molecular Mechanism of Berberine Towards Multiple Cancer Types Through Systems Pharmacology. *Front. Pharmacol.* 10, 857. doi: 10.3389/fphar.2019.00857

Huang, K. P., Zhang, Z. H., Li, R. M., and Chen, X. (2016). The Therapeutic Effects of the Chinese Herbal Medicine, Lang Chuang Fang Granule, on Lupus-Prone MRL/lpr Mice. *Evid Based Complement Alternat Med.* 2016, 8562528. doi: 10.1155/2016/8562528

Iraz, M., Ozerol, E., Gulec, M., Tasdemir, S., Idiz, N., Fadillioglu, E., et al. (2006). Protective effect of caffeic acid phenethyl ester (CAPE) administration on cisplatin-induced oxidative damage to liver in rat. *Cell Biochem. Funct.* 24 (4), 357–361. doi: 10.1002/cbf.1232

Itoh, A., Isoda, K., Kondoh, M., Kawase, M., Watari, A., Kobayashi, M., et al. (2010). Hepatoprotective effect of syringic acid and vanillic acid on CCl4-induced liver injury. *Biol. Pharm. Bull.* 33 (6), 983–987. doi: 10.1248/bpb.33.983

Kim, M. C., Kim, S. J., Kim, D. S., Jeon, Y. D., Park, S. J., Lee, H. S., et al. (2011). Vanillic acid inhibits inflammatory mediators by suppressing NF-kappaB in lipopolysaccharide-stimulated mouse peritoneal macrophages. *Immunopharmacol. Immunotoxicol.* 33 (3), 525–532. doi: 10.3109/08923973.2010.547500

Kyogoku, C., Smiljanovic, B., Grun, J. R., Biesen, R., Schulte-Wrede, U., Haupl, T., et al. (2013). Cell-specific type I IFN signatures in autoimmunity and viral infection: what makes the difference? *PloS One* 8 (12), e83776. doi: 10.1371/journal.pone.0083776

Kyriakidis, N. C., Kapsogeorgou, E. K., Gourzi, V. C., Konsta, O. D., Baltatzis, G. E., and Tzioufas, A. G. (2014). Toll-like receptor 3 stimulation promotes Ro52/TRIM21 synthesis and nuclear redistribution in salivary gland epithelial cells, partially via type I interferon pathway. *Clin. Exp. Immunol.* 178 (3), 548–560. doi: 10.1111/cei.12432

Lai, Z. W., Marchena-Mendez, I., and Perl, A. (2015). Oxidative stress and Treg depletion in lupus patients with anti-phospholipid syndrome. *Clin. Immunol.* 158 (2), 148–152. doi: 10.1016/j.clim.2015.03.024

Lampiasi, N., and Montana, G. (2016). The molecular events behind ferulic acid mediated modulation of IL-6 expression in LPS-activated Raw 264.7 cells. *Immunobiology* 221 (3), 486–493. doi: 10.1016/j.imbio.2015.11.001

Lee, H. T., Wu, T. H., Lin, C. S., Lee, C. S., Wei, Y. H., Tsai, C. Y., et al. (2016). The pathogenesis of systemic lupus erythematosus - From the viewpoint of oxidative stress and mitochondrial dysfunction. *Mitochondrion* 30, 1–7. doi: 10.1016/j.mito.2016.05.007

Lee, S. B., Shin, J. S., Han, H. S., Lee, H. H., Park, J. C., and Lee, K. T. (2018). Kaempferol 7-O-beta-D-glucoside isolated from the leaves of Cudrania tricuspidata inhibits LPS-induced expression of pro-inflammatory mediators through inactivation of

NF-kappaB, AP-1, and JAK-STAT in RAW 264.7 macrophages. *Chem. Biol. Interact.* 284, 101–111. doi: 10.1016/j.cbi.2018.02.022

Leng, R. X., Pan, H. F., Liu, J., Yang, X. K., Zhang, C., Tao, S. S., et al. (2016). Evidence for genetic association of TBX21 and IFNG with systemic lupus erythematosus in a Chinese Han population. *Sci. Rep.* 6, 22081. doi: 10.1038/srep22081

Li, X., An, J., Guo, R., Jin, Z., Li, Y., Zhao, Y., et al. (2010). Association of the genetic polymorphisms of the ACE gene and the eNOS gene with lupus nephropathy in northern Chinese population. *BMC Med. Genet.* 11, 94. doi: 10.1186/1471-2350-11-94

Li, J. Y., Wang, X. B., Luo, J. G., and Kong, L. Y. (2015). Seasonal Variation of Alkaloid Contents and Anti-Inflammatory Activity of Rhizoma coptidis Based on Fingerprints Combined with Chemometrics Methods. *J. Chromatogr Sci.* 53 (7), 1131–1139. doi: 10.1093/chromsci/bmu175

Li, B., Ma, C., Zhao, X., Hu, Z., Du, T., Xu, X., et al. (2018). YaTCM: Yet another Traditional Chinese Medicine Database for Drug Discovery. *Comput. Struct. Biotechnol. J.* 16, 600–610. doi: 10.1016/j.csbj.2018.11.002

Liu, P., Song, J., Su, H., Li, L., Lu, N., Yang, R., et al. (2013). IL-10 gene polymorphisms and susceptibility to systemic lupus erythematosus: a meta-analysis. *PloS One* 8 (7), e69547. doi: 10.1371/journal.pone.0069547

Liu, X., Vogt, I., Haque, T., and Campillos, M. (2013). HitPick: a web server for hit identification and target prediction of chemical screenings. *Bioinformatics* 29 (15), 1910–1912. doi: 10.1093/bioinformatics/btt303

Liu, H., Zeng, L., Yang, K., and Zhang, G. (2016). A Network Pharmacology Approach to Explore the Pharmacological Mechanism of Xiaoyao Powder on Anovulatory Infertility. *Evid Based Complement Alternat Med.* 2016, 2960372. doi: 10.1155/2016/2960372

Liu, D. Q., Chen, S. P., Sun, J., Wang, X. M., Chen, N., Zhou, Y. Q., et al. (2019). Berberine protects against ischemia-reperfusion injury: A review of evidence from animal models and clinical studies. *Pharmacol. Res.* 148, 104385. doi: 10.1016/j.phrs.2019.104385

Loram, L. C., Culp, M. E., Connolly-Strong, E. C., and Sturgill-Koszycki, S. (2015). Melanocortin peptides: potential targets in systemic lupus erythematosus. *Inflammation* 38 (1), 260–271. doi: 10.1007/s10753-014-0029-5

Luo, W., Pant, G., Bhavnasi, Y. K., Blanchard, S. G.Jr., and Brouwer, C. (2017). Pathview Web: user friendly pathway visualization and data integration. *Nucleic Acids Res.* 45 (W1), W501–w508. doi: 10.1093/nar/gkx372

Ma, Y. C., Lin, C. C., Li, C. I., Chiang, J. H., Li, T. C., and Lin, J. G. (2016). Traditional Chinese medicine therapy improves the survival of systemic lupus erythematosus patients. *Semin. Arthritis Rheum* 45 (5), 596–603. doi: 10.1016/j.semarthrit.2015.09.006

Marques, C. P., Maor, Y., de Andrade, M. S., Rodrigues, V. P., and Benatti, B. B. (2016). Possible evidence of systemic lupus erythematosus and periodontal disease association mediated by Toll-like receptors 2 and 4. *Clin. Exp. Immunol.* 183 (2), 187–192. doi: 10.1111/cei.12708

Marquez, A., Davila-Fajardo, C. L., Robledo, G., Rubio, J. L., de Ramon Garrido, E., Garcia-Hernandez, F. J., et al. (2013). IL2/IL21 region polymorphism influences response to rituximab in systemic lupus erythematosus patients. *Mol. Biol. Rep.* 40 (8), 4851–4856. doi: 10.1007/s11033-013-2583-6

Morris, D. L., Sheng, Y., Zhang, Y., Wang, Y. F., Zhu, Z., Tombleson, P., et al. (2016). Genome-wide association meta-analysis in Chinese and European individuals identifies ten new loci associated with systemic lupus erythematosus. *Nat. Genet.* 48 (8), 940–946. doi: 10.1038/ng.3603

Nam, Y. J., and Lee, C. S. (2018). Protocatechuic acid inhibits Toll-like receptor-4-dependent activation of NF-kappaB by suppressing activation of the Akt, mTOR, JNK and p38-MAPK. *Int. Immunopharmacol* 55, 272–281. doi: 10.1016/j.intimp.2017.12.024

Oates, J. C., Levesque, M. C., Hobbs, M. R., Smith, E. G., Molano, I. D., Page, G. P., et al. (2003). Nitric oxide synthase 2 promoter polymorphisms and systemic lupus erythematosus in african-americans. *J. Rheumatol* 30 (1), 60–67.

Papadimitraki, E. D., Choulaki, C., Koutala, E., Bertsias, G., Tsatsanis, C., Gergianaki, I., et al. (2006). Expansion of toll-like receptor 9-expressing B cells in active systemic lupus erythematosus: implications for the induction and maintenance of the autoimmune process. *Arthritis Rheum* 54 (11), 3601–3611. doi: 10.1002/art.22197

Pinero, J., Bravo, A., Queralt-Rosinach, N., Gutierrez-Sacristan, A., Deu-Pons, J., Centeno, E., et al. (2017). DisGeNET: a comprehensive platform integrating information on human disease-associated genes and variants. *Nucleic Acids Res.* 45 (D1), D833–d839. doi: 10.1093/nar/gkw943

Ru, J., Li, P., Wang, J., Zhou, W., Li, B., Huang, C., et al. (2014). TCMSP: a database of systems pharmacology for drug discovery from herbal medicines. *J. Cheminform* 6, 13. doi: 10.1186/1758-2946-6-13

Shimane, K., Kochi, Y., Suzuki, A., Okada, Y., Ishii, T., Horita, T., et al. (2013). An association analysis of HLA-DRB1 with systemic lupus erythematosus and rheumatoid arthritis in a Japanese population: effects of *09:01 allele on disease phenotypes. *Rheumatol. (Oxford)* 52 (7), 1172–1182. doi: 10.1093/rheumatology/kes427

Suarez-Fueyo, A., Barber, D. F., Martinez-Ara, J., Zea-Mendoza, A. C., and Carrera, A. C. (2011). Enhanced phosphoinositide 3-kinase delta activity is a frequent event in systemic lupus erythematosus that confers resistance to activation-induced T cell death. *J. Immunol.* 187 (5), 2376–2385. doi: 10.4049/jimmunol.1101602

Tang, H., Tan, G., Guo, Q., Pang, R., and Zeng, F. (2009). Abnormal activation of the Akt-GSK3beta signaling pathway in peripheral blood T cells from patients with systemic lupus erythematosus. *Cell Cycle* 8 (17), 2789–2793. doi: 10.4161/cc.8.17.9446

Tao, W., Xu, X., Wang, X., Li, B., Wang, Y., Li, Y., et al. (2013). Network pharmacology-based prediction of the active ingredients and potential targets of Chinese herbal Radix Curcumae formula for application to cardiovascular disease. *J. Ethnopharmacol* 145 (1), 1–10. doi: 10.1016/j.jep.2012.09.051

Veeranki, S., and Choubey, D. (2010). Systemic lupus erythematosus and increased risk to develop B cell malignancies: role of the p200-family proteins. *Immunol. Lett.* 133 (1), 1–5. doi: 10.1016/j.imlet.2010.06.008

Wallace, D. J. (2015). The evolution of drug discovery in systemic lupus erythematosus. *Nat. Rev. Rheumatol* 11 (10), 616–620. doi: 10.1038/nrrheum.2015.86

Wang, G., Zhou, C., Liu, W., and Gao, H. (1991). Pharmacological effects of Lang Chuang Wan. *Pharmacl Clin. Chin Mater Clin. Med.* 03), 28–31.

Wang, C., Ren, Q., Chen, X. T., Song, Z. Q., Ning, Z. C., Gan, J. H., et al. (2018). System Pharmacology-Based Strategy to Decode the Synergistic Mechanism of Zhi-zhu Wan for Functional Dyspepsia. *Front. Pharmacol.* 9, 841. doi: 10.3389/fphar.2018.00841

Wang, Z., Linghu, K. G., Hu, Y., Zuo, H., Yi, H., Xiong, S. H., et al. (2019). Deciphering the Pharmacological Mechanisms of the Huayu-Qiangshen-Tongbi Formula Through Integrating Network Pharmacology and In Vitro Pharmacological Investigation. *Front. Pharmacol.* 10, 1065. doi: 10.3389/fphar.2019.01065

Wang, Z. (1989). Clinical and laboratorial study of the effect of antilupus pill on systemic lupus erythematosus. *Chin J. Integr. Tradit West Med.* 08), 465–468.

Wong, H. K., Kammer, G. M., Dennis, G., and Tsokos, G. C. (1999). Abnormal NF-kappa B activity in T lymphocytes from patients with systemic lupus erythematosus is associated with decreased p65-RelA protein expression. *J. Immunol.* 163 (3), 1682–1689.

Wong-Baeza, C., Tescucano, A., Astudillo, H., Resendiz, A., Landa, C., Espana, L., et al. (2015). Nonbilayer Phospholipid Arrangements Are Toll-Like Receptor-2/6 and TLR-4 Agonists and Trigger Inflammation in a Mouse Model Resembling Human Lupus. *J. Immunol. Res.* 2015, 369462. doi: 10.1155/2015/369462

Wu, C. J., Guo, J., Luo, H. C., Wei, C. D., Wang, C. F., Lan, Y., et al. (2016). Association of CD40 polymorphisms and haplotype with risk of systemic lupus erythematosus. *Rheumatol Int.* 36 (1), 45–52. doi: 10.1007/s00296-015-3345-7

Xie, G., Peng, W., Li, P., Xia, Z., Zhong, Y., He, F., et al. (2018). A Network Pharmacology Analysis to Explore the Effect of Astragali Radix-Radix Angelica Sinensis on Traumatic Brain Injury. *BioMed. Res. Int.* 2018, 3951783. doi: 10.1155/2018/3951783

Xu, J., Wang, Y., Pan, F., Stankovich, J., Ye, D., Lian, L., et al. (2007). Association of ACE gene polymorphism with genetic susceptibility to systemic lupus erythematosus in a Chinese population: a family-based association study. *J. Rheumatol* 34 (12), 2408–2411.

Xu, X., Zhang, W., Huang, C., Li, Y., Yu, H., Wang, Y., et al. (2012). A novel chemometric method for the prediction of human oral bioavailability. *Int. J. Mol. Sci.* 13 (6), 6964–6982. doi: 10.3390/ijms13066964

Xue, R., Fang, Z., Zhang, M., Yi, Z., Wen, C., and Shi, T. (2013). TCMID: Traditional Chinese Medicine integrative database for herb molecular

mechanism analysis. *Nucleic Acids Res.* 41 (Database issue), D1089–D1095. doi: 10.1093/nar/gks1100

Yang, L., Zhou, X., Huang, W., Fang, Q., Hu, J., Yu, L., et al. (2017). Protective Effect of Phillyrin on Lethal LPS-Induced Neutrophil Inflammation in Zebrafish. *Cell Physiol. Biochem.* 43 (5), 2074–2087. doi: 10.1159/000484192

Yu, G., Wang, L. G., Han, Y., and He, Q. Y. (2012). clusterProfiler: an R package for comparing biological themes among gene clusters. *Omics* 16 (5), 284–287. doi: 10.1089/omi.2011.0118

Zhang, J. Y., Hong, C. L., Chen, H. S., Zhou, X. J., Zhang, Y. J., Efferth, T., et al. (2019). Target Identification of Active Constituents of Shen Qi Wan to Treat Kidney Yang Deficiency Using Computational Target Fishing and Network Pharmacology. *Front. Pharmacol.* 10, 650. doi: 10.3389/fphar.2019.00650

Zhao, H., Wang, L., Luo, H., Li, Q. Z., and Zuo, X. (2017). TNFAIP3 downregulation mediated by histone modification contributes to T-cell dysfunction in systemic lupus erythematosus. *Rheumatol. (Oxford)* 56 (5), 835–843. doi: 10.1093/rheumatology/kew508

Zhao, M., Chen, Y., Wang, C., Xiao, W., Chen, S., Zhang, S., et al. (2018). Systems Pharmacology Dissection of Multi-Scale Mechanisms of Action of Huo-Xiang-Zheng-Qi Formula for the Treatment of Gastrointestinal Diseases. *Front. Pharmacol.* 9, 1448. doi: 10.3389/fphar.2018.01448

Zhou, A., Liu, X., Xia, T., Li, F., Wang, J., and Li, J. (2017). Estrogen receptor alpha gene (ESR1) polymorphism and its interaction with smoking and drinking contribute to susceptibility of systemic lupus erythematosus. *Immunol. Res.* 65 (4), 951–956. doi: 10.1007/s12026-017-8935-x

**Conflict of Interest:** The authors declare that the research was conducted in the absence of any commercial or financial relationships that could be construed as a potential conflict of interest.

# Advantages of publishing in Frontiers

**OPEN ACCESS**
Articles are free to read for greatest visibility and readership

**FAST PUBLICATION**
Around 90 days from submission to decision

**HIGH QUALITY PEER-REVIEW**
Rigorous, collaborative, and constructive peer-review

**TRANSPARENT PEER-REVIEW**
Editors and reviewers acknowledged by name on published articles

**Frontiers**
Avenue du Tribunal-Fédéral 34
1005 Lausanne | Switzerland

**Visit us:** www.frontiersin.org
**Contact us:** frontiersin.org/about/contact

**REPRODUCIBILITY OF RESEARCH**
Support open data and methods to enhance research reproducibility

**DIGITAL PUBLISHING**
Articles designed for optimal readership across devices

**FOLLOW US**
@frontiersin

**IMPACT METRICS**
Advanced article metrics track visibility across digital media

**EXTENSIVE PROMOTION**
Marketing and promotion of impactful research

**LOOP RESEARCH NETWORK**
Our network increases your article's readership